



A University of Sussex PhD thesis

Available online via Sussex Research Online:

<http://sro.sussex.ac.uk/>

This thesis is protected by copyright which belongs to the author.

This thesis cannot be reproduced or quoted extensively from without first obtaining permission in writing from the Author

The content must not be changed in any way or sold commercially in any format or medium without the formal permission of the Author

When referring to this work, full bibliographic details including the author, title, awarding institution and date of the thesis must be given

Please visit Sussex Research Online for more information and further details

Mixed sand and gravel
beaches: accurate
measurement of active layer
depth to develop predictive
models of sediment transport

Amanda Holland

Thesis submitted for the award of Doctor of Philosophy

UNIVERSITY OF SUSSEX

November 2019

I hereby declare that this thesis has not been and will not be, submitted in whole or in part to another university for the aware of any other degree.

Signature:

Acknowledgements

First and foremost, thanks to my supervisors: Professor Cherith Moses, Professor David Sear, Dave Picksley, Dr Samantha Cope and Dr John Barlow. Thanks also to my examiners, Dr Malcolm Bray and Professor Roger Moore, for their helpful feedback after my first submission.

Many thanks to Havant Borough Council / the Eastern Solent Coastal Partnership for use of equipment and assistance with software. In particular: Simon, Clare, Dan and Louise provided vital support and assistance in the field.

Thanks to Linley Hastewell at Portsmouth University for allowing me use of their sediment ovens, and staff at Southampton University for fieldwork and software assistance, and to Dr Jo Nield for allowing me use of her surface roughness script (which was ultimately only used in the pilot study).

Huge thank yous to my family for keeping a roof over my head, helping with fieldwork and checking the final copies.

To Sam and the wakeboarding girls: thank you for sticking around.

Sorry to anyone I've forgotten, it's been a long road.

This thesis uses aerial imagery and wave buoy data from the Channel Coast Observatory, and tide data from The British Oceanographic Data Centre. Funding was provided as part of a joint project between NERC and Havant Borough Council.

Summary

This thesis addresses the need to calibrate longshore sediment transport equations for use on heavily managed mixed sediment beaches, which are becoming increasingly common but are still relatively understudied. This is achieved through the use of active layer measurements, tracer pebble experiments, and monitoring of morphodynamics over a total period of 16 months. It is unique in investigating a complex, artificially replenished, groyned mixed sand and gravel beach in this way. The groynes have a significant impact on beach morphology and sediment transport at Eastoke.

Beach levels were monitored using repeated profiles at three main locations within a groyne cell, allowing for the effect of these structures on beach profile shape and response to changing wave climates to be assessed. This provides a more accurate representation of morphodynamics than would otherwise be available from semi-annual profile surveys. The beach response to hydrodynamic conditions was shown to be rapid, and not always indicative of drift direction. Sediment sorting was observed, but was not strongly correlated with wave conditions.

A vast dataset of active layer measurements indicated significant variability, which has not been made clear by previous studies of active layer depth. The key finding of this thesis is that active layer depth as a percentage of wave height can be predicted from significant wave height using the equation $\ln(y) = -0.797x + 3.565$ ($R^2 = 0.578$), and this value can then be converted into a depth measurement. The prediction can be applied at a daily scale to the combined upper and mid beach as an estimate of the average active layer depth. Further field sites should be investigated to determine whether this equation can be applied to other mixed sediment beaches.

Short- and medium-term pebble transport patterns were observed using passive integrated transponder (PIT) tagged pebbles, deployed in stages throughout the research. Sediment transport volumes were estimated based on field data, and hydrodynamic data used to calculate a range of drift coefficients (k) for the commonly used CERC transport formula. Low detection rates ultimately limit the confidence which can be applied to final calculations of longshore transport volumes and values of k , but this study provides insight into the complexities associated with studying a site like this, and suggestions for improvements which could be made to future research.

Table of Contents

Chapter 1: Introduction

1.1 Motivation for the study.....	1
1.2 Aim and objectives.....	3
1.3 Specific research questions.....	3
1.4 Structure of the thesis.....	5

Chapter 2: Literature Review

2.1 Introduction.....	7
i. Definition of a beach.....	7
ii. Beach classifications.....	8
iii. Basic morphology.....	9
iv. Beach replenishment.....	11
2.2 Mixed sediment beaches.....	12
i. Sediments.....	12
ii. Classifications.....	13
iii. Distribution.....	13
iv. Morphological features.....	14
v. Differences between natural and artificial mixed beaches.....	15
vi. Sediment transport.....	16
vii. Forcing mechanisms.....	17
2.3 The active layer.....	23
i. Active layer research on sand beaches.....	24
ii. Active layer research on gravel and mixed sediment beaches.....	26
2.4 Predicting drift rates.....	31
2.5 Summary.....	33

Chapter 3: Site Description

3.1 Introduction.....	34
3.2 The Solent.....	38
3.3 Wave climate.....	39
i. Bi-modal waves.....	41
ii. Wave refraction.....	43
3.4 Tidal deltas.....	44

3.5 Flood and defence history.....	46
i. Replenishment schemes.....	46
ii. Eastoke Point Defence Scheme.....	50

Chapter 4: Methodology

4.1 Overview.....	51
4.2 Research design.....	51
4.3 Monitoring wave climate.....	59
4.4 Beach profile changes.....	60
4.5 Active layer depth.....	65
4.6 Sediment composition.....	74
4.7 Sediment transport.....	77
4.8 Summary.....	88

Chapter 5: Profile Shape and Evolution

5.1 Introduction.....	89
5.2 Results.....	89
i. Sedimentology.....	89
ii. Surface sediments.....	95
iii. Correlation between surface sediment codes and physical samples.....	100
iv. Profile shapes.....	101
v. Profile changes.....	104
vi. Berm dynamics.....	115
vii. Using CSA to estimate longshore transport rates.....	120
5.3 Discussion.....	122
i. Mixed sediment beach characteristics.....	122
ii. Profile types.....	126
iii. Profile changes.....	127
iv. Berm dynamics.....	128
5.4 Conclusions.....	128

Chapter 6: Active layer dynamics

6.1 Introduction.....	130
6.2 Methods.....	131
6.3 Results.....	132
i. Variation in AL depth.....	132

ii. Relationship with wave height.....	151
iii. Relationship with wave period.....	169
iv. Relationship with wave power.....	177
v. Relationship with wave direction.....	182
vi. Depth of disturbance rods.....	184
vii. Multiple Regression Analysis (MRA).....	186
6.4 Discussion.....	188
i. Variation in AL depth.....	188
ii. Relationship with wave height.....	191
iii. Relationship with wave period.....	197
iv. Relationship with wave power.....	198
v. Relationship with wave direction.....	198
vi. Depth of disturbance rods.....	199
vi. Multiple Regression Analysis (MRA).....	200
6.5 Conclusions.....	200

Chapter 7: Transport Rates and Volumes

7.1 Introduction.....	204
7.2 Methods.....	205
7.3 Results.....	206
i. Detection rates.....	206
ii. Short term transport.....	208
iii. Transport relative to deployment depth.....	212
iv. Medium term transport rates.....	217
v. Calculating longshore transport volumes.....	224
vi. Calibrating the CERC equation.....	227
7.4 Discussion.....	230
i. Reasons for low detection rates.....	231
ii. Transport rates.....	233
iii. Longshore transport volumes.....	233
iv. CERC calibration.....	237
7.5 Conclusions.....	238

Chapter 8: Conclusion

8.1 Introduction.....	240
-----------------------	-----

8.2 Aims of the thesis.....	240
8.3 Recap of methods used.....	241
8.4 Main findings.....	242
8.5 Final recommendations.....	244

References.....	246
------------------------	------------

Appendices

Appendix A: Wave conditions.....	A-1
Appendix B: dGPS profile surveys.....	B-9
Appendix C: Mean profile and profile envelope for each profile during each study period.....	C-31
Appendix D: Cross-shore variation between percentages of surface sediment codes during the first winter, with each profile's results shown separately.....	D-39
Appendix E: Comparison of surface codes to sieved sediment samples.....	E-43
Appendix F: Database of AL measurements by date and location.....	F-45
Appendix G: Mean, maximum and standard deviation of AL depths per day.....	G-54
Appendix H: Mean, maximum and standard deviations of daily AL measurements in relation to wave height, separated by study period.....	H-56
Appendix I: Mean, maximum and standard deviations of daily AL measurements in relation to wave period, separated by study period.....	I-58
Appendix J: i) Daily mean AL measurements of each study period, in relation to wave direction (Winter 1).....	J-60
ii) Daily mean AL measurements of each study period, in relation to wave direction (Winter 2).....	J-61
Appendix K: Relationship between average sand content and AL depth.....	K-62
Appendix L: Scatterplots showing relationship between wave height and AL depth within each elevation zone.....	L-63
Appendix M: Relationships between slope angle and AL depth for each profile.....	M-66

Appendix N: RFID detector tests.....	N-67
Appendix O: Pebble deployments and distance between survey detections.....	O-68
Appendix P: Pebble column detection rates in individual surveys.....	P-79
Appendix Q: Pilot Study (March 2014).....	Q-85
Appendix R: Tracer guide.....	R-94

Table of Figures

Figure 1.1 Thesis flowchart	6
Figure 2.1: The classification of beaches based on their proportions of coarse sediments (gravel and cobbles) versus sand, with the resulting differences in their morphologies	9
Figure 2.2: Conceptual model processes affecting, and affected by, sediment transport on a mixed sediment beach	18
Figure 2.3: Types of breaking waves as a function of wave-height, water depth and beach slope gradient	19
Figure 3.1: A) National, B) regional and C) local maps to indicate location of study site.	36
Figure 3.2: Eastoke Point	37
Figure 3.3: The Solent River, early to mid quaternary.	39
Figure 3.4: Significant wave heights (Hs) and directions (°) measured at the Hayling Island wave buoy, 10/07/2003 – 31/12/2016.	40
Figure 3.5: Annual wave height exceedance levels (Hs).	40
Figure 3.6: Joint distribution plots: percentage occurrences of wave heights, periods and directions July 2003 – December 2016.	41
Figure 3.7: Example of bimodal wave energy spectra, 19:05 14/01/2015.	42
Figure 3.8: Sediment Transport from Portsmouth Harbour Entrance to Chichester Harbour Entrance.	45
Figure 3.9: Net volumetric change above MLWS, relative to 2004 baseline survey	49
Figure 3.10: Eastoke Point proposed scheme design (from ESCP, 2012). Purple areas indicate locations of riprap, either as a groyne or positioned on the beach crest. Wooden groynes are denoted by thinner lines in the west side of the image.	50
Figure 4.1: Location of key groyne compartment within the context of Eastoke area.	52
Figure 4.2 Location of Wave Rider (triangle), in relation to field area (boxed area).	59
Figure 4.3: Location of profile lines, and neighbouring HBC baseline survey locations	63
Figure 4.4: From Caldwell and Williams, 1985 (p.133). “Average profiles for the ten morphological categories. Vertical bars indicate one standard deviation either side on the mean profile every 1 m down the beach. An idealized model for each configuration is inset.”	64
Figure 4.5: Depiction of how sliding indicator devices (SIDs) measure the active layer.	67
Figure 4.6: Using a bottomless metal dustbin to dig in unconsolidated sediment.	68
Figure 4.7: Depth of disturbance rod with washer on the surface of the beach.	69
Figure 4.8: SID locations, winter 2014-15	71
Figure 4.9: SID locations, winter 2015-16	72
Figure 4.10: Location of depth of disturbance rod measurements	73
Figure 4.11: Examples of tags and tagged pebbles.	80
Figure 4.12: Image of PIT tags, showing their internal structure.	80
Figure 4.13: Pebbles placed in a tray, ready to be sealed in place and water jetted.	82
Figure 4.14: Zingg classification of different geometric particles	83
Figure 4.15: Deployment method for tagged pebbles – columns within the beach sediment.	84
Figure 4.16: Pebble column deployment locations, Winter 2014-15 field periods.	85
Figure 4.17: Pebble column deployment locations, Winter 2015-16 field periods.	86

Figure 4.18: A) RFID detector. Loop is the antenna, backpack contains the datalogger and power source, small yellow device below the handle is a GPS tracker. B) Detector being used.	87
Figure 5.1: Cross-shore variation of sand content, December 2014 – March 2015.	91
Figure 5.2: Locations of sediment samples on 21/03/2015.	92
Figure 5.3: Locations and numbers of sampling points in December 2014.	93
Figure 5.4: Variation between samples taken at the location of SID1 in December 2014.	93
Figure 5.5: Variation between samples taken at the location of SID3 in December 2014.	94
Figure 5.6: Variation between samples taken at the location of SID4 in December 2014.	94
Figure 5.7: Variation between samples taken at the location of SID5 in December 2014.	94
Figure 5.8: Proportions of surface sediment codes compared by profile number.	95
Figure 5.9: Number of points in each surface sediment category for different elevations on the beach.	96
Figure 5.10: Surface sediments from profiles measured in January, February and March 2015.	97
Figure 5.11: Frequency of sediment codes at different elevations on Profile 1.	98
Figure 5.12: Frequency of sediment codes at different elevations on Profile 2	98
Figure 5.13: Frequency of sediment codes at different elevations on Profile 3.	99
Figure 5.14: Percentage of points in each category for different wave heights.	99
Figure 5.15: Comparison of surface sediment codes with sand content of physical samples	100
Figure 5.16: Comparison of surface sediment codes with D50 of physical samples	101
Figure 5.17: Number of each profile shape experienced per profile, associated with dominant drift directions: A) westerly waves (eastwards drift); B) easterly waves (westwards drift).	103
Figure 5.18: Limits of cross-sectional areas of Profile 3.	104
Figure 5.19: Percentage change between mean cross-sectional area of each profile between each survey period	106
Figure 5.20: Cross-sectional area under each profile throughout the study.	108
Figure 5.21: Change in cross-sectional area of each profile between surveys.	108
Figure 5.22: Percentage change in cross sectional area for varying wave heights.	109
Figure 5.23: Change in cross-sectional area in relation to wave period.	109
Figure 5.24: Change in cross-sectional area in relation to wave power	110
Figure 5.25: Patterns of positive and negative change in terms of wave height and direction on Profile 1.	111
Figure 5.26: Patterns of positive and negative change in terms of wave height and direction on Profile 2.	111
Figure 5.27: Patterns of positive and negative change in terms of wave height and direction on Profile 3.	112
Figure 5.28: Change in CSA as a function of both wave height and tidal range.	112
Figure 5.29: Location of maximum net change between profile surveys on Profile 1.	113
Figure 5.30: Location of maximum net change between profile surveys on Profile 2.	113
Figure 5.31: Location of maximum net change between profile surveys on Profile 3.	114
Figure 5.32: Scatterplot of maximum significant wave height against maximum net change between each measured profile.	115

Figure 5.33: Berm removal seen from dGPS profiles measured on Profile 1 during February 2015.	118
Figure 5.34: Berm removal, formation and rollover seen from dGPS profiles measured on Profile 2 during February 2015.	119
Figure 5.35: Transport directions as inferred from differences in profile changes, compared to dominant wave direction at the time.	121
Figure 5.36: Scatterplot of longshore wave power against longshore transport as estimated from profile changes	122
Figure 5.37: Clipping at the crest of Profile 3, 24/02/2015.	123
Figure 5.38: Cusps in the mid-beach portion of the profile. 16/12/2014.	124
Figure 5.39: Surface sediment codes on A) 11/02/2015, and B) 13/02/2015.	125
Figure 5.40: Surface sediment codes on 14/02/2015.	126
Figure 6.1: Active layer depth measurements by day.	133
Figure 6.2: Histogram showing frequency of occurrences of measured AL depths on the mixed sediment beach.	134
Figure 6.3: Mean and maximum daily AL depth measurements on each day studied during A) Winter 2014-15 (n=33) and B) Winter 2015-16 (n=30).	135
Figure 6.4: Variation in mean and maximum values of AL depth on the mixed sediment beach for each study period.	136
Figure 6.5: Frequency histograms of AL depth measurements for A) Profile 1, B) Profile 2, and C) Profile 3.	137
Figure 6.6: Variation in mean and maximum active layer measurements on three profile lines measured in A) November 2015, B) December 2015, and C) January 2016.	138
Figure 6.7: Active layer depth based on elevation of the beach surface at SID location.	139
Figure 6.8: Histograms indicating frequency of AL depths measured on A) the upper beach, B) the mid beach and C) the lower beach.	140
Figure 6.9: Separation of groyne compartment into nine sections.	141
Figure 6.10: Scatterplots showing relationships between sediment composition and AL depth. A) Sand content of samples taken before AL measurement, B) Sand content of samples taken after AL measurement, C) D50 of samples taken before AL measurement, D) D50 of samples taken after AL measurement.	144
Figure 6.11: A) Relationship between sand content and AL depth as daily averages, using sediment samples taken before AL measurements, and B) The same relationship using sediment samples taken after AL measurements	145
Figure 6.12: A) Relationship between daily average sand content and AL depth during Winter 1 (2014-15), and B) The same relationship during Winter 2 (2015-16)	145
Figure 6.13: Mean, maximum and standard deviation of AL measurements categorised by surface sediment types.	146
Figure 6.14: Mean, maximum and standard deviation of AL depths for “large” (n=48) and “small” (n=58) surface sediment codes.	147
Figure 6.15: Mean, maximum and standard deviation of AL depths for “pure” (n=45) and “mixed” (n=61) surface sediment codes.	147
Figure 6.16: Profile slope angle plotted against average AL depth.	148
Figure 6.17: Local bed slope at individual SID locations plotted against AL depth.	149
Figure 6.18: Scatterplot showing relationship between change in elevation and AL depth	150

Figure 6.19: Change in cross-sectional area of a profile plotted against average AL depth for the same profile.	151
Figure 6.20: Active layer depth plotted against significant wave height.	152
Figure 6.21: Histogram showing frequency of individual AL depth measurements when related to wave height.	153
Figure 6.22: Individual AL measurements as a percentage of significant wave height	153
Figure 6.23: Scatter plot of daily mean significant wave heights and mean AL depth measurements.	154
Figure 6.24: Scatterplot showing correlation between wave height (H_s) and AL depth as a percentage of H_s .	156
Figure 6.25: Relationships between sediment composition and AL depth as a percentage of wave height at individual SID locations. A) Sand content for sample taken at the start of AL measuring period ($n=30$), B) Sand content for sample taken at the end of AL measuring period ($n=32$), C) D50 for sample taken at the start of AL measuring period ($n=30$), D) D50 for sample taken at the end of AL measuring period ($n=32$).	157
Figure 6.26: A) Relationship between daily average sand content and AL depth as a percentage of wave height, using sediment samples taken before AL measurements, and B) The same relationship using sediment samples taken after AL measurements	158
Figure 6.27: Mean, maximum and standard deviation for AL depths as a percentage of significant wave height at locations coded according to surface sediment.	159
Figure 6.28: Mean, maximum and standard deviation of AL measurements as a percentage of wave height for “small” ($n=58$) and “large” ($n=48$) sediment codes.	159
Figure 6.29: Mean, maximum and standard deviation of AL measurements as a percentage of wave height for “pure” ($n=45$) and “mixed” ($n=61$) sediment codes.	160
Figure 6.30: Scatterplot showing relationship between overall profile slope angle and AL depth as a percentage of wave height	161
Figure 6.31: An example from February 2015 of individual AL depth values, expressed as a percentage of wave height, compared to the beach slope at the site where each measurement was taken.	162
Figure 6.32: Histograms indicating frequency of AL depth as a percentage of wave height measured on each of the three profiles. A) Profile 1, B) Profile 2, C) Profile 3.	163
Figure 6.33: Active layer measurements as a percentage of H_s at different elevations.	164
Figure 6.34: Scatterplot showing relationship between change in elevation and AL depth as a percentage of wave height.	168
Figure 6.35: Scatterplot showing mean AL depth (as a percentage of wave height) against change in cross-sectional area of the profile.	169
Figure 6.36: Relationships between wave period and AL depth: A) Peak period (T_p), B) mean period (T_z).	170
Figure 6.37: A) Scatterplot comparing mean wave period (T_p) to mean AL depth for each of the 72 study days. B) Scatterplot comparing wave period to AL depth as a percentage of H_s .	171
Figure 6.38: Scatterplots showing relationships between daily mean wave period (T_p) and AL depths, for significant wave heights A) below 1 m, and B) above 1 m	172
Figure 6.39: Scatterplot and regression lines for wave period against average AL depth on each profile per day (November 2015 – January 2016 field periods).	174
Figure 6.40: Scatterplot indicating relationship between wave power and individual measurements of A) AL depth, and B) AL depth as a percentage of wave height.	178

Figure 6.41: A) Scatterplot showing wave power plotted against daily mean AL depth, B) Scatterplot showing wave power plotted against daily mean AL depth as a percentage of wave height	178
Figure 6.42: Wave rose indicating direction and Hs during the 72 study days.	182
Figure 6.43: A) Scatterplot comparing mean wave direction to mean AL depth for the 72 study days. B) Scatterplot comparing wave direction with AL depth measurements as a percentage of wave height for the 72 study days.	183
Figure 6.44: Scatterplot of significant wave height against active layer depth obtained using depth of disturbance rods in the lower beach.	185
Figure 6.45: Relationship between wave height and AL depth as a percentage of wave height, measured using depth of disturbance rods.	185
Figure 6.46: Comparison of AL measurements taken using SIDs and depth of disturbance rods A) in measured values, and B) as a factor of wave height.	186
Figure 6.47: Average AL values (as a percentage of wave height) from published studies undertaken on beaches with varying slope angles, compared to average AL values (as a percentage of wave height) from each study period, and overall, within the current study.	194
Figure 6.48: AL depth as predicted by the Bertin et al. (2008) formula, versus the actual measured AL depth.	199
Figure 7.1: Direction and distance of pebble transport from deployment location after 1 day.	209
Figure 7.2: Longshore transport distances of pebbles recovered within 7 days of deployment or previous detection.	209
Figure 7.3: Total distance travelled in first day according to tracer mass.	210
Figure 7.4: Total distance travelled in first day according to B axis of tracer.	210
Figure 7.5: Longshore distance travelled in first day according to tracer mass (positive values indicate eastwards transport).	211
Figure 7.6: Longshore distance travelled in first day according to B axis of tracer (positive values indicate eastwards transport).	211
Figure 7.7: Relationship between burial depth and distance travelled during the first day after deployment.	212
Figure 7.8: Relationships between burial depth and distance travelled for different sized tags.	213
Figure 7.9: Directions of transport after 1 day for pebbles buried at different depths, 09/03/2015-10/03/2015	214
Figure 7.10: Directions of transport after 2 days for pebbles buried at different depths, 13/03/15-15/03/15.	214
Figure 7.11: Directions of transport after 1 day for pebbles buried at different depths, 16/03/15-17/03/15.	215
Figure 7.12: Directions of transport after 1 day for pebbles buried at different depths, 19/01/2016-20/01/2016.	215
Figure 7.13: Transport velocities for every tracer detection, compared to the number of days since either deployment or the most recent detection (where relevant).	218
Figure 7.14: Average tracer velocities (m/day) of tracers detected during each survey.	220
Figure 7.15: Number of days taken to bypass a groyne as a function of longshore wave power.	221
Figure 7.16: Transport distances and rates of pebbles deployed in March 2011	222
Figure 7.17: Tracer detections on full surveys.	223

Figure 7.18: Scatterplot of longshore wave power against immersed weight transport.	229
Figure 7.19: Scatterplot of longshore power against values of k .	230
Figure 7.20: Mean longshore wave power 2008-2018.	234
Figure 7.21: Coastline change, 19/10/2011-22/04/2015.	235

Table of Tables

Table 2.1: Details of previous studies on active layer depth	29
Table 3.1: Monthly averages for all wave data (2003-2016)	42
Table 3.2: Recycling and replenishment volumes for Hayling Island, past 3 years.	48
Table 4.1: Measurements taken on each day of fieldwork	55
Table 4.2: From Caldwell and Williams (1985). Ten identified morphological categories	64
Table 5.1: Sand content of samples taken on 21/03/2015.	91
Table 5.2: Classifications of mean profiles.	102
Table 5.3: Average cross section of each profile taken from measured profiles within each study period.	105
Table 5.4: CSA change (as a percentage of greatest CSA) between smallest and largest measured CSA on each Profile during each study period.	107
Table 6.1: Mean AL depth and standard deviations for the 3 measured profiles, November 2015 - January 2016.	137
Table 6.2: Means and standard deviations of AL measurements within upper, middle and lower sections of the beach	139
Table 6.3: Means and standard deviations of AL measurements within 1 m elevation bins.	141
Table 6.4: Minimum, mean and maximum AL depths for each of the 9 sections within the main groyne compartment.	142
Table 6.5: Pearson's correlations for different combinations of sediment descriptors and measurement timings.	143
Table 6.6: Spearman's correlation coefficients for different combinations of wave height and AL depth measurements.	155
Table 6.7: Relationships between daily mean AL depth and daily mean wave height for each study period	155
Table 6.8: Pearson's correlation coefficients for relationships between sediment composition and AL depth as a percentage of wave height	157
Table 6.9: Variation in AL depth as a percentage of wave height between Profiles 1-3 during November 2015-January 2016.	162
Table 6.10: Variation in AL depth as a percentage of H_s for different elevations at which it was measured	164
Table 6.11: Pearson's correlation coefficients for relationships between wave height and AL depth on the upper, middle, and lower beach	165
Table 6.12: Pearson's correlation coefficients for relationship between wave height and AL depth within 1 m elevation bins	165

Table 6.13: Pearson's correlation coefficients for relationships between wave height and AL depth of measurements, subset by position within the groyne compartment.	166
Table 6.14: Relationships between wave height and AL depth at locations with repeated measurements.	166
Table 6.15: Pearson's correlation coefficients for the relationships between wave height and AL depth at locations where measurements were repeated on multiple occasions.	167
Table 6.16: Relationships between daily mean wave period and daily mean AL depth for each study period.	170
Table 6.17: Pearson's correlation coefficients for the relationships between daily average wave period and AL depth for different wave heights.	172
Table 6.18: Regression equations and Pearson's correlation coefficients for the relationship between T_p and AL, individual measurements separated by profile	173
Table 6.19: Pearson's correlation coefficients for the relationship between wave period and daily average AL depth for each profile (November 2015 – January 2016).	173
Table 6.20: Regression equations and Pearson's correlations for relationships between wave period and AL depth (both raw measurements and as a percentage of wave height), for the upper, middle, and lower sections of the beach.	174
Table 6.21: Pearson's correlations between peak wave period and AL depth (both raw measurements and as a percentage of wave height) within elevation bins (indicating cross-shore differences)	175
Table 6.22: Regression equations for relationships between wave period and AL depth within each of the nine groyne sections	176
Table 6.23: Pearson's correlations between wave period and AL depth (both raw measurements and as a percentage of wave height) for specific locations at which repeated measurements were taken.	176
Table 6.24: Relationships between daily mean wave power and daily mean AL depth for each study period.	179
Table 6.25: Pearson's correlation coefficients for relationship between wave power and AL depth on each profile between November 2015 – January 2016.	179
Table 6.26: Pearson's correlation coefficients for relationship between average wave power and daily average AL depth on each profile (November 2015 – January 2016).	179
Table 6.27: Pearson's correlation values for relationships between wave power and AL depth for upper, middle and lower beach sections.	180
Table 6.28: Pearson's correlation coefficients for relationship between wave power and AL depth for different elevation bins	180
Table 6.29: Regression equations and Pearson's correlation coefficients for relationship between wave power and AL depth in 9 sections of the groyne compartment.	181
Table 6.30: Pearson's correlation coefficients for relationship between wave power and AL depth at specific measurement locations	181
Table 6.31: Relationships between wave direction and active layer depth during each study period	183
Table 6.32: Regression equations and R^2 values for relationships between AL depth and wave direction on each profile	184
Table 6.33: Summary of multiple regression analysis for individual AL depths	187
Table 6.34: Summary of multiple regression analysis for daily average AL depths.	187
Table 6.35: Summary of multiple regression analysis for squared daily average AL depths as percentages of wave height.	188

Table 7.1: B axes and mass measurements for tagged pebbles	205
Table 7.2: Number of pebbles deployed and cumulative recovery rates for each deployment.	206
Table 7.3: Recovery rates for pebbles of different shapes and sizes.	207
Table 7.4: Mean longshore and cross-shore transport distances after one day for pebbles buried at different depths	216
Table 7.5: Average tracer velocity per deployment (only deployments with >70 % recovery rates)	217
Table 7.6: Average tracer velocities of pebbles detected in full-coverage surveys	218
Table 7.7: Mean longshore wave power experienced during each study period.	219
Table 7.8: Velocities of tracers between full-coverage surveys.	219
Table 7.9: Tracer velocities and associated transport volumes for short time periods	224
Table 7.10: Calculations of k from 1-day tracer experiments.	228
Table 7.11: Values of k calculated from profile-based transport volumes	228
Table 7.12: K values previously calculated on coarse grained beaches	237

1. Introduction

1.1 Motivation for the study

Longshore sediment transport (LST) rates have long been of interest to coastal researchers and managers (e.g. Engelund and Hansen, 1967; USACE, 1984; Williams, 1989; Hardisty, 1990), but much of the research has been focussed on sand beaches. In the UK, many of the beaches acting as important coastal defences are composed of a mixture of sand and gravel (Moses and Williams, 2008). Rising sea levels and the projected increase in storm events necessitates an improved understanding of the processes involved in sediment transport on mixed sediment beaches (MSBs) so that adequate and cost-effective protection can be provided (SCOPAC, 2004).

Beach replenishment is a popular coastal protection method to mitigate the risks of erosion and flooding. However, the costs associated with sourcing and placing materials – and the quantities required to achieve high enough protection standards – have been increasing rapidly in recent years (Hanson *et al.*, 2002). As a result, beach recycling – where sediment is taken from the downdrift area of a beach and placed back updrift at regular intervals – has risen in popularity (Rogers *et al.*, 2010). To make this process as cost-effective as possible, coastal managers need to be able to accurately predict longshore transport of sediment under different wave climates.

There exist a wide range of available models for predicting longshore sediment transport (Van Wellen *et al.*, 1997), but no equation or model yet created is applicable to all coarse-grained beaches. The CERC equation (USACE, 1984) is a simple equation that relates LST to wave energy, but it requires calibration for the specific site where it is being used (Van Wellen *et al.*, 2000; Curoy, 2012), which can best be achieved through accurate measurement of longshore transport rates under a variety of wave conditions to represent the local wave climate.

Calculating longshore transport rates requires three measurements: the width of the active profile, the depth to which sediment is activated during tidal inundation, and the longshore velocity at which it is transported (Komar and Inman, 1970; Miller and Warrick, 2012). The active layer on mixed sand and gravel beaches is understudied compared to pure sand beaches (e.g. Curoy, 2012), and so it is still unclear what the relative impact of factors such as wave conditions, beach slope, and sediment composition is on the active layer and thus sediment transport.

This thesis attempts to address these deficiencies by analysing a vast dataset of active layer measurements, which were taken over a variety of hydrodynamic conditions, alongside sediment sampling and dGPS profiles, so that relationships could be drawn out. These active layer measurements are then combined with RFID tracer data to more accurately estimate longshore transport rates at Eastoke, to enable calibration of the CERC equation (USACE, 1984) for future use at this site and potentially other similar ones. Tracer studies have previously been undertaken on frontages along the Solent coastline, including Eastoke, where the current study is based, but these were focussed mainly on ensuring published transport pathways were accurate (ESCP, 2013) and not on providing accurate bulk transport rates.

The study site, Eastoke (Hayling Island, UK) is a mixed sand and gravel beach which undergoes regular replenishment and recycling to counteract long-term erosion. In November 2013, a £5 million defence scheme was completed here. These defences consist of a rock armour revetment, three rock groynes and approximately 35,000 m³ of recharge material (ESCP, 2013c). Recent comprehensive sediment sampling indicates that sand constitutes 40 % of the sediment mix, though this number is generally lower at the beach crest and increases seawards (Seastar Survey Ltd., 2017). The surface sediments can be highly variable, sometimes presenting a dominance of sand or gravel over the majority of the active beach face, but generally consisting of a gravel crest and storm berm(s), with a sandy mid-lower beach.

It is widely agreed that there are significant differences between MSBs and either pure sand or pure gravel beaches (e.g. Kirk, 1980; Jennings and Shulmeister, 2002) and that these differences influence sediment transport processes, but the nature of these differences is not yet fully understood. These differences are generally related to the influence that having a mixture of grain sizes exerts on permeability and hydraulic conductivity of the sediment, with Mason (1997) having shown that a sand content of 20 % can reduce the hydraulic conductivity of a mixed sediment beach by up to an order of magnitude compared to a pure gravel beach. Additionally, there are recognisable differences between natural mixed beaches and those that have undergone replenishment, which are often linked to beach reprofiling or the compaction of imported sediments (McFarland *et al.*, 1994; Whitcombe, 1996; She *et al.*, 2007).

The results of this study will aid local coastal management teams in their future calculations of required sediment volumes and residence times of material for replenishment projects under different wave scenarios, leading to a more cost-effective management system, and will also add to the knowledge database regarding artificially replenished mixed sediment beaches.

The RFID tracer methodologies adopted in this study have been used to update handbooks used by the Eastern Solent Coastal Partnership (Appendix R), while the sliding indicator devices used to measure active layer depth (Chapter 4.5.ii.a) have been adapted for use in measuring scour at the base of sea walls by a SCOPAC funded study (ESCP, 2018).

1.2 Aim and objectives

The aim of this study is to establish statistical relationships between active layer depth and wave energy in order to provide a much-needed data set to parameterise calculations of longshore transport rates on mixed sediment beaches.

In order to achieve this aim, the following objectives were created:

1. To measure variations in active layer depth at a high resolution for a longer period of time than has previously been published,
2. To confirm preliminary research that a predictive relationship between active layer depth and wave height can be established for mixed sediment beaches,
3. To statistically relate any further variations in active layer depth to location on the profile, distance from groynes, sediment composition, and/or beach slope,
4. To determine short- and medium-term (days to months) sediment transport patterns and volumes under a range of hydrodynamic conditions,
5. And to calibrate the CERC equation for predictive use at this complicated site.

The originality of the study exists in the total number of active layer measurements, the time scale and range of hydro- and morpho-dynamic conditions over which they were collected, and the complexity of the study site.

1.3 Specific research questions

The following research questions will be covered as part of this investigation:

1. *Do beach profiles provide an accurate representation of longshore sediment transport on groyned beaches?*

Previous research has indicated that they do not (e.g. Moon, 2003), but beach profiles continue to be used in the presence of groynes as a method for measuring longshore sediment transport. Repeated beach profiles can be useful for measuring sediment build up at terminal groynes on beaches with unidirectional longshore transport, but the impacts of groyne fields

on beach morphology are likely to negatively impact the analytical capabilities of this method (e.g. Dornbusch *et al.*, 2008). Further research is required to establish the exact influence that groynes exert on beach profile morphology.

2. *How is the active layer on this mixed sand and gravel beach linked to:*

- a. *Wave conditions?*
- b. *Beach slope?*
- c. *Sediment composition?*

There is some evidence that each of these factors has an impact on active layer depth (e.g. Anfuso, 2005), but most of the research has been undertaken on sand beaches (e.g. King, 1951; Jackson and Nordstrom, 1993; Anfuso, 2005), and on short time scales (e.g. Ciavola *et al.*, 1997; Ferreira *et al.*, 2000), meaning that it likely does not provide enough detail to accurately assess these relationships. Studying the active layer on a mixed sand and gravel beach will provide the opportunity to determine the level of influence that variations in sediment composition exert in a way which cannot be reliably assessed using data from multiple beaches with different sized sediments, as it provides a certain level of 'control' over other aspects of beach dynamics. It is expected that the range of morphodynamic and sedimentary characteristics exhibited on a mixed sediment beach will produce significant variations in active layer depth. As accurate inputs of active layer depth are vital to the reliability of longshore transport calculations, this study provides a larger number of measurements over a greater time period than any other of which the author is aware. The common methods used to measure it will be discussed further in Chapter 4, alongside methods of measuring a similar parameter in gravel-bedded rivers, known as scour depth (DeVries, 2000), because of their relative usefulness on a mixed sediment beach, where traditional sand-based measurement methods are unlikely to withstand the potential damage caused by entrained pebbles.

3. *Can the longshore transport rate be used to calibrate an empirical formula such as the CERC equation for this site, and will this calibration value be similar to other mixed sand and gravel beaches?*

Having a detailed data set should allow an accurate calculation of the longshore sediment transport rate relative to the wave conditions experienced during the study (Schoonees and Theron, 1993). Using this to calibrate an equation for this site will allow predictions to be made into the future, thereby providing value to local coastal practitioners. It is unlikely that the calculated value will be similar to other values for mixed sediment beaches due to the groynes

at Eastoke, which should exert a greater effect on longshore sediment transport than the sediment composition.

1.4 Structure of the thesis

Figure 1.1 indicates how the research objectives relate to the research questions, and maps them into the thesis.

Chapter 2 summarises previously published literature on beach morphodynamics, active layer depth and sediment transport calculations, focussing on the specific characteristics of mixed sediment beaches which can cause them to respond differently to wave energy than either pure sand or pure gravel beaches.

Chapter 3 describes the setting and reasons for the field site's suitability in this research.

Chapter 4 provides details on the available methods for measuring topographic changes, active layer depths, sediment composition, and sediment transport. It then proceeds to set out the survey design for this project, with justifications for the methods chosen, and details of any issues encountered.

Chapter 5 contains results from dGPS profile surveys, which are used to assess the morphological changes within a groyne compartment, both spatially and temporally. These are used to assess the suitability of current monitoring techniques used by the coastal management team.

Chapter 6 investigates temporal and spatial variability of the active layer depth in relation to wave conditions, sediment composition, and beach slope angle.

Chapter 7 provides results of tracer surveys conducted to assess the longshore transport rates at the eastern end of Hayling Island beach. These are combined with active layer measurements and beach profile lengths to produce a total sediment transport volume and a range of calibration values 'k' for the CERC equation for longshore transport.

Chapter 8 concludes the results and provides recommendations for future research.

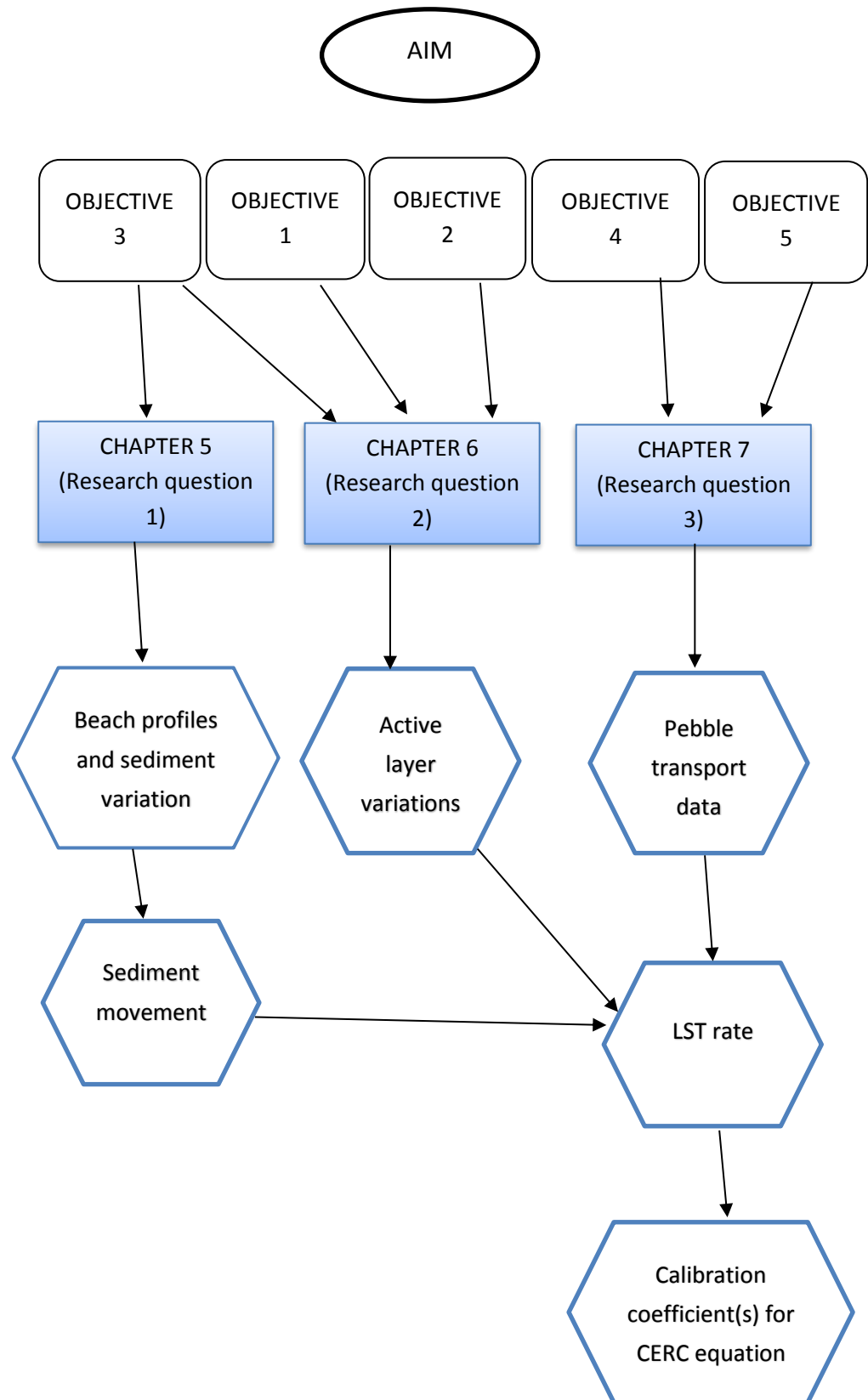


Figure 1.1: Thesis flowchart

2. Literature Review

2.1 Introduction

i. Definition of a beach

At its simplest, a beach can be defined as an unconsolidated accumulation of sediment at the coast (Thomas and Goudie, 2000), and using this definition, approximately 40% of the world's coastlines are beaches (Bird, 2008). This sediment can vary in size, but particles of sand to cobble sizes are most common. These sediments can be derived from local cliff outcrops, fluvial or glacial sources, and offshore sediment sinks or submarine outcrops, though Woodroffe (2003) states that they must be deposited by wave action for it to be classed as a beach. Some beaches are still receiving sediment from one or more of these sources, while others are now classed as 'relict beaches', with no additional sediment being deposited (Masselink *et al.*, 2011). Some beaches must be artificially replenished in order to maintain their current state, with this material often being sourced from local offshore sediment sinks (Rogers *et al.*, 2010). Most beaches are highly dynamic and constantly changing as a result of wave energy, tides and their associated currents, and other environmental influences.

Beaches can form in front of cliffs as the result of cliff erosion, or as a fringe on low-lying land. It is also possible for beaches to form separately from, but parallel to, land; these are referred to as 'barrier' beaches and usually have a back-barrier lagoon behind them. They are hypothesised to be the result of one of three processes: vertical growth of submarine bars, drowning of already-existing bars, or longshore sediment transport (Woodroffe, 2003).

Difficulties arise in determining the seaward limit of the 'beach' – the depth of closure is normally used to represent the separation between nearshore and offshore sediment transport processes (Hallermeier, 1978). It is the point at which there are no longer significant changes in bottom elevation, or significant sediment transport (Kraus *et al.*, 1998), but in reality this can be hundreds of metres offshore. The depth of closure is related to the occurrence of extreme waves at the given site, and the equation was only validated for grain sizes between 0.16 and 0.42 mm (Hallermeier, 1978; 1981). It can be calculated as follows:

$$D_c = 2.28H_e - 68.5 \left(\frac{H_e^2}{g T_e^2} \right) \quad (2.1)$$

where H_e is the nearshore storm-wave height that is exceeded for 12 hours during the time period of interest, T_e is the associated wave period, and g is acceleration due to gravity (Komar, 1998).

A simplification of this equation was suggested by Birkemeier (1985), and shown to provide a satisfactory representation of the depth of closure:

$$D_c = 1.57 H_e \quad (2.2)$$

Due to annual changes in storm activity, the profile closure depth can be misleading if only a small sample of wave data is used. As such, it is recommended that wave data averaged over several years is used in calculations, unless the profile closure depth for a specific event is required (Kraus *et al.*, 1998).

ii. Beach classifications

Beaches can be classified not only according to their sediment type - sand, gravel, or a mixture of the two – or their tidal range – microtidal (<2 m range), mesotidal (2-4 m range), or macrotidal (>4 m range) – but also according to their position on the dissipative-reflective continuum (Carter, 1989). Traditionally, there are three categories of beach: dissipative, reflective and intermediate. These are related to the wave energy, sediment type and slope angle of a beach: dissipative beaches are gently sloping, generally sandy, and, as the name suggests, dissipate a lot of the wave energy during breaking; reflective beaches are steeper, have a narrow surf zone, and are often at least partially composed of coarser sediments (Bird, 2008). There is some debate about the use of the term ‘reflective’ though, as pure gravel beaches, while steep, have been measured to reflect only 10% of incoming wave energy due to their ability to allow almost all of the swash to infiltrate between clasts (Powell, 1990). Wright and Short (1984) proposed that there are at least four separate intermediate beach types alongside the traditional dissipative and reflective ones. These four intermediate beach states are ‘longshore bar-trough’, ‘rhythmic bar-and-beach’, ‘transverse bar-and-rip’, and ‘low tide terrace’, with decreasing energy levels respectively (Aagaard *et al.*, 2013). Figure 2.1 shows the general profile shapes associated with beaches composed of different sediment sizes.

Sand beaches generally have a slope angle of less than 5 degrees and a wider area of wave impact than gravel beaches. Less infiltration of water between the small sediment particles means that swash and backwash have similar energies, which prevents sediment from

building up too steeply. Gravel beaches usually have a slope angle of over 10 degrees. Under normal (swell) conditions, greater rates of infiltration into the sediment means swash is stronger than backwash and so more energy is available to transport particles up the beach, creating the steeper slope (Pedrozo-Acuna *et al.*, 2006).

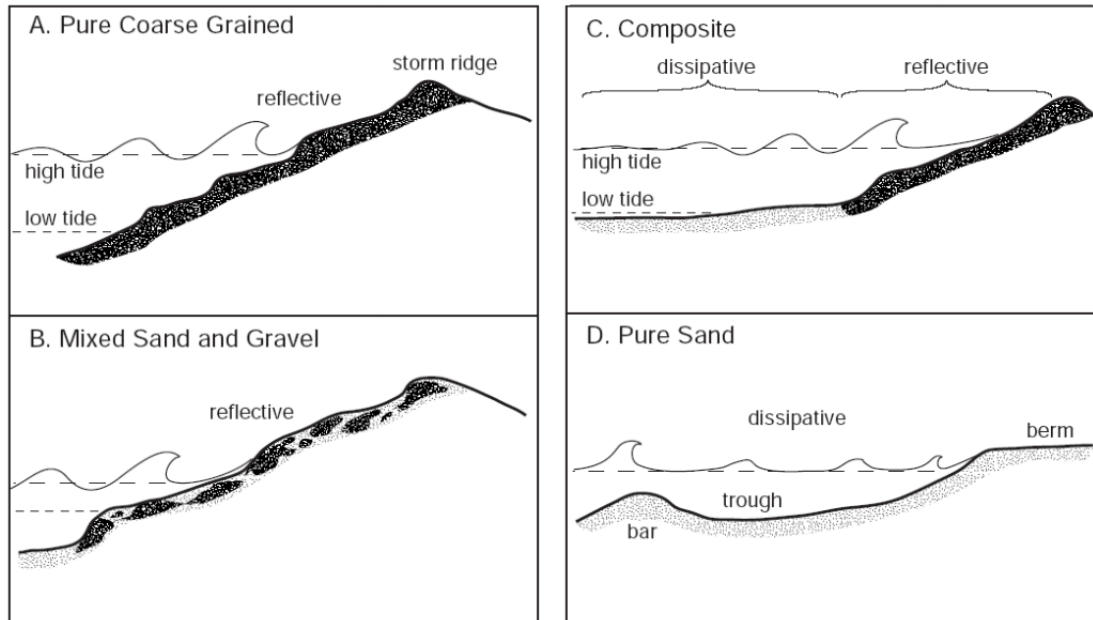


Figure 2.1: The classification of beaches based on their proportions of coarse sediments (gravel and cobbles) versus sand, with the resulting differences in their morphologies (extended from Jennings and Shulmeister (2002)). (Source: Napier City Council (2007))

iii. Basic morphology

Beaches are often considered in terms of their profile shape. Typical beach profile shapes displayed by sandy beaches can be concave, linear or convex (Sonu and Van Beek, 1971), and generally these are associated with accreting, stable and receding profiles respectively. It is generally accepted that all beaches have an ideal equilibrium profile towards which they are moving under calm or swell conditions (Komar, 1998). This can be altered drastically by storm events, causing rapid offshore movement of sediment and a flattening of the profile. Once normal conditions return, the beach will be gradually reworked by waves in an attempt to return towards equilibrium again (Austin and Masselink, 2006). Beaches often display different profile characteristics depending on the predominant wave processes. In calmer months (usually summer), a 'swell' profile may be in evidence due to the constructive energy of the waves: this will be steeper, convex and often contain at least one berm. In winter months a 'storm' profile is more likely: this will have a shallower, more concave slope than the summer profile (Sonu and Van Beek, 1971).

Common secondary morphological features include the beach crest, storm berms, cusps and longshore bars. These features may not exist on all beaches and can be present or absent under different circumstances.

a. Crest

Usually formed of the coarsest material on the beach, the beach crest is the result of clasts being pushed landward and forming a stable ridge at the back of the beach during storms.

b. Berm(s)

Also called ridges or beach terraces (Bird, 2008), these features run parallel to the shoreline, marking the extent of swash run up at high tide. They are formed by deposition and can be observed to increase in size and travel landward as the tide rises. Some beaches may have multiple berms marking different tide levels between spring and neap on the beachface. Berms are usually removed by erosive storm activity, and then reinstated during calmer conditions (Austin and Masselink, 2006).

c. Cusps

Beach cusps are regularly spaced crescent-shaped or triangular features composed of coarser material (Masselink *et al.*, 2011). They develop on many types of beaches, but are most common on beaches with slightly concave, reflective profiles (Kuenen, 1948) and low longshore transport rates (Komar, 1998). They can be formed or destroyed in hours. Little is understood about their initial formation, but two main theories exist. The first involves edge waves, which are shore parallel waves generated through reflection and subsequent refraction of incident waves (Guza and Inman, 1975). It is suggested that the wavelength of edge waves determines the spacing of cusps. The second theory is that small depressions in a flat beach attract wave energy, and this causes them to be further eroded, gradually becoming the 'bays' between cusp horns. The increase of energy in these locations leads to a subsequent decrease of energy in the horns, leading to deposition of larger particles. This causes the sediment sorting that is visible, and once it is occurring becomes a positive feedback loop, causing the cusps to continue growing in size (Masselink *et al.*, 2011). In this scenario, cusp spacing is a function of run up height (Thomas and Goudie, 2000). Coco *et al.* (2000) used computer simulations to show that cusps are self-organising features; once they start forming, a feedback loop develops that causes them to continue growing until

conditions change sufficiently to break the cycle. They can then be shifted or removed entirely by storms, but little is known about the processes that cause these changes (Masselink, *et al.*, 1997).

d. Low tide terrace

Usually composed almost completely of sand, this is a very shallow-sloping and often expansive section at the base of the profile, which is likely to be partially exposed by low tides (Pethick, 1984). Terraces can be observed not only on low-gradient sand beaches, but at the toe of some macrotidal gravel and mixed sediment beaches as well (Jennings and Shulmeister, 2002).

e. Longshore sand bars

These act as natural breakwaters (Carter, 1989), and are often formed when there are currents running parallel to the shoreline. These currents are more likely to occur during high energy events, and on microtidal beaches. The top of these bars may be exposed by very low tides, but usually they are submerged (Pethick, 1984). A different morphological feature known as onshore migratory swash bars (Bray, 2007; 2010) will be discussed in Chapter 3, in relation to the specific study site.

iv. Beach replenishment

Beach replenishment is the addition or replacement of sediments to increase beach volume. It is usually undertaken on eroding beaches and used as a means of protecting land, assets and infrastructure behind a beach (Rogers *et al.*, 2010). In most cases, replenishment material comes from offshore dredging, but it is sometimes possible to 'recycle' sediment from downdrift.

Beaches can be replenished with either sand or gravel, and it is normal to try and use a grain size similar to the native beach material, or slightly larger as theoretically larger clasts should be less susceptible to entrainment and thus remain on the beach for longer (James, 1974). Beach replenishment is usually accompanied by reprofiling, as managers will have created an ideal design profile which is intended to limit loss of the added sediments and maximise the protection provided by the beach. Much of the sediment required to achieve the design profile is unnecessary, and initial losses from replenishment projects are often high (e.g. Whitcombe, 1996). This can be combatted by more regular intervention (e.g.

Pevensey Bay, Ian Thomas, *pers. comm.*), which reduces the need for sediment but may increase labour costs and requires more ongoing management.

The UK has been using beach replenishment as a coastal defence since the 1950s, when it was common practice to use shingle (a mixture of sand, gravel and pebbles). Sand alone was not used until the 1970s, when the aesthetic of recreational beaches became more important. Since 1995, around 2.5 million m³ of sand and 550,000m³ of gravel have been used each year (Hanson *et al.*, 2002). Increase in recreational use is no longer a leading factor in decisions, but is viewed as secondary to the protection from coastal erosion and flooding. Defence schemes must consider the cost benefit ratio, the likely lifetime of the scheme, the level of protection it provides (e.g. 1 in 20 year event), and environmental impacts. Numerical models are used in the design of replenishment schemes, many of which are accompanied by groynes to help retain the material. However, more recently sediment 'recycling' has been used instead of groynes. This requires less constant maintenance: once it is known where the material travels to, it can be removed and put back at the updrift end of the beach. The cost of this is significantly lower than sourcing new material each time, too (Rogers *et al.*, 2010).

2.2 Mixed sediment beaches

i. Sediments

Mixed sediment beaches can be composed of a mixture of mud, sand and gravel sized particles (Blanco, 2003), but for this study the focus will be on mixed sand and gravel beaches.

Although the majority of coastal research has, in the past, been undertaken on sand beaches, gravel size clasts are a common component in beach sediments in mid to high latitudes, especially in the Northern hemisphere (Mason and Coates, 2001). This gravel is often derived from glacial deposits or erosion and weathering of cliffs.

McLean (1970) defined mixed sand and gravel beaches as having roughly equal proportions of sand and gravel, but in reality this can vary significantly: Mason and Coates (2001) reported sand content varying between 15 and 68 % for mixed sand and gravel beaches in the UK. A mixed sediment beach is classified as one with important sand and gravel fractions present both across the beach profile and with depth in the subsurface materials (Jennings and Shulmeister, 2002). Its sediment should range over three orders of

magnitude from fine sand (100 μm), through gravels (2 – 64 mm) and up to small boulders (>256 mm) (Coates and Damgaard, 1999), though there are no specified proportions of each class that make up a mixed sediment beach (Mason and Coates, 2001). MSBs are often categorised as bimodal, meaning that there are peaks in two sediment sizes, with the secondary size making up at least 30% of the mix.

Beach sediment grain size distributions have often been observed to grow finer in a seawards direction (e.g. Swift, 1970), and as a general rule, as particle size decreases, so does slope angle. As such, many gravel beaches have a sandy terrace, which may or may not be exposed at low tide (Jennings and Shulmeister, 2002).

ii. Classifications

There are three recognised types of MSB (Jennings and Shulmeister, 2002; Horn and Walton, 2007):

- ‘Mixed sand and gravel’, where both sand and gravel are present across the whole beach face (Figure 2.1B). Surface sorting is usually visible, with larger particles dominant on the upper beach and sand on the lower beach, but this sorting does not continue past the surface layer.
- ‘Composite’, where a steep reflective gravel upper beach is fringed by a shallow sloping sandy low tide terrace, so the sand and gravel components remain separated from each other (Figure 2.1C). Examples of these beaches in New Zealand were found by Jennings and Shulmeister (2002) to be slightly more steep than mixed sand and gravel beaches.
- ‘Composite mixed’, where a mixed sand and gravel upper beach is fringed by a sandy low tide terrace. This type of beach is particularly common in the UK (Horn and Walton, 2007).

iii. Distribution

Globally, there are few countries with significant numbers of MSBs and most of these are in paraglacial environments, which are found in the mid to high latitudes, as the main natural source of the larger sizes of sediment for such beaches is glacial sediment that has been made available at the coast and sorted by storm waves. Countries with MSBs include the UK, New Zealand and Japan, though MSBs are also found in the USA, Canada and much of the Mediterranean and South Atlantic coast.

MSBs are also frequently found where replenishment schemes use material that is coarser than the native sediment; it is widely accepted that coarser material is entrained at higher energy levels than sand and should therefore be less susceptible to erosion under normal

circumstances (Rogers *et al.*, 2010) and so coastal practitioners often choose to use a mixture of sand and gravel to prolong the lifespan of a replenishment as in theory it should remain on the beach for a longer period of time.

In England and Wales, between one quarter (Scott *et al.*, 2011) and one third (Fuller and Randall, 1988) of beaches are composed of mixed sand and gravel, but relatively little research has been done into maintaining these beaches efficiently in order to continue to protect the coastline (Curoy, 2012). It has been reported that approximately 19,000 km of beaches in the UK contain an important gravel component, with only 3,500 km of these classed as 'pure gravel' (Horn and Walton, 2007), meaning that mixed sediment beaches of various types constitute over 15,000 km of the UK's beaches. They are particularly common on the south coast of England (Fuller and Randall, 1988).

iv. Morphological features

Probably the most important morphological feature of coarse-grained beaches is the high tide berm. Austin and Masselink (2006) state that there are four key phases associated with berm dynamics. These are: regression, which is associated with a decreasing tidal range and relatively constant wave energy, whereby the berm migrates seaward; roll-over, associated with a neap to spring tidal transition and a landward migration of the berm; removal, usually associated with a high-energy wave event; and re-formation, where swell waves begin to re-build the berm.

Profile variation on a mixed sand and gravel beach has been studied by Curoy *et al.* (2009), who found four stages of profile evolution during a neap-spring-neap tidal cycle. As the berm accretes and moves seaward, the profile flattens out, with the break in slope becoming less marked. After this, a smooth, convex profile is formed as the berm is completely removed, leading to a shallower beach profile. Finally, the berm begins to rebuild and the upper profile steepens again, re-developing the break in slope and becoming relatively stable.

This process can be disrupted by storm events, during which the beach is generally eroded and the profile flattened as sediment is dragged offshore. In some cases, high energy waves can push or throw larger clasts (pebbles and cobbles) up the beach onto the crest. In extreme cases, on beaches without cliffs directly behind them, storms can combine with high tides to cause overtopping. This can reduce the height and increase the width of the

beach crest. In calmer weather, the sediments which had been moved beyond the low tide level can be gradually replaced back onto the beachface and berms re-formed.

The beach step, often formed of the coarsest material on the beach (Austin and Buscombe, 2008), has been observed to migrate onshore and increase in size as the tide rises, and retreat again as it falls, and may be completely absent at low tide (Masselink *et al.*, 2010). The breaking waves deposit sediment on the step, leading to a feedback loop as the increased size of the step forces wave breaking and deposition to continue occurring in the same location (Masselink *et al.*, 2011). The beach step is thought to be an important source of sediment for the building of berms (Masselink *et al.*, 2010). However on composite beaches the divide between the steep upper beach and the more shallow slope of the lower beach can be fairly mobile (Costa *et al.*, 2008) and the beach step is less likely to occur.

Beach cusps are believed to be more common on coarse grained beaches than on sand beaches (Masselink *et al.*, 1997), and due to the variety of grain sizes on a mixed sand and gravel beach can be found at multiple locations on the profile at the same time (Nolan *et al.*, 1999). However, this frequency of occurrence is obviously dependent on more than just the grain size of the beach: Curoy *et al.* (2009) observed cusps on only two days during an entire neap-spring-neap tidal cycle on a mixed sand and gravel beach, suggesting that they may not be common on all mixed sediment beaches, or under all hydrodynamic conditions.

The swash zone is the most important area in terms of sediment transport (Horn and Li, 2006), and the swash-dominated system is believed to be the main contributing factor for the presence of the beach step, berms and cusps on MSBs (Austin and Masselink, 2006). Due to the narrow surf zone caused by the steep gradient of the beach profile, bars are not found on reflective beaches (Aagaard *et al.*, 2013), but sand bars can form on the sand toe of composite beaches, which is the case at Pevensy Bay and parts of Hayling Island (Ian Thomas, *pers.comm.*). Morphological changes on coarse grained beaches tend to be of greater magnitude than on sand beaches (Van Wellen *et al.*, 2000; Austin and Masselink, 2006), perhaps in part due to the concentration of wave energy in a comparatively smaller area of the beachface (Pedrozo-Acuña *et al.*, 2006).

v. Differences between natural and artificial mixed beaches

Artificially replenished mixed sediment beaches are common on the south coast of the UK (Moses and Williams, 2008), and previous research has suggested that they do not behave

exactly as natural mixed sediment beaches would (McFarland *et al.*, 1994; Whitcombe, 1996). These differences are important for managers to understand and consider when planning replenishments, including sediment sizes, volumes and where to distribute the material on the profile.

Sherman (1991) found that replenishment created a beach profile that was more stable, even during storm events, but McFarland *et al.* (1994) noted that the presence of sand in 'gravel' nourishment material can lead to the formation of small cliffs on the beach face and a much more compact surface, reducing the protection offered by the beach and also its amenity value. This has been supported by Mason (1997), Blanco (2003) and She *et al.* (2006), all of whom determined that the porosity and hydraulic conductivity of bimodal replenishment material are negatively affected, altering the profile response (see section 2.3.ii for more detail about porosity, permeability and hydraulic conductivity).

She *et al.* (2006) used laboratory data to suggest that using gravel fill material with a sand content of 40% or higher causes cliffing, but there is also evidence that this threshold would be further influenced by the carbonate content of the material. Some of this sand moves seaward over time (Horn and Walton, 2007), but as the upper beach experiences the least tidal inundation, the sediments here remain less well-sorted and more susceptible to compaction and cliffing. Compaction by the heavy machinery often used to move sediment around when reprofiling during a replenishment can also make cliffing more likely (She *et al.*, 2006).

vi. Sediment transport

a. modes of sediment transport

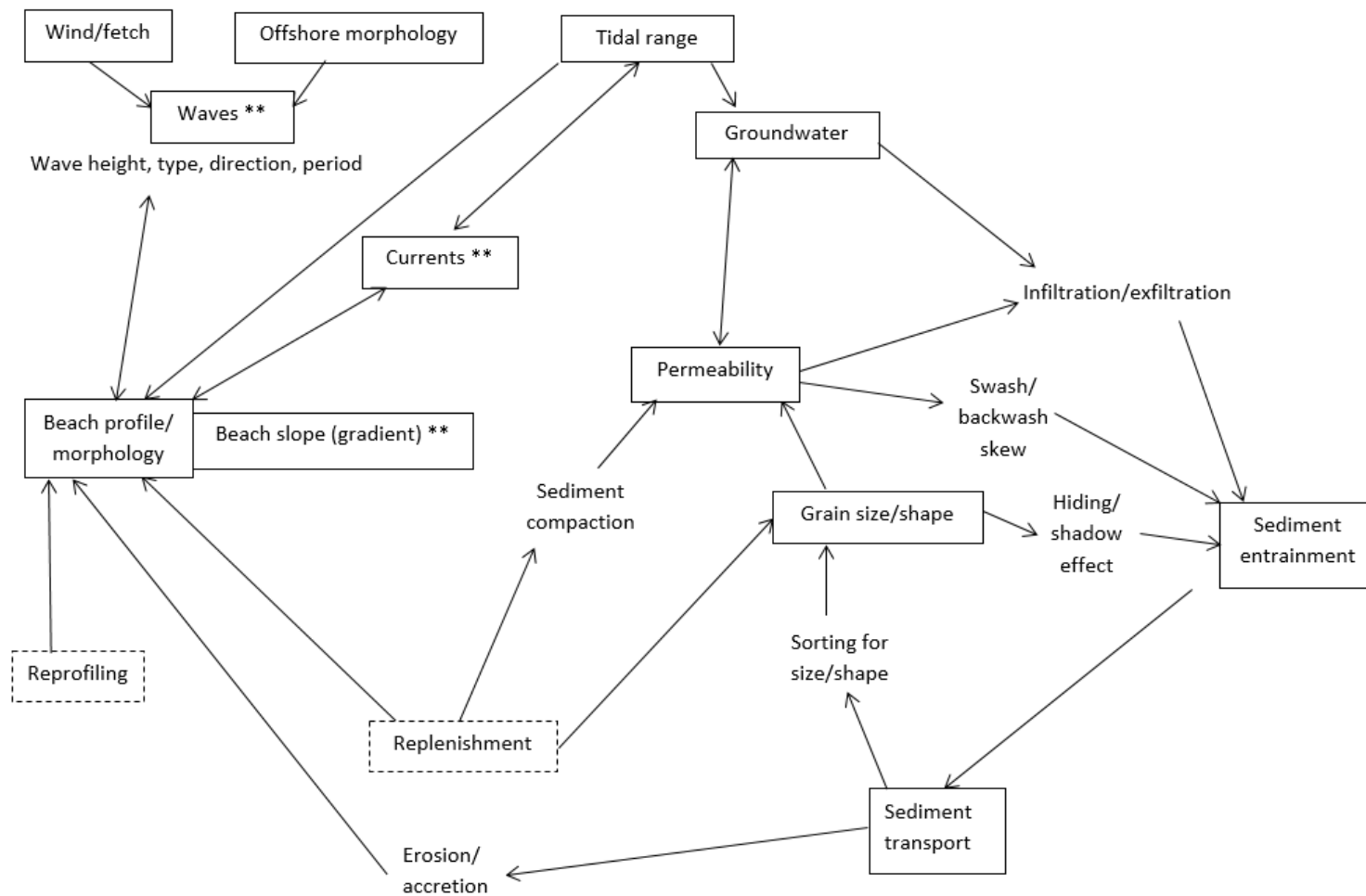
There are three modes of sediment transport: bed load, suspended load, and wash load (Komar, 1998). These modes of transport are correlated with the sediment type of a beach (Carter and Orford, 1984), as well as the energy from waves, tides and currents available to move sediment. Larger particles require more energy to be entrained and transported. As such, they tend to be transported as bed load, whereas sand is usually suspended in the water column.

Forces acting on a particle to encourage movement are wave-induced lift, and gravity (which can pull particles down a slope). The forces these are acting against is the submerged weight of the particle, which is reduced in water by the equivalent weight of water it has displaced (Bascom, 1960), and friction between particles.

Theoretically, when considering the range of particle sizes found on MSBs (coarse sand to cobbles) larger grains require a greater force in order to be entrained and transported. However, if large, angular clasts protrude into the flow, they have an increased friction surface and may have a lower resistance on the pivot point than some smaller particles, which makes their entrainment easier (Komar, 1987). These large clasts increase the surface roughness of the beachface, which creates more turbulent flows. It is also possible for the large clasts to shield sand particles, which is known as armouring, preventing them from being entrained. If there is a significant amount of silt or clay, this can bind larger particles together through cohesion, further increasing the energy required to entrain them (Woodroffe, 2003). The shape of the particles also influences contact friction, which can aid or hinder sediment entrainment.

vii. Forcing mechanisms

Sediment transport on MSBs is influenced by a large variety of inter-connected factors. Figure 2.2 is a conceptual model which indicates the complexity of relationships between morphological and hydrodynamic processes on a replenished mixed sediment beach. It is widely agreed that for the majority of beaches most of the energy for sediment transport comes from waves, but this is supplemented by tides, currents and groundwater flows (Curtiss *et al.*, 2009).



** = also directly influences sediment entrainment

Figure 2.2: Conceptual model processes affecting, and affected by, sediment transport on a mixed sediment beach

1) Wave energy

Wave height can provide a reasonable estimation of transport rates, but it is not the only variable to influence sediment transport; the type of breaking wave, its direction and period all affect the volume of sediment that will be transported and the direction of movement. For maximum longshore sediment transport, a wave approach angle of 45° is theoretically optimum (Dickson *et al.*, 2011), as waves approaching at this angle should provide greater longshore energy than waves approaching perpendicular to the coast. In the latter case, such waves will provide maximum energy for cross shore transport. It has also been observed that long period waves produce greater volumes of sediment transport in the swash zone than short period waves (Hoque and Asano, 2007).

Wave height is generally used as an indicator of energy, but the way in which the wave breaks can influence how that energy is transferred to the beach. The beach slope angle exerts significant influence on breaker type (Figure 2.3). Waves meeting a steep beach face will be forced to break more quickly, and thus will dissipate their energy more quickly, over a smaller area of beachface, which increases the potential for transport of large particles. Of the four breaker types, plunging breakers create the most turbulence (Pedrozo-Acuna *et al.*, 2006). The turbulence of a wave breaking can lead to suspension of sand-sized particles, which can then be transported to the lower zones of the beach if there is sufficient undertow (Van Rijn, 2010). Stronger rip currents created by storm waves can also be responsible for transporting sediment offshore.

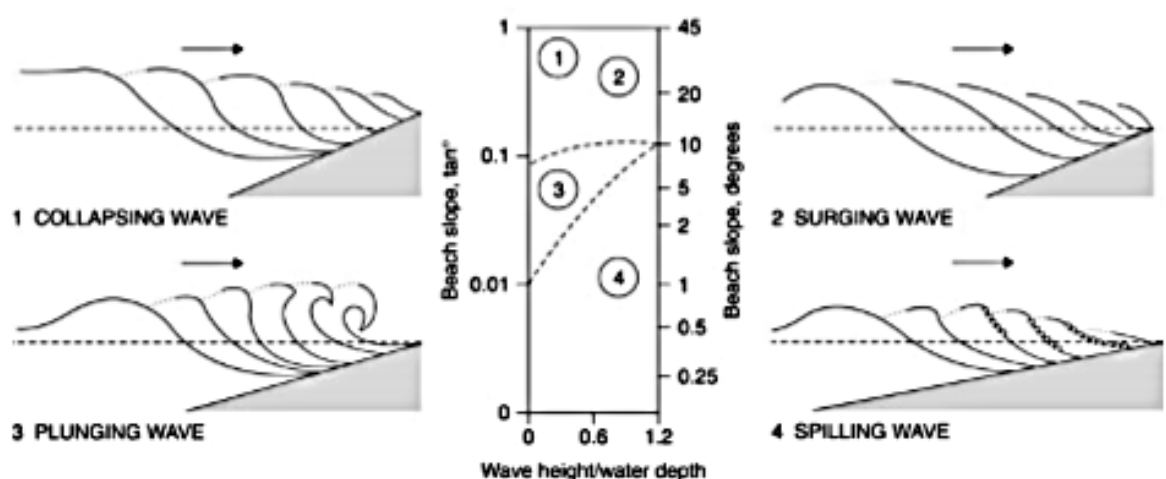


Figure 2.3: Types of breaking waves as a function of wave-height, water depth and beach slope gradient (from Smithson *et al.* 2002, p.533).

2) Tides

Tidal range can increase or decrease the area of the beach which is affected by wave breaking and swash and backwash processes, thus influencing the material available for transport. Tidal currents are created by the ebb and flow of the tide (Masselink and Hegge, 1995), and these can also influence sediment transport, more so on macrotidal beaches than in microtidal environments. Curtiss *et al.* (2009) have stated that the velocity of these currents by themselves is not enough to transport grains; they must be combined with energy from waves or vessel wakes in order to have a significant impact.

The general principle for swash-induced sediment movement (from Duncan, 1964) is that energy lost in moving up the beachface causes water to drop its sediment and infiltrate into unsaturated material, causing accretion. Then, as the tide recedes, exfiltration occurs, adding to the energy of the backwash and causing erosion. However, Kulkarni *et al.* (2004) observed a more complicated pattern than simply accretion on a rising tide and erosion on a falling tide. They found that, for a set location, as the tide started to rise, there was actually a short but significant phase of erosion before accretion began. They also found that the phase of accretion after the initial erosion occurred on both saturated and unsaturated sand, effectively disproving the idea that accretion is associated with infiltration. This may be because although infiltration increases the effective weight of sediment and reduces the likelihood of transport, it also increases the bed shear stress, which increases the likelihood of transport (Steenhauer *et al.*, 2011).

3) Beach groundwater

Groundwater levels are linked to the tide, with a sharp increase on the flood tide and a more gradual decrease on the ebb tide having been observed by Horn (2002). The lag behind the falling tide level results in a seepage face where groundwater exits and runs down the beachface (Masselink *et al.*, 2011). In general, infiltration occurs above the SWL (still water level), and exfiltration occurs below it (Massel and Pelinovsky, 2001). However, where the groundwater table is higher than the SWL, excess pore pressure can cause exfiltration. This can increase the amount of sediment transport by providing upward lift to particles, reducing their effective weight and thereby requiring less energy to transport them (Steenhauer *et al.*, 2011). These are sometimes known as 'unloading events' (Horn *et al.*, 1998) and may lead to increased erosion, but will have a much more significant impact on sand sized particles than gravels and so, depending on the surface sediment

characteristics of the MSB, may not be particularly relevant. Turner and Nielsen (1997) calculated that exfiltration flow speeds would need to exceed 50 mm.s^{-1} in order to fluidise fine to coarse sands.

Beaches with low water tables tend to accrete, and those with high water tables tend to erode (Horn, 2002). This may be due to the water table's effect on the hydraulic conductivity of the beach; a high water table creates a positive pore water pressure that decreases permeability and encourages exfiltration, which reduces the specific gravity of particles and makes them easier to transport offshore. The opposite is true of a low water table, where infiltration occurs, encouraging deposition of sediments on the beachface (Hoque and Asano, 2007). As such, beach drainage systems (also known as dewatering systems) have been implemented to reduce erosion on some beaches (Horn, 2002).

b. long- and cross-shore sediment transport

Longshore sediment transport can be measured as net transport or gross transport. The direction of transport can be altered by differences in approaching wave direction, meaning that some beaches can have high rates of gross transport but very little overall movement, while others will experience most of their transport in one direction, leading to greater net longshore transport rates (Komar, 1998). Net longshore transport is usually more significant than net cross-shore transport (Osborne, 2005), and as such is of greater importance to researchers and coastal managers alike.

Due to the generally coarser sediment found on reflective beaches, and its subsequent higher entrainment velocity, sediment transport rates on reflective beaches have been found to be up to an order of magnitude smaller than those of dissipative or intermediate beaches (Aagaard *et al.*, 2013).

Unlike sandy beaches, the majority of sediment transport on coarse grained beaches has been shown to occur in the swash zone rather than the surf zone. Van Wellen *et al.* (2000) suggest that 50-70% of longshore transport on a steep gravel beach occurs in the swash zone, and this may be similar on MSBs. On a mixed sediment beach, Curtiss *et al.* (2009) found the greatest transport rates high on the beachface. According to Turner and Masselink (1998), sediment transport in the swash zone is primarily affected by wave characteristics, bed characteristics and beach slope, and secondarily by in/exfiltration of the swash. Steeper beaches influence the way in which waves break, and generally produce

smaller surf zones and greater wave runup above the still water level, providing more energy for sediment transport to the swash zone.

There is some disagreement regarding the influence of particle size on sediment transport directions. Osborne (2005) states that smaller particles move preferentially across shore and larger clasts tend to move alongshore. However, Ciavola and Castiglione (2009) found that on a mixed sediment beach sand moves in a longshore direction, while gravel and pebbles mostly move cross-shore. This cross-shore movement involves the transport of pebbles offshore during high energy storm conditions, and the subsequent pushing of large pebbles back up the beach in the swash (Dickson *et al.*, 2011). Ciavola and Castiglione, (2009) also found that disc-shaped pebbles were more likely to be found higher up the beach and proposed that this was because they are less likely to roll back down the beach after being pushed up by the swash than more spherical pebbles.

Many aspects of sediment transport on mixed sediment beaches are unclear and require further research to clarify, support or disprove previous results.

c. Influence of groynes

Groynes are structures designed to limit longshore transport of sediment, and are common on UK beaches (Rogers *et al.*, 2010). They are usually constructed of wood, concrete or boulders, and are built perpendicular to the shoreline. Sediment within groyne compartment usually aligns itself to the direction of dominant wave approach, accumulating on the downdrift side of the compartment until there is a great enough volume to allow some bypassing.

Sediment can move past groynes in two main ways: 1) if sediment accumulation next to the groyne is high enough, it will begin to spill over the structure, and 2) by moving around the end of the groyne, in the lower region of the beach (Carter, 1989). The latter can also occur when storms transfer sediment offshore beyond the low tide level, and longshore processes then transport it before it can be replaced on the intertidal beach face during subsequent calmer conditions.

They do not stop cross-shore sediment exchange – and can actually increase offshore transport of sediment through the creation of rip currents (Scott *et al.*, 2016). Gourlay (1974) and Pattiaratchi *et al.* (2009) have both indicated that currents in the lee of groynes can create eddies, affecting local sediment transport patterns.

Rock groynes are more permeable to sediment, allowing potentially greater volumes of drift through them, but also dissipating greater amounts of wave energy than concrete groynes and thus potentially reducing the strength of rip currents. Dornbusch *et al.* (2008) indicated a rate of approximately 0.5-1.1 m³ of mixed sediment could pass through rock groynes on Saltdean beach and noted that the planform shape of the beach within the wooden groyne compartment was more concave than between rock groynes.

Sediment sorting patterns of mixed sediments within groyne compartments can be complex and vary according to wave conditions, but generally the coarsest material is deposited in the upper corner of the accumulating side of the compartment. Other than this there is often no visible sorting of sediments (Dornbusch *et al.*, 2008).

Research into sediment transport on mixed beaches has previously been dominated by studies on ungroynd sections of beaches, indicating the need to improve understanding of sediment transport on beaches where groynes play an important role in the morphodynamics (Dornbusch *et al.*, 2008).

2.3 The active layer

When measuring longshore sediment transport rates, the 'active layer' is an important factor. The spatial integration method states that three vectors of sediment transport are required for a bulk transport rate: the longshore velocity, the depth, and width of beach over which transport is occurring (Nicholls and Wright, 1991). These can then be multiplied together to provide the transport volume.

The sediment activation depth, or active layer depth, is most simply defined as the layer of sediment on the surface of the beach that is disturbed by wave breaking and other processes (Van Wellen *et al.*, 2000). There are other terms, including depth of disturbance and sediment mixing depth – all of these terms seem to have been used interchangeably over a range of timescales, depending on the author (Curoy *et al.*, 2009).

Anfuso (2005) recommends the following definitions:

- Mixing depth = short timescales (minutes to hours)
- Depth of disturbance = comparatively long timescales (one tide to a few days)

In fluvial environments, the sediment activation depth is usually referred to as scour depth (e.g. Hassan, 1990) and is a relatively constant measurement for a given location depending on river discharge at a given time.

It has been decided for this project to use the term ‘active layer’ to describe the layer of sediment that is transported on the beach by varying wave conditions, and ‘active layer depth’ to describe measurements. Available measurement techniques will be discussed and critiqued in Chapter 4.

i. Active layer research on sand beaches

The active layer depth of sand beaches has been studied for decades (e.g. King, 1951; Williams, 1971; Sunamara and Kraus, 1985; Anfuso *et al.*, 2000). It is generally agreed that there is a linear relationship between wave height and active layer depth (e.g. King, 1951; Kraus, 1985; Ferreira *et al.*, 2000; Osborne, 2005; Curtiss *et al.*, 2009). However, the exact value of this relationship varies between studies (Table 2.1). On sand beaches, active layer depth has been measured at anything from 2.7 % (Sunamara and Kraus, 1985) to 40 % (Williams, 1971) of wave height. King (1951) and Williams (1971) used the same methods, but their results differed by an order of magnitude -- King found AL depth to be 4 % of wave height, Williams 40 % -- which Williams (1971) suggested was due to shallow versus steep beach slopes respectively.

Whether wave period influences active layer depth is less universally accepted. Sunamara and Kraus (1985) found wave period to increase mixing depth on sand beaches for wave heights above 1.5 m when wave period was between 4 – 8 s. However this increase was lower for wave periods above 8 s. By contrast, Williams (1971) found no link between wave period and activation depth.

The angle of wave approach and its effect on active layer depth has not been investigated by many authors, perhaps because of the difficulty in measuring wave incidence at breaking point with any accuracy (Bertin *et al.*, 2008). Bertin *et al.* (2008) discovered that active layer depth was greater on a beach with increased wave incidence than on a beach with shore-normal approaching waves. They produced the following equation to allow wave direction to be factored into active layer depth calculations:

$$Z_0 = 1.6 \tan \beta H_s^{0.5} \sqrt{(1 + \sin(2 \alpha))} \quad (2.3)$$

(where Z_0 = sediment activation depth, β = beach face slope, α = the wave angle at breaking).

Foreshore slope is usually cited as the most important factor in the variation of sediment activation depths between studies on different beaches (e.g. Williams, 1971; Jackson and Nordstrom, 1993; Ferreira *et al.*, 2000; Anfuso, 2005). Ciavola *et al.* (1997) have indicated that there may be a difference in activation depth of up to an order of magnitude between shallow (<0.08) and steep (>0.08) beaches. They provide an equation:

$$Z_m = 0.27H_b \quad (2.4)$$

(where Z_m is activation depth and H_b is significant breaking wave height), which means activation depth on steep sand beaches equals 27 % of significant wave height. However, this is based on only five days of data collection spread across three sites and may therefore not be fully representative of all steep sand beaches. Ferreira *et al.* (2000) then created an equation with beach slope included as a parameter so that it could be used on beaches of any slope angle:

$$Z_m = 1.86H_b \cdot \tan\beta \quad (2.5)$$

(where Z_m is activation depth, H_b is significant breaking wave height, and $\tan\beta$ is the slope). Although this was created for sand beaches of varying slope angles, theoretically it may also be applicable to mixed sediment beaches.

Few authors seem to have studied the relationship between grain size and active layer depth, but of those who have, King (1951) found that a beach with coarser sand had an increased active layer depth as related to wave height, whereas Williams (1971) and Ciavola *et al.* (1997) found no such link. Additionally, Sunamara and Kraus (1985) found only limited differences in activation values for different grain sizes and thus concluded that sediment grain size has only a weak impact on active layer depth on sand beaches.

Cross-shore variability of active layer depth has been found by many authors (e.g. Williams, 1971; Kraus, 1985; Aagaard *et al.*, 2012), all of whom attributed this variation to the location of the wave breaking zone. Although some sediment disturbance does occur under non-breaking waves, the majority of sediment activation occurs in the wave breaking zone (Aagaard *et al.*, 2012). Another factor potentially affecting the active layer depth is the type of breaking wave: Anfuso (2000) offers the theory that plunging breakers relate to a deeper active layer than spilling breakers. This is likely due to the reduced area of beach impacted

by a plunging breaker compared to a spilling one, allowing plunging breakers to transfer more energy and thus affect sediment to a greater depth (Carter, 1989).

ii. Active layer research on gravel and mixed sediment beaches

The starting point for research onto beaches with larger grain sizes has been King's (1951) theory that gravel beaches would have a greater activation depth than sand beaches on the basis that larger particles also have larger pore spaces for the wave to travel through, allowing water (and its energy) to travel deeper into the beach.

The porosity of a sediment is simply the proportion of its volume that is void space. It is heavily influenced by sediment packing, sorting and shape, but not specifically by size (Blanco, 2003). Permeability is influenced by porosity, and can be defined as the rate at which fluid can flow through a porous material. It was found by Quick and Dyskerhuis (1994) that permeability is controlled by the finest fraction of sediment; likewise, Holmes *et al.* (1996) state that the finest 10% of sediment is the main controlling factor.

The working assumption for the active layer depth on mixed sand and gravel beaches is that it should be somewhere between that of pure sand or pure gravel beaches. This is due to the sand filling pore spaces between larger gravel particles affecting the permeability of the mix. Mason and Coates (2001) suggested that if the sand content is above 25 %, the hydraulic conductivity of a beach will be similar to a pure sand beach. Theoretically, these factors should exert a great amount of influence on active layer depth, and thus this 25 % sand value may also prove to be important in determining the active layer of a mixed sediment beach.

Though the two terms are often used interchangeably, hydraulic conductivity differs from permeability in that it is concerned not only with the properties of the sediment through which a fluid is flowing, but also with the fluid itself (Thomas and Goudie, 2000). It is influenced by beach groundwater levels; as groundwater levels increase, the ability of water to permeate into the beach is reduced (Horn, 2002). This in turn affects the extent to which wave run up impacts sediment transport (Bakhtyar *et al.*, 2011); if a beach is less permeable due to high groundwater levels, wave run up will be greater (and therefore active width will be greater), but the depth to which sediment is activated will be less. Hydraulic conductivity is also influenced by sediment size and grading, as well as fluid density and viscosity. Barnes (1995) found permeability values for sand and gravel mixtures to be comparable with pure sand, at $0.00001 - 0.01 \text{ m.s}^{-1}$, which is significantly smaller

than permeability of pure gravel sediments, given as $0.1-10 \text{ m.s}^{-1}$. This is due to infilling of the pores by smaller grain sizes, and an increase in tortuosity of the path that the fluid must take to get through the sediment, thus reducing hydraulic conductivity and slowing the rate of flow (Wilcock, 2001). She *et al.* (2006) found that the hydraulic conductivity of a mixed sand and gravel beach is comparable to a pure sand beach once the percentage of sand in the beach exceeds approximately 30 %. As such, well sorted sediments tend to have a higher permeability than poorly sorted sediments (Blanco, 2003). Mason and Coates (2001) determined the hydraulic conductivity of sediment to be the most important property that distinguishes a mixed beach from pure sand or gravel beaches.

However, when Saini *et al.* (2009) dug up three plots on a mixed sediment (but predominantly sand) beach and filled one each with sand, gravel, and a mixture of sand and gravel, they found no significant differences between the activation depths in each of these sediments.

Masselink *et al.* (2010) indicate that maximum active layer values on a fine gravel beach ($D_{50} = 2-10 \text{ mm}$) are 20-30 % of significant wave height. This is based on measurements taken at Slapton Sands (UK) but is not necessarily comparable with other authors as these are the maximum values, whereas most authors give an average value somewhere in this range, suggesting that their maximums would be higher.

Curoy *et al.* (2009) measured active layer depth at approximately 18 % of wave height, on average, for a mixed sediment beach composed of approximately 20 % sand. Miller and Warrick (2012) found an AL depth of 22% of significant wave height on a mixed sediment beach composed of approximately 40 % sand. The type and proportions of sediment are important factors influencing the active depth (Blanco, 2003). Thus, the difference between Curoy *et al.*'s (2009) values and Miller and Warrick's (2012) value could be due to differences in the proportion of sand within the sediment composition, indicating a requirement to monitor changes in sediment proportions as part of the current research.

One of the defining features of a mixed sediment beach is its steep main slope; therefore, it follows that the work of Ciavola *et al.* (1997), Ferreira *et al.* (2000) and Anfuso (2005) – who all found relationships between beach slope and active layer depth – may be broadly applicable to mixed beaches as well, despite a difference in sediment composition; both these factors require further investigation. However, initial research into this by Curoy *et al.* (2009) found that the active depth for given wave conditions is significantly lower for

MSBs than for similarly steep sand beaches (Ciavola *et al.*, 1997), possibly up to three times lower in the middle section of the profile.

Table 2.1: Details of previous studies on active layer depth

Author	Location (number of beaches)	Methods	Beach type. Grain size (slope angle: °/tanβ)	Wave heights	Active layer depth (as % of wave height)
King (1951)	UK (4)	Dyed sand plugs	Sand, mean grain size = 0.23 – 0.4 mm. (6°/0.1)	Up to 1.2 m	4 – 10 %
Williams (1971)	Hong Kong (3)	Tracer columns (total 56 columns)	Sand, mean grain size = 0.2 – 2.59 mm. (4-12°/0.07-0.21)	0 – 0.2 m	40 %
Greenwood and Hale (1980)	Kouchibouguac Bay, Canada (1)	Depth of disturbance rods (62 rods over 2 storm events)	Sand	1.5 & 2 m	15 & 35 %
Sunamara and Kraus (1985)	Japan (4)	Fluorescent sand tracers. (Total of 8 experiments)	Sand, mean grain size 0.18 – 0.59 mm. (0.5°,1°,6°/0.01,0.02,0.1)	0.6 – 1.6 m	2.31 – 7.22 %
Jackson and Nordstrom (1993)	Delaware Bay, USA (1)	Depth of disturbance rods	Sand, mean grain size = 0.46 mm. (6°/0.1)	0.06 – 0.52 m	18 - 26 %
Sherman <i>et al.</i> (1994)	Fire Island, NY (1)	Fluorescent sand tracers / cores (on shorter sub-tidal timescales)	Sand, mean grain size = 0.37 mm. (8°/0.14 upper beach, <0.5°/0.01 low tide terrace)	0.09 – 0.13 m	22 %
Ciavola <i>et al.</i> (1997)	Portugal (3)	Dyed sand tracers / cores. (Total of 4 tides)	Sand (6-8°/0.1-0.14)	0.36 – 0.8 m	21.02 – 29.44 %
Ferreira <i>et al.</i> (2000)	Portugal (4)	Some overlap with Ciavola <i>et al.</i> (1997). Varying combinations of tracers, plug holes and graduated rods. (7 experiments)	Sand	0.34 – 0.85 m	23 %
Anfuso <i>et al.</i> (2005) (from Anfuso <i>et al.</i> (2000), Anfuso <i>et al.</i> (2003) and Anfuso and Ruiz (2004))	Portugal (6)	Sand plugs, depth of disturbance rods. (Total of 10 tides)	Sand (1°-6°/0.02-0.11)	0.35 – 0.9 m	4.51 – 18 %
Austin and Masselink (2006)	Slapton Sands (1)	Depth of disturbance rods. 1 tidal cycle.	Fine gravel. D ₅₀ = 6 mm. (8.5°/0.15)	1.2 – 1.5 m	6.6 %

Bertin <i>et al.</i> (2008)	France (2)	Fluorescent sand plugs & fluorescent sand tracers/cores. 8 experiments.	Sand. $D_{50} = 0.18\text{-}0.22$ mm. ($9^\circ/0.015$)	0.4 – 2 m	2.5 – 3.7 %
			$D_{50} = 0.2\text{-}0.6$ mm. ($3.5^\circ/0.06$)	0.2 – 0.6 m	7.5 – 18.3 %
Saini <i>et al.</i> (2009)	Delaware Bay, USA (1)	Plot excavation/sediment replacement, depth of disturbance rods. 26 tides.	Mixed. ($9^\circ/0.15$, “predominantly sand”)	0.18 – 0.4 m	22 – 31 %
Curoy <i>et al.</i> (2009) (Curoy, 2012)	Cayeux-sur-Mer, France (Birling Gap, UK)	Tracer columns, 29 tides.	Mixed (20 % sand) ($7\text{-}10^\circ/0.12\text{-}0.17$).	$H_{st\max}$ 0.4 – 2.7 m	11-20 % (4 – 8%)
Masselink <i>et al.</i> (2010)	Slapton Sands, UK (1)	Fibreglass depth of disturbance rods, 10 days	Fine gravel ($D_{50} = 2\text{-}10$ mm)	0.5 – 1 m	20 – 30 %
Miller and Warrick (2012)	Elwha River delta, USA (1)	Depth of disturbance rods, RFID tracer pebbles (10 tracer deployments, March-September 2009)	Mixed (40 % sand). ($7^\circ/0.12$)	0.3 – 1.2 m	22 %

2.4 Predicting drift rates

Measurements of sediment transport can be used to test and calibrate transport equations, which can be of use to coastal managers, for example in planning beach recycling works. Techniques for measuring LST rates will be discussed in Chapter 4.

As the majority of beach research has been conducted on sand beaches, it makes sense that many longshore transport models have been created using data from sand beaches and laboratory experiments modelled after sand beaches. Osborne (2005) stated that some of the most important parameters to be considered in a transport model for mixed sediment beaches are infiltration, beach slope, and differential hydraulic conductivity. There have been models created for coarse-grained beaches, such as XBeach-G (Deltares, 2017), but these can still be unsuitable for use on mixed sand and gravel beaches. For example, XBeach-G does not consider groundwater sufficiently, and requires only a simple D_{50} grain size measurement for input, which does not adequately represent the range of grain sizes being transported.

The most common approach to calculating longshore sediment transport rates is to consider that transport is proportional to longshore wave power. One of the most widely used bulk longshore transport formula is the CERC (Coastal Engineering Research Center) equation (USACE, 1984):

$$I_l = k P_l \quad (2.6)$$

Where I_l is immersed transport weight, P_l is longshore wave power and k is the calibration coefficient. Wave power is generally calculated using H_{rms} (the square root of the mean of all squared wave heights, approximately $H_s / 1.4$). The value I_l is intended to include both suspended sediment and bed load, and can be related to the volumetric transport load Q_l as follows:

$$Q_l = \frac{I_l}{\tau} \quad (2.7)$$

where

$$\tau = \frac{(\rho_s - \rho)g}{1+e} \quad (2.8)$$

More complex profile-based models such as SANDS, SHINGLE (Powell, 1990) and BEACHPLAN (HR Wallingford), which attempt to predict how the profile shape will react to given hydrodynamic conditions, often make use of bulk transport equations derived from the CERC equation for predicting the longshore component of sediment transport.

The CERC formula seems flawed in that it does not account for any factors such as beach slope or grain size, which exert significant influence on sediment transport. However, Komar (1998) suggests that the value of k takes these factors into account. This may also explain why published values for k vary so widely.

The suggested value of k for sand beaches is 0.77 (USACE, 1984), though Schoonees and Theron (1993, 1994) used a more reliable selection of data and produced the value $k = 0.82$ for beaches with grain size of <1 mm, and $k = 0.02$ (though with a very low correlation coefficient of 0.11) on beaches with grain size >1 mm.

For coarse grained beaches the value of k has varied from 0.02 to 0.36 (Bray *et al.*, 1996). Nicholls and Wright (1991) provided a value of 0.02 from data collected at three sites, using tracers that covered a range of pebble sizes. Chadwick provided a less reliable range of values for k , 0.02-0.06, from sediment trap experiments in low energy conditions at Shoreham-by-Sea. Bray *et al.*'s (1996) experiments consisted of both electronic and aluminium tracers, with high (60-100 %) recovery rates and a wide range of sizes represented.

However, when Van Wellen *et al.* (2000) attempted to combine these data to produce one value of k for coarse grained beaches, they calculated $k = 0.22$ and admitted the level of confidence in this value was low, suggesting that the differences between coarse grained beaches mean that they cannot be represented as a group, and must therefore have transport equations calibrated at as many sites as possible. Both Nicholls and Wright (1991) and Van Wellen *et al.* (2000) noted that k increases with grain size, but this seems to be at odds with previously published data for sand beaches, where values for k were much closer to 1.

Most longshore transport equations provide the most accurate predictions for the sites at which they were created or calibrated. Van Wellen *et al.* (2000) assessed fourteen empirical formulae against data collected at Shoreham-by-Sea, a coarse-grained beach on the south coast of the UK, and determined that the best fits with the real data came from formulae which had been calibrated at Shoreham or similar nearby beaches. This highlights

how site specific formulae for gravel beaches need to be and justifies calibrating equations such as the CERC at as many beaches as possible.

2.5 Summary

Mixed sediment beaches are increasingly important as a defence against coastal erosion. Their use in this way is particularly common on the south coast of the UK (Moses and Williams, 2008), and studies aimed at better understanding their response to wave energy will be vital in ensuring their continued effectiveness as a coastal defence in the face of sea level rise and increased storminess as a result of climate change.

A significant body of research exists analysing the links between processes and beach morphodynamics on sand beaches, but less progress has been made in resolving the same issues on coarse grained, and especially mixed sediment beaches (Miller and Warrick, 2012). This is likely due to the increased complexity added to the system by the presence of multiple grain sizes in the sediment matrix. This affects sorting, packing and entrainment velocities (Wilcock, 2001), beach porosity and hydraulic conductivity (Mason and Coates, 2001), all of which have been shown to have significant influences on sediment transport (Blanco, 2003).

Being able to accurately predict longshore sediment transport rates is an important part of planning for beach replenishment schemes, a popular method of inhibiting coastal erosion. The calibration of equations for this purpose has been found to be very site-specific (Van Wellen *et al.*, 2000), justifying the need for detailed measurements to produce transport values against which a formula such as the CERC equation can be calibrated for use at the study site.

Additionally, there have been few studies into the active layer on mixed sediment beaches, though it has been theorised by Anfuso (2005) that beach slope angle may be more important than sediment composition in influencing the extent to which breaking waves activate the sediment. However, Curoy *et al.*, (2009) found conflicting results on a mixed sediment beach, and this certainly opens up the topic for further research.

3. Site Description

3.1 Introduction

To achieve the aim and objectives set out in Chapter 1, it was important to select an appropriate field site. The site needed to be variable in terms of its sediment and morphology so that the relationship between sediment composition and beach slope to active layer depth could be assessed. It was preferred that longshore transport be inhibited in some way, in order to keep the tracer survey area small enough to be realistically covered by one person in a single low tide. Additionally, there was a requirement for wave conditions to be measured nearby so that these could be related to variations in beach morphology, active layer depth and sediment transport patterns.

The selected field site was Eastoke Point, Hayling Island (Figures 3.1; 3.2). It is a replenished, groyned, mixed composite beach overlying a clay bed and compacted mainly sandy relict beach (Harlow, 1979), with a dominant eastwards littoral drift direction, tidal range of 4 m (ESCP, 2012) and relatively moderate wave climate (see section 3.3). The upper layers of sediment are the result of decades of beach replenishment and are highly variable both across and alongshore and with time, meaning that this site will allow for relationships between sediment composition and active layer depth to be established. During calm conditions, the distinction between the coarse upper beach and sandy lower beach is marked, but during storm conditions sediments tend to be mixed across shore (NFDC, 2017). The beach is actively eroding under most conditions, hence the need for regular replenishment.

A sediment sampling study undertaken in January 2017 indicates that the average sand content of the whole Hayling coastline is approximately 37 %. This increases to 40 % for samples taken within the Eastoke area, with sand content shown to be highest overall for the most easterly corner of the beach and decreasing sand content northwards into the harbour entrance. Sand content was generally shown to increase in a seawards direction, from approximately 15 % on average at the crest to approximately 47 % on average at MLW (Seastar Survey Ltd., 2017).

This surface sediment variation is relatively common for mixed sediment beaches (Ciavola and Castiglione, 2009) and will allow the relationship between sediment composition and

active layer depth to be analysed at both spatial and temporal scales. Previous studies linking grain size with active layer depth have mainly used measurements from entirely different beaches, or been undertaken in laboratories (e.g. Anfuso, 2005; Ciavola *et al.*, 2005; 2013), so the current study should provide a useful new insight into this relationship.

There are both wooden and rock groynes forming the defences within the study site, providing the opportunity to investigate whether differences in transport rates can be detected between the two types. The groynes will also serve to limit longshore transport velocities and allow for medium-term (months to a year) tracing experiments as well as the short term ones which are more common (e.g. Miller and Warrick, 2012).

A nearby wave buoy provides hydrodynamic data, and its location makes Eastoke a more suitable site than others in the Solent (such as Lee-on-the-Solent), which would be further from the wave buoy and subject to much different hydrodynamic conditions than those being measured, as wave refraction patterns within the Solent are complex (SCOPAC, 2004).

The addition of a second field site as a comparison was considered. Options for this included ungroined stretches of coast such as Shoreham-by-Sea (where much of the research into mixed sediment beaches in the UK has taken place), so that the impact of groynes at Eastoke may become more obvious in comparison, or a natural composite beach, where differences between natural and replenished mixed sediment beaches could be compared. Ultimately it was decided that timing and personnel constraints would not allow data to be collected simultaneously from two sites, which would limit direct comparisons between the sites anyway. A larger body of data from one site, especially a beach with fluctuating profile shape and sediment composition, was considered preferable. This would allow for data to be collected under a wider array of hydrodynamic conditions and provide a better basis for calibration of the CERC longshore transport equation. The methodology chapter will discuss exact locations of fieldwork measurements within the study area.

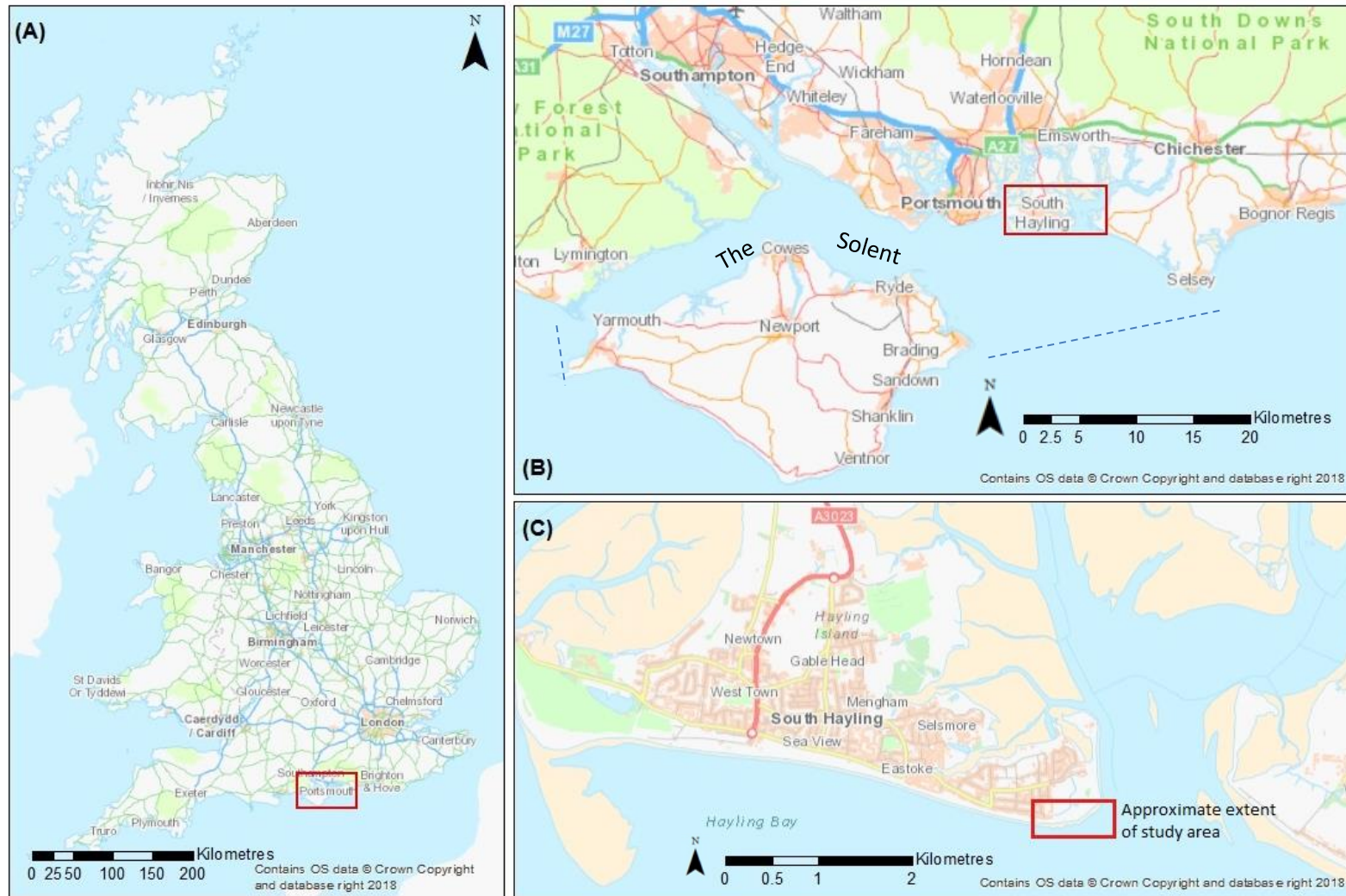


Figure 3.1: A) National, B) regional and C) local maps to indicate location of study site.



Figure 3.2: Eastoke Point (Aerial imagery courtesy of CCO, 2016).

3.2 The Solent

The Solent is the stretch of water between the UK mainland and the Isle of Wight; its limits are usually defined at Hurst Spit to the west and Selsey Bill to the east (Figure 3.1B).

The current Solent is part of a drowned river system; during the Pleistocene, the Solent River would have flowed eastwards between what is now the Isle of Wight and Hampshire, before heading south as a tributary of the Flueve Manche, or Channel River (Allen and Gibbard, 1993) (Figure 3.3). It was later flooded by eustatic and isostatic sea level rise during the Holocene. The evidence for this theory comes from a series of terraces and aggradational gravel deposits between 125 m O.D. and approximately -37 m O.D., believed to be the result of braided rivers in periglacial conditions (e.g. Dyer, 1975; West, 1980). The Eastern Solent contains the deepest part of this drowned riverbed, where it is incised to approximately -46 m O.D. and contains over 30 m of sediment, most of which is Holocene-era muds and shingle (Hampshire County Council, 2010).

The underlying geology of the Eastern Solent is Barton clays in the north and Becton and Barton sands further south. These are overlain by periglacial gravel beds from the drowned Solent river system, which is believed to have been a major source of sediment for Hayling Island beach in the past, though no current research has shown any evidence of onshore transport from these sources (NFDC, 2017).

The low lying Solent coastline is composed mainly of mixed sediment barrier beaches, separated by tidally influenced harbours, many of which have developed spits across their entrances. It is thought that the spits confining Chichester Harbour entrance (of which Eastoke Point is one) have developed since the 18th century (NFDC, 2017).

Recession of this coastline may be in the region of 2 km in the past 800 years, though much of this recession may be due to a series of 'superstorms' in the thirteenth century. These storms are believed to have permanently inundated the land behind the barrier beach, causing rollover (Thomas, 1953; Wallace, 1990). Relict barriers of cemented gravel exist several kilometres offshore (Harlow, 1980; Wallace, 1990; Whitcombe, 1995), and these can be used to assume that previous coastlines may have consisted of offshore barrier beaches, with backing lagoons and possibly salt marshes. As sea levels rose and these barriers retreated, they would have eventually attached to the mainland, creating a coastline more similar to the current one. However, the coastline has been subject to

manmade defences over the past century (section 3.5) which makes it difficult to relate it to its 'natural' form.

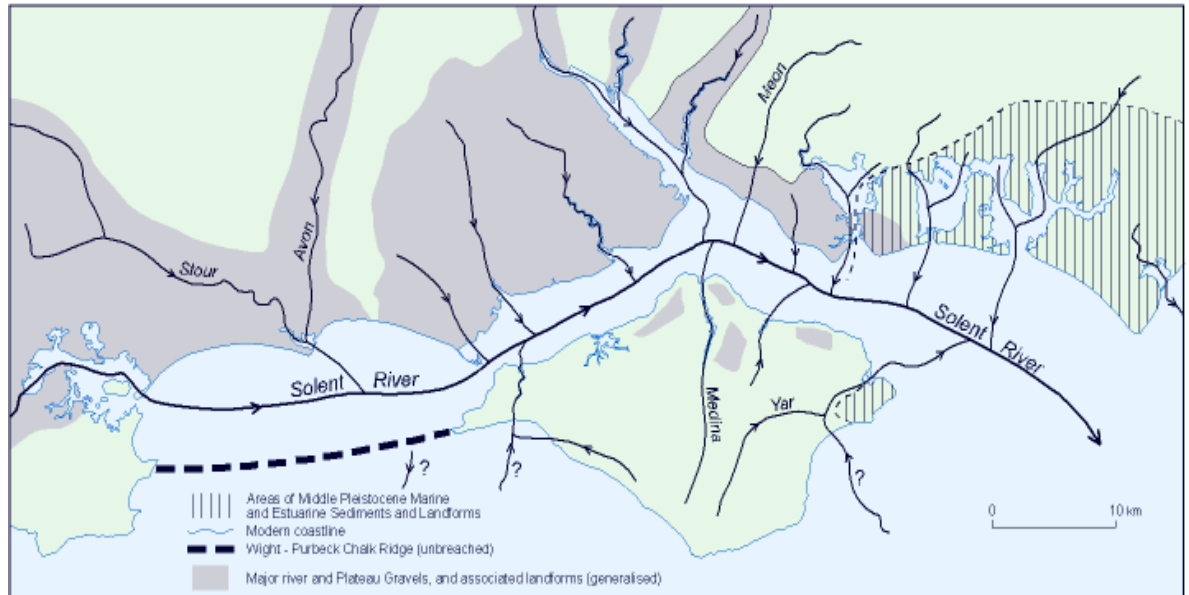


Figure 3.3: The Solent River, early to mid quaternary. (Source: SCOPAC, 2004)

3.3 Wave climate

A directional wave buoy is located approximately 5 km directly offshore of Eastoke in the Solent; this has been in place since 2003. Data from the wave buoy shows that the majority of waves approach from the south and south-south-west (Figure 3.4) and that 90 % of significant wave height are under 1.3 m in most years (Figure 3.5). The largest waves generally approach from approximately 200 degrees, but the waves with the longest period tend to approach from a more direct southerly direction (Figure 3.6). The peak wave period (T_p) has two distinct sections (Figure 3.6), indicating a combination of wind waves and swell waves affect this coast.

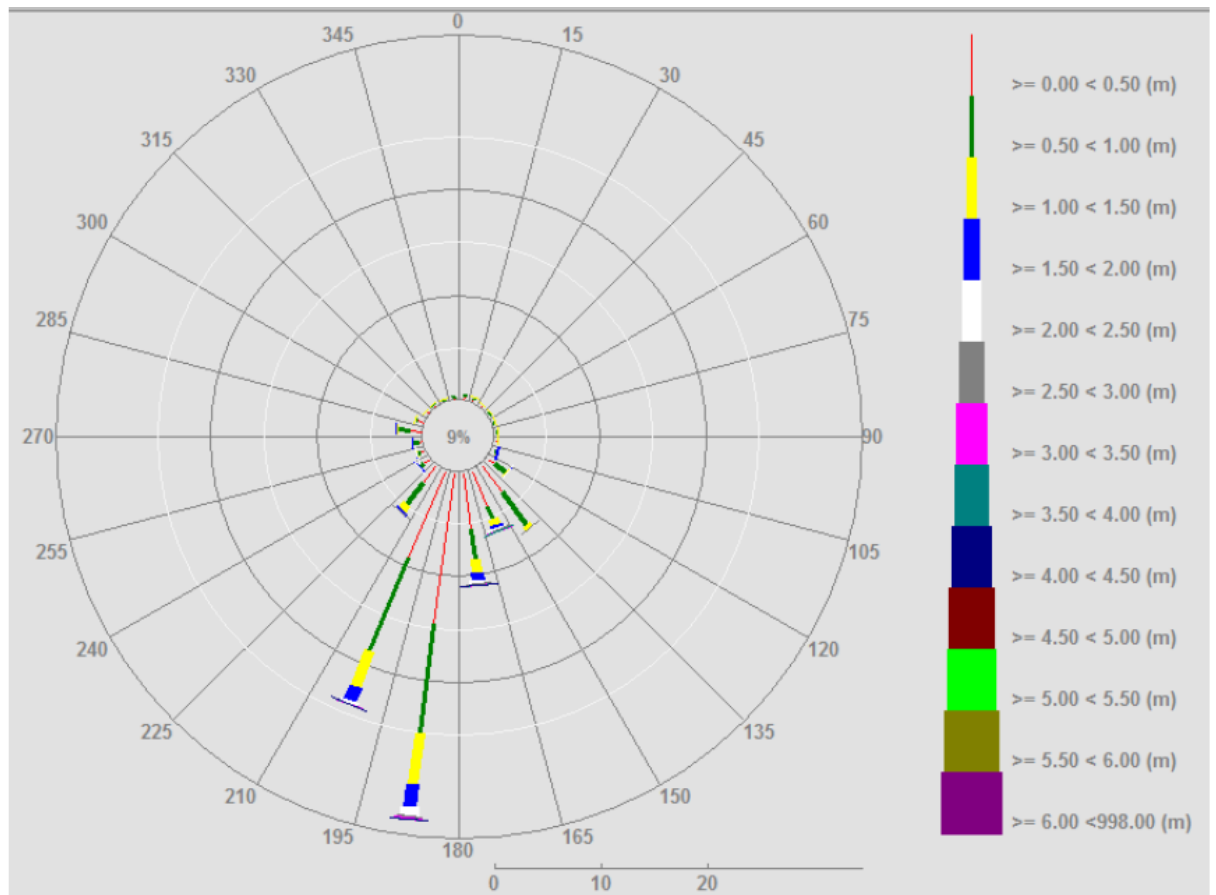


Figure 3.4: Significant wave heights (H_s) and directions ($^\circ$) measured at the Hayling Island wave buoy, 10/07/2003 – 31/12/2016. (Source: CCO, 2017)

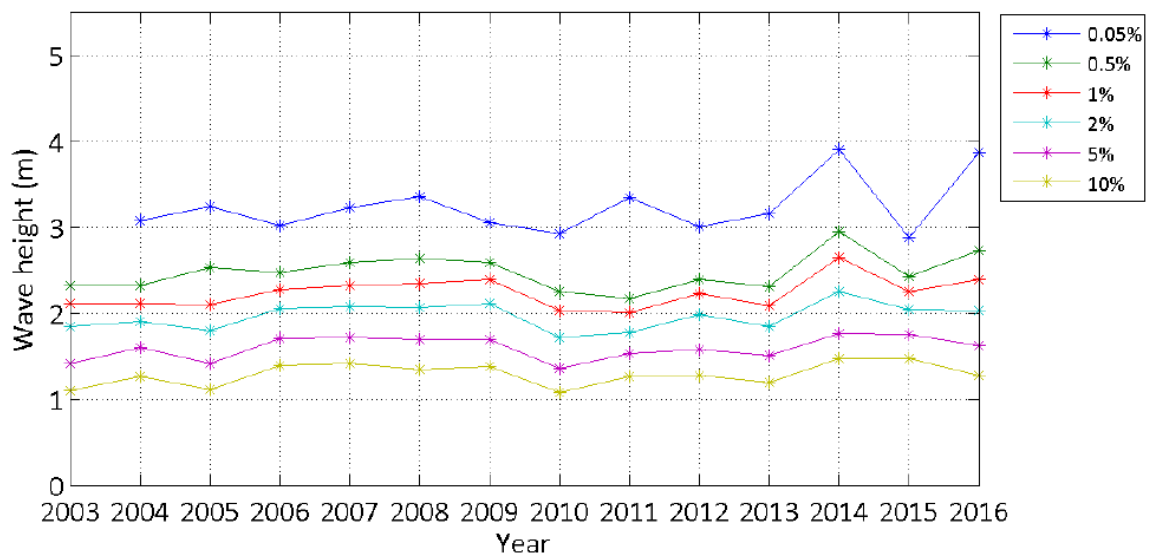


Figure 3.5: Annual wave height exceedance levels (H_s). (Source: CCO, 2017)

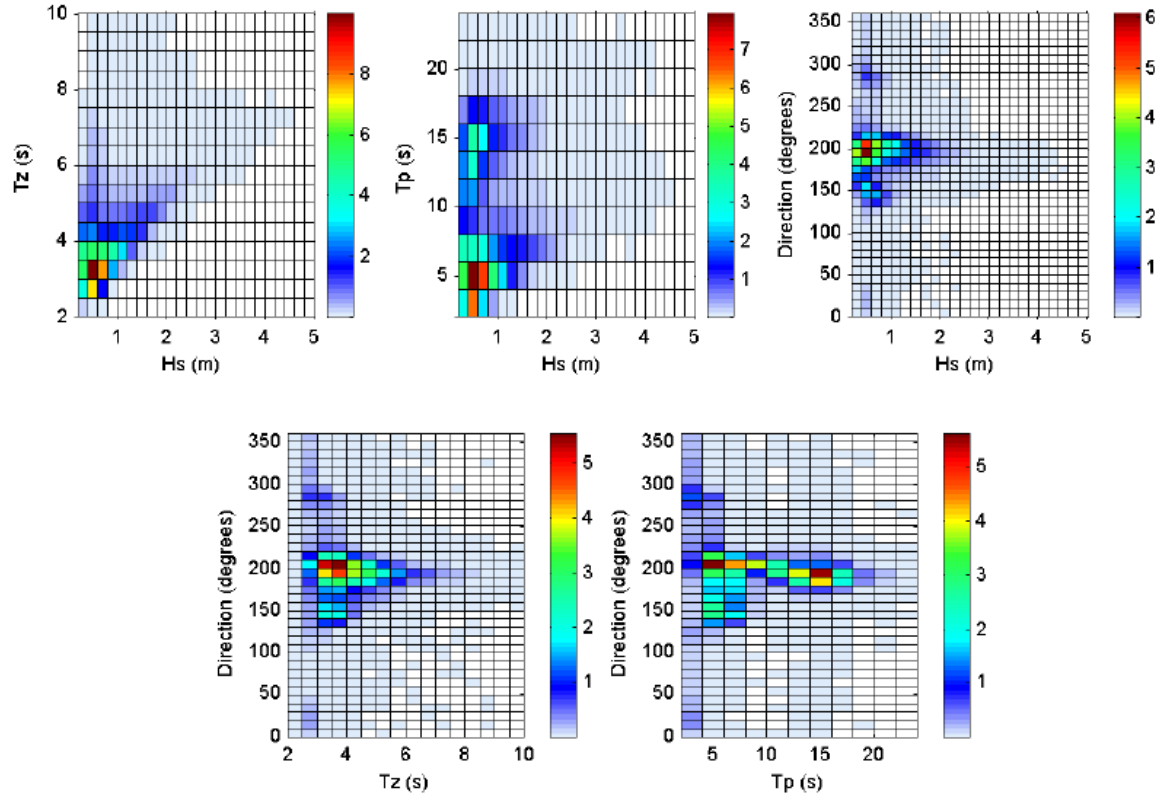


Figure 3.6: Joint distribution plots: percentage occurrences of wave heights, periods and directions July 2003 – December 2016. (Source: CCO, 2017)

i. *Bi-modal waves*

Bi-modal storm events occur when long period swell waves combine with local storm waves, and are associated with a greater likelihood of beach erosion and defence overtopping (Bradbury *et al.*, 2007; Wilson, 2017).

They can be seen in spectral analysis (Figure 3.7) and are defined as events when there are spectral peaks in both sea and swell waves. To qualify, the following criteria must be met (Mason *et al.*, 2008): significant wave height must be greater than 0.5 m; the smaller peak must be at least one third as large as the larger peak, and must contain at least $0.4 \text{ m}^2\text{Hz}^{-1}$ energy (about 0.2 m Hs equivalent); and the energy in the trough must be less than half the energy of the smaller peak, providing a clear separation frequency (usually around 0.1 Hz).

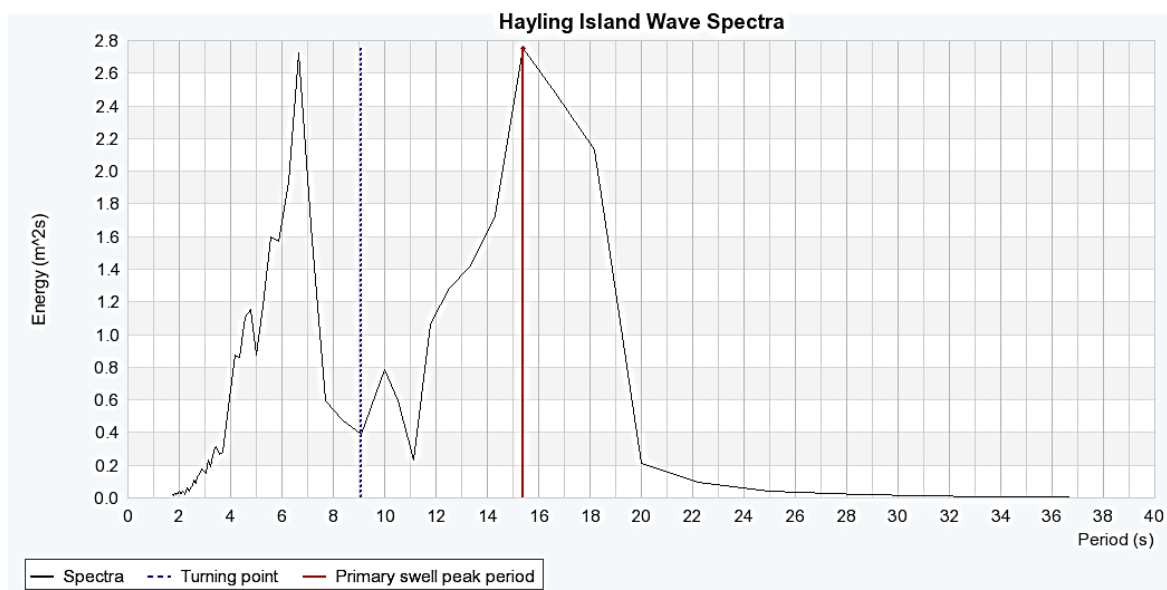


Figure 3.7: Example of bimodal wave energy spectra, 19:05 14/01/2015. (Source: channelcoast.org)

Bimodal events are more commonly associated with open coastlines where swell waves can travel uninterrupted over long distances, to combine with local wind waves. However, they have been found to be relatively common at Hayling Island (Bradbury *et al.*, 2007; 2009), occurring on average around 6 % of the time, and up to 25 % during some winter months. For storm events this number becomes much more significant: over 40 % of storm events are bimodal (Mason *et al.*, 2008). Table 3.1 shows the average monthly occurrences of bi-modal waves using data since Wave Rider records at this location began (CCO, 2017).

Table 3.1: Monthly averages for all wave data (2003-2016) (Source: CCO, 2017)

Month	H _s (m)	T _p (s)	T _z (s)	Dir. (°)	SST (°C)	Bimodal seas (%)
January	0.96	10.3	4.3	184	7.4	15
February	0.82	10.5	4.3	182	6.4	9
March	0.67	9.5	4.0	185	6.9	4
April	0.53	8.1	3.7	182	9.5	2
May	0.53	6.5	3.4	186	12.6	2
June	0.49	6.1	3.3	188	15.7	1
July	0.52	5.5	3.2	198	17.9	1
August	0.53	5.4	3.2	200	18.7	1
September	0.56	6.8	3.4	189	17.5	1
October	0.74	7.4	3.7	184	14.9	4
November	0.84	8.1	3.9	191	12.0	7
December	0.88	9.3	4.1	187	9.0	11

The importance of bimodal wave conditions may be detectable in the data collected for the current study. It is likely that wave period will play a significant role in measured morphological changes.

ii. Wave refraction

The wave climate in the Solent is complicated by the presence of the Isle of Wight, which causes complex wave refraction patterns. This leads to variable wave energies and directions even along the 6 km coast of Hayling. Eastoke does not benefit as much from the Isle of Wight's wave shadow as the western end of Hayling Island (Whitcombe, 1996). This means that approximately 45% of waves approach Eastoke from the southwest (Moon, 2003). Due to the increased fetch from this direction, these waves are larger than waves from any other direction. As such, the significant wave heights for given return periods are higher at Eastoke than for the rest of the island. Using hindcast data from 1971 to 2006, the maximum significant wave heights have been modelled as 5.19 m for a one year return period, 6.45 m for a 10 year, and 7.31 m for a 50 year return period (compared to 3.3 m, 4 m and 4.48 m at central Hayling for the same return periods) (HR Wallingford, 2008). This wave focussing increases erosion rates at Eastoke compared to other parts of Hayling Island.

The difference in direction of wave approach caused by refraction around the Isle of Wight has created a local drift divide (Figure 3.8). With minimal onshore sediment sources (Whitcombe, 1995), the drift divide leads to a shortage of sediment available for longshore transport and would lead to significant erosion if not offset by artificial beach replenishment (section 3.5.i). The exact position of the drift divide is slightly variable as it depends on the dominant direction of wave approach. For approximately 7% of the year, waves approach from a south-easterly direction, and this causes longshore transport at Eastoke to switch temporarily to a westerly direction (Moon, 2003). Because the drift divide would add an extra layer of complexity to an already complicated study, the specific area selected for the study site is located approximately half a kilometre east of the divide. This should mean that sediment transport pathways are broadly similar across the whole study area.

3.4 Tidal deltas

Hayling Island is situated between two harbour entrances: Chichester in the east and Langstone in the west. The currents at these locations complicate patterns of sediment transport around this coastline (Figure 3.8), creating tidal deltas. The tidal delta of most relevance to the study site is West Pole Sands – it can be seen in Figure 3.2 and is marked on Figure 3.8.

The dominant sediment transport at both Eastoke and West Wittering is towards the harbour entrance, where sediment interacts with tidal currents and is generally moved seawards. The flood currents of the harbour entrances are of longer duration than the ebb currents, and as such the ebb currents have a greater capacity for sediment transport. Scour channels up to 20 m deep have been observed (SCOPAC, 2004), but once the water has passed through the harbour entrances on the ebb tide, it slows down and deposits this sediment, helping to create the sandbanks. At Chichester Harbour, this sediment accumulation extends up to 4 km offshore for sand and 2 km offshore for gravel, with a potential total volume of 25 million m³ (Webber, 1979).

West Pole Sands provides some level of protection to Eastoke, as it dissipates wave energy as it approaches the shore. It may also provide a source for onshore transport of sand during southerly storms (Harlow, 1980). Bray (2007; 2010), working on the east of Chichester Harbour entrance, found that sediment from the tidal delta could be observed to move onshore as part of migratory bars up to 150 m wide and approximately 1 m high which then weld to the existing beach. Bray (2010) suggests that this process can take up to four years to be completed.

Tidal currents are not believed to contribute to sediment transport in the nearshore zone, having been measured to have velocities of less than 0.5 ms⁻¹ during spring tides (Hydraulics Research, 1992). However, in the harbour entrance, when combined with wave energy, their effects can be significant. Tidal currents can also influence approaching waves, diminishing wind waves and thus reducing their impact on the beach north of Eastoke Point towards Black Point (Figure 3.8), where sediment is transported north but at a slower rate (NFDC, 2017).

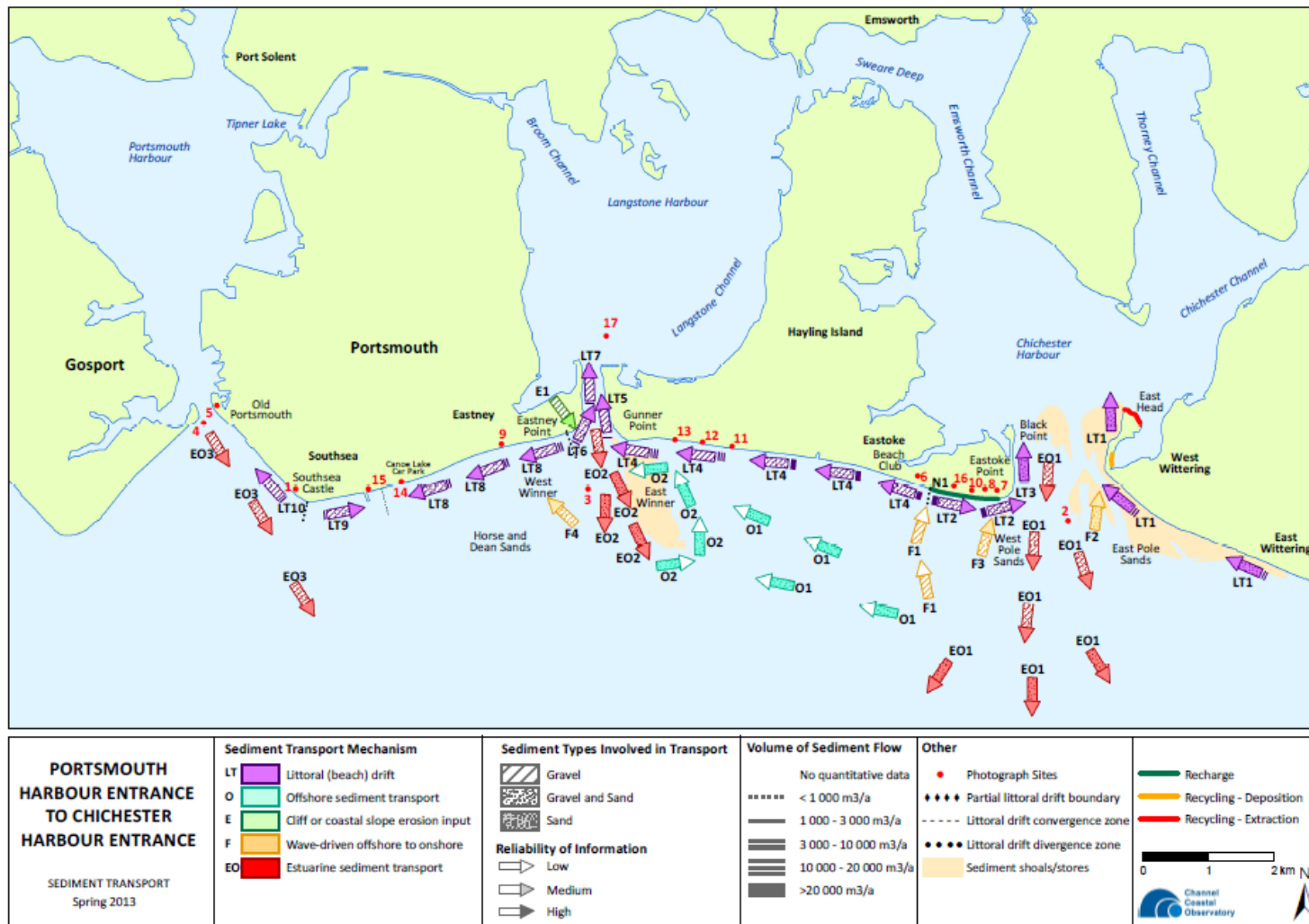


Figure 3.8: Sediment Transport from Portsmouth Harbour Entrance to Chichester Harbour Entrance. (Source: NFDC, 2017)

3.5 Flood and defence history

Eastoke has historically (20th century) been the most frequently flooded part of Hayling Island (Ruocco *et al.*, 2011), and remains an area of interest in terms of maintaining and adapting flood defences due to its high population density.

Hayling Island - and particularly Eastoke - has a long history of coastal management. The sea wall at Eastoke was constructed between 1939 and 1954 to prevent further retreat of the barrier beach, but depletion of the beach levels seaward of the wall caused it to be quickly undermined; major repairs were required by 1978, with an additional splash wall being constructed in the early 1980s (ESCP, 2012). Some groynes were in place prior to 1985, but new groynes were put in place between 1987 and 1991. In January 1991, a terminal rock groyne was built at Eastoke Point; some material could then be recycled from here. To increase stability of the beach crest at Eastoke Point, a rock revetment was constructed in 1992.

Hayling Island is currently managed by the Eastern Solent Coastal Partnership (ESCP), mainly through annual replenishment schemes, but also through groynes and revetments (both rock and wooden). The preferred management strategy for the entire open coast of Hayling Island is to hold the line (New Forest District Council, 2010; ESCP, 2012), i.e. prevent any further erosion from taking place along this coastline.

i. Replenishment schemes

The first replenishment scheme at Hayling Island was undertaken in 1985, between April and December. This was in response to an estimated net sediment loss of 13,000 m³ per annum (Hydraulics Research, 1980; Harlow, 1985). It involved the addition of approximately 530,000 m³ of sediment to a 2.2 km stretch of beach at Eastoke, at a cost of £4 million (McFarland *et al.*, 1994).

The sediment was dredged from Owers Bank, which is located to the southeast of Selsey Bill. The James Renourishment Factor (James, 1974) was used to determine its suitability for Eastoke (this states that replenishment sediment should be slightly larger than the native material and preferably poorly sorted as this should help to increase its retention time and therefore the lifespan of the replenishment). Sediment was deposited by shallow draught barges on the lower foreshore, and then reprofiled by bulldozers to create a beach crest approximately 5.6 m OD and 30 m in width to reduce the risk of overtopping and

provide a significant barrier against flooding (Grant, 1986). The beach naturally aligned itself to a 1 in 9 slope and rapid sorting of surface sediments occurred. Gravel clast size decreased from the beach crest to toe and increased both east and west away from the littoral drift divide (Harlow, 1985). However, much of the replenishment material remained unaffected by wave action and became compacted to $2,000 \text{ kg/m}^3$; the original design specification was $1,750 \text{ kg/m}^3$, so this represented a fairly major difference that produced steep cliffs on the upper beach (McFarland et al., 1994). It is thought that a high calcium carbonate content may have aided in the formation of these cliffs by weakly cementing sediment together. More recent research has shown that the poorly sorted material can be compacted by the heavy machinery, and affected by rainwater percolating through it, creating layers of cemented sediment which do not seem to interact with the previous beach surface (Zarkogiannis *et al.*, 2018).

Post-replenishment sediment volumes showed significant variation, but there was an overall trend for net erosion (Whitcombe, 1995). Figures for the net sediment transport rate vary (due to the inherent error that comes from calculating volumes using the DEM method - an error of a few mm in elevation measurements can increase exponentially when multiplied over a larger area (Moon, 2003)), but all seem to agree that initial rates of erosion were significantly higher than later averages. Rates of longshore transport were also much greater than those measured prior to the replenishment project; this is assumed to be because of the increased volume of sediment available for transport, and also because some of the original groynes were either completely or partially buried by replenishment material, leading them to become redundant in preventing or limiting longshore transport. New timber groynes were constructed in 1987 to reduce the rates of longshore sediment transport.

Hydraulics Research (1987) calculated that initial loss of recharge material during the first year was $88,000 \text{ m}^3\text{a}^{-1}$, though other estimates indicated that between February 1986 and 1987, longshore transport rates were approximately $53,000 \text{ m}^3\text{a}^{-1}$. This decreased to approximately $30,000 \text{ m}^3\text{a}^{-1}$ for the period following until 1993, and then to 25,000 between 1994 and 1996.

The beach crest retreated at $2\text{-}3 \text{ m.a}^{-1}$ according to initial observations, which reduced to 1.5 m.a^{-1} for the period between 1990 and 1995, and finally to 0.5 m.a^{-1} (HBC, 1999; 2000). By 1994, just under 55% of the replenishment material had been lost (HR Wallingford, 1995). This was compensated for by recycling of material from observed accumulations, for

example in front of Hayling Golf Club at the west of the island. Recycling volumes totalled over 100,000 m³ between 1985 and 1993 (Whitcombe, 1995), indicating a reasonably fast transport rate along this coast. Direct offshore losses – for example of the fine material from the replenishment fill (She *et al.*, 2006) – are unknown, but likely to be significant.

Storm losses were shown to be limited, with the majority of sediment lost to each event recovered later during calm conditions (SCOPAC, 2004). The main area of loss is at Eastoke, east of the drift divide. Total averaged net loss between 1985 and 2000 has been estimated at 5,000 m³a⁻¹ (gross transport was 25,000 m³a⁻¹, with annual replenishment volumes of 20,000 m³a⁻¹). This is believed to be mainly due to the interruption of longshore transport by currents at Chichester Harbour entrance.

Since replenishment began in 1985, the only significant flood event to occur was in November 2005, when bimodal waves combined with extreme water levels resulted in overtopping along much of South Hayling. However, the flooding on this occasion was still not as severe as events prior to 1985, indicating the replenishments were beneficial (ESCP, 2012).

Replenishment is now generally undertaken every five years (ESCP, 2012). The preferred particle size for recharge material is D₅₀ = 20-40 mm, and it should be as well sorted as possible to reduce the fine content, which can negatively impact the beach's post-replenishment adjustments.

There are also annual recycling schemes which help to prevent too much of the replenishment material being lost and reduces the amount of dredging that needs to occur locally. This is much more cost effective as it does not require the purchase of new sediment. Despite regular replenishment, the average annual net loss since 2004 has been calculated at 4,920 m³ for the whole of South Hayling, which is reflected in the proportions of recycled to imported sediment (Table 3.2). This was worked out based on volumetric calculations from annual dGPS profile surveys taken at MLWS. Distribution of erosion and accretion can be seen in **Figure 3.9**.

Table 3.2: Recycling and replenishment volumes for Hayling Island, past 3 years. (Data from ESCP, 2017)

Year	Recycled (m ³)	Imported (m ³)	TOTAL (m ³)	% recycled
2013-14	43,437	4,396	47,833	90.8
2014-15	31,610	2,477	34,087	92.7
2015-16	44,863	1,683	52,819	84.9

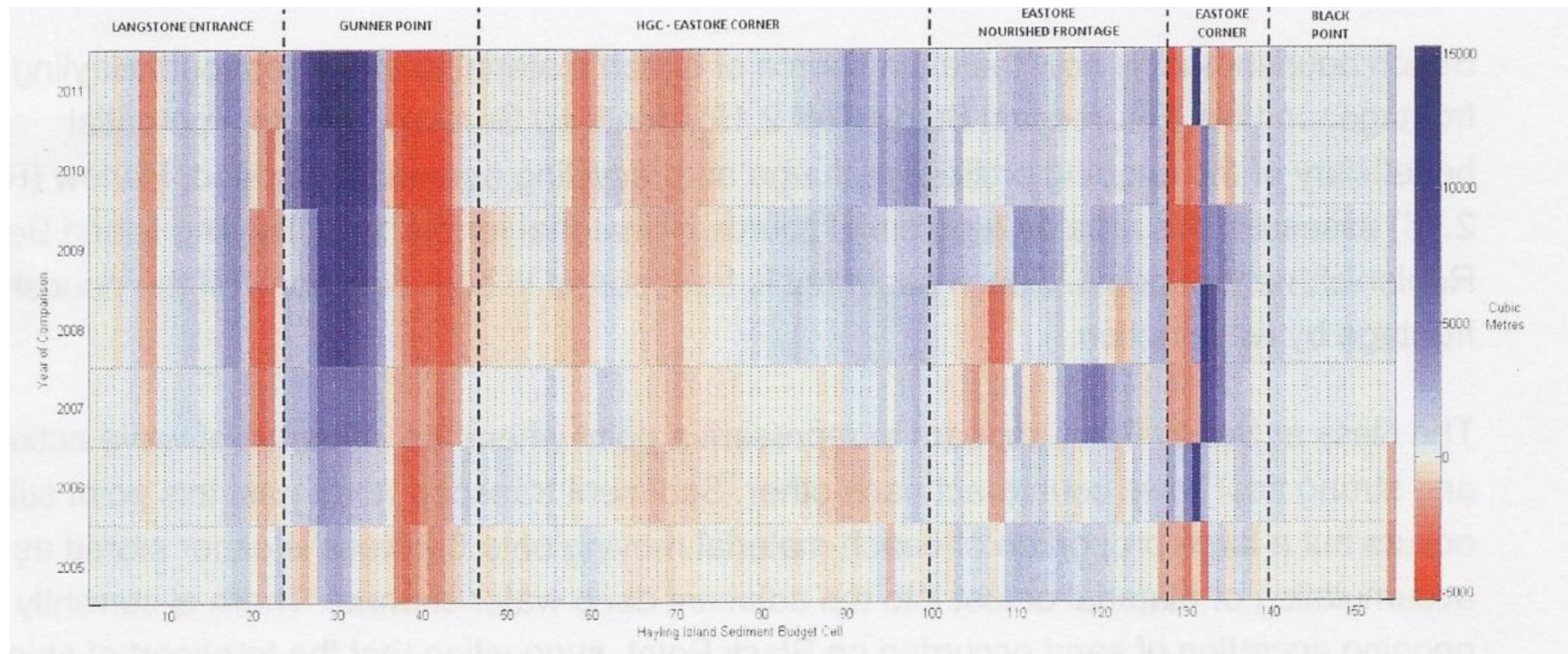


Figure 3.9: Net volumetric change above MLWS, relative to 2004 baseline survey (from ESCP, 2012)

ii. 2013 Eastoke Point Defence Scheme

In November 2013, a new defence scheme for Eastoke Point was completed to protect over 1,700 homes against a 1 in 200 year flood event. It consisted of 650 m of new rock armour revetments and three rock groynes at Hayling Island's south east corner (Figure 3.10) and cost a total of £5 million, which was provided by funding from the Environment Agency. Works took 6 months to complete, including the import of 75,000 tonnes of Norwegian granite, and the addition of 35,000 m³ of sand and gravel, dredged from Owers Bank.

The rock revetment that forms the crest of the beach is 6 m above OD, which, combined with the crest width of 18 m, is considered to provide the required protection against overtopping and crest failure. Each rock groyne extends approximately 100 m from the revetment. The works were designed to be adaptable, with the possibility of altering the length of the rock groynes if they were found to allow too much or too little sediment to pass over, around or through them.

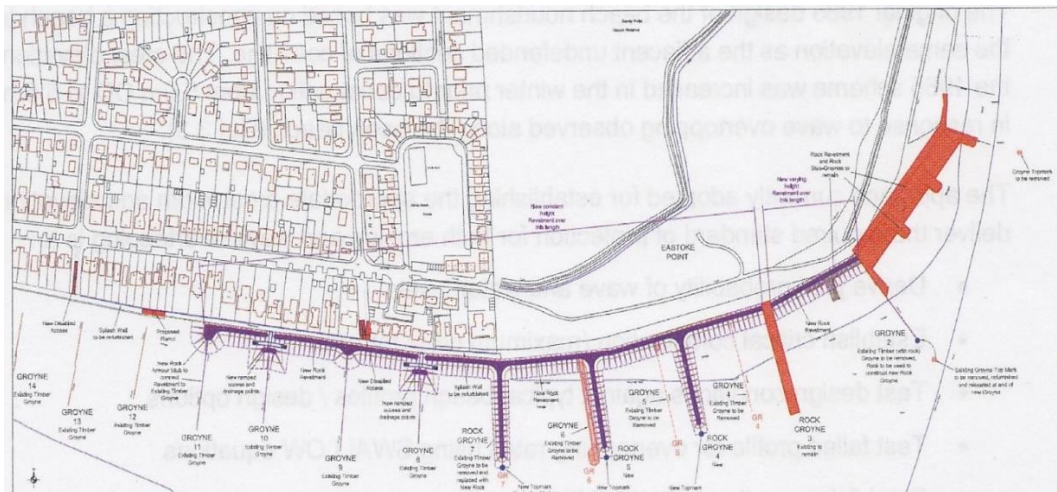


Figure 3.10: Eastoke Point proposed scheme design (from ESCP, 2012). Purple areas indicate locations of riprap, either as a groyne or positioned on the beach crest. Wooden groynes are denoted by thinner lines in the west side of the image.

During severe storms in the winter of 2013/14, these new defences successfully protected the houses immediately behind them by limiting wave overtopping and preventing breaching, which almost definitely would have occurred prior to the defences. A significant volume of the replenishment material was transported below the low tide level in an offshore direction, however, reducing the beach volume significantly - observations of post-storm beach recovery indicates that very little of this material returned to the active beach face. Relatively major cliffing of the remaining sediment also occurred, with cliffs up to approximately half a metre in height being observed.

4. Methodology

4.1. Overview

This chapter details the sample design used to collect data intended to fulfil the aim and answer the research questions associated with the thesis (Chapter 1).

Active layer depth was measured with sliding indicator devices (SIDs) adapted from fluvial research (e.g. DeVries, 2002). This, combined with dGPS profiling, regular sediment sampling, and RFID tracer techniques provides new insight into the morphodynamics of a managed mixed sediment beach, from which attempts have been made to calibrate longshore sediment transport formula for future use.

4.2 Research Design

To achieve research objectives 1 and 2 (Chapter 1.2), a study was created that would provide results from a range of hydrodynamic conditions. Coarse grained beaches are known to experience significant morphological and sedimentological changes, even at short timescales (Buscombe, 2008; Curoy *et al.*, 2009). Thus it was necessary to sample across the entire range of environmental conditions experienced at the site. A series of nine field periods were created, during which daily measurements could be taken. Data collection began in late September 2014 (referred to as the October 2014 field period, because most of the data collection occurred in October). After this data would be collected for approximately one to two weeks out of each month.

During these periods, monitoring of beach profile changes (section 4.4), AL depths both across and alongshore (section 4.5), changes in sediment properties (section 4.6), and sediment transport (section 4.7) were undertaken. This provided a large dataset that enabled relationships between different processes to be analysed for the mixed sand and gravel beach at Eastoke, at both short (semi-diurnal) and medium (monthly/seasonal) time scales, accomplishing research objectives 3 and 4 (Chapter 1.2). All of these data need to be linked to high resolution wave data (section 4.3) (available from the Channel Coast Observatory (CCO)) for research objectives 2 and 5, and tide data (available from the British Oceanographic Data Centre (BODC)).



Figure 4.1: Location of key groyne compartment within the context of Eastoke area. Aerial imagery courtesy CCO, 2016.

As discussed in Chapter 3, the field site was selected to be representative of managed mixed sediment beaches. A small area was chosen for the study to take place, as it would constrain some of the variables, with the intention of strengthening the observed influences of the most dominant driving forces and links between measured variables, given that mixed sediment beaches are particularly complex (Blanco, 2003; Horn and Walton, 2007). A groyne compartment at the western end of the granite defences was selected for monitoring of all aspects of this study; dominant sediment transport in this area is to the east, so this allowed tracer surveys to span the length of the 2013 Defence Scheme area. The location of the groyne cell in relation to the Eastoke frontage can be seen in Figure 4.1. Dornbusch *et al.* (2008) have shown that behaviour within neighbouring groyne bays can be similar even if they are different sizes, so this data should be able to be upscaled to the rest of the area.

All beach surveys and measurements were undertaken at low tide, when the maximum beach profile length was exposed. Priority was given to dGPS surveys and tracer detections as needing to be completed at the full extent of low tide, while burial of tracers (section 4.7.iv) and resetting of sliding indicator devices (section 4.5.iii) could be completed either side of low tide with the slightly higher water level not impacting the process or results.

For simplicity, the field periods can be separated into two 'winters', the first consisting of field periods 1-5 (October 2014, December 2014, January-March 2015) and the second consisting of field periods 6-9 (October 2015-January 2016). There was not a field period in November 2014 as changes were required to the components of the active layer-measuring sliding indicator devices (SIDs) to make them more durable. This issue had not surfaced during the pilot study and so had not been planned for.

The dates of the fieldwork periods were intended to provide a range of wave and tide conditions at the site; one long study period would not have ensured a range of conditions could be studied. The data collection was focused during Autumn/Winter months to ensure that some higher energy conditions were measured, which would allow results and subsequent transport calculations and calibrations to be applicable to a wider range of wave scenarios. Table 4.1 shows measurement types taken on each day during each of the field periods. On some occasions, timings of tides and daylight hours meant limited or no data was collected.

During October 2014, dGPS profiles were taken, but have been excluded from results as they did not follow exact profile lines. AL measurements stopped after 05/10/14 because all SIDs had been damaged. Pebble survey data was corrupted during download and thus has no

location data associated with it. The surface codes collected during this month were used to create a more detailed and representative coding system which was used in subsequent field periods.

The set profile of Profile 2 began on 11/12/2014. A fault with the datalogger meant pebble surveys could not be completed during December 2014. A different fault during January 2015 meant that pebble surveys did not have location data associated with them, so only the tag IDs of detected pebbles are known. Data from 24-27/01/15 was collected mainly to compare physical sediment samples to the surface coding system.

Issues with the dGPS kit allowed only partial profile measurements on February 16th and 25th 2015, and no measurements on the 19th, 26th and 27th. On 23/11/15, the dGPS disconnected from the base station after one profile had been measured and could not be reconnected. There were also occasions during January 2016 when the dGPS kit did not function correctly.

The focus of field period 5 was on pebble deployments and surveys. Additional pebble surveys were undertaken during April and May 2015, and unsuccessful attempts were made to recover pebbles and log their burial depths during July 2015. A further pebble survey was undertaken after all other fieldwork had finished, on 27/02/2016.

Table 4.1: Measurements taken on each day of fieldwork

	Date	dGPS points at SID locations	Profile 1	Profile 2	Profile 3	AL depth - SIDS	Pebble deployment	Pebble survey	Surface codes	Sediment sampling
Field Period 1 – October 2014	30.09.14									
	01.10.14									
	02.10.14									
	03.10.14									
	04.10.14									
	05.10.14									
	06.10.14									
	07.10.14									
	21.10.14									
Field Period 2 – December 2014	01.12.14									
	02.12.14									
	03.12.14									
	04.12.14									
	05.12.14									
	06.12.14									
	10.12.14									
	11.12.14									
	12.12.14									
	13.12.14									
	14.12.14									
	15.12.14									
	16.12.14									
Field Period 3 – January 2015	09.01.15									
	10.01.15									
	11.01.15									
	12.01.15									
	13.01.15									
	14.01.15									
	15.01.15									
	16.01.15									
	17.01.15									
	18.01.15									
	19.01.15									
	20.01.15									
	24.01.15									
	25.01.15									
	26.01.15									
	27.01.15									

	Date	dGPS points at SID locations	Profile 1	Profile 2	Profile 3	AL depth - SIDS	Pebble deployment	Pebble survey	Surface codes	Sediment sampling
Field Period 4 -February 2015	11.02.15									
	12.02.15									
	13.02.15									
	14.02.15									
	15.02.15									
	16.02.15									
	17.02.15									
	18.02.15									
	19.02.15									
	20.02.15									
	22.02.15									
	23.02.15									
	24.02.15									
	25.02.15									
	26.02.15									
	27.02.15									
Field Period 5 – March 2015	09.03.15									
	10.03.15									
	11.03.15									
	12.03.15									
	13.03.15									
	14.03.15									
	15.03.15									
	16.03.15									
	17.03.15									
	18.03.15									
	19.03.15									
	20.03.15									
	21.03.15									
	22.03.15									
	23.03.15									
	24.03.15									

	Date	dGPS points at SID locations	Profile 1	Profile 2	Profile 3	AL depth - SIDS	AL depth – DoD rods	Pebble deployment	pebble survey	Sediment sampling
Field Period 6 – October 2015	28.09.15									
	29.09.15									
	30.01.15									
	01.10.15									
	02.10.15									
	03.10.15									
	04.10.15									
	05.10.15									
	06.10.15									
	20.10.15									
	21.10.15									
Field Period 7 – November 2015	04.11.15									
	05.11.15									
	06.11.15									
	07.11.15									
	08.11.15									
	09.11.15									
	10.11.15									
	11.11.15									
	12.11.15									
	13.11.15									
	14.11.15									
	17.11.15									
	18.11.15									
	19.11.15									
	23.11.15									
	26.11.15									
Field Period 8 – December 2015	02.12.15									
	03.12.15									
	04.12.15									
	08.12.15									
	09.12.15									
	10.12.15									
	11.12.15									
	14.12.15									
	15.12.15									
	16.12.15									

	Date	dGPS points at SID locations	Profile 1	Profile 2	Profile 3	AL depth - SIDS	AL depth – DoD rods	Pebble deployment	Pebble survey	Sediment sampling
Field Period 9 – January 2016	01.01.16									
	04.01.16									
	05.01.16									
	06.01.16									
	07.01.16									
	08.01.16									
	09.01.16									
	10.01.16									
	11.01.16									
	12.01.16									
	13.01.16									
	14.01.16									
	15.01.16									
	16.01.16									
	18.01.16									
	19.01.16									
	20.01.16									
	24.01.16									
	25.01.16									
	28.01.16									
	31.01.16									

It had been anticipated that at least one of the field periods could be timed to occur immediately after a beach replenishment event. Unfortunately, despite the length of the study, this was not possible. Though the replenishment would have added a useful and significant comparative dataset, the variety of hydrodynamic, morphological and sedimentological conditions under which measurements were taken is much broader than most AL studies, and provides a reasonable representation of this type of beach. Since the 2013 defences have been put in place, major replenishment works have not been the norm, and beach recycling operations deposit most of the sediment at the drift divide to the west of the study site, meaning that there is less interference by heavy machinery or the initial post-nourishment sorting processes on beach dynamics.

A pilot study for measuring the active layer depth was undertaken in March 2014 (Appendix Q) which gave an indication of the time required to take readings from SIDS and reset them.

Additional analyses undertaken during this pilot study were deemed to be too complex, expensive or time consuming to undertake on the regular basis required by this project, but might be considerations for future research projects on similar beaches.

4.3 Monitoring wave climate

The local wave climate was monitored using a wave buoy operated by the Channel Coastal Observatory (CCO). It is a Datawell Directional Wave Rider MK III, which was deployed in July 2003 and has been providing reliable data on wave height, period and direction since February 2004. The buoy is located at $50^{\circ} 43.91' \text{ N } 00^{\circ} 57.56' \text{ W}$ (Figure 4.2), approximately 5 km south of the field site at Eastoke in 10 m CD water depth; it is classed as a nearshore wave buoy.



Figure 4.2 Location of Wave Rider (triangle), in relation to field area (boxed area). (Aerial imagery from ESRI.)

Outputs are given for 30 minute periods, and can be downloaded in monthly or annual files. These were manually separated according to the time of low tide (to coincide with measurements taken on the beach at this time). Mean averages, maximums and minimums were calculated for each day. Graphs of monthly wave data can be seen in Appendix A.

Wave power and longshore wave power were calculated using equations in Chapter 2 (section 2.4), with an angle of 185 degrees from North considered 'perpendicular' for the calculation of the longshore component.

This Wave Rider is the best available local data source and is used by HBC for planning and calculations, so any future predictions based on the results of this project will be made using data from it. Thus, in the absence of a calibrated propagation model for this shoreline, it makes sense to use this data when looking for relationships.

4.4 Beach profile changes

i. Methods available

The most basic method for measuring beach profiles would be to use a compass, tape measure and clinometer to record the profile angles and how these change cross-shore. However, the most common technique currently is to use a differential GPS antenna on a pole. This can provide x,y and z coordinates which are accurate to a few millimetres and is also very quick once the user is comfortable with the equipment.

Certain studies, including Curoy *et al.* (2009) and Dornbusch (2010), used a bicycle wheel on the base of the antenna pole to undertake continuous topographical surveys, whereby the GPS system is set to automatically take a measurement once per second, and the researcher simply rolls the wheel along a profile line. Theoretically, this is a quick and easy way to produce detailed profile lines. However, on coarse grained beaches, where steep beach slopes are experienced, the size of the wheel can lead to inaccurate measurements (Dornbusch, 2010).

On wide stretches of relatively flat, sandy beach, it is possible to use the GPS system to run continuous surveys from a quadbike (Baptista, *et al.*, 2008). This covers large areas of morphologically barren beach very quickly, but is not suitable for use on the narrow, steep and morphologically varied beach at Eastoke.

Other recent studies, such as Almeida *et al.* (2015) have used a laser scanner to create a high-resolution point cloud of the beach face, from which beach profiles can be extracted if needed. This particular example of research was done on a gravel beach, suggesting that it would also be feasible on a mixed sediment beach. However, positioning a laser scanner to limit point shadows created by berms (which are common on mixed sediment beaches) would be difficult without a raised area on which to place it (Dornbusch, 2010). The only other way to combat point shadows is to scan from two locations, which would take too long. In intertidal areas the time taken for even a single scan to be completed would be an issue, as the encroaching tide would cover areas needing to be scanned. Further errors would be introduced to the data by the researcher, who would need to be moving around on the beachface, measuring and resetting SIDs (4.5.ii) and taking sediment samples (section 4.6.iii).

ii. Chosen method

dGPS beach profiles were selected as being the simplest and most efficient way to collect the data required at this temporal resolution. Its positional accuracy is similar to laser scanning

(Dornbusch, 2010), but it is considerably faster and more appropriate for use on a steeply sloping beach.

Previous studies have shown the inaccuracies associated with using dGPS profiles to estimate LST rates (e.g. Moon, 2003), but the practice is still commonly used among coastal practitioners. The profile data collected during this study is mainly intended to provide morphological data against which to assess patterns in AL depth. However, beach profiles can also be processed in SANDS to produce cross-sectional areas, which can be compared from survey to survey as an indication of erosion and accretion. Having measured three profiles in the same groyne compartment, the changes in each of these profiles can be used together to estimate longshore sediment transport within the groyne compartment under varying wave conditions. This method is not capable of producing a longshore sediment transport rate for the whole section of coastline, but results can be compared to short term pebble tracer experiments to determine whether both methods produce similar results.

iii. The dGPS system

The RTK-dGPS system used in this study was provided by Havant Borough Council. It consisted of a Trimble R8 antenna and a Trimble TSC3 handheld controller. A permanent base station located on the other side of Chichester Harbour can be accessed via an internet connection in the TSC3 controller. This provides real time data corrections for the GNSS satellite data used by the antenna to calculate its position. The data obtained from this system has a vertical accuracy of ± 30 mm and a horizontal accuracy of ± 15 mm. This error is of the same order of magnitude as the error which Curoy *et al.* (2009) suggest would be caused by minor topographical differences because of the packing of larger grain sizes; the surface is not flat, so a few centimetres of lateral movement could result in two different elevations being measured; steps have been taken to minimise the influence of this in the data. Additionally, coarse sediment is unstable, and walking on it can cause the grains to shift. The overall error is assumed to be approximately equivalent to the D_{50} of the coarsest material on the beach, which at Hayling has variously been reported to be 20-40 mm.

iv. Survey design

For the current project, measurement of location and elevation was required daily at positions where sliding indicator devices were deployed to measure the active layer (section 4.5.iii), so it was deemed simpler and quicker to use a detail pole for all measurements. This study used a pole with a pointed end; flat ended poles can be used on beaches with gentle slope, but where

the slope angle is significant, the flat end can make it difficult to accurately position and level the pole and thus provide inaccurate measurements (Dave Picksley, *pers.comm.*).

In order to account for the precision required when using a pointed detail pole, all surveys were completed by one surveyor, enabling a consistent method to be used: when measurements were taken in gravel-dominated locations, the point was gently rested on the surface of a pebble which did not extrude excessively from its general surroundings; on sand dominated sections of the beach, the point was rested on the surface and not allowed to sink below the surface. The pole to which the handset and antenna are attached has a levelling bubble to allow the surveyor to hold it as vertical as possible, thus reducing human-induced error. Points were taken approximately every 5 m along the profile, or when morphological changes occurred – such as a change in slope angle.

Beach profiles were intended to be measured on a daily basis during each field period. In October 2014 profiles were not taken in consistent locations every day and so have not been used in the data set. From 11/12/2014 onwards, a HBC baseline survey location was followed as the central profile in the main groyne compartment studied. Two additional profiles were also monitored during this time (approximately symmetrically spaced between the HBC baseline profile and the wooden groynes to either side). These later became Profiles 1 and 3, but during December 2014, the profile lines to be followed had not been set into the dGPS and so some lateral movement between actual measured profiles occurred. Profile locations can be seen in Figure 4.3. The variation in volume under each profile can be calculated and compared to hydrodynamics (especially wave direction) to monitor possible sediment circulation patterns within the groyne bay.

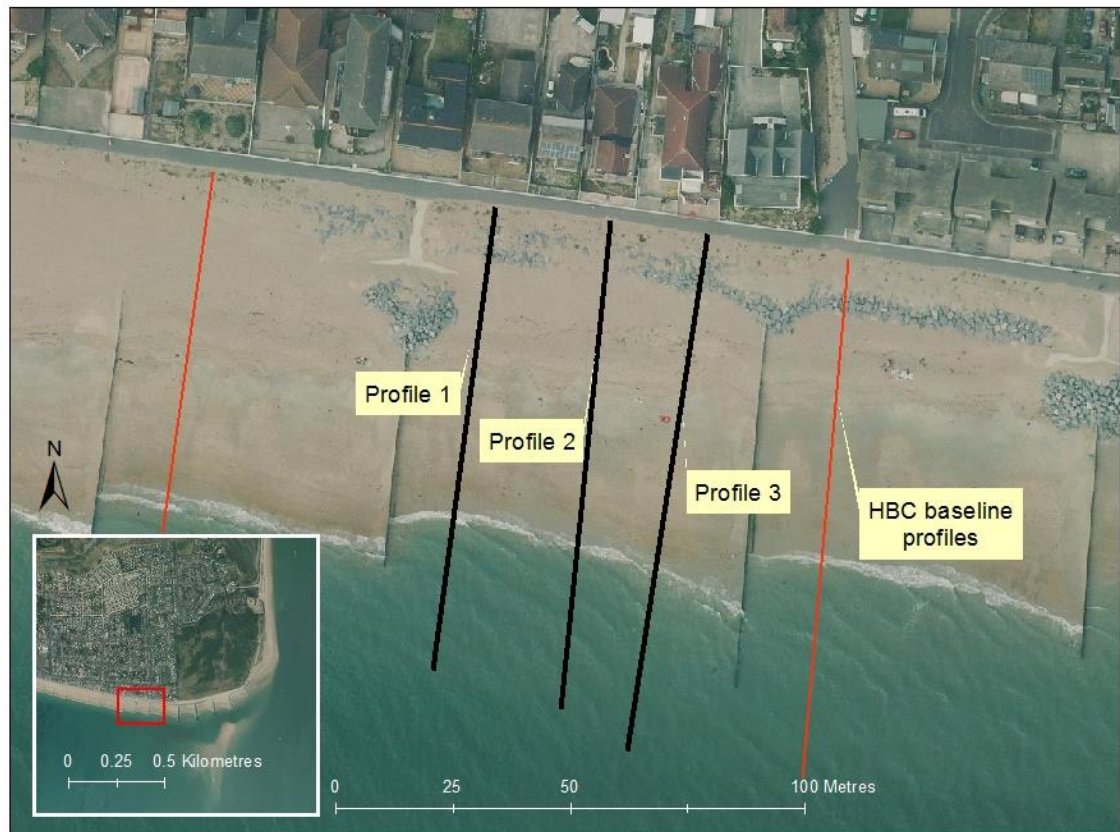


Figure 4.3: Location of profile lines, and neighbouring HBC baseline survey locations

Classifying the shapes of beach profiles according to categories allows further insights to be gained relating these shapes to the beach response to wave conditions, and may also be useful in terms of future replenishment schemes; if a particular shape is most common or stable, it might be possible to design a beach to be this shape in an attempt to increase the stability of the beach. Caldwell and Williams (1985) determined statistically, using 402 profiles measured over almost three years on two gravel beaches in South Wales ($D_{50} = 2\text{-}10\text{ mm}$), that there were 10 potential coarse clastic beach profiles. These consisted of five linear profiles and five concave profiles, each with corresponding berm placements (or no berm) (Table 4.2, Figure 4.4). Their visual classification system is relatively simple to use, and so all profiles were classified accordingly. This also provides insight into the similarity (or lack thereof) between pure gravel and mixed sand and gravel beaches in terms of overall profile shape, as it gives an indication of the relevance of each of these profile types on a mixed sand and gravel beach.

Table 4.2: From Caldwell and Williams (1985). Ten identified morphological categories

Code	Definition	No. of profiles	Figure 2
CCNB	Concave, no berm	90	A
CCUB	Concave, upper berm	66	B
CCMB	Concave, mid-berm	74	C
CCLB	Concave, lower berm	16	D
CCCB	Concave, composite berm	37	E
LNB	Linear, no berm	41	F
LUB	Linear, upper berm	35	G
LMB	Linear, mid-berm	21	H
LLB	Linear, lower berm	11	I
LCB	Linear, composite berm	11	J

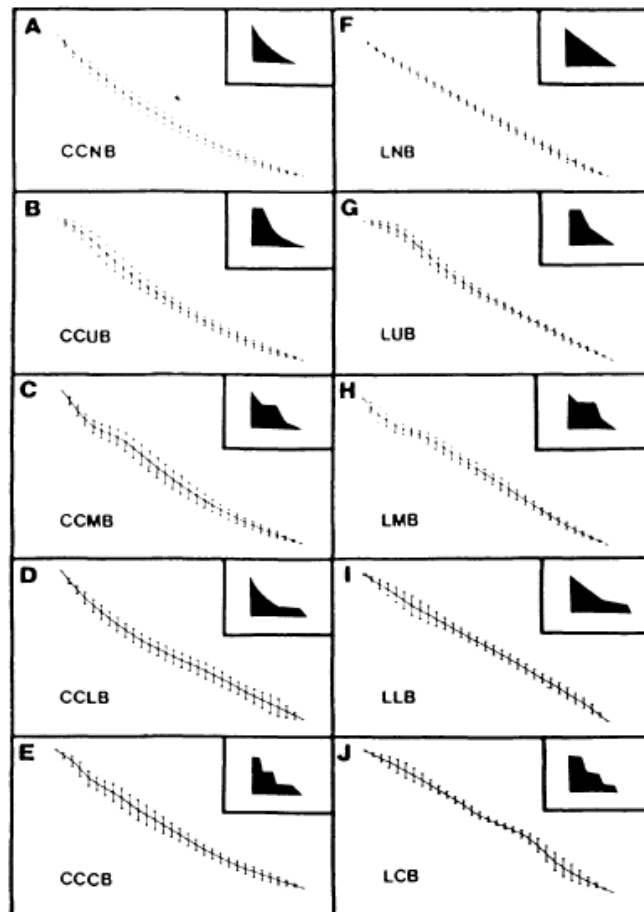


Figure 4.4: From Caldwell and Williams, 1985 (p.133). “Average profiles for the ten morphological categories. Vertical bars indicate one standard deviation either side on the mean profile every 1 m down the beach. An idealized model for each configuration is inset.”

v. Issues experienced

The main limitation of this method is that the profiles do not extend past the low water level, which provides different lengths of profile depending on the exact stage of the tide and the amount of run up contributed by waves. This meant the potential existence and dynamics of the beach step, an important aspect of coarse grained beaches (Buscombe and Masselink, 2006) could not be assessed.

On some days a bad network connection meant it was not possible to connect to the CHINET base station via internet. This could normally be resolved by walking around the beach until a good enough phone and internet signal was found to complete the connection – once the connection had been made, the handset usually stayed connected, even when returning to the original location where the problem had arisen. Technical problems occurred with greater regularity during the second winter. High wind days also affected GPS surveys by making it too difficult to hold the pole and antenna upright and level while points were measured.

4.5 Active layer depth

i. Methods available

One popular technique for determining AL depth on beaches is to use buried columns of tracers. These can take the form of dyed sand (e.g. Williams, 1971; Sunamara and Kraus, 1985) or painted pebbles (e.g. Whitcombe, 1996; Curoy, 2012). Using this method, columns of visually distinct (e.g. painted) pebbles are buried within the active layer. Their precise locations are marked either with metal stakes or GPS coordinates. After a tidal cycle, the researcher returns to the same spot and digs the column back up to determine the number of pebbles which have been entrained and transported during this time, and thus the AL depth. Miller and Warrick (2012) pioneered the use of passive integrated transponder (PIT) tagged pebbles for this, improving on the previous painted pebble methods by allowing the direction and distances of pebble movements to be tracked.

Depth of disturbance rods are commonly used on sand beaches (e.g. Greenwood and Hale, 1980; Jackson and Nordstrom, 1993; Saini *et al.*, 2009; Miller and Warrick, 2012). They are thin metal rods or stakes, usually around 1 m in length, which are inserted vertically into the beach. A loose-fitting metal washer is placed around the rod at the beach surface and moves downwards to indicate the extent of the active layer as the sediment underneath it is disturbed by wave action. Greenwood and Hale (1980) found these to be fairly reliable,

although problems were experienced in locating buried rods, rod bending, and difficulty of excavation where there was a significant depth of disturbance. In a high energy environment, as many mixed sand and gravel beaches are, they may be less suitable. Researchers must also bear in mind that the rods can create a tripping hazard to the general public when they protrude from the beach surface and may thus not be suitable for use on popular public beaches.

In gravel-bedded rivers, scour chains are a common technique to measure the fluvial equivalent of the active layer, which is known as the scour depth (e.g. Foley, 1978; Laronne and Duncan, 1989). Chains made of nylon or metal are buried below the surface (deep enough to not be excavated under normal flow conditions) and anchored in place. The chains bend at the point of deepest sediment activation so that the tip is pointing in the direction of flow and is then buried under the continually moving sediment above it. However, scour chains are not particularly appropriate for coastal environments, mainly due to the difficulty in locating a buried metal chain, especially after high-energy or accretionary events.

Similar to scour chains, but more appropriate for coastal environments, are sliding indicator devices (SIDs), which usually consist of wire strung with buoyant objects, for example plastic practice golf balls (e.g. DeVries, 2002). The wire is then attached to a heavy piece of wood or metal and buried deep in the sediment. As the beach sediment is activated by waves, the buoyant objects buried below the surface float upwards in the water column. A knot is tied in the end of the wire to prevent the balls floating away completely. After a tidal cycle, the researcher can return and count the number of balls now exposed; this, multiplied by the diameter of each ball, gives an indication of the active layer depth. This method is usually accurate to within a few centimetres, but could be made more precise by using smaller indicators, such as foam discs rather than balls. Sliding indicator devices are cheap and relatively easy to produce, and so in a high energy environment where equipment is easily damaged, they are a very suitable option.

Another technologically advanced technique is to use 'Tell-Tail' scour monitors (e.g. Van Wellen *et al.*, 1997). These consist of pieces of metal pipe with monitors attached at approximately 10 cm intervals. Each monitor can detect when the sediment around it is moving, and sends this information to a data logger. This can give real time active layer depth measurements at a much higher resolution; it is not limited to a maximum depth at that location for each tidal event. Another benefit of this device is that it does not need to be reset (i.e. dug up and reburied) as long as there is still space in the data loggers. It is much more expensive though, which gives less scope to gather results from multiple locations on the

beach face for a single event. In a high energy environment it would also be very easily damaged by pebble and cobble sized clasts.

ii. Chosen method

a) Sliding indicator devices

Sliding indicator devices (SIDs) based on techniques used by DeVries (2002) were selected as the most appropriate method for use on this beach. They can be reburied after every tide/measurement, making them exceptionally cost effective, especially when compared to tracer-based methods, which would require the production of thousands of tracers to produce results at the resolution this study required. The anchor buried in the beach should help to make them more resilient than depth of disturbance rods, and the buoyancy of the indicators means they are easy to find above the surface of the beach except in cases of extreme accretion. Additionally, they are less intrusive to local beach-goers, and less likely to cause injury to wildlife than long, thin steel rods.

The devices were made using plastic coated steel wire, connected at one end to a block of wood (these were from groyne offcuts provided by HBC). Foam practice golf balls of 42 mm diameter were then threaded onto the string and a float attached at the other end to keep the string above the surface of the beach.

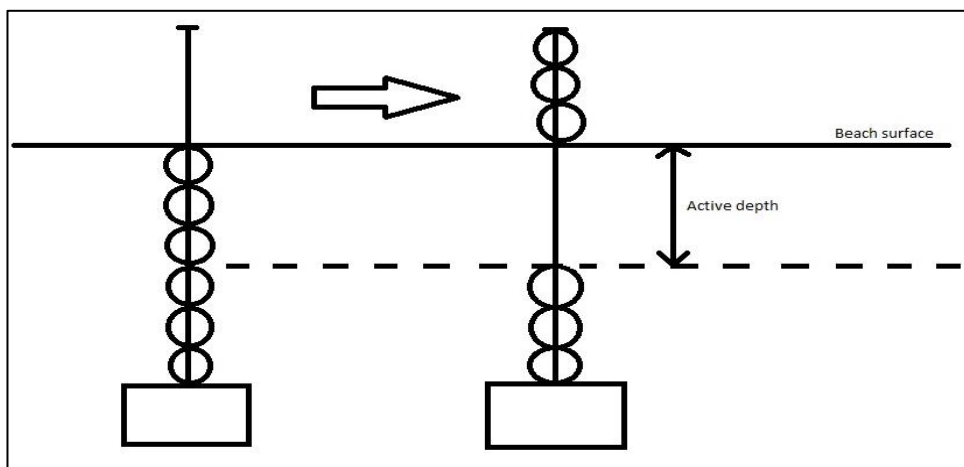


Figure 4.5: Depiction of how sliding indicator devices (SIDs) measure the active layer.

A pilot study was completed in March 2014 to test this method (Appendix Q). During this pilot study, two types of ball (indicator) were used: foam golf balls and hollow plastic ones.

Anecdotal evidence showed that the plastic ones, which had holes in their surface, were liable to fill with sand. It was not obvious whether this affected their ability to float (and thus may have caused them to underestimate AL depth), so only foam balls were used for later experiments.

The devices were buried to depths of at least 0.5 m (measured to the top of the anchor) in rows between high and low tide level. In order to keep track of elevation changes as well, dGPS readings were taken at every point where the AL depth was measured. The location information would also allow the influence of position on the beach profile on the active depth to be measured.

In particularly unconsolidated sediment, where it was difficult to dig a deep enough hole in which to bury SIDs, a sawn off metal dustbin was inserted into the hole and gradually dug down to prop up the sides (Figure 4.5).



Figure 4.6: Using a bottomless metal dustbin to dig in unconsolidated sediment.

The number of exposed balls were counted each day during fieldwork periods and compared to the number which had been left exposed the previous day to provide a measurement of the active depth. The devices were then 'reset' by digging to replace the exposed balls. Any devices which were damaged were replaced as soon as possible when necessary.

b) Depth of disturbance rods

Due to high groundwater in the lower beach, sliding indicator devices proved difficult to bury here. Depth of disturbance rods – metal stakes with loose fitting washers around them (Greenwood and Hale, 1980) – were used in the lower beach instead. The washer moves down

the stake as sediment underneath it is disturbed by wave action, providing an indication of the maximum sediment activation depth between deployment and measurement.



Figure 4.7: Depth of disturbance rod with washer on the surface of the beach.

As it is a public beach and is often used by dog walkers, even during the winter, these rods had fluorescent orange flags attached to the top to make them visible and prevent injuries (Figure 4.6). Like the sliding indicator devices, the depth of disturbance rods were measured and reset daily during fieldwork periods, and removed from the beach when not required.

iii. Survey Design

a) SIDs

Previous experiments (e.g. Curoy, 2012; Miller and Warrick, 2012) have indicated that best practice for measuring AL depth is to deploy devices in rows from the beach crest to low tide level (or as close as is possible), with devices approximately every 5 m. During the second winter of data collection, SIDs were buried along existing measured profile lines to simplify the experiment. Device locations can be seen in Figures 4.7 and 4.8.

Most active layer studies deploy a greater number of devices but over very short timescales – often only a single tide (e.g. Austin and Masselink, 2006). However the lack of personnel in this case meant that the number of measurements taken on each day had to be limited, hence the

requirement for a larger number of experiments in order to provide a large enough volume of data points to even attempt to represent the variability of a mixed sediment beach.

No new devices were buried for the March 2015 study period, as the focus was placed on tracer pebble experiments as a priority during this month. Additionally, wave conditions were predicted to be very low energy, and AL depth had been previously measured under low energy conditions in October 2014. The AL measurements from March 2015 were not used in the majority of calculations – anything requiring a daily average AL depth – as two measurements was not considered to be representative of the whole beach face.

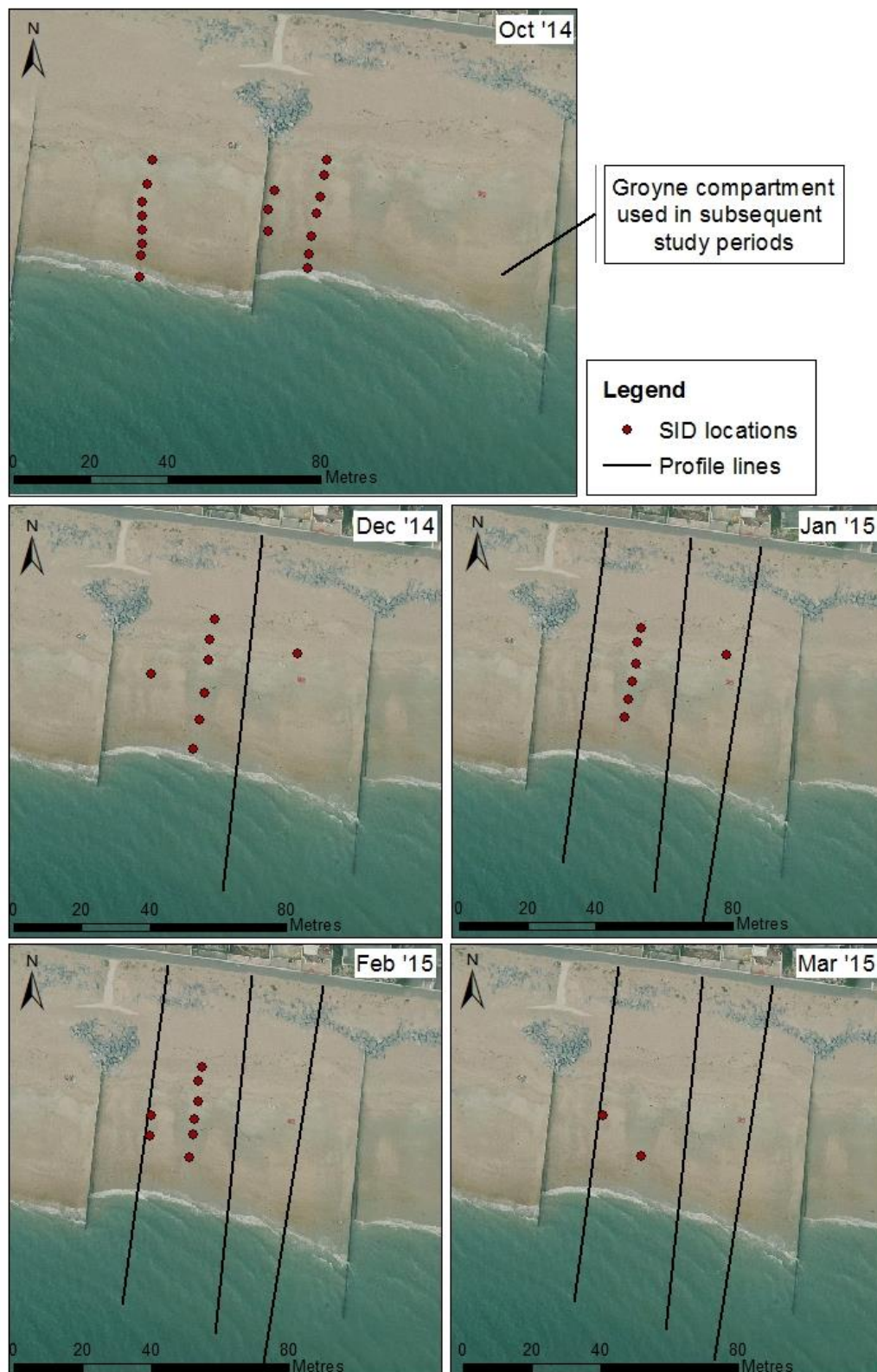


Figure 4.8: SID locations, winter 2014-15

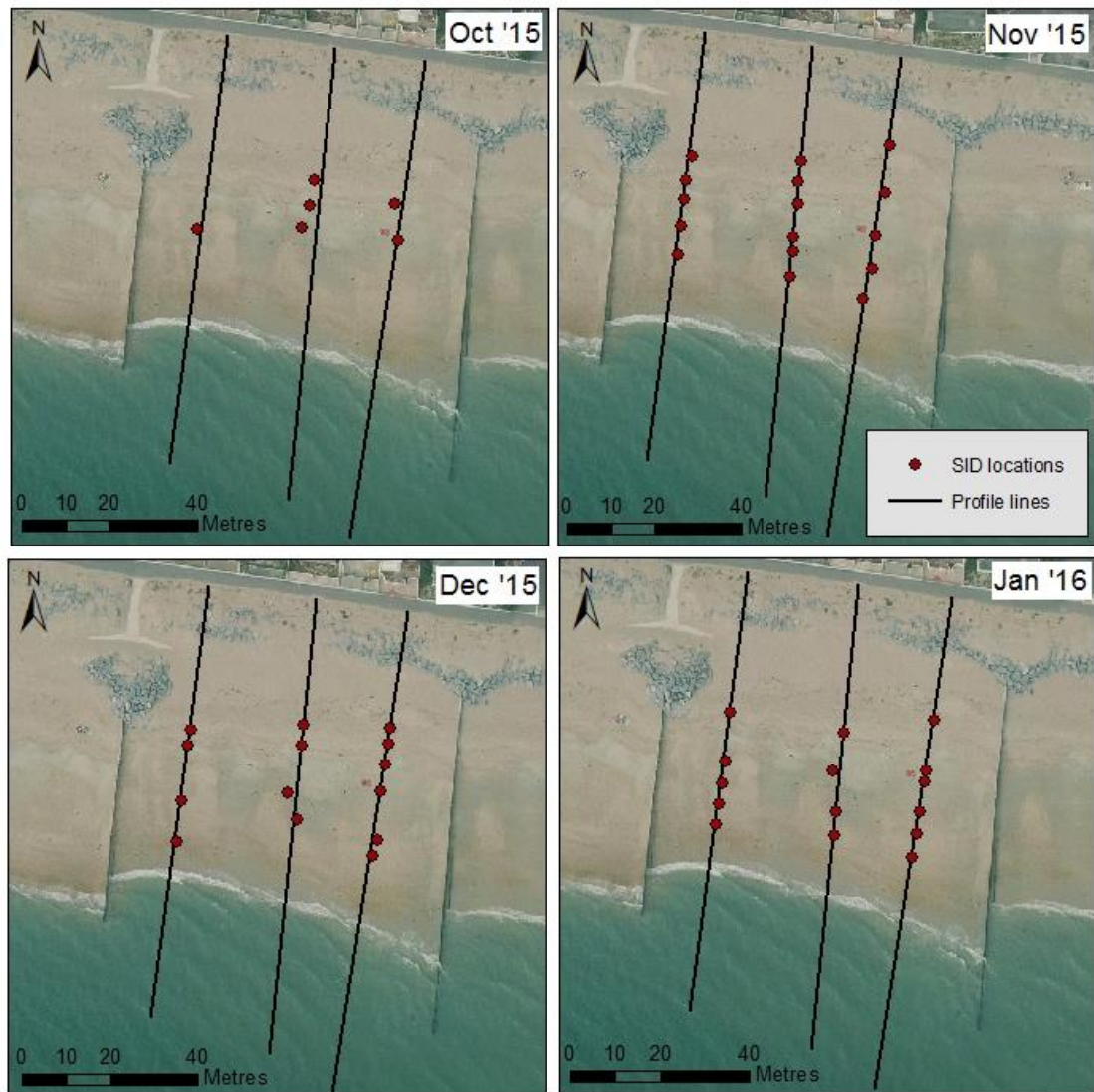


Figure 4.9: SID locations, winter 2015-16

b) Depth of disturbance rods

Depth of disturbance rods were used to provide additional measurements of AL in the lower beach during November 2015, December 2015 and January 2016 field periods, on days when the tide exposed a wider area of the beach face (i.e. closer to spring tides). Two rods were deployed at a time, as they could be difficult to install, taking time to avoid hitting larger clasts within the beach matrix while hammering the rods into place. The rods were deployed along the same profile lines as the SIDs, at approximately equal spacing, but closer to the low tide line than was possible with SIDs (Figure 4.9).

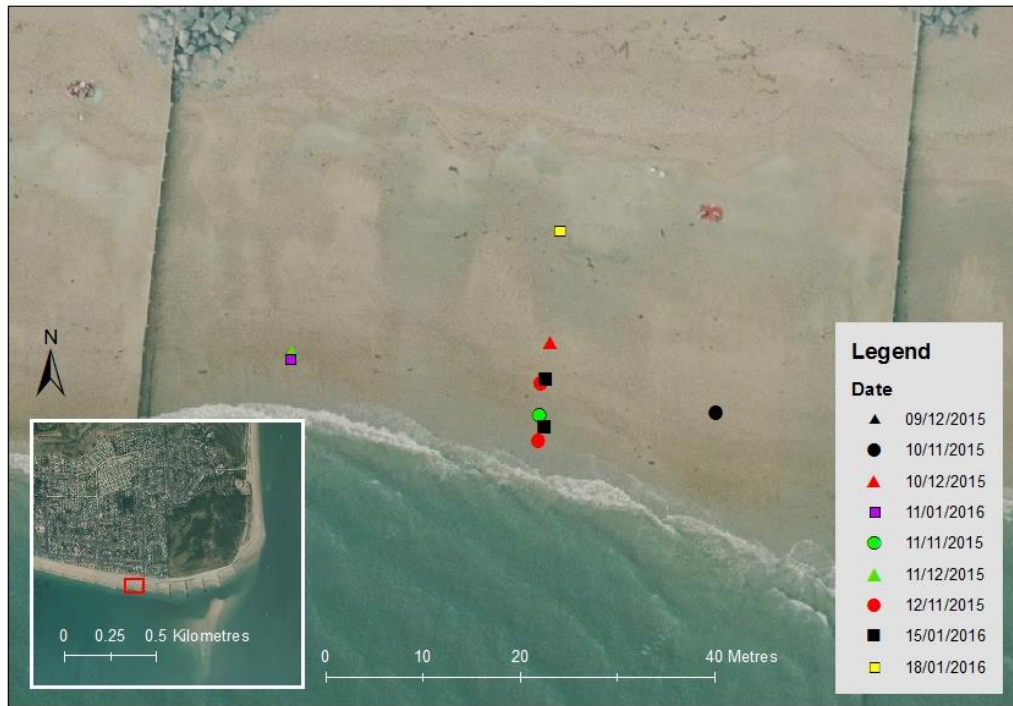


Figure 4.10: Location of depth of disturbance rod measurements

iv. Issues encountered

In this highly dynamic environment, erosion and accretion can occur rapidly. If the beach eroded significantly during a tidal cycle, the anchors became exposed and the SIDs could wash away. If the beach accreted, the chains could become buried; often this meant that they were too deep to be dug out by hand and the researcher was forced to wait until a large erosive event occurred to remove the device after the end of a study period.

High groundwater levels in the mid to lower beach, and areas of particularly unconsolidated sediment, sometimes made it impossible to dig a deep enough hole in which to bury a device. One solution to this problem was to prop the sides of the hole with a sawn-off metal dustbin, but this was not possible in every situation. The majority of the data is for the upper and mid sections of the tidally inundated beach face, leaving the potentially important low tide terrace relatively unstudied.

It was difficult to time field periods to occur with high energy events, as these cannot be predicted in advance and some winters experience higher energy conditions than others. This means that the data collected can only be relied on to a particular wave height, above which any calculations would require extrapolation of the dataset. Likewise, the data is only valid for the range of sediment compositions exhibited during these field periods. It was unfortunate that measurements could not be taken directly following a beach replenishment event, as this would have provided a comparison.

Depth of disturbance rods were discovered to be much more likely to eject from the beach during a tidal inundation, perhaps because the method does not allow them to be anchored in place. The depth of disturbance rods were easily removed from the beach by waves, and experienced issues with bending due to the large clasts within the beach. They produced a comparatively small dataset, with only 18 successful measurements and a much higher failure rate than SIDs. This method would not be recommended for future use in coarse sediment beaches.

4.6 Sediment composition

i. Methods available

Traditionally, sediment characteristics are assessed by taking samples from the beach, drying, and sieving them. Traditional methods (e.g. Gale and Hoare, 1992) suggest that for a sample to be representative it must contain at least 100 particles from each $\frac{1}{2}$ phi interval. For beaches with a significant gravel portion these samples can be very large; Van Wellen (1999) calculated that a sample size of 70 kg would be required. This produces issues with collection, transport and sieving.

Due to the spatial and temporal changes in sediment distributions on mixed sand and gravel beaches, BAR (2005) suggests that a more representative view of beach sediments would be gained by taking a larger number of 2-5 kg samples, rather than singular large volume samples. This technique, which has since been utilised by Horn and Walton (2007) allows for more frequent spatial and temporal sampling without removing so much material that the volume of sediment on the beach is significantly affected.

Analysis of surface sediments can be completed in two main ways. The simplest is to categorise areas based on the dominant grain size characteristics expressed at the surface (Watt *et al.*, 2008). Appropriate coding systems can be created for individual field sites depending on the number of grain sizes displayed on the beach surface, but it is difficult to ensure categories are consistent if multiple surveyors are used. Needing to refer to measurement tables or photographs to ensure consistency between surveyors would increase the time taken to complete surveys.

Authors such as Buscombe (2008) and Miller and Warrick (2012) have used photographic analysis of the beach surface to determine sediment characteristics. This technique involves taking photographs either at a set distance from the beachface, or containing a scale object. These photographs can then be analysed using specialised software to produce information

about grain size proportions and distributions. However, they can be difficult to calibrate, and tend to require very high powered computers. Bosnic *et al.* (2011) extended this technique below the beach surface by taking sediment cores and analysing images of these. However, this is limited to areas above the groundwater table, due to the inability to remove sediment samples from a water logged beach without disturbing their packing and sorting patterns, which would exclude at least the lower third of the beach at Eastoke. Additionally, coring does not tend to work when large particles are included in the sediment mixture.

ii. Chosen method(s)

It is necessary to take physical sediment samples from the active layer for results to be truly representative of the sediment dynamics that may be influencing active layer depth. Samples were collected to a depth of approximately 20 cm to correlate with the measured active depth.

The BAR (2005) method is becoming more widely used on mixed sediment beaches (e.g. Horn and Walton, 2007; Curoy *et al.*, 2009) where spatial and temporal patterns of sediment change need to be observed for sampling to be truly representative of the nature of the beach material, and thus able to be linked to other beach parameters.

It was not, however, within the scope of this project to take enough samples on each of the three dGPS monitored profiles (Figure 4.3) to be representative of overall sediment patterns for every day on which other variables were measured, and so a supplementary method was utilised to provide an overview of the visible sediment sorting patterns. This supplementary method needed to be quick and simple, as it has already been suggested that the surface sediments of mixed beaches are not representative of the internal structure of their active layer (Ciavola and Castiglione, 2009); however, the relationship between surface sediments and the composition of the active layer is still relatively understudied, so it is worthwhile producing another dataset to combine with previous research.

Surface sediment codes based on those used by Watt *et al.* (2008) were adapted for Eastoke beach, and a code added to each dGPS point as the beach was surveyed.

iii. Sample design

a) Physical samples

Sediment characteristics in this research were intended for use in conjunction with active layer measurements, thus physical samples taken from locations of SIDs would allow the direct

relationship between sediment composition and individual active layer measurements to be assessed.

The BAR (2005) method for sediment sampling was utilised, with samples of between 2-5 kg being collected in each location. Due to the large number of AL data points being collected, sampling at every location on every day of measurement would have created an unreasonable number of samples to sieve; three or four SID locations were selected for sampling on a few days during each short field period between October 2014 and March 2015. Dates of samples in these periods can be seen in Table 4.1.

Physical sediment samples were dried overnight at 105°C, and sieved in a mechanical shaker for 15 minutes each with sieve sizes of 0.5 mm, 0.75mm, 1 mm, 2 mm, 4 mm, 8 mm, and 16 mm.

Preliminary data analysis during the summer of 2015 suggested that there was no significant correlation between the physical sediment samples and their corresponding active layer measurements. There was, however, a correlation between the average sediment composition and the average active layer measurement. This was unexpected, so the method was adapted for the second winter season to determine whether the same relationship continued to exist when samples were taken from other areas on the profile which were not specific to the active layer measurement points.

During the second winter samples were taken at four evenly spaced locations on the central profile, starting at the high tide line and ending near low water (not including the sandy low tide terrace if this was exposed, as it is generally viewed as a separate entity in definitions of mixed sand and gravel beaches (e.g. Jennings and Shulmeister, 2002)). The overall number of samples within each field period remained similar, as it was still not realistic to take samples every day. See Table 4.1 for dates of samples.

b) Surface codes

The surface sediment of mixed sand and gravel beaches has been shown to be highly variable, even on short time scales (Watt *et al.*, 2008), which can have significant impacts on the morphodynamics of the beach (Horn and Walton, 2007). It would not have been possible to collect and process enough physical samples to provide detailed insight into these changes, so in addition to these physical samples, a representative coding system for the surface sediment was produced. This was based on work by Watt *et al.* (2008) and consisted of the following categories:

1. S / Sand
2. H / Granules (broken up pieces of shell, common at this site; approx. 1 – 4 mm)
3. P / Small gravel (up to approx. 20 mm)
4. G / Medium/large gravel (>20 mm)
5. MS / Mixed, mainly sand
6. MH / Mixed, mainly granules
7. MP / Mixed, mainly small gravel
8. MG / Mixed, mainly med/large gravel
9. R / Rock (exposed granite sea defences)

These categories were selected based on anecdotal observations of the beach surface during the field period in October 2014, and were subsequently applied to every dGPS point until the end of March 2015. Chapter 5 analyses the results of these surface surveys in relation to wave conditions and profile morphology, as well as discussing the surface codes as they relate to physical samples taken at the same locations. Chapter 6 sections 6.3.i.e and 6.3.ii.d relate surface codes to active layer measurements. Overall, the coding system was found to be of limited use and so was not continued during the second winter, as it took longer to measure each dGPS location if a code had to be added each time.

iv. Limitations

The main limitation of the sediment sampling for this project is with representation. Taking only a few samples at a time does not realistically represent the variety of sediment compositions on this type of beach, but surface sediments on mixed beaches are often better sorted than the sediments just a few millimetres or centimetres down. However, it was simply not within the scope of the project to complete full sampling regimes on every field day. If a similar project is undertaken in the future, it is recommended that a separate study of sediment composition and variation (both spatially and temporally) run alongside the AL and transport research, so that the two datasets can be fully combined.

4.7 Sediment transport

i. Methods available

Physical measurements of sediment transport are achieved through three general techniques:

1. Topographic surveys
2. Sediment traps
3. Sediment tracers

Topographic surveys and sediment traps are widely stated to be inaccurate predictors of sediment transport, particularly on coarse grained or mixed sediment beaches (Bray *et al.*, 1996). SCOPAC (2004) indicate that using dGPS surveys of inter-groyne beach volumes to infer longshore transport does not provide an accurate solution. On beaches with a significant coarse fraction, sediment traps are affected by the significant amounts of on and off-shore sediment transport, perhaps causing them to overestimate longshore rates (Lee *et al.*, 2000).

Tracers are not without their own issues, however. Coastal sediment tracing has been researched for over a century, and during this time three categories of tracer have been devised: visual tracers, passive tracers and active tracers. Visual tracers include painted particles (e.g. Jolliffe, 1964) and non-native particles (e.g. Carr, 1971); passive tracers include magnetic particles, radioactive particles (though these are no longer legal due to public health concerns), and radio tagging; active tracers can also be called 'smart' pebbles, and can be remotely traced from a signal transmitted regularly to a remote location, thus enabling data to be collected at a higher resolution than the tidal basis of most other methods.

Visual tracers are limited to surface detection, and so are likely to overestimate LST (Van Wellen *et al.*, 1998; Sear *et al.*, 2000), as pebbles on the surface have a much greater likelihood of being entrained and transported long distances, whereas pebbles below the surface may only move very short distances, if they are ever actually entrained. A major problem with painted particles is that abrasion is going to quickly chip away at the paint coating the pebble, further lowering detection rates over time. Exotic lithology does not experience the issue of paint removal by abrasion, but the exotic pebbles are often different in size, shape or density than the natural sediment and thus are likely to react differently to wave conditions than native sediments.

Magnetic particles (e.g. Wright *et al.*, 1978) can be detected below the surface by using a metal detector, which increases their detection rates compared to visual tracers (Sear *et al.*, 2000). Detection rates can be exceptionally high – Osborne (2005) experienced a 93% recovery rate for magnetic tracers – but are more likely to be between 40-85 %. They can provide a more accurate representation of total longshore transport rates due to their ability to continue to be detected while mixing into the beach matrix, but it is time consuming to dig individual pebbles up to trace their movements over time, so they are mostly used when only a bulk view of transport is required.

Nichols (2004) and Lamarre *et al.* (2005) were the first to use the Radio Frequency Identification (RFID) tracking system, in gravel-bed rivers. In this environment it is possible to

deploy a large detector (or multiple detectors) which monitors tracers as they travel across it and thus monitor transport downstream. Allan *et al.* (2006) then adapted it for coastal use, where it has since become common for pebble transport studies (e.g. Curtiss *et al.*, 2009; Dickson *et al.*, 2011; Miller and Warrick, 2012). Detection rates for PIT tagged pebbles are usually comparable with magnetic tracers, and are generally found to decrease over time. This is thought to occur as pebbles become buried or are transported offshore.

Bertoni *et al.* (2010) adapted the system for underwater use with scuba gear. This was found to increase the detection rate by providing access to pebbles that had been transported just offshore, to areas that were still underwater at low tide.

Miller and Warwick (2012) used deployed RFID-tagged pebble in columns, noting the initial burial depth of each pebble, to measure longshore transport rates throughout the active layer. As expected, they found that pebbles nearer the surface travelled faster than ones further down; this provides evidence to suggest that tracers should not be deployed on the surface of the beach, but spread throughout the active layer in this way.

ii. Chosen method

The most appropriate method for this study was to use sediment tracing, specifically RFID technology. The groynes along this stretch of beach are expected to limit longshore transport of grains, and the unique ID associated with detection of each tracer would allow individual particles to be traced and patterns in transport over time investigated in more detail than would be afforded by other tracing techniques.

It is uncertain whether size or shape of sediment have an effect on the rate of transport. It was found by Richardson (1902), Jolliffe (1964), Caldwell (1983) and Cooper *et al.* (1996) that larger particles moved more quickly than smaller ones, but Carr (1971, 1974) had inconclusive results, with both positive and negative correlations. Most studies have failed to find any link between particle shape and either transport rate or cross-shore position, despite the fact that cross-shore size and shape sorting has been frequently reported on gravel and mixed beaches (Osborne, 2005). One of the main benefits of the unique ID stored in each PIT tag is that information on pebble size, shape and mass can be collected in a database before deployment, making the process of investigating these relationships comparatively simple.

Tracers can be inserted/deployed using either the Eulerian method or the Lagrangian method. The Eulerian method injects tracers at a constant rate over a set time, and the Lagrangian method releases tracers all at the same time, but over a set area (Larson *et al.*, 1997). For this

study, gradual release of the pebbles in multiple deployments would provide better insight into short-term transport patterns under a variety of wave conditions.

The pebbles were deployed in columns after Miller and Warrick (2012) (section 4.7.iv.b) to create a degree of mixing and reduce the likelihood of overestimation of transport rates. This creates the additional benefit of allowing transport rates at different depths to be studied to determine if the same correlation that Miller and Warrick (2012) found, whereby speed of transport decreases approximately logarithmically with depth, exists within this dataset.

iii. The RFID system

Passive Integrated Transponder (PIT) tagged pebbles are usually natural clasts which have been drilled to allow the insertion of a tag which can be detected by an antenna swept across the beach face (Figure 4.10). The tags (Figure 4.11) contain a coil of copper wire, which enables the tag ID to be transmitted to the detector when a signal from the detector is received (Allan *et al.*, 2006).



Figure 4.11: Examples of tags and tagged pebbles. (Source: HBC. Photo credit: unknown).



Figure 4.12: Image of PIT tags, showing their internal structure.

Curtiss *et al.* (2009) measured detection ranges of up to 0.4 m for 32 mm tags, and up to 0.2 m for 12 mm tags (dependent on tag orientation) in a mixed sand and gravel beach overlain by pebble and cobble deposits. However Dickson *et al.* (2011) measured ranges of 0.4-0.8 m for the 32 mm tags. Appendix N contains results from a brief test to determine the range of the

detector in different sediments at Eastoke, which indicate results closer to Curtiss *et al.*'s (2009) results.

Each tag has a unique ID built in, which the detector's on-board datalogger can store alongside its GPS coordinates; this is an advantage over magnetic tracers, as it allows for easy tracking of individual pebbles across surveys. Published recovery depths for the two methods are comparable, though both vary depending on the environment in which they were deployed.

Published recovery rates for RFID detections range from 0-60 % by Dickson *et al.* (2011), who associated the differences in detection rates between three studied sites as being caused by differences in across-shore pebble transport during storms, to much higher rates of detection measured by Curtiss *et al.* (2009), who experienced minimum detection rates of 78 % during two year-long studies on a mixed sand and gravel beach overlain by pebble and cobble deposits.

The PIT tags do not require an internal battery, and so could theoretically remain in-situ and provide data for 30-50 years (Allan *et al.*, 2006), but previous studies completed by ESCP (2013) have indicated that after 2-3 years, recovery rates are close to 0, likely due to the highly active nature of the beaches along the Solent coastline, and the regular addition of material to each frontage.

HBC had previously used the RFID system in tracer experiments along Hayling Island and Portsmouth frontages (ESCP, 2013), so much of the survey design was based on these experiences. Any additional knowledge and experience obtained during the present study was included in new handbooks which the author produced for future HBC research (Appendix R).

iv. Survey design

a. Tagging pebbles

Tracer pebbles were selected based on the D_{50} of the coarse fraction of the replenishment material (approximately 40 mm), but also based on the relative detection ranges of different tag sizes, to increase the likelihood of detection. Conservative published detection ranges for different sizes of tag suggest that 12 mm tags can be detected in up to 20 cm sediment depth (Curtiss *et al.*, 2009), with a gradual increase in range experienced up to a maximum of 40 cm for 32 mm tags.

Whitcombe (1996) found that active depths on beaches at Hayling Island were generally 5-15 cm, with a maximum of up to 40 cm during storms. This would indicate that the use of 12 mm tags may not be appropriate here, but a mixture of 23 and 32 mm tags would provide

adequate possibility for detection. Using smaller tags allowed for smaller pebbles to be used, thus better representing the coarse fraction of the beach material at Eastoke.

Approximately 400 'native' pebbles were collected from the recently replenished beach in November 2013. Research by Allan *et al.* (2006) suggests that the tags are more easily detected if they are perpendicular to the antenna, meaning that the tags needed to be inserted into the C axis. A ruler was used to ensure that each pebble selected had a C axis long enough for a tag to be inserted, with at least 6 mm extra length to allow for the resin which would hold it in place.

The pebbles were laid out in trays in a grid pattern (Figure 4.12), sealed in place with expanding foam, and sent to be water jetted so that each had a hole into which the tag could be inserted. It is necessary to water jet pebbles because drilling can cause the flint to shear. A 10 % failure rate is associated with water jetting, but this was accounted for in collection of pebbles.

After water jetting was complete, pebbles were scrubbed to remove the expanding foam, and sorted approximately by size so that appropriate length tags could be inserted into each pebble. A 2-part clear cast epoxy resin was used to seal the tags in place.



Figure 4.13: Pebbles placed in a tray, ready to be sealed in place and water jetted. (Source: HBC, photo credit: unknown.)

After the resin had dried, pebbles were catalogued to a database. As a means of identifying pebbles without needing to scan them before deployment, each pebble had a 3-digit number written in permanent marker on the side, running consecutively from 000. Numbers which

could be viewed differently if seen upside down were underlined to ensure mistakes were not made during deployment. Each pebble was then swiped past the RFID detector to reveal its unique ID code, which was copied into the spreadsheet.

The A, B and C axes of each pebble, measured with callipers to the nearest millimetre, were added to the database, along with each pebble's mass. The axes measurements were then used to calculate the shape of each pebble according to the Zingg classification system. This is achieved by dividing the C axis measurement by the B axis measurement, and then the B axis measurement by the A axis measurement. These two values are referred to as p and q, and their relation to each other dictates the shape of the pebble (Figure 4.13).

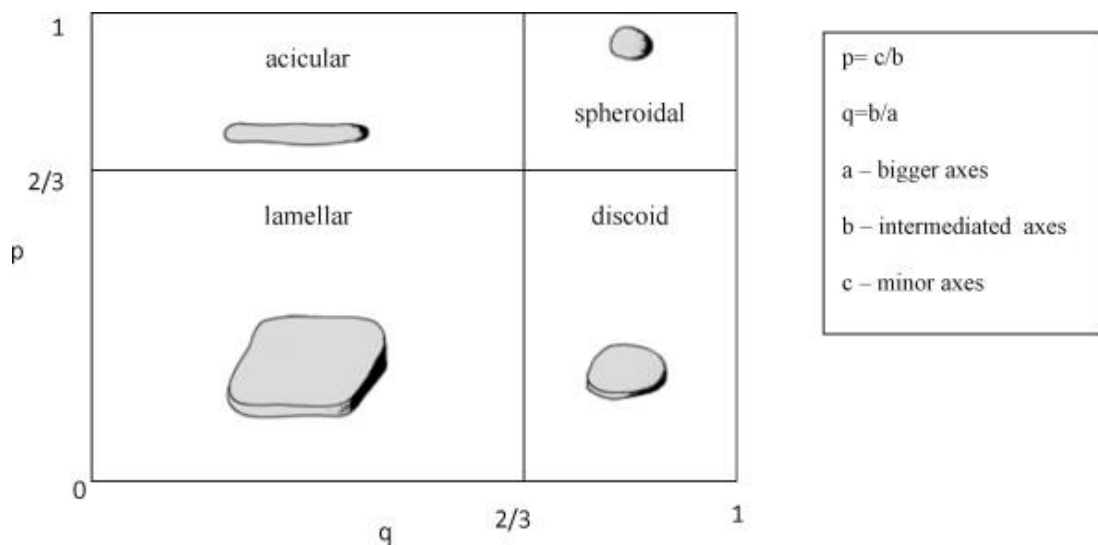


Figure 4.14: Zingg classification of different geometric particles (Source: Viana *et al.*, 2011).

b. Deployments

As stated previously, pebbles were deployed in columns below the beach surface (Figure 4.14) to enable conclusions to be drawn about the relationship between depth and rate of transport. Pebble numbers were noted as they were deployed, along with their burial depth. Previous research by ESCP (2013) has focussed on longer term transport patterns around this coastline, with larger, less frequent deployments, and monthly to semi-annual surveys. The current research project provides additional data into the shorter term sediment transport patterns by using this new deployment method.

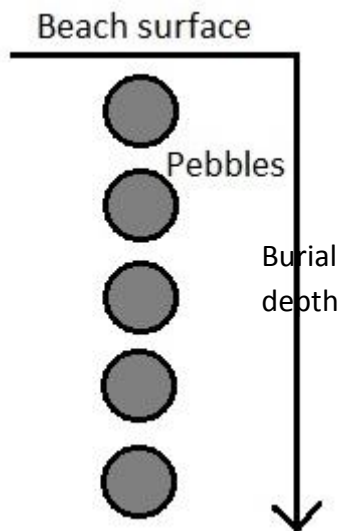


Figure 4.15: Deployment method for tagged pebbles – columns within the beach sediment.

Initially, holes of approximately 25-30 cm were dug, and approximately 6-8 tracers placed into each hole, between layers of sediment; the depths to which tracers were buried was based on the pilot study (Appendix Q), and findings by Whitcombe (1995) from research on Hayling Island beaches. The precise depth of burial of each tracer measured to the nearest centimetre and recorded alongside the ID written on the pebble. In order to improve and simplify comparability between columns, during the second winter, pebbles were simply buried in approximately 5 cm increments. For all columns a mixture of 23 mm and 32 mm tagged pebbles were used.

The deployment locations were selected based on profile locations and sliding indicator device (SID) burials. As tracers were deployed in small numbers regularly throughout the fieldwork, columns were generally located within the main study groyne cell (Figures 4.15 and 4.16), between SIDs. This provide a link between the two datasets, whereby the AL depth measured by the SIDs could be compared to the depth of activated pebbles within the column.

The first deployment was larger than the others, releasing a greater number of tracers into the system to begin the long-term tracer study. It consisted of 61 pebbles, deployed in 10 columns across two groyne bays (the main one, and one to the west of this) on 30/09/14. These were surveyed daily from 01/10/14-4/10/14. Unfortunately, the files were corrupted and no location data is associated with any pebble detections for these dates, but it can nevertheless be used as an indicator of recovery rates for these short term studies. The total number of deployment dates was 14, 10 of which occurred after the detection kit had been fixed. The locations of these can be seen in Figures 4.15 and 4.16.

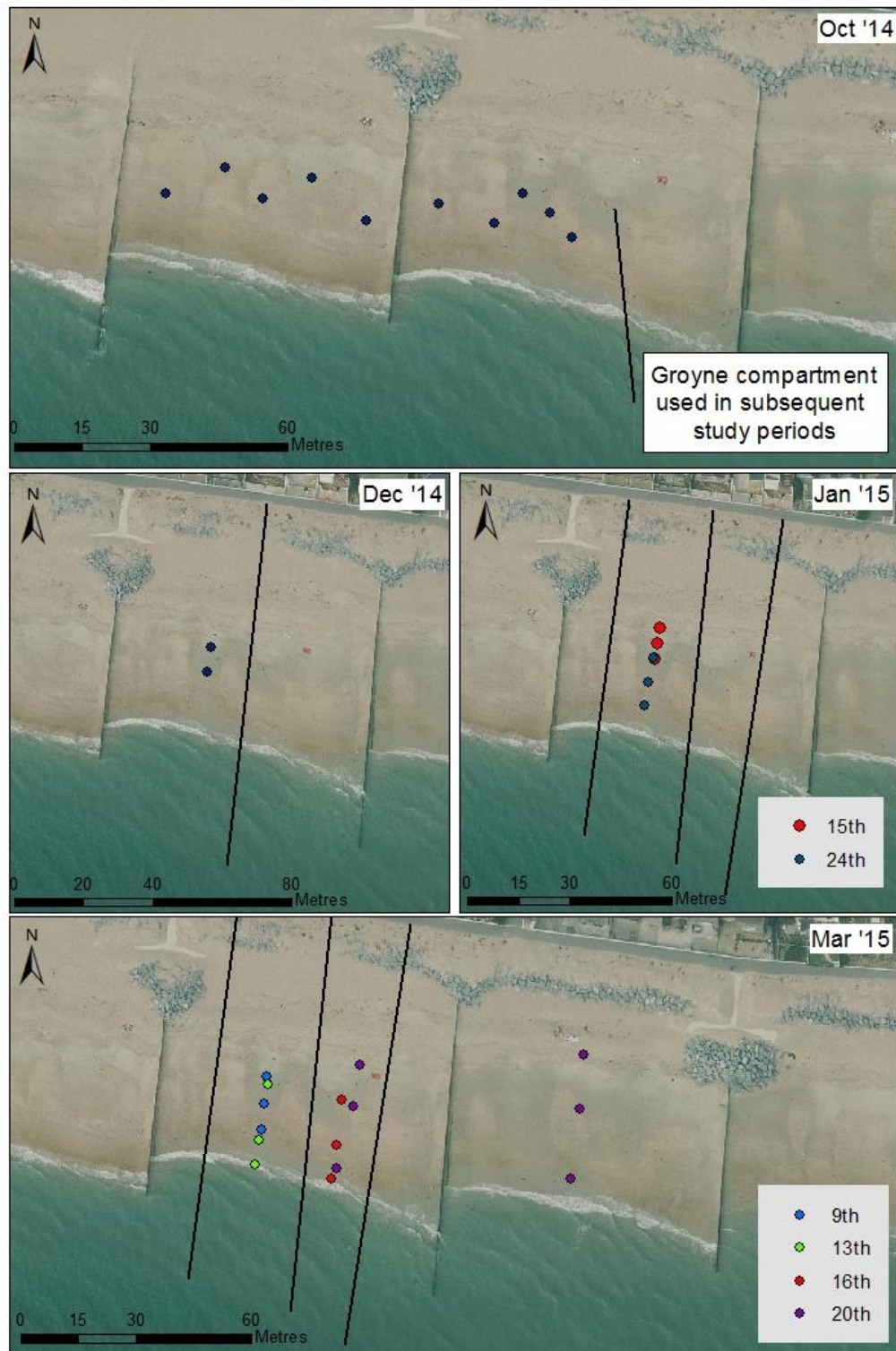


Figure 4.16: Pebble column deployment locations, Winter 2014-15 field periods.

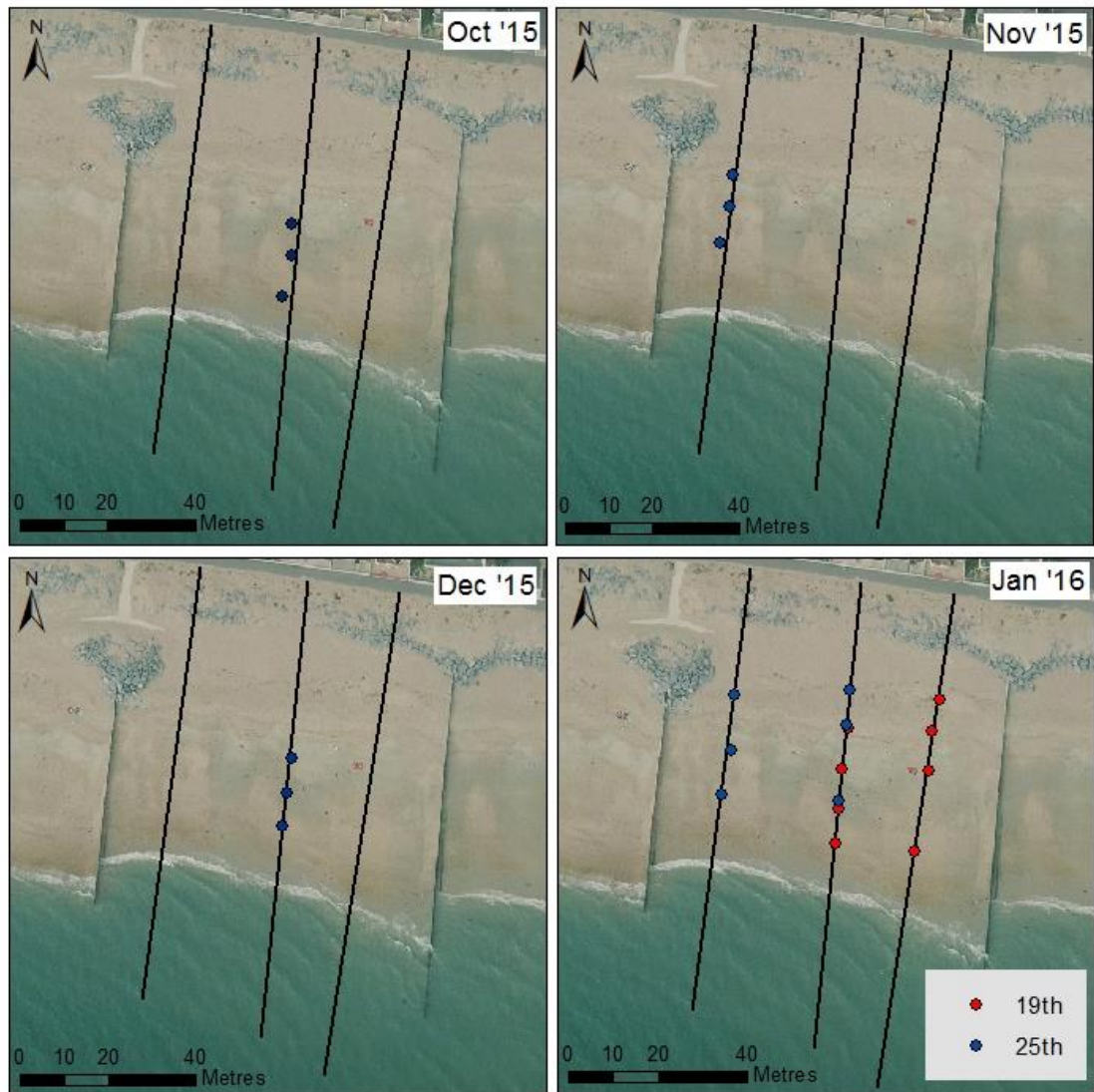


Figure 4.17: Pebble column deployment locations, Winter 2015-16 field periods.

c. Detections

To detect pebbles within the beach sediments, the surveyor must hold the detector so that the antenna (Figure 4.17A) is level with and only a few centimetres away from the beach surface (Figure 4.17B). Regularly spaced (approximately every 2 m) transects are walked at a normal walking speed, while sweeping the antenna from side to side in a regular pattern.

The RFID reader automatically logs and time stamps any detections, and the GPS device, in continuous logging mode, provides location data which can later be processed to match up with the tracer detections. The device also beeps and a light flashes when a tracer is detected, but there is no reason for the surveyor to stop walking.



Figure 4.18: A) RFID detector. Loop is the antenna, backpack contains the datalogger and power source, small yellow device below the handle is a GPS tracker. B) Detector being used.

Evidence from the previous tracer study undertaken at Eastoke (ESCP, 2013) indicates that tracers did not travel further than one groyne cell either side of where they were deployed within the first week. Thus for the surveys which were intended to trace movements within the first few days of each deployment, generally only two or three groyne cells were walked.

It took approximately 20 minutes to survey each groyne compartment, meaning that surveys covering the entire study area were not possible to undertake on every day of fieldwork. These were completed on 5 occasions during the timeframe of the experiments: in April, May, November and December 2015, and January 2016.

v. *Issues encountered*

For a significant period during the start of the winter 2014-15 fieldwork months, the RFID detector experienced technical issues which first resulted only in an error message whenever the datalogger was switched on. Pebble deployments were temporarily halted while this issue was repaired. Unfortunately, once the first error had been fixed, a different problem occurred, which resulted in pebble detections not being logged with a correct time stamp, meaning that they could not be correlated with the GPS data recorded. This means that surveys during January 2015 had pebble numbers associated with them, but no locations.

4.8 Summary

The large number of processes influencing the morphodynamics and sediment transport of mixed sediment beaches necessitate studies that measure multiple variables concurrently (Schoonees and Theron, 1993), as this study has attempted. Concurrent measurement enables conclusions to be drawn about the links between observed beach morphology, on a tidal and monthly frequency, with sediment dynamics, active layer depth, and sediment transport. By studying one groyne compartment in this level of detail and over multiple fieldwork periods, patterns of short to medium term dynamics and evolution can begin to be observed.

The use of daily dGPS profile measurements, repeated in specific locations, enabled beach profile evolution to be related to wave action and tidal influence to a scale that would not be economically viable as part of long-term beach management strategies. This method is convenient and relatively quick, and has the added benefit of being directly relatable to semi-annual surveys collected by HBC using the same method. Surface sediment codes were noted between December 2014-March 2015, providing both an overview of the surface sediment distributions during this time, and details of the influence of wave energies on sorting patterns.

Collection of active layer measurements from repeated locations spread out across- and along-shore within the groyne cell account for as many influences as possible. SIDs were used in the main mixed sediment beach, providing a relatively robust yet inexpensive method that was almost perfectly suited to this environment. An issue with high groundwater levels was partially combatted by deploying depth of disturbance rods in the sandy lower foreshore, so that the active layer measurements could be continued further along the beach profiles.

Sediment samples taken from the active layer of the beach have been related to the active depth measurements, as have morphological changes and slope angles calculated from dGPS profiles.

Sediment transport was measured through the use of PIT tagged tracer pebbles, over both tidal and annual time scales, which was intended to allow short- and long-term transport patterns to be identified.

Wave characteristics were measured at a nearshore Wave Rider wave buoy located approximately 5 km from the study site. These are output in 30-minute increments, and were linked to daily profile measurements, sediment samples, and active layer depth measurements.

5. Profile Shape & Evolution

5.1 Introduction

This chapter describes results of dGPS surveys at Eastoke, Hayling Island during a total of 66 days over 8 field periods between December 2014 and January 2016. Exact dates of surveys can be seen in Chapter 4.2.

The aim of this chapter is to investigate the morphological variability of a groyned, replenished mixed sand and gravel beach, at both short and medium temporal scales, and assess whether sediment transport can be inferred from morphological change.

The research question stated in Chapter 1 is:

- Do beach profiles provide an accurate representation of longshore sediment transport on groyned beaches?

It is common practice to use beach profiles as a method for estimating longshore transport rates, but this practice is mainly limited to open stretches of coastline. Profiles on mixed sediment beaches in general are likely to be more variable, as they are generally considered to be an intermediate beach state. The presence of groynes further complicates profile dynamics and sediment sorting patterns, knowledge of which is required to create effective defences against coastal erosion and flooding, providing justification for this investigation. Previous research has indicated that profiles within a groyne compartment are not usually identical (e.g. Dornbusch *et al.*, 2008), which can pose issues when selecting how many profiles are required and where they should be positioned.

5.2 Results

i. Sedimentology

One of the most important factors affecting beach processes is the sediment composition. Bimodality of sediments is commonly associated with mixed sediment beaches, and can have a significant influence on beach processes and sediment transport. Mixed sand and gravel beaches in the UK are reported to contain between 15 to 68 % sand (Mason and Coates, 2001). Sediment size often decreases seawards on natural mixed sand and gravel beaches, but artificially replenished beaches are more complex. Beaches replenished with a mixture of sand

and gravel have been shown to rapidly sort themselves, usually decreasing in size towards the low tide line. However, the upper beach and the crest, where waves rarely reach, can remain poorly sorted.

Harlow (1979) has previously described the beach sediments at Eastoke as a coarser “shingle” upper beach, with a gradual shift through the central section to a sandy lower beach. This was many years ago, and as has been previously discussed, one of the main defining and controlling features of MSG beaches is their sediments; thus, it was necessary to investigate sediment sorting in relation to measured beach profiles for the current dataset.

Sediment samples were taken as part of the active layer research (Chapter 6), which can also be used to provide some insight into the sediment composition of this beach. Monthly averages from all samples taken during each study period can be seen in Appendix K. For additional insights into surface sorting processes, a coding system (Chapter 4.6) was used to classify each of the dGPS points taken during four of the field periods (December 2014 – March 2015 inclusive).

For the purposes of this beach, the term ‘sand’ refers to particles smaller than 1 mm. Visual observations of the particles within each of the sieves indicated that particles larger than this are pieces of broken shell, and are thus marked as ‘granules’, which correlates better with the sediment coding system used for surface sediments. The majority of the fine material at this site was measured to be under 0.5 mm in diameter.

The sand content within these samples ranged from 0 to 98.5 %, with a mean of 25.2 %. 76 % of all samples were visually assessed as bimodal; these samples were associated with sand percentages of approximately 15 – 60 %. These values are similar to the values suggested by Mason and Coates (2001) as the proportions for considering a beach ‘mixed’.

In general, sand content increases seaward, as would be expected. Figure 5.1 indicates a weak negative correlation between elevation (as a proxy for cross-shore position) and sand content within a sample. Only sediment samples from December 2014 – March 2015 were associated with specific elevation measurements and could thus be used in this analysis. The sample associated with the highest sand content was from the low tide terrace, which is only exposed during spring tides.

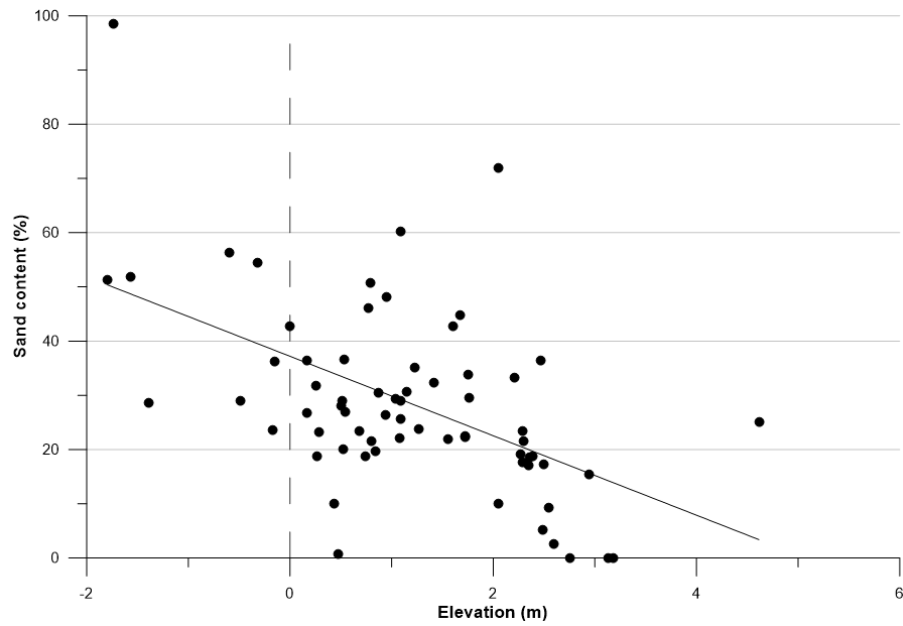


Figure 5.1: Cross-shore variation of sand content, December 2014 – March 2015. ($y = -7.328x + 37.135$, $R^2 = 0.278$.) $N=67$.

Table 5.1 provides details on the spatial variations of sediment composition during a more comprehensive sample set taken on 21/03/2015 (Figure 5.2 indicates the locations from which samples were taken). This snapshot shows an increase in sand content seawards and, in general, eastwards, which indicates that sorting processes have been more effective on the upper-west part of this groyne cell.

Table 5.1: Sand content of samples taken on 21/03/2015. Locations of profiles in Figure 5.2.

Cross-shore position	Profile 1 (% sand)	Profile 2 (% sand)	Profile 3 (% sand)
Crest	-	-	25.08
Upper	0.03	0.03	36.55
Middle	28.1	36.63	26.96
Lower	28.72	51.95	51.36

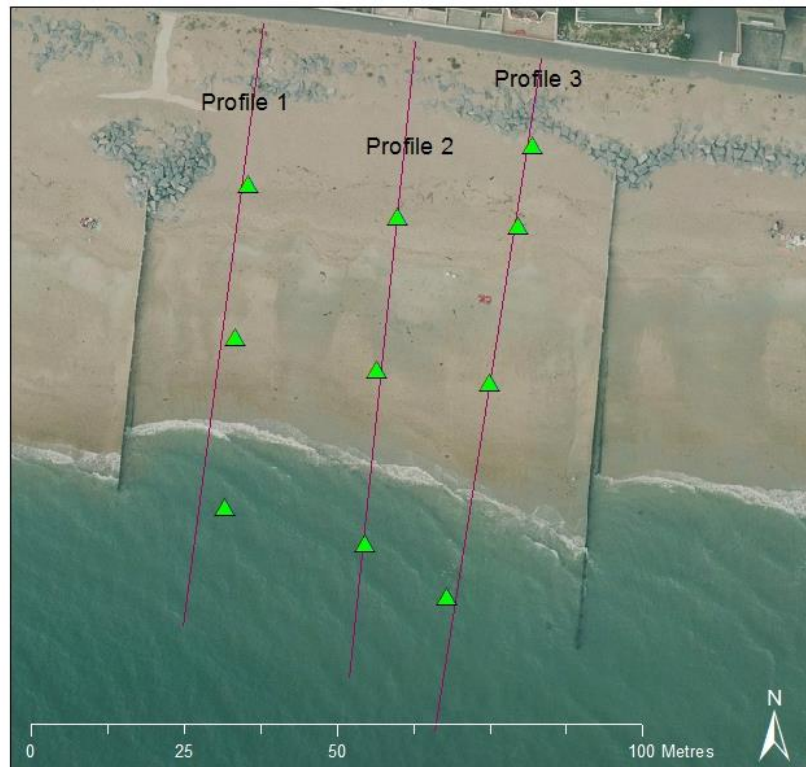


Figure 5.2: Locations of sediment samples on 21/03/2015. Aerial imagery courtesy CCO, 2016.

It must be noted that variability is one of the defining features of mixed sediment beaches. Samples taken in the same location on multiple occasions do not contain consistent proportions of different grain sizes. Samples were taken to be associated with active layer measurements (Chapter 6), and so there are occasions when an exact location was sampled repeatedly within a short space of time. Figure 5.3 shows the locations of four examples of this, and Figure 5.4 - Figure 5.7 show analysis of sieving. The greatest change occurs at location 1 (Figure 5.4) which contained over 70 % sand on December 4th, but less than 15 % sand by December 10th. The percentage of grains categorised in the largest sieve was also much higher on December 10th for this location. The changes do not appear to be consistent between locations, indicating that a link between wave conditions and sediment proportions would be difficult to find.

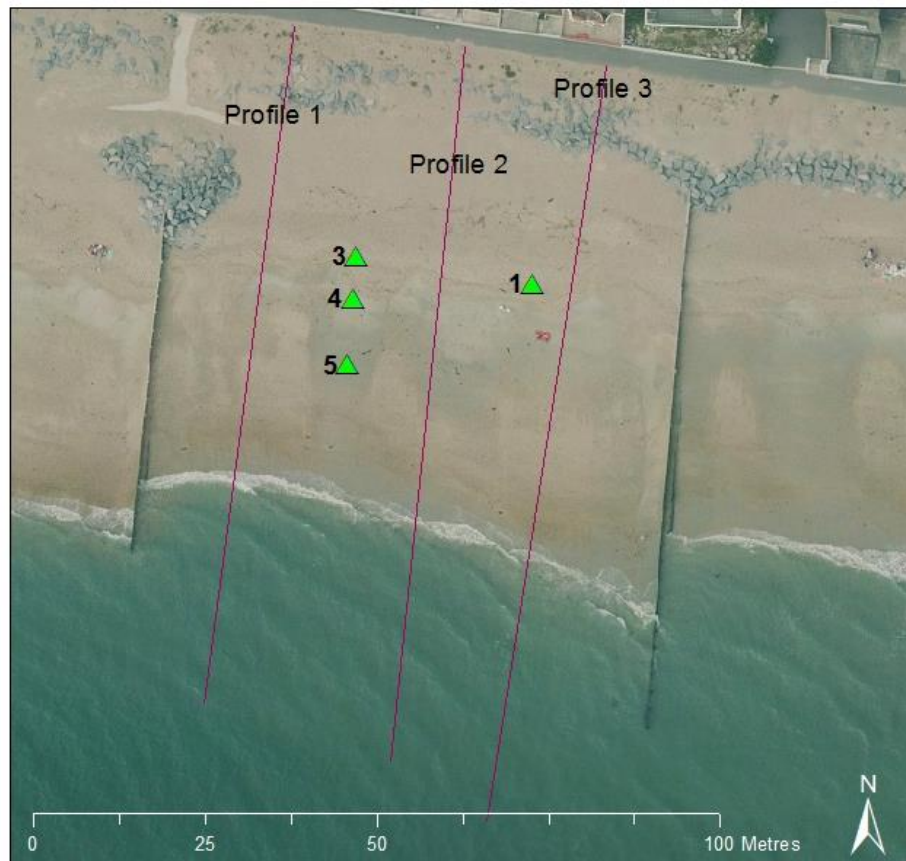


Figure 5.3: Locations and numbers of sampling points in December 2014. Aerial imagery courtesy CCO, 2016.

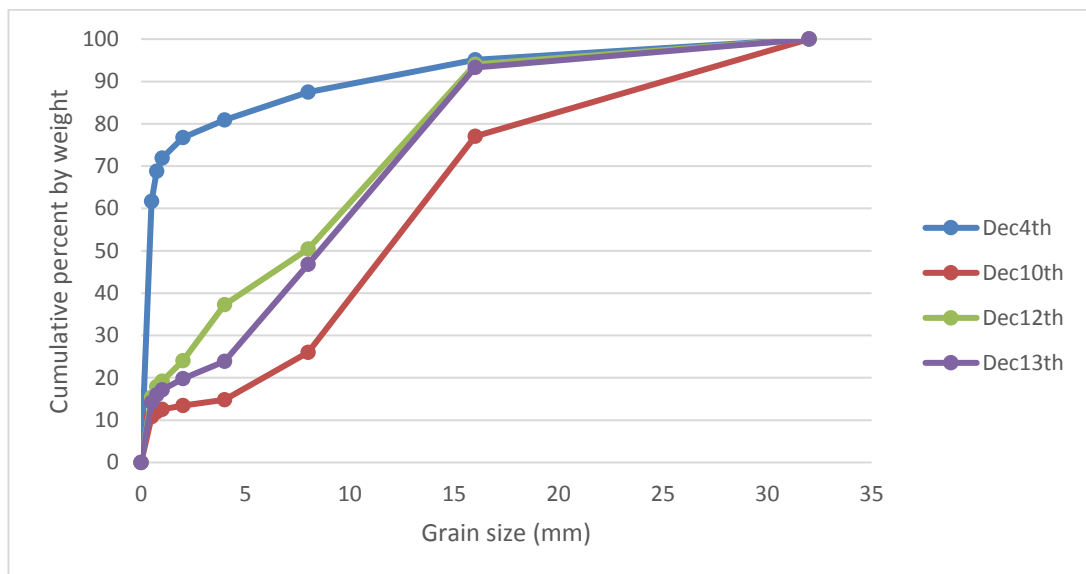


Figure 5.4: Variation between samples taken at the location of SID1 in December 2014.

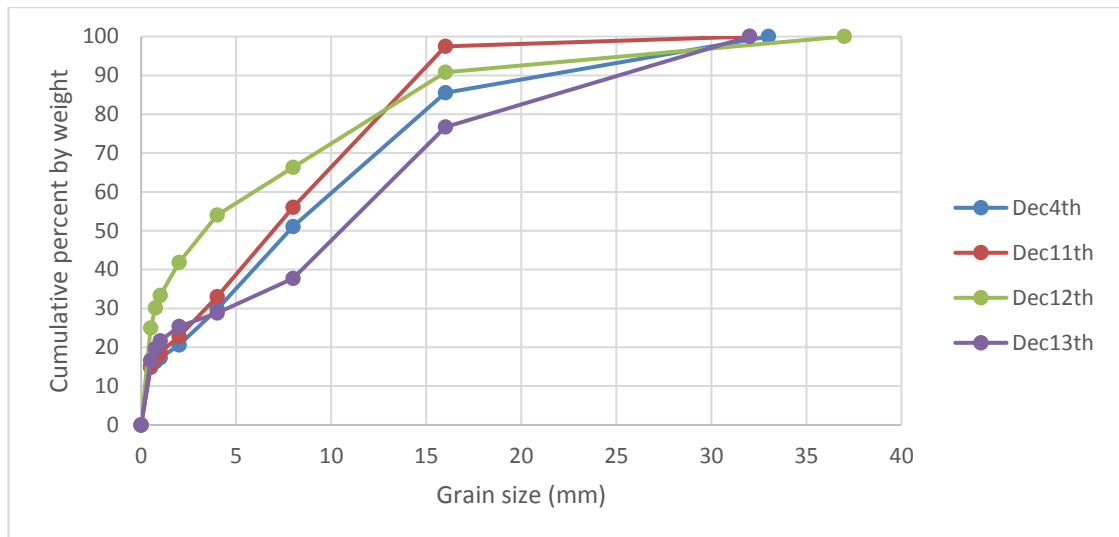


Figure 5.5: Variation between samples taken at the location of SID3 in December 2014.

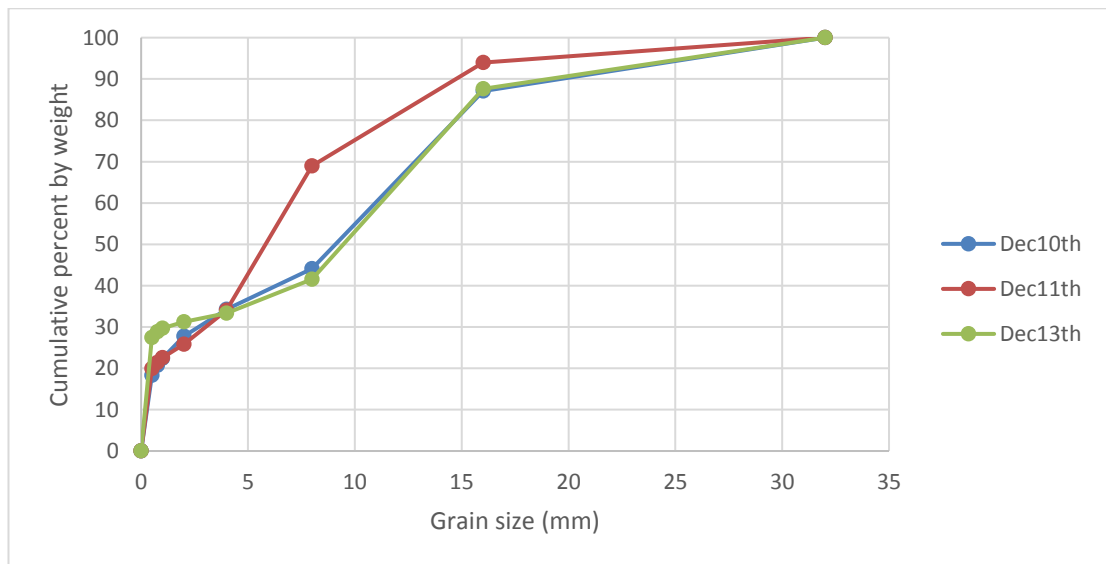


Figure 5.6: Variation between samples taken at the location of SID4 in December 2014.

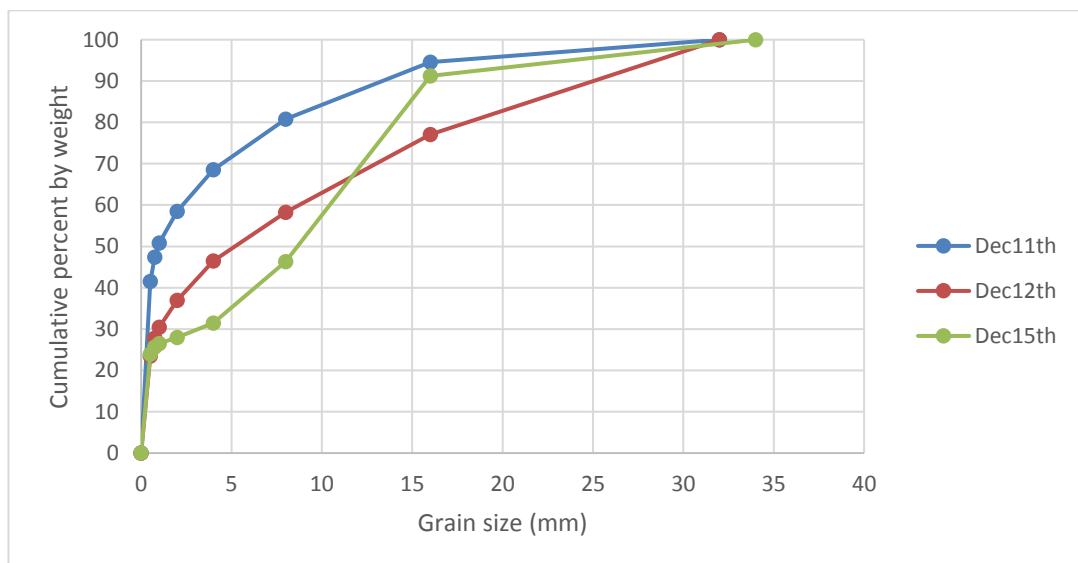


Figure 5.7: Variation between samples taken at the location of SID5 in December 2014.

ii. Surface sediments

Despite the new methodology created by the BAR (2005) project, wherein smaller 2-5 kg samples are used, it was not within the scope of this project to fully assess the variability of sediment dynamics of the beach at Eastoke with physical samples. A faster technique for assessing sediment distributions is to mark each dGPS point with a code (e.g. Watt *et al.*, 2005). dGPS points were categorised according to the system set out in Chapter 4, section 4.6.iii.b.

An assessment of the differences in codes used on each profile (Figure 5.8) indicates that sorting patterns are not perfectly consistent across the three profiles. Overall, Profile 3 has a much higher proportion of ‘mainly sand’ points and a lower proportion of ‘small gravel’ points than the other two profiles.

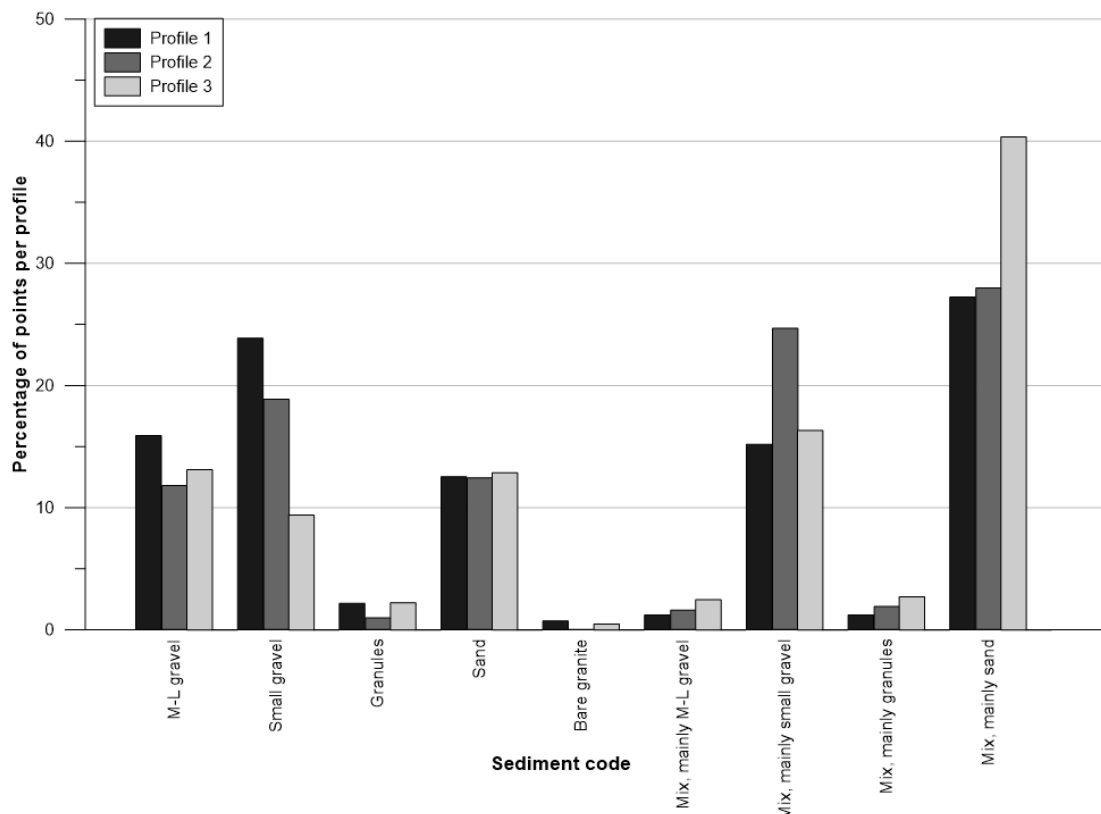


Figure 5.8: Proportions of surface sediment codes compared by profile number.

The dominant overall category on the beach is ‘mainly sand’, followed by ‘small gravel’ and ‘mainly small gravel’. This is not consistent across the beach profile though (Figure 5.9). Below -1 m elevation, ‘sand’ and ‘mainly sand’ dominate, while between -1 and 1 m elevation ‘small gravel’ starts to occur at greater numbers of points, though still less so than ‘sand’ combinations. From 2-4 m elevation, ‘medium/large’ and ‘small gravel’ become dominant,

while 4-5 m elevation indicates a more even split between ‘medium/large gravel’, ‘small gravel’ and ‘mainly small gravel’ and ‘mainly sand’. The final elevation category, which generally represents the beach crest, is dominated by ‘mainly small gravel’ points.

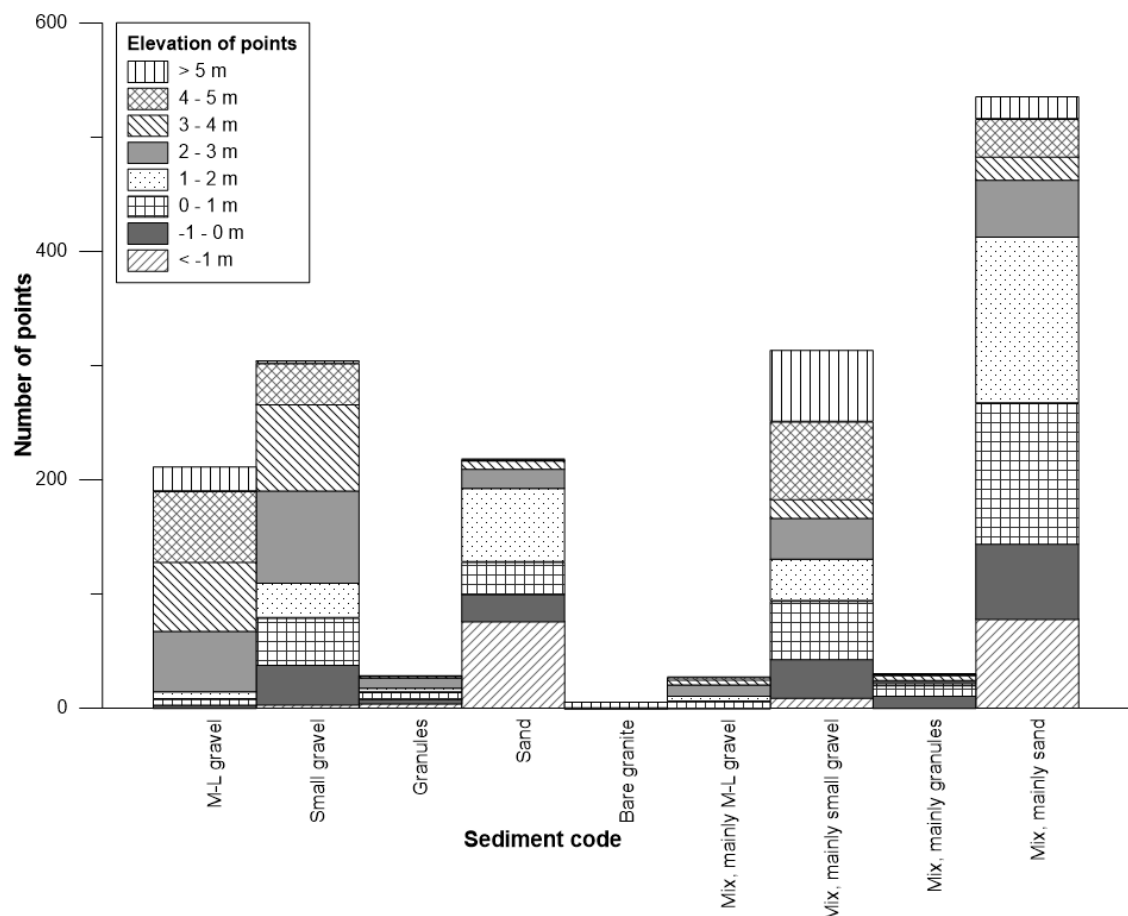


Figure 5.9: Number of points in each surface sediment category for different elevations on the beach. n=1671.

This general pattern of grain size decreasing seawards along each profile can be seen in Figure 5.10, with sand dominating the lower quarter of the beach. There are some occasions when sand can be seen along a greater proportion of each profile. All three profiles have smaller gravel on the top of the beach crest. The traditional sediment sorting does not begin until the base of the crest, where the coarser gravel code is used. However, even here, especially on Profile 1, there are bands of coarser gravel between patches of small gravel, indicating that sorting patterns on this artificially replenished beach are not as simple as may be expected.

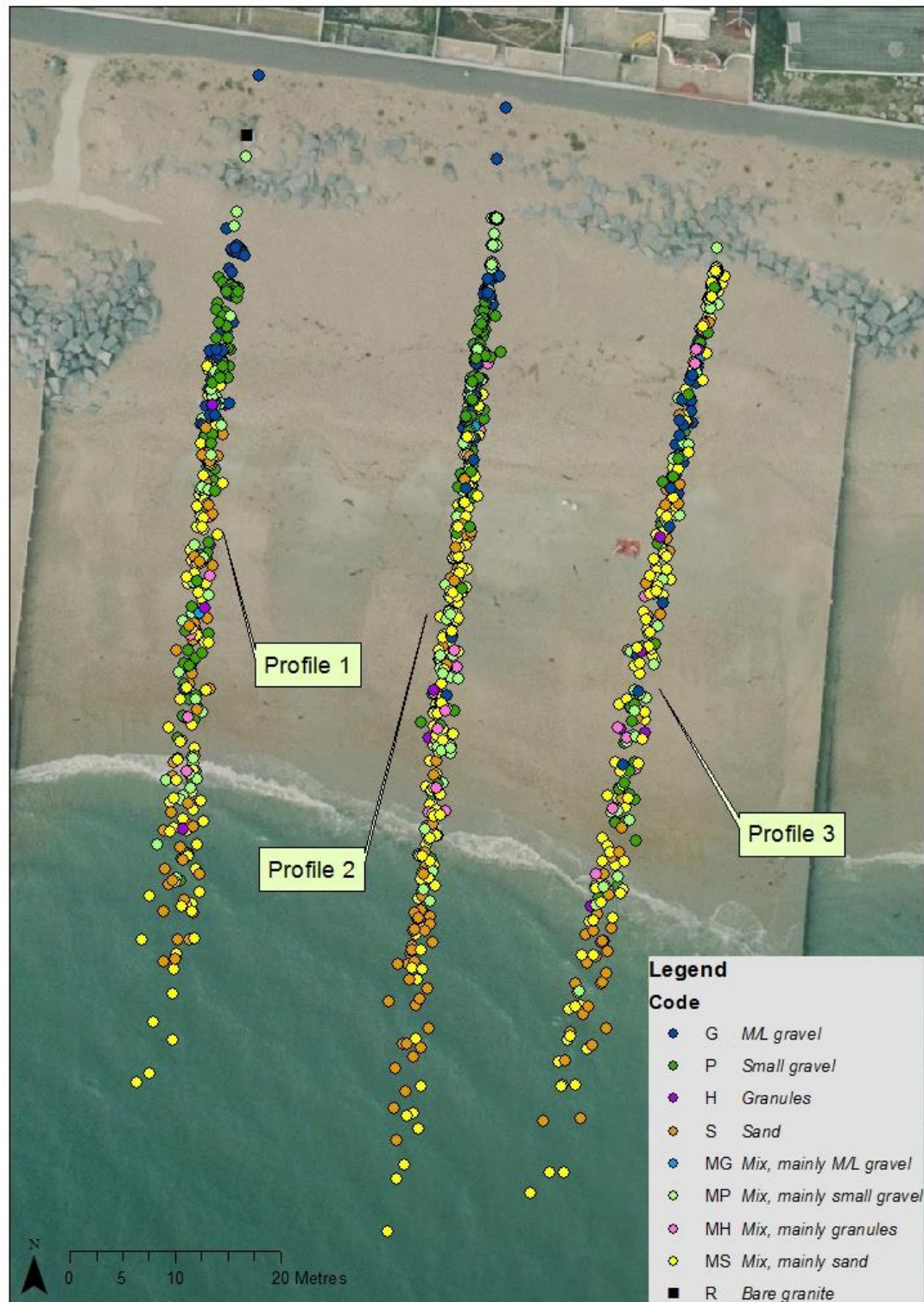


Figure 5.10: Surface sediments from profiles measured in January, February and March 2015. Aerial imagery courtesy CCO, 2016.

Profiles 1 and 2 are more similar in terms of the overall proportions of each code reported (Figure 5.11, Figure 5.12). Profile 3 is marked by a dominance of ‘mainly sand’ (Figure 5.13), indicating that sediment sorting is not as efficient in this section of the beach. This area likely experiences more interference from refracted waves due to groyne interaction. The upper beach (> 4 m) of Profile 1 is better sorted than on Profiles 2 and 3.

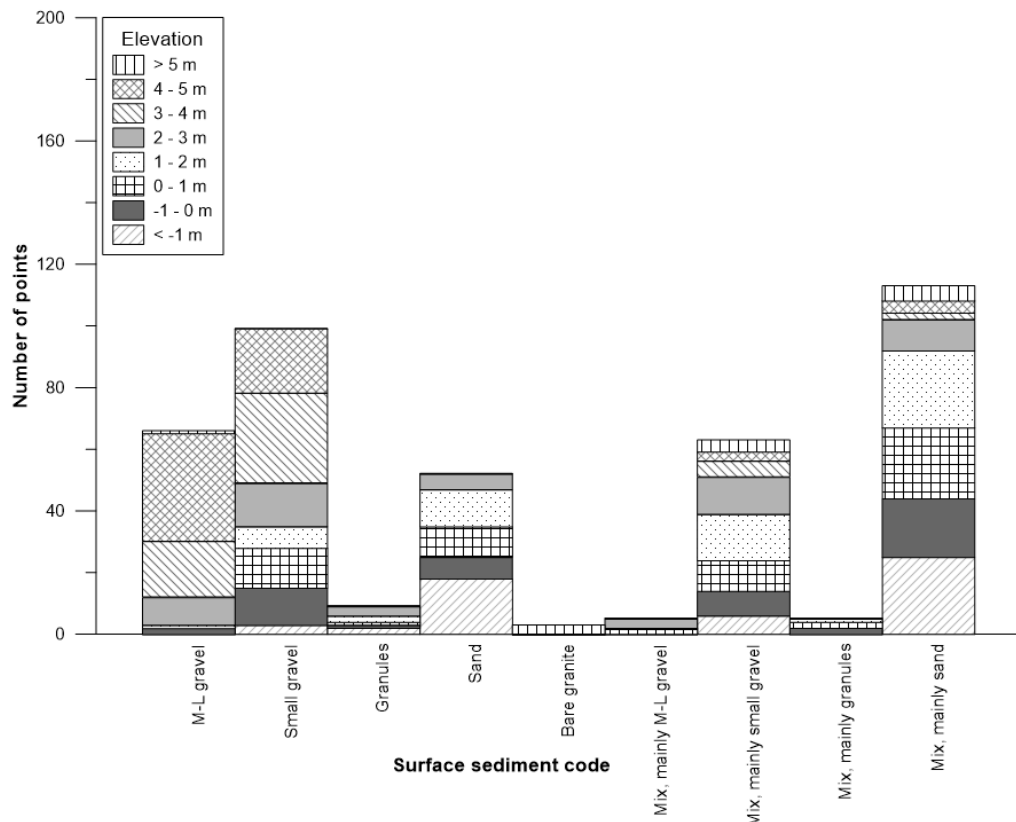


Figure 5.11: Frequency of sediment codes at different elevations on Profile 1. N=415.

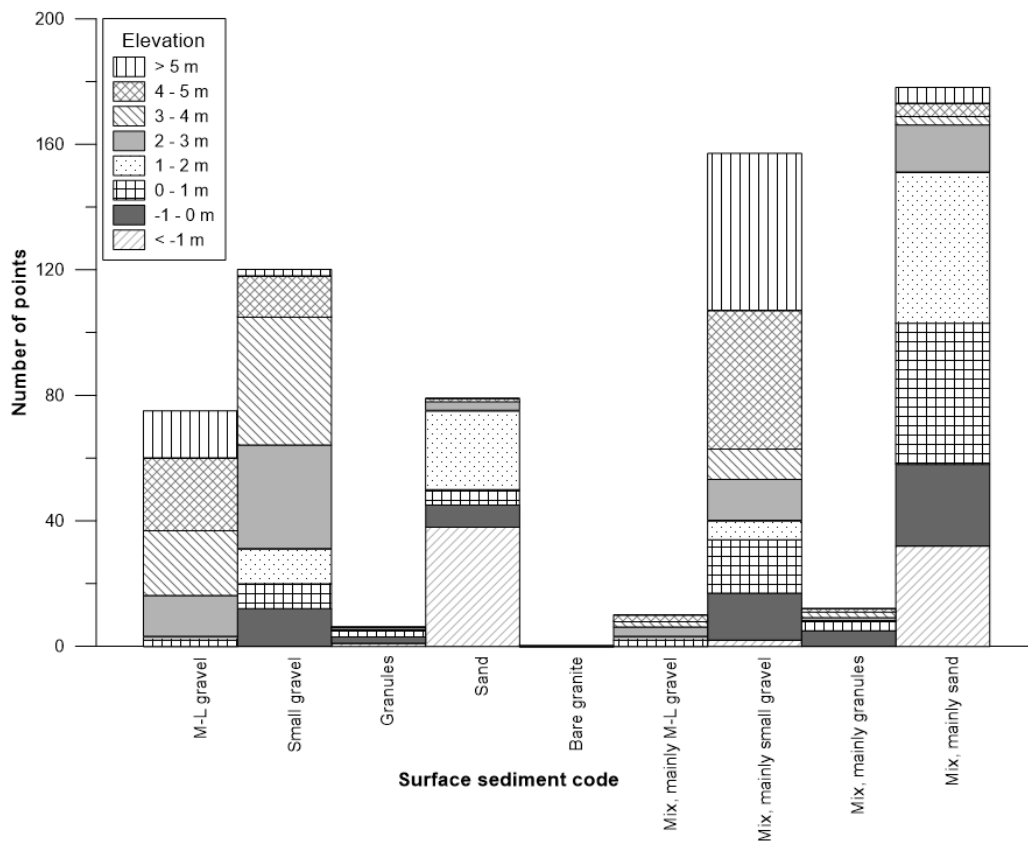


Figure 5.12: Frequency of sediment codes at different elevations on Profile 2. N=637.

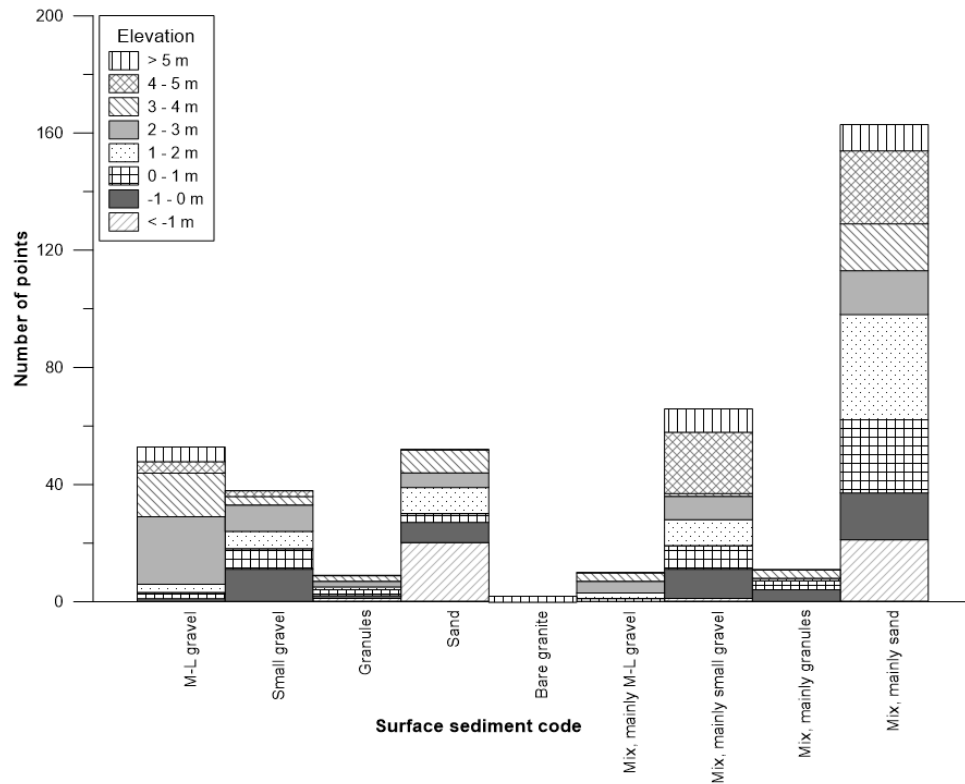


Figure 5.13: Frequency of sediment codes at different elevations on Profile 3. N=404.

To investigate whether dominance of certain categories was more likely under particular wave conditions, Figure 5.14 was created.

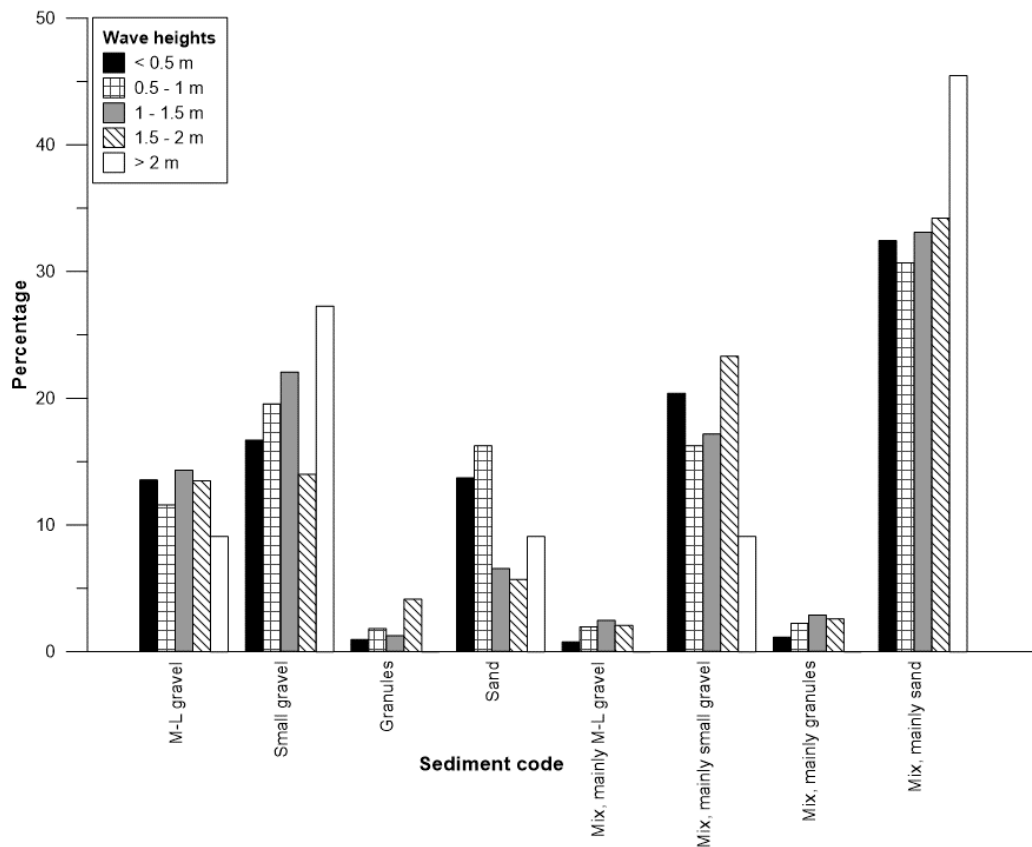


Figure 5.14: Percentage of points in each category for different wave heights.

The proportion of ‘mainly sand’ points increases drastically with wave heights over 2 m; the proportion of ‘small gravel’ points is also higher for this group, and overall seems to increase with wave height apart from an anomaly between 1.5-2 m wave height. These changes broadly correlate with opposing changes in the ‘mainly small gravel’ category, suggesting that increased wave heights are sorting these grain sizes better.

The proportion of pure sand points appears to be higher under low wave energy conditions (< 1 m). No other obvious patterns exist in this data.

iii. Correlation between surface sediment codes and physical samples

Sorting on mixed sand and gravel beaches is often limited to the very surface layer (Jennings and Shulmeister, 2002), and does not continue into the full active layer. Physical samples were compared to relevant surface codes to determine how representative this coding system is (Figure 5.15). A table of these comparisons can be seen in Appendix E.

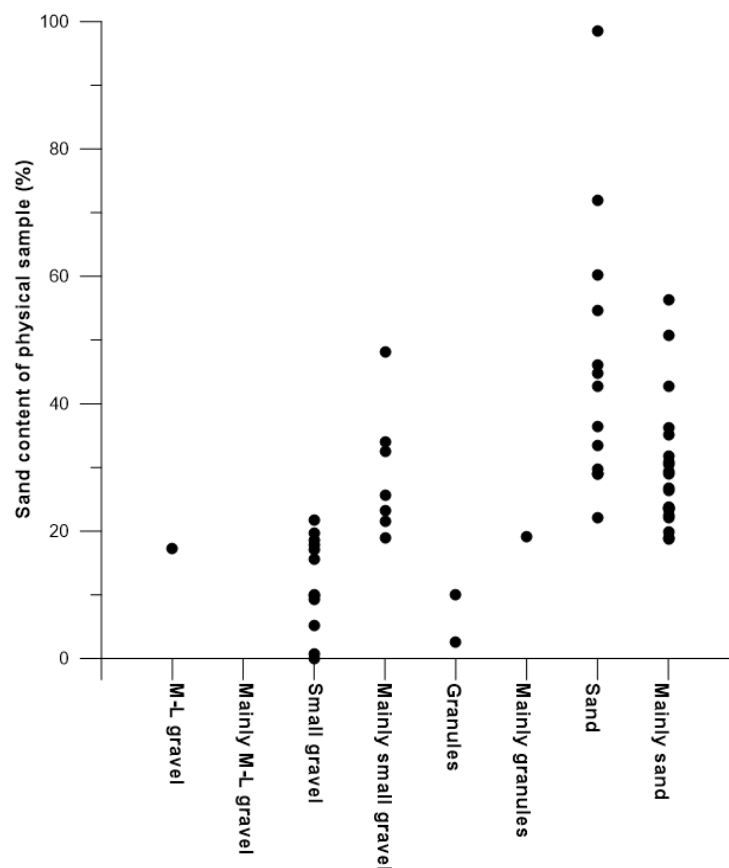


Figure 5.15: Comparison of surface sediment codes with sand content of physical samples. N=57.

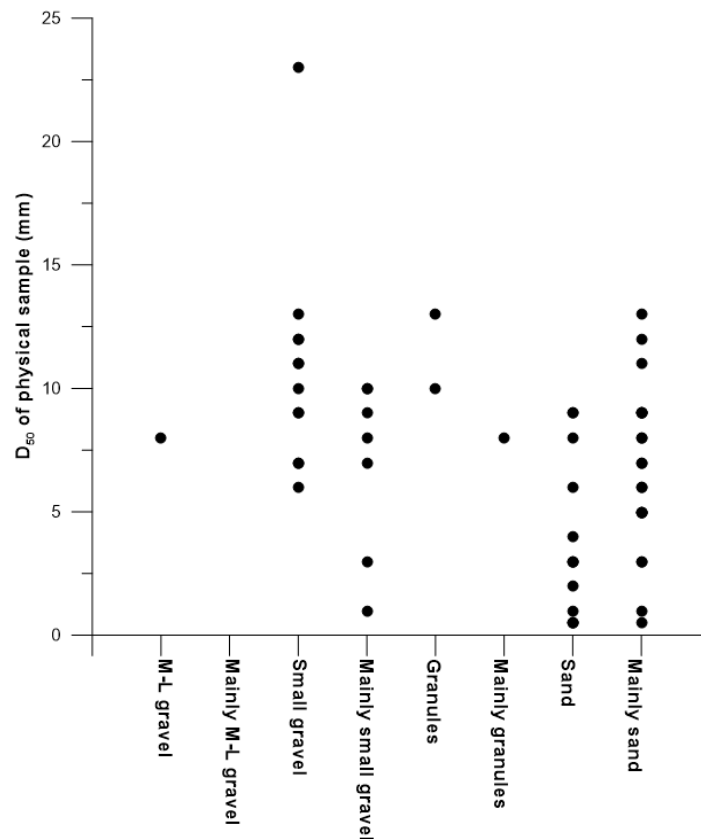


Figure 5.16: Comparison of surface sediment codes with D₅₀ of physical samples. N=57.

There is a broad correlation between the surface codes and their respective physical samples. Figure 5.15 indicates higher proportions of sand in areas marked with ‘sand’ or ‘mainly sand’ codes, and lower proportions of sand in ‘small gravel’ and ‘granule’ areas compared to the mixed categories of both those grain sizes.

Figure 5.16 indicates less of a correlation between surface codes and the D₅₀ of samples, but there are still some patterns. D₅₀s are generally lower for sand-dominant codes, and for ‘mixed’ codes. The D₅₀ for the sole M-L gravel point is an outlier and would be expected to be higher. This could be explained by the existence of only a thin upper layer – known as armour – of large gravel, with sand or other smaller particles underneath, which would be included in the physical sample but not in the coding.

iv. Profile shapes

As this is a managed beach, it may be helpful to know whether particular profile formations are more common (the inference from this being that they are more stable), in order to plan future replenishments in terms of where on the profile it may be best to deposit sediment. Each individual profile was visually categorised according to Caldwell and Williams’ (1985) classification system (Chapter 4.4.iv), to provide a relatively simple way to compare profiles

both spatially and temporally. According to the original methodology used to create the system, only the ‘active’ part of each profile was used. A total of 152 profiles were categorised, 44 along Profile 1, 61 along Profile 2, and 47 along Profile 3 (Figure 5.10 shows locations of profiles).

In addition to this, the 22 mean profiles (from each profile during each study period) were categorised (Table 5.2) (all mean profiles can be viewed in Appendix C). Profile 1 exhibits the most variation between codes, while Profiles 2 and 3 both have multiple cases of a particular categorisation (LUB and CCMB, respectively). The means of the three profiles are consistently different shapes in terms of berm location, though on one occasion (February 2015) Profiles 1 and 3 were categorised to the same code. However, the lack of cases where all profiles match indicates potentially large amounts of morphological discrepancy within the cell, which could result from frequent re-orientation of the beach, perhaps due to changes in drift direction.

Table 5.2: Classifications of mean profiles. Profiles 1 and 3 were not measured during December 2014.

	Profile 1	Profile 2	Profile 3	Drift direction
December 2014	--	CCMB	--	East
January 2015	CCLB	CCUB	CCMB	East
February 2015	CCMB	CCUB	CCMB	West
March 2015	CCUB	LUB	CCMB	West
October 2015	LMB	CCCB	LNB	West
November 2015	CCMB	LUB	CCLB	East
December 2015	LCB	LUB	CCLB	West
January 2016	LUB	CCLB	LMB	East

The drift direction column was added to investigate whether dominant drift direction had a discernible influence on berm placement. It seems reasonable to expect that berms are more likely to form on the western-most profile (Profile 1) when the dominant drift direction is to the west, and vice versa during eastwards drift periods. An obvious pattern does not emerge from these mean profile shapes, with berms on both profiles common under both drift directions.

All three profiles experienced significant variation at a daily scale as well. Profiles 1 and 2 most frequently have upper berms but are fairly evenly split between concave and linear, while Profile 3 has a dominant concave shape. The least common profile overall is LLB, though mid berms are also infrequent (Figure 5.17).

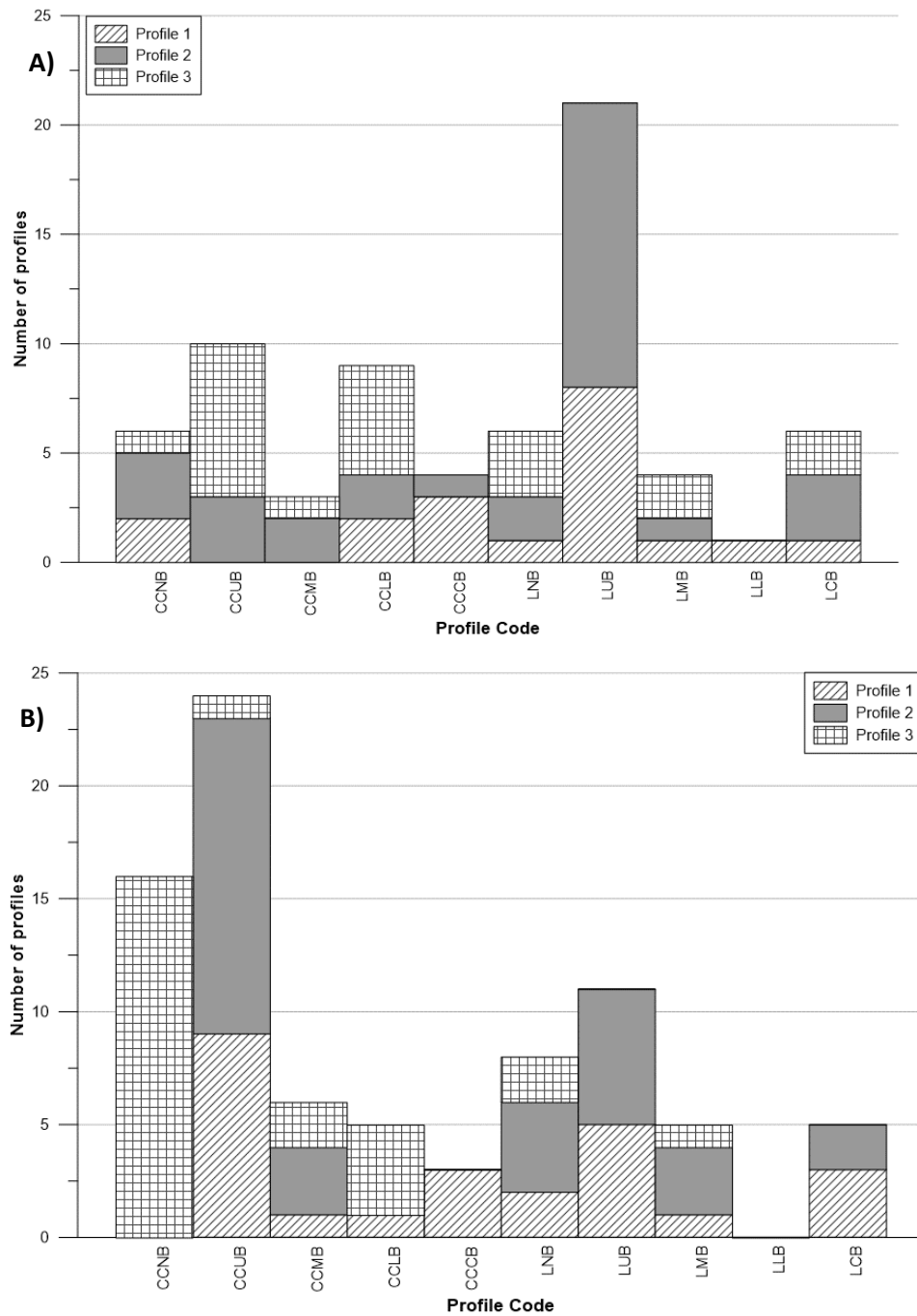


Figure 5.17: Number of each profile shape experienced per profile, associated with dominant drift directions: A) westerly waves (eastwards drift); B) easterly waves (westwards drift).

Daily profiles were separated by dominant preceding wave direction to determine what influence this has on differences in profile shapes between the three profiles (Figure 5.17). The most striking difference is in the distribution of shapes exhibited on Profile 3: under westerly waves, there was a much more even split of profiles shapes, whereas under easterly waves the profile shape CCNB dominates.

Similarly, the upper berm – especially for overall concave shaped profiles, but also to a lesser extent for the linear shape – becomes more dominant on Profile 1 under easterly waves.

Profile 1 also exhibits a greater number of concave profiles under easterly waves.

Profile 2 experiences a dominance of LUB categorisations under westerly approaching waves, and a dominance of CCUB under easterly waves. Overall, almost two thirds of the shapes on Profile 2 are concave under westerly waves, and this split becomes much more even under easterly waves.

v. Profile changes

a. Medium term profile changes

Cross-sectional areas were calculated using a ‘master profile’ for each of the three measured profiles. These took into consideration the length of the shortest profile measured (due to changes in the level of low water throughout the study) and the depth of the clay bed layer, which exists at approximately -1 m OD beneath the upper beach and slopes very gently seaward. The cross-sectional areas do not include the whole beach crest, which is composed mainly of large granite boulders and was not overtopped at any point during this study. Figure 5.18 shows the example for Profile 3 of the area considered. The cut-off points for Profiles 1 and 2 were 18-52 m and 15-50 m chainage respectively. Thus the volumes consider only the upper to mid sections of the active profile.

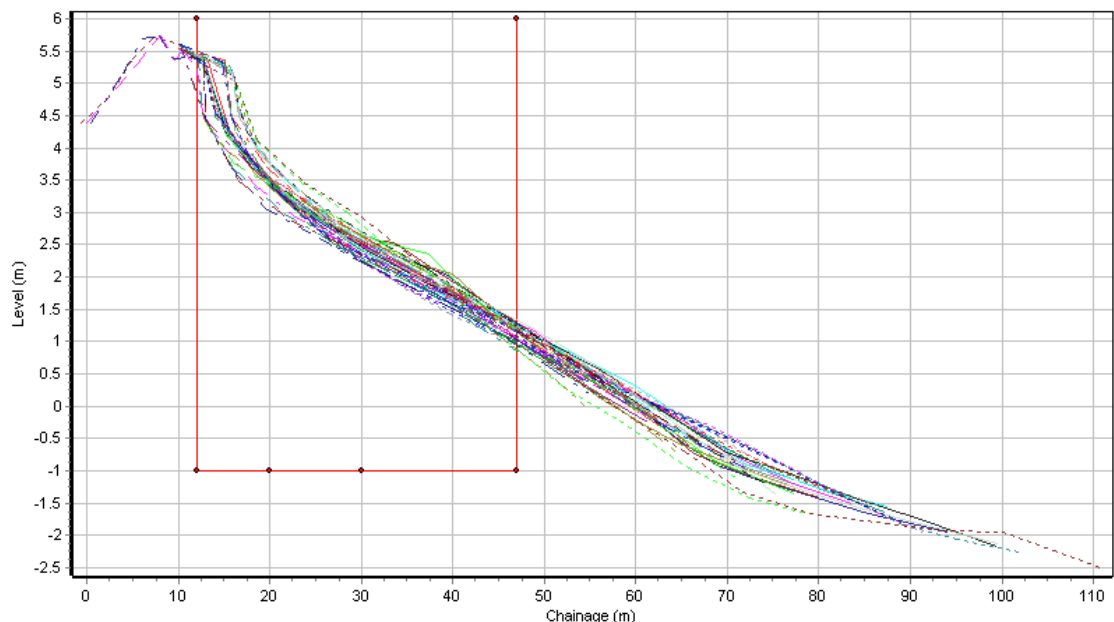


Figure 5.18: Limits of cross-sectional areas of Profile 3.

The average cross-sectional area under this area of each profile during each study period is shown in Table 5.3, along with the combined volume of the three profiles to give an indication

of overall erosion or accretion in the upper and mid sections of the beach. As all three profiles are within the same groyne bay, these figures can be used to give an indication of the direction of sediment transport. The expected dominant drift direction (based on wave data across each study period) is also listed in the Table. Shorter term profile changes will be discussed in section b.

Table 5.3: Average cross section of each profile taken from measured profiles within each study period.

Month	Profile 1 (m²)	Profile 2 (m²)	Profile 3 (m²)	TOTAL	Expected dominant drift direction
Dec14	-	117.63	-		East
Jan15	109.58	123.25	131.04	363.72	East
Feb15	110.83	128.34	130.89	370.06	West
Mar15	104.79	122.31	126.03	353.13	West
Oct15	121.02	130.50	138.51	390.03	West
Nov15	111.27	124.83	136.36	372.46	East
Dec15	103.77	124.88	131.33	359.98	West
Jan16	113.50	118.61	124.87	356.98	East

Profile 3 is the most easterly profile, and as such would be expected to increase in size during periods of eastwards drift, while Profile 1 would be expected to increase in size during periods of westwards drift. This pattern holds true in February 15, where Profiles 1 and 2 increase in volume, while Profile 3 experienced a loss (Figure 5.19), indicating that some sediment was travelling west within the groyne bay. This pattern does not appear to hold true during March 2015, which was also predicted to have a westward drift direction; here instead Profile 3 experienced the smallest loss of all three profiles, which does not suggest sediment being transferred from Profile 3 towards Profile 1.

The increase between March 2015 and October 2015 is partly due to beach recycling further east, and partly due to expected accretion during the calmer summer months (this can be seen from the TOTAL column, which increases significantly during October 2015 but then decreases to similar values during the following months). Profile 1 experienced the greatest increase here, followed by Profile 3; the increase under Profile 2 was much lower.

Between October 2015 and November 2015, all three profiles experienced a loss in volume, however the loss under Profile 3 was smaller than under Profiles 1 and 2, indicating that the drift direction was as expected.

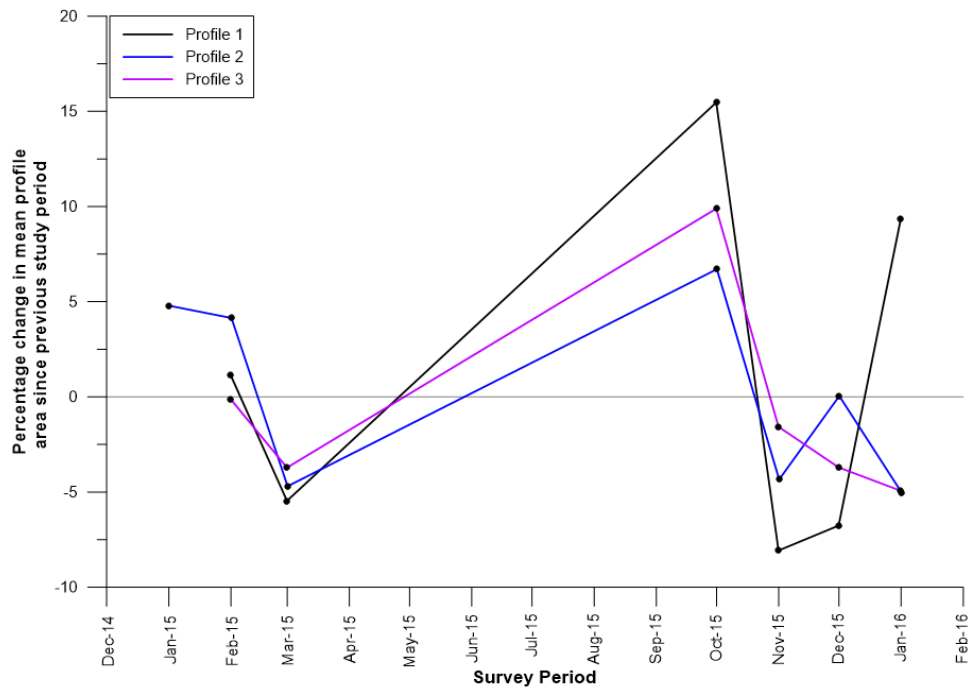


Figure 5.19: Percentage change between mean cross-sectional area of each profile between each survey period

The volume of Profile 2 stayed very stable between November and December 2015, but both Profiles 1 and 3 reduced in volume, not indicating any particular drift direction. The data for January 2016 also disagrees with the predicted drift direction: Profile 1 increases while Profiles 2 and 3 decrease, which would suggest either a westward drift direction, or that sediment is indeed travelling east, but is being transported over the top of groynes, thus depleting the east side of the groyne bay while building the west side. The latter seems unlikely though; in that situation, sediment would be expected to travel relatively evenly through the groyne bay, and would certainly not accumulate at the western side.

The profile envelopes in Appendix C can be used as an indicator of the amount of change and where on each profile it occurred during each study period. While they do not show daily profile changes, they do provide an overview of the total variation experienced across each profile, which can be considered alongside the overall wave climate.

The profile envelopes generally exhibit quite high levels of variation across the beach. In general, the envelopes on Profile 3 are smaller than on the other two profiles. During some months, for example March 2015, all three profiles have very small profile envelopes. However during others, some have small envelopes while others have comparatively large ones – for example in October 2015, this difference is especially pronounced between Profiles 1 and 3. Profile 1 has a very wide envelope, while Profile 3 has almost none.

Figure 5.4 shows the percentage change in cross-sectional area between the greatest and smallest CSA on each profile in each study period. Compared to the profile envelopes in Appendix C, these values seem small and generally more consistent between profiles. This may indicate cross-shore movement of sediment, which makes profile envelopes appear larger than the changes they represent.

Table 5.4: CSA change (as a percentage of greatest CSA) between smallest and largest measured CSA on each Profile during each study period.

Month	Profile 1 (%)	Profile 2 (%)	Profile 3 (%)	Mean H _s (m)	Daily mean H _s range (m)
Dec14	-	1.81	-	0.97	0.40-1.85
Jan15	4.05	5.00	4.90	1.05	0.31-1.89
Feb15	5.44	3.00	2.92	0.82	0.50-1.31
Mar15	3.50	3.40	3.25	0.53	0.41-0.74
Oct15	3.81	4.06	4.31	0.62	0.46-0.77
Nov15	6.78	4.49	3.41	1.17	0.86-1.68
Dec15	4.07	2.61	5.50	1.59	1.23-1.99
Jan16	11.29	9.33	8.49	1.37	0.96-1.93

b. Short term variation

The change in cross-sectional area can also be considered on a survey-by-survey basis. Figure 5.20 provides the calculated CSAs for each profile on every occasion they were measured through the study, with Figure 5.21 showing the amount of change. All three profiles are highly variable, and many of the patterns of change are consistent between them, but there are occasions when this is not the case. For example, between late January 2015 and mid-February 2015, Profiles 1 and 2 increase while Profile 3 decreases.

In mid-November 2015, Profiles 1 and 2 both decrease in volume, while Profile 1 increases slightly. When Profiles 2 and 3 experience a large reduction in volume at the end of December 2015, Profile 1 retains its volume.

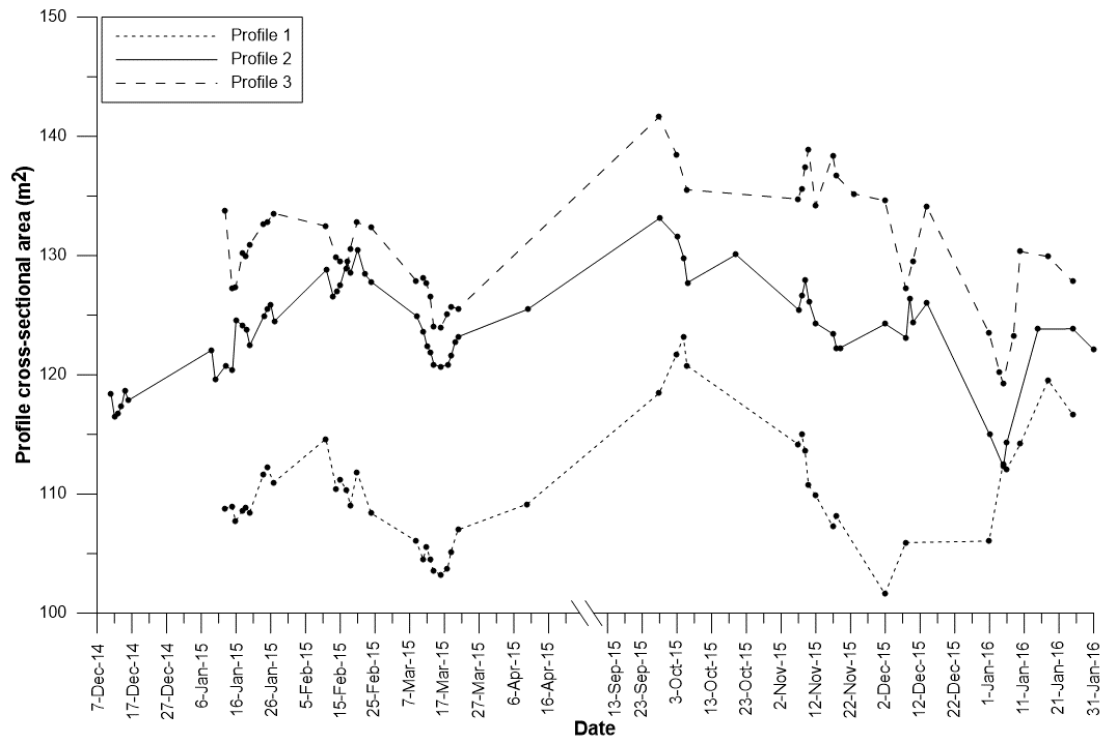


Figure 5.20: Cross-sectional area under each profile throughout the study.

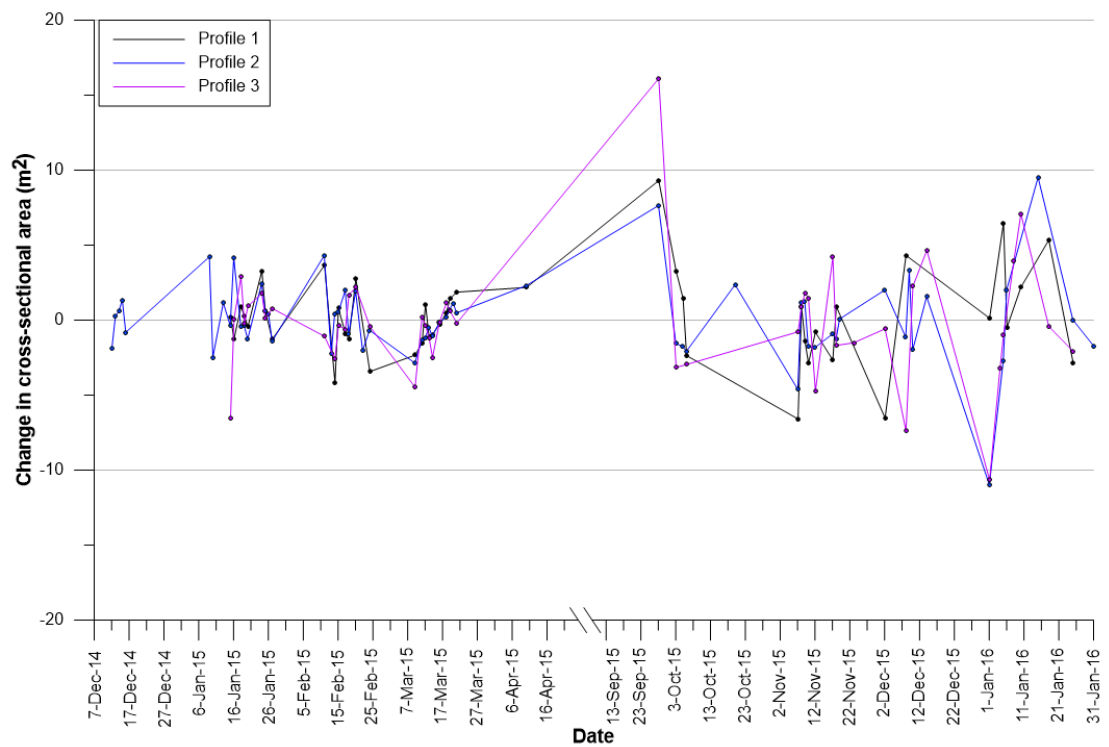


Figure 5.21: Change in cross-sectional area of each profile between surveys.

These changes in cross-sectional area were related to wave height (Figure 5.22) to determine whether a causal link could be found. In general, changes were larger for bigger wave heights. The changes on Profile 2 are overall smaller than changes on Profiles 1 and 3.

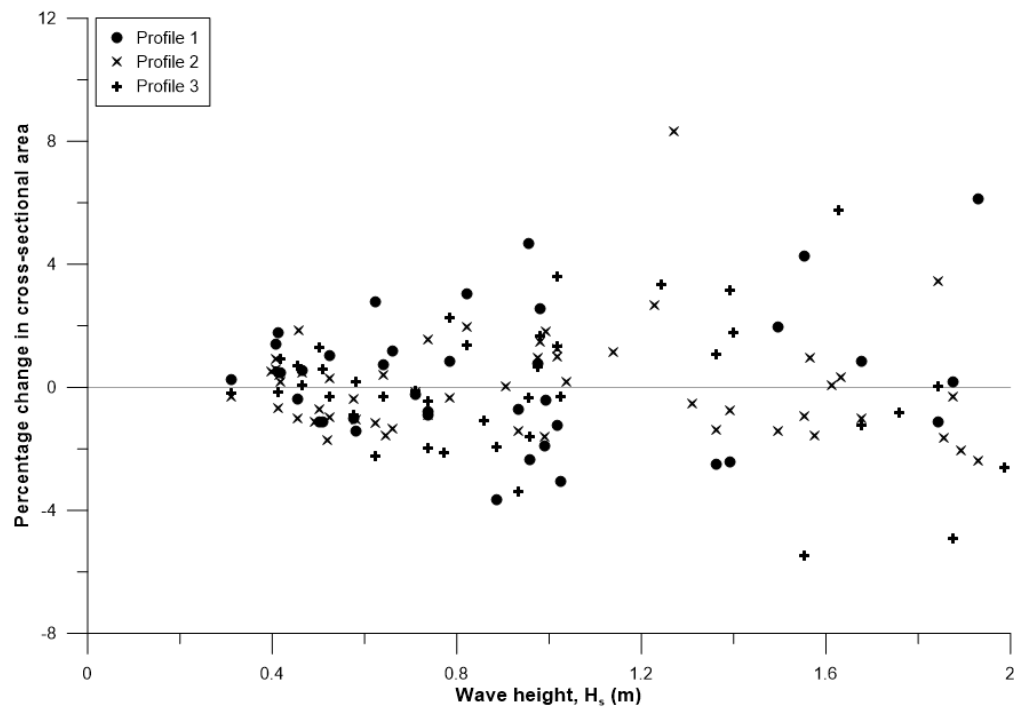


Figure 5.22: Percentage change in cross sectional area for varying wave heights.

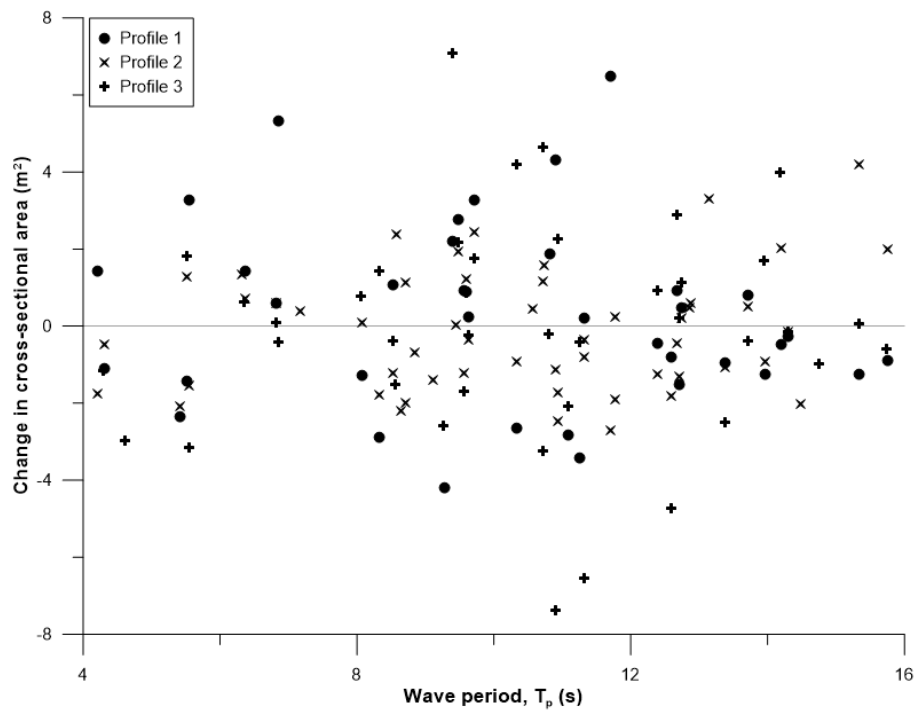


Figure 5.23: Change in cross-sectional area in relation to wave period.

Due to the frequency of bimodal wave events at this site (Chapter 3.3.i), changes were also compared to wave period to determine whether they were more likely to happen under storm or swell waves. No correlation was found. Likewise, there is no apparent link between CSA change and wave power, likely because of the inclusion of wave period in this calculation.

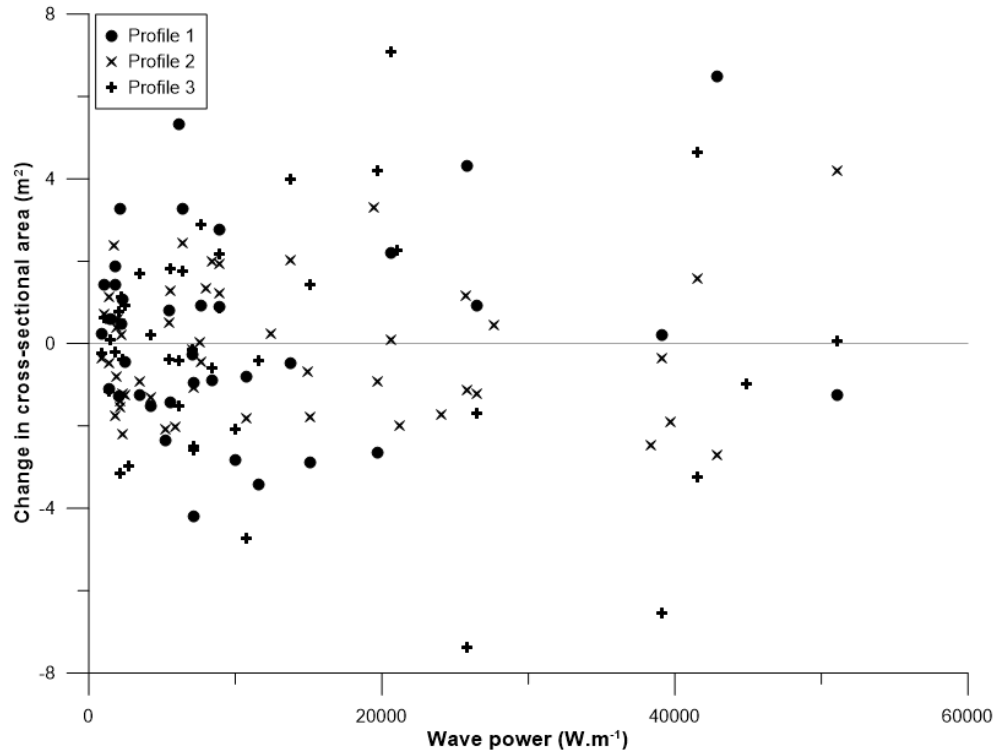


Figure 5.24: Change in cross-sectional area in relation to wave power.

To test whether wave directions had an influence on whether differences measured were positive or negative, bubble plots were created (Figure 5.25-Figure 5.27). These show the relative size of change (and whether it was positive or negative) for the experienced wave height and direction. Profile 1 would be expected to experience erosive events for wave directions >185 degrees, and Profile 3 would be expected to experience erosive events for wave directions <185 degrees, which is the approximate orientation of the groynes. There are no clear-cut separations between positive and negative changes for different wave directions on either profile.

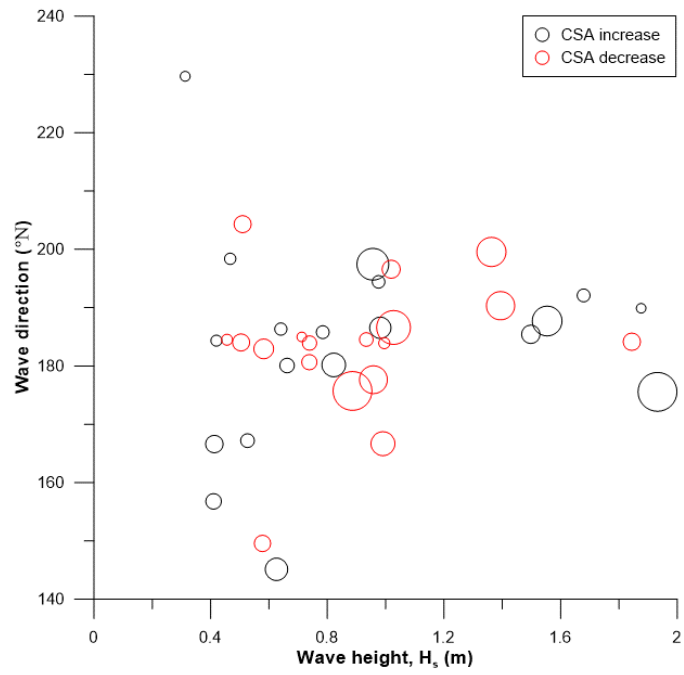


Figure 5.25: Patterns of positive and negative change in terms of wave height and direction on Profile 1.

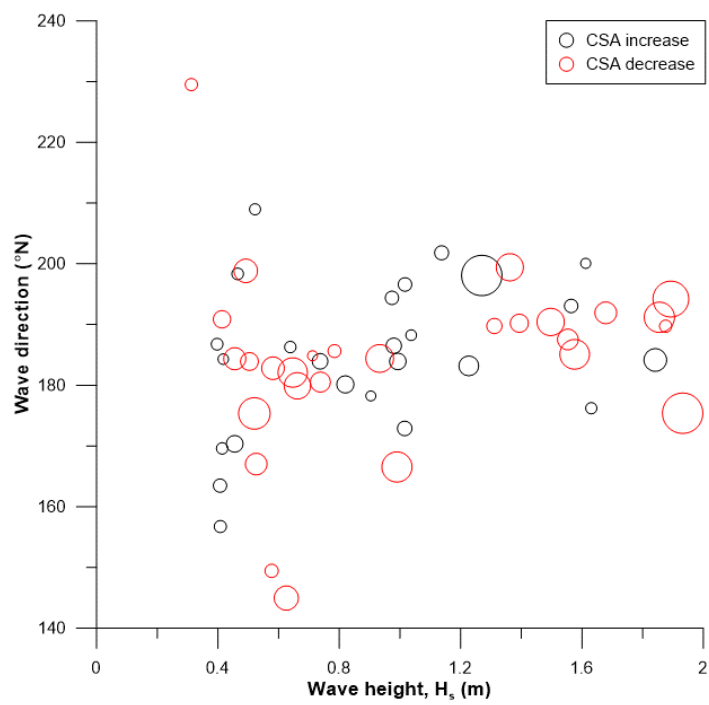


Figure 5.26: Patterns of positive and negative change in terms of wave height and direction on Profile 2.

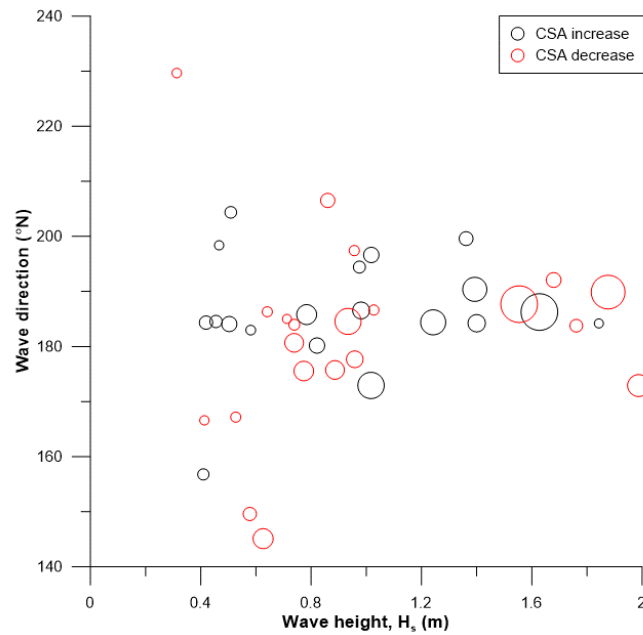


Figure 5.27: Patterns of positive and negative change in terms of wave height and direction on Profile 3.

It has been suggested (e.g. Kroon and Masselink, 2002) that waves are more effective during neap tides; theoretically, if they have a smaller width of beach to cover, more energy can be transferred to each part of the beach, leading to greater changes (Reichmüth and Anthony, 2007).

If this were true of these results, the largest values of profile change should be found in the top left corner of Figure 5.28 (at the point where wave height is largest and tidal range is smallest). There is no correlation between these variables.

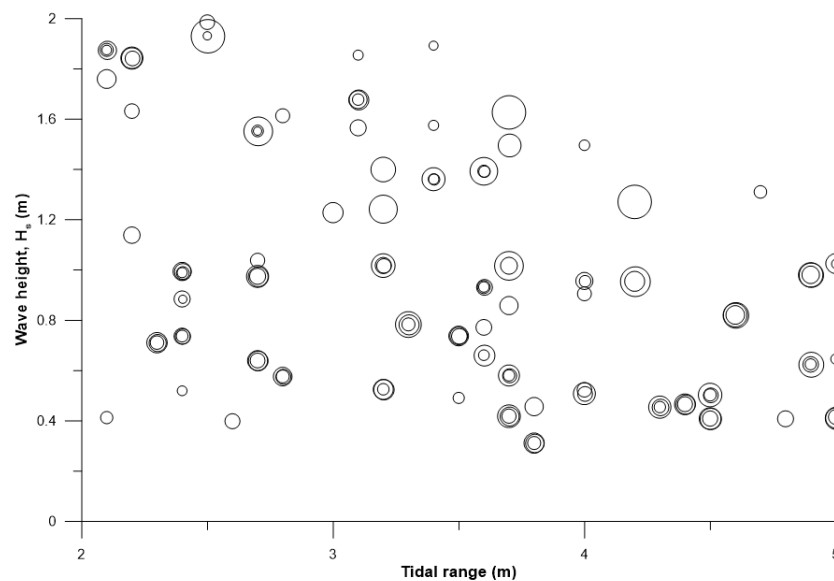


Figure 5.28: Change in CSA as a function of both wave height and tidal range.

c. Locations of maximum net change

The majority of change on coarse grained beach profiles is usually thought to be a product of berm dynamics (Curoy *et al.*, 2009). To test this, locations of maximum net change between surveys were plotted for each of the three profiles (Figure 5.29-Figure 5.31). There are more points for Profile 2 (Figure 5.30) than Profiles 1 and 3, because this profile was more frequently surveyed.

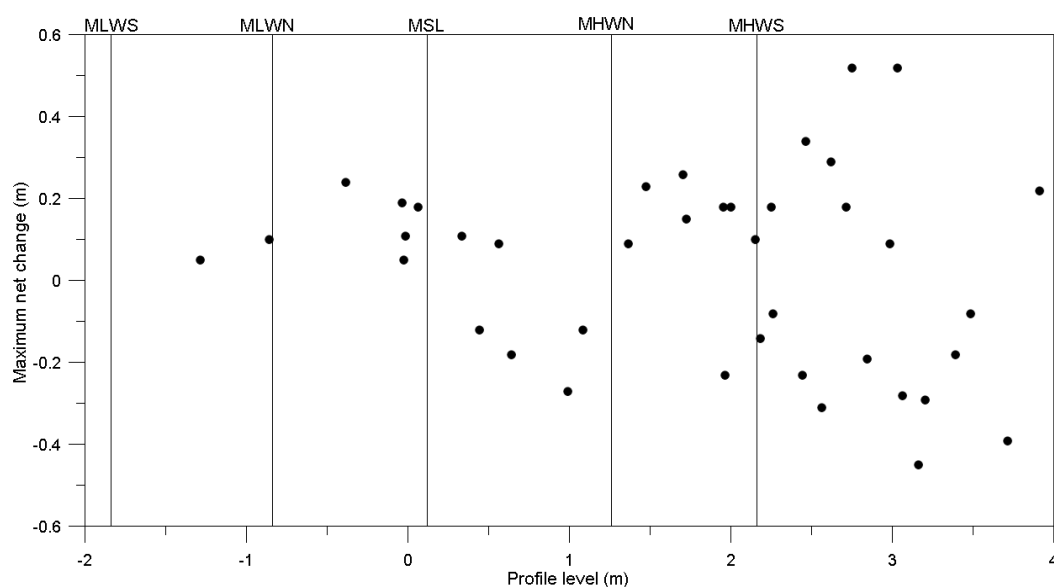


Figure 5.29: Location of maximum net change between profile surveys on Profile 1.

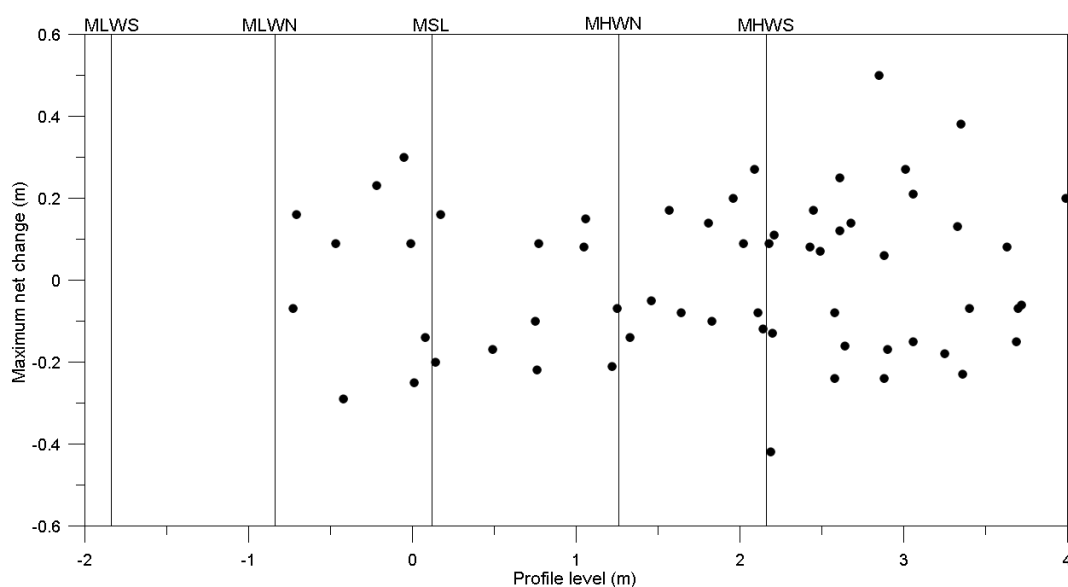


Figure 5.30: Location of maximum net change between profile surveys on Profile 2.

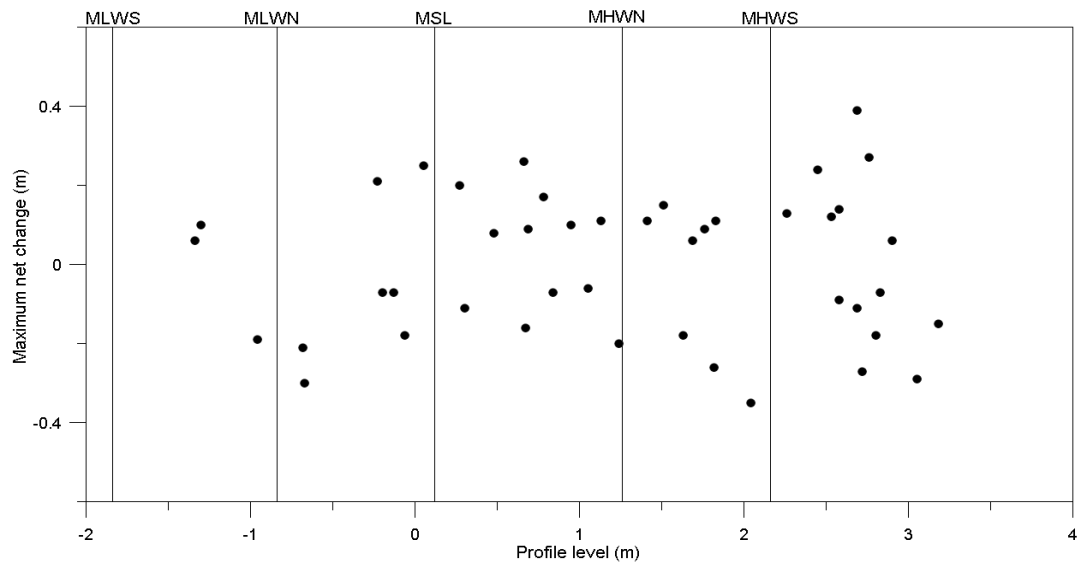


Figure 5.31: Location of maximum net change between profile surveys on Profile 3.

All three profiles show an indication that the most significant changes usually occur in the upper half of the profile. The majority of points of maximum net change are above MHWN, indicating that high tide berms are most frequently experiencing the greatest changes compared to the rest of the profile. Profile 3 has the most even spread of locations of maximum change. This is perhaps due to the limited morphological change (in terms of berm formation, transition and removal) experienced on this profile compared to the others.

Profile 1 experiences only positive maximum changes below MSL. This could be indicative of cusp emergence, especially for the slightly larger measurements between MLWN and MSL.

All three profiles experienced maximum change events above the level of MHWS, which is commensurate with the addition of wave height and run-up. There does not appear to be a pattern between the maximum change measured between two surveys and the position of this change on the profile.

Theoretically, it makes sense that the maximum change on a profile would be more closely related to maximum significant wave height than mean significant wave height for the time over which the change occurred. Thus, these two variables were correlated (see Figure 5.32), producing two linear relationships: one for positive maximum change and one for negative maximum change. The relationship for positive maximum changes ($r = 0.61$, $p < 0.001$, $n=77$) is stronger than for negative maximum changes ($r = 0.40$, $p < 0.001$, $n=67$).

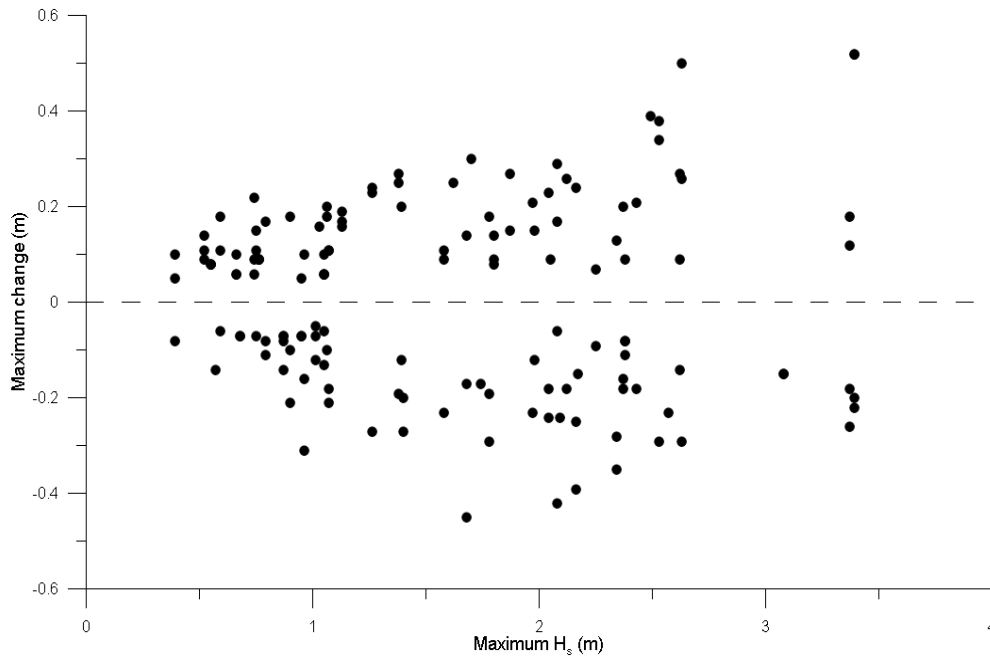


Figure 5.32: Scatterplot of maximum significant wave height against maximum net change between each measured profile.

vi. *Berm dynamics*

While medium to long term beach profile evolution is a useful tool for coastal managers, it is also important to understand how the different profiles react on a smaller scale, for example after a storm event, or in relation to a spring-neap-spring tidal phase to help ensure that protection schemes are designed as efficiently and effectively as possible in the face of rising sea levels and increasing storm activity (Dornbusch, 2017).

All beach profiles can be seen in Appendix B, but a few examples will be discussed here in terms of berm dynamics, storm response and alongshore variation.

Perhaps the best examples of the berm transitions discussed by Austin and Masselink (2006) can be seen in profiles measured during February 2015. This is one of the months with the most variable wave climates, and as a result experiences three out of the four transitions.

On all three profiles (Figure 5.33, Figure 5.34), berms that existed on 11/02/2015 are removed before 14/02/2015. These berms initially existed in different places on the profiles, but the larger wave heights experienced between these two surveys smoothed out all three profiles.

Profile 2 can then be seen to experience berm reformation between 15/02/2015 and 17/02/2015 (Figure 5.34), as more moderate waves occurred. This berm then experiences roll-over between 18/02/2015 – 24/02/2015, which would normally be associated with tides

transitioning towards springs. However, in this case, the largest tidal ranges were on 21/02/2015, yet the berm continues to roll-over after this point. The difference in range was smaller than the added wave height, which explains why run up was still high enough to cause berm roll-over. That more energy came from the waves may also help to explain why the profile directly below the berm is steeper on 24/02/2015 than previously.

The only transition which was not observed in February 2015 was berm retreat, probably because while the tidal range was decreasing towards neaps wave height was over 1.5 m, which became the dominant factor in shaping the beach profile. However, berm retreat can be seen in January 2015, on Profiles 1 and 3, though at different times. On Profile 1 it was observed from 20/01/2015 to 24/01/2015, while on Profile 3 it was between 25/01/2015 and 27/01/2015. During the timeframe when Profile 1 experienced berm retreat, the tidal range remained fairly constant, but significant wave heights gradually decreased and were consistently measured at approximately 0.5 m until a small spike (up to just over 1 m) shortly before the profile was taken. The berm retreat on Profile 3 is more easily explained: between 25/01/2015 and 27/02/2015 the tidal range decreased slightly and wave heights remained small and constant.

Other examples of berm roll-over can be seen on Profile 1 in November 2015 (07/11/2015 – 09/11/2015) and January 2016 (06/01/2016 – 18/01/2016), and on Profile 2 in December 2015 (08/12/2014 – 14/12/2015) and January 2016 (06/01/2016 – 25/01/2016).

November 2015 is the only other month to exhibit berm removal. This happens on Profile 1 between 09/11/2015 and 10/11/2015 where waves of approximately 1.5 m were experienced, and again between 12/11/2015 and 17/11/2015, where waves of 1-2 m occurred.

Berm reformation also happens on Profile 2 in December 2015, between 02/12/2015 and 08/12/2015. During this time the tidal range increased and wave height varied between 1-2.5 m, which is perhaps larger than would be expected to create a berm.

The profile response to storms (generally classified as having a peak significant wave height over 3 m at this location) is seen in December 2014 and January 2015 (Appendix A & B). In December 2014, the only profile being measured was Profile 2, which experiences erosion between approximately 15 and 30 m chainage from 11/12/2014 – 12/12/2014 (Appendix A & B), in line with the occurrence of the storm. There were no berms on the profile for the storm waves to remove, however, so this erosion merely creates a more concave profile. Later in the

month, as the wave heights are lower, the profile begins to recover, seen as accretion between approximately 35 and 50 m chainage.

A storm with peak wave heights over 3 m also occurred between profiles taken on 13/01/2015 and 15/01/2015 (Appendix A & B). Profile 1 experienced steepening of the profile, with erosion in the beach below approximately 1.7 m elevation, and accretion above this point. Profile 2 remained almost unchanged, with just a slight flattening near the top of the profile where a small berm had been positioned. Profile 3 experienced a fairly evenly spread amount of erosion across the whole active profile. Profile 3 experienced a significant reduction in volume of the mid and upper beach: 4.9 % of previous volume. This is one of the highest percentage losses for this profile.

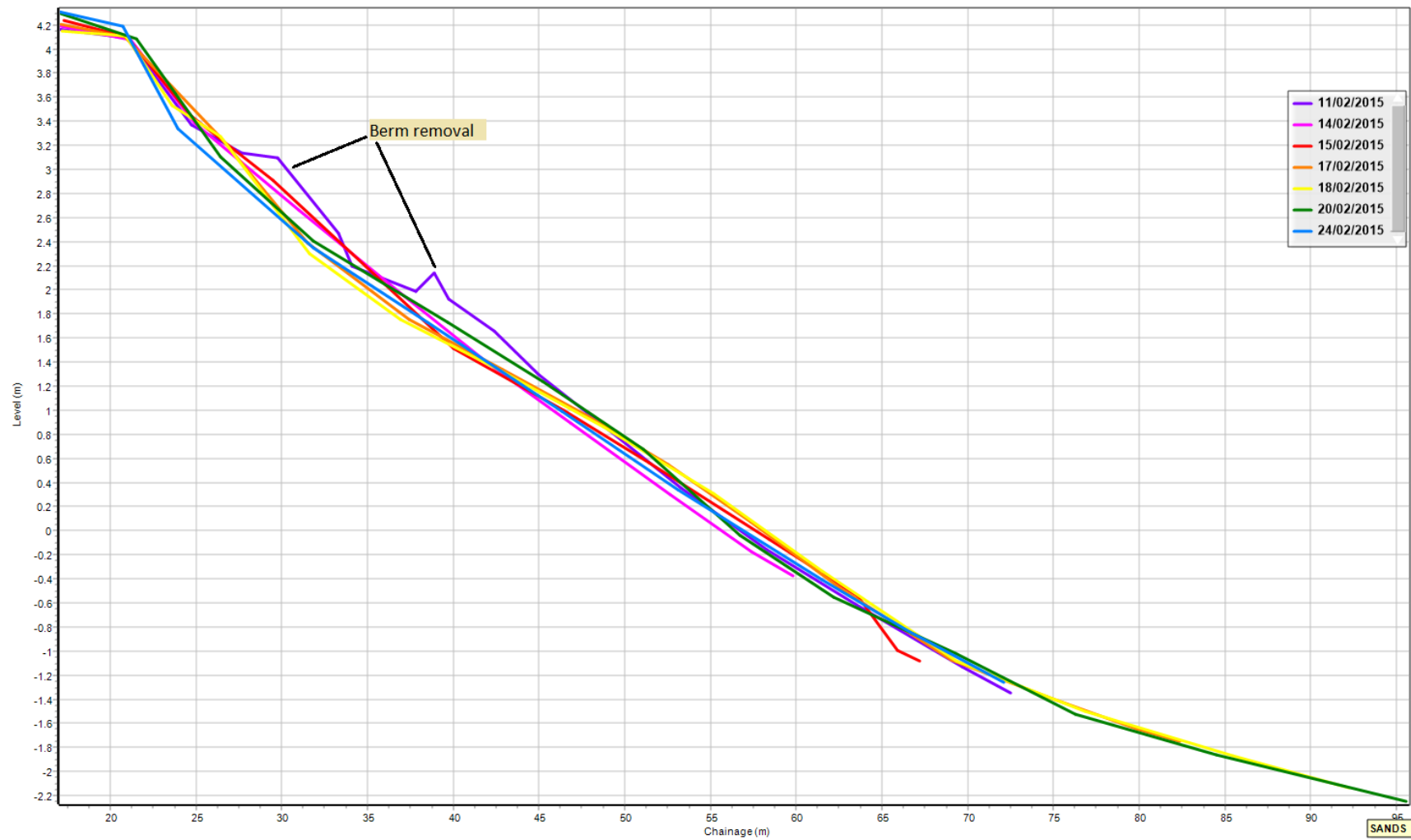


Figure 5.33: Berm removal seen from dGPS profiles measured on Profile 1 during February 2015.

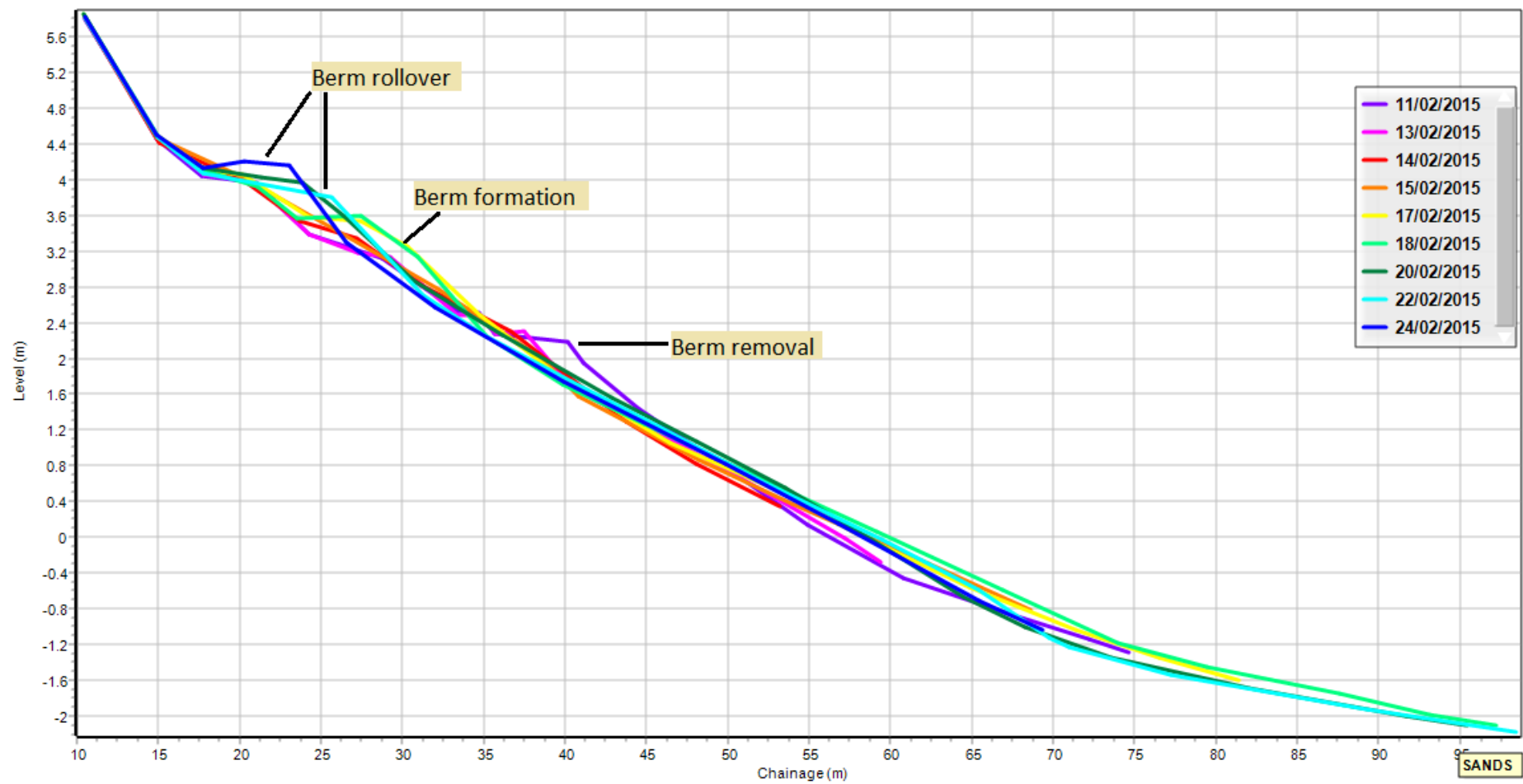


Figure 5.34: Berm removal, formation and rollover seen from dGPS profiles measured on Profile 2 during February 2015.

vii. Using CSA to estimate longshore transport rates

Using profiles to estimate LST volumes can be done using SANDS, where either the CERC (USACE, 1984) or Kamphuis (1991) equations are used. However, this requires inshore wave data. Propagation is a time-consuming process and ideally requires verification from real measurements, so there is no guarantee the inshore wave data would be accurate. Additionally, the groynes at Eastoke are transport limiting, and so the rates calculated using the suggested coefficients for one of these calculations – based solely on grain size and without calibration from measured transport rates – would likely massively over-estimate LST at this site.

Concurrent changes between neighbouring profiles within a groyne bay can be utilised to infer the dominant transport direction. For example, if the CSA of the western-most profile (in this case, Profile 1) increases, while the eastern-most profile (Profile 3) decreases, the assumption is a dominant westwards transport direction. If both profiles decrease, but one much more so than the other, longshore transport is assumed to be towards the less eroded profile. Results produced by visually assessing the differences in CSA do not indicate any sustained periods of drift in either direction, instead suggesting that it switches between east and west very regularly.

These inferred LST directions were compared to the dominant wave direction associated with each set of measurements (Figure 5.35), indicating that though the range of values for eastwards transport is almost exactly what would be expected, westwards transport can be inferred from profile changes under almost any wave directions.

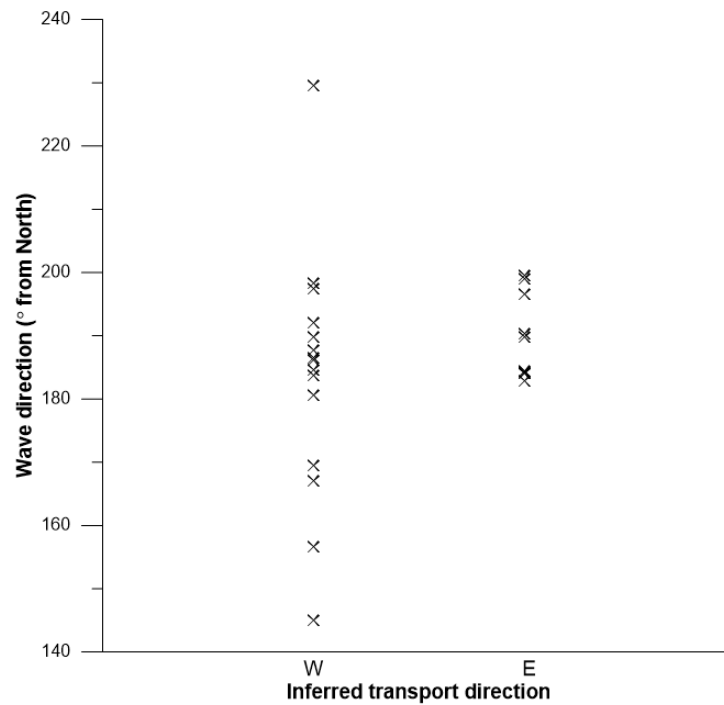


Figure 5.35: Transport directions as inferred from differences in profile changes, compared to dominant wave direction at the time.

It is very difficult to accurately quantify longshore transport rates from profile changes, even within a groyne compartment where the sediment is more restricted than on an open beach and so generally accumulates on the downdrift side of the compartment. Erosion and accretion (cross-shore transport) are also affecting the measured cross-sections. In a perfect world, the increase/decrease would be mirrored on Profiles 1 and 3, indicating no overall change in beach volume and thus all change could be said to be due to LST, but this was only the case on one occasion (18-19/02/2015, $P1 = +0.24 \text{ m}^2$, $P3 = -0.24 \text{ m}^2$). In this case, a crude calculation would allow the change in CSA to be multiplied by the distance between the two profiles (approximately 45 m), to provide a volumetric transport rate of 10.8 m^3 westwards per day.

In more complex cases, determining the change in cross-sectional area by which to multiply the distance was almost impossible, but to provide a level of consistency between measurements, the smaller change value was used – for example, if Profile 1 increase by 0.3 m^2 , but Profile 3 decreased by only 0.12 m^2 , the value for Profile 3 was used and multiplied by the distance between the two profiles. These calculations can be used to give some indication of daily transport rates, but their accuracy is highly questionable. More complex calculations would need to allow for overall accretion or erosion of the beachface, which may significantly alter the actual estimates of transport. There were also multiple occasions when Profile 2

increased in volume despite both Profiles 1 and 3 decreasing, which cannot be explained with this theory.

Figure 5.36 shows the correlation between the calculated values of longshore transport and average longshore wave power during the same time frame; the correlation is not strong. Only two quadrants on the scatterplot should have any points in them – the lower left and upper right – if CSA change were to be reliably linked to wave energy. However, there are plenty of occasions suggesting westward transport under opposing wave conditions. These estimates of sediment transport will be further utilised in Chapter 7.

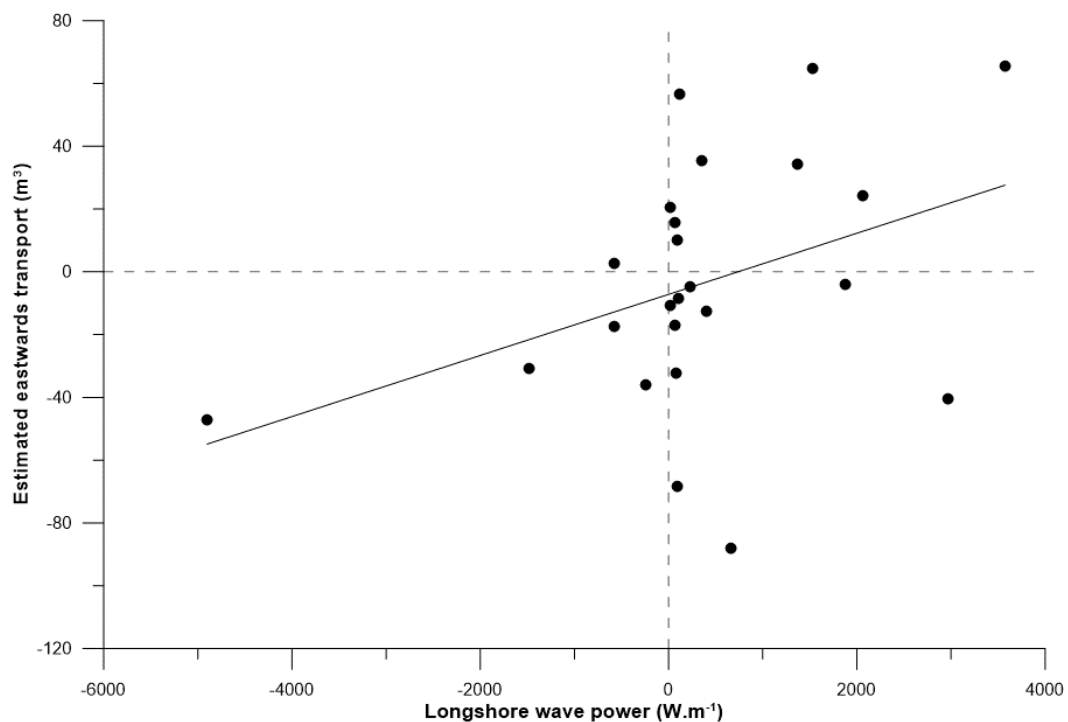


Figure 5.36: Scatterplot of longshore wave power against longshore transport as estimated from profile changes. N=26.

5.3 Discussion

i. Mixed sediment beach characteristics

The beach at Eastoke displays most of the characteristics of a mixed sand and gravel beach, with additional features of a replenished and defended beach also in evidence. It has a steep beach crest, which in this case has been artificially created with rip rap and beach recharge. Beyond the beach crest, the beach slope quickly decreases and becomes more gentle for the majority of the active beachface, with a gradually decreasing slope. There is a gently sloping

sandy low-tide terrace which is generally only exposed on the lowest spring tides. The beach exhibits berms of varying sizes, most commonly at the high water level and in conjunction with swell waves.

It is well-documented that mixed sand and gravel beaches often have well-sorted surface sediments (e.g. Jennings and Shulmeister, 2002; Watt *et al.*, 2008). These sediments are also subject to short term changes; Masselink *et al.* (2010) found changes occur even on a wave-by-wave basis. The sediment is visibly mixed in terms of grain size, and displays some surface sediment sorting, with a general pattern of coarser material in the upper beach and finer material lower on the profile. Additionally, the low number of mixed 'mainly m/l gravel' points indicates that larger gravels are one of the better sorted grain types as they are more often found alone. However, this could also just be because this is rarely the dominant grain size. Overall the sorting was not definitive, likely because this is an artificial mixed beach.

It must also be noted that especially on Profile 3, the beach crest is marked by a dominance of sand. This is common on replenished beaches (Horn and Walton, 2007), where the crest is designed to be high enough that it is not reached by waves or tides except in very extreme events, so the fine sediment is not filtered out. This can lead to compaction – particularly at Eastoke, where heavy trucks drive along the beach crest to deliver sediment further along the coast during recycling operations – which then makes cliffing more likely when waves do start to erode or change the shape of the profile directly below the beach crest (Figure 5.37).



Figure 5.37: Cliffing at the crest of Profile 3, 24/02/2015.

Most of the time there is no clear separation between the coarse upper beach and the sandy lower beach. This agrees with previous research by Costa *et al.* (2008), who indicate that this boundary is fairly mobile. It has been reported that replenished mixed beaches experience more complicated patterns of sediment distribution than their natural counterparts

(Dornbusch *et al.*, 2008). This may be an explanation for the lack of continuity between surface sediment sorting patterns experienced during the first winter of this study.

Sediment sorting and cusp formation are intrinsically linked, though it is still unclear whether one is caused by the other. It seems more likely that a feedback loop exists, whereby the beginnings of a cusp cause preferential deposition of larger grain sizes, which in turn increases the size of the cusps (Coco *et al.*, 2000). Cusps are also likely to be related to instances where the maximum level change on the profile occurs lower on the beach profile, as they represent a significant morphological change (Bird, 2008).



Figure 5.38: Cusps in the mid-beach portion of the profile. 16/12/2014.

Patterns of day-to-day surface sediment change were investigated to determine whether Costa *et al.*'s (2008) observations – that sand moves onshore during moderate swells and offshore during storm events – could be seen at Eastoke. First, the wave data (Appendix A) was inspected to find time periods when these changes were most likely to occur.

The consistent calm conditions during March 2015 would seem to be an ideal time to investigate the claim that the surface would contain a higher proportion of sand during moderate swells. There is some evidence to suggest that sand is more dominant higher up the profile during March 2015, but due to the limitations of using a sediment coding system, it is not possible to be conclusive about this; there may well be a higher proportion of sand, but it would still be coded as 'MS', and thus appears the same when viewing the results.

The stormy conditions which occurred at the beginning of the study period in February 2015 should, according to Costa *et al.* (2008), have led to a decrease in sand on the profile, which may be expressed in the results as an increase in larger particles. It does appear that there is more small gravel lower on Profile 2 after these waves (Figure 5.39), but this could be related to the removal of the upper berm and subsequent spreading out of this sediment across a wider area of the beach face. By 14/02/2015, Profile 1 has more sand higher up the profile, while Profiles 2 and 3 have a similar distribution of codes to 11/02/2015.



Figure 5.39: Surface sediment codes on A) 11/02/2015, and B) 13/02/2015. Aerial imagery courtesy CCO, 2016.

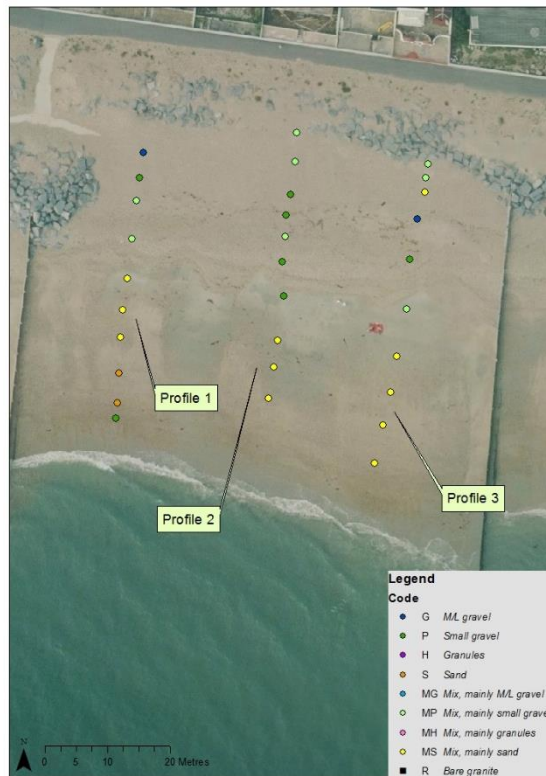


Figure 5.40: Surface sediment codes on 14/02/2015. Aerial imagery courtesy CCO, 2016.

ii. Profile Types

Of the ten profile types identified by Caldwell and Williams (1985) (Chapter 4.4.iv), concave and linear shapes with an upper berm were most common overall, with LUB dominating both Profile 1 and 2. This trend was not consistent across the three profiles though; Profile 3 did not ever display a profile categorised as LUB and was generally much less likely to have a berm of any kind. This identifies a significant difference in morphology related to placement of profile line within the groyne compartment.

The dominance of CCNB on Profile 3 under easterly waves, while Profile 1 experienced a dominance of ‘upper berm’ codes during these same waves theoretically makes sense. Easterly waves should be causing westwards transport, away from Profile 3 and onto Profile 1.

Issues do arise with categorising profiles in this way when cusps are considered. Depending on where in the groyne cell a profile is measured, it may pass over the horn or trough of a cusp, providing different profile shapes. Cusps were observed to exist periodically on this beach, potentially playing an important role both in profile shape and surface sediment distributions.

iii. Profile changes

Medium term profile changes and variation within the groyne compartment did not appear to be correlated with dominant wave direction.

In general, larger wave heights were linked with greater changes in cross-sectional area, but a predictive relationship could not be produced. The cross-sectional areas covered only the upper and mid sections of the beach, and so may be over- or under-estimating actual profile changes; erosion from one area can often be balanced out, at least partially, by accretion in another area (Theuerkauf and Rodriguez, 2012).

When inspecting the daily profile graphs (Appendix B) for morphological changes, most of the changes relate to berm building, agreeing with results by Curoy *et al.* (2009) and Austin and Masselink (2006), and are easily explained by wave and tide action. However, the size of the change does not always directly correlate with wave height, tidal range or a combination of the two. Though relationships can be seen for maximum profile change in relation to maximum wave height, these correlations are more or less symmetrical when comparing positive and negative change values. Thus, it would not be possible to use them to predict whether the change could be expected to be positive or negative, only its approximate magnitude.

The groynes clearly have an impact on beach profiles, as Curoy (2012) found little variation between profiles along an unmanaged section of mixed sand and beach, but at Eastoke there are significant differences between the shapes and dynamics of neighbouring profiles. But separating profiles and investigating based on dominant wave direction did not provide an explanation for the lack of correlation between erosion and accretion.

Carter (1989) indicates that the beach within each groyne cell will align towards the predominant wave direction. While this does appear to happen at Eastoke, it does not seem to create the 'equilibrium' state which he suggests it can; if the beach were in 'equilibrium' it would be much less dynamic, especially under moderate wave energies. The lack of equilibrium states on mixed sediment beaches is also a generally accepted piece of knowledge (Woodroffe, 2003), especially on replenished beaches, where the profiles and sediments are continuously adjusting from an original 'design' profile (James, 1974; Dornbusch, 2017).

Groynes have been shown to cause rip currents during storms, which allow sediment to be dragged offshore. This is likely to alter profiles in some parts of the groyne cell (i.e. those closest to the groynes) more than others. It was not possible to measure the currents in the

vicinity of the groynes here, but considering the scale of the defences at this beach, it would be almost impossible for them not to have some effect on wave and current directions and speeds.

Results do not agree with Kroon and Masselink's (2002) theory that wave action has a greater impact when the tidal range is reduced. It is possible that the lack of relationship is caused by preceding profile shape, which may limit the potential influence that waves of a given height would exert on the beach anyway, thus decreasing the impact that a slower moving tide might have. It is also possible that the variations in tidal range are too small to produce noticeable differences at this site.

iii. Berm dynamics

All four aspects of berm development were displayed at one time or another across the three profiles, but Profile 3 was much less likely to experience any of these processes, as upper berms were infrequently observed on this profile. In most instances it was possible to associate berm removal and re-building events with the wave climate, and berm roll-over and retreat with tidal range; this is to be expected (Austin and Masselink, 2006). However, the process of berm retreat did not always occur as the tide transitioned from springs towards neaps. It is possible for the berm to become stranded above the extent of wave run-up, until either spring tides occur once more or larger waves come and increase the run-up height on the beach profile.

There was a surprising lack of berm growth during March 2015. The waves were generally between 0.5-1 m in height, so according to Mason and Hanson (1989), who suggested change occurs with waves over 0.5 m in height, this should be enough to induce morphological change. This is possibly a case in which the berm had become stranded and so further wave action did not reach it and thus did not build on it. However, if this were the case, a second smaller berm might be expected to form slightly lower on the profile, and this does not occur on any of the three measured profiles.

5.4 Conclusions

There was a broad overall correlation between physical sediment samples and surface codes, but the codes cannot realistically represent the full sediment composition of a location. If suitable codes for a particular beach are used, the system can provide a broad overview of sediment composition and surface changes. Surface coding systems are perhaps better suited

to more natural mixed beaches, where sorting is more uniform and so fewer 'mixed' points would be expected. At this site, the coding system indicated sorting patterns which conflict with Dornbusch *et al.* (2008)'s theory that the coarsest sediment would be found in the upper corner on the accumulating side of the groyne; this was attributed mainly to the fine material within replenishment sediments, which had not been sorted out by wave action.

Profile shape and volume within the groyne compartment are highly variable, as is to be expected for a mixed sediment beach over this timeframe. Overall, however, the volume of the upper beach remained similar on a seasonal basis, indicating that the management practices here are working and the beach recovers sediment onto the upper profile during calmer summer months.

The research question for this chapter was "Do beach profiles provide an accurate representation of longshore sediment transport on groyned beaches?"

Profile changes and variations between profiles within the groyne compartment were not found to correlate well with longshore wave power, indicating that this method for calculating transport volumes is inaccurate. Chapter 7 discusses this further.

Only approximately half of the active profile was included in the cross-sectional areas; it is possible that surveys which extended into the water would have dulled the effects of cross-shore transport and thus provided a clearer view of longshore transport within the groyne. This would still not necessarily provide an accurate representation of longshore transport for the whole beach, however, as changes within the groyne compartment may appear larger and thus produce greater transport volumes than the beach as a whole is experiencing, as the groynes limit longshore transport.

Regular small-scale changes are relatively unpredictable. Infrequent surveys are not capturing all the details of these changes, and thus may be wildly inaccurate as an indicator of seasonal changes in beach volume. On decadal timescales as markers of overall shoreline position and larger scale changes these inaccuracies become less relevant and so surveys are more useful. It must also be considered that the profile lines surveyed by HBC extend beyond low water level, so as long as the sediment has not moved fully out of the reach of waves it will still be included in the volume, which increases seasonal accuracy. New surveys often make use of laser scanning, as this can provide a better overview of morphological patterns within the cell (Dornbusch, 2010), but the downside to this technique is that it cannot be extended beyond low water level.

6. Active layer dynamics

6.1 Introduction

This chapter describes results of measurement of the depth and width of the active layer at Eastoke during a total of nine study periods between October 2014 and January 2016. It addresses the main aim of the thesis by providing a large and varied dataset of active layer (AL) measurements and attempting to determine which factors are most important in being able to accurately predict AL depth.

Knowing the active layer depth and width is essential in calculating longshore sediment transport volumes (Lee *et al.*, 2000). Understanding how and why the active layer changes, based on accurate field data, also enables more accurate predictions of LST volumes to be made.

The aims are to determine whether relationships exist between these measurements of active layer depth and the hydrodynamic conditions – wave height, period and direction – the influence of sediment composition and beach slope, and investigate longshore and cross-shore variations, with an overall intention of determining the relative influences of each of these factors on AL depth in order to more accurately predict it.

The main research question to be answered in this chapter is:

How is the active layer on this mixed sand and gravel beach linked to:

- a. Wave conditions*
- b. Beach slope*
- c. Sediment composition*

As a reminder, the objectives for this, as laid out in the Introduction chapter were:

- To measure variations in active layer depth at a high resolution for a longer period of time than has previously been published,
- To confirm preliminary research that a predictive relationship between active layer depth and wave height can be established for mixed sediment beaches,
- To statistically relate any further variations in active layer depth to location on the profile, sediment composition, and/or beach slope.

While data of this sort has been relatively well-researched for decades on sand beaches (e.g. Williams, 1971; Greenwood and Hale, 1980; Sunamara and Kraus, 1985; Jackson and Nordstrom, 1993; Anfuso, 2000; Bosnic *et al.*, 2011), similar data for mixed sediment beaches has only more recently been collected (e.g. Whitcombe, 1996; Roman Blanco, 2003; Saini *et al.*, 2009; Curoy *et al.*, 2009; Miller and Warrick, 2012). Variations in active layer depth have previously been attributed to different wave conditions (e.g. Sunamara and Kraus, 1985; Bertin *et al.*, 2008), sediment size (King, 1951), beach slope angle (Williams, 1971; Jackson and Nordstrom, 1993; Ciavola *et al.*, 1997; Ferreira *et al.*, 2000; Anfuso, 2005)), and position of the wave breaking zone (Williams, 1971; Kraus, 1985; Aagaard *et al.*, 2012). Mixed sediment beaches are complex, and the current site is further complicated by the presence of groynes and riprap, and regular sediment recycling. The results presented here are more detailed and taken over a longer time period than any other available published research on sand or mixed sediment beaches of which the author is aware, allowing for more accurate and reliable interpretations to be made about correlations and their causes.

6.2 Methods

Full descriptions and justifications for the methods chosen can be found in Chapter 4, along with maps of the field area, locations of measurements, and timings of field periods.

To recap, sliding indicator devices (SIDs) were used for most AL measurements. These were based on devices used by DeVries (2002) in gravel-bedded rivers, and the current project is the first major use of this technique on mixed sand and gravel beaches.

Depth of disturbance rods were used for a total of 18 measurements to capture data from the lower beach, which had high groundwater levels that were not conducive to successful burial of SIDs. These rods experienced much higher rates of failure than SIDs, and because they represent only the sandy lower portion of the beach are considered separately in section 6.3.vi.

Wave data was taken from the CCO Wave Rider buoy located in 10 m water depth approximately 5 km due south of the field site. The Wave Rider outputs values in 30-minute time periods which have then been converted into daily averages of significant wave height and other properties, in order to correspond with active layer measurements. If, for example, the SIDs were deployed during a low tide at 10 am on one day, and then retrieved during low tide the following day (after 2 full tides, due to the semidiurnal tidal cycle experienced at this

location), then all 30-minute periods of significant wave height between these two times would be used to calculate the mean average significant wave height for this day (Chapter 4.3).

Data were sub-set both spatially and temporally to investigate possible patterns and relationships between AL depth and other variables. In the following results section, data will be analysed broadly in terms of the relationship between AL depth and wave conditions, and sub-set under each of these to determine whether patterns exist at different temporal or spatial scales.

6.3 Results

i. Variation in AL depth

Unless otherwise specified, the following sections discuss only results obtained from the SIDs, which were located on the mixed sediment portion of the beach and thus do not include the sandy lower beach/foreshore, which is considered separately in Section 6.3.vi. In total, 555 measurements of the active layer depth were taken using SIDs on the mixed sand and gravel beach (as described in Chapter 4.5); this excludes devices which were located above the maximum run-up height on any given day. General variations will be described first, and later sections will consider patterns by sub-setting the data according to factors such as wave conditions, location, beach morphology and sediment.

Measured values of the active layer depth on the mixed sediment beach range from 4.2 to 37.8 cm. There was one measurement of 42 cm on 3rd October 2014, but none of the other values this day was greater than 16.8 cm so this value has been excluded from all calculations on the basis that the chain may have been tampered with by a member of the general public; it was close to the beginning of the study, and from personal experience this seems likely.

Figure 6.1 provides an indication of the variation in measurements – overlap exists where multiple points of the same value were measured on a particular day, so this graph does not necessarily show every measurement. A full database of AL measurements can be seen in Appendix F.i, with locations for each of the SIDs in Appendix F.ii. There are significant spatial and temporal variations within the data.

The mean value of the remaining 554 measurements is 14.7 cm, with a median of 12.6 cm and a standard deviation of 7.1 cm. The highest frequency of measurements falls between 12 – 16 cm (Figure 6.2). The measurements do not follow a normal distribution due to a positive

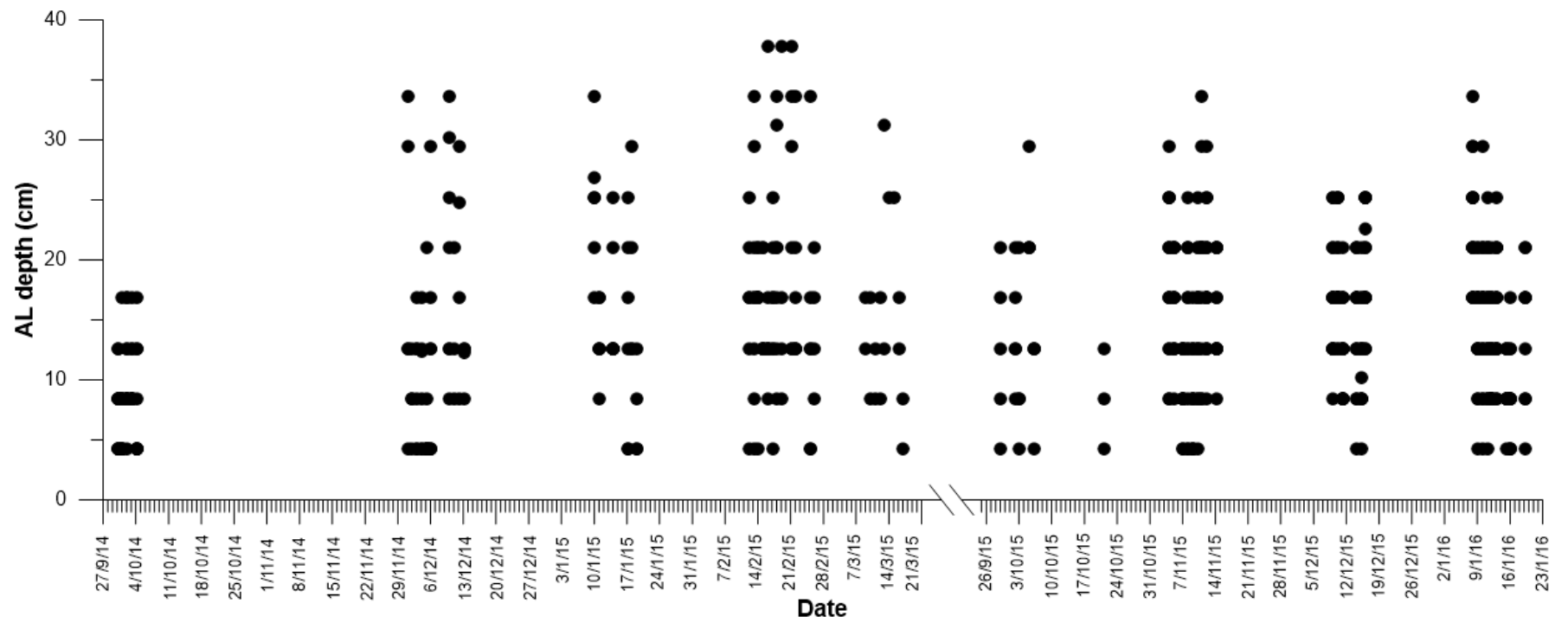


Figure 6.1: Active layer depth measurements by day. N=554.

skewness of 0.631 (standard error = 0.104). Additionally, a Shapiro-Wilk test provides a p-value of $p < 0.001$, thus indicating a non-normal distribution.

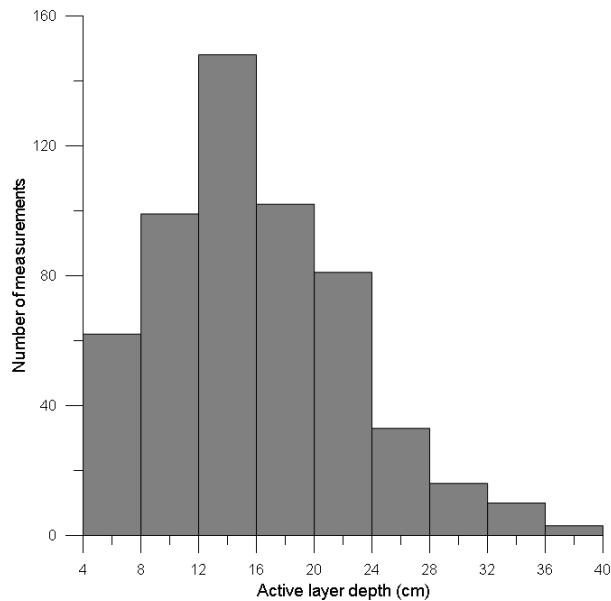


Figure 6.2: Histogram showing frequency of occurrences of measured AL depths on the mixed sediment beach. N=554.

Investigating AL data at a daily scale has been common practice in other studies, some of which have investigated AL depth only over a single tide (e.g. Ciavola *et al.*, 1997). Figure 6.3 provides an overview of the mean and maximum measurement for each day, as well as the standard deviation of that day's measurements. Appendix G provides separate graphs of each of the study periods. These data are averaged across all profiles where applicable; separated profiles will be considered later in Section 6.3.i.a. Data from March 2015 are not included in Figure 6.3 because each day had too few AL measurements to allow for calculation of reliable or representative average values. The shortest fieldwork period was during October 2014, where only 5 consecutive days of measurement occurred. This was due to equipment tampering by members of the public. The greatest range of mean values exist in January 2015, but a relatively broad spectrum of AL depths was measured in each field period (Figure 6.2).

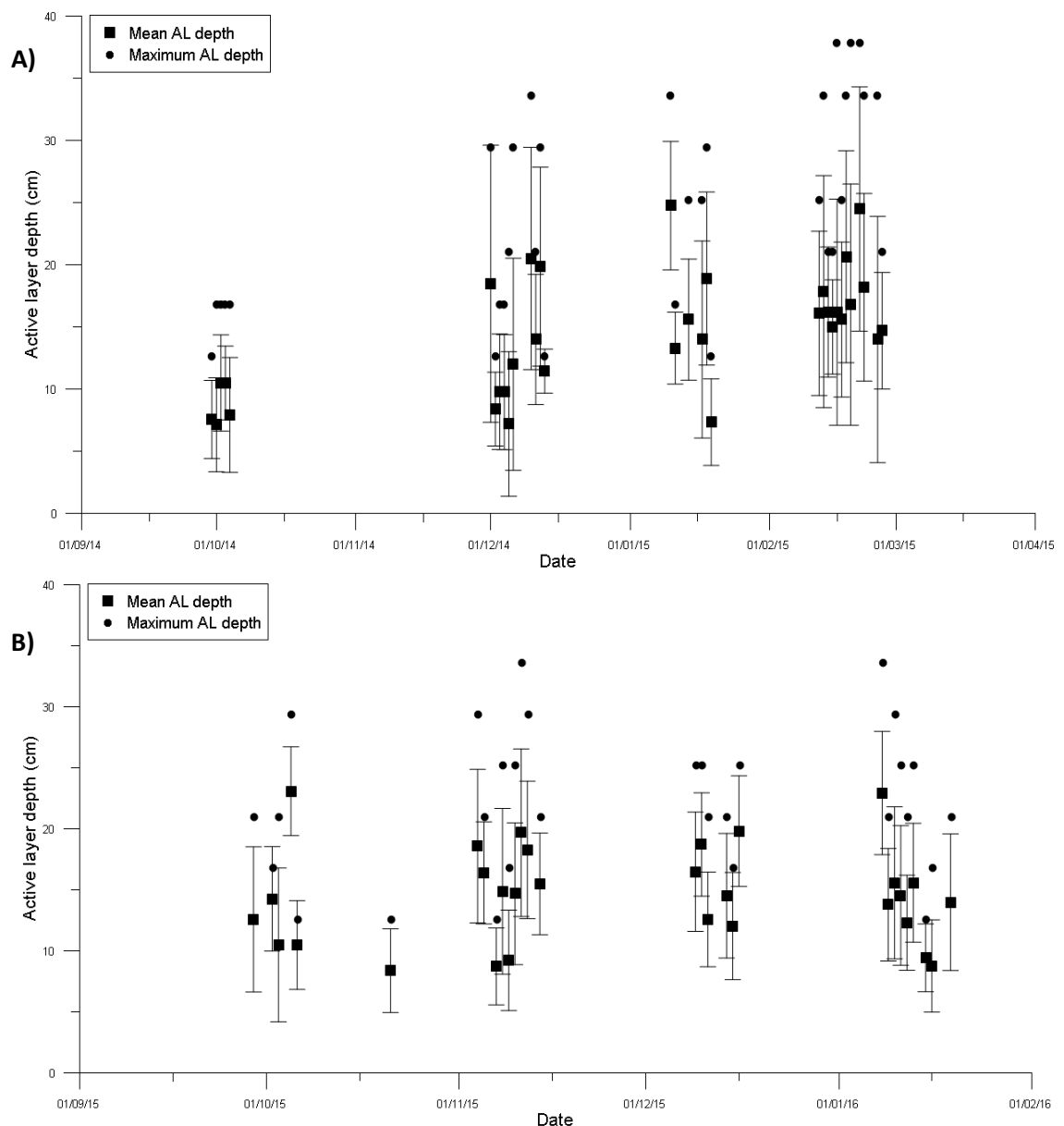


Figure 6.3: Mean and maximum daily AL depth measurements on each day studied during A) Winter 2014-15 (n=33) and B) Winter 2015-16 (n=30). Bars represent one standard deviation from the mean.

Another common way for AL data to be presented has been as a value or range of values over study period (e.g. King, 1951; Jackson and Nordstrom, 1993; Anfuso *et al.*, 2005). Since many of the previous studies have been only a few days in length, each of the study periods here can be considered separately (Figure 6.4). Apart from October 2014, all study periods have broadly similar results: means between 13 cm and 17 cm, maximums between 25.2 cm and 37.8 cm, standard deviations between 6.3 cm and 8.4 cm. During the October 2014 field period measurements were smaller: the mean was 8.7 cm, the maximum was 16.8 cm, and the standard deviation was 4 cm. There is a trend of increasing mean AL depth from October 2014 to February 2015, which is not apparent during the following winter.

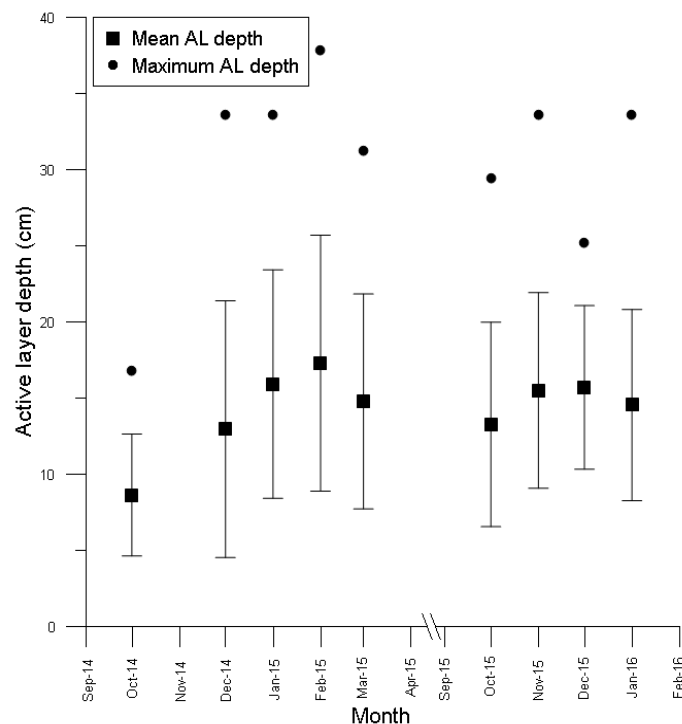


Figure 6.4: Variation in mean and maximum values of AL depth on the mixed sediment beach for each study period. Bars represent one standard deviation from the mean.

a. Alongshore

Few authors seem to have investigated whether variation exists in active layer measurements alongshore. Those that have investigated this parameter have usually found minimal alongshore variation in active layer depth for points at the same location on neighbouring profiles (e.g. Curoy, 2012). However, these results were from open, uninterrupted stretches of beach; Eastoke has regular groynes (approximately every 60 m), and thus offers an opportunity to investigate whether distance from the groyne has an influence on AL depth.

Data from Winter 2015-16 were investigated for any potential variation between profiles (Table 6.1, Figure 6.5). A one-way ANOVA test was run to compare the means of measurements from each of the three profiles. The data must meet certain assumptions to allow this test to be run with any level of confidence. The data contain no outliers, and despite being non-normally distributed each group had a similar sample size and skewness, so this should not affect the robustness of the test. A Levene's test for equality of variances indicates that the assumption of homogeneity of variances is met ($p = 0.207$). Thus, the final result of the ANOVA test indicates that there is no statistically significant difference between the means of the three measured profiles during Winter 2015-16 ($F(2, 300) = 1.771, p = 0.172$).

Table 6.1: Mean AL depth and standard deviations for the 3 measured profiles, November 2015 - January 2016.

	Mean AL depth (cm)	Standard Deviation
Profile 1	14.5	5.7
Profile 2	15.1	6.6
Profile 3	16.1	6.1

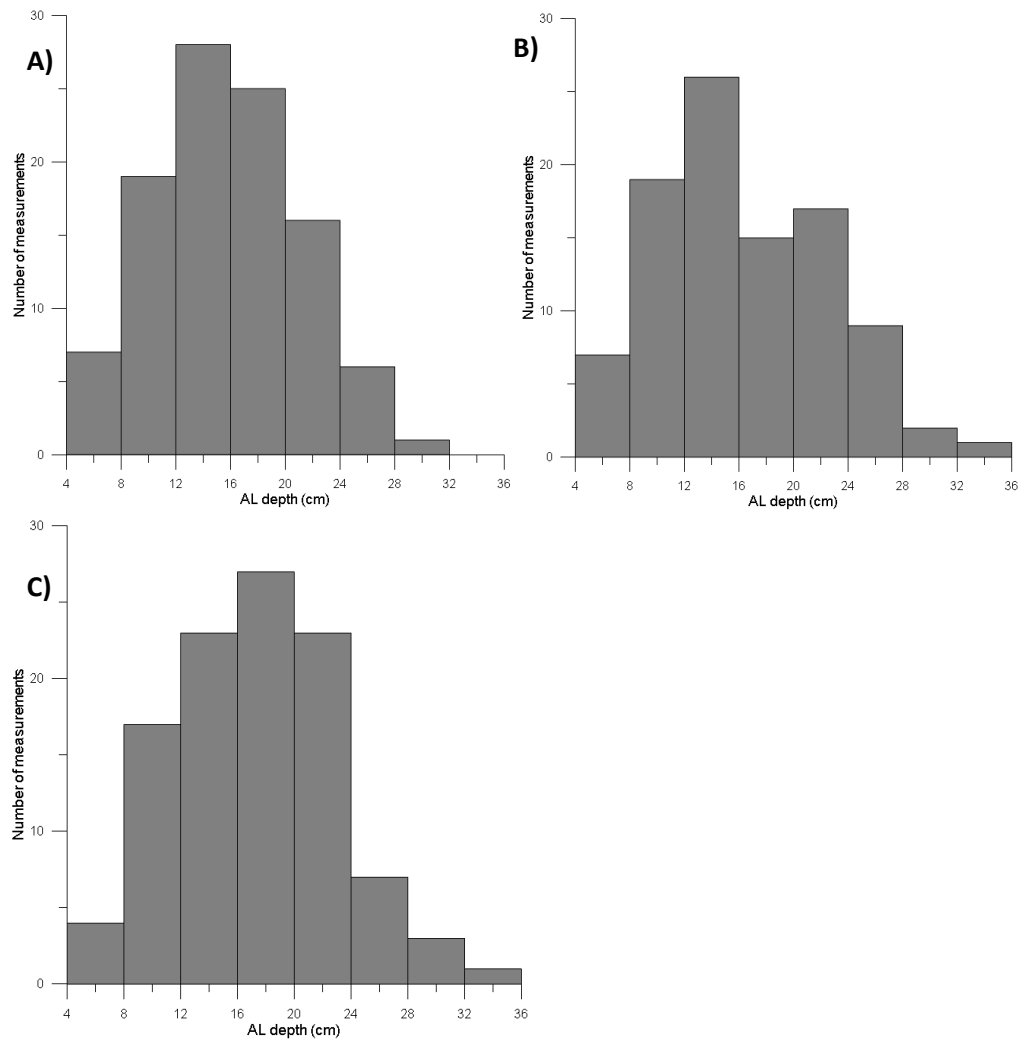


Figure 6.5: Frequency histograms of AL depth measurements for A) Profile 1, B) Profile 2, and C) Profile 3.

Figure 6.6 indicates that the variations between profile lines were not consistent across all months. In November 2015, the mean active layer depth increased slightly between profiles 1 to 3, while the maximum increased more drastically. In December 2015, the maximum values were broadly similar, yet the mean for profile 2 was much lower than the others. In January 2016, all three profile lines displayed approximately equal active layer depths, with only slight variation in the standard deviation and a higher maximum value on the central profile (Profile 2). These variations are discussed in relation to wave direction in section 6.3.ii.

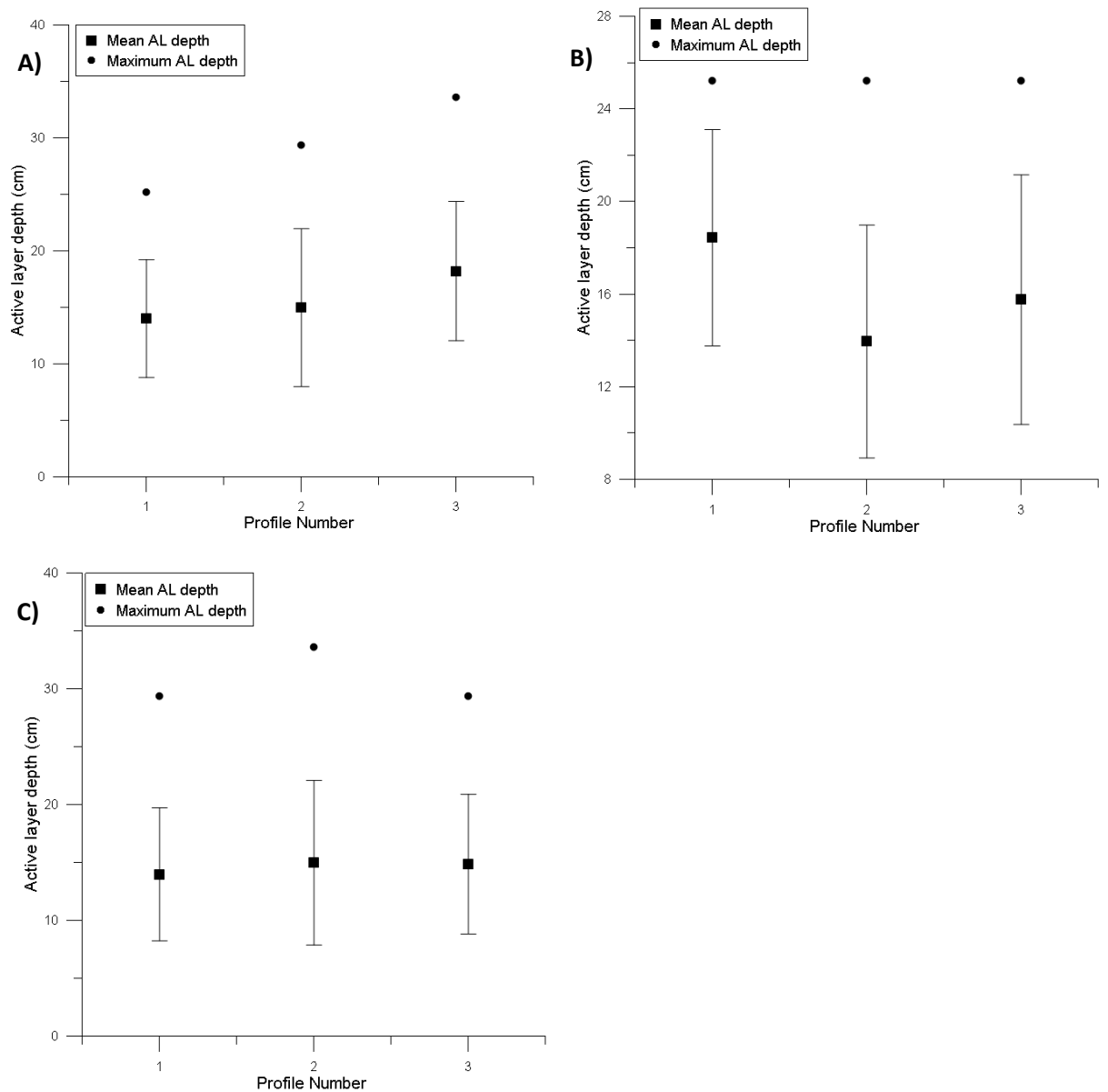


Figure 6.6: Variation in mean and maximum active layer measurements on three profile lines measured in A) November 2015, B) December 2015, and C) January 2016. Bars represent one standard deviation from the mean.

b. Across shore

It is generally accepted that active layer depth varies cross-shore, on both sand beaches (e.g. King, 1951, Williams, 1971) and mixed sediment beaches (e.g. Curoy, 2012), but it is important to determine whether the relationship here is obvious too. Site observations indicated a high groundwater level, which decreases hydraulic conductivity (Blanco, 2003), so it is expected that AL measurements in the lower part of the beach will be smaller due to the reduced ability of waves to infiltrate the beachface.

Using dGPS measurements taken at the location of each active layer measurement point, it is possible to assess how active layer depth differs depending on elevation. Figure 6.7 shows that to some extent the AL depth is more variable in the middle of the profile but does not indicate a relationship between elevation and AL depth. Further analysis of this relationship will be discussed in relation to wave conditions in later sections.

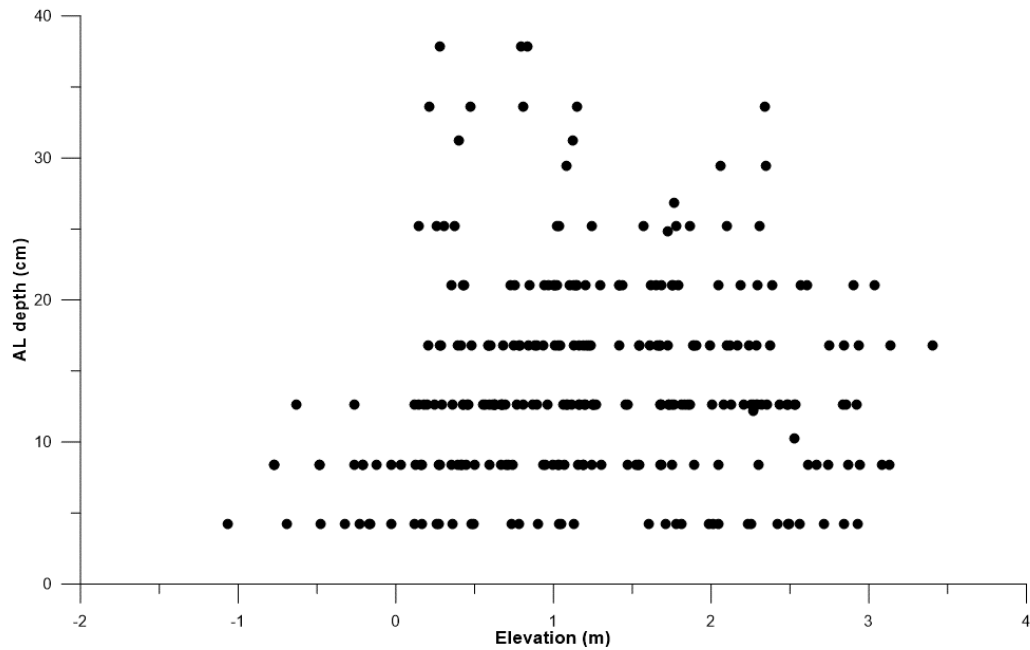


Figure 6.7: Active layer depth based on elevation of the beach surface at SID location. N=275.

The elevations were separated arbitrarily into upper (> 2 m), middle ($0.5 - 2$ m), and lower (< 0.5 m) beach areas. The average AL depth in the middle is higher than for the upper and lower beach, though the lower beach has a higher standard deviation of measurements than the other two areas (Table 6.2).

Table 6.2: Means and standard deviations of AL measurements within upper, middle and lower sections of the beach

	Upper (> 2 m) n=64	Middle ($0.5 - 2$ m) n=146	Lower (< 0.5 m) n=65
Mean AL depth (cm)	13.54	15.07	12.24
Standard Deviation	6.81	6.72	8.06

Measurements on the mid-section of the beach outnumber the upper and lower beach by far, and follow a slightly more normal distribution, though all three areas are positively skewed

(Figure 6.8). A Kruskal-Wallis test was run, which determined that the distributions of AL depths were statistically significantly different between groups, $\chi^2(2) = 12.855$, $p = 0.002$. A post-hoc pairwise comparison (using Dunn's (1964) procedure with a Bonferroni correction for multiple comparisons) revealed that a statistically significant difference exists between mean ranks of the lower (110.7) and mid beach (152.04) ($p = 0.001$), but not between the lower and upper (133.7) ($p = 0.284$), or mid and upper beach ($p = 0.351$).

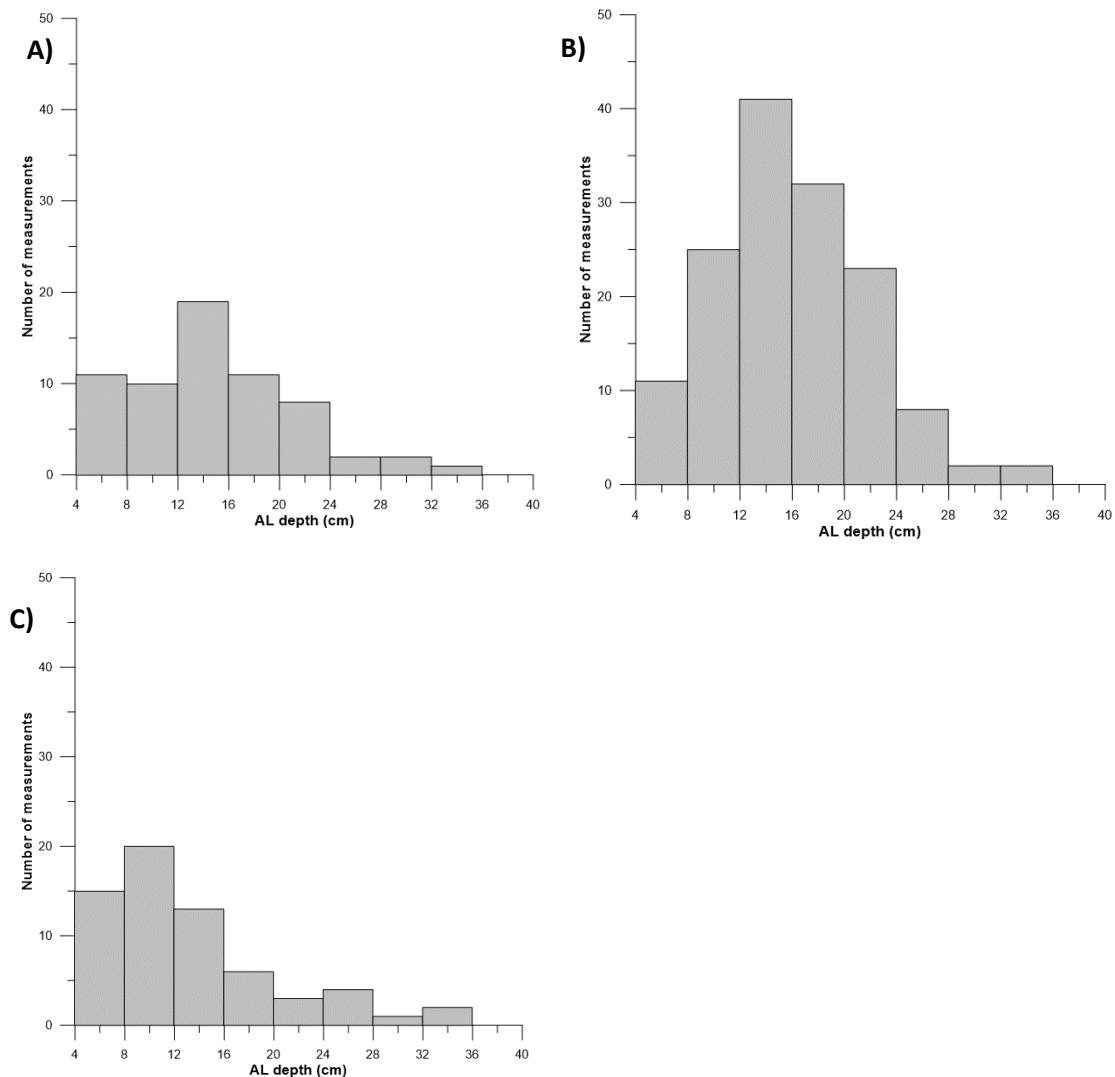


Figure 6.8: Histograms indicating frequency of AL depths measured on A) the upper beach, B) the mid beach and C) the lower beach.

Separating the measurements into arbitrary upper, middle and lower sections does not really draw out definitive patterns, so measurements were also split into elevation bins of 1 m each. Table 6.3 contains the means and standard deviations for each of these sections. The beach below 0 m OD has an average of approximately half that of each of the other elevation bins, which all have broadly similar means and standard deviations.

Table 6.3: Means and standard deviations of AL measurements within 1 m elevation bins.

	< 0 m	0 – 1 m	1 – 2 m	2 – 3 m	> 3 m
Average AL depth (cm)	7.07	14.52	15.26	13.48	14.28
Standard Deviation	2.74	7.89	6.48	6.93	5.04

c. By area within the groyne

Due to the likely influence of the groynes at this site, an attempt to determine the patterns between a combination of long- and cross-shore position is necessary. In order to determine whether relationships with wave conditions became more consistent within smaller areas of measurement, the main groyne bay was split into 9 approximately equally sized boxes (Figure 6.9). This means that some compartments had a higher number of measurements within them, but this is more representative than attempting to split the measurements evenly between sections.

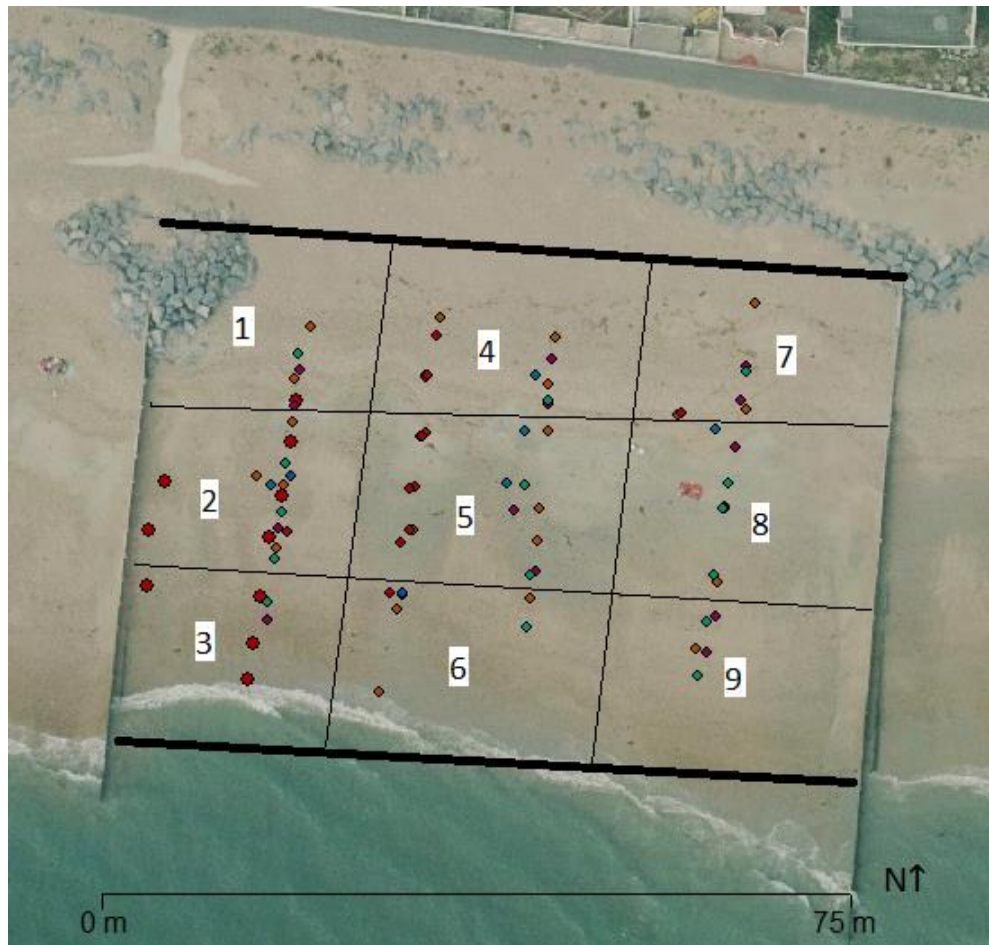


Figure 6.9: Separation of groyne compartment into nine sections. Aerial imagery courtesy CCO, 2016.

Table 6.4: Minimum, mean and maximum AL depths for each of the 9 sections within the main groyne compartment.

Section	N	Minimum AL depth (cm)	Mean AL depth (cm)	Maximum AL depth (cm)
1	33	4.2	15.78	25.2
2	100	4.2	15.47	37.8
3	27	4.2	8.24	16.8
4	61	4.2	15.37	33.6
5	126	4.2	15.34	33.6
6	56	4.2	14.43	37.8
7	29	4.2	12.55	25.2
8	65	4.2	17.90	33.6
9	32	4.2	12.86	21

Not all sections contained SIDs during each field period, so variations in wave climates experienced between field periods could explain the differences – for example the much lower mean and maximum values for section 3 compared to the others (Table 6.4). This possibility will be discussed further in later sections.

d. By sediment composition

Previous studies have been inconclusive about the role of sediment size and composition on active layer depth, with some authors (e.g. King, 1951) finding a link between sediment size and active layer depth, and others (e.g. Williams, 1971; Saini *et al.*, 2009) finding no such correlation. Sediment composition can fluctuate significantly on a mixed sediment beach, and thus may be a vital contributing factor to AL depth at Eastoke. Samples were taken from the active layer across the beach face on multiple occasions, then dried, sieved and weighed (Chapter 4.6). In accordance with a time-saving methodology for sampling gravel beaches produced by BAR (2005) and later used by Horn and Walton (2007), multiple smaller samples (2-5 kg each) were taken on each day (dates of samples can be seen in Chapter 4.2). During the first winter, sediment samples were taken from the active layer at the exact locations where SIDs were located, in order to assess the level of the relationship between sediment composition and active layer depth at a high spatial resolution.

Because of its importance to the hydraulic conductivity and profile response of a mixed sediment beach (Mason and Coates, 2001), the percentage of sand in a sample is used as an indicator of sediment composition, similar to Curoy (2012). This was done by totalling the weight of sediment smaller than 1 mm (Chapter 4.5) and calculating its proportion of the whole sample. The median grain size, or D_{50} , for each sample was then estimated using

cumulative frequency graphs. Sediment on the surface of mixed sediment beaches can change rapidly, even under relatively small amounts of wave action. For this reason, active layer measurements were correlated with sand content and D_{50} of sediment samples taken at both the beginning and the end of the two-tide cycle on which active layer depth was measured (Table 6.5; Figure 6.10). This allowed for any difference in the relationships to be investigated; the strongest relationship exists when sand content from before the AL measurement is used, but this relationship is still only weak to moderate.

Neither sand content nor D_{50} is a good predictor of AL depth at this scale (Figure 6.10). Both will be considered in relation to wave conditions in later sections, but due to the importance of proportional sand content within a mixed sediment beach, this is the statistic which was used to analyse the relationship between sediment and AL depth at a broader scale.

Table 6.5: Pearson's correlations for different combinations of sediment descriptors and measurement timings.

	Start of AL measurement (n=30)	End of AL measurement (n=32)
Sand content	-0.336	0.022
D_{50}	0.168	-0.159

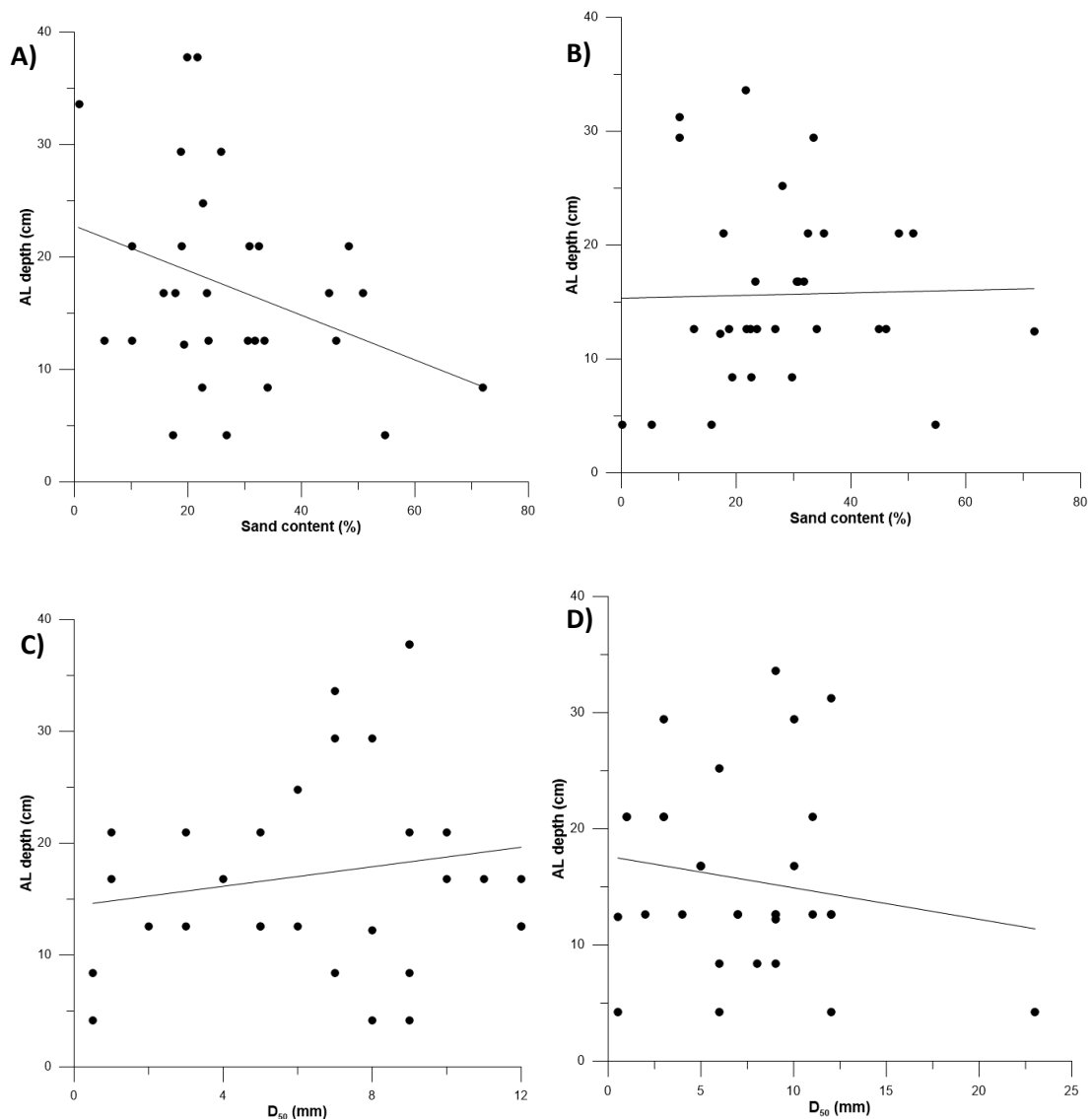


Figure 6.10: Scatterplots showing relationships between sediment composition and AL depth. A) Sand content of samples taken before AL measurement, B) Sand content of samples taken after AL measurement, C) D₅₀ of samples taken before AL measurement, D) D₅₀ of samples taken after AL measurement.

Figure 6.11 indicates the relationship between daily average AL depth and the average sand content of samples taken either at the start (A) or end (B) of the AL measuring period. The relationship is much stronger when samples from the end of the measurement period are used. This relationship is strengthened further when the two winters are considered separately (Figure 6.12), with a much stronger relationship apparent during the second winter. This is likely due to the slightly altered sampling technique (Chapter 4.5), which meant that the average of all samples was more generally representative of the beach face but could not be associated with individual AL measurements.

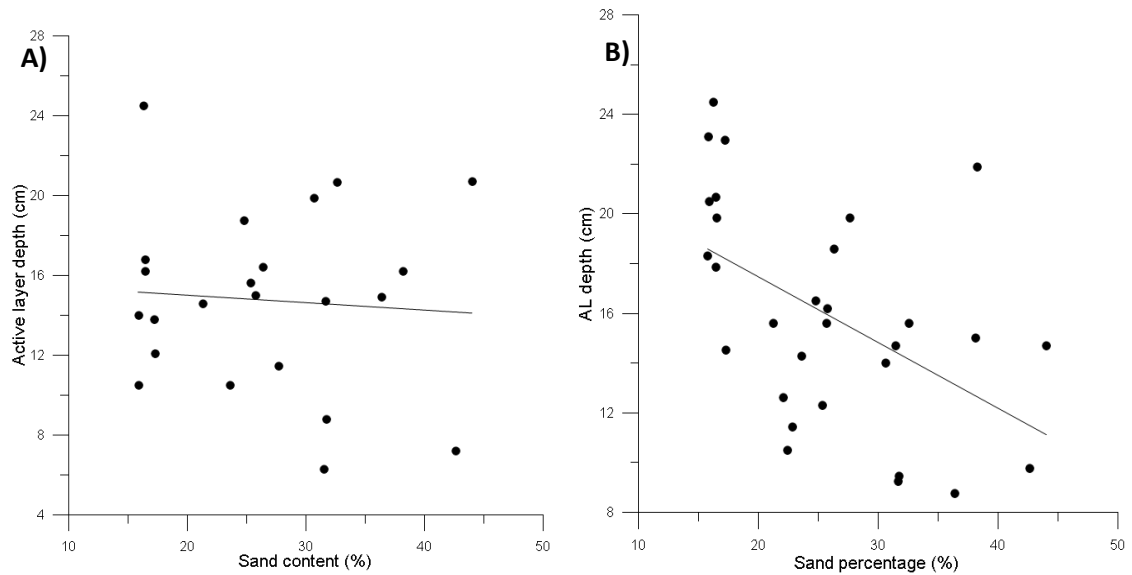


Figure 6.11: A) Relationship between sand content and AL depth as daily averages, using sediment samples taken *before* AL measurements ($y = 0.005x + 16.581$, $R^2 = 0.003$, $n=23$), and B) The same relationship using sediment samples taken *after* AL measurements ($y = -0.264x + 22.772$, $R^2 = 0.256$, $n=30$).

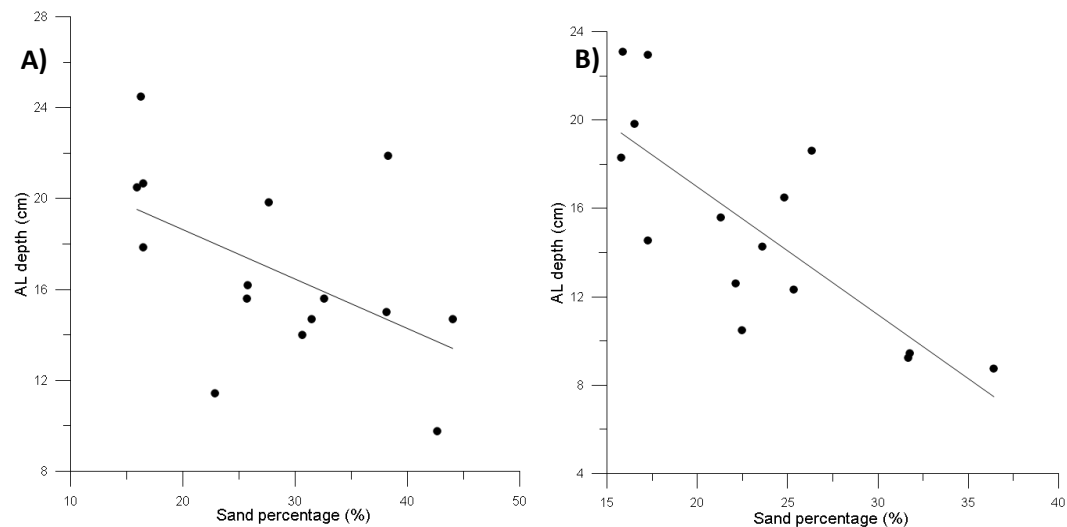


Figure 6.12: A) Relationship between daily average sand content and AL depth during Winter 1 (2014-15) ($y = -0.218x + 22.982$, $R^2 = 0.274$, $n=15$), and B) The same relationship during Winter 2 (2015-16) ($y = -0.579x + 28.545$, $R^2 = 0.6$, $n=15$).

e. By surface sediment

Collecting and analysing sediment samples is very time consuming and as such could not be used on a broader scale in this experiment. A popular way of quickly categorising sediment is to attribute codes to dGPS points (Watt *et al.*, 2005), which was done during the first winter of fieldwork for this project. The overall results from this are described in Chapter 5. Since dGPS points were taken to track the elevation at each SID on most days, there are also sediment

codes associated with AL depth measurements. Figure 6.13 indicates the mean, maximum and standard deviation of measurements for each surface sediment code. The number of points measured in each category is listed in the caption of Figure 6.13; gravel- and granule-dominated points were much rarer than those dominated by either sand or small gravel and so cannot be visually assessed from this graph with any degree of reliability. ‘Small gravel’ and ‘mainly small gravel’ points have higher means and maximums than ‘sand’ and ‘mainly sand’, but also have much greater standard deviations.

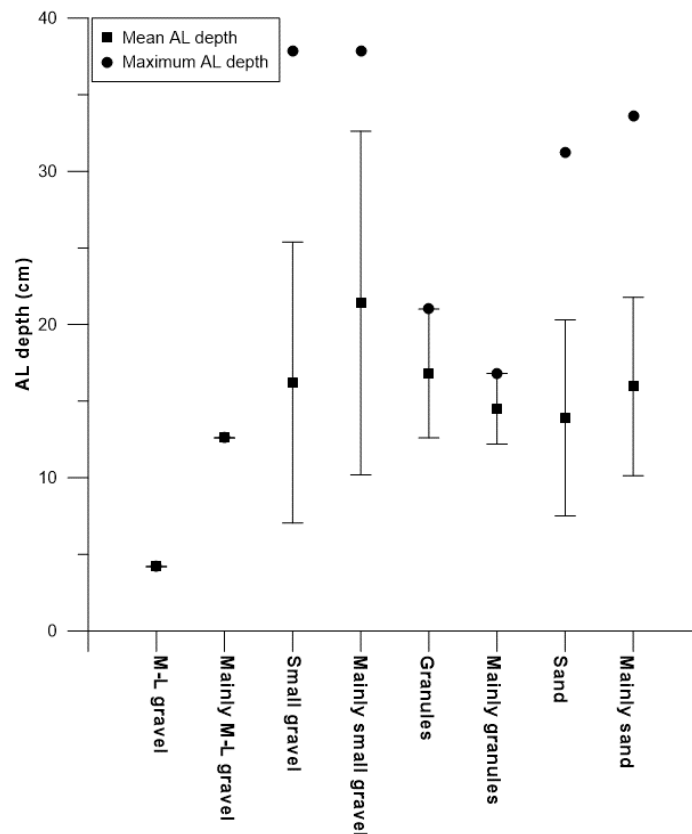


Figure 6.13: Mean, maximum and standard deviation of AL measurements categorised by surface sediment types. (Number of points in each category: G=4, MG=1, P=28, MP=15, H=2, MH=2, S=11, MS=43.)

There are 8 codes overall – too many to detect meaningful patterns from, especially as some were much more frequent than others – so two types of separation were attempted to investigate patterns. King (1951) believed that larger grain sizes would correlate with greater AL depths, so codes were separated into “small” and “large” categories as follows: “small” = sand, mainly sand, granules, mainly granules; “large” = m/l gravel, mainly m/l gravel, small gravel, mainly small gravel. The standard deviation is much greater for the “large” points, and the maximum is slightly larger, but the means are similar (Figure 6.14).

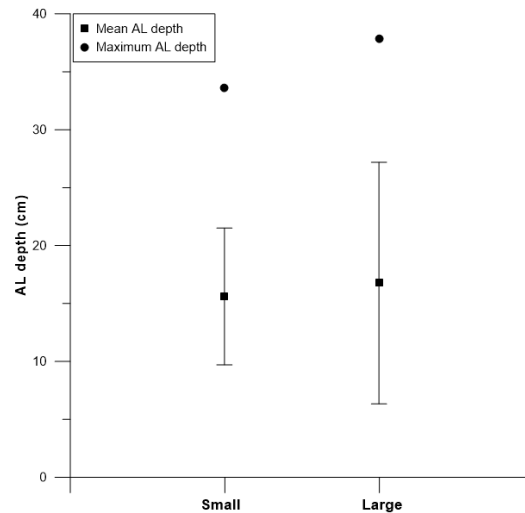


Figure 6.14: Mean, maximum and standard deviation of AL depths for “large” (n=48) and “small” (n=58) surface sediment codes.

Research into hydraulic conductivity implies that the lower porosity and permeability of mixed sediments would produce a lower AL depth, regardless of the size of particles (Blanco, 2003). In this case the codes were separated into “pure” and “mixed” categories, with any of the codes containing “mainly” counting towards the “mixed” category. The mean for “mixed” points is slightly larger, but the maximums are the same and standard deviations are similar (Figure 6.15).

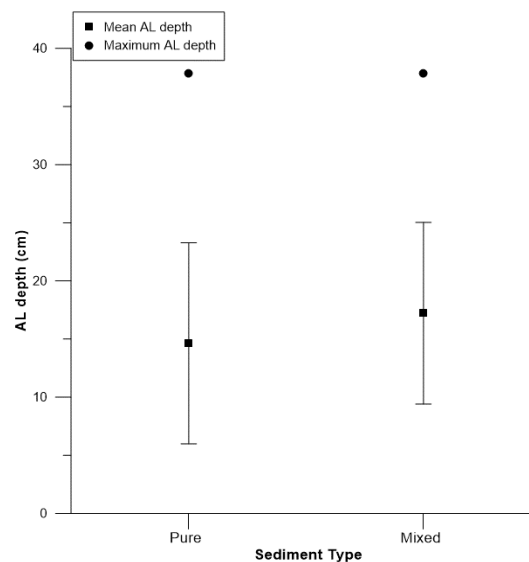


Figure 6.15: Mean, maximum and standard deviation of AL depths for “pure” (n=45) and “mixed” (n=61) surface sediment codes.

f. By slope angle

It has been suggested by Ciavola *et al.* (1997) that beach slope has a strong influence on AL depth, which can be up to an order of magnitude larger on steep (>0.08) sand beaches compared to more gently sloping (<0.08) beaches.

As a replenished, groyned, mixed sediment beach, the profile shape and slope angles at Eastoke can change frequently (Chapter 5), and so can be considered at a smaller scale, both spatially and temporally. It was important to determine whether minor changes in overall slope angle would have a noticeable effect on AL depth. To this end, slope angles were calculated from dGPS measurements, and compared to average AL depth measured on that same profile. Figure 6.16 shows the results: no correlation can be found at this scale between slope angle and AL depth. The relationship does not become clearer if the three profiles are investigated separately. This relationship will be analysed further, in terms of wave conditions, in later sections.

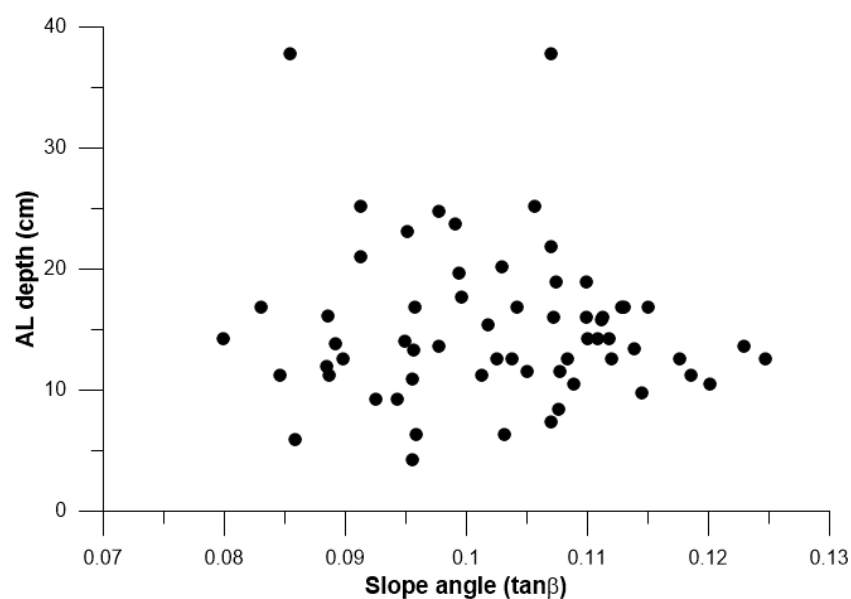


Figure 6.16: Profile slope angle plotted against average AL depth. N=62.

The selection of a site as complex as Eastoke provides an opportunity to test whether small changes in slope at a particular site can significantly affect AL depth. Mixed sediment beaches often do not have consistent slopes across the whole beach face, as the beach slope can transition from steep on the upper beach, to much more shallow on the lower beach. Horn (2002) has indicated that one of the aspects of mixed sediment beaches which is not often considered in studies of beach dynamics is the local bed slope. A selection of points from February 2015 were analysed to determine whether a relationship existed between local bed slope at each measurement site and AL depth (Figure 6.17). There is a very weak negative correlation between these variables.

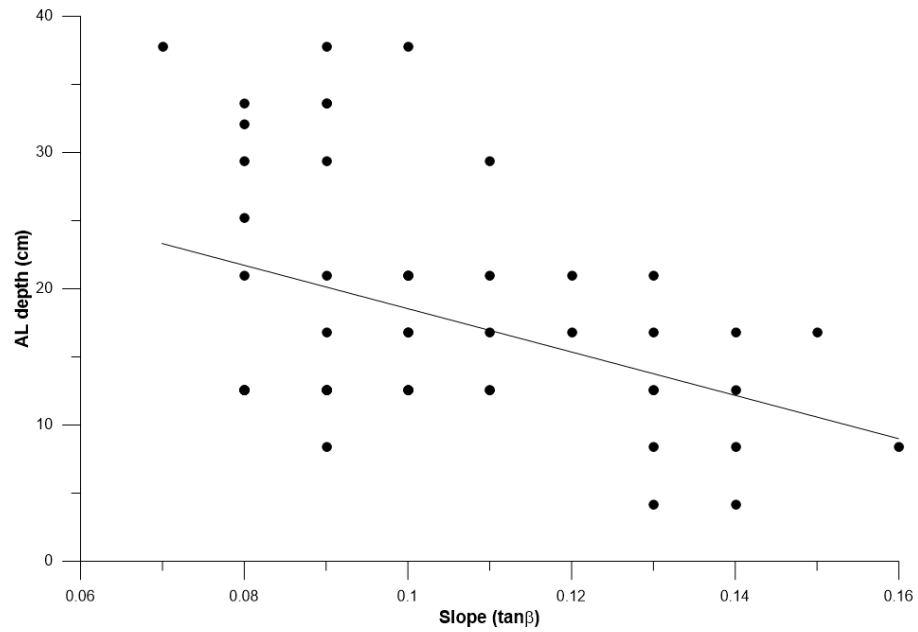


Figure 6.17: Local bed slope at individual SID locations plotted against AL depth. ($y = -159.125x + 34.462$. $R^2 = 0.161$. $n=54$.)

g. By change in elevation

Measuring elevation change is easier than measuring AL depth, so if a relationship can be found between these two variables, it could prove useful for predictions of AL depth and longshore transport in the future. Figure 6.18 shows the relationship between the change in elevation and the AL depth of specific SIDs: there is no correlation between these two variables. Wave height will be factored into this relationship in section 6.3.ii.

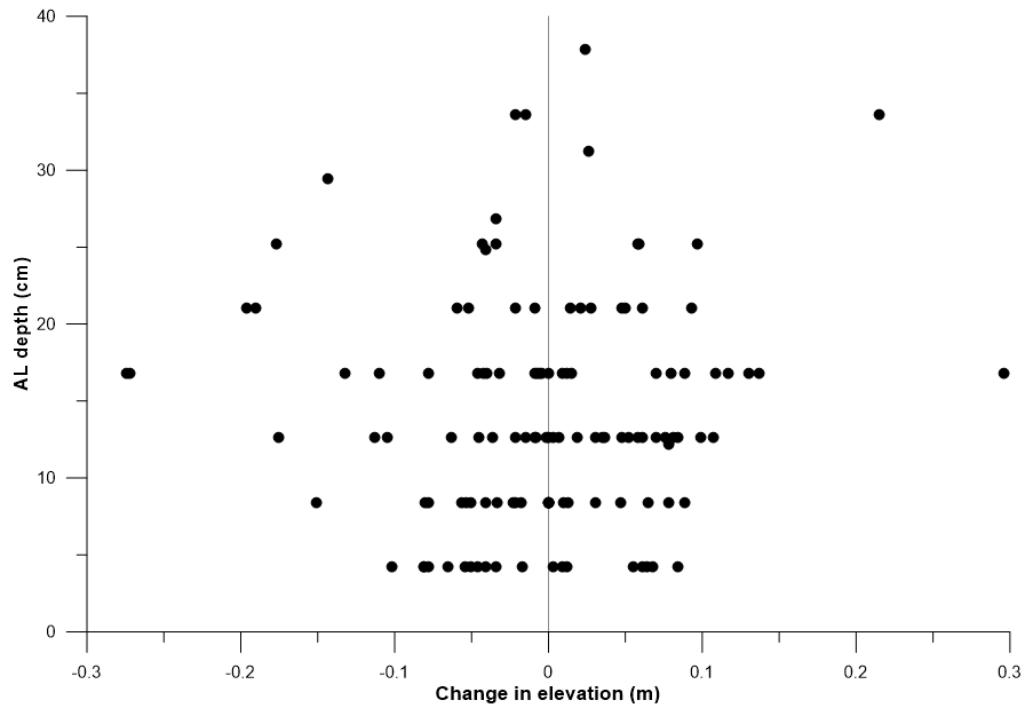


Figure 6.18: Scatterplot showing relationship between change in elevation and AL depth. n=122

h. By change in cross-sectional area (CSA)

It is also possible to consider the change of each profile (Chapter 5.2.v) against AL measurements taken during the same time frame. There are limited occasions when both sets of measurements match up perfectly, with multiple AL depths from which to produce a mean for the profile. Figure 6.19 indicates the results: there is not a strong correlation between these variables. The correlation between negative CSA change and AL depth is stronger than for positive values of CSA change, but there are also fewer points on the negative side. This relationship will be considered in terms of wave height in a later section.

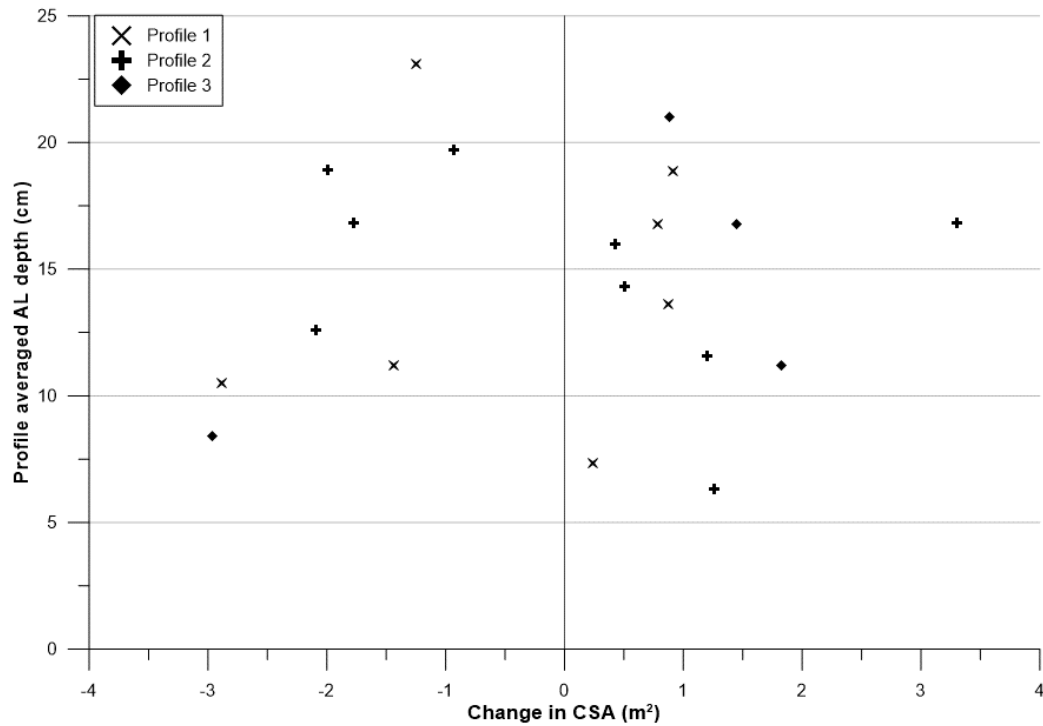


Figure 6.19: Change in cross-sectional area of a profile plotted against average AL depth for the same profile.

ii. Relationship with wave height

a. Overall

The key driver associated with active layer depth is wave height (e.g. King, 1951; Williams, 1971; Ciavola *et al.*, 1997; Curoy *et al.*, 2009) which appears to be the basis for every study previously undertaken on this topic (Chapter 2.3). Wave data from a nearshore Wave Rider (5 km offshore) was used to investigate this relationship at Eastoke (Chapter 4.3). More detailed wave conditions for each month can be seen in Appendix A.

Each AL measurement can be seen plotted against significant wave height (H_s) in Figure 6.20. There is no apparent correlation between these variables at this scale, with a Pearson's correlation coefficient of 0.241, indicating that wave height is perhaps not the dominant factor controlling AL depth that past research has implied. The spatial variations of this relationship are considered in section f onward.

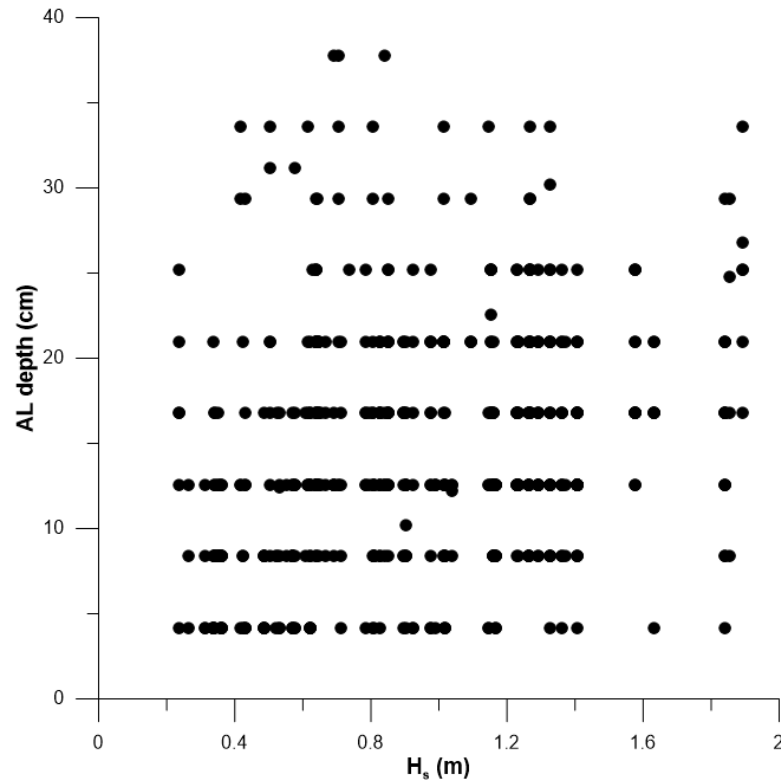


Figure 6.20: Active layer depth plotted against significant wave height. $n=554$.

Because previous authors (e.g. Masselink *et al.*, 2010; Miller and Warrick, 2012) have referred to the active layer depth as a percentage of wave height, a value was calculated for every individual measurement of the active layer depth. This was done by dividing each raw active layer measurement by the mean significant wave height for the time period during which it was measured, to give a percentage. These percentages allow results to be directly compared to values for other beaches which may have different wave conditions, as well as allowing other factors to be taken into consideration alongside wave height. These percentages are displayed as a histogram in Figure 6.21. The average active layer depth for individual measurements (554 points in total) is 18.0 % of wave height, but this varies from a minimum of 2.3 % to a maximum of 107 %; the standard deviation is 12.3. The Pearson's correlation coefficient between these individual values and actual wave height is -0.450, which indicates a moderate strength relationship.

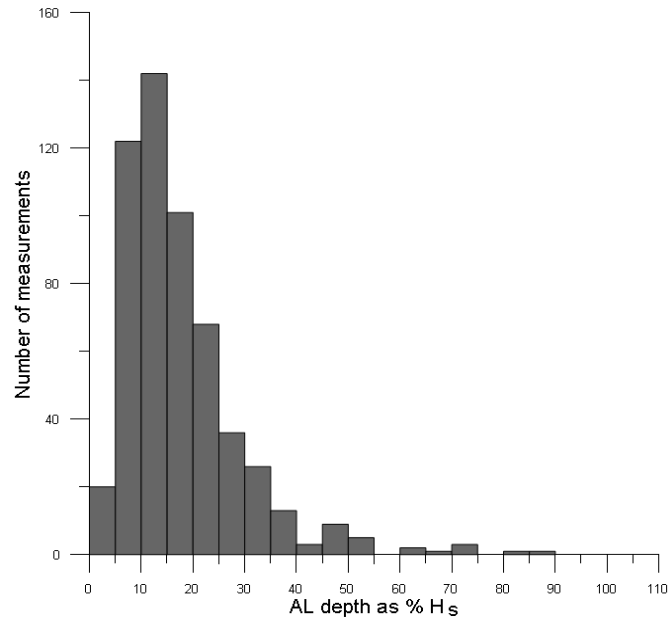


Figure 6.21: Histogram showing frequency of individual AL depth measurements when related to wave height. n=554.

b. Temporally

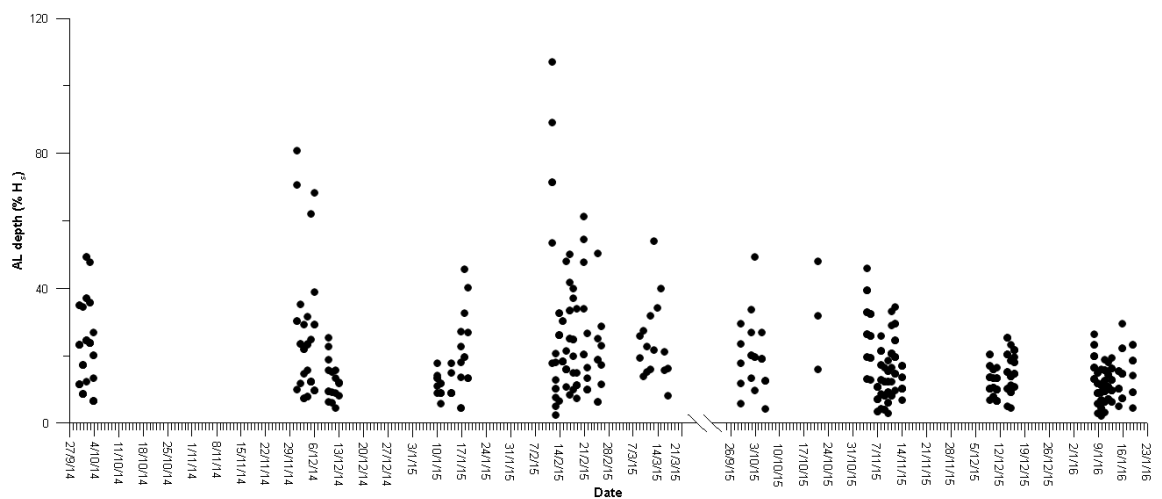


Figure 6.22: Individual AL measurements as a percentage of significant wave height. n=554

Figure 6.22 shows the variation in values of AL as a percentage of wave height for each day during the study. The greatest spread of values occurred during February 2015. Other authors tend to investigate their data on a daily scale and not as individual measurement points, so average values were then also calculated for the 72 days. The mean daily AL depth is 20.1 % of

wave height, the maximum is 68.5 %, the minimum is 7.5 % and the standard deviation is 10.0 %.

Only a weak correlation was found between daily average significant wave height and daily mean active layer depth (Figure 6.23), with a Pearson's correlation coefficient of 0.436 indicating a moderate relationship. A T-Test was undertaken to investigate whether there was any statistically significant difference between the populations of mean active layer measurements taken on days when wave height was <1 m and >1 m. This showed no statistically significant difference, further indicating a lack of correlation between the two variables.

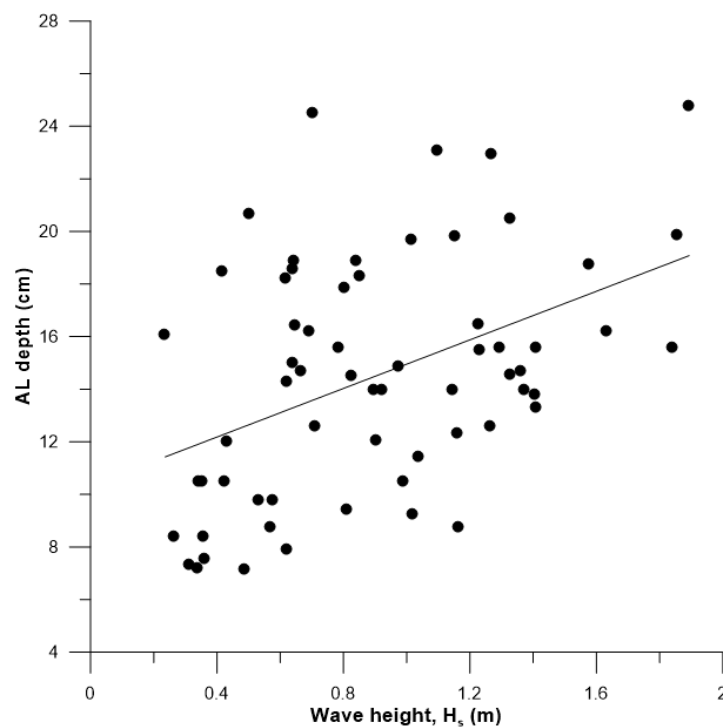


Figure 6.23: Scatter plot of daily mean significant wave heights and mean AL depth measurements. ($y = 4.618x + 10.341$, $R^2 = 0.190$. $n=63$.)

Ferreira *et al.* (2000) found a ratio between mean and maximum sediment activation depths whereby $Z_{\max} = 1.8 Z_m$ for steep (slope > 0.08) sand beaches. For the daily values at Eastoke, the average ratio is 1.59, ranging from 1 to 2.92. This inconsistency supported the idea that one of these variables (i.e. mean AL depth or maximum AL depth) could have a better relationship with wave height than the other. However, a grid of correlation values indicates that the strongest relationship exists between mean H_s and mean AL depth (Table 6.6) and so this is what has been used in calculations.

Table 6.6: Spearman's correlation coefficients for different combinations of wave height and AL depth measurements.

	Mean AL	Max AL
Mean H _s	0.396 (p < 0.01)	0.321 (p < 0.01)
Max H _s	0.382 (p < 0.01)	0.325 (p < 0.01)

The number of days over which AL data was collected for this project is much greater than all previous AL research of which the author is aware (see Table 2.1 in Chapter 2). As such, the measurements can be separated according to field period and still provide an adequate number of data points. Plots of daily mean, maximum and standard deviations can be seen in Appendix H. None of the study periods show a clear link between wave height and AL depth, though some show better correlation than others (Table 6.7). None of the correlations can be said to be statistically significant due to the small number of points used (equal to the number of days). Similarly, when considering the two winters separately, lines of best fit produce the following correlations: $R^2 = 0.247$ during the first winter (excluding March as there were only one or two AL measurements per day, which cannot be said to produce a representative average value), and $R^2 = 0.131$ during the second.

Table 6.7: Relationships between daily mean AL depth and daily mean wave height for each study period

Study period (month)	Number of days	Regression line equation	R ²
October 2014	5	$y = -7.707x + 12.058$	0.327
December 2014	10	$y = 6.157x + 8.071$	0.460
January 2015	6	$y = 7.042x + 7.993$	0.488
February 2015	12	$y = -1.76x + 18.685$	0.042
March 2015	9	$y = 32.995x - 4.550$	0.218
October 2015	6	$y = 11.5x + 5.360$	0.493
November 2015	9	$y = -6.826x + 21.876$	0.190
December 2015	6	$y = 6.247x + 8.473$	0.279
January 2016	9	$y = 6.219x + 6.817$	0.318

Despite only a weak correlation existing between wave height and active layer depth (section 6.4.ii), a much more significant secondary link can be found. The daily mean active layer measurement was calculated as a percentage of mean significant wave height for the same period. By comparing these values with significant wave heights, it is apparent that greater wave heights have a reduced proportional impact on AL depth, producing a smaller percentage value (Figure 6.24). A Spearman's Rank correlation test on these variables gives a correlation value of -0.79 (p < 0.01), which indicates a strong negative correlation. This is a stronger

correlation than is produced by a Pearson's correlation ($r = -0.67$, $p < 0.01$) indicating that the relationship is non-linear. An exponential curve was found to produce the best fit (Figure 6.24).

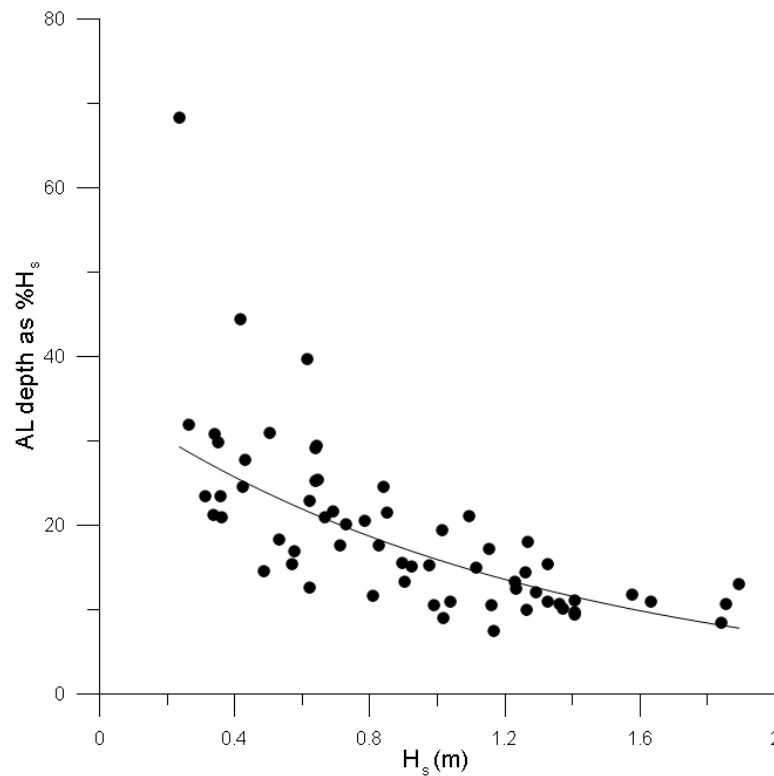


Figure 6.24: Scatterplot showing correlation between wave height (H_s) and AL depth as a percentage of H_s . Trendline sits at $\ln(y) = -0.797x + 3.565$. (where $R^2 = 0.578$, $p < 0.01$, $n=63$).

c. By sediment composition

For sediment samples taken at specific SID locations, there is not a strong relationship between AL depth as a percentage of wave height and either sand content (Figure 6.25A & B) or D_{50} (Figure 6.25C & D). Pearson's correlation coefficients (Table 6.8) indicate that the strongest relationship exists when samples from the end of the measurement period are used, and when sand content is used instead of D_{50} . This is slightly different to results for pure AL depth at the same scale, where a better relationship exists if sediment samples from before the AL measurement were used.

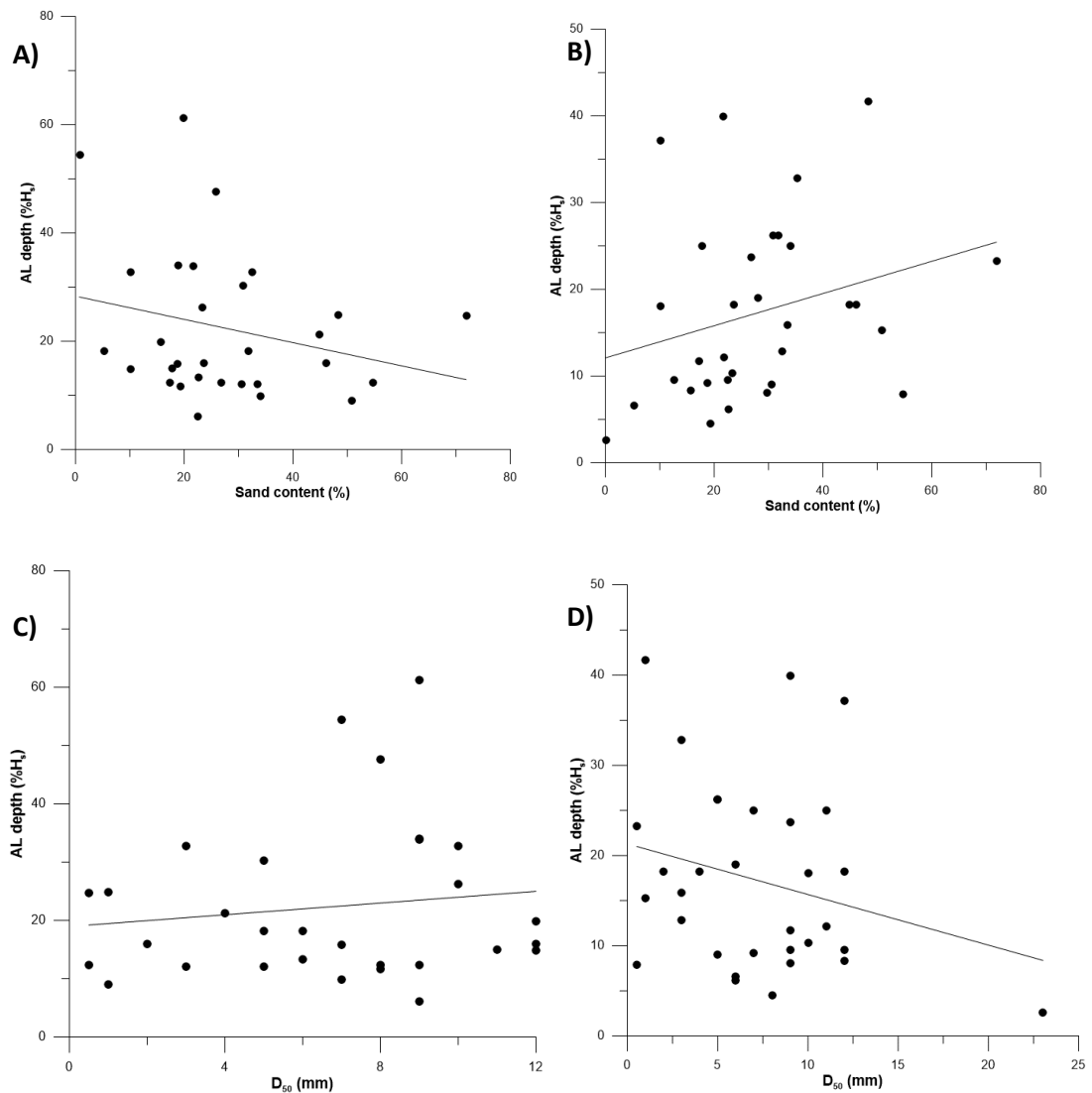


Figure 6.25: Relationships between sediment composition and AL depth as a percentage of wave height at individual SID locations. A) Sand content for sample taken at the start of AL measuring period (n=30), B) Sand content for sample taken at the end of AL measuring period (n=32), C) D₅₀ for sample taken at the start of AL measuring period (n=30), D) D₅₀ for sample taken at the end of AL measuring period (n=32).

Table 6.8: Pearson's correlation coefficients for relationships between sediment composition and AL depth as a percentage of wave height.

	Start of AL measurement	End of AL measurement
Sand content	-0.246	0.273
D ₅₀	0.131	-0.252

When values were averaged across the beach face and compared to daily average AL depth, there is a slight improvement in the relationship when sediment samples from the day before are used (Figure 6.26). However, this relationship is not as strong as the relationship for pure AL depths shown in section 6.3.i.d.

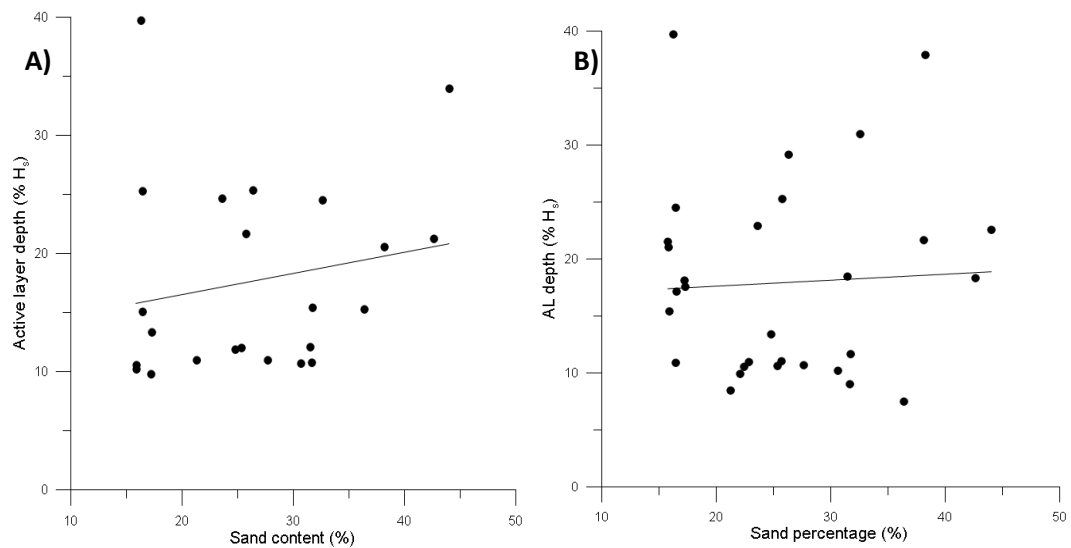


Figure 6.26: A) Relationship between daily average sand content and AL depth as a percentage of wave height, using sediment samples taken *before* AL measurements ($y = 0.179x + 12.925$, $R^2 = 0.036$, $n=23$), and B) The same relationship using sediment samples taken *after* AL measurements ($y = 0.052x + 16.581$, $R^2 = 0.003$, $n=30$).

d. By surface sediment

As mentioned in section 6.3.i.e, dGPS points taken during the first winter were coded according to the surface sediment composition. These codes can be attributed to specific AL measurements to determine whether there were obvious differences between the response of the beach for different surfaces. Figure 6.27 shows the mean, maximum and standard deviation of AL depths (as a percentage of wave height) experienced at points coded under each sediment type.

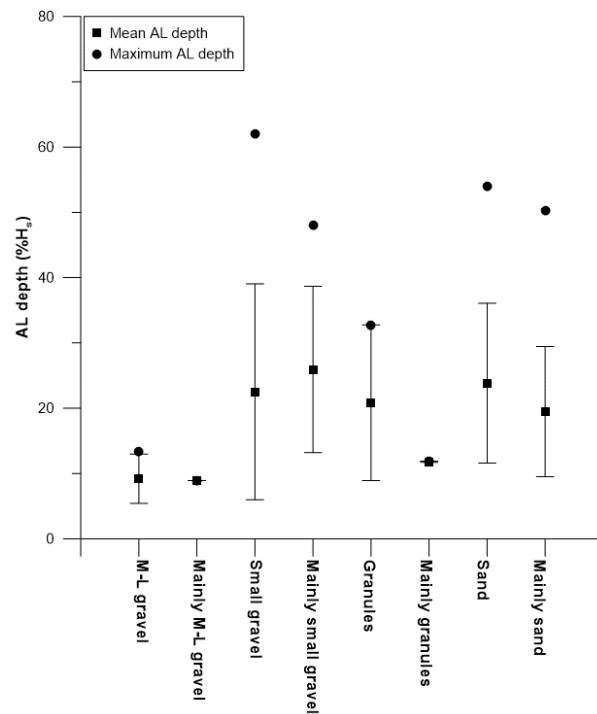


Figure 6.27: Mean, maximum and standard deviation for AL depths as a percentage of significant wave height at locations coded according to surface sediment. (Number of points in each category: G=4, MG=1, P=28, MP=15, H=2, MH=2, S=11, MS=43.)

The codes were separated according to the size of the dominant particle (Figure 6.28). Both size groups have similar means (small = 20.3 %, large = 22.2 %), though the maximum and standard deviation of the “large” sediment group is greater.

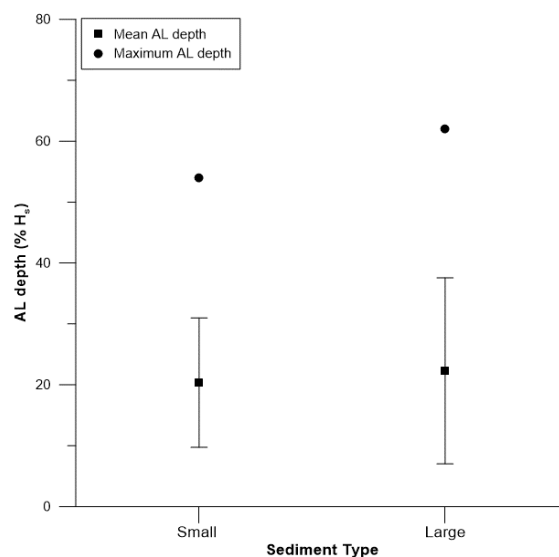


Figure 6.28: Mean, maximum and standard deviation of AL measurements as a percentage of wave height for “small” (n=58) and “large” (n=48) sediment codes.

Surface codes were also categorised according to whether they were composed of a mixture of grain sizes (Figure 6.29). Again, the mean values are very similar (pure = 21.6 %, mixed = 20.7 %), but pure sediments experienced a greater range of values.

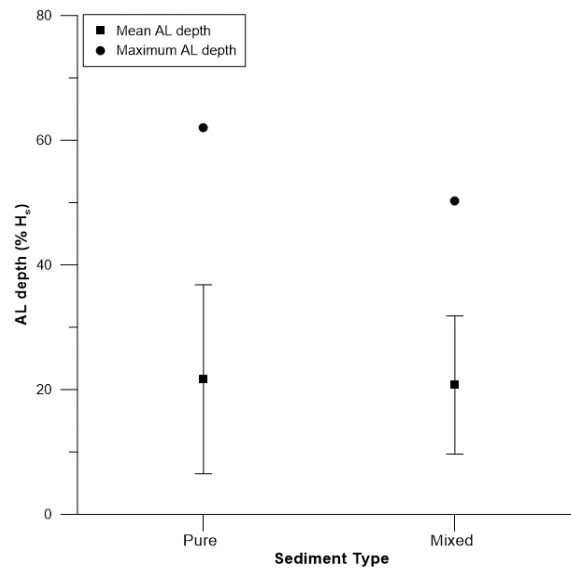


Figure 6.29: Mean, maximum and standard deviation of AL measurements as a percentage of wave height for “pure” (n=45) and “mixed” (n=61) sediment codes.

e. By slope angle

It has been stated by Ciavola *et al.* (1997) and Anfuso (2005) that the overall slope angle of a beach affects active layer depth; steeper beaches have greater AL depths. The average beach slope for this site was calculated to be $\tan\beta = 0.1$, from low tide level to approximate maximum run-up level. The average from daily values of active layer depth as a percentage of wave height is 20.1 %. These values will be discussed in relation to previous research in section 6.4.

To discern whether beach slope affected AL depth at a smaller scale than this, slope angles were calculated for individual profiles and compared to average AL depths for that same profile. Figure 6.30 shows the correlation between the slope angle of individual profiles and AL depth as a percentage of wave height, which is minimal.

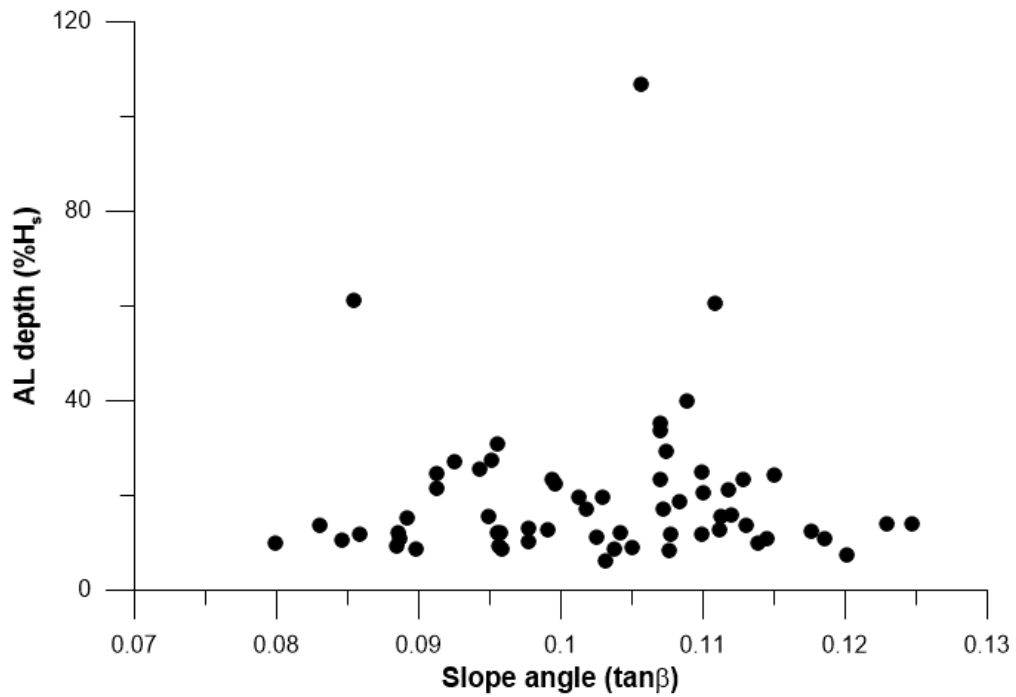


Figure 6.30: Scatterplot showing relationship between overall profile slope angle and AL depth as a percentage of wave height (n=62).

Local bed slopes – slope angle at specific SID locations – were correlated with AL depth as a percentage of wave height (Figure 6.31). At this scale, a moderate linear relationship appears to exist, whereby as slope angle increases, the active layer depth decreases, indicated by a Pearson's coefficient of -0.38 ($p < 0.01$). However, this relationship is slightly weaker than when raw AL depth measurements were used (section 6.3.i.f).

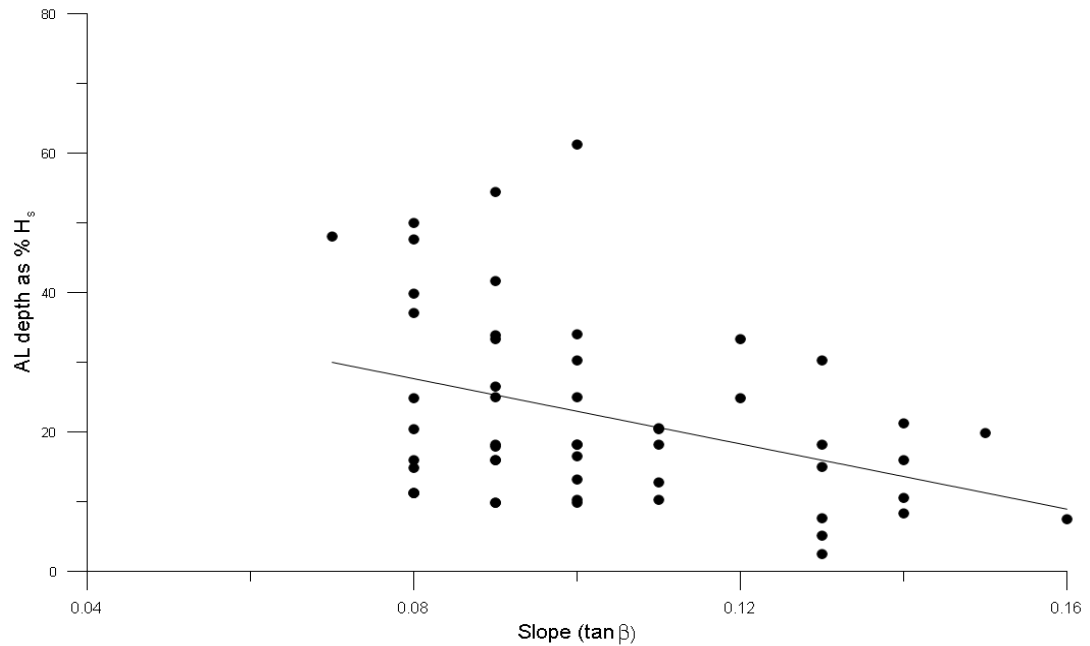


Figure 6.31: An example from February 2015 of individual AL depth values, expressed as a percentage of wave height, compared to the beach slope at the site where each measurement was taken. $n = 53$. Trendline sits at $y = -233.96x + 46.374$. $R^2 = 0.147$ ($p < 0.01$).

f. Alongshore

Chapter 5 showed that the three profiles within this groyne cell respond uniquely to wave conditions, so it was necessary to separate measurements from each profile and consider them individually. The mean AL depths as percentages of wave height are relatively similar between the three profiles (Table 6.9), but the distributions look quite different (Figure 6.32). A Kruskal-Wallis test indicated that there was no statistically significant difference between the median values from the three profiles, $X^2(2) = 0.837$, $p = 0.658$.

Table 6.9: Variation in AL depth as a percentage of wave height between Profiles 1-3 during November 2015-January 2016.

	Mean AL depth (% H_s)	Standard Deviation
Profile 1 (n=102)	13.75	6.30
Profile 2 (n=96)	14.75	7.98
Profile 3 (n=105)	15.08	7.54

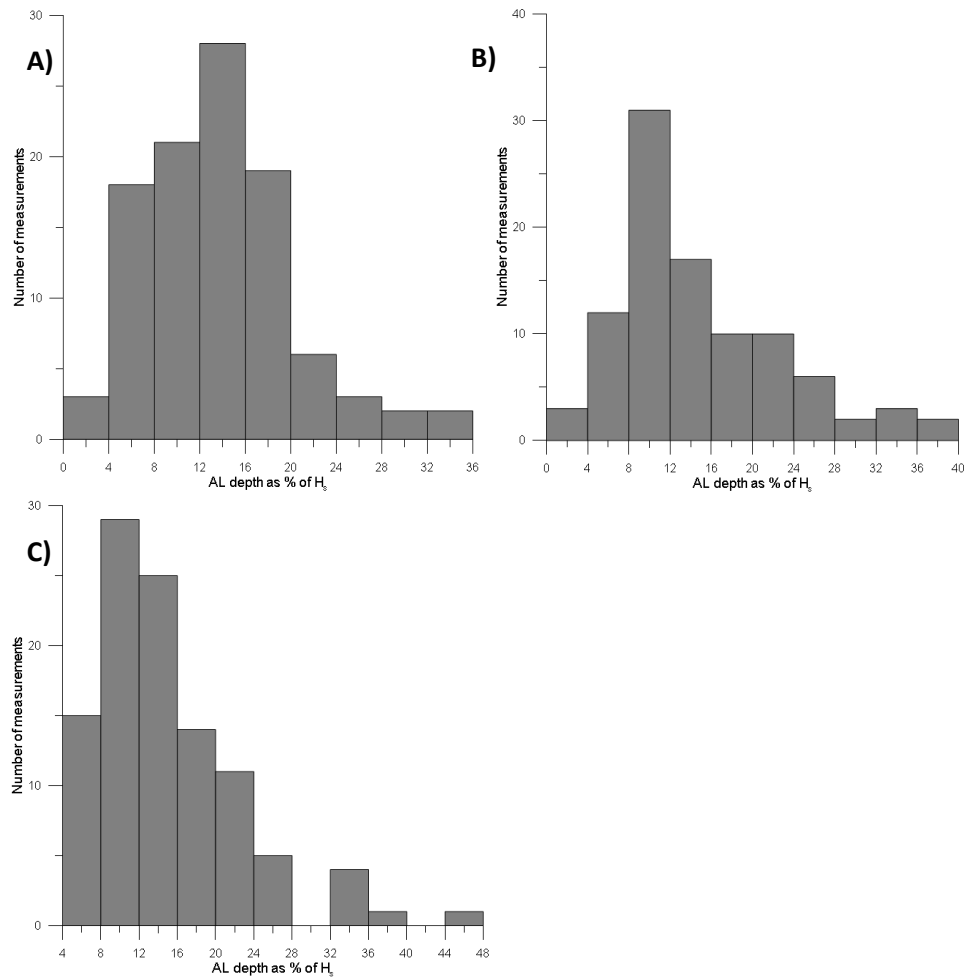


Figure 6.32: Histograms indicating frequency of AL depth as a percentage of wave height measured on each of the three profiles. A) Profile 1, B) Profile 2, C) Profile 3.

g. Across shore

There is no clear relationship between elevation and AL depth as a percentage of wave height (Figure 6.33). Generally, the greatest active layer depths as a percentage of wave height were recorded between 0-2 m elevations, as is evidenced by the mean values in Table 6.10, but there is still huge variation in measurements taken at these elevations. There is less variation between the minimum measurements for each elevation bracket, but the same pattern is broadly true for maximum measurements, apart from between 0-0.5 m elevation, which experienced the second highest maximum of any section of the profile.

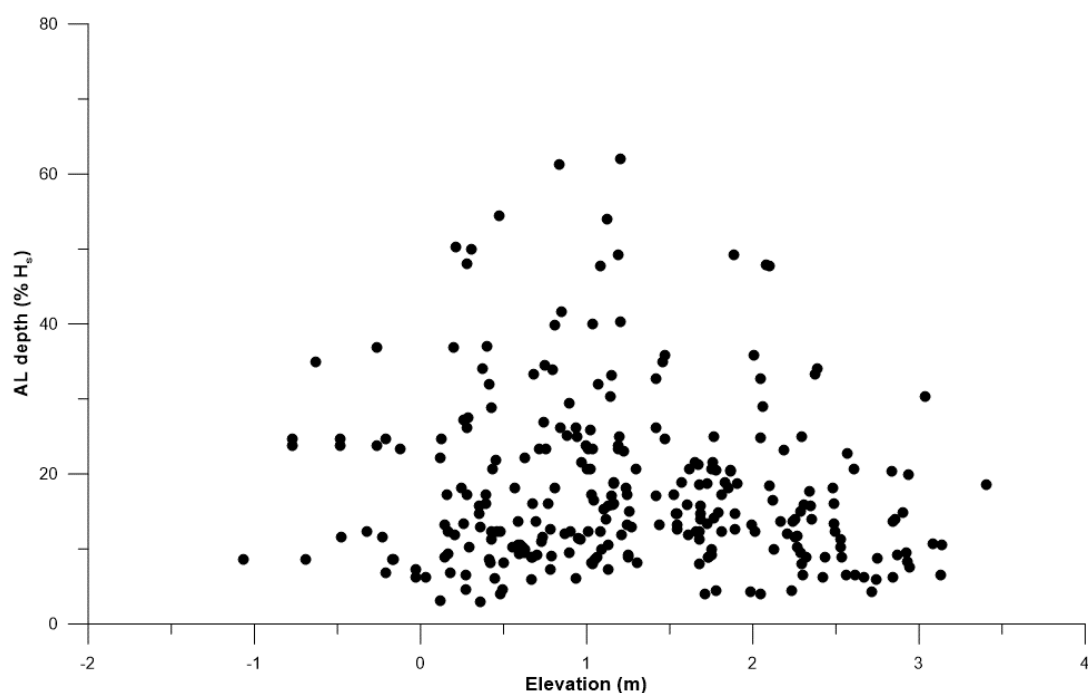


Figure 6.33: Active layer measurements as a percentage of H_s at different elevations. (n=275)

Table 6.10: Variation in AL depth as a percentage of H_s for different elevations at which it was measured

Elevation	Min AL (% H_s)	Mean AL (% H_s)	Max AL (% H_s)
<0 m	6.33	17.46	36.99
0- 0.5 m	3.08	18.76	54.53
0.5 -1 m	5.98	18.11	61.35
1-1.5 m	7.38	21.69	62.01
1.5-2m	4.12	15.69	49.32
2-2.5m	4.12	17.74	47.95
>2.5m	4.31	12.06	30.39

A Kruskal-Wallis test determined that there is a statistically significant difference in the mean ranks of values between measurements when separated into upper, middle and lower beach, $X^2(2) = 6.219$, $p = 0.045$. A post-hoc pairwise comparison (using Dunn's (1964) procedure with a Bonferroni correction for multiple comparisons) revealed this difference to be between the mean ranks of the upper (117.95) and mid beaches (147.58) ($p = 0.039$), with no statistically significant difference between either the upper and lower (136.22) ($p = 0.577$), or mid and lower beach ($p = 1$). This is different to results for standard AL measurements, which had a statistically significant difference between the lower and mid beach, but not any other combinations.

Results also indicate that separating the beach into upper, middle and lower sections does not improve the relationship between wave height and AL depth. Table 6.11 provides Pearson's correlation coefficients for the relationship between wave height and AL depth for these different cross shore areas. These follow the same general pattern as the whole beach, with no area having a particularly good correlation; the lower beach has the worst relationship.

Table 6.11: Pearson's correlation coefficients for relationships between wave height and AL depth (both raw measurements and as a percentage of wave height), on the upper, middle, and lower beach

	Upper (> 2 m)	Middle (0.5 – 2 m)	Lower (< 0.5 m)
H _s vs AL (cm)	0.331	0.327	0.230
H _s vs AL (%H _s)	-0.444	-0.421	-0.342

The relationships between wave height and AL depth were also assessed for 1 m elevation bins (Table 6.12). The coefficients for the relationship between wave height and true AL depth are surprisingly low in the <0 m and 0-1 m bins, and much higher – but still only a moderate strength – in the 1-2 and 2-3 m bins.

For the relationship between wave height and AL depth as a percentage of wave height, areas with lower numbers of measurements have noticeably stronger relationships, but the areas with greater numbers of measurements have similar Pearson's coefficients to those produced in the upper/middle/lower split.

Table 6.12: Pearson's correlation coefficients for relationship between wave height and AL depth within 1 m elevation bins.

	H _s vs AL	H _s vs %H _s
<0 m (n=19)	0.015	-0.538
0-1 m (n=93)	0.070	-0.398
1-2 m (n=99)	0.458	-0.425
2-3 m (n=59)	0.355	-0.433
>3 m (n=5)	-0.107	-0.618

h. By area within the groyne

Individual measurements were separated according to the nine sections in Figure 6.9. The relationship between wave height and AL depth remains relatively weak within each section, with a range of Pearson's correlation coefficients between 0.056 and 0.321 (Table 6.13). The relationships improve when AL depth as a percentage of wave height is used, with a range of Pearson's coefficients between -0.315 and -0.689, which can be considered moderate strength

relationships. The strongest relationships between wave height and AL depth as a percentage of wave height exist in the lower west and upper east segments.

Table 6.13: Pearson's correlation coefficients for relationships between wave height and AL depth of measurements, subset by position within the groyne compartment.

Box Number	N	Pearson's correlation coefficient H_s vs AL (cm)	Pearson's correlation coefficient H_s vs AL (% H_s)
1	33	0.261	-0.562
2	100	0.056	-0.490
3	27	0.195	-0.669
4	61	0.260	-0.401
5	126	0.295	-0.463
6	56	0.131	-0.315
7	29	0.102	-0.689
8	65	0.321	-0.399
9	32	0.271	-0.404

i. At specific measurement locations

Due to the length of time over which AL measurements were taken in the present study, it was possible to track specific locations and determine whether relationships between AL depth and other variables became stronger when the potential influence of the groynes and position on the profile were minimised. Eight locations were identified where SIDs had been deployed in multiple field periods to produce a reasonable number of AL measurements under a variety of wave conditions. The results from each of these locations were analysed separately, and regression equations produced for each location (Table 6.14). The average AL depth as a percentage of wave height is inconsistent across locations, with a wide range of percentages experienced at each.

Table 6.14: Relationships between wave height and AL depth at locations with repeated measurements.

SID number	Easting	Northing	N	Mean AL as % H_s	Relationship between H_s and AL	Relationship between H_s and % H_s
Dec14 C4 / Jan15 C4 / Feb15 C5	474433.9	98002	26	15.1 % (range: 4.6 – 32.8 %)	$Y = 9.404x + 3.79$ $R^2 = 0.438$	$Y = 12.381x^{-0.363}$ $R^2 = 0.173$
Dec14 C5 / Feb15 C3	474433.2	97992.4	22	26.2 % (range: 9.06 – 70.7 %)	$Y = 17.214x^{0.257}$ $R^2 = 0.097$	$Y = 46.575e^{-0.909x}$ $R^2 = 0.468$
Jan15 C3 / Feb15 C4	474432.8	97996.7	9	26.9 % (range: 8.9 – 71.4 %)	$Y = 2.871x + 15.299$ $R^2 = 0.166$	$Y = 62.393e^{-1.049x}$ $R^2 = 0.820$

Nov15 C14 / Dec15 C12 / Jan16 C12	474464.8	97994.8	22	18.0 % (range: 9.1 – 46.1 %)	$Y = -0.639x + 19.035$ $R^2 = 0.002$	$Y = 44.632 e^{-0.891x}$ $R^2 = 0.497$
Nov15 C16 / Dec 15 C14	474462	97980.3	13	14.1 % (range: 6.6 – 26.0 %)	$Y = -4.381x + 17.025$ $R^2 = 0.037$	$Y = 36.938 e^{-0.995x}$ $R^2 = 0.369$
Nov15 C15 / Jan16 C13	474464	97987.2	16	19.8 % (range: 7.4 – 39.5 %)	$Y = 17.303 x^{0.507}$ $R^2 = 0.088$	$Y = -13.49 \ln(x) + 19.833$ $R^2 = 0.164$
Dec15 C5 / Jan 16 C7	474445.6	97988.2	15	14.0 % (range: 6.8 – 26.5 %)	$Y = -14.115x^2 + 36.111x - 6.122$ $R^2 = 0.099$	$Y = 28.67 e^{-0.692x}$ $R^2 = 0.285$
Dec15 C7 / Jan16 C9	474446.9	98005.3	12	14.0 % (range: 9.0 – 25.4 %)	$Y = 2.345x + 14.171$ $R^2 = 0.013$	$Y = 30.513 e^{-0.658x}$ $R^2 = 0.265$

Almost all locations had a stronger relationship between wave height and AL as a percentage of wave height than between wave height and raw AL depth measurements (Table 6.15). The Pearson's coefficients indicate that the strongest relationship by far was at the location in row three of the table, though this location had only 9 measurements, the lowest of all selected points. The Pearson's correlation for the H_s vs AL (as % H_s) relationship for the daily average values was -0.67, so most of these individual locations actually exhibit a weaker relationship than this.

Table 6.15: Pearson's correlation coefficients for the relationships between wave height and AL depth at locations where measurements were repeated on multiple occasions.

SID number	H_s vs AL (cm)	H_s vs AL (% H_s)
Dec14 C4 / Jan15 C4 / Feb15 C5	0.662	-0.415
Dec14 C5 / Feb15 C3	0.214	-0.618
Jan15 C3 / Feb15 C4	0.408	-0.846
Nov15 C14 / Dec15 C12 / Jan16 C12	-0.041	-0.658
Nov15 C16 / Dec 15 C14	-0.002	-0.667
Nov15 C15 / Jan16 C13	0.126	-0.423
Dec15 C5 / Jan 16 C7	0.128	-0.463
Dec15 C7 / Jan16 C9	0.115	-0.497

j. By change in elevation

Section 6.3.i.g indicated that there was no relationship between the change in elevation and pure AL depth. Figure 6.34 shows that the same is true when AL depth as a percentage of wave height is used.

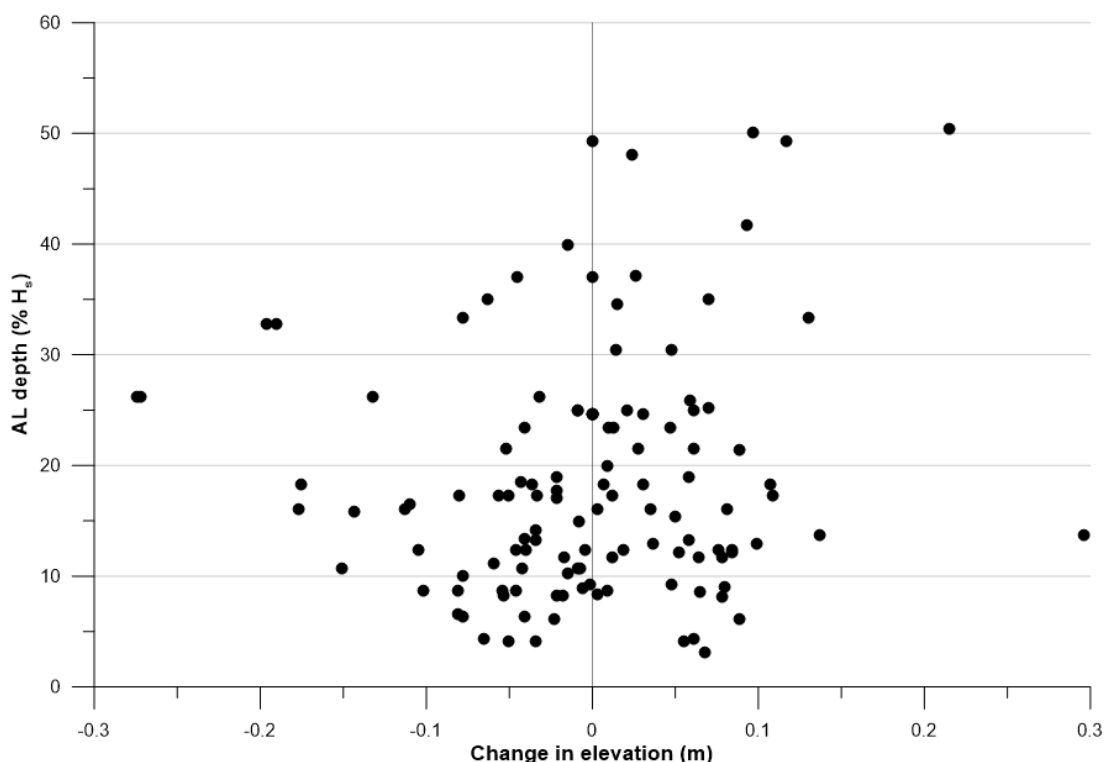


Figure 6.34: Scatterplot showing relationship between change in elevation and AL depth as a percentage of wave height. N=122.

k. By change in CSA

There is a clear correlation between profile change and AL depth as a percentage of wave height: AL depth is greatest when the profile experiences little change (Figure 6.35). The pattern appears fairly symmetrical (meaning it does not matter if change is positive or negative), so if all change values are converted to positives, the Pearson's correlation coefficient between profile change and AL depth as a percentage of wave height is -0.629, which indicates a moderate to strong relationship between increasing CSA change and decreasing AL depth as a percentage of wave height. With all change converted to positive values, the linear regression equation $y = -5.238x + 24.424$ explains 39.6 % of the variation in AL depths.

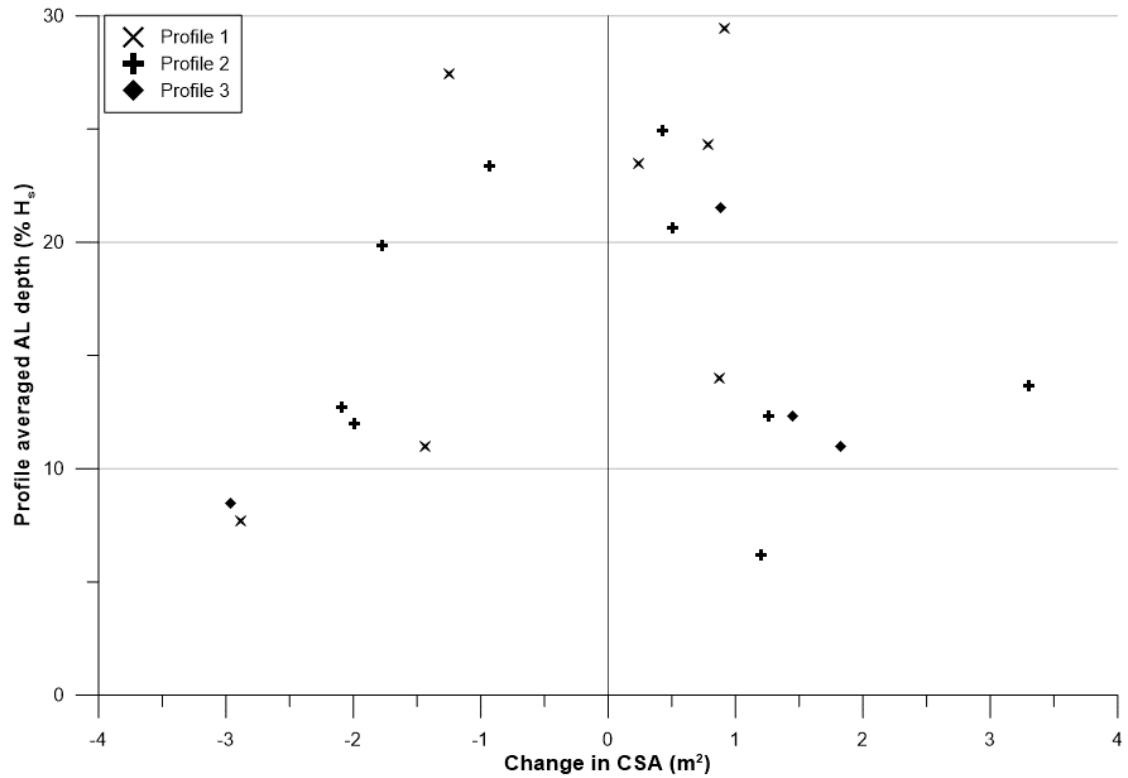


Figure 6.35: Scatterplot showing mean AL depth (as a percentage of wave height) against change in cross-sectional area of the profile. N=20.

iii. Relationship with wave period

a. Overall

In previous studies, conflicting results have been reported regarding the influence of wave period on active layer depth (Chapter 2.3), but the pilot study undertaken in March 2014 (Appendix Q) indicated that wave period was a strong influence on daily average AL depth at Hayling. Due to the bimodal nature of the wave climate in this area (Chapter 3.3.i), it was unclear whether mean period (T_z) or peak period (T_p) would provide a clearer relationship, though a sensible assumption is that T_p would be more indicative of the wave conditions, and therefore more influential. T_p was used in the pilot study and so was expected to provide similar results in this case, but to be sure, all possible options were considered.

Across all 554 measurements, no clear relationship with either T_p or T_z was apparent (Figure 6.36), with correlation coefficients of 0.060 and 0.067 respectively. At every other scale, T_p had better correlations than T_z , so peak wave period was chosen; it better represents the actual wave conditions, by indicating the period at which the most significant waves are travelling.

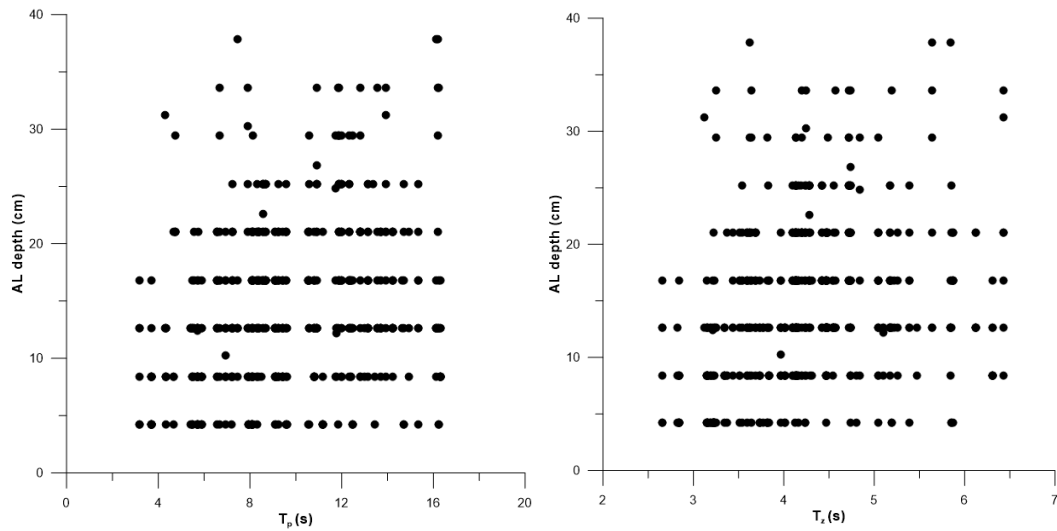


Figure 6.36: Relationships between wave period and AL depth: A) Peak period (T_p), B) mean period (T_z). $n=554$.

b. Temporally

As with wave height (section 6.4.ii), the relationship between wave period and active layer depth was investigated using daily averages from each of the short field periods, in order to conform with previous research, most of which has been done to this scale. These are displayed graphically in Appendix I, and the lack of correlation between the variables can be seen in Table 6.16. Most months show an exceptionally weak correlation between wave period and active layer depth, however, the R^2 values for October 2014, November 2015 and January 2016 are much higher than for other months. It is not possible to state whether these values are statistically significant because the sample sizes are too small.

Table 6.16: Relationships between daily mean wave period and daily mean AL depth for each study period.

Study period (month)	Number of days	Regression line equation	R^2
October 2014	5	$Y = 0.282x + 6.177$	0.615
December 2014	10	$Y = 0.409x + 9.133$	0.093
January 2015	6	$Y = 0.006x + 15.726$	0.000004
February 2015	12	$y = -0.013x + 17.496$	0.0002
March 2015	9	$Y = -0.331x + 19.935$	0.029
October 2015	6	$Y = 1.229x + 7.109$	0.032
November 2015	9	$Y = 1.027x + 4.969$	0.694
December 2015	6	$Y = 0.348x + 12.607$	0.066
January 2016	9	$Y = 1.313x + 3.197$	0.545

The correlation between daily mean peak wave period and mean is non-linear, but only of moderate strength (Figure 6.37A); a Spearman's rank correlation test yielded a result of 0.38 ($p < 0.01$). There is no statistically significant correlation between peak wave period and active layer depth as a percentage of wave height (Figure 6.37B).

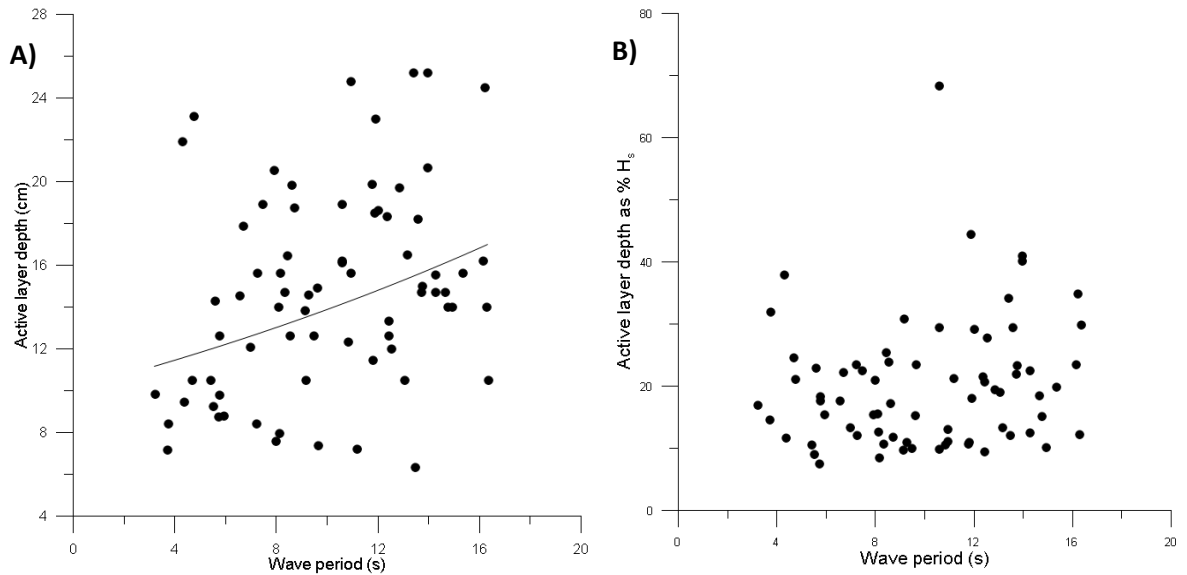


Figure 6.37: A) Scatterplot comparing mean wave period (T_p) to mean AL depth for each of the 72 study days. Trendline sits at $y = 10.088e^{0.032x}$ where $R^2 = 0.114$. B) Scatterplot comparing wave period to AL depth as a percentage of H_s .

c. By wave height

When the daily averages are split according to wave height, it becomes apparent that the relationship between peak period and AL depth is stronger when significant wave heights are below 1 m. For the 38 data points which fit into this category, a scatterplot was produced (Figure 6.38A), with an R^2 value of 0.250; the same scatterplot produced for wave heights greater than 1 m (Figure 6.38B) yielded a much poorer correlation ($R^2 = 0.009$, $n = 25$). However, the spread of data points in Figure 6.38A indicates that predicting AL depth from wave period would be unsuccessful.

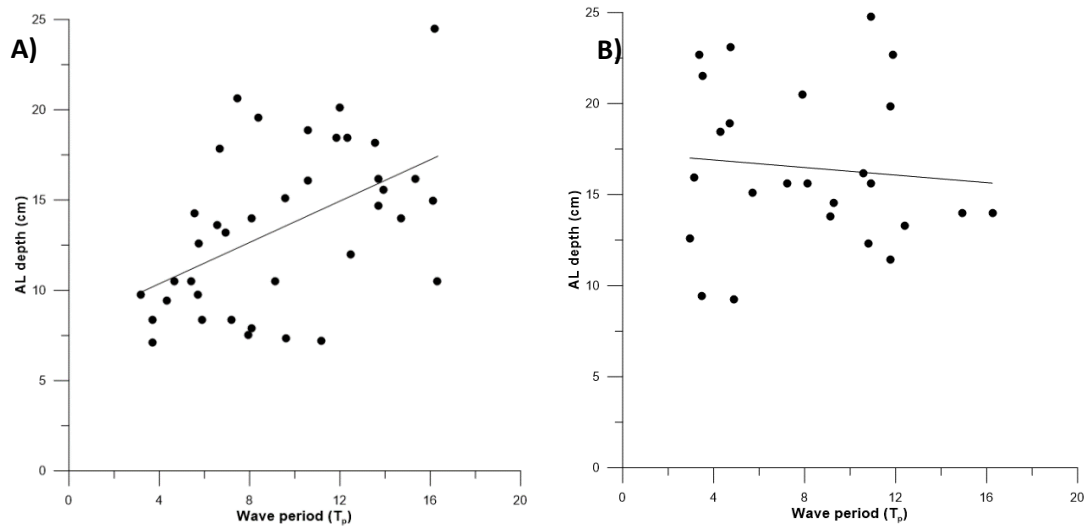


Figure 6.38: Scatterplots showing relationships between daily mean wave period (T_p) and AL depths, for significant wave heights A) below 1 m ($y = 0.613x + 7.646$, $R^2 = 0.298$, $n=38$) and B) above 1 m ($y = 0.057x + 15.549$, $R^2 = 0.002$, $n=25$)

The Pearson's correlation coefficients for the relationship between wave period and AL depth, and wave period and AL depth as a percentage of wave height, for daily average wave heights below and above 1 m are listed in Table 6.17, and indicate that a relationship between daily average wave period and AL depth does not exist once wave heights pass 1 m. Wave period is also a better predictor of pure AL depth than AL depth as a percentage of wave height.

Table 6.17: Pearson's correlation coefficients for the relationships between daily average wave period and AL depth for different wave heights.

	T_p vs AL (cm)	T_p vs AL (% H_s)
$H_s < 1$ m	0.546	0.367
$H_s > 1$ m	0.040	0.003

d. Alongshore

The relationship between peak wave period and AL depth is no clearer when individual measurement points from November 2015 – January 2016 are separated according to profile number. Table 6.18 contains the regression equations and R^2 values, along with Pearson's correlation coefficients for each profile. The correlation is worse when AL depth is considered as a percentage of wave height (Table 6.18, rows 4-6).

Table 6.18: Regression equations and Pearson's correlation coefficients for the relationship between T_p and AL, individual measurements separated by profile

Profile Number	N	Regression Equation	R^2	Pearson's correlation coefficient
1	102	$y = 0.662x + 8.345$	0.090	0.300
2	96	$y = 2.4542x^{0.771}$	0.199	0.407
3	105	$y = 1.027x + 6.699$	0.173	0.416
1 (% H_s)	102	$y = 0.502x + 9.097$	0.042	0.205
2 (% H_s)	96	$y = 0.98x + 5.467$	0.101	0.317
3 (% H_s)	105	$y = 0.866x + 7.175$	0.036	0.281

The average daily values for AL depth on each profile – during the months when three distinct profiles were monitored (November 2015 – January 2016) – were related to wave period to determine whether this made correlations stronger, or whether any differences existed at this scale (Table 6.19). An improvement in the relationship with pure AL depth is seen, but the Pearson's correlation coefficients for the relationship between wave period and AL depth as a percentage of wave height are not strengthened as much. The correlation and regression lines are similar for each of the three profiles (Figure 6.39).

Table 6.19: Pearson's correlation coefficients for the relationship between wave period and daily average AL depth for each profile (November 2015 – January 2016).

	N	T_p vs AL	T_p vs AL as % H_s
Profile 1	24	0.560	0.295
Profile 2	24	0.627	0.393
Profile 3	24	0.670	0.394

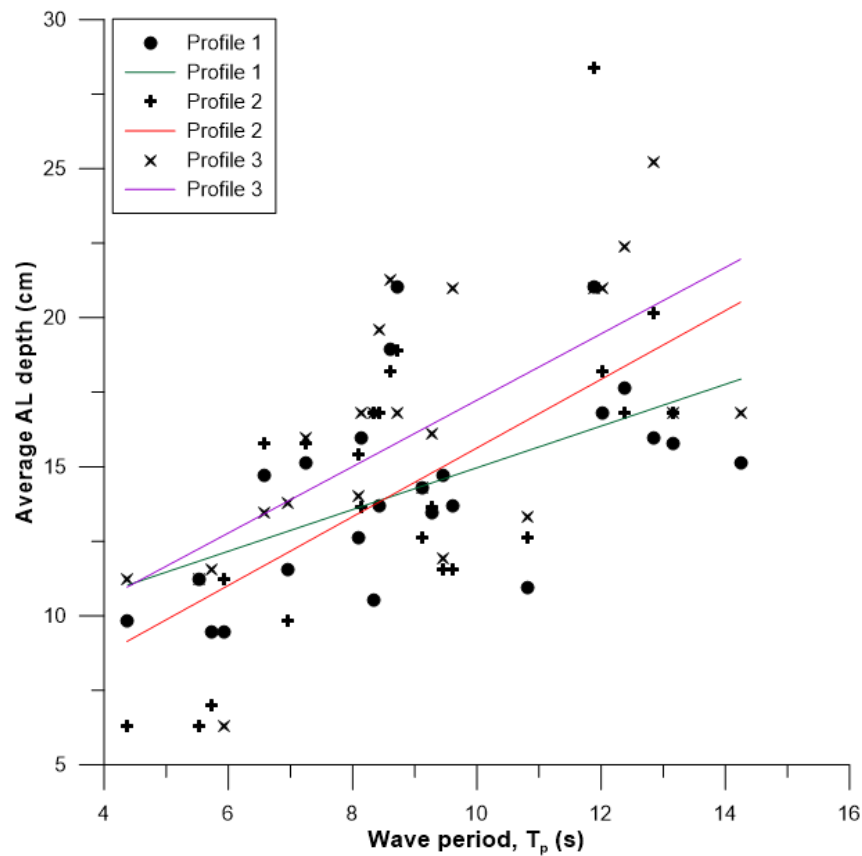


Figure 6.39: Scatterplot and regression lines for wave period against average AL depth on each profile per day (November 2015 – January 2016 field periods). (Profile 1: $y = 0.70x + 7.959$, $R^2 = 0.314$, $n=24$. Profile 2: $y = 1.152x + 4.118$, $R^2 = 0.393$, $n=24$. Profile 3: $y = 1.114x + 6.103$, $R^2 = 0.449$, $n = 24$).

e. Across shore

When measurements were separated into upper, middle, and lower sections of the beach, the strongest relationship between wave period and AL depth is found in the lower beach, and when using raw AL depth measurements rather than as a percentage of wave height (Table 6.20). However, this relationship can still only be classed as ‘moderate’.

Table 6.20: Regression equations and Pearson’s correlations for relationships between wave period and AL depth (both raw measurements and as a percentage of wave height), for the upper, middle, and lower sections of the beach.

		Tp vs AL (cm)	Tp vs AL (%H _s)
Upper	Regression equation	$y = 0.174x + 11.601$	$y = 0.634x + 8.351$
	R ²	0.007	0.043
	Pearson’s correlation coefficient	0.081	0.207
Middle	Regression equation	$y = 0.769x + 6.989$	$y = 9.237 e^{0.052x}$

	R ²	0.130	0.091
	Pearson's correlation coefficient	0.242	0.197
Lower	Regression equation	$y = 0.319x + 4.187$	$y = 0.953x + 8.850$
	R ²	0.221	0.161
	Pearson's correlation coefficient	0.579	0.513

Using the 1 m elevation bins, Pearson's correlation coefficients follow the same pattern, and are strongest in areas under 1 m elevation (Table 6.21). But even in these areas there is still only a 'moderate' link between wave period and AL depth, and a slightly weaker link between period and AL depth as a percentage of wave height.

Table 6.21: Pearson's correlations between peak wave period and AL depth (both raw measurements and as a percentage of wave height) within elevation bins (indicating cross-shore differences)

	Tp vs AL	Tp vs %Hs
<0 m (n=19)	0.470	0.401
0-1 m (n=93)	0.459	0.427
1-2 m (n=99)	0.264	0.166
2-3 m (n=59)	0.102	0.208
>3 m (n=5)	-0.220	0.194

f. By area within the groyne

The regression equations for the relationship between peak period and AL depth within each section (Figure 6.9) are seen in Table 6.22. There are large differences in the strength of the relationship between sections, and no consistent pattern to indicate whether pure AL depth or AL depth as a percentage of wave height has the better relationship. Sections 6 and 9 are the areas of Profiles 2 and 3 closest to low tide level, and section 8 is the middle section of Profile 3, so this would indicate that the influence of wave period is strongest in the lower and east area of the groyne compartment. The relationship in these areas is still only weak to moderate though.

Table 6.22: Regression equations for relationships between wave period and AL depth within each of the nine groyne sections

Box Number	N	Regression equation	R ²	Pearson's correlation coefficient	Pearson's T _p vs AL (%H _s)
1	33	Y = 0.345x + 12.311	0.024	0.154	0.378
2	100	Y = 0.372x + 11.786	0.031	0.177	0.213
3	27	Y = 0.292x + 5.709	0.079	0.282	0.119
4	61	Y = -0.111x + 16.598	0.003	-0.050	0.136
5	126	Y = 0.379x + 11.532	0.039	0.196	0.113
6	56	Y = 1.257x + 1.377	0.225	0.474	0.449
7	29	Y = 0.171x + 10.935	0.009	0.093	0.144
8	65	Y = 1.472x + 5.578	0.352	0.593	0.255
9	32	Y = 0.755x + 5.821	0.160	0.400	0.277

g. At specific locations

The relationship between wave period and AL depth was not found to be consistent at each of the selected SID locations (Table 6.23). Most locations had a stronger correlation between wave period and raw AL depth rather than AL depth as a percentage of wave height. The relationship is generally stronger for SIDs measured during the second winter, which agrees somewhat with earlier findings based on the individual field periods (section b). The strongest correlation was found at Nov15 C15 / Jan16 C13, which was located in the mid-east area of the groyne compartment. It is not clear why there is no continuity of positive and negative relationships for the two sets of variables; this perhaps indicates that wave period is not a dominant predictive factor at this scale.

Table 6.23: Pearson's correlations between wave period and AL depth (both raw measurements and as a percentage of wave height) for specific locations at which repeated measurements were taken.

SID number	Number of measurements	Correlation between T _p and AL	Correlation between T _p and AL as %H _s
Dec14 C4 / Jan15 C4 / Feb15 C5	26	0.179	0.235

Dec14 C5 / Feb15 C3	22	-0.040	-0.023
Jan15 C3 / Feb15 C4	9	0.111	-0.251
Nov15 C14 / Dec15 C12 / Jan16 C12	22	0.583	0.365
Nov15 C16 / Dec 15 C14	13	0.522	0.488
Nov15 C15 / Jan16 C13	16	0.844	0.739
Dec15 C5 / Jan 16 C7	15	0.477	0.092
Dec15 C7 / Jan16 C9	12	0.170	-0.058

iv. Relationship with wave power

a. Overall

King (1951) indicated that wave power can be used as a predictor for AL depth; her results showed that AL depth increases with wave power. However, since that study, it does not appear that any others have investigated this further. Due to the weak relationship between wave height and AL depth, it was decided to investigate the potential correlation with wave power. To assess this relationship in the current study, wave power values were required to be calculated from the measurements taken at the CCO Wave Rider.

Equations for wave power can be relatively complicated and vary from deep to shallow water, and as such, it is difficult in this case to select an appropriate equation. The deep water equation for wave energy flux using Airy wave theory is

$$P = EC_g = \frac{\rho g^2 T H^2}{32 \pi} \quad (\text{eq. 6.1})$$

Where ρ is water density, g is acceleration due to gravity, T is wave period and H is wave height. In this case, because the variations in water density are unknown, ρ is a constant value ($1,025 \text{ kg.m}^{-3}$), as are g and π . This equation then simplifies to $P = 981.211 H_s^2 T$. A power value was calculated for each 30 minute measurement interval as provided by the Wave Rider, and these were then averaged across the time period over which AL depth measurements were taken (approximately 24 hours) to provide an average wave power value for each day.

Figure 6.40 indicates the overall relationship between wave power and AL depth for individual measurements across the whole study. The correlation is stronger when the percentage of wave height is used, rather than pure AL depth.

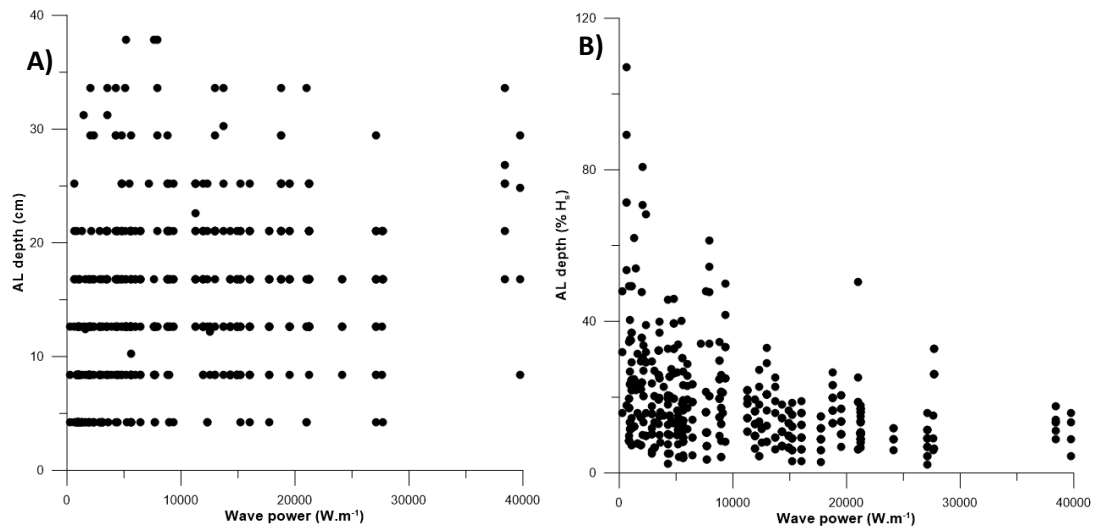


Figure 6.40: Scatterplot indicating relationship between wave power and individual measurements of A) AL depth, and B) AL depth as a percentage of wave height. N=554.

b. Temporally

A scatterplot showing average daily wave power plotted against average daily active layer depth indicates a weak relationship between the two variables (Figure 6.41A). There is a slightly stronger correlation when AL depth as a percentage of wave height is used (Figure 6.41B).

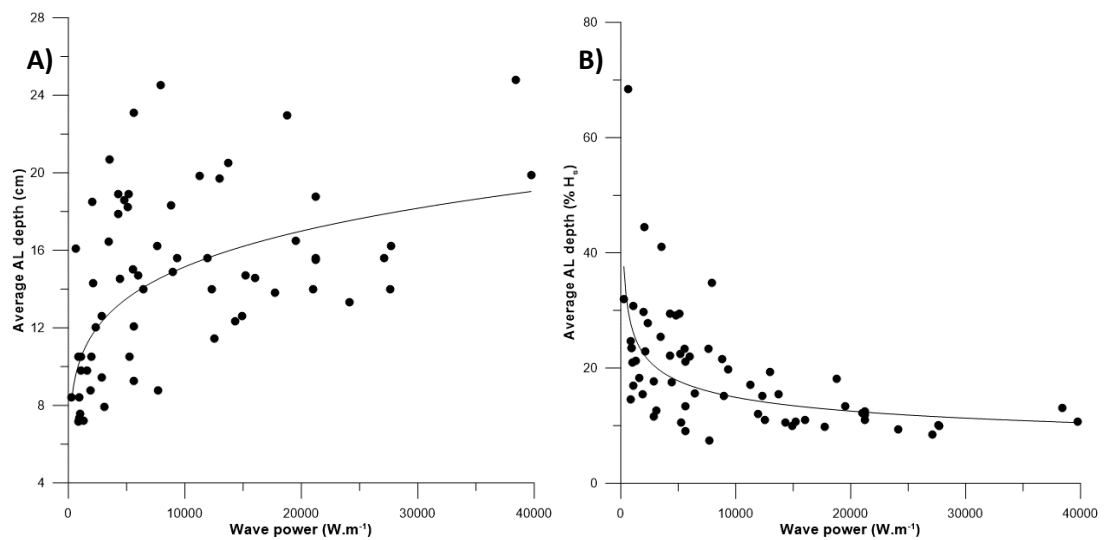


Figure 6.41: A) Scatterplot showing wave power plotted against daily mean AL depth ($y = 3.309x^{0.165}$, $R^2 = 0.353$, $n=63$.), B) Scatterplot showing wave power plotted against daily mean AL depth as a percentage of wave height ($y = 150.619x^{-0.251}$, $R^2 = 0.412$, $n=63$).

When these daily averages are split into the study periods, the strength of the relationship between wave power and AL depth varies significantly (Table 6.24). The months with the best

fitting regression lines align with months where wave height was a stronger predictor (section 6.3.ii.b); they do not align with wave period predictions (section 6.3.iii.b).

Table 6.24: Relationships between daily mean wave power and daily mean AL depth for each study period.

Study period (month)	Number of days	Regression line equation	R ²
October 2014	5	$Y = 4.359 x^{0.094}$	0.056
December 2014	10	$Y = 2.905 x^{0.177}$	0.495
January 2015	6	$Y = 1.897 x^{0.222}$	0.543
February 2015	12	$Y = 18.245 e^{-0.000007x}$	0.111
March 2015	9	$Y = 11.802 e^{0.00004x}$	0.058
October 2015	6	$Y = 0.001x + 9.083$	0.584
November 2015	9	$Y = 13.556 e^{0.000007x}$	0.019
December 2015	6	$Y = 2.722 x^{0.186}$	0.299
January 2016	9	$Y = 1.350 x^{0.251}$	0.649

c. Alongshore

The relationship between wave power and AL depth for individual measurements (both raw measurements and as a percentage of wave height) does not change dramatically between the 3 profiles (Table 6.25).

Table 6.25: Pearson's correlation coefficients for relationship between wave power and AL depth on each profile between November 2015 – January 2016.

	Profile 1	Profile 2	Profile 3
P / AL (cm)	0.262	0.207	0.179
P / AL (%H _s)	-0.341	-0.321	-0.346

For daily averages of measurements on each profile (Table 6.26), the correlations overall are improved, but still follow the same pattern as for the individual measurements, with the strongest correlation existing on Profile 1 (Table 6.25). Profile 3 is the only one for which AL depth as a percentage of wave height has a stronger correlation than pure AL depth.

Table 6.26: Pearson's correlation coefficients for relationship between average wave power and daily average AL depth on each profile (November 2015 – January 2016).

	Profile 1	Profile 2	Profile 3
P / AL (cm)	0.496	0.378	0.261
P / AL (%H _s)	-0.457	-0.323	-0.409

d. Across shore

The relationship between wave power and AL depth is consistent between the upper, middle and lower sections of the beach (Table 6.27). When AL depth is considered as a percentage of wave height, the relationship is slightly better for the upper beach (but still relatively weak), and weakest on the lower beach.

Table 6.27: Pearson's correlation values for relationships between wave power and AL depth for upper, middle and lower beach sections.

	U	M	L
P / AL (cm)	0.358	0.346	0.347
P / AL (%H _s)	-0.319	-0.292	-0.175

Splitting the data into 1 m elevation bins indicates that the relationship between wave power and AL depth is strongest between 1-2 m elevation, but when AL depth is considered as a percentage of wave height that changes; in this case, the strongest relationship exists at elevations greater than 3 m. However, there are only 5 data points in this category (Table 6.28).

Table 6.28: Pearson's correlation coefficients for relationship between wave power and AL depth for different elevation bins.

	Power vs AL	Power vs %H _s
<0 m (n=19)	0.176	-0.373
0-1 m (n=93)	0.173	-0.244
1-2 m (n=99)	0.483	-0.280
2-3 m (n=59)	0.382	-0.306
>3 m (n=5)	-0.176	-0.636

e. By area within the groyne

Using the sections from Figure 6.9, relationships between wave power and AL depth were assessed for separate areas within the groyne compartment. None of the nine individual sections have a strong relationship between wave power and AL depth, as evidenced by the low R² and Pearson's values in Table 6.29. The Pearson's coefficients are generally stronger when wave power is related to AL depth as a percentage of wave height rather than using the raw AL data; this is true for six of the sections.

Table 6.29: Regression equations and Pearson's correlation coefficients for relationship between wave power and AL depth in 9 sections of the groyne compartment.

Box Number	N	Regression equation	R ²	Pearson's correlation coefficient	Pearson's correlation coefficient: Power vs AL%H _s
1	33	$Y = 0.0003x + 12.652$	0.092	0.303	-0.441
2	100	$Y = 0.0001x + 14.483$	0.012	0.109	-0.346
3	27	$Y = 0.00002x + 8.256$	0.002	0.282	-0.555
4	61	$Y = 0.0002x + 13.095$	0.059	0.242	-0.348
5	126	$Y = 0.0002x + 13.004$	0.097	0.312	-0.315
6	56	$Y = 0.0003x + 12.191$	0.053	0.229	-0.155
7	29	$Y = 0.00003x + 12.207$	0.002	0.049	-0.575
8	65	$Y = 0.0004x + 14.005$	0.150	0.388	-0.269
9	32	$Y = 0.0003x + 9.384$	0.141	0.375	-0.247

f. At specific locations

The relationship between wave power and AL depth can be classed as moderate to strong for two of the SID locations, though one is a better relationship when raw AL depth is used (Table 6.30, row 1), and the other is better when AL depth as a percentage of wave height is used (Table 6.30, row 3). There are two others which have moderate strength relationships (Table 6.30, rows 2 and 4). Out of eight SID locations, six have a stronger correlation when the percentage of wave height is used instead of raw AL depth.

Table 6.30: Pearson's correlation coefficients for relationship between wave power and AL depth at specific measurement locations

SID number	Number of measurements	Correlation between P and AL(cm)	Correlation between P and AL(%H _s)
Dec14 C4 / Jan15 C4 / Feb15 C5	26	0.674	-0.336
Dec14 C5 / Feb15 C3	22	0.109	-0.550
Jan15 C3 / Feb15 C4	9	0.437	-0.772
Nov15 C14 / Dec15 C12 / Jan16 C12	22	0.114	-0.495

Nov15 C16 / Dec 15 C14	13	0.257	-0.370
Nov15 C15 / Jan16 C13	16	0.378	-0.167
Dec15 C5 / Jan 16 C7	15	0.230	-0.340
Dec15 C7 / Jan16 C9	12	0.209	-0.394

v. Relationship with wave direction

Miller *et al.* (2011) and Bertin *et al.* (2008) have previously found relationships between wave direction and active layer depth, though they contradict each other: Miller *et al.* (2011) states that active layer depth decreases under oblique waves, whereas Bertin *et al.* (2008) suggests that the opposite is true. Although the range of angles of wave approach at Eastoke is small (Figure 6.42), it is nonetheless necessary to determine whether a relationship exists between wave angle and active layer depth at this site.

Figure 6.42 includes data from the Wave Rider on all days that active layer measurements were collected. The majority of waves approached from angles between 180 and 200 degrees. The beach where AL measurements were taken is orientated approximately S-SSW (its shore normal is at approximately 185°), meaning that these waves approached almost perpendicular to the shoreline.

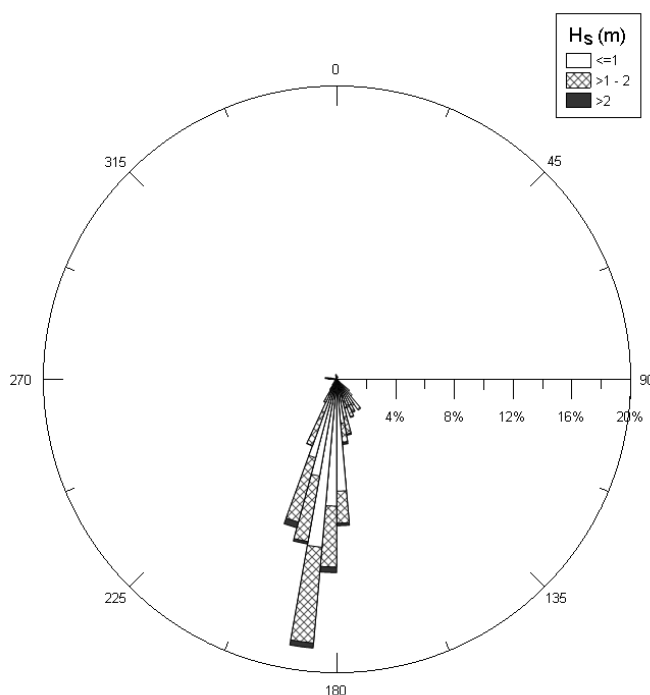


Figure 6.42: Wave rose indicating direction and H_s during the 72 study days.

The Pearson's correlation coefficient between wave direction and AL depth (n=554) is -0.133, indicating a very weak relationship. When AL depth as a percentage of wave height is used, this value is -0.140, which does not constitute a real difference.

When the daily average AL depth is compared to wave direction, the correlations are -0.200 for average AL depth and -0.167 for average AL as a percentage of wave height. There is no statistically significant correlation between wave direction and depth, both for raw measurements (Figure 6.43A) and as a percentage of wave height (Figure 6.43B).

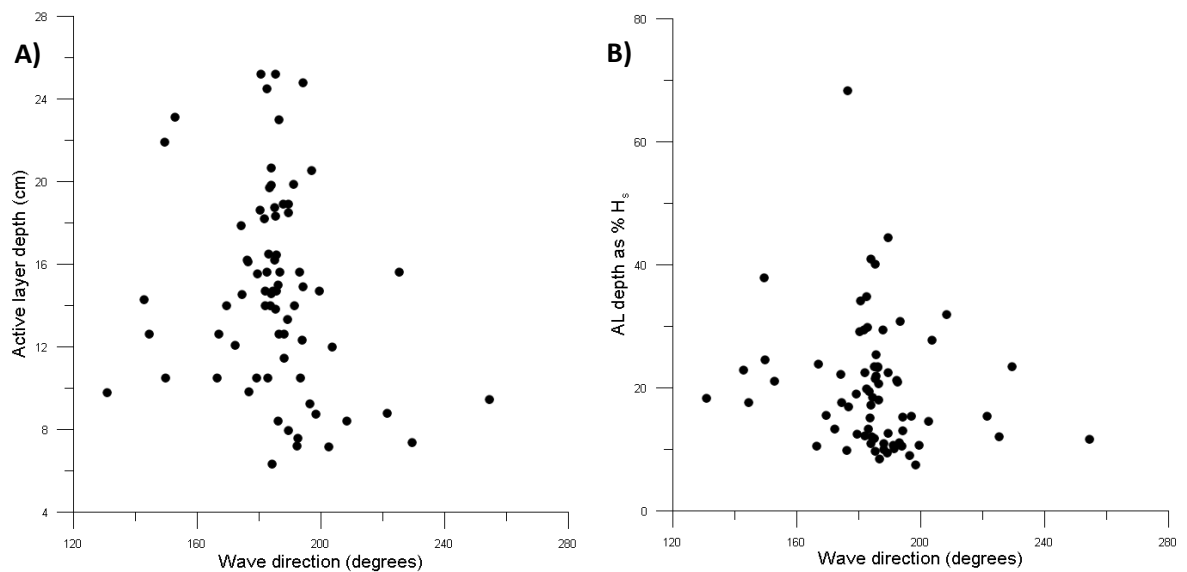


Figure 6.43: A) Scatterplot comparing mean wave direction to mean AL depth for the 72 study days. B) Scatterplot comparing wave direction with AL depth measurements as a percentage of wave height for the 72 study days.

The daily wave direction and active layer data were investigated for relationships within each monthly study period (Appendix J; Table 6.31). Most months show a general downward trend, indicating that as wave angle increases, active layer depth decreases. However, the highest R^2 value – in November 2015 – still indicates only a moderate strength relationship, and as has been mentioned previously, the number of days in each study period does not allow statistically significant conclusions to be drawn. Similar relationships exist when comparing wave direction to active layer as a percentage of wave height.

Table 6.31: Relationships between wave direction and active layer depth during each study period.

Month	Number of days	Trendline	R^2
October 2014	5	$Y = -0.144x + 36.33$	0.389
December 2014	10	$Y = 0.081x - 1.776$	0.112
January 2015	6	$Y = -0.203x + 55.55$	0.339
February 2015	12	$Y = 0.038x + 10.414$	0.003

March 2015	9	$Y = -0.129x + 38.814$	0.054
October 2015	6	$Y = -0.099x + 29.102$	0.217
November 2015	9	$Y = -0.369x + 84.97$	0.566
December 2015	6	$Y = 0.217x - 23.696$	0.183
January 2016	9	$Y = -0.078x + 29.781$	0.262

a. Variation between Profiles 1-3

Table 6.32: Regression equations and R^2 values for relationships between AL depth and wave direction on each profile.

	Regression equation	R^2
Profile 1	$y = -0.075x + 28.797$	0.050
Profile 2	$y = -0.112x + 36.044$	0.047
Profile 3	$y = -0.085x + 31.265$	0.036
Profile 1 (%Hs)	$y = -0.056x + 24.452$	0.023
Profile 2 (%Hs)	$y = -0.091x + 31.565$	0.076
Profile 3 (%Hs)	$y = -0.088x + 32.733$	0.061

The relationship between wave direction and AL depth does not improve when data are separated by the profile on which they were measured (Table 6.32). The differences (or lack thereof) between AL depths on different profiles discussed in previous sections are also not believed to be linked to wave direction; no relationships were found when correlating the differences between average daily AL depths as a percentage of wave height from Profiles 1-2, 2-3, or 1-3 with average wave directions for the same timeframe.

vi. Depth of disturbance rods

Anfuso and Ruiz (2004) found different relationships with wave height for the foreshore as opposed to the low tide terrace, so it was necessary to ensure active layer measurements were undertaken on as much of the beach profile as possible. Due to difficulties obtaining measurements in the lower third of the beach during the first fieldwork winter (2014-15), depth of disturbance rods were inserted in this area on some days during the second winter (2015-16). These were not particularly well-suited to this relatively high energy environment and more often than not were unsuccessful, but a total of 18 measurements were collected during November 2015, December 2015 and January 2016 under a variety of wave conditions. Figure 6.44 indicates a lack of correlation between these two variables, but they do fit into the broader range of active layer values measured using SIDs (Figure 6.46).

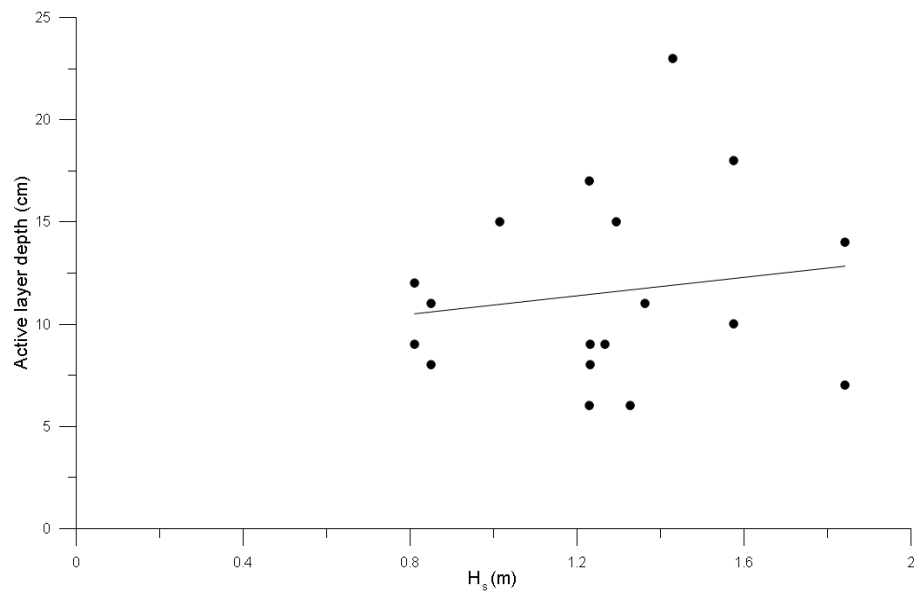


Figure 6.44: Scatterplot of significant wave height against active layer depth obtained using depth of disturbance rods in the lower beach. $n=18$. Mean AL depth = 11.6 cm, maximum = 23 cm, minimum = 6 cm. Trendline sits at $y = 2.2577x + 8.7004$. $R^2 = 0.0243$.

These active layer measurements were then plotted as a percentage of wave height (Figure 6.45) to determine whether a relationship existed similar to the SID results (section 6.4.iii). There is a general downward trend, which agrees with the SID measurements (Figure 6.46), but the correlation coefficient is relatively low suggesting this is only a weak relationship. The average result for AL as a percentage of wave height is 9.6 %.

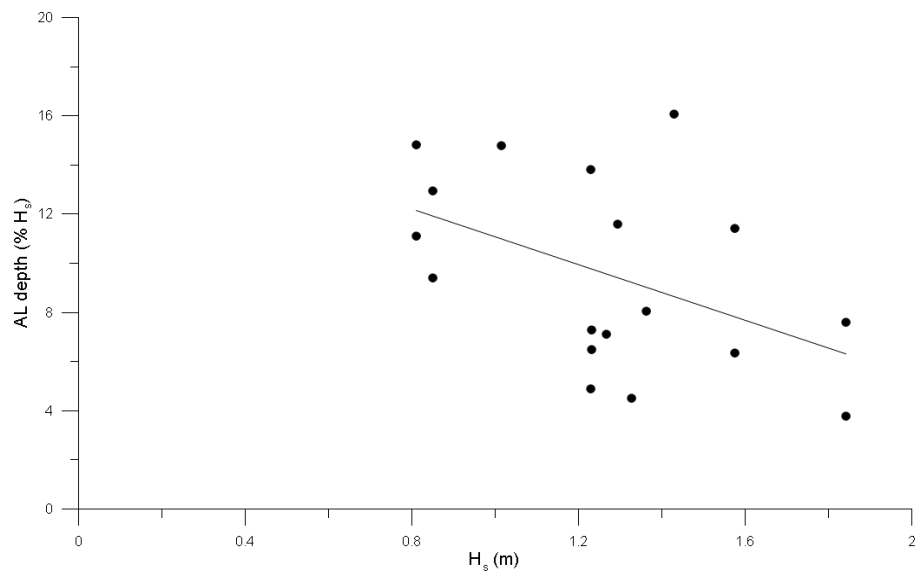


Figure 6.45: Relationship between wave height and AL depth as a percentage of wave height, measured using depth of disturbance rods. Trendline sits at $y = -5.658x + 16.722$. $R^2 = 0.217$. $n=18$.

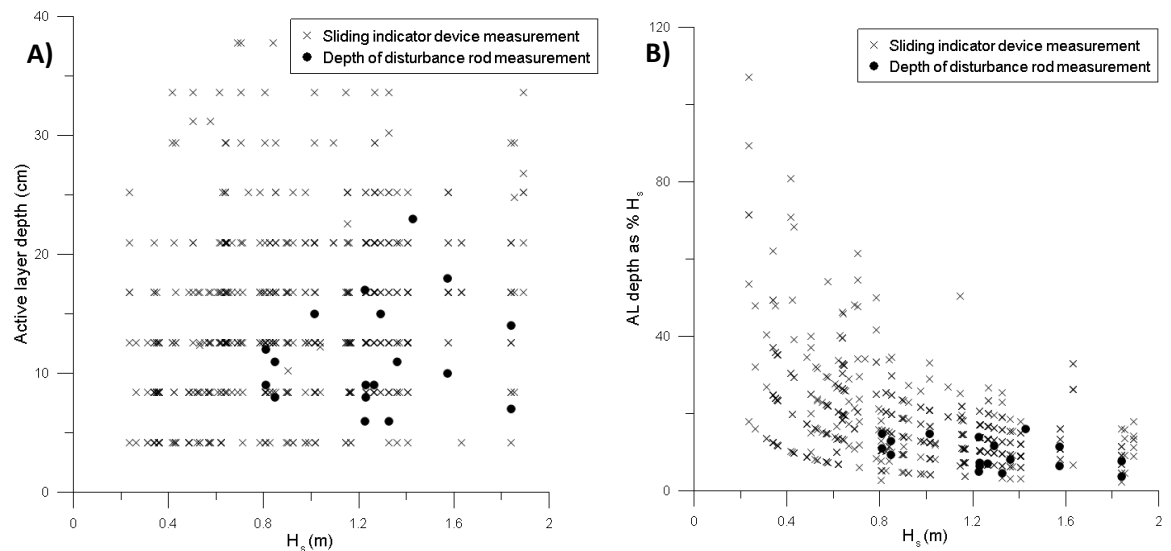


Figure 6.46: Comparison of AL measurements taken using SIDs and depth of disturbance rods A) in measured values, and B) as a factor of wave height. $n=572$.

vii. Multiple Regression Analysis (MRA)

Individually, none of these variables can adequately predict active layer depth. Multiple Regression Analysis (MRA) can be used to produce an equation to predict AL depth by incorporating multiple independent variables. Standard multiple regression was chosen over stepwise multiple regression in this case, as this research is seeking to explain theoretically which variables may be the most influential, rather than practically assessing how few variables need to be measured for the model to provide the best fit.

MRAs were run both with data from individual AL measurements and with daily averages. The individual measurements were analysed based on wave height, period, direction, tidal range, slope angle at the point of measurement, sediment properties (sand content versus D_{50}), and elevation and distance of point from the groyne (as proxies for position on the beach). The majority of these variables were not found to be statistically significant to the model.

The final model produced with individual measurements was found to be statistically significant $F(3,550) = 27.601$, $p < 0.001$. However, the adjusted R^2 is only 0.126. It is not surprising that this value is so low; the only independent variables found to be statistically significant were wave conditions (Table 6.33), which means there are multiple AL depths for each combination of variables.

Table 6.33: Summary of multiple regression analysis for individual AL depths

Variable	B	Standard error of B	Beta	<i>p</i>
Constant	15.899	3.341		<0.001
Wave height, H_s	4.253	0.698	0.243	<0.001
Wave period, T_p	0.488	0.086	0.226	<0.001
Wave Direction	-0.054	0.017	-0.129	0.001

Predicting AL depth to a reasonable degree of accuracy at this scale is impossible with the current results. The errors would then be scaled up as multiple points would need to be predicted across the beach face. To reduce this error, multiple regression was run for daily average AL depths. Daily averages were compared only to wave height, period and direction. Of these variables only wave height and period were found to have a statistical significance (Table 6.34), producing an equation with an adjusted R^2 value of 0.292. The model was shown to statistically significantly predict active layer depth: $F(2,60)=13.784$, $p<0.001$.

Table 6.34: Summary of multiple regression analysis for daily average AL depths. n=63.

Variable	B	Standard error of B	Beta	<i>p</i>
Constant	6.266	1.705		<0.001
Wave period, T_p	4.073	1.176	0.373	<0.001
Wave height, H_s	0.496	0.139	0.382	<0.001

The adjusted R^2 value increases if squared values of AL depth as a percentage of wave height are used as the dependent variable (they have to be squared before use in order to produce linear relationships with the independent variables, which is one of the assumptions that must be met before multiple regression analysis can be run). Various points were highlighted as outliers or leverage points in the analysis, so the final equation has $n=59$. The model was found to statistically significantly predict squared AL depth as a percentage of wave height, $F(2,56)=28.517$, $p<0.001$, adjusted $R^2 = 0.487$ (Table 6.35).

Table 6.35: Summary of multiple regression analysis for squared daily average AL depths as percentages of wave height.

Variable	B	Standard error of B	Beta	<i>p</i>
Constant	609.534	90.523		<0.001
Wave period, T_p	-491.366	66.273	-0.712	<0.001
Wave height, H_s	22.613	7.788	0.279	0.005

Using daily averages for each profile allowed for the inclusion of variables such as slope angle and percentage profile change. However, with pure AL depth as the dependent variable, wave height and period were still the only variables with statistical significance in the analysis. This did not change when the squared values of AL depth as a percentage of wave height was used instead; in this case, only wave period appeared to be statistically significant.

Therefore, the most accurate predictions using multiple regression techniques still do not explain as much of the variation at a daily scale as a simple pair of calculations based on significant wave height (section 6.3.ii.b).

6.4 Discussion

i. Variation in AL depth

Overall, the range of values for the active layer depth found during this study correlate fairly well with Whitcombe's (1996) results, which are also from beaches on Hayling Island. Using tracer columns he found active layer depths of 5-15 cm, with 40-45 cm experienced during storm conditions. The smaller maximum readings from the current study could be due to the limited wave heights experienced during measurement periods: none of the active layer measurements in this study were taken over periods when prolonged wave heights >2 m occurred.

There is a high degree of variability in the measurements of active layer depth at Eastoke. This variability is often not apparent in previous studies of active layer depth. If each study period is considered by itself, the number of measurements and days over which these occurred is more similar to previous studies by other authors. In general, this does not reduce the amount of variation experienced.

Figure 2.2 in Chapter 2 indicated some of the complex interactions between morphology and hydrodynamics on mixed sediment beaches. It is most likely that the variation experienced is a result of the complexity of mixed sediment beaches in general, combined with the effects of

groynes, which can cause wave refraction and scour. This can lead to marked variations in profile shape within groyne cells (Chapter 5.2.iv), thus also affecting slope angle, which should have a strong influence on AL depth (e.g. Williams, 1971; Ferreira *et al.*, 2000).

Section 6.3.i detailed the temporal and spatial variations in AL depth without relating them to wave conditions. The first key point to take away from this section is that no statistically significant differences were found between active layer measurements on the three profiles used in Winter 2015-16. This is contrary to what might have been expected, as the beach profiles were often different shapes, which could reasonably have been expected to alter their reactions to wave conditions. Additionally, the presence of groynes is known to cause wave reflection, refraction and localised rip currents, all of which would influence the power of water to entrain and transport sediment. These localised changes would have been expected to cause differences between AL measurements on different profiles. However, it is possible that the hydrodynamics and groynes do not always interact in the same way, leading to the overall lack of variation even though small variations can be seen sometimes.

There is significant variation in active layer depth across the beach face, with areas near the high and low tide lines experiencing smaller active layer depths than areas in the middle of the profile. A statistically significant difference was found between measurements taken on the lower beach (< 0.5 m elevation) and those on the mid beach (0.5 – 2 m elevation). This agrees with previous results by King (1951), Williams (1971) and Curoy (2012), who theorise that the cause of this variation is related to where waves break on the profile at different points of the tidal cycle; the greatest impact from waves breaking throughout the course of a tidal cycle is in the middle section of a beach. The relationship is limited however, with Figure 6.7 indicating no clear correlation between cross-shore position and AL depth, which could be explained by the type of beach. If, as authors have suggested in the past, cross-shore variation is due to the position of the wave breaking zone, the shorter distance between low and high tide at this beach (due to its steeper slope) may explain why the variation is less observable than in previous research. Wave breaking is heavily influenced by the size and position of the beach step (Austin and Masselink, 2006). They found that their maximum AL depth measurements occurred at approximately the positions of the step at high tide and just before low tide. There was not scope within this study to track the position of the step throughout tidal cycles, so the current results cannot provide further evidence for this claim.

The overall smaller AL depth in section 3 of the 9 areas within the groyne compartment is likely due to the orientation of the beach – the elevation here is lower, and anecdotally the

groundwater level was higher here than in equivalent areas on Profiles 2 and 3. High groundwater decreases AL depth by reducing the ability of waves to infiltrate within the sediment, as the pore spaces are already filled with water (Blanco, 2003).

The best explanation for the variation, without considering wave conditions, was sediment composition – and in particular sand content. Possibly because of the pre-existing relationships between beach slope angle and active layer depth (e.g. Williams, 1971; Anfuso, 2005) and the relative difficulties associated with sediment sampling in comparison to measuring beach slope, many previous studies have not considered the link between sediment size and active layer depth, with only a few authors doing detailed enough studies to be able to investigate a potential relationship (e.g. Saini *et al.* 2009). Beach-wide averages were found to have stronger correlations (with average AL depth) than individual samples with their respective AL measurement, especially during the second winter when samples were taken spaced along the central profile rather than at specific SID locations. 15 data points is not enough to state with certainty that this relationship is statistically significant, but it seems likely that further research would find a similar relationship.

The permeability of mixed sediments is more dependent on the smaller grains in the mix (Mason and Coates, 2001), so it is unsurprising that a better relationship with AL depth was found for the percentage of sand in sediment samples than for D_{50} . This agrees with previous research on mixed beaches (e.g. Blanco, 2003), which often indicates the inadequacy of the D_{50} measurement to accurately represent the range and proportions of grain sizes.

For the individual measurements and samples, sediment samples taken at SID locations directly prior to AL measurements had a better correlation than those taken afterwards, which disagrees with the averaged results. The relationship is weak, with a Pearson's correlation coefficient of only -0.336, so the level of confidence in this finding is low. This limited relationship is not what would be expected if sediment is a controlling variable in active layer depth; it would be expected that a better relationship should be found by taking samples at individual measurement points, rather than by averaging them over the whole beach face. The dominant grain size of a beach is generally linked with overall beach slope, which has already been suggested by multiple authors to be the "most important" influencer of AL depth (e.g. Williams, 1971; Anfuso, 2005); perhaps the fact that overall beach slope is less influenced by small-scale differences in sediment composition explains the limited correlation between individual samples and their respective AL depths.

There was also minimal overall variation in AL depth associated with different surface sediment codes, though any true patterns may be obscured by the dominance of certain codes over others. Sediment coding systems have proven difficult to use on mixed sediment beaches, as the number of codes required to accurately portray the proportions of different grain sizes at particular points would be far too high (Chapter 5). It is likely that the simplification of sediments into the 8 chosen codes is at least partially to blame for the lack of correlation here.

There was no relationship between profile slope angle and average AL depth. There was also only a weak inverse relationship with local bed slope – this is the opposite of what would be expected based on the overall trend for steeper beaches to have greater AL depths (e.g. Ciavola *et al.*, 1997; Anfuso, 2005), and is a new finding as far as the author is aware.

Individual dGPS measurements of elevation change showed no correlation between elevation change and AL depth. Comparing these results with profile changes in Chapter 5 also indicates that the maximum AL depth does not usually correlate with areas of maximum erosion or accretion – the ‘middle’ section of the beach often experiences the greatest AL depth, despite experiencing limited morphological change, whereas the greatest morphological change often occurs around high tide level on mixed sediment beaches as berms are formed, moved or removed.

At a larger scale, active layer depth can be great even when consecutive daily profiles experience minimal change in cross sectional area, indicating that change in beach profile is not sufficient to show that sediment transport is occurring. This agrees with results found by Curoy (2012). The relationship between change in cross-sectional area and profile averaged AL depth is better than elevation change at individual points, and is clearer when the beach is eroding than when it is accreting.

ii. Relationship with wave height

The range of values produced when each measurement is converted to a percentage of wave height is much greater than ranges supplied by previous authors, likely due to the complexity of this site. There was less variation in percentages during the second winter, possibly because of a general increase in wave heights, which tends to create lower percentage values.

The overall relationship for the average daily values can be expressed as $Z_m = 0.2H_s$, which correlates well with results from other coarse clastic beaches (for example, Masselink *et al.*

(2010) and Miller and Warrick (2012) – see Chapter 2 Table 2.1). However this does not take into consideration the large amount of variation which exists within the data. Ciavola *et al.* (1997) identified a relationship whereby $Z_m = 0.27H_b$ on steep sand beaches, which could reasonably have been expected to apply to a mixed beach as well. However, both Curoy (2012) and the present study found that the Ciavola *et al.* (1997) equation produced values for active layer depth which were greater than those measured. Compared to Ciavola's equation ($Z_m = 0.27H_b$) for steep sand beaches, Curoy's (2012) results were 26 % (Cayeux-sur-Mer) and 70-85 % (Birling Gap) lower than expected. This study produced results more similar to the results from Cayeux-sur-Mer, though it used significant wave height (H_s) rather than breaking wave height (H_b) indicated by Ciavola *et al.* (1997). Though breaking waves are normally higher than the same waves measured before shoaling, in this case the wave data used was from an offshore buoy, so the waves will have lost some of their height due to energy dissipation in decreasing water depth before increasing in height again at break point.

This difference in measured values versus predicted values could be caused by a much larger volume of data used in the present study compared to Ciavola *et al.* (1997), who had only five days of data spread across three beaches – two of the beaches they studied only had one day of data collection – so in light of the variability shown at Eastoke, Ciavola *et al.*'s (1997) data cannot be considered representative of those beaches under different hydrodynamic conditions; their experiments covered only situations where wave heights were between 0.36 to 0.8 m. The relationship between significant wave height and daily average AL depth is stronger within almost every study period than for all days combined, which perhaps goes some way to explaining why previous authors have been so adamant that a strong relationship exists between wave height and AL depth, as each of these study periods was closer in length to the majority of previous studies on this topic.

There is a good relationship between wave height and daily average AL depth as a percentage of wave height, meaning that a regression equation could be created and used to predict (to a relatively good degree of accuracy) daily average AL depth. Though this does not account for small scale variations experienced across the beach face, it is at a more similar scale to what would be required to predict longshore sediment transport rates in the future. It also provides a counterpoint to Williams' (1971) assertion that the difference in percentage values between his research (40 %) and that of King (1951) (4 – 10 %) was due to beach slope: in actuality, it may have been due to the differences in wave conditions between the two projects. King (1951) measured AL depth under wave heights up to 1.5 m, whereas the maximum wave

height experienced during Williams' (1971) project was only 0.2 m. The current project indicates that percentage values are much higher for lower wave heights, which may help to explain the discrepancy between these values.

This relationship is not dissimilar to results found by Sunamara & Kraus (1985) who found that AL depth increases linearly with wave height up to 1.5m significant wave height, and after that, the rate of increase decreases as the wave height increases. They related this to the shear stress, suggesting that the friction coefficient decreases for increased wave heights. This would potentially result in the energy of the wave being spread over a wider area of beach and thus decrease the active layer depth while increasing its width. Another potential theory comes from Puleo *et al.* (2014), who indicates that larger waves produce more turbulence, which may decrease the amount of energy available for sediment transport, which would prevent the active layer depth from increasing linearly with wave height. This would also suggest that sediment size distributions may be key, as these can change rapidly on mixed sand and gravel beaches, and different particle sizes and mixtures would require different amounts of energy to be transported.

Surface sediment codes indicate that areas classified as either "pure" or "large" have greater maximum values, but the means are similar to the "mixed" and "small" groups, so there is no clear distinction, despite previous research indicating that larger sediments have greater AL depths (e.g. Blanco, 2003) and the theory that mixed sediments would have more limited infiltration and thus smaller AL depths. The second could be caused by the grouping of pure gravel points and pure sand points, but there were insufficient numbers of each of these codes to produce three comparable groups.

The relationship between AL depth and sand content does not improve when the percentage wave heights are used instead of pure AL depth measurements. Sand content is still a better predictor than D_{50} , but it is surprising that including wave height does not explain some of the variation in this relationship. Theoretically, these two variables were expected to exert the strongest influence on active layer depth, but it appears that, at least at this small scale within the beach, sediment composition is not a good predictor of AL depth. This does agree with Saini *et al.* (2009), who did not find significant differences between three patches with different proportions of sand and gravel on the same beach.

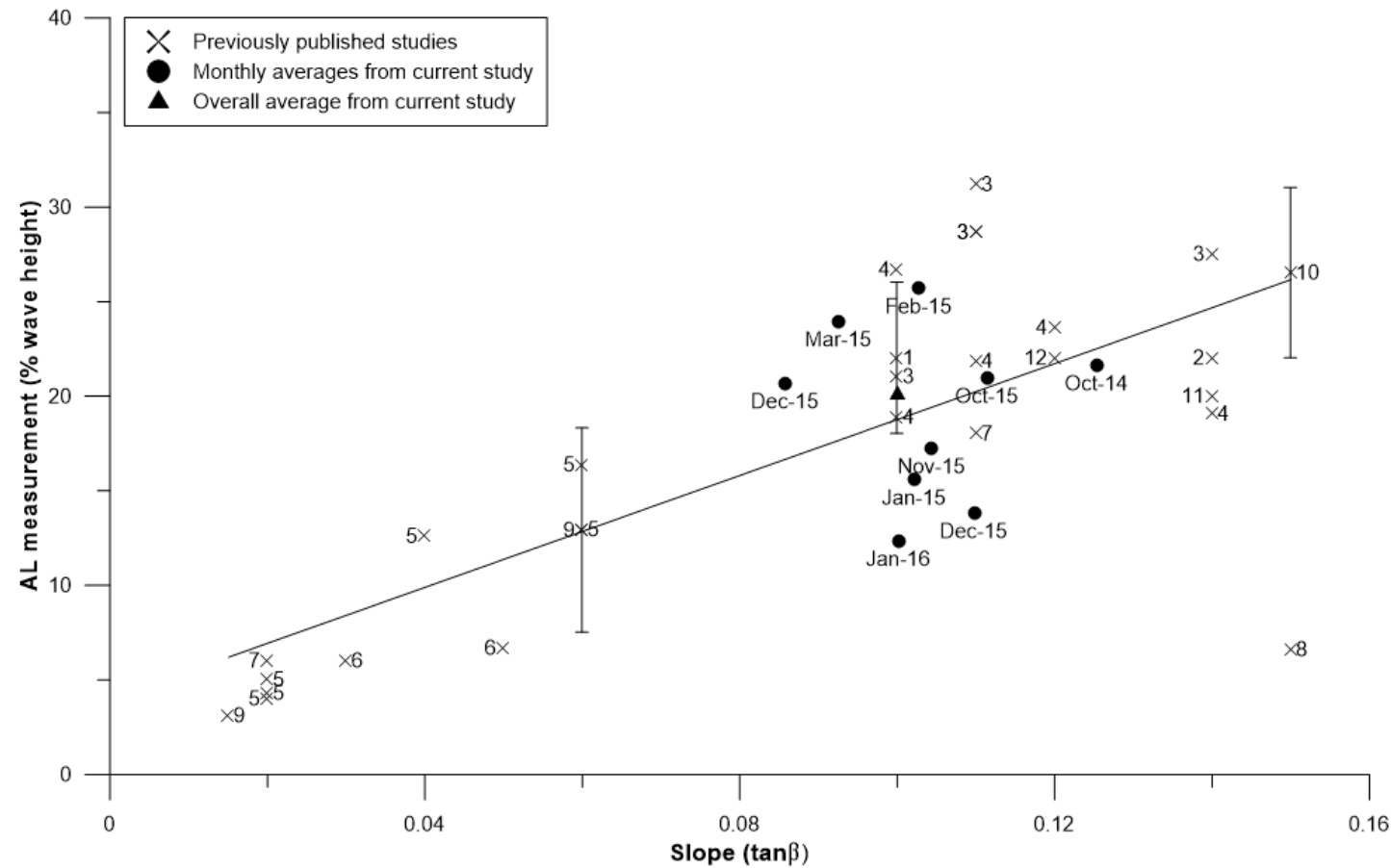


Figure 6.47: Average AL values (as a percentage of wave height) from published studies undertaken on beaches with varying slope angles, compared to average AL values (as a percentage of wave height) from each study period, and overall, within the current study. Error bars were used for studies where a range of values was provided. (Study numbers relate to the following studies: 1) Jackson and Nordstrom (1993); 2) Sherman *et al.* (1994); 3) Ciavola *et al.* (1997); 4) Ferreira *et al.* (1998); 5) Anfuso *et al.* (2000); 6) Anfuso *et al.* (2003); 7) Anfuso and Ruiz (2004); 8) Austin and Masselink (2006); 9) Bertin *et al.* (2008); 10) Saini *et al.* (2009); 11) Curoy (2012); 12) Miller and Warrick (2012).) Regression line fits previously published studies.

Individual measurements comparing active layer depth to local bed slope were inconclusive (section 6.3.ii.e), and there was no correlation between profile slope and profile averaged AL depth. However, the average beach slope of $\tan\beta = 0.1$ (calculated from daily profiles), combined with the average AL depth of 20.07 % of significant wave height, sits close to the regression line produced by amalgamating many previous studies into active layer depth (Figure 6.47). Furthermore, many of the studies used in Figure 6.47 are from sand beaches, indicating that active layer measurements of mixed sediment beaches may be broadly similar, as has been suggested in the past (e.g. Mason and Coates, 2001).

The overall average value of 20.1 % is lower than Ciavola *et al.*'s (1997) value for steep foreshores (27 %), but is at least in the same order of magnitude, as opposed to 4 % for King (1951) working on gently sloping sand beaches.

Using Ferreira *et al.*'s (2000) equation $Z_m = 1.86H_s \tan\beta$, and the average values for significant wave height (0.87 m) and beach slope ($\tan\beta = 0.1$), a value for the mixing depth of 16.1 cm is calculated. Though this is relatively close to the average measured AL value of 14.7 cm, it is apparent from the lack of a relationship at a daily scale that this calculation would not provide accurate results for this beach in short term experiments.

As far as the author is aware, this is the first study which has investigated the role of beach slope in active layer depth on the scale of local bed slope. The data does not agree with the hypothesis, extrapolated from studies investigating the relationship between overall beach slope and active layer depth, that steeper slopes correlate with greater active layer depths. The most likely explanation for this lies in the morphology of mixed sand and gravel beaches. One of the key features of such beaches is the beach step, which is located just below the low tide level (Masselink *et al.*, 2010). This has been shown to change size and location as the tide rises and falls and exists in a feedback loop with wave height, whereby it is both affected by incoming waves and can cause wave breaking patterns to change (Masselink *et al.*, 2010). Additionally, the variation in slope angle is relatively minimal both spatially and temporally, so it may be less of an influence at this scale as it is when comparing a shallow sloping beach to a steep one.

There was a statistically significant difference of measurements of AL depth as a percentage of wave height between the upper and mid beach areas. This is likely due to the difference in wave breaking as the tide reaches different stages on the beach. However, the relationship between wave height and AL depth did not improve if the upper, middle and lower beach were

considered separately, and no overall correlation was found between elevation and AL depth as a percentage of wave height. In terms of sediment transport, it is useful to know if there are certain areas of the beach which experience greater amounts of transport, and AL depth is a relatively good indicator of this. Producing a 2D model of AL depth across shore for specific wave conditions would have been ideal, but unfortunately the relationship is not strong enough to justify this.

Splitting the beach into 9 sections indicates that some of the cross-shore variation is explained by proximity to groynes, but although the relationships are stronger in each of these sections, good predictive equations for each section cannot be produced.

Repeating measurements at exact locations should be dulling the effects of groynes and minimising variation, allowing good predictive equations to be created for each location individually, but relationships were still not straightforward. Multiple types of regression lines provided best fit for different points, and most of these did not explain the variation well, indicating that it would be difficult to produce a model that could predict beach-wide variations in AL depth.

There was no relationship between change in elevation and AL depth as a percentage of wave height at individual points, but when profile averaged values and change in cross-sectional area were used there was a relatively strong inverse relationship. The relationship between change in profile CSA and AL depth as a percentage of wave height is perhaps not surprising, given that Chapter 5 showed a link between lower wave heights and smaller amounts of profile change, and this chapter has shown that the AL depth as a percentage of wave height is highest for smaller waves.

Williams (1971) suggested that AL depth was best measured on stable beaches where no profile change is occurring. These results corroborate this statement to some degree, but also indicate that only measuring AL depth when there is no profile movement would not provide realistic real-world insights, as profiles on this type of beach are rarely stable. It does, however, indicate that rates of longshore transport may be higher when cross-shore transport (indicated by profile change) rates are lower. It is indicative of the inability of profile change to provide meaningful values for rates of LST.

iii. Relationship with wave period

Due to the bimodal nature of wave conditions at Eastoke beach, it was expected that a link would be found between wave period and AL depth. However, overall results show no correlation between these variables. This is at odds with the initial pilot study for this project, which was undertaken during March 2014 and is discussed in Appendix Q.

Sunamara and Kraus (1985) found that wave periods of 4 – 8 s could influence active layer depth. This pattern was specifically apparent for wave heights above 1.5 m. For the current study, there were only 19 days with wave periods between 4 – 8 s, and none of these had wave heights above 1.5 m. Different beaches experience different wave conditions, but even considering all 19 days and investigating separately the links for mean active layer measurements and AL as a percentage of wave height for each of these days, no similar relationship was found between wave period and AL depth. There is however a weak correlation between wave period and AL depth when only data from days with wave heights under 1 m is used, which may be related to the strong relationship found during the Pilot study, which also experienced predominantly small wave heights.

Wave period was found to be a better predictor of AL depth in the lower east sections of the groyne compartment. This is likely due to the influence of the groyne on wave refraction patterns, and is an important finding which the author does not believe has been shown in any previous studies.

There was also no overall correlation between wave period and AL depth as $\%H_s$, but some study periods have stronger correlations: notably, October 2014, November 2015 and January 2016 for daily average values. However, each of these includes very few data points.

The correlation between wave period and AL depth is slightly stronger when profiles are considered separately, but this may be linked to the fact that the second winter did have slightly better correlations, and this is also the winter when three profiles were consistently monitored.

The standard deviation in daily active layer measurements shows some correlation with wave period. As far as the author is aware, this has not been discovered by any authors previously, but could perhaps be explained by the fact that larger wave periods transfer greater energy to the beach. If AL depth is larger in areas of breaking waves, and the standard deviation is generally indicative of cross-shore variation, this could explain why the standard deviation is higher for longer wave periods.

iv. Relationship with wave power

Perhaps surprisingly, most authors do not consider the influence of wave power on active layer depth. King (1951) indicated that though there was a relationship, it was more scattered than the relationship between wave height and AL depth. She suggests that the reason the relationship between wave power and AL depth appears to exist is because of the inclusion of wave height within the wave power equation. The current project produced similar results, indicating that overall wave height is a better predictor than wave power, so despite the prevalence of bimodal wave conditions at this site (Chapter 3.3.i), it appears that wave period is not a useful predictor of AL depth.

It would be interesting to further investigate this relationship by more directly measuring wave power at the shoreline. This might also make it more feasible to measure differences in wave power throughout the tide, and attribute specific wave energies to particular cross-shore locations.

v. Relationship with wave direction

Unlike Miller *et al.* (2011), no link was found between active layer depth and wave direction. This is potentially due to the limited wave directions experienced at this location; the majority of waves approach more or less perpendicular to the shoreline, and as such Miller *et al.*'s (2011) finding that more oblique waves produce greater active layer depths could not be sufficiently investigated at Eastoke.

However, it was still possible to test Bertin *et al.*'s (2008) equation for AL depth on sand beaches, which incorporates beach slope, significant wave height, and angle of incidence:

$$Z_0 = 1.6 \tan \beta H_s^{0.5} \sqrt{(1 + \sin(2 \alpha))}$$

(where Z_0 = sediment activation depth, β = beach face slope, α = the wave angle at breaking). Using the average values for each of these variables across the whole study period, $\tan \beta = 0.1$, $H_s = 0.866$, and $\alpha = 0$. This produces a value whereby $Z_0 = 0.149$ m, or 14.9 cm. This is exceptionally close to the measured average value of 14.7 cm, though the caveat that wave data was not measured directly at the shoreline must be applied. It must also be considered that the angle of incidence was only estimated based on ortho-rectified aerial imagery and not from direct measurements. Still, the apparent accuracy of this equation suggests that these three factors may be important in terms of estimating average AL depth.

However, when daily values (separated into average value per profile) were tested for fit with this equation, its fit worsened (Figure 6.48). While many of the data points are predicted within 5 cm of the actual measurements, there are also some points which were massively underpredicted. The reason for this is unclear, but it must be noted that Bertin *et al.* (2008) specify that the angle of the breaking wave should be used; anything else would not be accurate enough. Those data are not available for Eastoke, and so only the wave angle from the nearby wave buoy could be used. It is possible that this does not perfectly correlate with angles of incidence experienced as waves break, which could explain why no relationship was found at Eastoke.

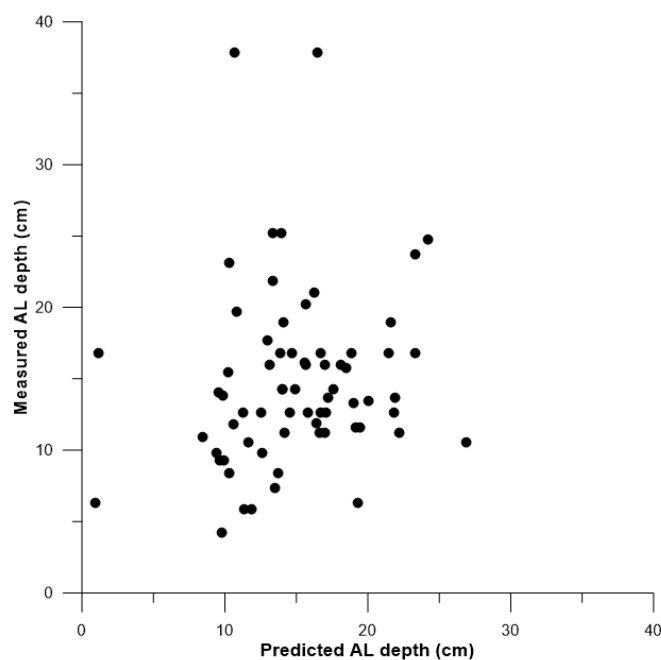


Figure 6.48: AL depth as predicted by the Bertin *et al.* (2008) formula, versus the actual measured AL depth. Each point represents the daily mean value for one profile.

It could have been argued that the lack of variation in AL depth between the three profiles was caused by a variety of wave direction approaches, leading results to even out over the study. However, no correlation was found between wave direction and differences on the profiles.

vi. Depth of disturbance rods

Anfuso and Ruiz (2004) found different relationships with wave height for the foreshore as opposed to the low tide terrace, with the active layer measured at 18 % and 6 % of wave height respectively. These results are remarkably similar to what was found at Eastoke in this study, with the foreshore presenting an average of 18.0 % and the lower beach 9.6 % of significant wave height. The measurements taken at Eastoke were not exclusively of the low

tide terrace, which is why they are referred to as the 'lower beach'. This may help to explain the slight discrepancy between these results (9.6 %) and Anfuso and Ruiz's (2004) (6 %).

Future research should investigate whether different patterns of sediment transport are occurring in this lower portion of the beach, which is less hindered by groynes, and is composed of mainly sand.

vii. Multiple Regression Analysis (MRA)

Multiple Regression Analysis was run to provide insight into the combined predictive capabilities of variables affecting AL depth. Many variations were tested using individual measurements, profile averages and daily averages, but in the end the best equation could still only provide a moderate fit with the data, and only variables concerned with wave conditions were found to statistically significantly affect the model outcome.

The main issue with running this type of analysis in this situation is the interconnected nature of the variables influencing AL depth, especially on such a complex beach (Chapter 2, Figure 2.2). This causes many combinations of variables to violate one of the assumptions of MRA, which is that there must be no collinearity.

Another part of the problem is the difficulty encountered in aligning measurements of all independent variables. The limited number of cases associated with all input variables meant multiple smaller combinations of variables needed to be analysed. A future study would need to be more meticulously planned to provide a greater number of data points. The current study provides a good basis from which to continue, however.

6.5 Conclusions

The results described in this chapter show a high level of variability in active layer depth for this managed mixed sediment beach. This variability has not been previously highlighted. It is likely that much of this variability can be attributed to the influence of varying sediment mixtures, and refraction and currents caused by the groynes at this particular study site, but more concentrated research into each of these factors would be required to confirm this suggestion, as inshore wave conditions and currents were not measured, and only a weak link was found between AL depth and sediment composition.

The aim of this chapter was to provide further insight into the controls on AL depth on mixed sediment beaches, to improve the accuracy of predictions which can then be fed into

longshore transport estimates. This was achieved by asking how the active layer on this mixed sand and gravel beach was linked to:

- *Wave conditions*

Overall, these results do suggest that wave height is the most significant factor influencing AL depth, though this relationship is not as simple as has been indicated by previous shorter studies which may not have experienced a wide range of wave heights (e.g. Sherman *et al.*, 1994, Williams, 1971). Instead, active layer depth was found to be best predicted by a two step-process involving significant wave height. Wave height was a good predictor of the percentage value, by means of the equation $\ln(y) = -0.797x + 3.565$, $R^2 = 0.578$ (Figure 6.24). Once calculated, the percentage value can then be used to calculate the predicted actual active layer depth for the upper and mid beach at a daily average scale. This is the key finding of this chapter, and could potentially be applied to other mixed sediment beaches, though calibration of the initial equation may be required for different sites.

Unlike in the pilot study (Appendix Q), wave period was not found to be a good predictor of AL depth, and as such wave power was a worse predictor than significant wave height. Wave period was more influential in certain areas of the groyne compartment than others – specifically the southeast corner.

Wave direction was not found to have a significant influence on AL depth, or cause differences between the three profiles measured within the groyne compartment. Though Bertin *et al.* (2008)'s equation including angle of wave approach gave a very close result for the overall average AL depth, it was found to be insufficient to explain all of the daily variations experienced.

- *Beach slope*

Beach slope was not found to be a good predictor of AL depth. Ferreira *et al.* (2000)'s equation incorporating wave height and beach slope was found to be insufficient to predict short-term changes in AL depth, despite providing a good prediction for the overall average at this site.

The overall slope of the beach and average value for AL depth as a percentage of wave height fitted very well onto a regression line created from previous studies on other beaches with varying slope angles. However, the sheer variability of AL depth at this location means that the “average” value is essentially irrelevant.

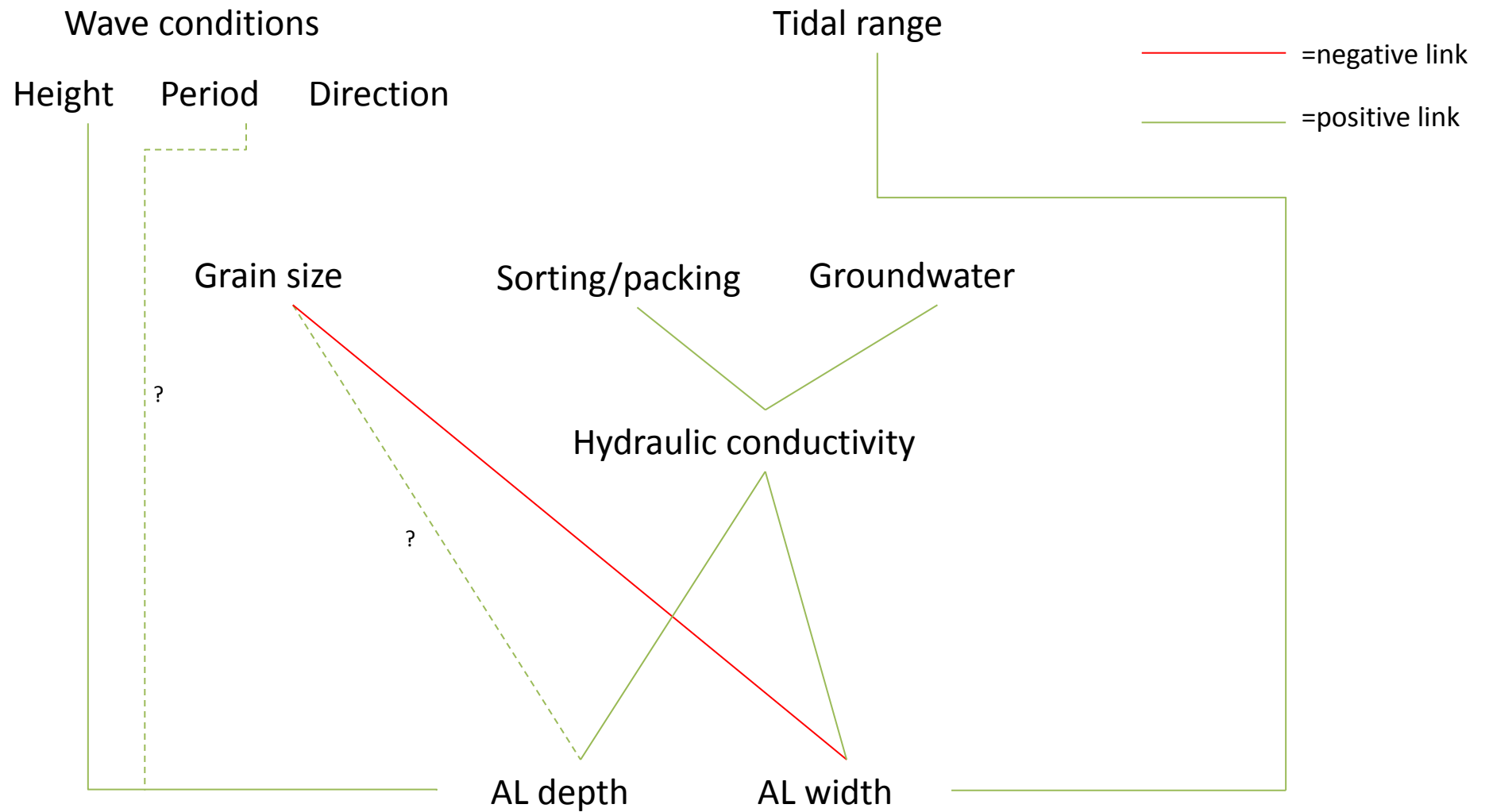


Figure 6.49: Conceptual model of factors likely to have significant impacts on AL depth and width.

- *Sediment composition*

The sediment composition was expected to exert a greater influence on AL depth than the results showed. Despite taking sediment samples from the exact locations of AL measurements in order to directly link sediment proportions with AL depth, only a very weak correlation was found. As sediments on mixed beaches have been shown to change rapidly, a suggestion for improvement in future research would be to allow only one tide to occur between measurements, thus allowing more definitive conclusions to be drawn about the role of sediment composition on AL depth. Additionally, studying the permeability and packing patterns of sediments on mixed beaches is likely to provide further insights into this relationship (Blanco, 2003).

Despite attempts to measure multiple variables alongside AL measurements to determine the relative importance of different factors, it is still difficult to draw any definitive conclusions. Average AL depth across the beach face is much easier to predict with any degree of accuracy than AL depth at a specific location, even when variables such as slope angle, sediment composition, distance from groyne and cross-shore position are known. Figure 6.49 presents a conceptual model of factors believed to be of importance to active layer depth on mixed sediment beaches. This study indicated that wave period may not be important, and grain size (sediment composition) may not be as influential as had been expected.

Other significant findings from this chapter include the relationship between active layer depth and profile cross-sectional area change – indicating that the active layer depth is greatest when the wave energy is not being used to alter the overall shape or steepness of the beachface – and the lack of relationship between wave power and active layer depth. King (1951) had indicated that AL depth increased with wave power, but Figure 6.41A did not show convincing evidence for this theory; the relationship between wave power and AL depth was weaker than the relationship between significant wave height and AL depth for the same data.

The final point of note is that attempts to produce a multiple regression model from the data were mostly unsuccessful. It was not possible to produce a statistically significant model using variables other than wave height and period, meaning that the final model is less useful than the previously mentioned equation for predicting average AL depth from significant wave height. Future research should focus on controls on the hydraulic conductivity as a priority for accurate prediction of active layer depth.

7. Transport Rates & Volumes

7.1 Introduction

This chapter provides results of Radio Frequency Identified (RFID) tracer pebbles deployed on 61 occasions over a total of 8 months between October 2014 and January 2016.

Longshore and cross-shore transport patterns are investigated. These are combined with findings presented in Chapter 6 to produce approximations of transport volumes along this stretch of the coast, which was the site of a new coastal defence project by the Eastern Solent Coastal Partnership (ESCP) in 2013 (Chapter 3.5.ii).

This chapter focuses on research question 3:

- Can the longshore transport rate be used to calibrate an empirical formula such as the CERC equation for this site, and will this calibration value be similar to other mixed sand and gravel beaches?

The intentions of this chapter are to:

- determine short and medium term transport patterns at the Eastoke Defence Scheme part of Hayling beach,
- provide an estimated sediment transport rate for the coarse fraction of the beach at Eastoke,
- combine this with results from previous chapters to produce an estimate for the longshore transport volume along this groyned section of replenished beach,
- calibrate the commonly-used CERC transport equation (USACE, 1984) for future use at this site.

With the costs associated with sourcing suitable replenishment material constantly rising (Moses and Williams, 2008), beach recycling is a more cost-effective way to distribute sediment to areas where it is most necessary. Longshore transport volumes are useful to the ESCP in terms of beach recycling and replenishment, as they can be used to assess how much of the required sediment can potentially be recycled, where from, and how often.

The particular importance of Eastoke as a defence against coastal flooding provides a basis to further this research. Longshore transport calculations for coarse and mixed beaches are understudied compared to sand beaches, which provides a strong rationale for calibrating equations for use on such beaches.

Sediment tracing using the RFID technique has been previously undertaken along stretches of the Solent coastline by the ESCP to determine directions and approximate rates of sediment transport (ESCP, 2013a). However, the previous studies provide only longer-term measurements – monthly surveys with low recovery rates, and so may not show the relative impact of individual wave events, which is addressed in this chapter.

Incorporating active layer data (from Chapter 6) along with tracer velocity rates allows more accurate volumes of transport to be produced. Longshore volume changes calculated from beach profiles in Chapter 5 will be compared to values calculated from tracer data. Calibration values for the CERC equation (USACE, 1984) will be determined and discussed in relation to previous values for coarse grained beaches (e.g. Bray *et al.*, 1996; Curoy, 2012).

7.2 Methods

Approximately 400 pebbles were selected from ‘native’ replenishment material to have B axes long enough to insert a tag of either 23 mm or 32 mm with 6 mm of extra space to allow it to be sealed in place with resin. A smaller number of pebbles were selected to contain 12 mm tags, but a previous study undertaken at Lee-on-the-Solent suggests that the recovery rate for these is so low (5-20 % after one month) that they were not likely to provide any data points (ESCP, 2013a).

The collected pebbles were then drilled, and tags inserted and sealed in place with resin (Chapter 4.7.iv). Three axes and the mass of each pebble were measured, and key statistics for each category can be seen in Table 7.1.

Table 7.1: B axes and mass measurements for tagged pebbles

Tag size	D ₅₀ (mm)	D ₁₆ (mm)	D ₈₄ (mm)	Mean mass (g)	Minimum mass (g)	Maximum mass (g)
12 mm	35.6	31.7	40.6	61.9	40.2	98.2
23 mm	41.0	35.7	49.0	98.0	37.6	255.3
32 mm	55.1	48.6	64.4	217.7	101.2	356.8
ALL	47.5	37.1	58.5	145.0	37.6	356.8

The axes measurements were used to place each pebble within a Zingg shape category (Chapter 4.7.iv). Of the pebbles used in deployments, 79.2 % were classed as ‘spheres’, 8.2 % as ‘rods’, and 12.6 % as ‘discs’.

The pebbles were deployed in columns below the beach surface, following Curoy *et al.* (2009) and Miller and Warrick (2012), with the depth of each pebble measured relative to the surface of the beach.

Evidence from the previous tracer study undertaken at Eastoke (ESCP, 2013) indicates that tracers did not travel further than one groyne cell either side of where they were deployed within the first week. Thus for the surveys which were intended to trace movements within the first few days of each deployment, generally only two or three groyne cells were walked. The main survey area extends to an area known as the Ness (Chapter 3.1), and full surveys were undertaken in April, May, November and December 2015, and January 2016. Results from these can be seen in Figure 7.17.

7.3 Results

i. Detection rates

Total detection rates were not as high as would have been expected based on previous use of this technology, which have been consistently reported to be around 70 % (e.g. Allan *et al.*, 2006; Curtiss *et al.*, 2009; Bertoni *et al.*, 2010). Of the 317 pebbles deployed as part of the study, only 197 were ever detected again, for a total detection rate of 62.1 %. Of these, 114 (34.0 %) were detected during more than one survey. Potential reasons for this are discussed in section 7.4.

Table 7.2 contains separate cumulative recovery rates for each deployment. Only one deployment had a 100 % recovery rate, but eight out of the 14 deployments had recovery rates over 70 %, which is generally considered acceptable for this technology.

Table 7.2: Number of pebbles deployed and cumulative recovery rates for each deployment.

Deploy date	Number of pebbles (number of columns)	Recovery rate
30/9/14	60 (10)	51.7 %
4/12/14	11 (2)	27.3 %
15/1/15	15 (3)	86.7 %
24/1/15	18 (3)	72.2 %
9/3/15	18 (3)	94.4 %
13/3/15	15 (3)	100 %
16/3/15	14 (3)	92.9 %

20/3/15	22 (6)	90.9 %
20/10/15	16 (3)	43.8 %
9/11/15	12 (3)	83.3 %
2/12/15	13 (3)	38.5 %
6/1/16	29 (5)	27.6 %
19/1/16	43 (8)	76.7 %
25/1/16	32 (6)	12.5 %

Recovery rates of each column for every survey date can be seen in Appendix P, along with cumulative recovery rates for each column. The cumulative rates of individual columns vary between 0 and 100 %. Out of 62 columns deployed, 19 had a 100 % cumulative recovery rate, while 24 had a cumulative recovery rate of 50 % or less.

Tracers containing 32 mm tags had a higher recovery rate than tracers containing 23 mm tags (65.6 % and 60.7 % respectively), indicating that the smaller detection range of the 23 mm tags (ESCP, 2013; Appendix N) may be influencing the accuracy of the study. Too few 12 mm tracers were deployed to determine whether the much lower detection rate of these is statistically significant.

Tracer data was also analysed to determine whether tracer shape had any effect on recovery rate. Table 7.3 indicates that differences in recovery rates were minimal between the three different Zingg shapes represented in the tracer population. The total number of rod-shaped tracers in the 32 mm tag population means no definitive conclusion can be drawn from the 100 % recovery rate here, especially because the recovery rate for 23 mm tagged rods is almost exactly the same as those for spheres and rods in this size category.

Table 7.3: Recovery rates for pebbles of different shapes and sizes.

	32 mm tags				23 mm tags				12 mm tags
	Sphere	Rod	Disc	TOTAL	Sphere	Rod	Disc	TOTAL	Sphere
Deployed	102	3	17	122	145	23	23	191	4
Recovered	67	3	10	80	88	14	14	116	1
% Recovery	65.7	100	58.8	65.6	60.7	60.9	60.9	60.7	25.0

Initial recovery rates for pebbles from individual columns when surveys were done within 3 days of deployment ranged between 0 – 100 %. The disparity between these recovery rates can sometimes be seen between individual columns buried on the same day, but on different parts of the profile. Pearson's correlation tests were run to determine whether position on the profile had any bearing on the recovery rate of pebbles from particular columns (n=61). Using the overall recovery rates produced a result of $r = -0.384$ ($p < 0.005$), which is a moderate relationship, and statistically significant result. However, no statistically significant relationship was found for the initial recovery rates, on which this would be expected to have a greater influence.

It is unclear whether tracers are more likely to be detected on particular parts of the profile in the long term. Figure 7.17 indicates that tracers detected in the fourth groyne bay from the west were all located at approximately the same beach level. However, this pattern is not repeated in other groyne compartments.

ii. Short term transport

From the successful surveys done within one day of deployment, a clear pattern of transport direction does not emerge. Tracers certainly are not subject to the dominant transport direction of this coastline as a whole, which is to the east. Figure 7.1 shows the initial directions and distances of travel of all tracer pebbles detected after only one day in-situ. Cross-shore transport distances are generally smaller than alongshore distances for the same time period. The mean longshore distance travelled by tracers in their first day was 3.97 m, with a mean cross-shore distance of 0.62 m seaward. However, the mean absolute distance travelled was 20.03 m; this number is much larger because it is not balanced out by tracers travelling in opposite directions. These numbers are based on only 44 measurements (approximately 14 % of all deployed tracers) and so should be treated with some degree of caution; they are likely quite representative of transport during March 2015, when most of these successful 1-day recoveries were made, but may not be representative of any longer term change.

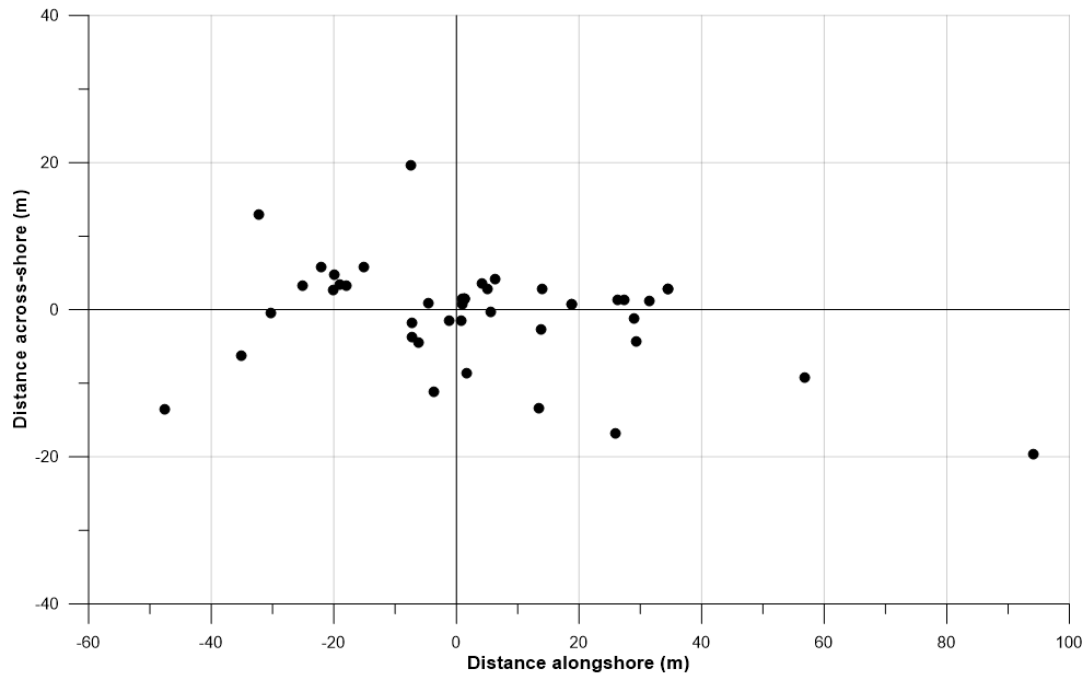


Figure 7.1: Direction and distance of pebble transport from deployment location after 1 day. N=44.

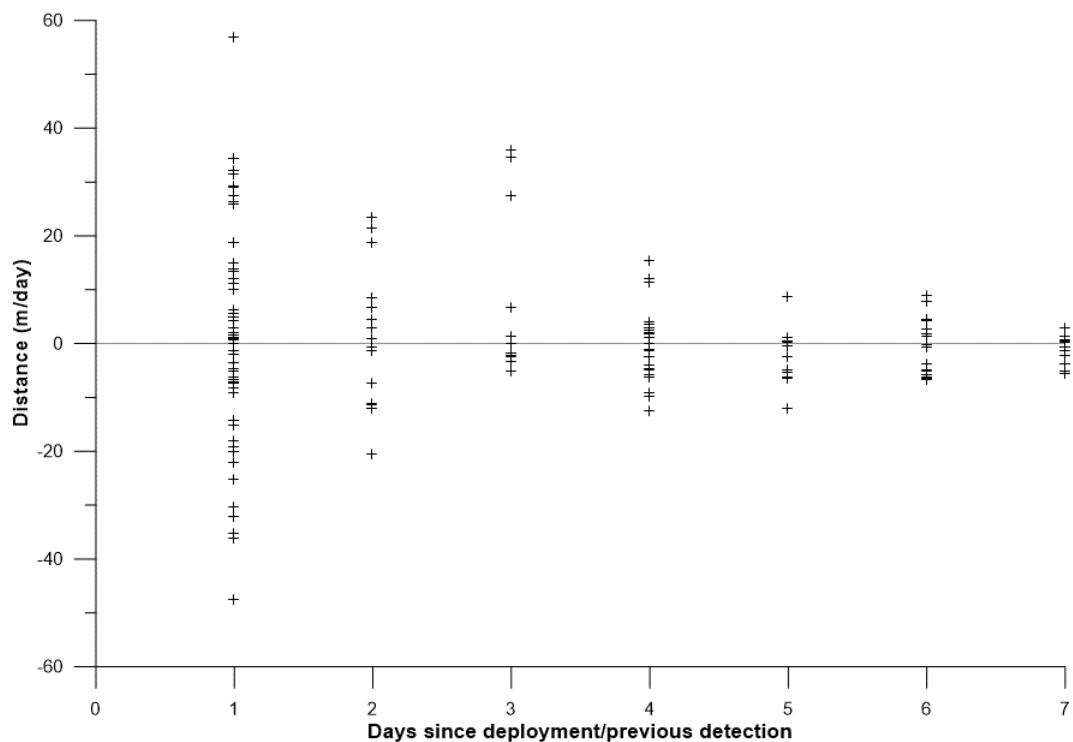


Figure 7.2: Longshore transport distances of pebbles recovered within 7 days of deployment or previous detection. N=165.

The tracers were investigated to determine whether size of the pebbles had any influence on transport directions or distances in this initial period. Neither pebble mass nor B axis length was found to affect total distance travelled in the first day after deployment (Figure 7.3, Figure 7.4). Pebble mass was found to be a slightly better predictor of longshore

transport distance than B axis length (Figure 7.5, Figure 7.6). However, neither measurement had a strong relationship with distance.

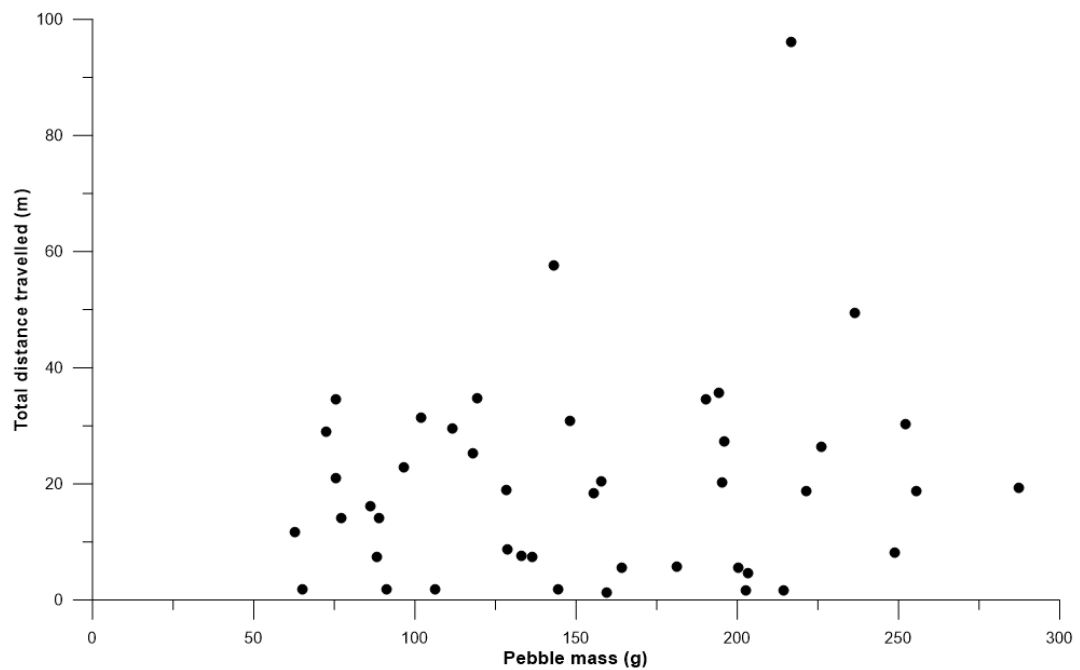


Figure 7.3: Total distance travelled in first day according to tracer mass. N=44.

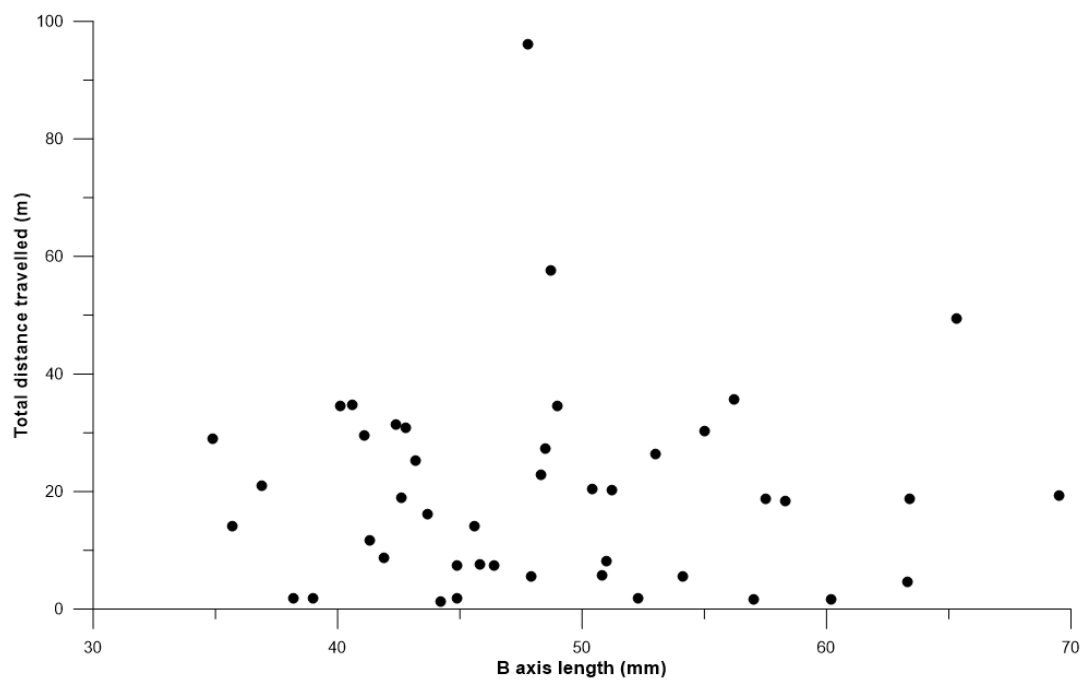


Figure 7.4: Total distance travelled in first day according to B axis of tracer. N=44.

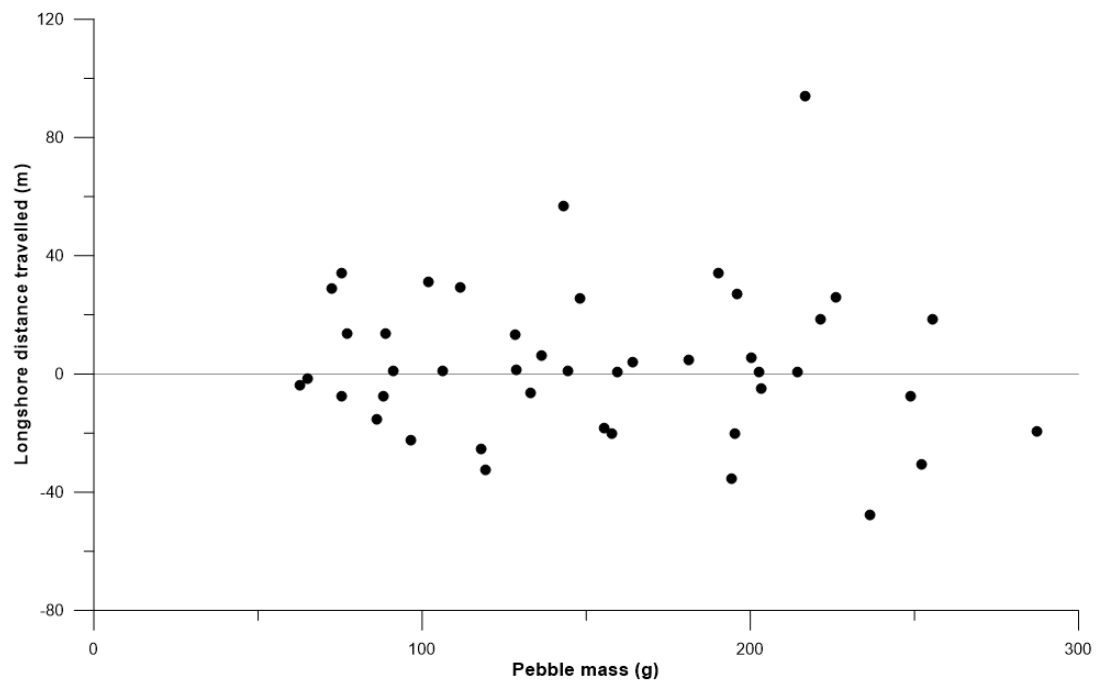


Figure 7.5: Longshore distance travelled in first day according to tracer mass (positive values indicate eastwards transport). N=44.

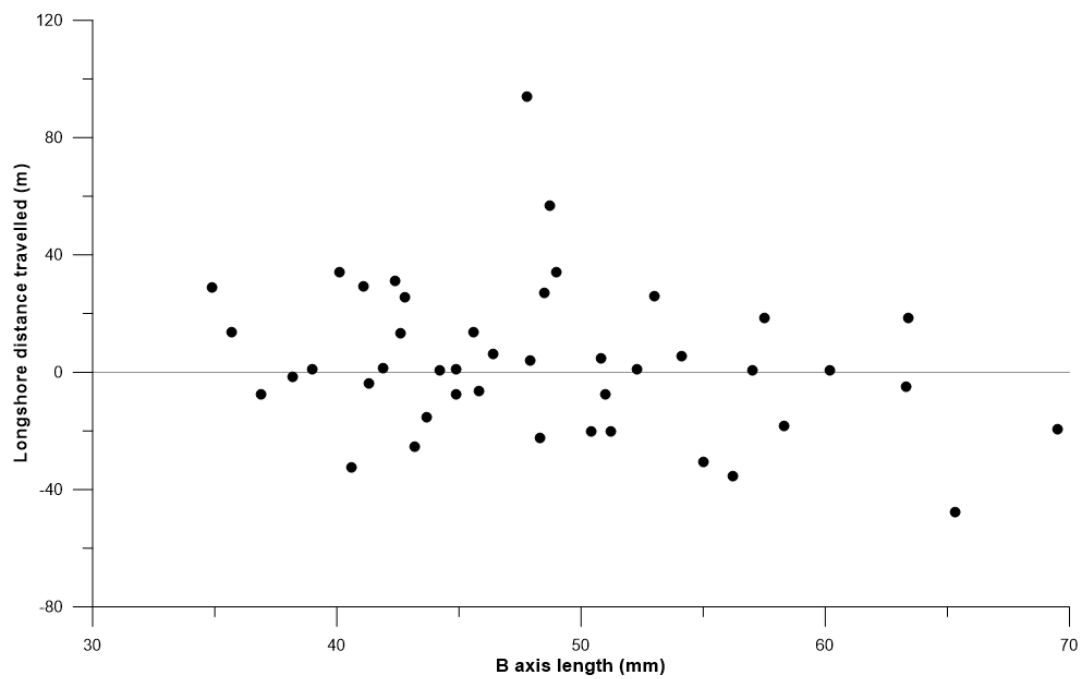


Figure 7.6: Longshore distance travelled in first day according to B axis of tracer (positive values indicate eastwards transport). N=44.

iii. Transport relative to deployment depth

Part of the reasoning behind burying pebbles in columns was to produce an indication of the possible existence of differential transport rates at different depths within the active layer, to provide further evidence towards Miller and Warrick's (2012) research indicating that pebbles buried lower in the active layer had a slower rate of transport than those nearer the surface. Figure 7.7 shows that no real relationship can be detected between burial depth and distance travelled; the Pearson's correlation coefficient for this set of data is -0.235, indicating a very weak relationship whereby increased burial depth decreases initial distance travelled.

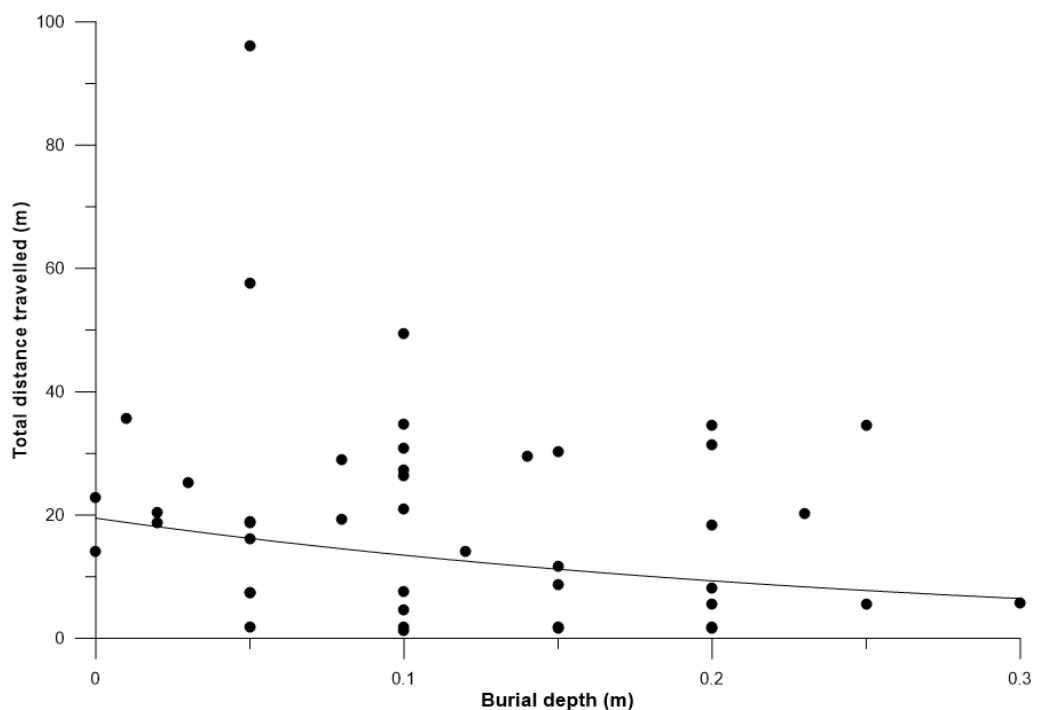


Figure 7.7: Relationship between burial depth and distance travelled during the first day after deployment. ($y = 19.491e^{-3.688x}$, $R^2 = 0.064$).

These relationships are weaker for distance east (0.041) and distance north (0.105). This seems to have little to do with wave conditions. Using only the 20 distances of pebbles deployed on 19/01/2016 and detected the following day, the Pearson's correlation coefficient is 0.077 (and not statistically significant).

Slight differences in the relationship are apparent when data is separated by tag size (32 mm or 23 mm) (Figure 7.8).

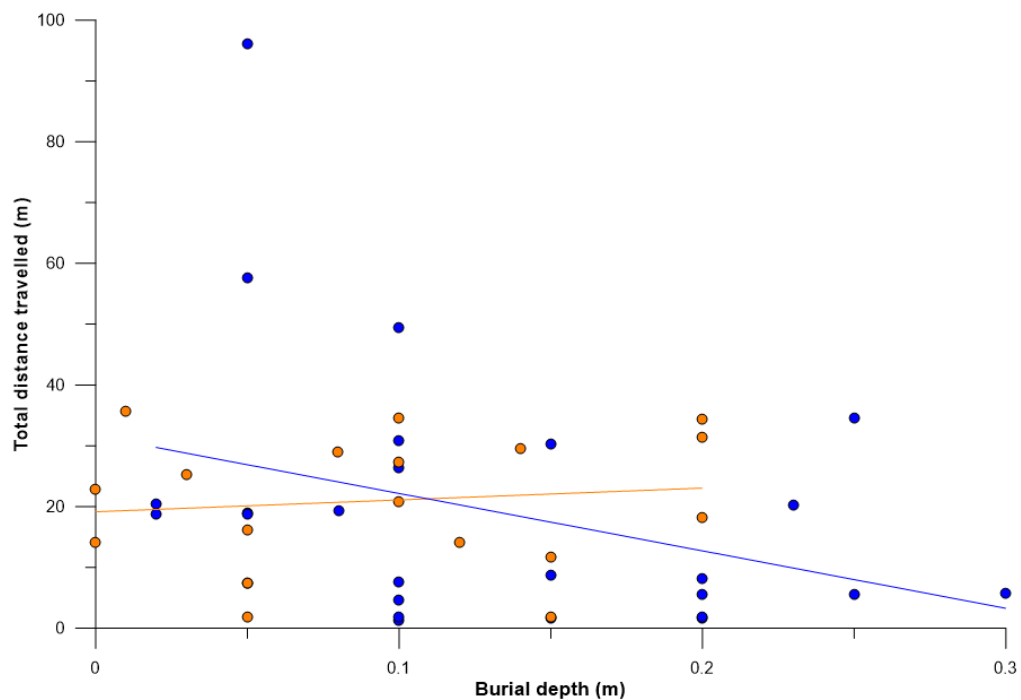


Figure 7.8: Relationships between burial depth and distance travelled for different sized tags. Blue points indicate 32 mm tags ($y = -55.802x + 23.684$, $R^2 = 0.083$), orange indicates 23 mm tags ($y = 19.463x + 19.095$, $R^2 = 0.015$).

Figure 7.9-Figure 7.12 show some examples of initial transport directions and distances with indicators of the depth at which each pebble was initially buried. These show how unpredictable transport is, with none of these deployments showing a dominant transport direction during this short timeframe. Table 7.4 includes results from all surveys successfully completed approximately 24 hours after tracer deployment, indicating mean long and cross-shore transport rates for pebbles buried at different depths.

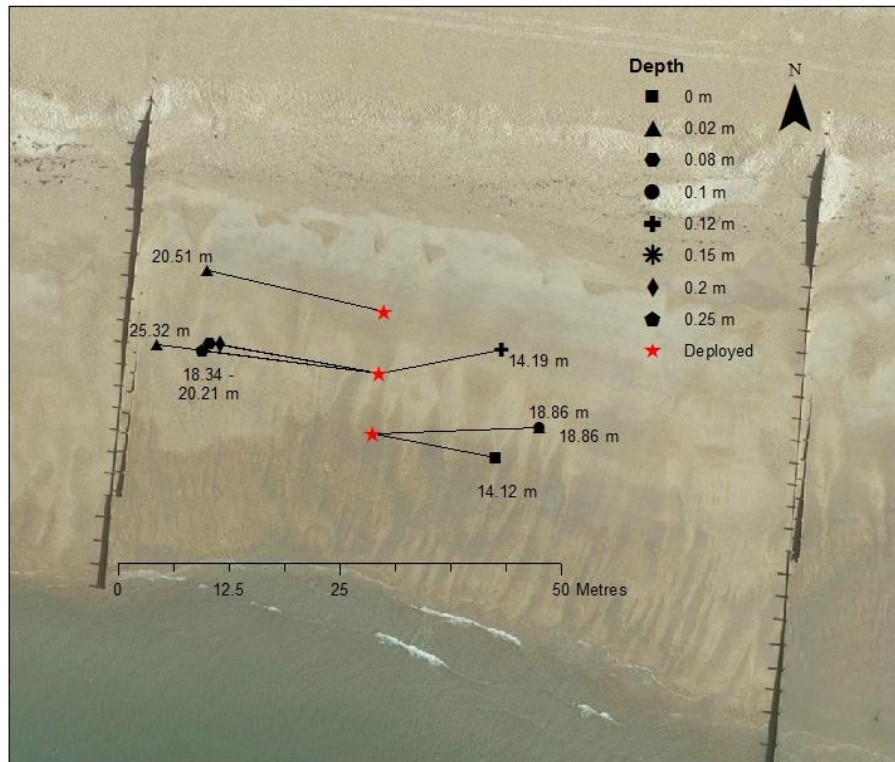


Figure 7.9: Directions of transport after 1 day for pebbles buried at different depths, 09/03/2015-10/03/2015. Aerial imagery courtesy CCO, 2008.

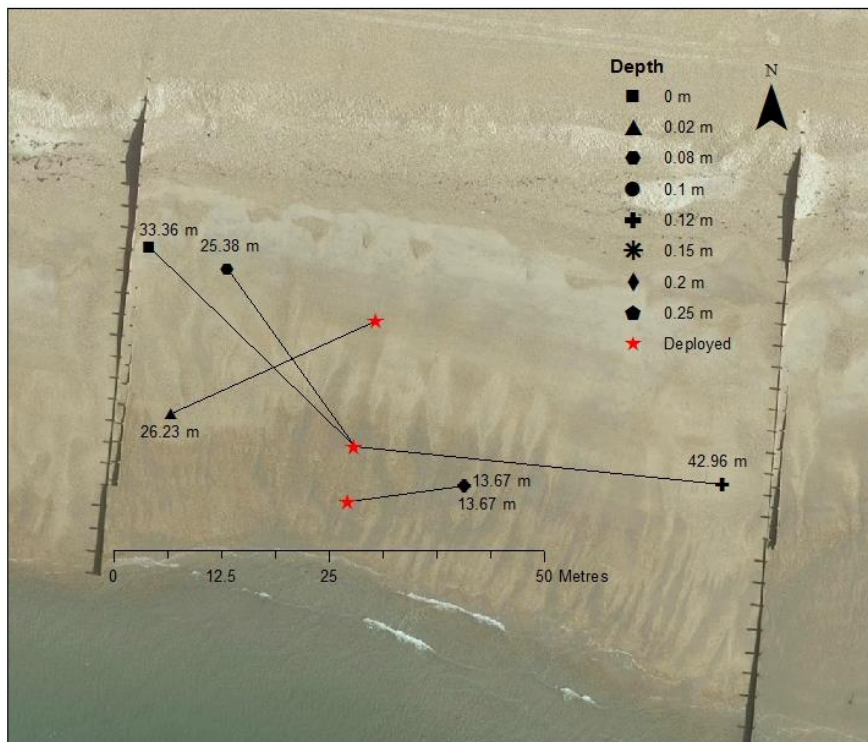


Figure 7.10: Directions of transport after 2 days for pebbles buried at different depths, 13/03/15-15/03/15. Aerial imagery courtesy CCO, 2008

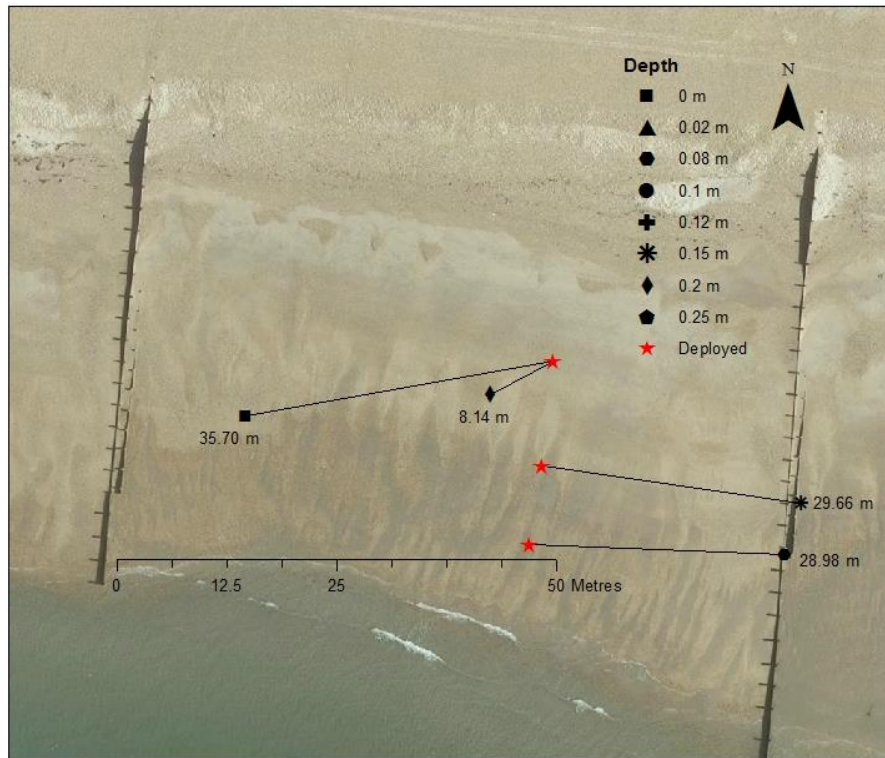


Figure 7.11: Directions of transport after 1 day for pebbles buried at different depths, 16/03/15-17/03/15. Aerial imagery courtesy CCO, 2008

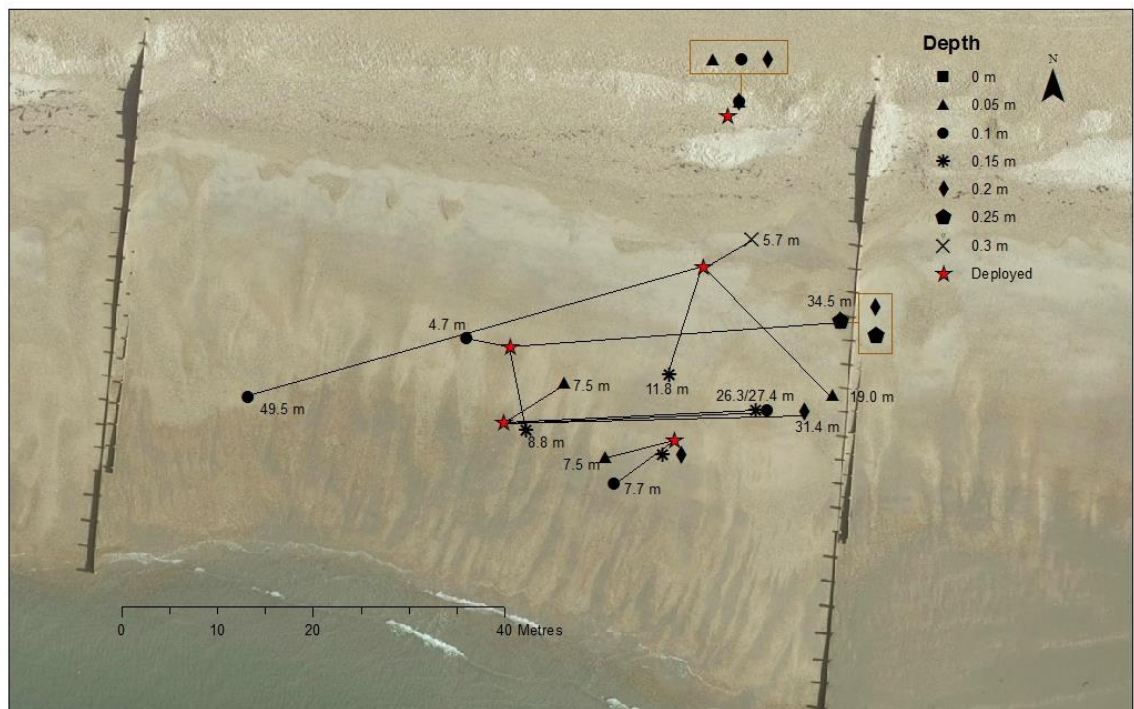


Figure 7.12: Directions of transport after 1 day for pebbles buried at different depths, 19/01/2016-20/01/2016. Aerial imagery courtesy CCO, 2008

Table 7.4: Mean longshore and cross-shore transport distances after one day for pebbles buried at different depths. Negative longshore distances indicate westwards transport, negative cross-shore distances indicate southwards/offshore transport.

Burial Date	N	Mean wave height, Hs (m)	Mean wave direction	Mean longshore transport (m)	Mean cross shore transport (m)	Initial burial depth								
						0-9 cm			10-19 cm			20-30 cm		
						N	Mean longshore transport (m)	Mean cross shore transport (m)	N	Mean longshore transport (m)	Mean cross shore transport (m)	N	Mean longshore transport (m)	Mean cross shore transport (m)
09/03/15	9	0.61	186.5	-4.09	2.09	5	-6.29	1.89	2	16.38	1.72	2	-19.05	2.95
16/03/15	4	0.52	184.4	3.98	-3.87	2	-3.10	-3.68	1	29.34	-4.36	1	-7.22	-3.77
09/11/15	3	1.36	199.5	29.44	-8.76	1	56.85	-9.27	1	25.94	-16.76	1	5.53	-0.25
02/12/15	4	1.30	190.0	-18.71	7.69	2	-18.60	5.80	2	-18.83	9.59	0		
06/01/16	5	1.46	182.6	-11.72	6.02	0			4	-11.10	5.66	1	-14.19	7.48
19/01/16*	17	0.49	186.4	6.74	-2.07	3	4.15	-3.66	8	-1.00	-4.49	6	18.35	1.93

*excluded 3 points where it seemed likely the pebbles had not moved.

iv. Medium term transport rates

It is difficult to calculate a definitive medium-term transport rate from the current study's tracers due to the issues with low detection rates. These issues mean that it is not as simple as finding the final location of each pebble and calculating the distance travelled since its deployment; some pebbles were only located within the first few days after deployment, and because sediment transport patterns within the groyne compartment are so complex, these may not initially be representative of longer-term sediment transport patterns. Additionally, the gradual deployment of pebbles means each deployment experienced a different set of wave conditions.

The average rate of transport based on every detection (n=388) was 1.05 m/day to the east. However, this includes all surveys, not just ones covering the full area, and so it is biased towards pebbles that stayed closer to their deployment location and is thus believed to underestimate the true average.

Table 7.5 shows the average velocities of pebbles from each survey, using only surveys with a cumulative recovery rate of more than 70 %. There is significant variation within the data.

Table 7.5: Average tracer velocity per deployment (only deployments with >70 % recovery rates)

Deploy Date	Average tracer velocity (all subsequent surveys) (m/day)
15/1/15	0.94
24/1/15	-0.30
9/3/15	0.75
13/3/15	1.33
16/3/15	1.71
20/3/15	-0.40
9/11/15	10.86
19/1/16	2.22

Transport rates decrease as the number of days since deployment or previous detection increases (Figure 7.13), but this allows broader patterns of transport to be drawn out. Tracer velocity rates can be calculated for slightly longer time frames, to provide an indication of whether a dominant direction begins to appear in the data. Using only data

where more than 30 days had elapsed since the pebble's deployment or a previous detection, a velocity of 0.87 m/day (to the east) is produced.

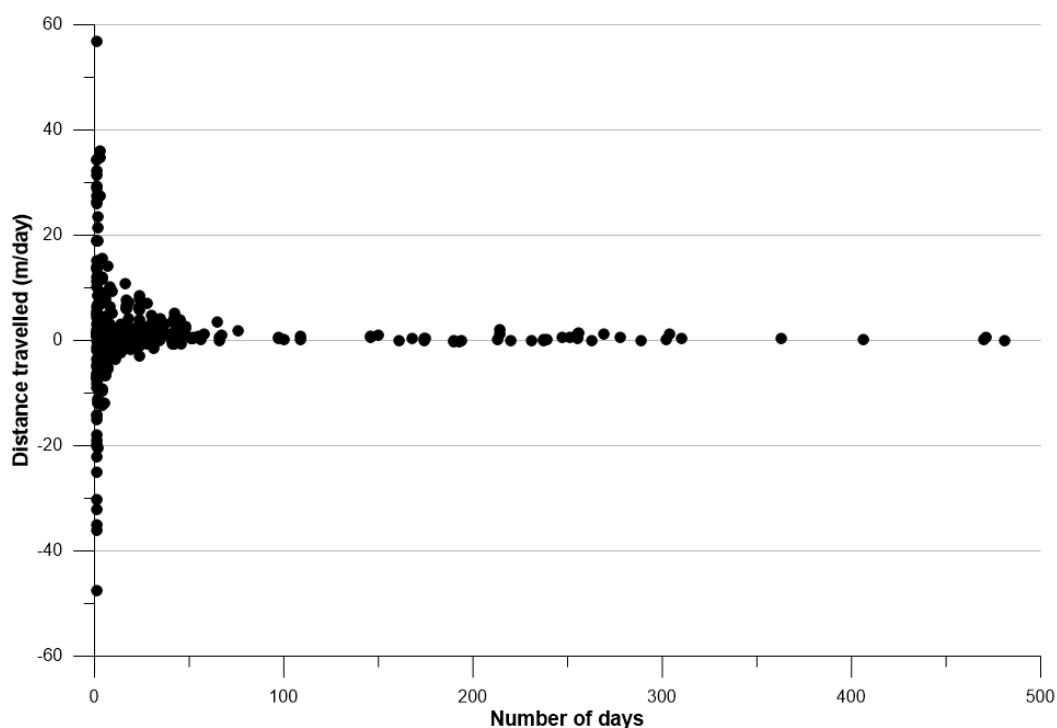


Figure 7.13: Transport velocities for every tracer detection, compared to the number of days since either deployment or the most recent detection (where relevant). Negative distance values indicated westwards transport, positive values indicate eastwards transport.

When only full-coverage surveys were included in the calculations, an average rate of 1.93 m/day was produced. This is closer to the rate originally calculated by ESCP (2013) for this same stretch of coastline (Figure 7.16), but as Table 7.6 indicates, the values on which this is based were not all similar. One potential reason for this is the variation in wave energies experienced (Table 7.7).

Table 7.6: Average tracer velocities of pebbles detected in full-coverage surveys.

Survey Date	Number of pebbles	Average distance/day of all detected pebbles	Annual velocity
20&21/4/15	20	0.89 m EAST	324.85
4/5/15	26	1.29 m EAST	470.85
10/11/15	15	6.32 m EAST	2,306.80
3&4/12/15	21	2.18 m WEST	-795.70
13&14/1/16	23	0.31 m EAST	113.15

Table 7.7: Mean longshore wave power experienced during each study period.

Study Period/Month	Mean LS Power
Oct14	-459.249
Dec14	761.7475
Jan15	663.4938
Feb15	-268.963
Mar15	-88.0373
Oct15	-1454.63
Nov15	1243.28
Dec15	-17.663
Jan16	-977.795

Using only tracers detected in multiple full-coverage surveys gives very few results for each survey period (Table 7.8).

Table 7.8: Velocities of tracers between full-coverage surveys.

Surveys	Average velocity (m/day)	N
April – May 2015	0.57	5
May – November 2015	-0.16	2
May – December 2015	0.91	3
Nov – December 2015	2.36	5
April 15 – Jan 16	0.64	2
May15 – Jan 16	0.96	2
November15 – Jan16	3.53	1
December15 – Jan16	2.65	5

Figure 7.14 provides information on the average velocities of tracers detected at each survey. These numbers do not necessarily represent transport for specific periods of time, as the number of repeat detections was low.

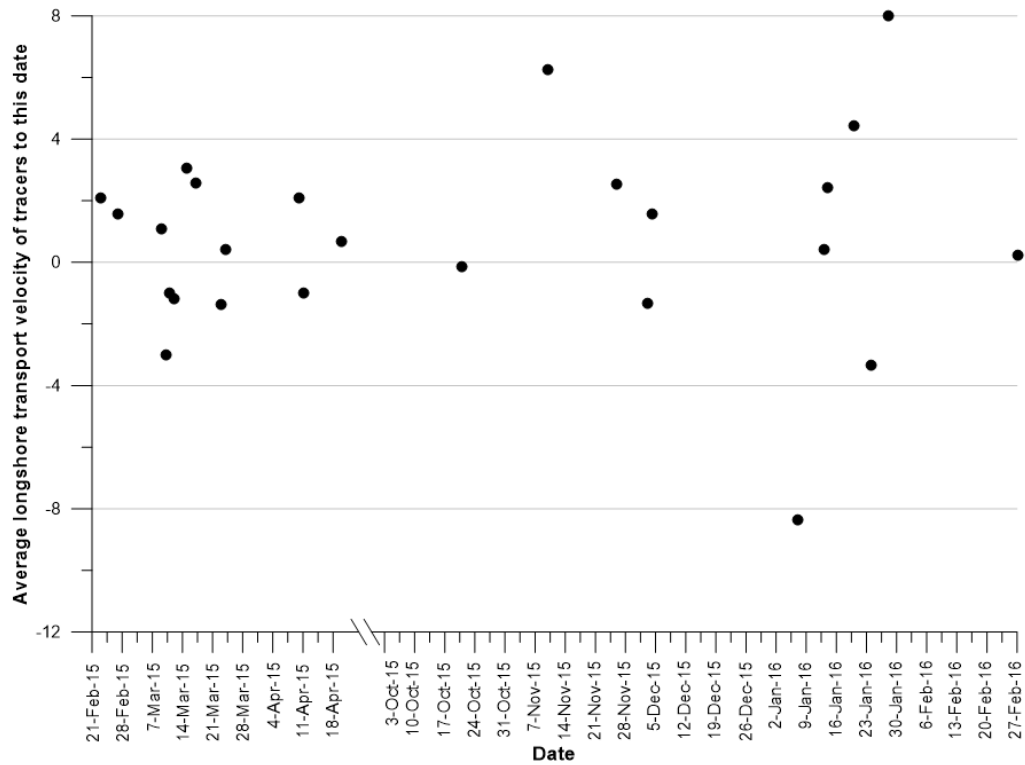


Figure 7.14: Average tracer velocities (m/day) of tracers detected during each survey.

The groynes also complicate transport patterns and thus add complexity to calculations of longer term transport rates. Location data from each detection was used to determine in which groyne compartment pebbles were located during each survey. The window during which pebbles had travelled past a groyne was then calculated, along with longshore wave energy during that window (Figure 7.15). Overall, the results are as expected: greater longshore wave power leads to faster groyne bypassing. The tracers observed to bypass groynes even under average negative longshore powers likely moved over a groyne during a period of positive longshore power, and did not transfer back again when the wave direction changed.

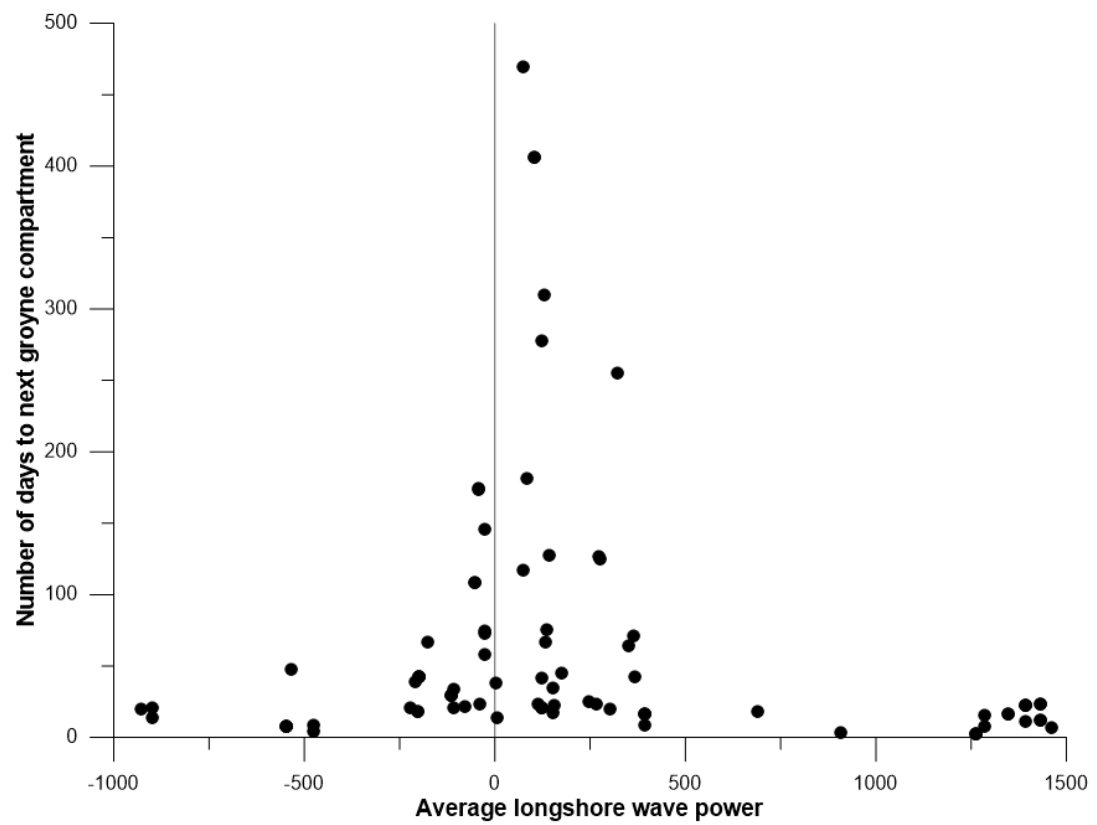


Figure 7.15: Number of days taken to bypass a groyne as a function of longshore wave power.



Figure 7.16: Transport distances and rates of pebbles deployed in March 2011 (source: ESCP, 2013, pp.18).



Figure 7.17: Tracer detections on full surveys. Though the survey area extended approximately 150 m further east than the area shown in this map, no other tracers were detected. Aerial imagery courtesy CCO, 2016.

v. Calculating Longshore Transport Volumes

Using the SIM calculation (e.g. Sear *et al.*, 2000), longshore transport can be broken down into three components: active layer depth, width, and rate of transport. These components then simply need to be multiplied together to produce a volume for longshore sediment transport (Table 7.9; depth, width, and velocity columns multiply together to produce volume column).

The width of the active layer can be estimated based on a combination of the level to which beach profile changes occur and the limit of wave run-up (Lee *et al.*, 2000) (see Chapter 5), and the depth of the active layer was discussed in Chapter 6. The active depth has been shown to be highly variable due to a large number of influencing factors (Chapter 6), and low pebble recovery rates limit our ability to rely on calculations of transport rates based upon these measurements.

Table 7.9: Tracer velocities and associated transport volumes for short time periods

Dates	H_s (m)/ T_p (s) /Dir (deg)	LS Wave Power (W/m)	AL depth (m)	AL width (m)	W--E tracer velocity (m/day)	Volume (m ³ / day)
9-10/03/15	0.61, 12.4, 186.5	204.64	0.126	50	-4.09	25.7 WEST
16- 17/03/15	0.52, 13.5, 184.4	2.55	0.063	60	3.98	12.5 EAST
9-10/11/15	1.36, 8.3, 199.5	3574.29	0.092	45	29.44	135.4 EAST
2-3/12/15	1.30, 10.5, 190.0	1130.99	*0.163	45	-18.71	152.5 WEST
6-7/1/16	1.46, 8.5, 182.6	-2021.59	*0.161	50	-11.72	93.3 WEST
19-20/1/16	0.49, 12.5, 186.4	127.82	*0.117	50	6.74	39.4 EAST

* estimated from data presented in Chapter 6 (Figure 6.24). H_s was used to estimate the approximate AL depth as a percentage of H_s , which can then be converted to an estimated AL depth.

The wave conditions experienced between deployment and recovery for the first two experiments in Table 7.9 were similar, yet the first experienced net westerly transport

while the second experienced net easterly transport (the dominant transport direction at this site). A wave direction of 190 degrees should indicate eastwards sediment transport, yet the transport direction of tracers measured between 02/12/2015 and 03/12/2015 was westwards. This was based on only 3 recovered tracers, but all three tracers had moved westwards.

The best estimate of longshore sediment transport speeds should be obtained by using only results from full-coverage surveys. The position of each tracer found during a survey was used to calculate its distance travelled eastwards (as the dominant transport direction and approximate alignment of the beach), either since it had been deployed or since its most recent detection where relevant (Appendix O). These distances were then divided by the number of days that had passed, to produce an average 'distance per day'. The distances per day from full coverage surveys were the only ones used to calculate an average daily transport rate of 1.93 m/day. Full coverage surveys were undertaken on 20/04/15, 04/05/15, 10/11/15, 03-04/12/15, and 13-14/01/16.

This method does mean that some pebbles had been deployed or previously detected more recently than others, but low re-detection rates mean that choosing a more specific time frame would not have given enough data to produce a reliable result. As such it is difficult to assess the relationship between tracer transport and wave conditions in order to produce a more accurate upscaling of the data.

Average significant wave height during 2015 was 0.74 m. This was calculated from the entire annual data set from the CCO's Hayling Island wave buoy, which produces an average significant wave height for each 30-minute time period. Using the equation $\ln(y) = -0.797x + 3.565$ (Figure 6.24), this equates to a predicted active layer depth of 19.59% wave height. 19.59 % of 0.74 m is 0.145 m, or 14.5 cm. The errors involved in upscaling this value to the annual scale relate to the variability in AL depth measurements, shown in Chapter 6. This equation was shown to account for 57.8 % of the variability at a daily average scale, and this margin of error is then multiplied when it is applied more broadly.

The active layer width is estimated from profile envelopes (Appendix C) during February 2015, when the average wave height was close to the annual average (0.79 m in February compared to 0.74 m for the annual average). Although the upper limit of interaction between waves and sediment changes depending on the tide and wave height, the methodology used to collect the profile data did not allow the full extent of the active

beachface below the low tide level to be determined. Thus, for simplicity, the whole profile envelope area is assumed to be approximately representative of the overall average active beachface. The length of the profile envelope on Profile 1 during the February 2015 field period was 50 m, Profiles 2 and 3 were 70 m each. This creates an average value of 63 m, which was used as an approximation of active width. Extrapolating in this way has the potential to bring a large amount of inaccuracy into the calculation. The errors are introduced by the limits of the surveyable beach, and the low number of measurements of AL depth in the lower beach. Averaging over the entire year also does not necessarily consider the potential impacts of storm events, during which greater reserves of sediment from the crest of the beach may be accessed and transported. A more accurate method would include factors such as variations in tidal range throughout the year, as well as the likelihood of storm events occurring during spring tides and at high tide.

Multiplying the average values for active depth (0.145 m), width (63 m) and tracer velocity (1.93 m/day) together and then multiplying by 365 (for days in the year) provides an estimated longshore transport volume of 6,435, or approximately 6,400 m³/year. Upscaling in this way is the simplest option and therefore comes with huge potential for error and its accuracy is given low confidence; it does not take into consideration the effect of storms, which some authors (e.g. Whitcombe) have suggested may explain the majority of sediment transport. If the longshore transport rates are significantly higher during storms at Eastoke, using the average wave height rather than proportions throughout the year will likely be significantly underestimating the overall longshore transport rate. Upscaling in this way is however the only feasible option given the sparsity of pebble tracer data; there were not enough successful short-term experiments to allow accurate estimations of LST during different hydrodynamic conditions.

On a groyned beach, the important aspect of longshore transport is how quickly sediment transits past each groyne. Using the data from Figure 7.15 the following equation was produced (for the positive values of longshore wave power): $y = 72.937e^{-0.001x}$, $R^2 = 0.372$. With the average longshore wave power from 2015 being 217 W.m⁻¹, this gives a value of 90.6 days to bypass a groyne. The groynes on average are 90 m apart, so the transport velocity is essentially 1 m/day under 'average' conditions for the study period.

vi. Calibrating the CERC equation

As discussed in the literature review, the basis of the CERC equation is that sediment transport is proportional to longshore wave energy, via a coefficient 'k', which varies by location and beach type (Komar, 1998). So far, there has been no agreement on a constant value for k that can be applied to all coarse grained or mixed beaches (Curoy, 2012), so it must be calibrated for use at individual sites (Van Wellen *et al.*, 2000). It is generally only calibrated on open stretches of coastline, so the transport-limiting groynes at this site present a unique calibration opportunity.

First, it is necessary to convert volumetric transport rates into immersed weights so that the units of measurement are the same as those of wave power (Watts per metre, or Joules per second per metre) (Equation 2.7 in Chapter 2).

Bray *et al.* (1996) indicate that the R value for flint gravel beaches is 10807, and used this value in their calculations at Shoreham beach. It has been deemed acceptable as a value for this experiment, as it describes the properties of the flint tracers which were used. Thus, these values can only be said to represent longshore transport of the gravel portion of this beach. The only slight issue with using this value is that the packing patterns of mixed sediment are different than those of pure gravel, which is likely to have some effect on the rate of gravel transport. Refining this calculation for mixed sand and gravel beaches by accurately measuring density, porosity and packing patterns is suggested as a future branch of research.

To calculate the longshore wave power at this site, the following equation is used:

$$P_l = EC_g \sin \theta \cos \theta$$

where θ is the angle of wave approach from normal.

It is technically for deep water energy, but the buoy from which the data comes is located in 10 m water depth, and it is more convenient to calibrate using the same data source which would be used in future estimates.

Using the one day volumes from section 7.3.v, the calibrations listed in Table 7.10 were produced. This is a wide range of k values, with k in general being highest for the lowest values of wave power.

Table 7.10: Calculations of k from 1-day tracer experiments.

Dates	Volume (m ³ /day)	Equivalent Immersed Weight (W/m)	Longshore Power (W/m)	k
9-10/03/15	25.77	3.22	204.64	0.0157
16-17/03/15	15.04	1.88	2.55	0.7379
9-10/11/15	121.88	15.25	3574.29	0.0043
2-3/12/15	137.24	17.17	1130.99	0.0152
6-7/1/16	94.35	11.80	2021.59	0.0058
19-20/1/16	39.43	4.93	127.82	0.0386

Calculations from beach profile data provide an even wider array of k values (Table 7.11).

These are given an even lower degree of trust, due to consisting of only partial profiles (the upper and mid areas) and using the most basic of calculations.

Table 7.11: Values of k calculated from profile-based transport volumes.

Date	LS wave power	LS volume Q	LS volume I	k
15/01/2015	1874.711575	4.275	0.53472135	0.0003
16/01/2015	584.8445008	2.7	0.33771875	0.0006
19/01/2015	8.562337432	10.8	1.350875	0.158
20/01/2015	14.53097044	20.25	2.532890625	0.174
25/01/2015	222.8395599	4.95	0.61915104	0.003
27/01/2015	354.9316522	35.1	4.39034375	0.012
15/02/2015	67.72814074	56.25	7.035807292	0.104
18/02/2015	110.354437	12.825	1.60416406	0.015
20/02/2015	398.5624379	33.975	4.249627604	0.011
24/02/2015	1364.339527	9.9	1.238302083	0.0009
11/03/2015	94.41940307	17.55	2.19517188	0.023
12/03/2015	584.790086	68.4	8.55554167	0.015
14/03/2015	94.59145892	15.525	1.941882812	0.021
18/03/2015	62.51220369	36	4.50291667	0.072
19/03/2015	250.3259882	8.55	1.06944271	0.004
21/03/2015	98.36012803	31.05	3.88376563	0.039
03/10/2015	1485.339661	64.8	8.10525	0.005
09/11/2015	1526.09437	65.25	8.161536458	0.005

10/11/2015	3574.294642	88.2	11.0321458	0.003
12/11/2015	656.345692	24.03	3.005696875	0.005
17/11/2015	2060.444814	40.5	5.06578125	0.002
18/11/2015	2962.557941	32.325	4.04324392	0.001
08/12/2015	72.45160483	47.3625	5.92414974	0.082
05/01/2016	4902.348066	2.3625	0.29550391	0.00006

Figure 7.18 compares wave power to values of immersed weight transport, estimated both from tracer experiments and beach profile changes. Unfortunately, there is not a correlation, which explains why the coefficient k varies so greatly. There is not even a consistent separation between direction of longshore wave power (indicated by positive or negative values) and direction of immersed weight transport (also indicated by positive or negative values), so it would not be feasible to use k to estimate longshore transport direction, only its magnitude.

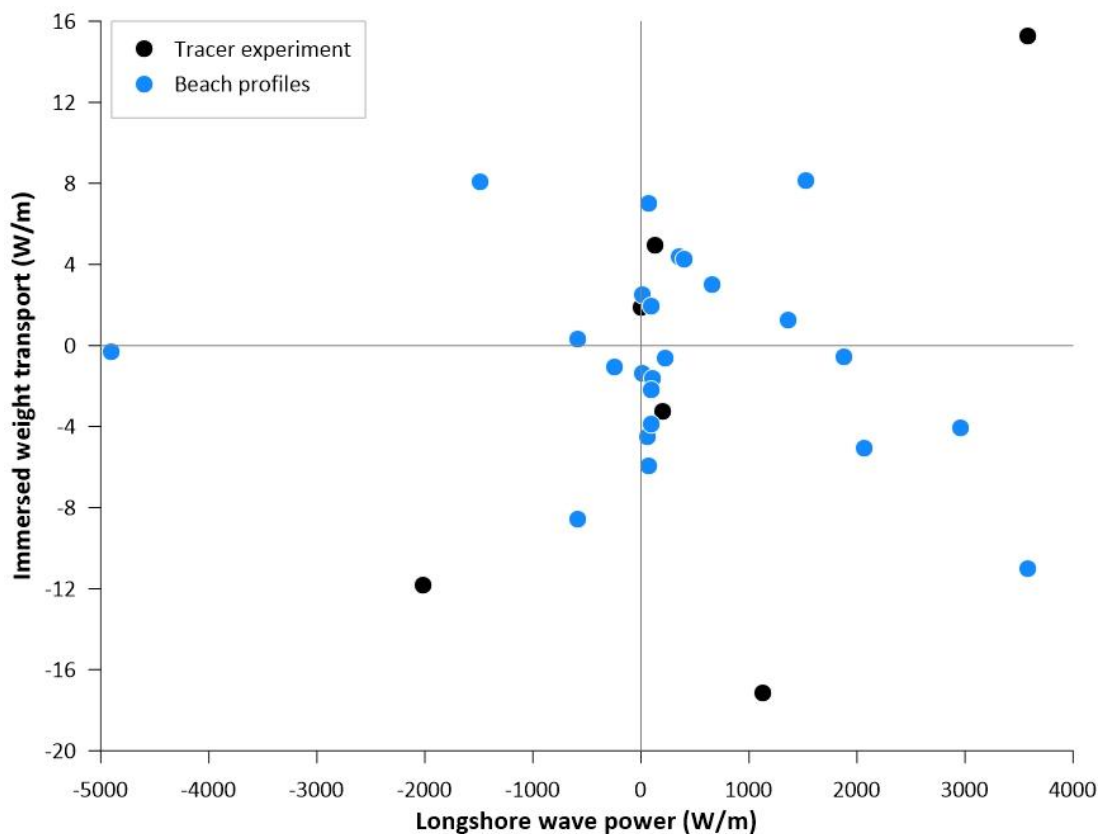


Figure 7.18: Scatterplot of longshore wave power against immersed weight transport for all data from tables 7.10 (black) and 7.11 (blue).

Since k cannot be negative – it is a dimensionless coefficient – the direction of power and transport were removed and only the magnitude used in the calculation of k values. As a

general rule, the value of k decreases as wave power increases, fitting well to a curve with equation $y = 1.814 x^{-0.908}$ ($R^2 = 0.723$) (Figure 7.19).

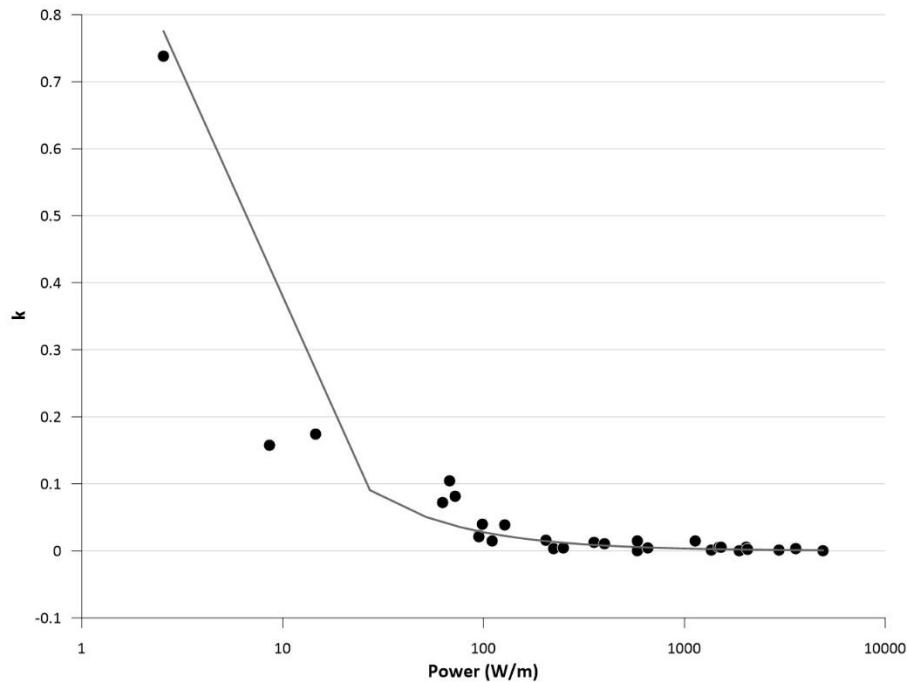


Figure 7.19: Scatterplot of longshore power against values of k for data from tables 7.10 and 7.11.

7.4 Discussion

In agreement with previous studies (e.g. Allan *et al.*, 2006; ESCP, 2013), detection rates decrease with time after deployment. This has a negative effect on the ability to reliably estimate longshore transport rates; with so few pebbles detected, it is difficult to assess the speed of transport.

However, the current study had much lower detection rates even at shorter timescales than have been previously reported in the literature. It is unclear whether this may be related to the groynes and the overall erosive nature of beaches along the Solent coastline. Previous studies by the ESCP have found similarly low detection rates, but it had been expected that by doing more surveys within the first two weeks after deployment, tracers would have a higher likelihood of multiple detections.

It is possible that the lack of correlation between burial depth and distance travelled was due to the 24-hour period between deployment and surveying, where two high tides occurred. Results may have been clearer after only 1 tide, and this should have been taken into consideration when timing these deployments, so that attempts could be made to recover tracers at the directly subsequent low tide.

i. Reasons for low detection rates

The likelihood of detecting a pebble is generally assumed to decrease with time after deployment, but this does not explain the low recovery rates in the days immediately following pebble deployments. Dickson *et al.* (2011) found that their lowest detection rates actually correlated with the timings of larger wave heights and not increased time in the field; directly after storms, fewer tagged pebbles were detected on the beach. It is true that the best recovery rates for surveys done within a few days of deployment were found in March 2015, when the wave climate was calm all month (see Appendix A), but none of the tracers deployed on 20/10/2015 were recovered during the survey the following day, and wave heights reached a maximum of only 0.8 m during this time.

By contrast, Allan *et al.* (2006) found that in summer, the accretion on the beach reduced detection rates. All major surveys apart from May 2015 had some recently deployed pebbles to boost their recovery rates. Thus comparing these to results from May 2015 to determine whether accretion on the beach may have led to a decreased detection rate would provide misleading results. Additionally, no topographic surveys were undertaken at this time, so it would not be possible to assess the change in beach volume and provide a meaningful analysis.

Fast movement of tracers alongshore, out of the regularly surveyed zones, is a possibility to consider as a reason for the low detection rates. However, even the full area surveys suffered from low detection rates, indicating that there are other factors at play. It is possible that due to the time between large surveys some pebbles were travelling much faster than anticipated and had been transported out of the survey area, but the average time taken to pass each groyne suggests that the majority of tracers would have remained in the study area.

More likely than rapid longshore transport is offshore transport, removing tracers beyond the scope of surveys. Bertoni *et al.* (2010) used a specially adapted waterproof RFID system to discover that up to 60 % of their detected pebbles (with an overall 77 % detection rate) were found below low tide level. This indicates that the potential for seaward transport of tracer pebbles might be relatively high. Even if the pebbles are not actually below the water level, the lower third of the beach at Eastoke experiences high groundwater levels – frequently high enough to cause visible seepage. The addition of this much salt water into the sediment matrix has been shown by Bertoni *et al.* (2010) to significantly dampen the

radio signal and reduce the range of the detector. This would suggest that any pebbles which are not directly on the surface in this lower section of the beach may go undetected.

Some pebbles may have been 'buried' to depths below the range of the detector. This could be caused by a specific event where AL depth was large, or by accretion on the beachface. It is also possible that the detector did not achieve maximum depth range during actual use. The detector kit, when tested, had a reasonable range (ESCP, 2013b; Appendix N) which agreed with published ranges, but this was under optimum conditions – although sediment types and dampness were considered as variables in testing, knowing exactly where the tracer is buried and thus where to swipe the antenna does not represent real-world surveys. The tags are made out of glass, and despite being fully encased within the pebble, it is still possible that there were some breakages.

More representative rates of transport for the whole active layer are provided by burying the pebbles in columns. However, this method also has one major disadvantage: it is not possible to tell from the surface whether all pebbles within the column are in transit. Previous research using tracer columns has required each column to be re-dug after a tidal inundation to determine the depth to which pebbles were activated by waves. Detection depths of the RFID kit had been published at much greater depths than pebbles were buried, and so it had been expected that pebbles would be detected if they remained at the burial site, negating the need to re-dig. After analysis of the data, it seems likely that the detection range of the RFID kit is much lower than previously published, and perhaps even lower than testing indicated (Appendix N). This would potentially explain the low detection rates in most surveys.

It is possible to estimate the depths to which columns were activated for deployments which were timed to coincide with AL measurements (Chapter 6), which gives an initial indication of how many pebbles may have been in transit. But due to the prolonged nature of the experiment, it is not possible to calculate whether pebbles may have been moved at a later date, and if so, when.

No tracers were detected around the Ness. This is believed to be due to accretion in this area, which can be seen in aerial imagery (Figure 7.21). The fact that the estimated annual accretion at the Ness is much higher than the longshore transport rate would suggest it should be indicates a secondary source of sediment input, for example the tidal delta known as West Pole Sands, which can be seen to increase in size and move towards the

shoreline in Figure 7.21. In this case, it is possible that sediment is being transported offshore and transported by tidal currents outside the bounds of the surveyable area. If the sediment is then held within the tidal delta for significant amounts of time, those pebbles may not have moved back to the surveyed beach area within the time frame of the experiments.

If this experiment were repeated, it would be preferable to release tracers in larger groups, immediately before a two-week field period so that consistent measurements of AL depth could be applied to tracer movements.

ii. Transport rates

It was not uncommon for tracers to be detected multiple times in similar locations, often within one groyne compartment over many months. This is indicative of the cyclical nature of groyne cell transport, and potentially agrees with Ciavola and Castiglione's (2009) theory which suggested that on a mixed sediment beach, the gravel sized particles are more likely to experience cross-shore transport. It does not agree with Osborne (2005) though; he suggested that the smallest particles in a mixed sand and gravel beach would move shorter distances, and predominantly cross-shore, whereas larger particles move longshore.

No evidence was found to corroborate Miller and Warrick's (2012) claim that speed of transport decreases logarithmically with depth.

Different medium-term rates of transport can be calculated by separating the data according to deployment, survey date, or length of time the field prior to detection. There was not a strong correlation between wave conditions and tracer transport rates, suggesting that the different rates calculated are not due to variations in wave energy throughout the study. This casts a significant amount of doubt on any transport rate calculated from this data: it is not possible to know which tracers are 'most representative'.

iii. Longshore transport volumes

The estimated transport rate of approximately 6,400 m³ per year is much lower than the current rate of loss used by HBC, which has been calculated to be approximately 20,000 m³ per year; approximately 10,000 m³ of sediment accumulates each year at the Ness (Samantha Cope, *pers.comm.*), which is measured using repeated topographic surveys,

and a similar amount is dredged annually from Chichester Bar, which is believed to be fed by littoral drift from Eastoke (SCOPAC, 2004; NFDC, 2017).

The longshore wave power at this stretch of coastline varies significantly year-on-year (Figure 7.20), but was relatively 'normal' during 2015 – there are four other years in this 10 year period with very similar mean annual wave energies.

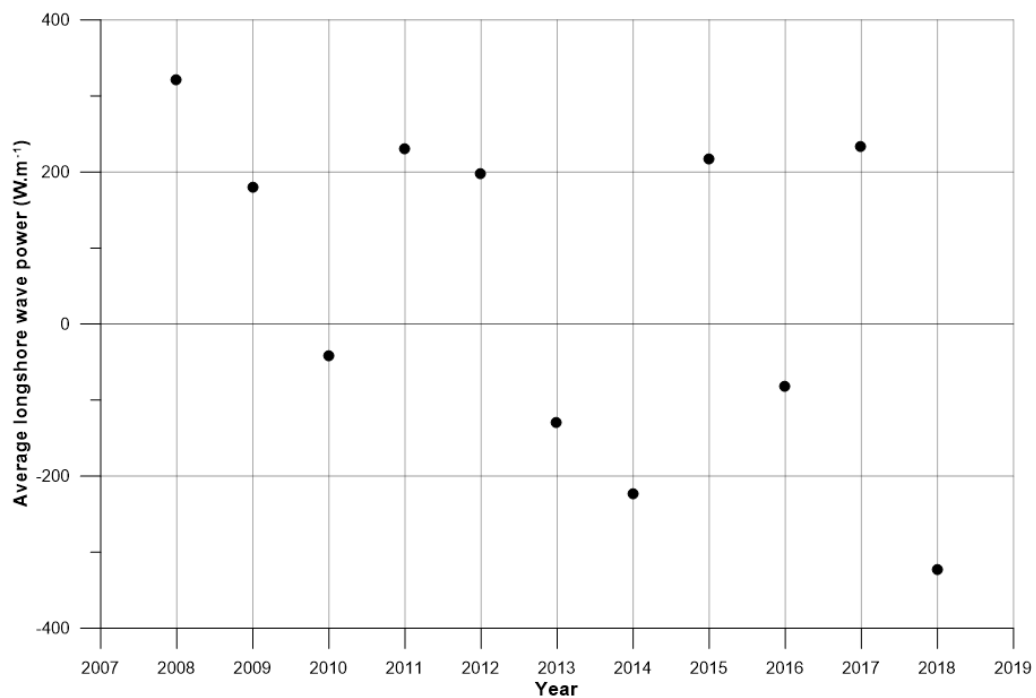


Figure 7.20: Mean longshore wave power 2008-2018.

As discussed in Chapter 5, the longshore adjustments of beach profiles are not a reliable method for measuring longshore transport rates, especially when groynes are causing certain parts of the beach to change differently and the profile lines are not all positioned in the same part of a groyne compartment. However, the HBC estimate is also based on a convergence zone at the Ness where sediment accumulates (ESCP, 2012). While it is possible that the stretch of beach on which these surveys were undertaken is not the only sediment source for that accumulation, there is not yet any research to suggest otherwise.



Figure 7.21: Coastline change, 19/10/2011-22/04/2015. [Source: Google Earth].

The presence of onshore-migrating swash bars has been documented on the other side of Chichester Harbour Entrance by Bray (2007; 2010), so it is certainly possible that a similar process occurs here, transporting sediment onshore from West Pole Sands to the beach at Eastoke. Satellite imagery taken just over three years apart shows significant change in the shape and position of West Pole Sands (Figure 7.21); it certainly seems that it may be moving onshore and could therefore be considered as a possible source of sediment.

Additionally, the Ness appears much larger, suggesting a significant source of sediment. This may be longshore drift of replenishment material from the Eastoke Scheme. Alternatively, it may be material lost 'offshore' during the stormy winter of 2013-14 (immediately after the Scheme was completed), which then travelled alongshore in the low tide zone before moving back onto the intertidal beachface at the Ness.

It is likely that the size of the tracers and thus their inability to represent the full range of sediment sizes is an influential factor in producing this lower estimate. Aagaard *et al.* (2013) found transport rates on reflective beaches to be up to an order of magnitude lower than on dissipative and intermediate beaches and attributed this to the relative difficulty of entraining and transporting larger sediments. This would suggest that on a mixed sand and gravel beach, sand-sized particles are preferentially transported alongshore. Certainly, previous evidence collected by the ESCP (2012) indicates that there is less gravel towards the distal end of Eastoke spit due to the decrease in wave energy within the harbour but does not fully explain the slower gravel transport along the more open stretch of coastline in this study.

In an ideal world, it would have been preferable to extend the survey area further in both directions to ensure as many tracers are recovered as possible, and to do surveys only on spring tides so that the largest possible area of beach is exposed. This may have provided extra insights into gravel behaviour, but the research seems to be indicating that sand is perhaps the more important aspect requiring study here.

In the future, it would be suggested that simultaneous sand tracing experiments are undertaken. However, on a mixed sand and gravel beach, taking cores to measure sand transport throughout the active layer of the beach would, as far as the author is aware, be impossible using currently available methods due to the larger grains. This would potentially leave only the option of tracing sand at the surface, which as previously discussed is not representative of all transport and may provide an over-estimation (Van Wellen *et al.*, 2000).

It is also possible that the estimate for the active profile width is smaller than the reality. As surveys were not continued below low water level, it is not possible to determine how far below this point the active profile extends. Given the short surf zone generally found on steep beaches (Van Wellen *et al.*, 2000), the extra distance is often assumed to be negligible, but it must be considered that there is a significantly shallower sandy terrace at

Eastoke, much of which may be influenced by breaking waves at low tide. This would combine with the theory that sand transport is greater, as this area contains almost purely sand sized particles, and is not restricted by groynes. If longshore currents are in evidence, which is certainly likely especially given the proximity to the harbour entrance, it is certainly possible that a significant volume of longshore transport occurs in this unmeasured area just below low water level.

iv. CERC calibration

Table 7.12 provides k values from some of the prominent studies on coarse grained beaches. Technically the CERC equation should use H_{rms} rather than H_s . This value is approximately equivalent to $H_s/1.4$ and is rarely used in modern coastal research. In the past, some researchers have used H_{rms} , while others have used H_s (Table 7.12). K values produced using H_s can be approximately doubled to compare with those calculated using H_{rms} . There is some variability between k values from previous research, indicating the necessity to calibrate this equation specifically for the site at which it is intended for use.

Table 7.12: K values previously calculated on coarse grained beaches

Authors/Year	K value	Data used
Curoy (2012)	0.04	H_s Birling Gap Tracers
Komar (1988)	0.1	H_{rms} Hattori and Suzuki's (1978) tracers Suruga Bay, Japan (surface only)
Nicholls and Wright (1991)	0.02	H_s Hengistbury, Long Beach, Hurst Castle Spit. Tracer experiments
Chadwick (1989)	0.02-0.06	H_{rms} Shoreham Sediment traps
Bray <i>et al.</i> (1996)	0.02-0.36 depending on wave energy	H_{rms} Shoreham Sediment traps and tracers.

The average k value for this study was 0.052, but this is based on a wide range of values from 0.00006 to 0.7379. The lowest value is much lower than other published results and the highest is much higher. However, the values for data from tracer experiments ranged from 0.0043 to 0.7379.

The results align with Bray *et al.*'s (1996) finding that the value of k varies according to wave energy, and thus suggests that the efficiency of transport is reduced in larger waves. This also mirrors results from Chapter 6 which indicated that the efficiency with which waves disturb the active layer reduces as the wave height increases (Figure 6.24).

However, the lack of relationship between direction of wave power and observed direction of transport must be taken into account when considering the reliability and usefulness of these results. The mismatches between direction of wave energy and direction of transport mean that even though the value of k could be relatively accurately predicted based on wave power, it cannot then be used to predict direction of transport – only magnitude. This is likely due to flaws with the data used to estimate longshore transport in the first place. The limited tracer results affect the reliability of longshore transport calculations, and multiple previous researchers (e.g. Moon, 2003) have shown inaccuracies arising from the use of beach profiles to estimate LST.

7.5 Conclusions

The main research question associated with this chapter was: *Can the longshore transport rate be used to calibrate an empirical formula such as the CERC equation for this site, and will this calibration value be similar to other mixed sand and gravel beaches?*

A range of k values from 0.0043 to 0.738 were produced from tracer experiments at this site. An additional range of k values from 0.00006 to 0.174 were produced from differences between dGPS profile surveys at different locations within the groyne compartment. K was shown to decrease as wave power increased, indicating that sediment transport becomes less efficient in higher energy waves.

These values are given extremely low confidence however, due to the data from which they were calculated. The tracer experiments had low recovery rates at the scale required to calibrate this equation, while beach profiles alone are generally not considered an acceptable method for estimating drift volumes.

It is possible that slightly better correlations between longshore transport and wave energy would have been produced using inshore measured or propagated wave data. This is recommended for future investigation.

Results from buried columns of tracer pebbles, combined with estimates for active layer depth and width, produced an estimated longshore transport volume of 6,400 m³/year. This is significantly lower than the value which has been estimated based on sediment accumulation at the end of the cell, suggesting that one or more inputs to the calculation is underestimated. While it is possible that the active width is wider than can be estimated from profiles measured only above low water level (Chapter 5), the reduction in active layer depth in the sandy lower beach (Chapter 6) would imply that the additional length would contribute minimally to the overall volume. However, this area is beyond the limit of the groynes and thus has less inhibited longshore transport. The growth of West Pole Sands in aerial imagery indicates significant longshore transport, mainly of sand. Therefore this value of 6,400m³/year is only applicable to gravel transport within the groyned width of the beach, and even then only with low confidence.

This overall volume would give a k value of 0.004, based on the average wave power for 2015. However, the gradual injection of tracers and low numbers of repeat detections means this value is not representative of all wave conditions experienced at the site.

Previously, RFID tracer studies along the Solent coastline have been assumed to be representative of overall sediment transport. The disparity between annual longshore transport volumes and the measured sediment accumulations indicates that although tracers may be indicative of overall pebble transport, they hugely underestimate the sand component of littoral drift at this coastline. Further measurements of the rates of sand transport, especially on the low tide terrace, are recommended.

Realistically, sediment transport needs to be measured for a much longer period of time to gather a clear picture of trends and patterns. Schoonees (2000) suggests that studies need to be continued for 5-8 years to truly be representative. Considering the low detection rates experience in this and the previous Eastoke tracer survey, it would be an expensive exercise to collect enough data to create an accurate accounting of coarse sediment transport on Hayling. The main finding of this chapter was the variability of short-term pebble transport on this groyned mixed sediment beach, further highlighting the necessity to numerically model these processes in future.

8. Conclusion

8.1 Introduction

A replenished mixed sand and gravel beach at Eastoke, Hayling Island, was studied during a total of 9 field periods between October 2014 and January 2016 to provide additional insights into the morphodynamics and sediment transport, a notoriously complex area of coastal research, especially on mixed sediment beaches (Blanco, 2003).

This particular beach was chosen for the study because of its importance as a coastal defence, and the general lack of research into the morphodynamics of complex, managed mixed sediment beaches. With sea levels set to rise significantly in the next few decades and the cost of supplying adequate-quality replenishment sediment increasing as well, it is vital that such beaches can be utilised as efficiently as possible.

Results from this study add to the global knowledge base of mixed sand and gravel beaches – in particular, heavily managed ones – which have received significantly less research attention than their sand counterparts. Specifically, the study provides a new method for the prediction of active layer depth on such beaches, which could be used both as part of longshore transport estimates and to help predict the volume of sediment required on a beach to protect against coastal erosion.

The ESCP manage the coast from Lee-on-Solent to Hayling Island, which is fronted almost in its entirety by mixed sediment beaches (NFDC, 2010). Developing the most cost effective and sustainable method for managing the shoreline is key to providing future protection from erosion and flooding, and this project was an essential part of this effort.

8.2 Aims of the thesis

This thesis set out to establish statistical relationships between active layer depth and wave energy in order to provide a much-needed data set to parameterise calculations of longshore transport rates on mixed sediment beaches.

The research questions associated with this aim were:

1. Do beach profiles provide an accurate representation of longshore sediment transport?

2. How is the active layer on this mixed sand and gravel beach linked to:
 - a. Wave conditions?
 - b. Beach slope?
 - c. Sediment composition?
3. Can the longshore transport rate be used to calibrate an empirical formula such as the CERC equation for this site, and will this calibration value be similar to other mixed sand and gravel beaches?

8.3 Recap of methods used

Beach morphodynamics were studied in 8 short field periods over 16 months, providing a detailed yet temporally representative dataset. Beach morphology was monitored on three evenly-spaced profiles within one groyne compartment, using RTK-dGPS profiles, as a basis for understanding the specific morphodynamics associated with groyned beaches. Most other measurements (excluding tracer surveys, which extended further east to track long term sediment transport) were also undertaken in this groyne compartment, to allow links to be made between the datasets and also in an attempt to constrain some of the variables that could influence the variables being measured.

Beach slope angles were created from this data to be compared to active layer measurements; this allowed the study to be compared to previously published research which has found that wave energy causes greater active layer depths on steep beaches compared to gentle ones (Anfuso, 2005).

The active layer was measured using sliding indicator devices (SIDs) (DeVries, 2000) in the main mixed beach, and depth of disturbance rods (Greenwood and Hale, 1980) in the lower beach, where groundwater levels were too high for SIDs to be buried. This was completed at a higher resolution covering a wider range of hydrodynamic conditions and on a greater temporal scale than any study of which the author is aware, providing a unique dataset.

Surface sediment data was collected using a coding system created specifically for this site and recorded alongside dGPS points for all measurements taken between December 2014 and March 2015. Physical sediment samples were taken from the active layer, dried and sieved, to allow active layer measurements to be associated with sediment composition.

PIT tagged tracer pebbles and an RFID tracking system were used to conduct short- and long-term tracer surveys, with attempts made to correlate burial depth with the rate of transport.

8.4 Main findings

Chapter 5 analysed the beach profile results and surface sediment data in order to provide an answer to research question 1. The key finding of this chapter in relation to the original aim was that profile lines vary significantly depending on where they are located in the groyne compartment. Profiles express different shapes, and react in different ways to wave energies, agreeing with previous work by Dornbusch (2010) and Theuerkauf and Rodriguez (2012). Surface sediment compositions and patterns of sorting were inconsistent between the three profiles, which is believed to be related to the variation in profile dynamics.

The placement of transects within groyne cells has a significant impact on its morphological features and reactions to forcing mechanisms. Based on this evidence, it is suggested that the semi-annual baseline surveys completed along this coastline by HBC may be inadequate for displaying patterns of change. At decadal time scales, there is no doubt that changes would likely be sufficient enough for these profiles to be useful, but using them to measure annual erosion and accretion patterns may lead to inaccuracies where measured profile lines are positioned differently in relation to groyne spacing. More importantly, this could lead to discrepancies when calculating rates of longshore transport based solely on topographic surveys.

Chapter 6 investigated the factors influencing the active layer depth and in doing so produced one of the largest datasets on this topic, and developed methods for the prediction of active layer depth on mixed sand and gravel beaches.

This study highlights the variability of active layer depth within such a complex setting. The major contribution of this chapter and the thesis in general is the finding of a non-linear relationship between active layer depth and wave height. Previous authors (e.g. Williams, 1971; Ferreira *et al.*, 2000) have assumed, often from high resolution but short scale studies (e.g. Ciavola *et al.*, 1997) that the relationship between active layer depth and wave height is straightforward. This research shows that, for a mixed sand and gravel beach at least, this is certainly not the case. It builds on a body of work investigating the influence of sediment mixtures on hydraulic conductivity and sediment transport, producing a key

equation ($\ln(y) = -0.797x + 3.565$, $R^2 = 0.578$) which allows for the prediction of active layer depth on a mixed sand and gravel beach, and which may be applicable to other beaches after verification with field experiments. The predictions can be used for the upper and mid sections of the wave activated beachface. The lower beach, which is composed mainly of sand and has a shallower slope, had a smaller average active layer depth, but too few measurements were successful to allow creation of a similar equation for this region of the beach.

The results also suggested that sediment composition perhaps does not play as strong a role in AL depth as would be expected, and that whether the profile cross-sectional area changes is a much more influential factor; AL depth is greatest when the beach system is not using its energy to rearrange the overall beach shape.

Chapter 7 detailed attempts to study sediment transport patterns both within the groyne compartment and alongshore in the direction of dominant transport. The low recovery rates even when tracers had only been in the field for one day highlight the energetic and unpredictable nature of mixed sand and gravel beaches, and provide justification for future studies to further investigate complex beaches like this, with the ultimate aim of reliably modelling the transport processes occurring.

A total longshore transport volume of approximately $6,400 \text{ m}^3/\text{year}$ was calculated for the study area using long term tracer velocities. This value is only representative of gravel transport in the groyned area of the beachface, and is given low confidence due to the low tracer detection rates from which it was calculated. It is suggested that longshore sand transport may be of greater volume at this beach than had previously been proposed by Whitcombe (1996), who indicated that gravel sized sediment would travel faster due to its preferential sorting into the upper, more active, beach. If this is the case, tracer pebbles could have been following a pattern found by Bertoni *et al.* (2012), who found tracers were preferentially transported seawards, to a location just below the beach step. From here they may have been lost even further seaward due to tidal currents. Future experiments should attempt to measure sand transport, and determine the rate of transport in the lower beach and low tide terrace, where sediment is less restricted by groynes.

Attempts to calibrate the CERC equation (USACE, 1984) for use at this site produced values for coefficient k ranging from 0.00006 to 0.7379. K was found to decrease as wave power increases.

Successfully calibrating the CERC equation would allow beach managers to use the equation to estimate longshore transport for sediment recycling purposes in future, and save time and money usually spent on surveys. However, the low reliability of the current study must be acknowledged, and so realistically it is unlikely that the equation can be used. It is possible that further data from this site could be added to the database of calibrations though.

The main limitation with this study was the low detection rates of the tracer pebbles. The premise of this technique is still better than other methods used to determine transport velocities, but with such low recovery rates in this particular case, little confidence can be assigned to any results obtained.

8.5 Final recommendations

One of the major shortcomings of this project was the use of offshore wave data. The impact of groynes on wave refraction patterns cannot be properly assessed from this data, and it is believed that they had a strong influence, making many of the studied relationships appear weaker than they may have on an unaffected coastline. In order to rectify this, a good start would be to monitor the inshore wave climate at Eastoke with a wave recorder. This data could then be used to calibrate a wave propagation model that could be applied to Hayling wave buoy long term climate, allowing reliable estimates to be produced for inshore wave height and period, which may produce a clearer relationship between these variables and beach morphodynamics (Bertin *et al.*, 2008).

An intensive sampling regime, perhaps using both surface photography methods (Buscombe, 2008) and physical sediment samples of the active layer, at a much higher resolution than was attempted by the current study, would likely provide a more accurate overall picture of the sediment composition and long- and cross-shore sorting patterns under a variety of wave climates. Results and previous research (e.g. Mason and Coates, 2001; Blanco *et al.*, 2006) would suggest that potentially the most complex aspect of a mixed sand and gravel beach – particularly a replenished one – is its sediment and the variability it can display on both short and long temporal scales (Horn and Walton, 2007). A more quantitative analysis of surface sediment data may be able to reveal a link between this and the active layer.

The transport of sand is likely to be of increased importance in the sandy lower foreshore just beyond the limit of low water and the extent of the groynes, where it is possible material is being transported alongshore at a faster rate than the tracers deployed within the confines of a groyne bay. A tracer study in this area of the beach would likely provide valuable insights into sediment transport dynamics at Eastoke, and perhaps on other similar beaches.

Assessing cross-shore variations in active layer depth and transport velocities would enable the creation of a one line model, which if calibrated for a variety of wave conditions, could lead to more accurate future estimates of longshore transport both in the intertidal zone and on the lower foreshore, where longshore currents may be more influential than wave power.

References

- Aagaard, T., Greenwood, B. and Hughes, M. (2013) 'Sediment transport on dissipative, intermediate and reflective beaches'. *Earth-Science Reviews*, 124, pp.32-50.
- Aagaard, T., Hughes, M., Baldock, T., Greenwood, B., Kroon, A. and Power, H. (2012) 'Sediment transport processes and morphodynamics on a reflective beach under storm and non-storm conditions'. *Marine Geology*, 326-328, pp. 154-165.
- Allan, J.C., Hart, R. and Tranquili, V. (2006) 'The use of Passive Integrated Transponder (PIT) tags to trace cobble transport in a mixed sand-and-gravel beach on the high-energy Oregon coast, USA'. *Marine Geology*, 232 (1), pp.63–86.
- Allen, L.G. and Gibbard, P.L. (1993) 'Pleistocene evolution of the Solent River of Southern England'. *Quaternary Science Reviews*, 12 (7), pp.503-528
- Almeida, L.P., Masselink, G., Russell, P.E., and Davidson, M.A. (2015) 'Observations of gravel beach dynamics during high energy wave conditions using a laser scanner'. *Geomorphology*, 288, pp.15-27
- Anfuso, G. (2005) 'Sediment-activation depths for gentle and steep beaches'. *Marine Geology*, 220 (1-4), pp101-112.
- Anfuso, G., Gracia, F.J., Andrés, J., Sánchez, L., Del Río, and López-Aguayo, F. (2000) 'Depth of Disturbance in Mesotidal Beaches during a Single Tidal Cycle'. *Journal of Coastal Research*, 16 (2), pp.446-457.
- Anfuso, G., Benavente, J., Del Rio, L., Castiglione, E., and Ventorre, M. (2003) 'Sand transport and disturbance depth during a single tidal cycle in a dissipative beach: La Barrosa (SW Spain). *Proceedings of the 3rd IAHR Symposium on River, Coastal and Estuarine Morphodynamics*, 2, pp.1176-1186.
- Anfuso, G., Ruiz, N. (2004) 'Morphodynamics of a mesotidal, exposed, low tide terrace beach (Faro, South Portugal)'. *Cienc. Mar.* 30 (4), pp.575-584.
- Austin, M.J. and Buscombe, D. (2008) 'Morphological change and sediment dynamics of the beach step on a macrotidal gravel beach'. *Marine Geology*, 249 (3-4), pp.167-183.

- Austin, M.J. and Masselink, G. (2006) 'Observations of morphological change and sediment transport on a steep gravel beach'. *Marine Geology*, 229 (1-2), pp.59-77.
- Bakhtyar, R., Brovelli, A., Barry, D.A. and Li, L. (2011) 'Wave-induced water table fluctuations, sediment transport and beach profile change: Modelling and comparison with large-scale laboratory experiments'. *Coastal Engineering*, 58, pp.103-118.
- Baptista, P., Bastos, L., Bernardes, C., Cunha, T., and Dias, J. (2008) 'Monitoring sand shores morphologies by dGPS – a practical tool to generate digital elevation models'. *Journal of Coastal Research*, 24 (6), pp.1516-1528.
- BAR. (2005) 'Beach material properties'. In: University of Sussex. *Beaches at Risk*. Falmer: pp. 25
- Barnes, G.E. (1995) *Soil Mechanics Principle and Practice*. MacMillan Press Ltd.
- Bascom, Willard (1960) 'Beaches'. *Scientific American*, 203 (2), pp.80-94.
- Bertin, X., Castelle, B., Anfuso, G. and Ferreira, O. (2008) 'Improvement of sand activation depth prediction under conditions of oblique wave breaking' *Geo-Mar Lett*, 28, pp. 65-75.
- Bertoni, D., Sarti, G., Benelli, G., Pozzebon, A. and Raguseo, G. (2010) 'Radio Frequency Identification (RFID) technology applied to the definition of underwater and subaerial coarse sediment movement'. *Sedimentary Geology*, 228 (3-4), pp.140-150.
- Bertoni, D., Sarti, G., Benelli, G., Possebon, A. and Raguseo, G. (2012) 'Transport trajectories of "smart" pebbles on an artificial coarse-grained beach at Marina di Pisa (Italy): implications for beach morphodynamics'. *Marine Geology*, 291-294, pp.227-235.
- Bird (2008) *Coastal Geomorphology* (2nd edition). Chichester: John Wiley & Sons.
- Birkemeier, W.A. (1985) 'Field data on seaward limit of profile change'. *Journal of Waterway, Port and Coastal Engineering*, 111 (3), pp.598-602.
- Blanco, B. (2003) 'Dynamics of mixed, sand and gravel, beaches'. PhD Thesis, University of London.

Bosnic, I., Cascalho, J., Taborda, R., Ribeiro, M., Oliveira, A., Rodrigues, A. and Lira, C. (2011) 'Textural characterisation of the beach active layer'. *Journal of Coastal Research*, Special Issue 64, pp.40-44.

Bradbury, A.P., Mason, T.E., and Poate, T. (2007) 'Implications of the spectral shape of wave conditions for engineering design and coastal hazard assessment – evidence from the English Channel'. *10th International Workshop on Wave Hindcasting and Forecasting and Coastal Hazard Symposium*. [Online] Available from: <http://www.waveworkshop.org/10thWaves/Papers/IMPLICATIONS%20OF%20THE%20SPECTRAL%20SHAPE%20OF%20WAVE%20CONDITIONS.pdf> [Accessed 24/05/2019]

Bradbury, A.P. and Mason, T.E. (2009) 'An inter-comparison of hindcast and measured wave data: implications for beach recharge design'. *11th International Workshop on Wave Hindcasting and Forecasting and Coastal Hazard Symposium*. [Online] Available from: <http://citeseerx.ist.psu.edu/viewdoc/download?doi=10.1.1.730.1590&rep=rep1&type=pdf> [Accessed 24/05/2019]

Bray, M. (2007) *East Head and West Wittering: Interpretation of Beach Changes 2003-06*. Technical Report. Chichester District Council. [Online] Available from: <https://www.researchgate.net/publication/269394970> [Accessed 24/05/2019]

Bray, M. (2010) *East Head, West Wittering and Cakeham: Interpretation of beach changes 2004-09*. Technical Report. Chichester District Council/East Head Coastal Issues Advisory Group. [Online] Available from: <https://www.researchgate.net/publication/269395206> [Accessed 24/05/2019]

Bray, M., Workman, M., Smith, J., Pope, D. (1996) 'Field measurements of shingle transport using electronic tracers'. *Proceedings of the 31st MAFF Conference of River and Coastal Engineers*, pp.10.4.1. – 10.4.13.

Buscombe, D. (2008) 'Estimation of grain-size distributions and associated parameters from digital images of sediment'. *Sedimentary Geology*, 210 (1-2), pp.1-10.

Buscombe, D. and Masselink, G. (2006) 'Concepts in beach gravel dynamics'. *Earth-Science Reviews*, 79 (1-2), pp.33-52.

Caldwell, N.E. (1983) 'Using tracers to assess size and shape sorting processes on a pebble beach'. *Proceedings of the Geologists' Association*, 94 (1), pp.86-90.

- Caldwell, N.E. and Williams, A.T. (1985) 'The Role of Beach Profile Configuration in the Discrimination between Differing Depositional Environments Affecting Coarse Clastic Beaches'. *Journal of Coastal Research*, 1 (2), pp.129-139.
- Carr, A.P. (1971) 'Experiments on longshore transport and sorting of pebbles: Chesil Beach, England.' *Journal of Sedimentary Research*, 41 (4), pp.1084-1104.
- Carr, A.P. (1974) 'Differential movement of coarse sediment particles'. *Proceedings of the 14th Coastal Engineering Conference*. ASCE, p851-870.
- Carter, R.W.G. (1989) *Coastal Environments – An Introduction to the Physical, Ecological and Cultural Systems of Coastlines*. London: Academic Press.
- Carter, R.W.G. and Orford, J.D. (1984) 'Coarse clastic beaches: a discussion of the distinctive dynamic and morphosedimentary characteristics'. *Marine Geology*, 60, pp.377-389.
- CCO (2017) *Annual Wave Report 2016: Hayling Island Directional Waverider Buoy*.
- Ciavola, P., Billi, P., Armaroli, C., Preciso, E., and Salemi, E. (2005) 'Morphodynamics of the Bevano Stream outlet: the role of bedload yield'. *Geologica tecnica e ambientale*, 1, pp.41-57.
- Ciavola, P., Contestabile, P., Aristodemo, F. and Vicinanza, D. (2013) 'Beach sediment mixing under drained and undrained conditions'. *Journal of Coastal Research*, SI 65: Proceedings of the 12th International Coastal Symposium ICS 2013, 2, pp.1503-1508
- Ciavola, P. and Castiglione, E. (2009) 'Sediment dynamics of mixed sand and gravel beaches at short time-scales'. *Journal of Coastal Research*, SI 56 (Proceedings of the 10th International Coastal Symposium), pp.1751-1755.
- Ciavola, P., Taborda, R., Ferreira, O. and Dias, J.A. (1997) 'Field observations of sand-mixing depths on steep beaches'. *Marine Geology*, 141 (1-4), pp.147-156.
- Coates, T.T., Brampton, A.H., and Powell, K.A. (2001) 'Shingle beach recharge in the context of coastal defence'. In: *Ecology and geomorphology of coastal shingle* (J.R. Packham, R.E. Randall, R.S.K. Barnes, and A. Neal Eds.), pp.394-403. Westbury: Otley.

- Coates, T.T. and Damgaard, J.S. (1999) 'Towards improved management of mixed grain beaches'. *Proceedings of HYDRALAB workshop in Hannover*, pp.69-73.
- Coco, G., O'Hare, T.A. and Huntley, D.A. (2000) 'Investigation of a self-organisation model for beach cusp formation and development'. *Journal of Geophysical Research*, 105, pp.21991-22002.
- Cooper, N.J., Bray, M.J., King, D.M. (1996) 'Field measurements of fine shingle transport'. *Proceedings of Tidal '96*.
- Costa, S., Levoy, F., Monfort, O., Curoy, J., De Saint Léger, E. and Delahaye, D. (2008) 'Impact of sand content and cross-shore transport on the morphodynamics of macrotidal gravel beaches (Haute-Normandie, English Channel)'. In: Hequette A. and C. Moses (eds) (2008). *Beaches at Risk. Zeitschrift für Geomorphologie N.F. 52, Supplementband 3*, pp.41-62.
- Curoy, J. (2012) *Morphological and longshore sediment transport processes on mixed beaches*. PhD thesis, University of Sussex.
- Curoy, J., Moses, C.A., Robinson, D.A. and Williams, R.B.G. (2009) 'Profile evolution and active layer measurements on a macrotidal composite gravel beach, Somme Estuary, France'. *Zeitschrift für Geomorphologie*, 53 (3), pp.387-409.
- Curtiss, G.M., Osborne, P.D. and Horner-Devine, A.R. (2009) 'Seasonal patterns of coarse sediment transport on a mixed sand and gravel beach due to vessel wakes, wind waves and tidal currents'. *Marine Geology*, 259, pp.73-85.
- Deltares (2017) XBeach-G software. [online] Available from: <https://oss.deltares.nl/web/xbeach/xbeach-og> [Accessed 12-06/2019].
- DeVries, P. (2000) '*Scour in low gradient gravel bed streams: patterns, processes, and implications for the survival of salmonid embryos*'. PhD Thesis, University of Washington.
- DeVries, P. (2002) 'Bedload layer thickness and disturbance depth in gravel bed streams'. *Journal of Hydraulic Engineering*, 128, pp.983-991.
- Dickson, M.E., Kench, P.S. and Kantor, M.S. (2011) 'Longshore transport of cobbles on a mixed sand and gravel beach, southern Hawke Bay, New Zealand'. *Marine Geology*, 287, pp.31-42.

- Dornbusch, U. (2010) 'Ground survey methods for mixed sand and gravel beaches in intertidal environments: a comparison'. *Journal of Coastal Research*, 20 (3), pp.451-464.
- Dornbusch, U. (2017) 'Design requirement for mixed sand and gravel beach defences under scenarios of sea level rise'. *Coastal Engineering*, 123, pp.12-24.
- Dornbusch, U., Robinson, D.A., Moses, C.A. and Williams, R.B.G. (2008) 'Variation in beach behaviour in relation to groyne spacing and groyne type for mixed sand and gravel beaches, Saltdean, UK'. In: Hequette A. and C. Moses (eds) (2008). *Beaches at Risk*. Zeitschrift für Geomorphologie N.F. 52, Supplementband 3, pp.125-143.
- Duncan, J.R. (1964) 'The effects of water table and tide cycles on swash-backwash sediment distribution and beach profile development'. *Marine Geology*, 2, pp. 186-197.
- Dunn, O.J. (1964) 'Multiple comparisons using rank sums'. *Telenometrics*, 6 (3), pp.241-252.
- Dyer, K.R. (1975) 'The buried channels of the 'Solent River', southern England.' *Proceedings of the Geologists' Association*, 86 (2), pp.239-245.
- Engelund, F. and Hanson, E. (1967) 'A monograph on sediment transport.' Teknisk Forlag, Copenhagen, Denmark.
- ESCP (2012) *South Hayling Beach Management Plan, Version 2.1*. Havant: Eastern Solent Coastal Partnership (Report Number: ESCP-HBC-SHBMP-001)
- ESCP (2013a) *Beach Sediment Tracer Study 2010-2012: Beach Tracer Report for Portsmouth & Hayling Island Frontage*. Havant: Eastern Solent Coastal Partnership.
- ESCP (2013b) *Tracer Study Burial Depth Detection Range*. Havant: Eastern Solent Coastal Partnership. https://scopac.org.uk/wp-content/uploads/2018/11/FINAL_Tracer-burial-depth-experiment-LeeOnSolent.pdf [Accessed 09/06/2019].
- ESCP (2013c) *Coastal defence project now complete*. [Online] Available from: <https://www.escp.org.uk/news/coastal-defence-project-now-complete> [Accessed 12-06/2019]
- ESCP (2017) *South Hayling BMP 2017-22*. Technical Report SHBMP1722.

ESCP (2018) *SCOPAC/ESCP Minor Fund Toe Scour Research Project*. [Online] Available from: www.scopac.org.uk/research/beach-response [Accessed 11/12/2018].

Ferreira, O., Bairos, M., Pereira, H., Ciavola, P., and Dias, J.A. (1998) 'Mixing depth levels and distribution on steep foreshores'. *Journal of Coastal Research*, 26, pp.292-296.

Ferreira, O., Ciavola, P., Taborda, R., Bairos, M. and Dias, J.A. (2000) Sediment mixing depth determination for steep and gentle foreshores. *Journal of Coastal Research*, 16 (3), pp.830-839.

Foley, M.G. (1978) 'Scour and fill in steep, sand-bed ephemeral streams'. *Geological Society of America Bulletin*, 89 (4), pp.559-570.

Fuller, R.M. and Randall, R.E. (1988) 'The Orford Shingles, Suffolk, UK – Classic conflicts in coastline management'. *Biological Conflicts*, 46, pp.95-114.

Gale, S.J. and Hoare, P.G. (1992) 'Bulk sampling of coarse clastic sediments for particle-size analysis'. *Earth Surface Processes and Landforms*, 17, pp.729-733.

Gourlay, M.R. (1974) 'Wave set-up and wave generated currents in the lee of a breakwater or headland'. *Coastal Engineering 1974: Proceedings of the 14th International Conference*. New York: American Society of Civil Engineers. pp.1976-1995.

Grant, T.D. (1986) *Hydraulic model investigation of the shingle nourished beach at Hayling Island*. Unpublished BSc report, Department of Civil Engineering, Southampton University.

Greenwood, B. and Hale, P.B. (1980) 'Depth of activity, sediment flux and morphological change in a barred nearshore environment'. *Geological Survey of Canada*, 80 (10), pp.89-109.

Guza, R.T. and Inman, D.L. (1975) 'Edge waves and beach cusps'. *Journal of Geophysical Research*, 80 (21), pp.2997-3012.

Hallermeier, R.J. (1978) 'Uses for a calculated limit depth to beach erosion'. *Proceedings of the 16th Coastal Engineering Conference*, pp.1493-1512.

Hallermeier, R.J. (1981) 'A profile zonation for seasonal sand beaches from wave climate'. *Coastal Engineering*, 4, 253-277.

Hampshire County Council (2010) *Eastern Solent*, Hampshire County.

Hanson, H., Brampton, A., Capobianco, M., Dette, H.H., Hamm, L., Laustrop, C. Lechuga, A. and Spanhoff, R. (2002) 'Beach nourishment projects, practices, and objectives – a European overview'. *Coastal Engineering*, 47 (2), pp.81-111.

Hardisty, J. (1990) *Beaches: Form and Process*. London: Unwin Hyman.

Harlow, D.A. (1979) 'The littoral budget between Selsey Bill and Gilkicker Point and its relevance to coast protection works on Hayling Island'. *Quarterly Journal of Engineering Geology*, 12 (4), pp.257-265.

Harlow, D.A. (1980) *Sediment Processes, Selsey Bill to Portsmouth*. Unpublished PhD thesis, Department of Civil Engineering, University of Southampton.

Harlow, D.A. (1985) 'Hayling Island beach replenishment scheme'. In: S.M. Bevan (ed.) *Shingle Beaches: Renourishment and Recycling*. London: Thomas Telford.

Hassan, M.A. (1990) 'Scour, fill and burial depth of coarse material in gravel bed streams'. *Earth Surface Processes and Landforms*, 15, pp. 341-356.

Havant Borough Council, Technical Services Department (1999). *Beach Management Strategy Plan for the Southern Frontage of the Eastoke Peninsula*. Coast Protection Unit, pp.35.

Havant Borough Council, Technical Services Department (2000). *Chichester Harbour Approach Channel. Navigational Dredging: Appropriate Assessment*. Coast Protection Unit, pp.26.

Holmes, P., Baldock, T.E., Chan, T.C. and Neshaei, M.A.L. (1996) 'Beach evolution under random waves'. *Proceedings of the 25th International Conference on Coastal Engineering*, American Society of Civil Engineers, pp.3006-3019.

Hoque, M.A. and Asano, T. (2007) 'Numerical study on wave-induced filtration flow across the beach face and its effects on swash zone sediment transport'. *Ocean Engineering*, 34, pp.2033-2044.

- Horn, D.P., Baldock, T.E., Baird, A.J. and Mason, T.E. (1998) 'Field measurements of swash induced pressure gradients within a sandy beach'. *Proceedings of the 26th International Conference on Coastal Engineering*, American Society of Civil Engineers.
- Horn (1997) 'Beach research in the 1990s'. *Progress in Physical Geography*, 21 (3), pp.454-470.
- Horn, D.P. (2002) 'Beach groundwater dynamics'. *Geomorphology*, 48 (1-3), pp.121-146.
- Horn, D.P. and Li, L. (2006) 'Measurement and modelling of gravel beach groundwater in response to wave run-up: effects on beach profile changes'. *Journal of Coastal Research*, 22 (5), pp.1241-1249.
- Horn, D.P. and Walton, S.M. (2007) 'Spatial and temporal variations of sediment size on a mixed sand and gravel beach'. *Sedimentary Geology*, 202 (3), pp.509-528.
- HR Wallingford (1995) *Pagham Harbour to River Hamble Coastal Strategy Study, Volume 1: Pagham Harbour to Portsmouth Harbour*. Report EX3121. Report to Pagham to Hamble Coast Strategy Group, pp.134.
- HR Wallingford (2008) *Eastoke Point Coastal Defence Strategy*
- Hydraulics Research (1987) *Hayling Island Beach Replenishment Scheme*, Report to Havant Borough Council, 29pp.
- Hydraulics Research (1992) *Selsey Bill, Hayling Island and the Isle of Wight: Effects of dredging on nearshore wave conditions*. Report EX 2696.
- Jackson, N.L. and Nordstrom, K.F. (1993) 'Depth of activation of sediment by plunging breakers on a steep sand beach'. *Marine Geology*, 115 (1-2), pp.143-151.
- James, W.R. (1974) 'Beach fill stability and borrow material texture'. *Proceedings of the 14th International Conference on Coastal Engineering*, pp.1334-1349.
- Jennings, R. and Shulmeister, J. (2002) 'A field based classification scheme for gravel beaches.' *Marine Geology*, 186, pp.211-228.
- Jolliffe, I.P. (1964) 'An experiment designed to compare the relative rates of movement of different sizes of beach pebble'. *Proceedings of the Geologists' Association*, 75(1), pp.67-76.

- King, C.A.M. (1951) 'Depth of Disturbance of Sand on Sea Beaches by Waves'. *Journal of Sedimentary Petrology*, 21 (3), pp.131-140.
- Kirk, R.M. (1980) 'Mixed sand and gravel beaches: morphology, processes and sediments'. *Progress in Physical Geography*, 4 (2), pp. 189-210.
- Komar P.D. (1987) 'Selective Grain Entrainment by a Current from a Bed of Mixed Sizes: A Reanalysis'. *Journal of Sedimentary Research*, 57 (2), pp.203-211.
- Komar, P.D. (1988) 'Environmental controls on littoral sand transport'. In *Proceedings of the 21st Coastal Engineering Conference*, ASCE, Spain, pp.1238-1252.
- Komar, P.D. (1998) *Beach processes and sedimentation* (2nd edition). Prentice Hall: New Jersey.
- Komar, P.D., and Inman, D.L. (1970) 'Longshore transport on beaches'. *Journal of Geophysical Research*, 75, pp.5514-5527.
- Kraus, N.C. (1985) 'Field experiments on vertical mixing of sand in the surf zone'. *Journal of Sedimentary Petrology*, 55, pp.3-14.
- Kraus, N.C., Larson, M., and Wise, R.A. (1998) *Depth of Closure in Beach-fill Design*. Coastal Engineering Technical Note CETN II-40, 3/98. US Army Engineer Waterways Experiment Station, Vicksburg, MS.
- Kroon, A. and Masselink, G. (2002) 'Morphodynamics of intertidal bar morphology on a macrotidal beach under low-energy wave conditions, North Lincolnshire, England'. *Marine Geology*, 190 (3-4), pp. 591-608.
- Kuenen, H. (1948) 'The formation of beach cusps'. *The Journal of Geology*, 56 (1), pp.34-40.
- Kulkarni, C.D., Levoy, F., Monfort, O. and Miles, J. (2004) 'Morphological variations of a mixed sediment beachface (Teignmouth, UK)'. *Coastal Shelf Research*, 24, pp.1203-1218
- Lamarre, H., MacVicar, B., and Roy, A.G. (2005) 'Using Passive Integrated Transponder (PIT) tags to investigate sediment transport in gravel-bed rivers'. *Journal of Sedimentary Research*, 75 (4), pp.736-741.

- Larone, J.B. and Duncan, M.J. (1989) 'Constraints on duration of sediment storage in a wide, gravel-bed river, New Zealand'. *International Association of Hydrological Sciences Publication 184*, pp.165-172.
- Larson, R., Morang, A. and Gorman, L. (1997) 'Monitoring the coastal environment; part II: sediment sampling and geotechnical methods'. *Journal of Coastal Research*, 13 (2), pp.308-330.
- Lee, M.W.E., Bray, M.J., Workman, M., Collins, M.B., and Pope, D. (2000) 'Coastal Shingle Tracing: A Case Study Using the Electronic Tracer System (ETS)'. In: Foster, D.L. ed. *Tracers in Geomorphology*. Chichester: John Wiley & Sons, pp.413-436.
- Mason, S.J. and Hansom, J.D. (1989) 'A Markov model for beach changes on the Holderness coast of England'. *Earth Surface Processes and Landforms*, 14 (8), pp. 731-743.
- Mason, T. (1997) *Hydrodynamics and sediment transport on a macro-tidal, mixed (sand and shingle) beach*. Unpublished PhD thesis, University of Southampton.
- Mason, T., Bradbury, A., Poate, T., and Newman, R. (2008) 'Nearshore wave climate of the English Channel – evidence for bimodal seas'. *Coastal Engineering 2008: Proceedings of the 31st International Conference*, Vol.1, pp.605-616.
- Mason, T. and Coates, T.T. (2001) 'Sediment transport processes on mixed beaches: a review for shoreline management'. *Journal of Coastal Research*, 17 (3), pp.645-657.
- Massel, S.R. and Pelinovsky, E.N. (2001) 'Run-up of dispersive and breaking waves on beaches'. *Oceanologia*, 43 (3), pp.61-97.
- Masselink, G. and Hegge, B. (1995) 'Morphodynamics of meso- and macrotidal beaches: examples from central Queensland, Australia'. *Marine Geology*, 129 (1-2), pp.1-23.
- Masselink, G., Hughes, M.G. and Knight, J. (2011) *Coastal Processes & Geomorphology*. 2nd ed. London: Hodder Education.
- Masselink, G., Hegge, B.J. and Pattiaratchi, C.B. (1997) 'Beach cusp morphodynamics'. *Earth Surface Processes and Landforms*, 22, pp.1139-1155.

- Masselink, G., Russell, P., Blenkinsopp, C. and Turner, I. (2010) 'Swash zone sediment transport, step dynamics and morphological response on a gravel beach'. *Marine Geology*, 274, pp. 50-68.
- McFarland, S., Whitcombe, L. and Collins, M. (1994) 'Recent shingle beach renourishment schemes in the UK: some preliminary observations'. *Ocean and Coastal Management*, 25 (2), pp.143-149.
- McLean, R.F. (1970) 'Variations in grain-size and sorting on two Kaikoura beaches'. *New Zealand Journal of Marine and Freshwater Research*, 4 (2), pp.141-164.
- Miller, I.M. and Warrick, J.A. (2012) 'Measuring sediment transport and bed disturbance with tracers on a mixed beach'. *Marine Geology*, 299-302, pp.1-17.
- Miller, I.M., Warrick, J.A. and Morgan, C. (2011) 'Observations of coarse sediment movements on the mixed beach of the Elwha Delta, Washington'. *Marine Geology*, 282 (3-4), pp.201-214.
- Moon, C. (2003) 'Assessing the Accuracy of Beach Volume Estimates for Hayling Island'. MSc thesis, University of Southampton.
- Moses, C.A. and Williams, R.B.G. (2008) 'Artificial beach recharge: the South East England experience'. In: Hequette A. and C. Moses (eds) (2008). *Beaches at Risk*. Zeitschrift für Geomorphologie N.F. 52, Supplementband 3, pp.107-124.
- Napier City Council (2007) The dynamics of mixed sand-and-gravel beaches and the Hawke's Bay monitoring programme. [Online] Available from: <https://ref.coastalrestorationtrust.org.nz/documents/the-dynamics-of-mixed-sand-and-gravel-beaches-and-the-hawkes-bay-monitoring-programme/> [Accessed 12-06-2019]
- New Forest District Council (2010) North Solent Shoreline Management Plan.
- New Forest District Council (2017). 2012 Update of Carter, D., Bray, M., & Hooke, J., 2004 SCOPAC Sediment Transport Study, www.scopac.org.uk/sts.
- Nicholls, R.J. and Wright, P. (1991) 'Longshore transport of coastal pebbles: experimental estimates of K'. *Proceedings of the Conference on Coastal Sediments '91*, pp.920-933.

- Nichols, M.H. (2004) 'A radio frequency identification system for monitoring coarse sediment particle displacement'. *Applied Engineering in Agriculture*, 20 (6), pp.783-787.
- Nolan, T.J., Kirk, R.M. and Shulmeister, J. (1999). 'Beach cusp morphology on sand and mixed sand and gravel beaches, South Island, New Zealand'. *Marine Geology*, 157, pp.185-197.
- Osborne, P.D. (2005) 'Transport of gravel and cobble on a mixed-sediment inner bank shoreline of a large inlet, Grays Harbour, Washington'. *Marine Geology*, 224, pp.145-156.
- Pattiaratchi, C., Olsson, D., Hetzel, Y., and Lowe, R. (2009) 'Wave-driven circulation patterns in the lee of groynes'. *Continental Shelf Research*, 29, pp.1961-1974.
- Pedrozo-Acuña, A., Simmons, D.J., Otta, A.K. and Chadwick, A.J. (2006) 'On the cross-shore profile change of gravel beaches'. *Coastal Engineering*, 53, pp.335-347.
- Pethick, J. (1984) *An introduction to Coastal Geomorphology*, Arnold Heinemann, London.
- Powell, K.A. (1990) *Predicting short term profile response for shingle beaches*. HR Wallingford. (Report SR 219).
- Puleo, J.A., Lanckriet, T. and Blenkinsopp, C. (2014) 'Bed level fluctuations in the inner surf and swash zone of a dissipative beach'. *Marine Geology*, 349, pp.99-112.
- Quick and Dyksterhuis (1994) 'Cross-shore transport for beaches of mixed sand and gravel.' *International Symposium: Waves – physical and numerical modelling*. Canadian Society of Civil Engineers, pp.1443-1452.
- Reichmuth, B. and Anthony, E.J. (2007) 'Tidal influence on the intertidal bar morphology of two contrasting macrotidal beaches'. *Geomorphology*, 90, pp.101-114.
- Richardson, N.M. (1902) 'An experiment on the movement of a load of brickbats deposited on the Chesil Beach'. *Proceedings of the Dorset Natural History and Archaeological Society*, pp.123-133.
- Rogers, J., Hamer, B., Brampton, A., Challinor, S., Glennerster, M., Brenton, P. and Bradbury, A. (2010) *Beach Management Manual* (2nd edition). London: CIRIA.

- Ruocco, A.C., Nicholls, R.J., Haigh, I.D., and Wadey, M.P. (2011) 'Reconstructing coastal flood occurrence combining sea level and media sources: a case study of the Solent, UK since 1935'. *Natural Hazards*, 59, pp.1773-1796.
- Saini, S., Jackson, N.L. and Nordstrom, K.F. (2009) 'Depth of activation on a mixed sediment beach'. *Coastal Engineering*, 56 (7), pp.788-791.
- Schoonees, J.S. (2000) 'Annual variation in the net longshore sediment transport rate'. *Coastal Engineering*, 40 (2), pp.141-160.
- Schoonees, J.S. and Theron, A.K. (1993) 'Review of the field-data base for longshore sediment transport'. *Coastal Engineering*, 19, pp.1-25.
- Schoonees, J.S. and Theron, A.K. (1994) 'Accuracy and applicability of the SPM longshore transport formula'. *Proceedings of the 24th International Conference on Coastal Engineering*. Kobe: American Society of Civil Engineers. Pp2595-2609.
- SCOPAC (2004a) *Portsmouth Harbour Entrance to Chichester Harbour Entrance*.
- SCOPAC (2004b) *Portsmouth, Langstone and Chichester Harbour*.
- Scott, T., Masselink, G. and Russell, P. (2011) 'Morphodynamic characteristics and classification of beaches in England and Wales'. *Marine Geology*, 286 (1-4), pp.1-20.
- Scott, T., Austin, M., Masselink, G., and Russell, P. (2016) 'Dynamics of rip currents associated with groynes – field measurements, modelling and implications for beach safety'. *Coastal Engineering*, 107, pp.53-69.
- Sear, D.A., Lee, M.W.E, Oakey, R.J., Carling, P.A., and Collins, M.B. (2000) 'Coarse Sediment Tracing Technology in Littoral and Fluvial Environments: A Review'. In: Foster, D.L. ed. *Tracers in Geomorphology*. Chichester: John Wiley & Sons, pp.21-56.
- Seastar Survey Ltd (2017) Hayling Island Particle Size Analysis, January 2017.
- She, K., Horn, D., and Canning, P. (2006) 'Porosity and hydraulic conductivity of mixed sand-gravel sediment'. *Conference of Flood and Coastal Risk Management*. [Online] Available from: <http://www.researchgate.net/publication/261481567> [Accessed 24/05/2019]

- She, K., Horn, D., and Canning, P. (2007) *Influence of permeability on the performance of shingle and mixed beaches*. Defra/Environment Agency. (R&D Technical Report FD1923/TR.)
- Sherman, D.J. (1991) 'Gravel beaches'. *National Geographic Research and Exploration*, 7, pp.442-452.
- Sherman, D.J., Nordstrom, K.F., Jackson, N.L., and Allen, J.R. (1994) 'Sediment mixing-depths on a low-energy reflective beach'. *Journal of Coastal Research*, 10 (2), pp.297-305.
- Smithson, P., Addison, K., and Atkinson, K. (2002) *Fundamentals of the Physical Environment* (3rd edition). London: Routledge.
- Sonu, C.J. and Van Beek, J.L. (1971) 'Systematic beach changes on the outer banks, North Carolina'. *The Journal of Geology*, 79 (4), pp.416-425.
- Steenhauer, K. Pokrajac, D., O'Donoghue, T. and Kikkert, G.A. (2011) 'Subsurface processes generated by bore-driven swash on coarse-grained beaches'. *Journal of Geophysical Research*, 116 (C04013), pp.1-17.
- Sunamara, T. and Kraus, N.C. (1985) 'Prediction of average mixing depth of sediment in the surf zone'. *Marine Geology*, 62 (1-2), pp.1-12.
- Swift, D.J.P. (1970) 'Quaternary shelves and the return to grade' *Marine Geology*, 8 (1), pp. 5-30.
- Theuerkauf, E.J. and Rodriguez, A.B. (2012) 'Impacts of transect location and variations in along-beach morphology on measuring volume change'. *Journal of Coastal Research*, 28 (3), pp.707-718.
- Thomas (1953) *The King Holds Hayling*. Havant: Pelham Books.
- Thomas, D.S.G. and Goudie, A. (2000) *The Dictionary of Physical Geography*. 3rd ed. Oxford: Blackwell.
- Trim, L.K. She, K. and Pope, D.J. (2002) 'Tidal effects on cross-shore transport on a shingle beach'. *Journal of Coastal Research*, Special Issue 36, pp.708-715.

- Turner, I.L. and Masselink, G. (1998) 'Swash infiltration-exfiltration and sediment transport'. *Journal of Geophysical Research*, 103 (C13), pp. 30813-30824.
- Turner, I.L and Nielsen, P (1997) 'Rapid water table fluctuations within the beach face: implications for swash zone sediment mobility?' *Coastal Engineering*, 32 (1), pp.45-59.
- USACE (1984) *Shore Protection Manual*. Department of the Army, US Corps of Engineers, Washington, DC 20314.
- Van Rijn, L.C., 2010. Modelling erosion of gravel/shingle beaches and barriers. EU FP6 project: Concepts and Science for Coastal Erosion Management (CONSCIENCE), report D13b.
- Van Wellen (1999) *Modelling of swash zone sediment transport on coarse grained beaches*. Unpublished PhD Thesis, University of Plymouth.
- Van Wellen, E., Chadwick, A.J., Bird, P.A.D., Bray, M., Lee, M. and Morfett, J. (1997) 'Coastal sediment transport on shingle beaches'. *Coastal Dynamics '97: Proceedings of the third Coastal Dynamics Conference*, Plymouth, UK, pp.38-47.
- Van Wellen, E., Chadwick, A.J., Lee, M., Baily, B. and Morfett, J. (1998). 'Evaluation of longshore sediment transport models on coarse grained beaches using field data: a preliminary investigation'. *Proceedings of 26th International Conference on Coastal Engineering*, ASCE, Copenhagen, pp.2640, 2653.
- Van Wellen, E., Chadwick, A.J. and Mason, T. (2000) 'A review and assessment of longshore sediment transport equations for coarse-grained beaches'. *Coastal Engineering*, 40 (3), pp.243-275.
- Wallace, H. (1990) *Sea level and shoreline between Portsmouth and Pagham for the past 2,000 years*. Privately published by author.
- Watt, T., Robinson, D.A., Moses, C.A. and Dornbusch, U. (2008) 'Patterns of surface sediment grain size distribution under the influence of varying wave conditions on a mixed sediment beach at Pevensey Bay, southeast England'. In: Hequette A. and Moses, C. (eds) (2008). *Beaches at Risk*. Zeitschrift für Geomorphologie N.F. 52, Supplementband 3, pp.63-77.

- Webber, N.B. (1979) *An investigation of the dredging in Chichester Harbour approach channel, and the possible effects on the Hayling Island coastline*. Report to Chichester Harbour Conservancy, Havant Borough Council and Francis Concrete Ltd.
- West, I.M. (1980) 'Geology of the Solent Estuarine System'. In: *The Solent Estuarine System: an Assessment of Present Knowledge*. N.E.R.C. Publication, Series C, 22, pp.6-18.
- Whitcombe, L.J. (1995) 'Sediment transport processes, with particular reference to Hayling Island'. PhD thesis, University of Southampton.
- Whitcombe, L.J. (1996) 'Behaviour of an artificially replenished shingle beach at Hayling Island, UK'. *Quarterly Journal of Engineering Geology and Hydrology*, 29 (4), pp.265-271
- Wilcock, P.R. (2001) 'Toward a practical method for estimating sediment-transport rates in gravel-bed rivers'. *Earth Surface Processes and Landforms*, 26, pp.1395-1408.
- Williams, A.T. (1971) 'An analysis of some factors involved in the depth of disturbance of beach sand by waves'. *Marine Geology*, 11 (3), pp.145-158.
- Williams, J.J., Ruiz de Alegria-Arzaburu, A., McCall, R.T., and Van Dengeren, A. (2012) 'Modelling gravel barrier profile response to combined waves and tides using XBeach: Laboratory and field results.' *Coastal Engineering*, 63, pp.62-80.
- Wilson, M (2017) *To model and map historical bimodal storm conditions off Hayling Island*. Unpublished MSc Thesis. University of Portsmouth.
- Woodroffe, C. (2003) *Coasts: Form, process and evolution*. Cambridge: University Press.
- Wright, P., Cross, J.S., and Webber, N.B. (1978) 'Aluminium pebbles: a new type of tracer for flint and chert pebble beaches'. *Marine Geology*, 27 (1-2), pp.M9-M17.
- Wright, L.D. and Short, A.D. (1984) 'Morphodynamic variability of surf zones and beaches: a synthesis'. *Marine Geology*, 56, pp.93-118.
- Zarkogiannis, S.D., Kontakiotis, G., Vousdoukas, M.I., Velegrakis, A.F., Collins, M.B., and Antonarakou, A. (2018) 'Scarping of artificially-nourished mixed sand and gravel beaches: sedimentological characteristics of Hayling Island beach, Southern England'. *Coastal Engineering*, 133, pp.1-12.

Appendices

Appendix A : Wave conditions

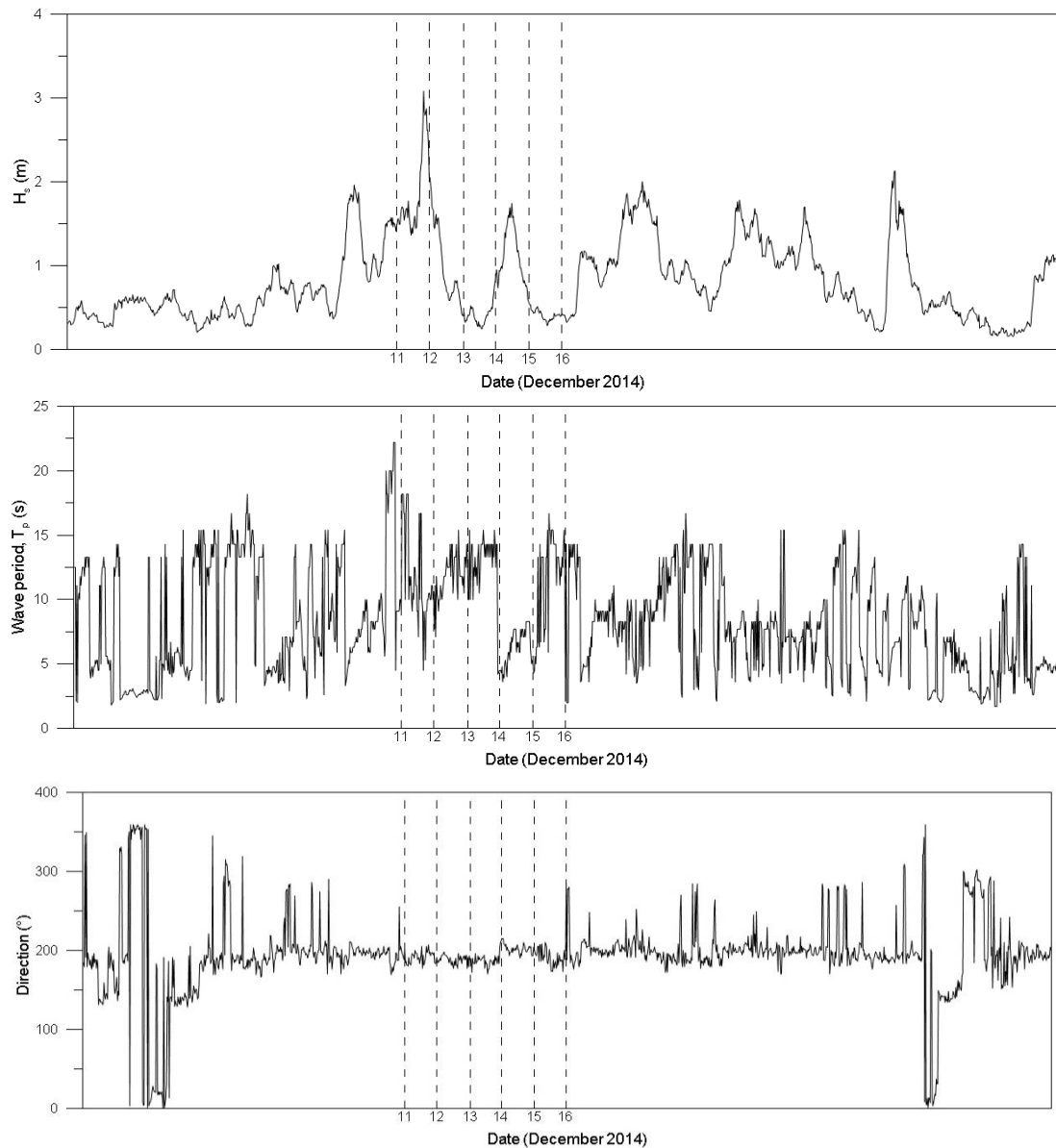


Figure A-1: Wave conditions during December 2014, with profile survey dates marked by dashed lines. Data from CCO.

December 2014 (Figure A-1)

The maximum significant wave height (3.08 m) occurs between the profiles measured on the 11th and 12th. This peak occurs shortly before low tide, but wave heights between these two surveys were sustained at around 1.5 m. After this, H_s drops to below 1 m apart from another smaller peak, at a maximum of 1.74 m between surveys on the 14th and 15th. This peak coincides approximately with low tide. Peak wave period is similar between most surveys, the exception being December 14th-15th, where it is much lower. Wave direction stays constant during this field period, approaching from approximately 200 degrees, or SSW. This is close to perpendicular to the shoreline.

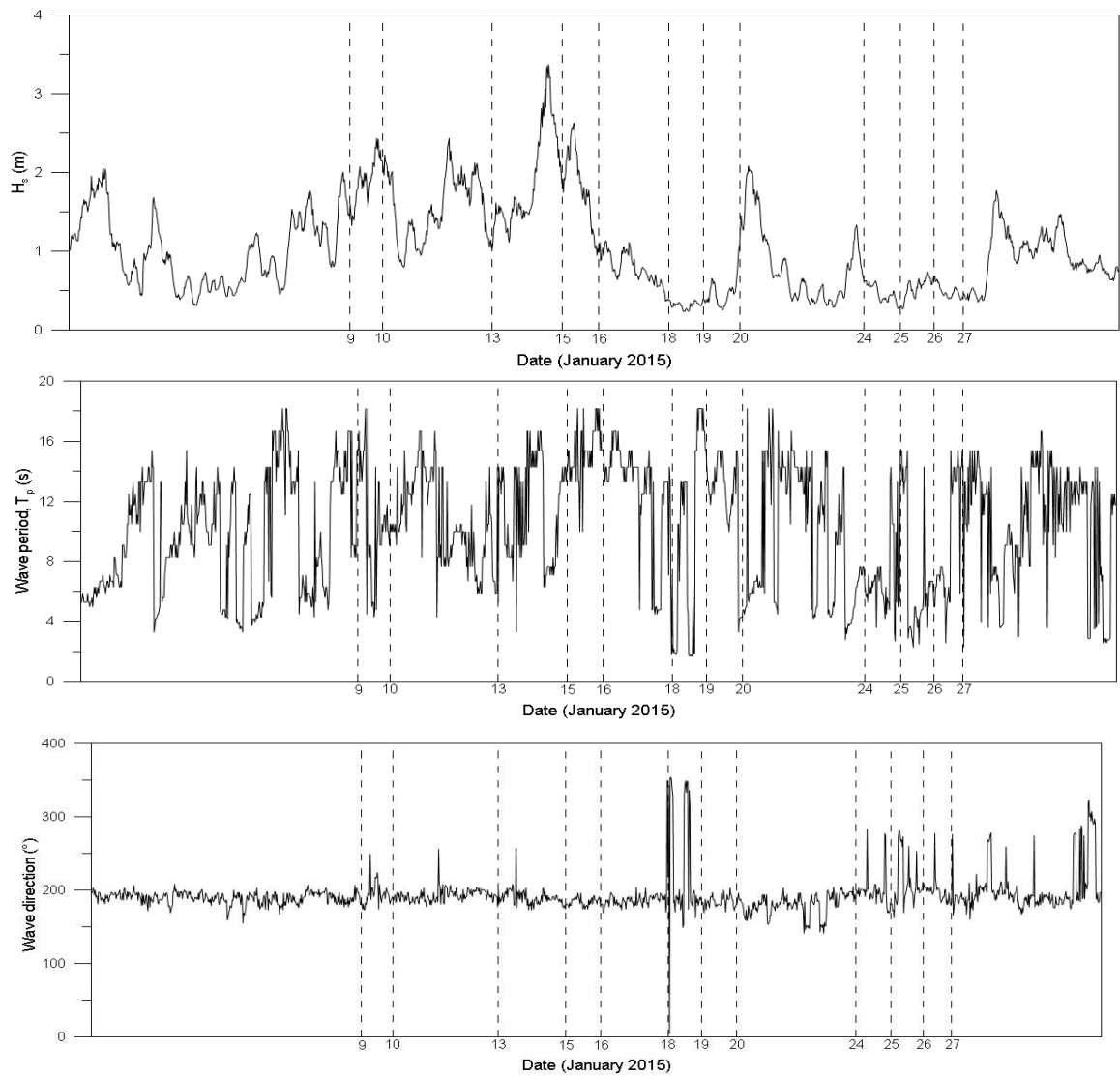


Figure A-2: Wave conditions during January 2015, with profile survey dates marked by dashed lines. Data from CCO.

January 2015 (Figure A-2)

Significant wave heights during January 2015 were varied, with a peak of 3.37 m and a minimum of 0.23 m. The largest waves occurred in the first half of the month, with surveys after the 16th generally experiencing waves of around 0.5 m. The exception to this is a peak of approximately 2 m shortly after the survey on January 20th took place, and another smaller peak shortly before the survey on the 24th.

Peak wave periods were varied but generally high, around 12-16 seconds. Wave direction once again stayed fairly constant at around 200 degrees, with a few spikes at 250 degrees and then some waves approaching from a more northerly direction around the survey on the 18th. These coincide with small wave heights on these dates due to the angle of the coastline; the offshore buoy being 5 km offshore allows a small amount of fetch for northerly waves, but at the beach these would be non-existent.

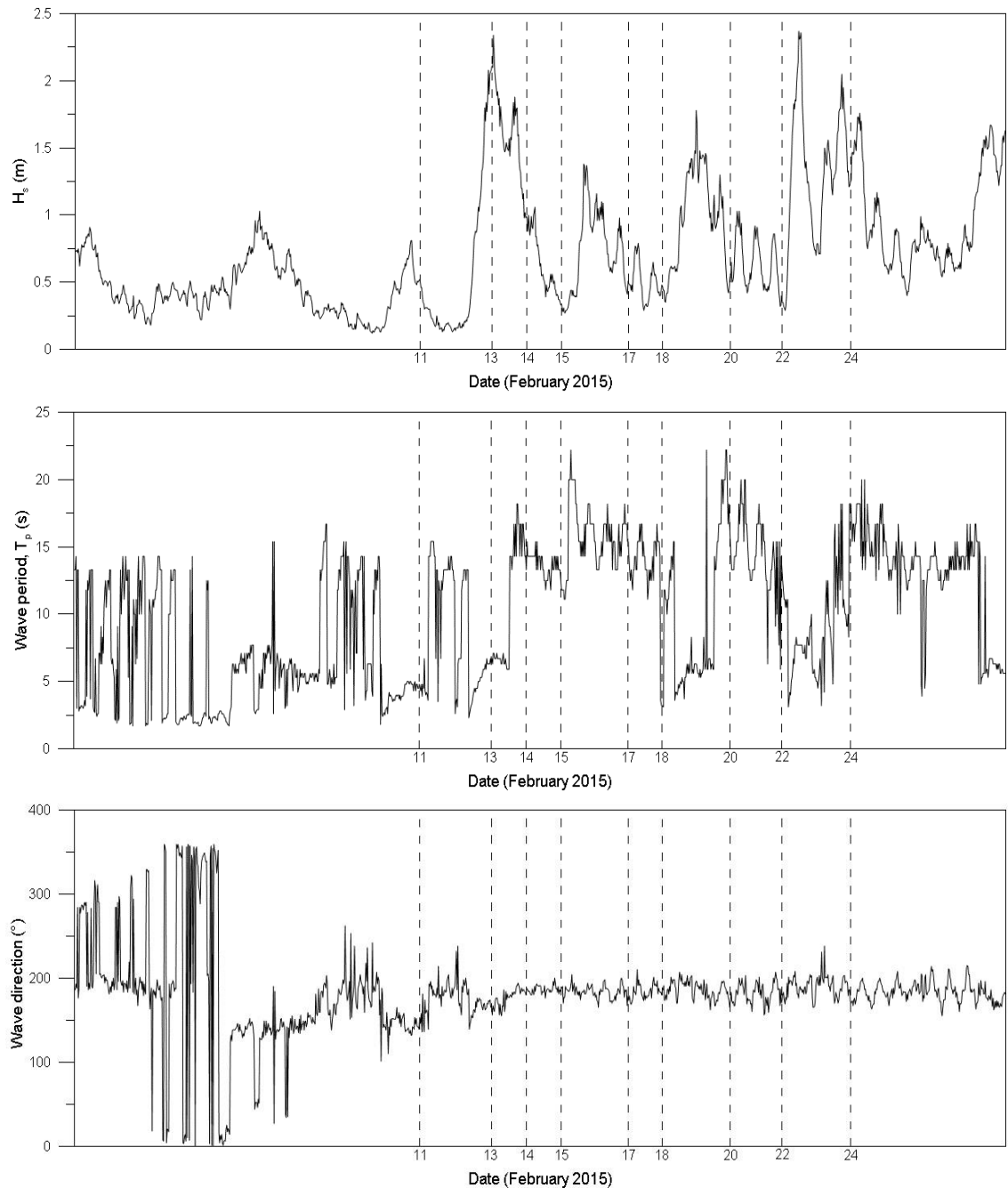


Figure A-3: Wave conditions during February 2015, with profile survey dates marked by dashed lines. Data from CCO.

February 2015 (Figure A-3)

After the first survey undertaken on the 11th of February 2015, significant wave heights became more varied, with peaks over 2 m occurring on the 13th and 22nd. These peaks represent sustained periods of higher waves of at least 24 hours each.

Wave periods fluctuated between approximately 5 and 20 seconds, though most measurements during the surveyed part of the month seem to be between 12-16 seconds once more. As in previous months, the wave direction for the surveyed part of February remains at approximately 200 degrees.

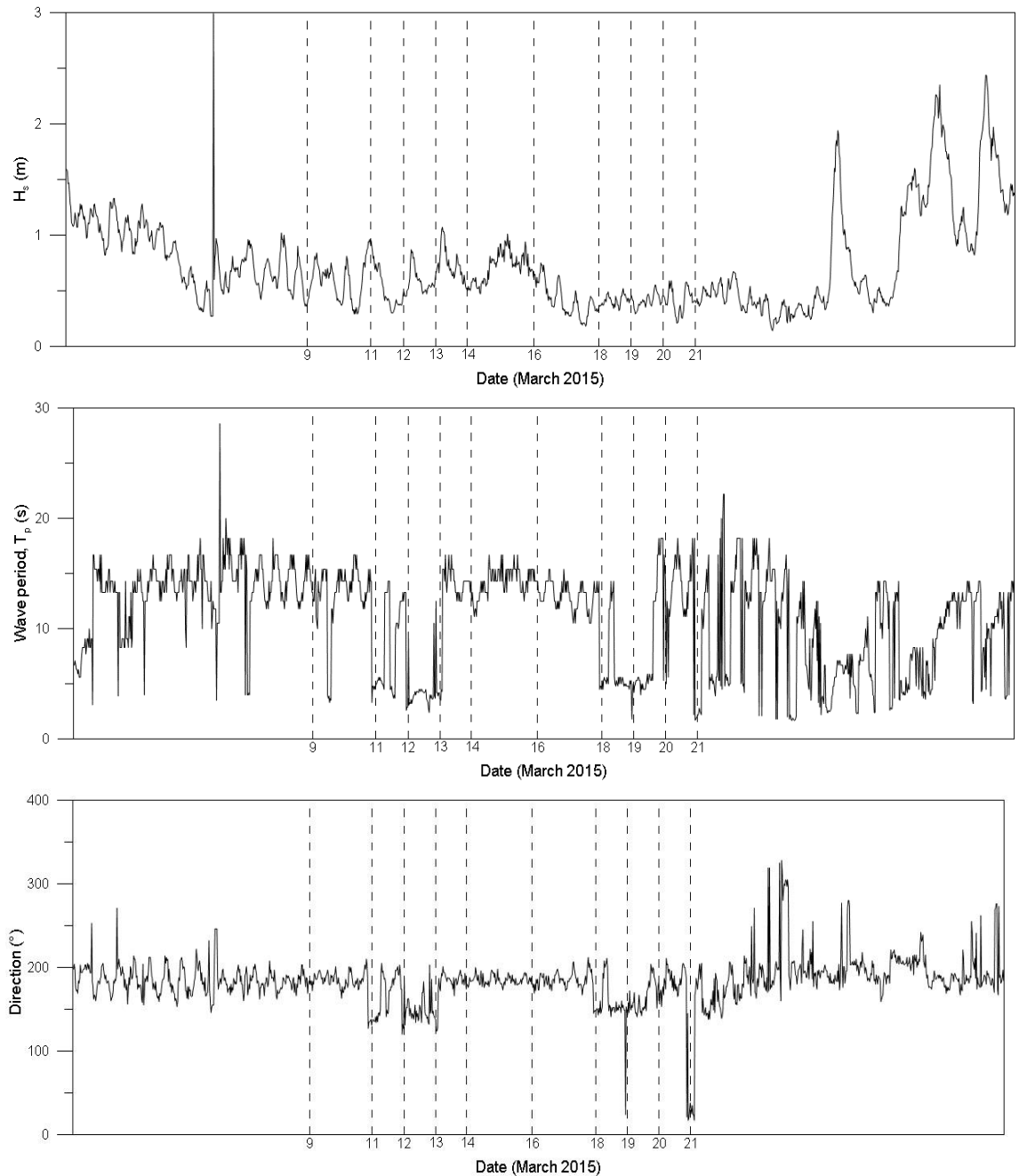


Figure A-4: Wave conditions during March 2015, with profile survey dates marked by dashed lines. Data from CCO.

March 2015 (Figure A-4)

Significant wave heights during March 2015 were consistently below approximately 1 m. This combined with wave periods around 15 seconds, though certain days – between the 12th and 13th, and the 18th-20th, for example – experienced smaller periods of approximately 5 seconds. The direction of wave approach was more varied than in previous months, fluctuating between 150-200 degrees on similar timescales to the troughs in wave period.

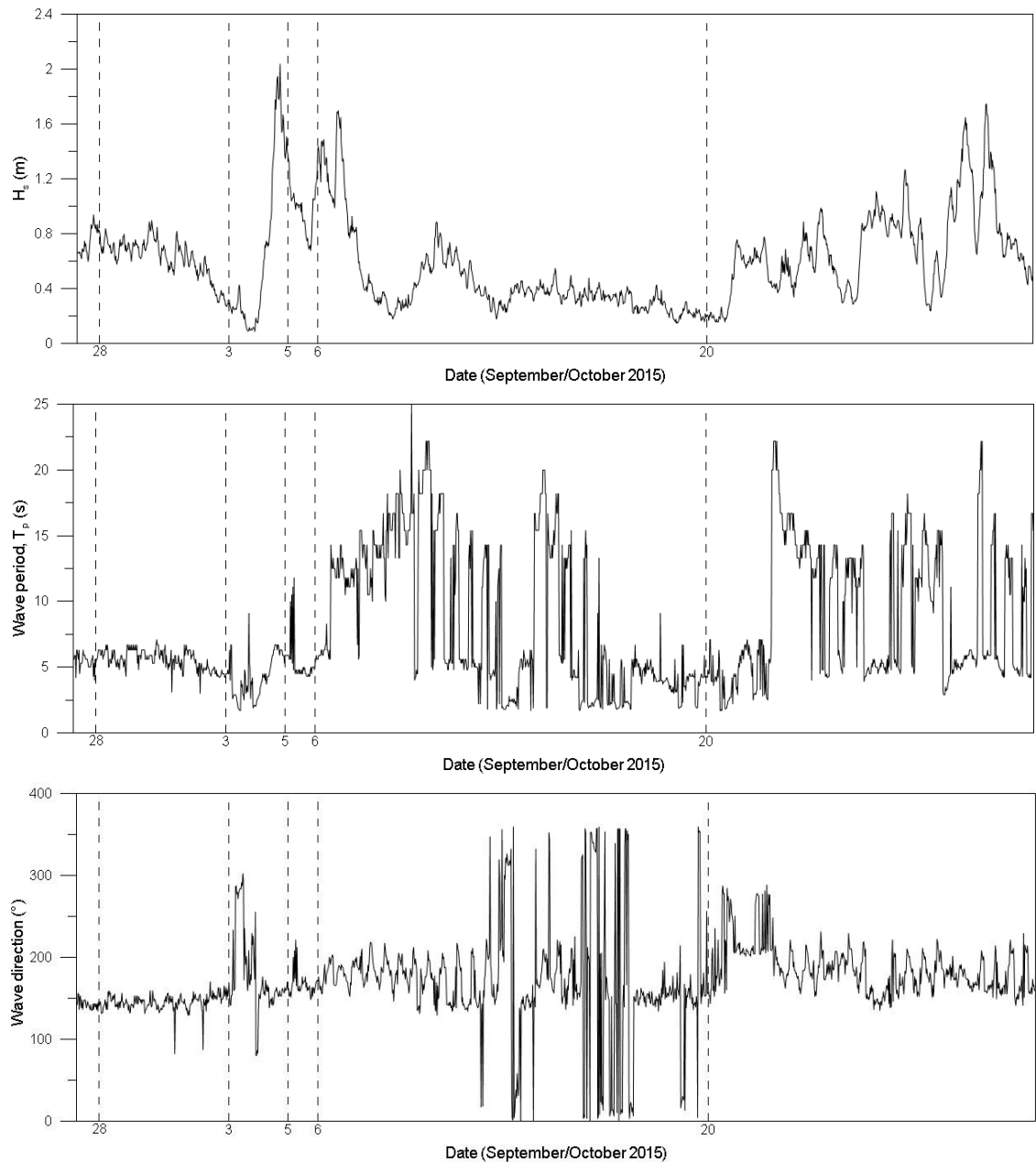


Figure A-5: Wave conditions during late September and October 2015, with profile survey dates marked by dashed lines. Data from CCO.

October 2015 (Figure A-5)

The waves occurring between the first survey, on September 28th, and the second, on October 3rd, are of consistent height (between 0.7-0.8 m), period (5-6 seconds) and direction (approximately 150 degrees, or southeasterly). There is a peak in wave height which coincides approximately with high tide before the survey on October 5th. Wave heights leading up to the survey on the 20th are very small, generally below 0.5 m, but the wave period and direction during this time fluctuate: wave period between 2 and 20 seconds; wave direction from 0/360 degrees through to approximately 150 degrees.

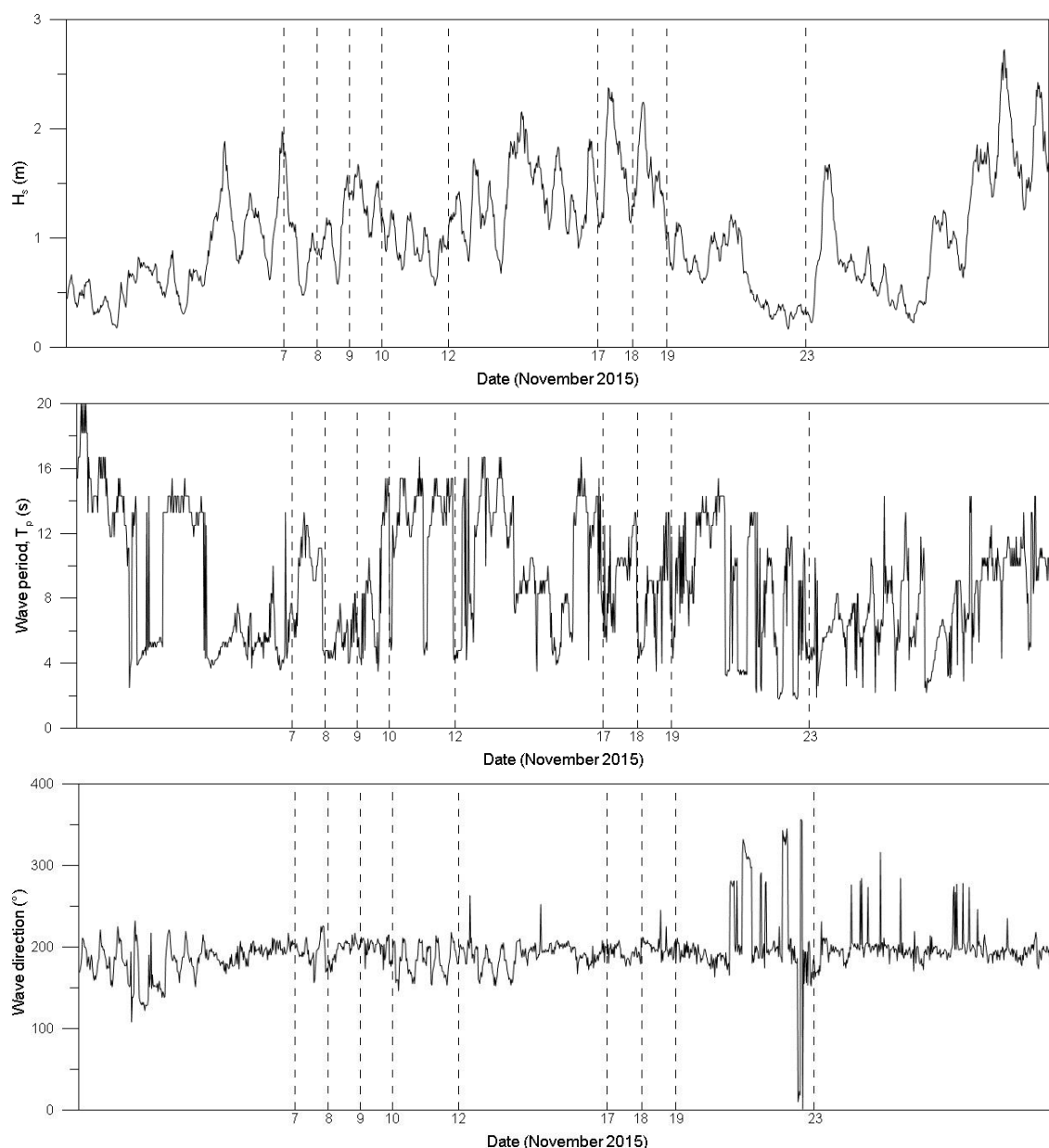


Figure A-6: Wave conditions during November 2015, with profile survey dates marked by dashed lines. Data from CCO.

November 2015 (Figure A-6)

Significant wave height during November was generally moderate (1-2 m). During the survey period, the highest waves occurred between the 17th and 18th, with the lowest waves before the survey on the 23rd.

Wave period ranges between 2-4 seconds, with the shortest periods occurring between the 8th and 9th of November, and the longest between the 8th and 14th. Wave direction stays at around 200 degrees until the 21st, when it varies a little more. This coincides with the smaller wave heights, as waves approaching from directions other than southeast to southwest are small due to limited fetch.

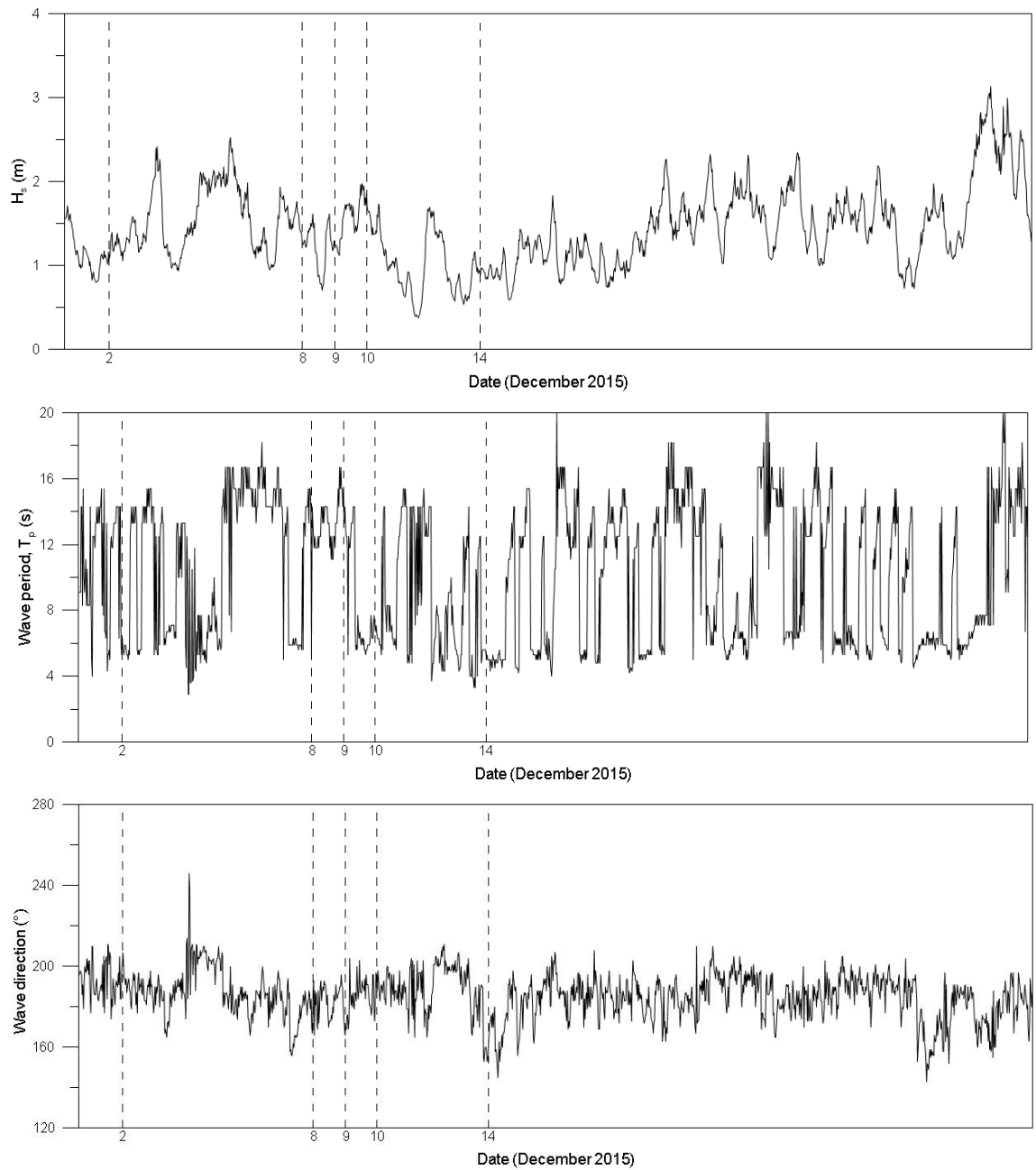


Figure A-7: Wave conditions during December 2015, with profile survey dates marked by dashed lines. Data from CCO.

December 2015 (Figure A-7)

Wave heights during the survey period in December were moderate to high, ranging from 1-2.5 m until the 10th and between 0.5-1.6 m between the 10th and 14th. Wave period fluctuated during this time, though less so than during other surveys; between approximately 5 and 15 seconds. Wave direction remained within a range of approximately 20 degrees: from 180-200 degrees for most of the survey period.

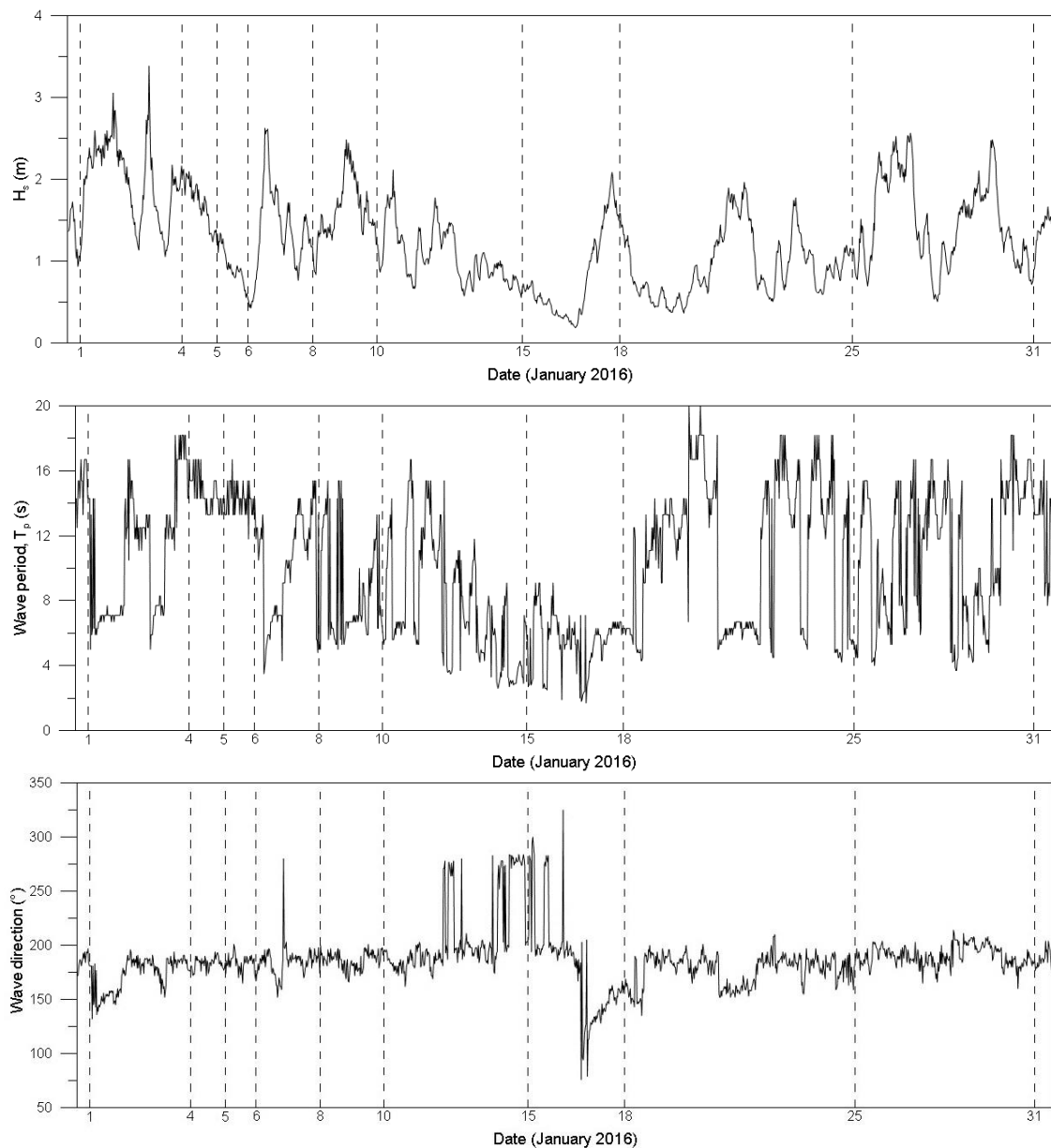


Figure A-8: Wave conditions during January 2016, with profile survey dates marked by dashed lines. Data from CCO.

January 2016 (Figure A-8)

As can be seen on the December 2015 graphs (Figure A-7), a prolonged period of stormy waves occurred prior to the January 1st survey. These reached a maximum of over 3 m. This continued between the 1st and 4th, marked by generally high waves and shorter periods. These waves approached from a more southeasterly direction than the majority of waves experienced during other surveys. Between the 4th and 6th, wave heights gradually decreased from 2 m to 0.5 m, and wave period remained long, at around 14-16 seconds. Additionally, the direction for these waves was generally 180 degrees, or southerly. Further peaks of approximately 2.5 m wave height occurred between the 6th and 8th and 8th and 10th, both coinciding with mid flood tide. Wave heights and periods between the 10th and 15th gradually decreased, with short wave periods and a peak in wave height of approximately 2 m occurring before the survey on the 18th. Towards the end of the month there was another period of larger waves with periods between 4-18 seconds. Wave direction stayed reasonably constant, apart from a period between the 12th and 17th which involved many waves approaching from 280-300 degrees, as well as a short period when they approached from 80-100 degrees. These coincide with short wave periods and low wave heights.

Appendix B : dGPS Profile Surveys

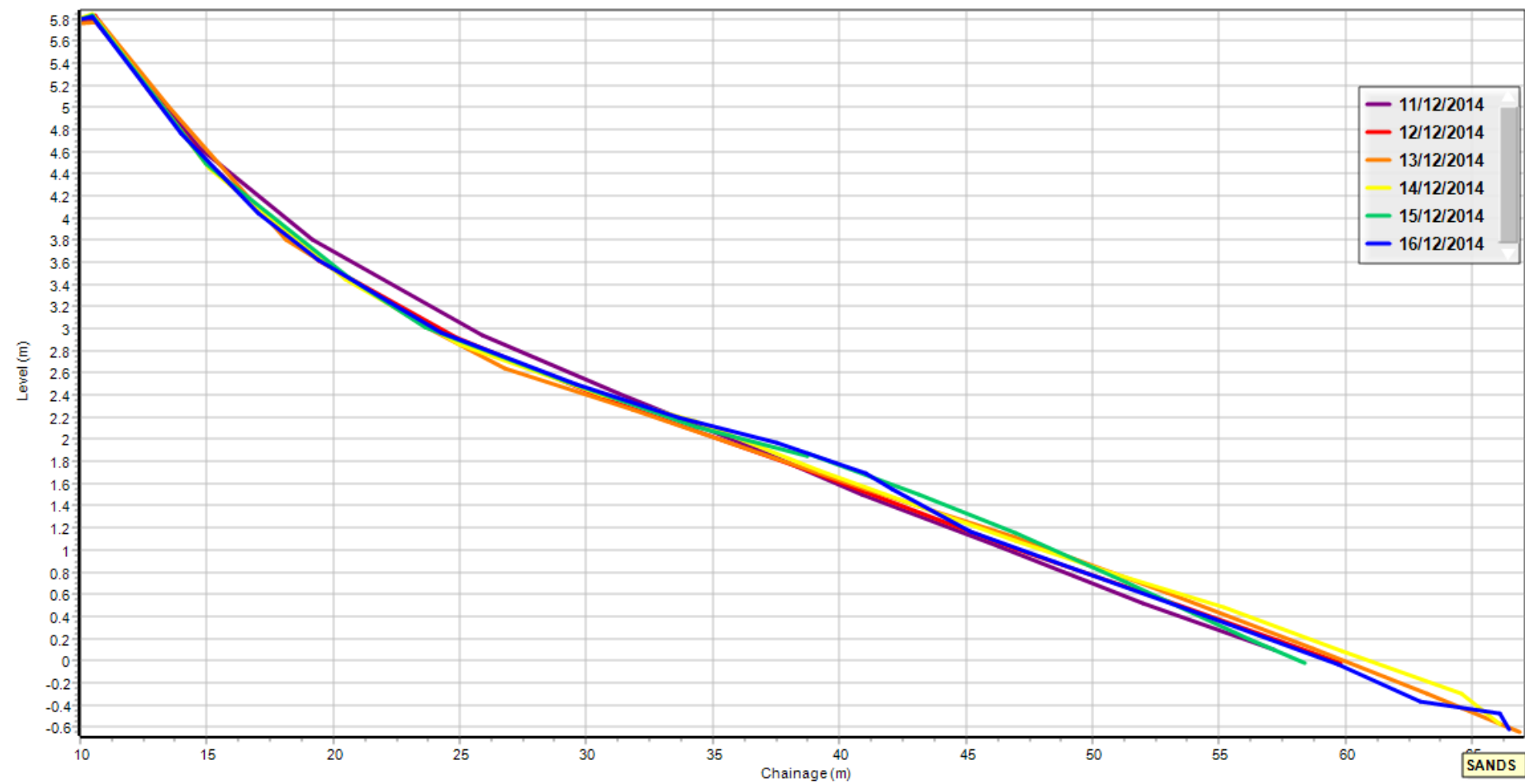


Figure B-1: dGPS profiles measured on Profile 2 during December 2014

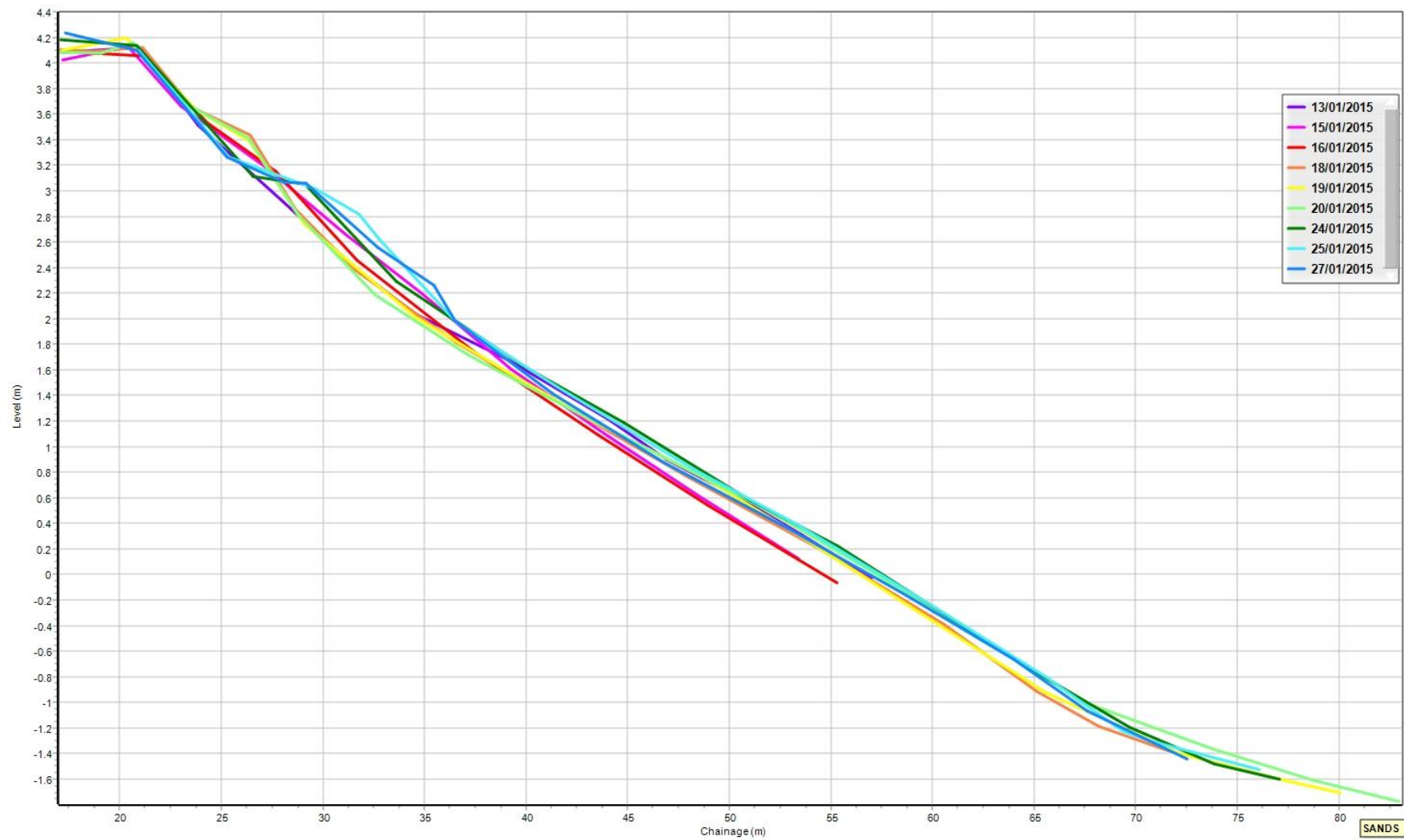


Figure B-2: dGPS profiles measured on Profile 1 during January 2015.

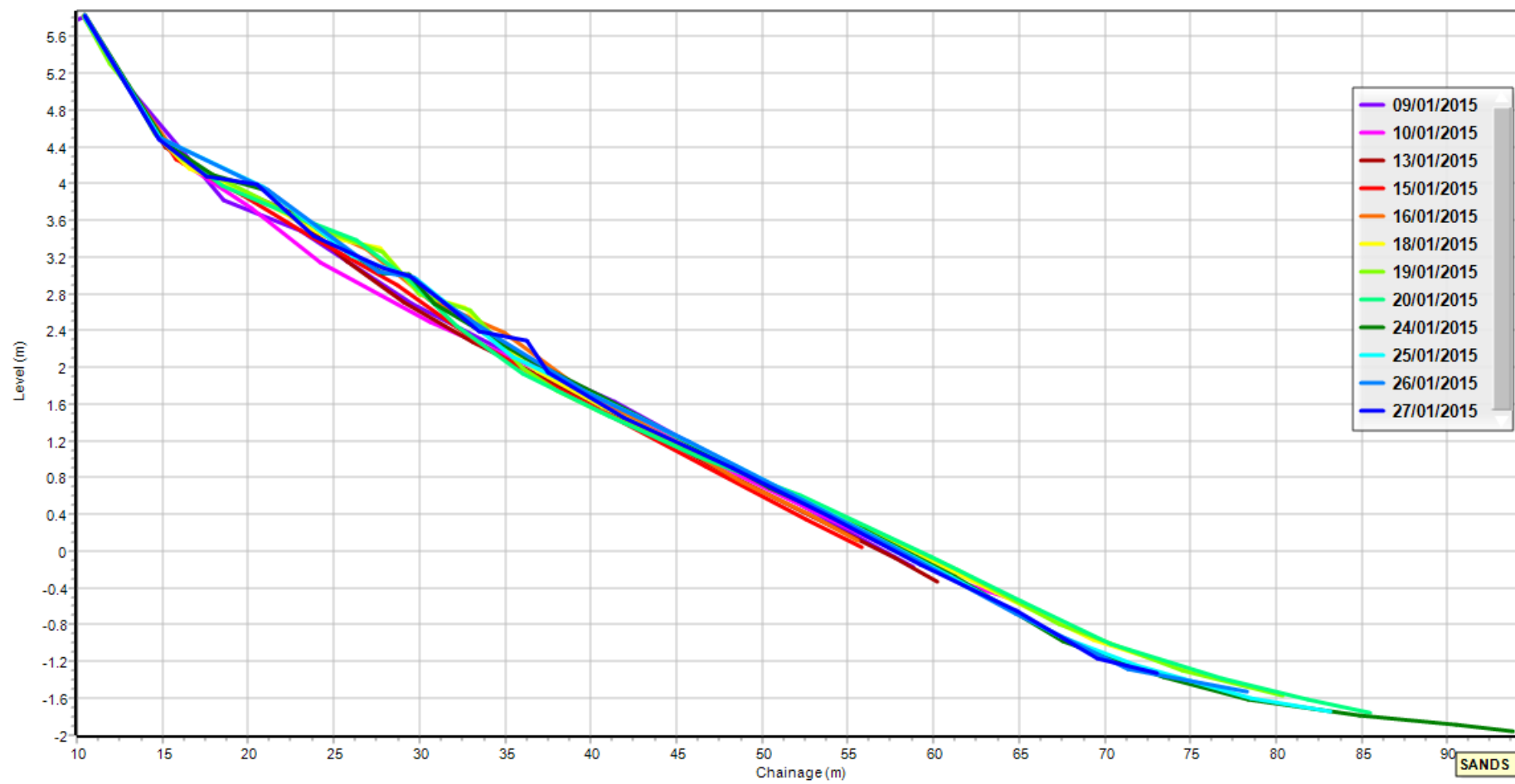


Figure B-3: dGPS profiles measured on Profile 2 during January 2015.

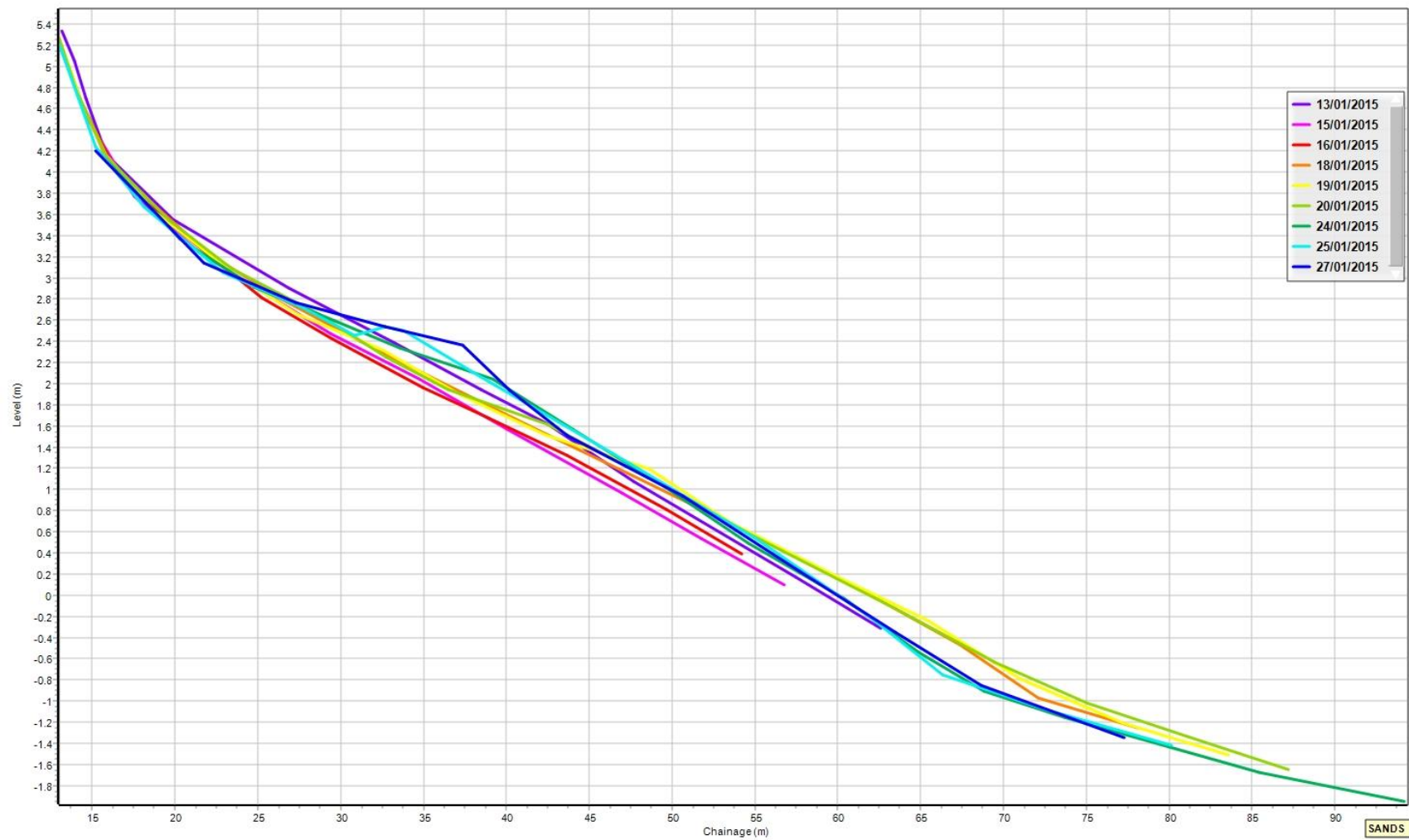


Figure B-4: dGPS profiles measured on Profile 3 during January 2015.

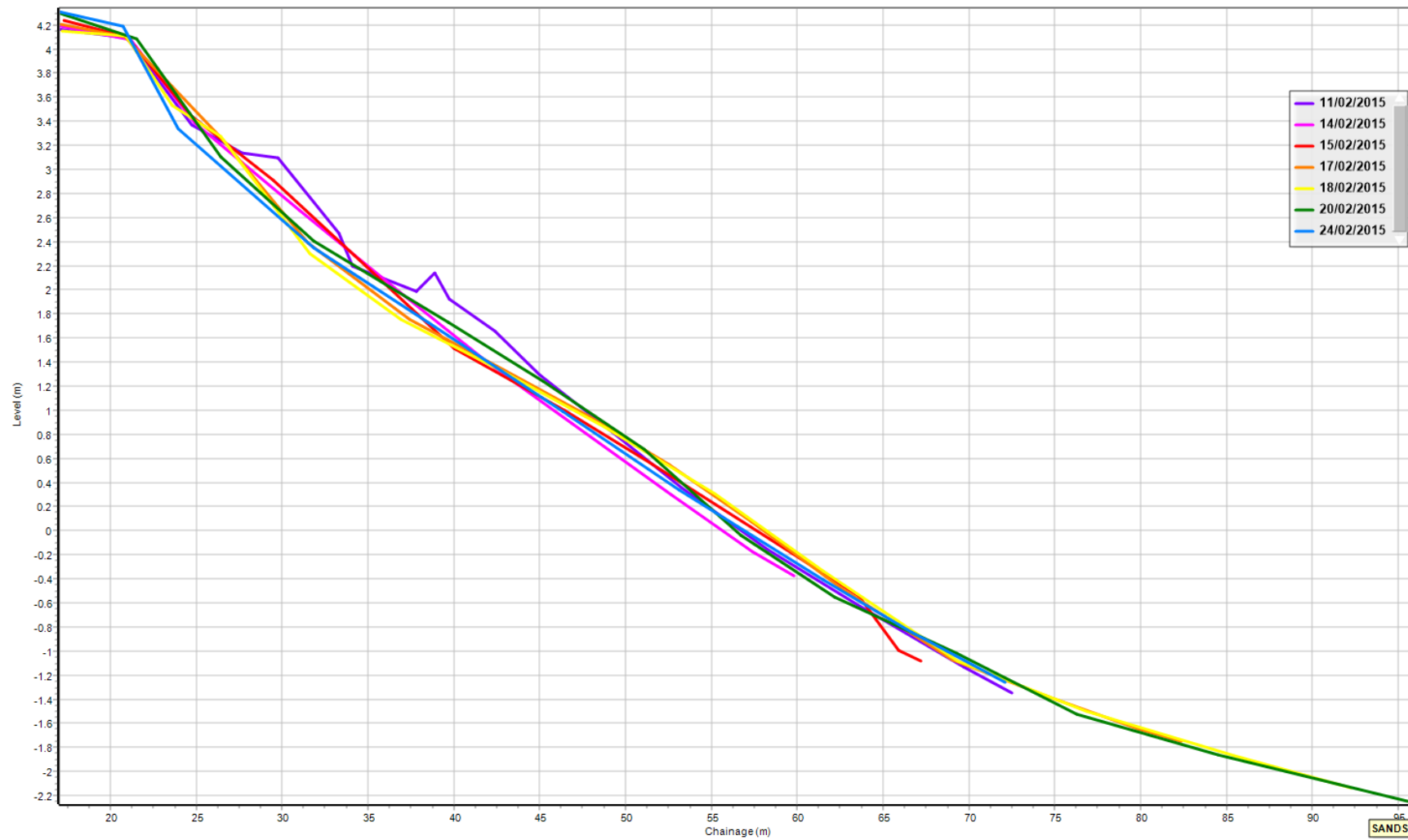


Figure B-5: dGPS profiles measured on Profile 1 in February 2015.

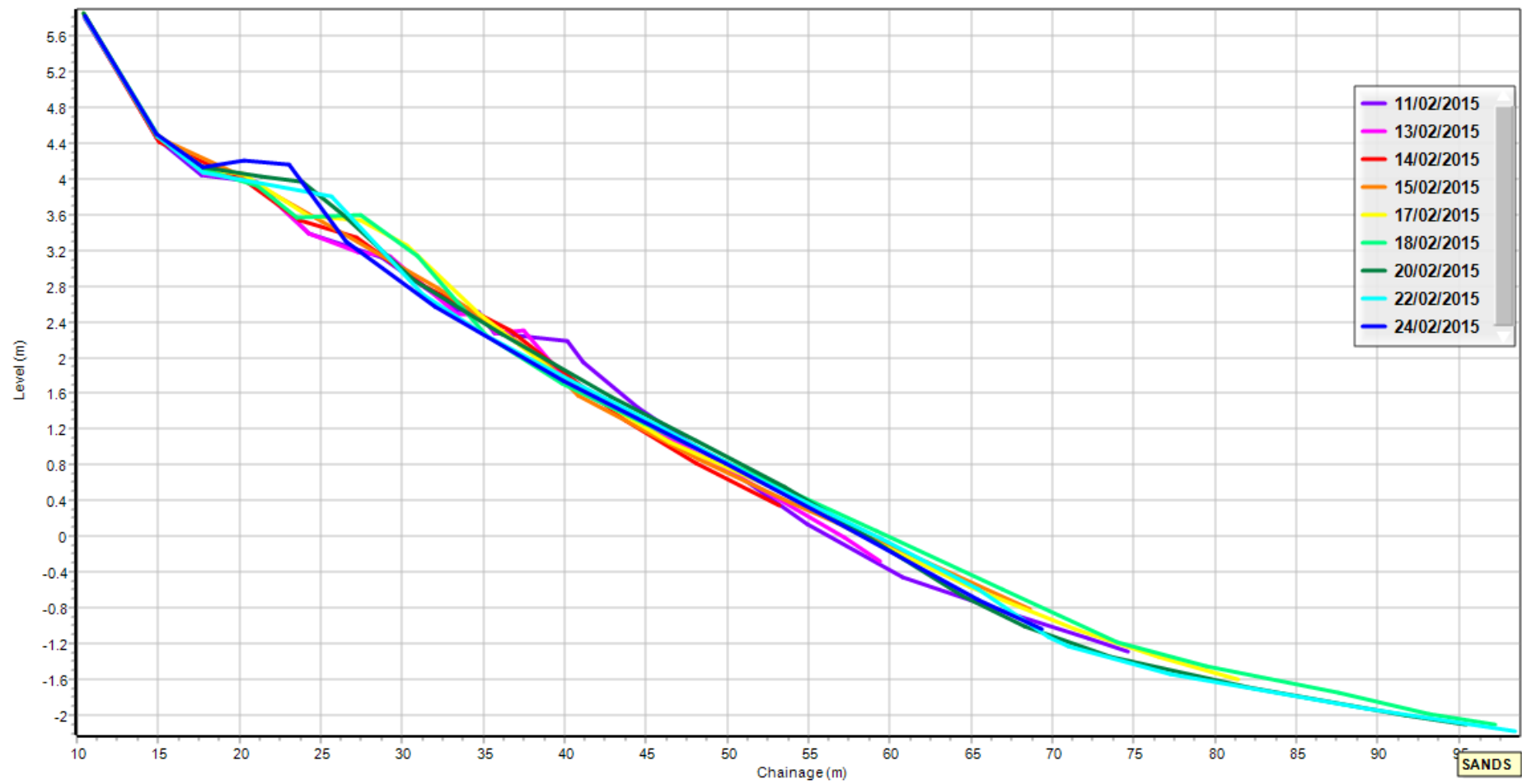


Figure B-6: dGPS profiles measured on Profile 2 in February 2015.

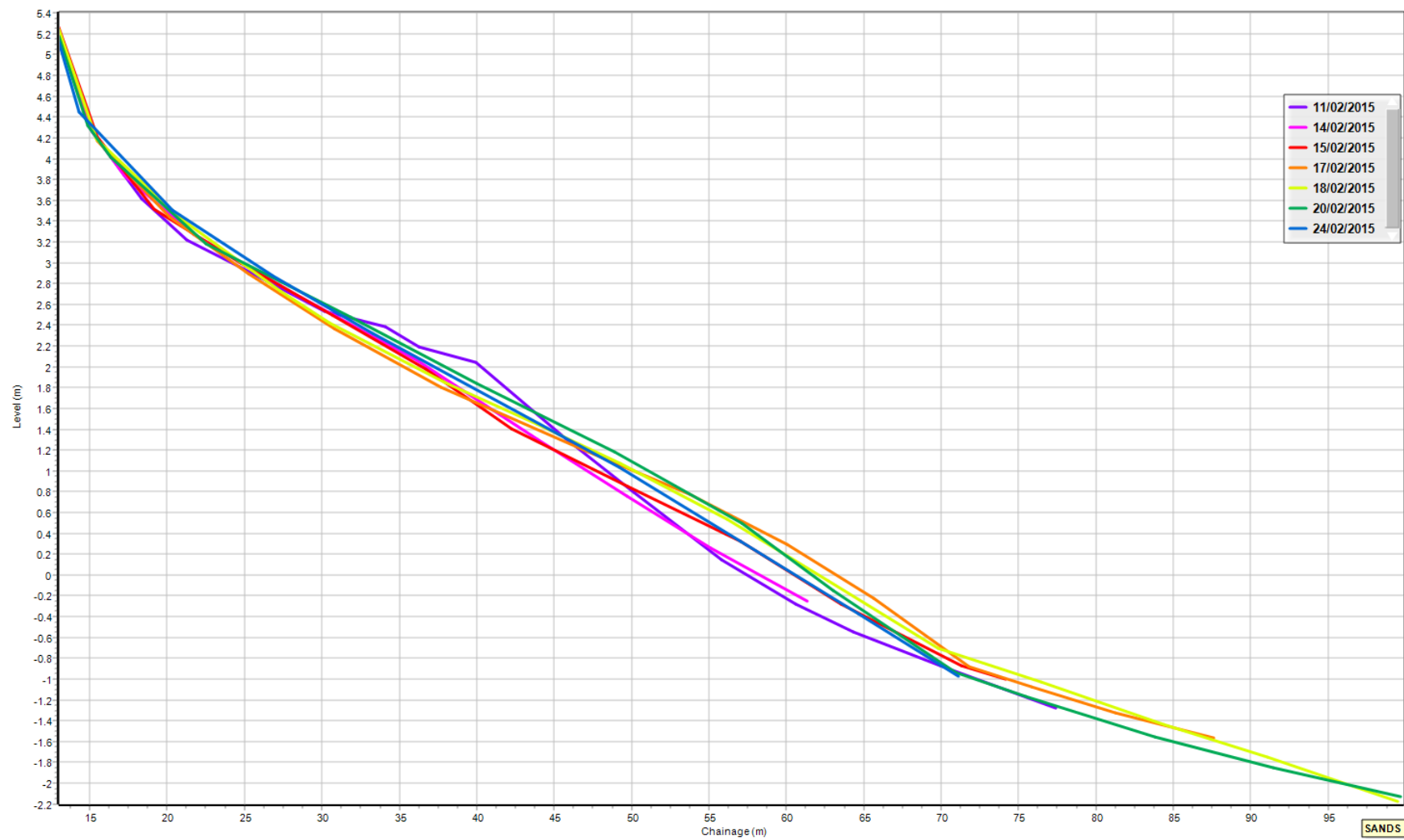


Figure B-7: dGPS profiles measured on Profile 3 during February 2015.

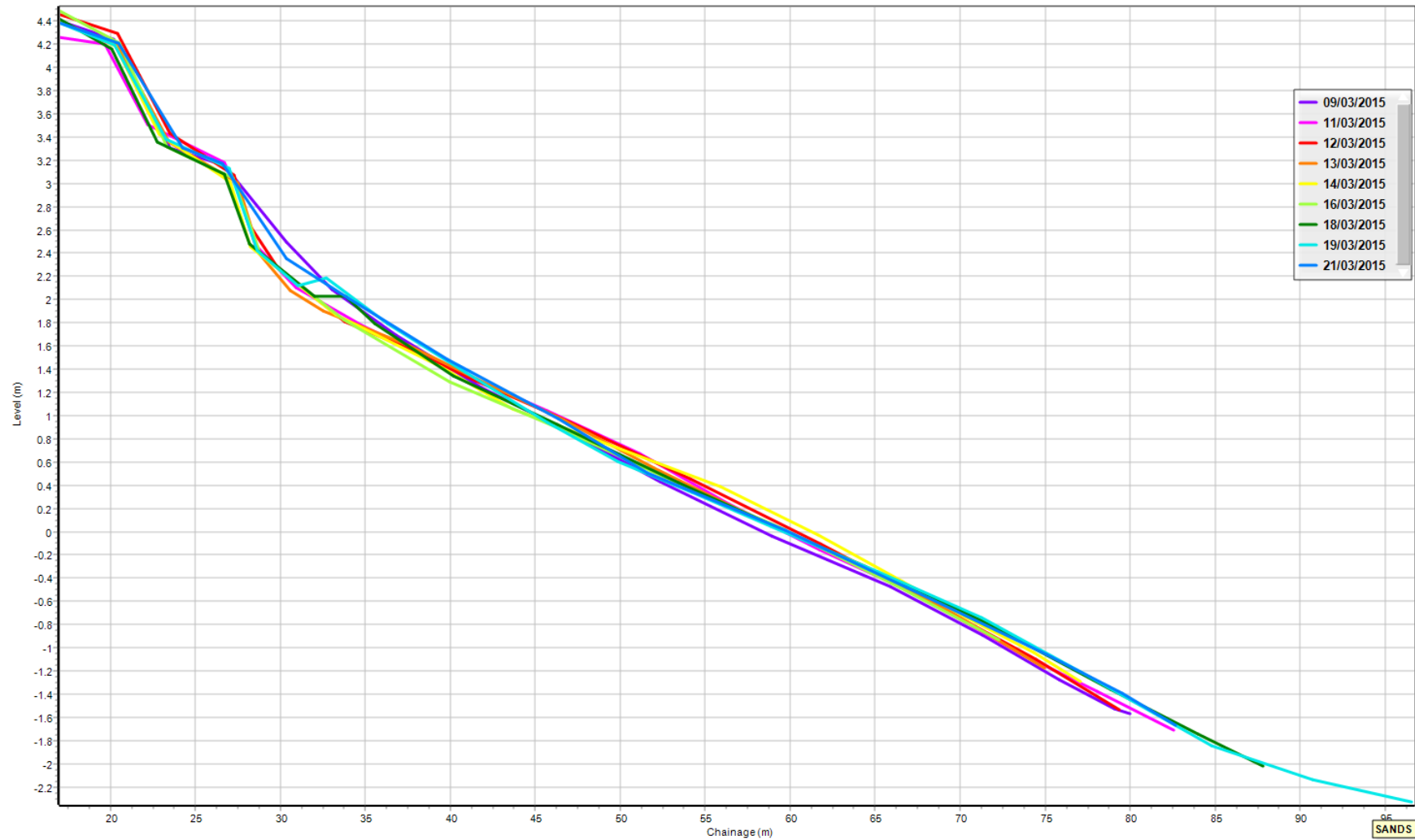


Figure B-8: dGPS profiles measured on Profile 1 during March 2015.

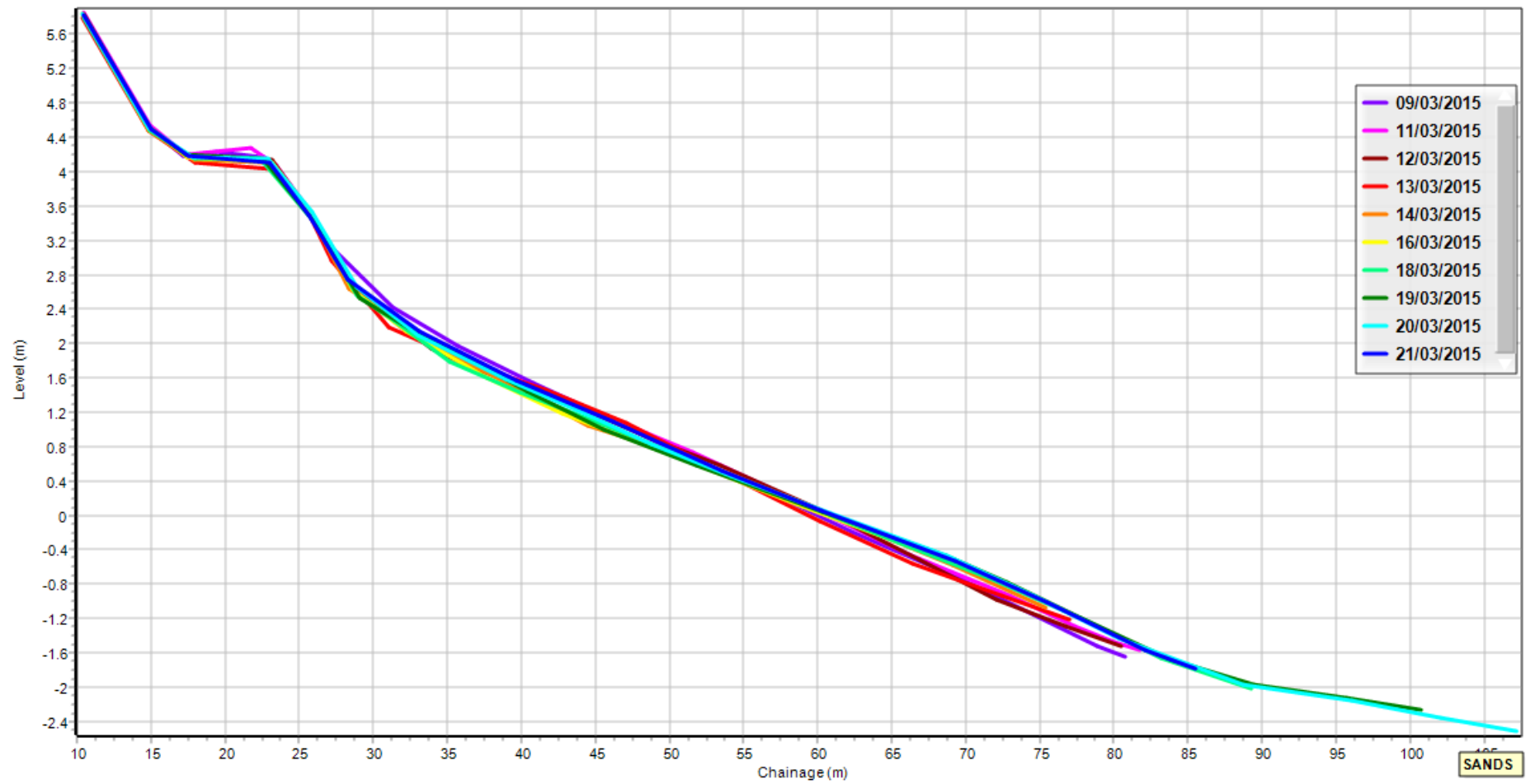


Figure B-9: dGPS profiles measured on Profile 2 during March 2015.

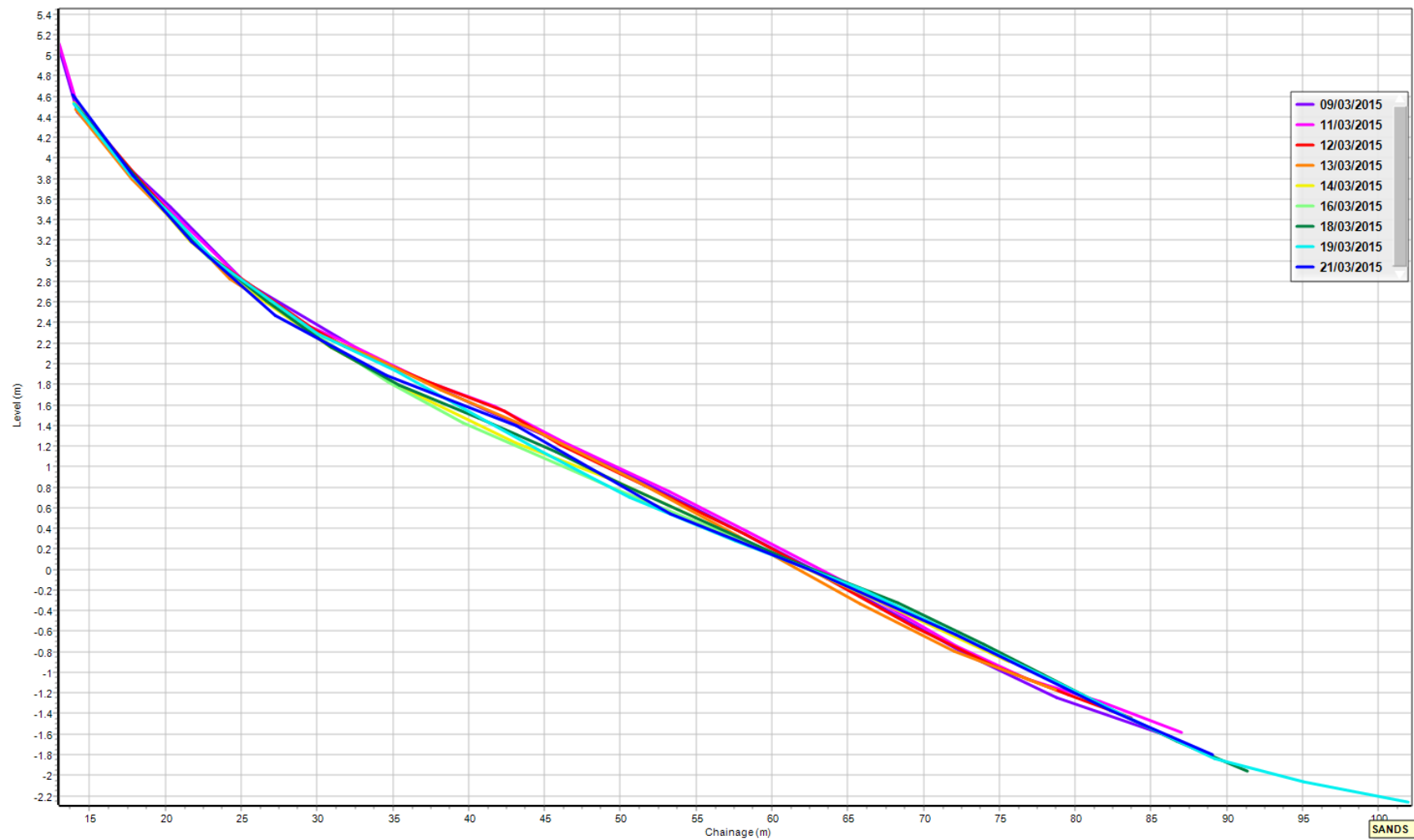


Figure B-10: dGPS profiles measured on Profile 3 during March 2015.

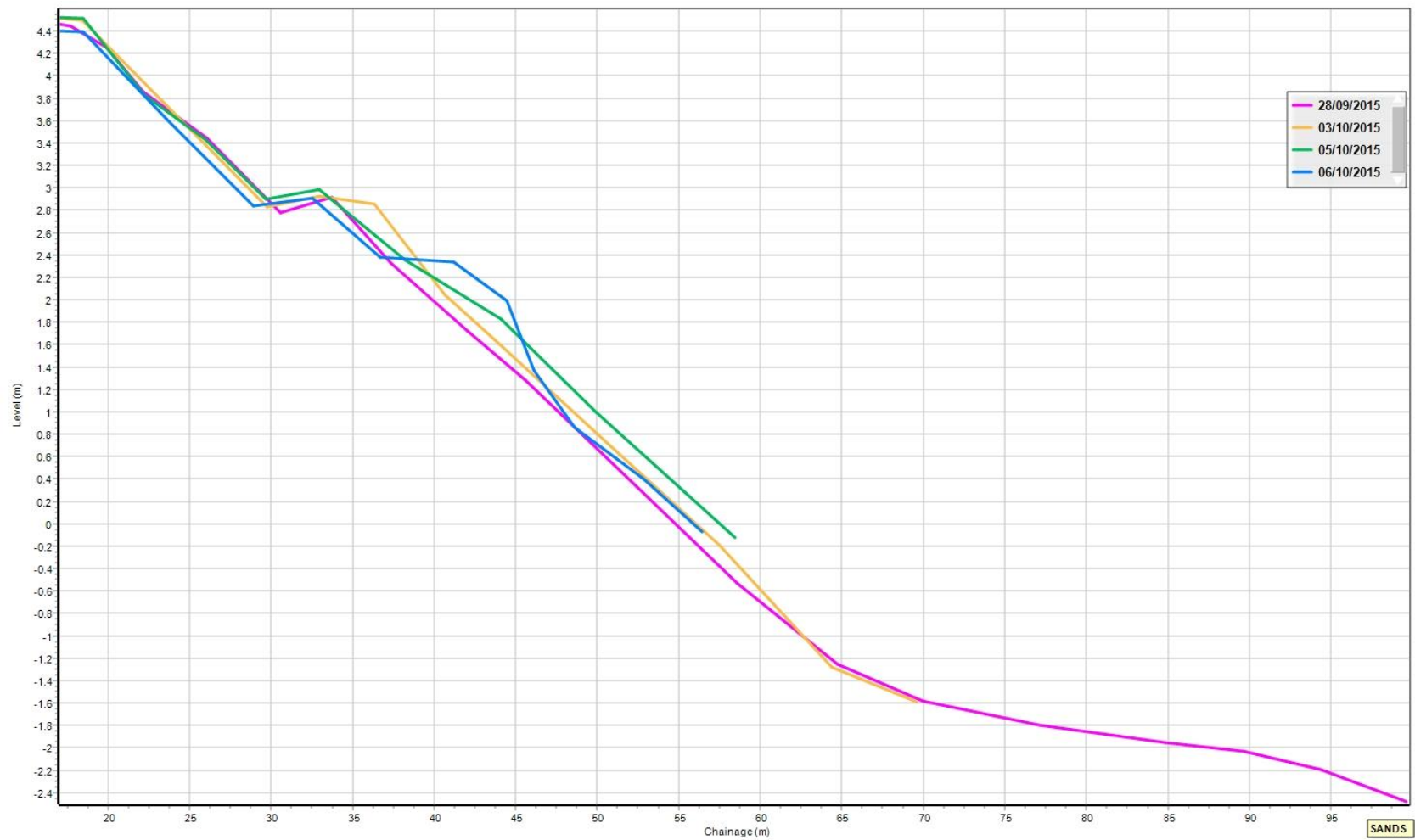


Figure B-11: dGPS profiles measured on Profile 1 during September/October 2015.

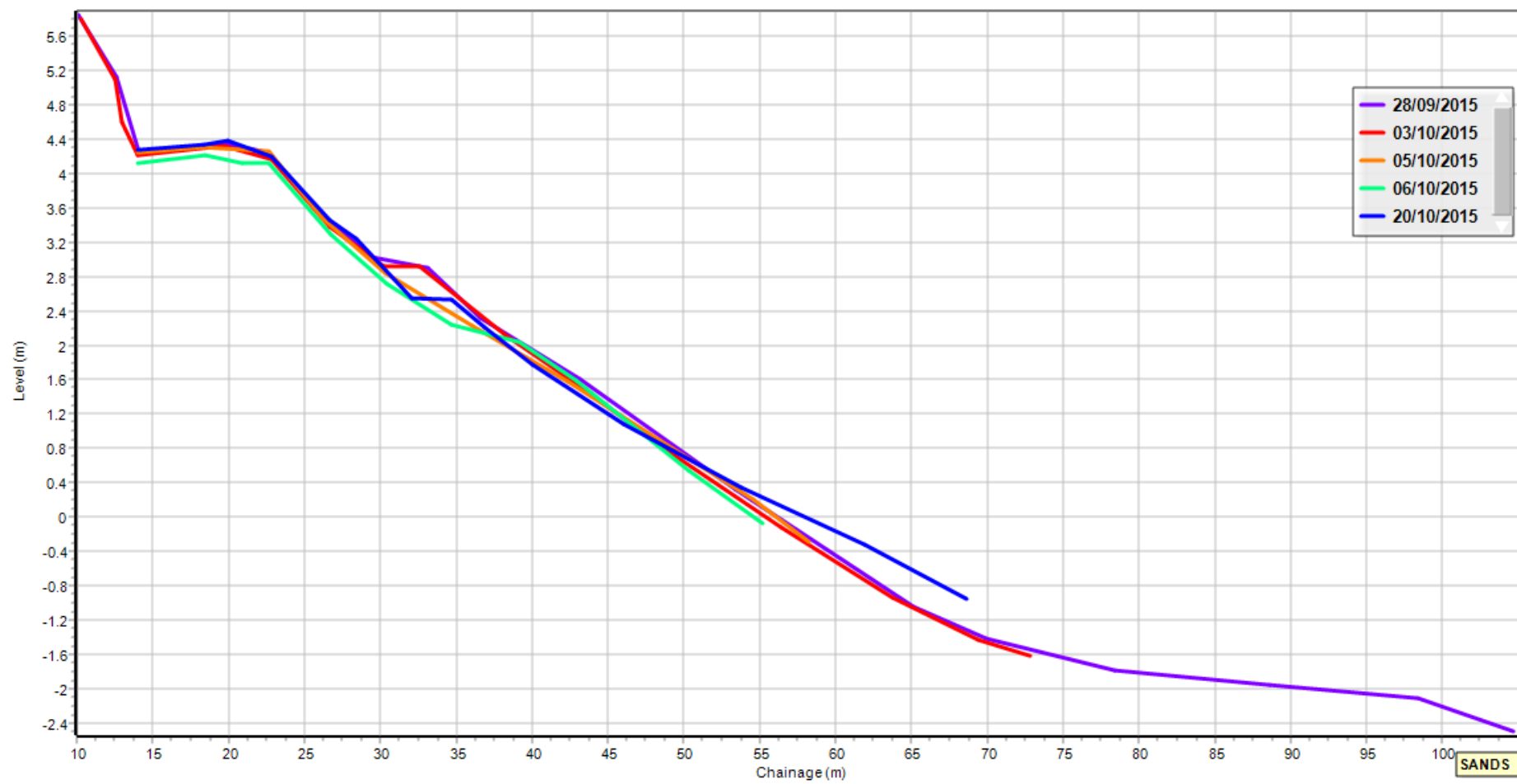


Figure B-12: dGPS profiles measured on Profile 2 during September/October 2015.

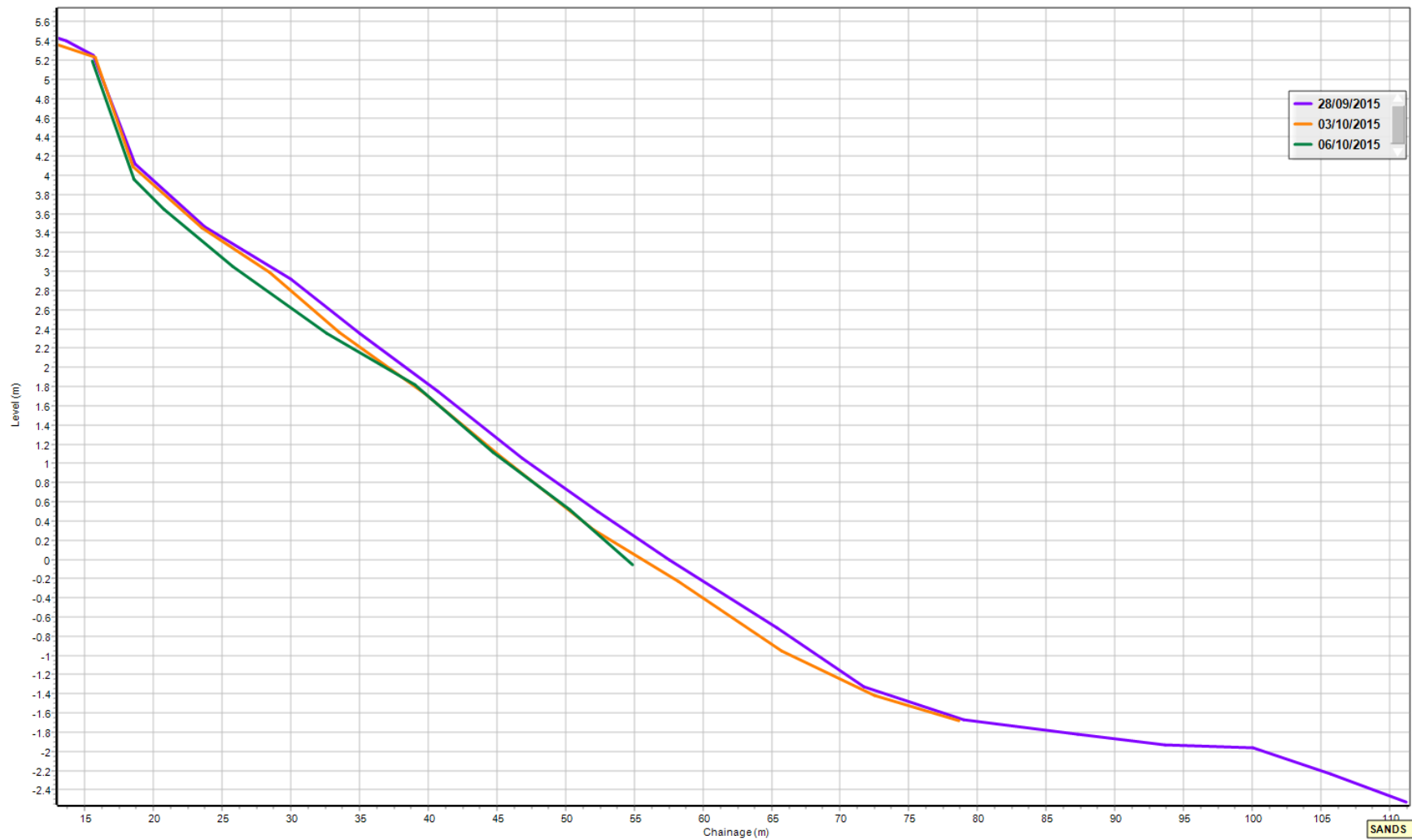


Figure B-13: dGPS profiles measured on Profile 3 during September/October 2015.

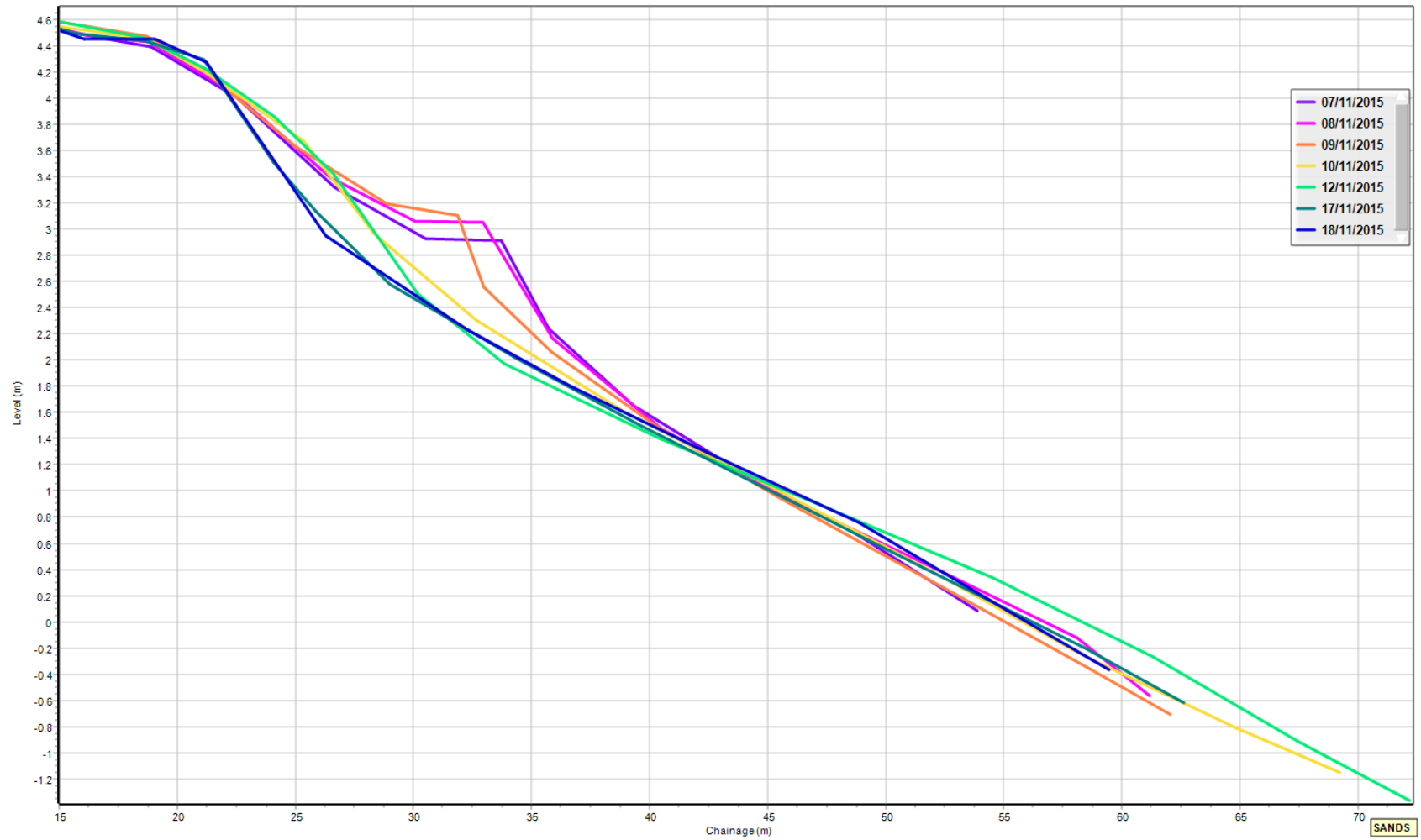


Figure B-14: dGPS profiles taken on Profile 1 during November 2015.

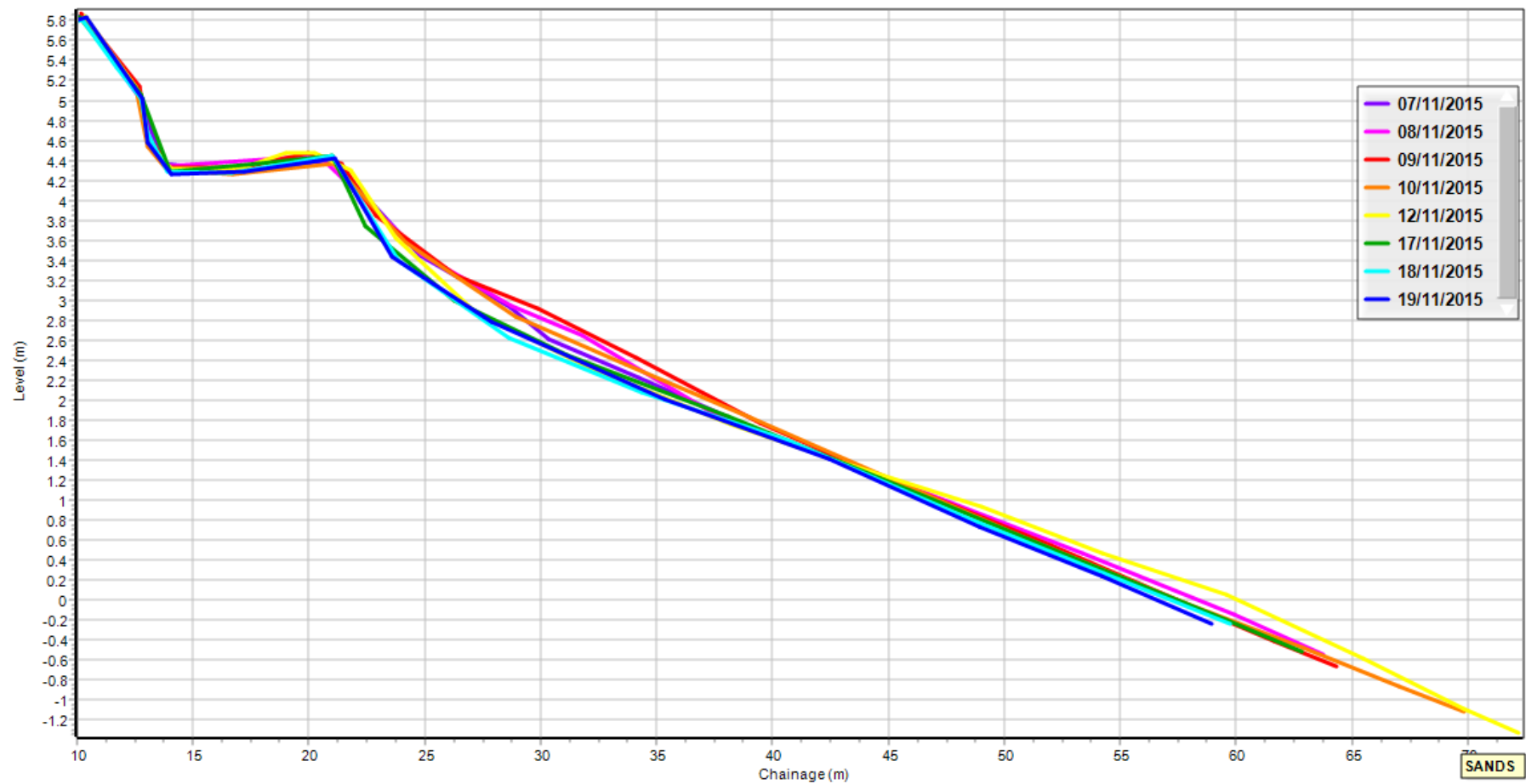


Figure B-15: dGPS profiles taken on Profile 2 during November 2015.

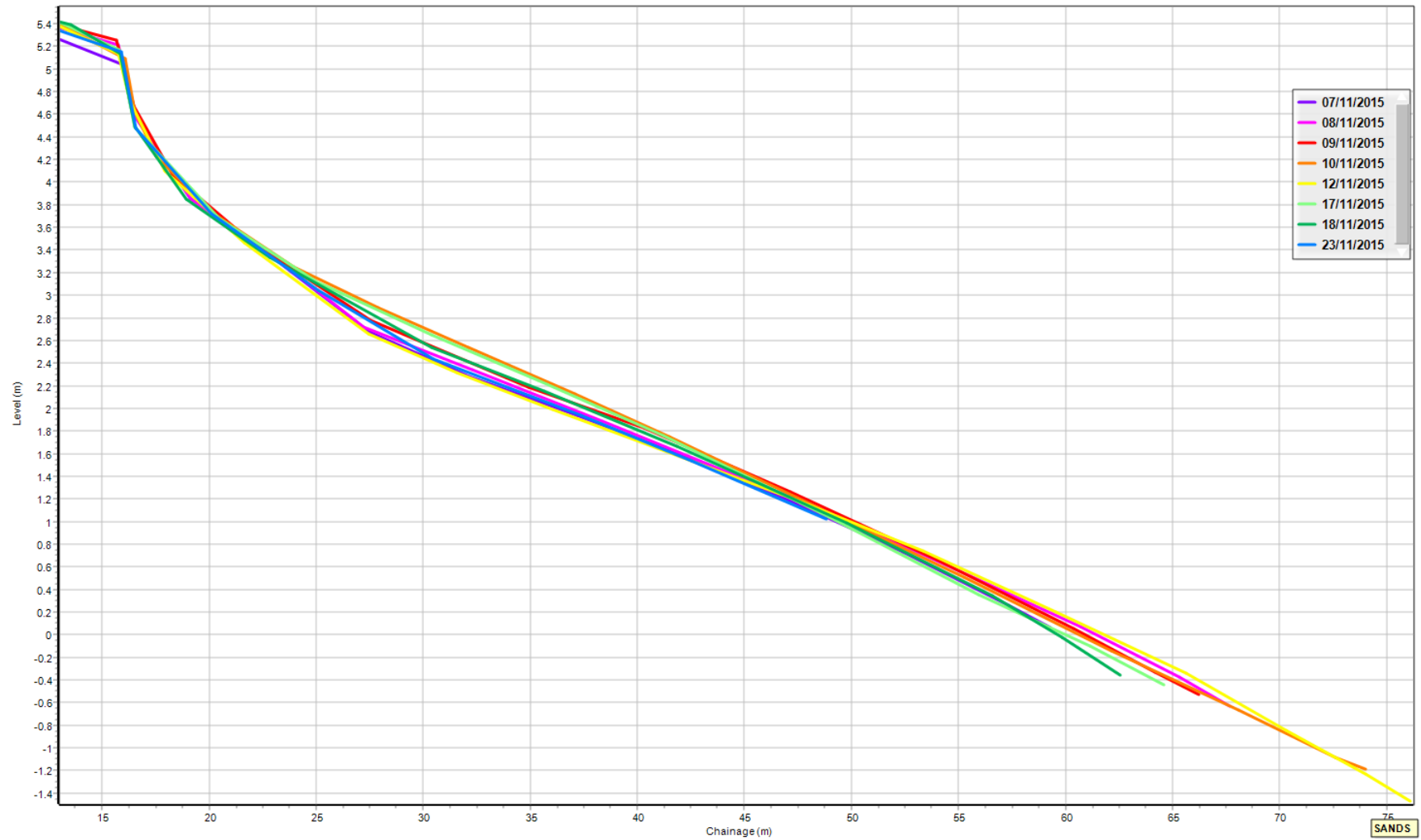


Figure B-16: dGPS profiles taken on Profile 3 during November 2015.

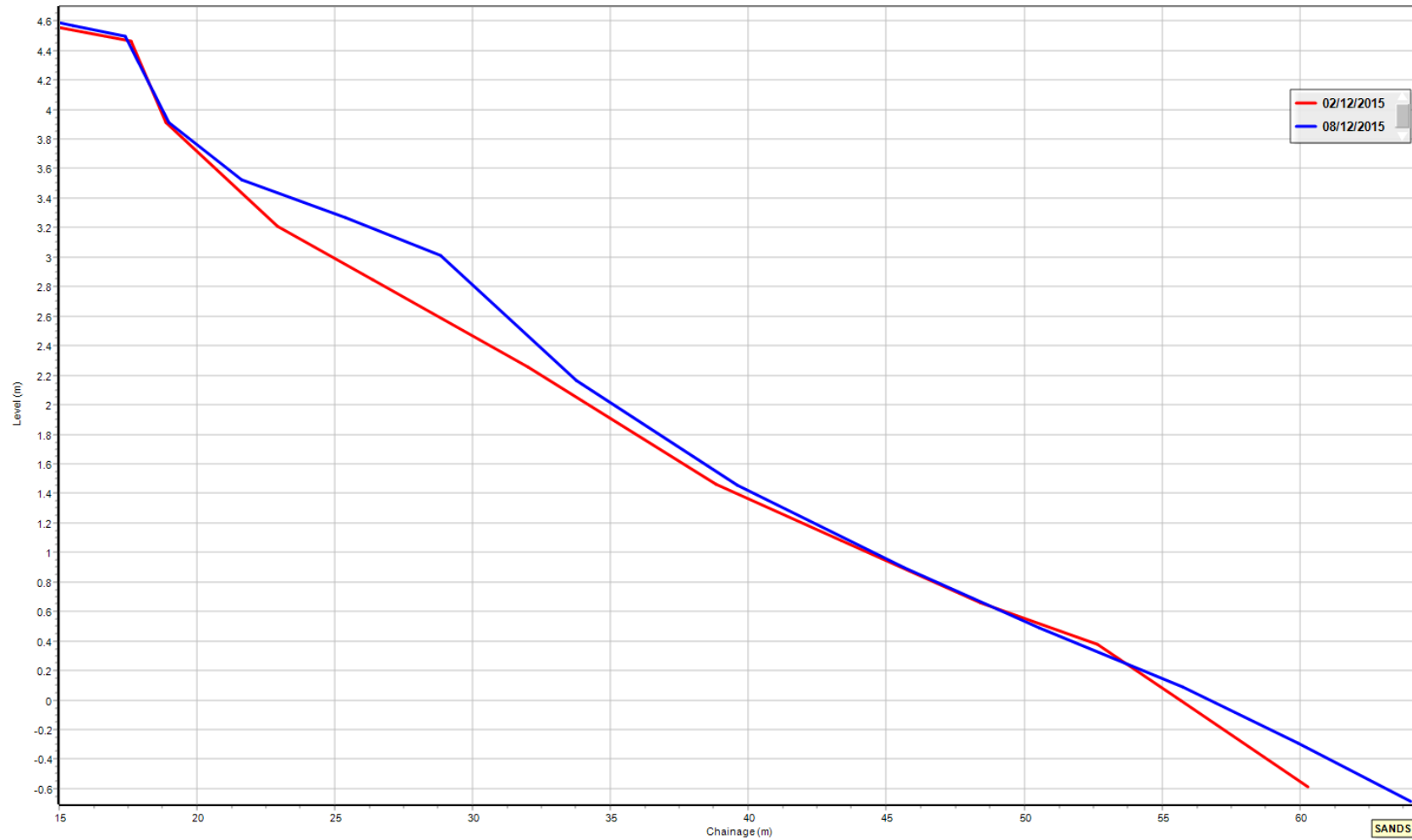


Figure B-17: dGPS profiles measured on Profile 1 in December 2015.

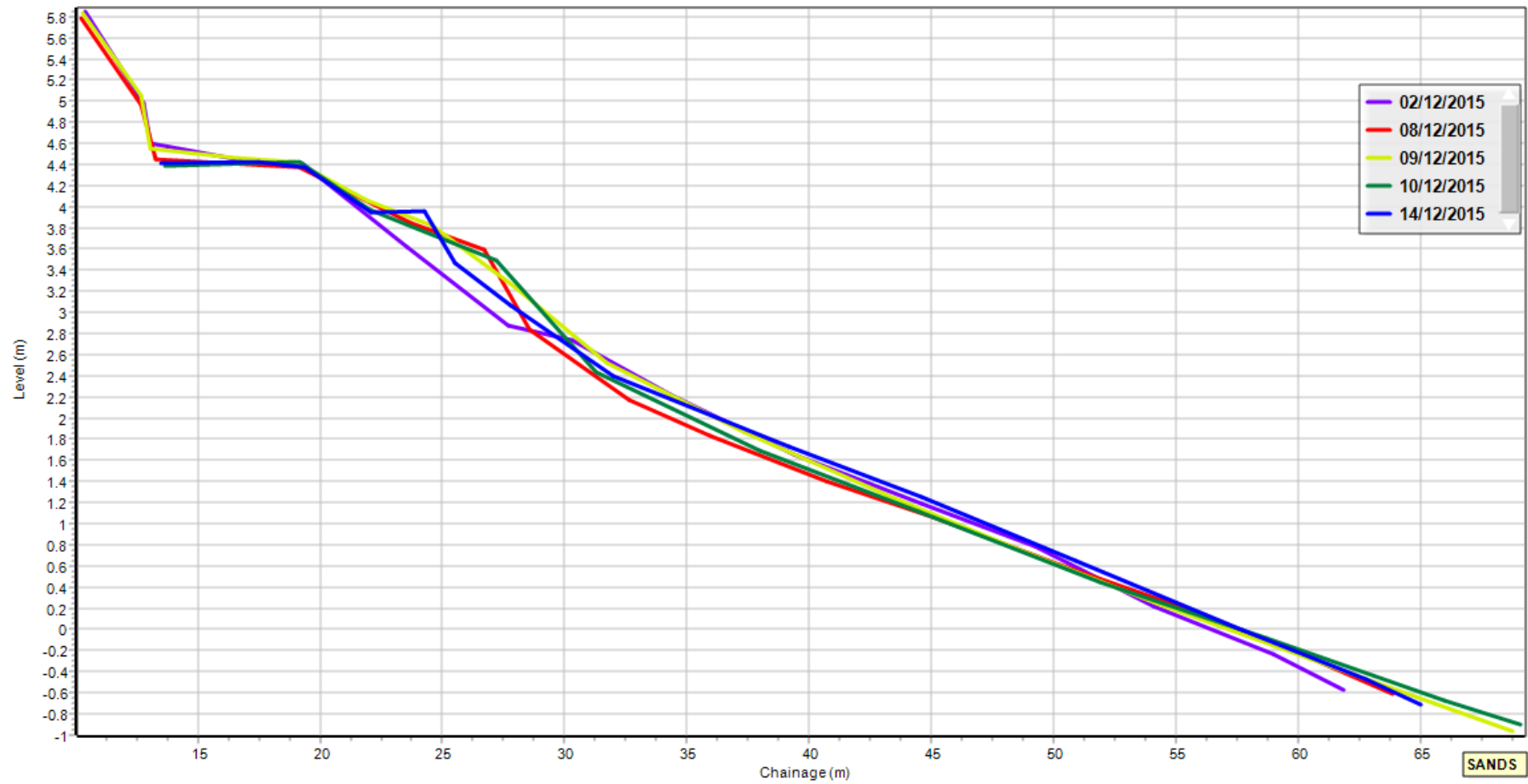


Figure B-18: dGPS profiles measured on Profile 2 during December 2015.

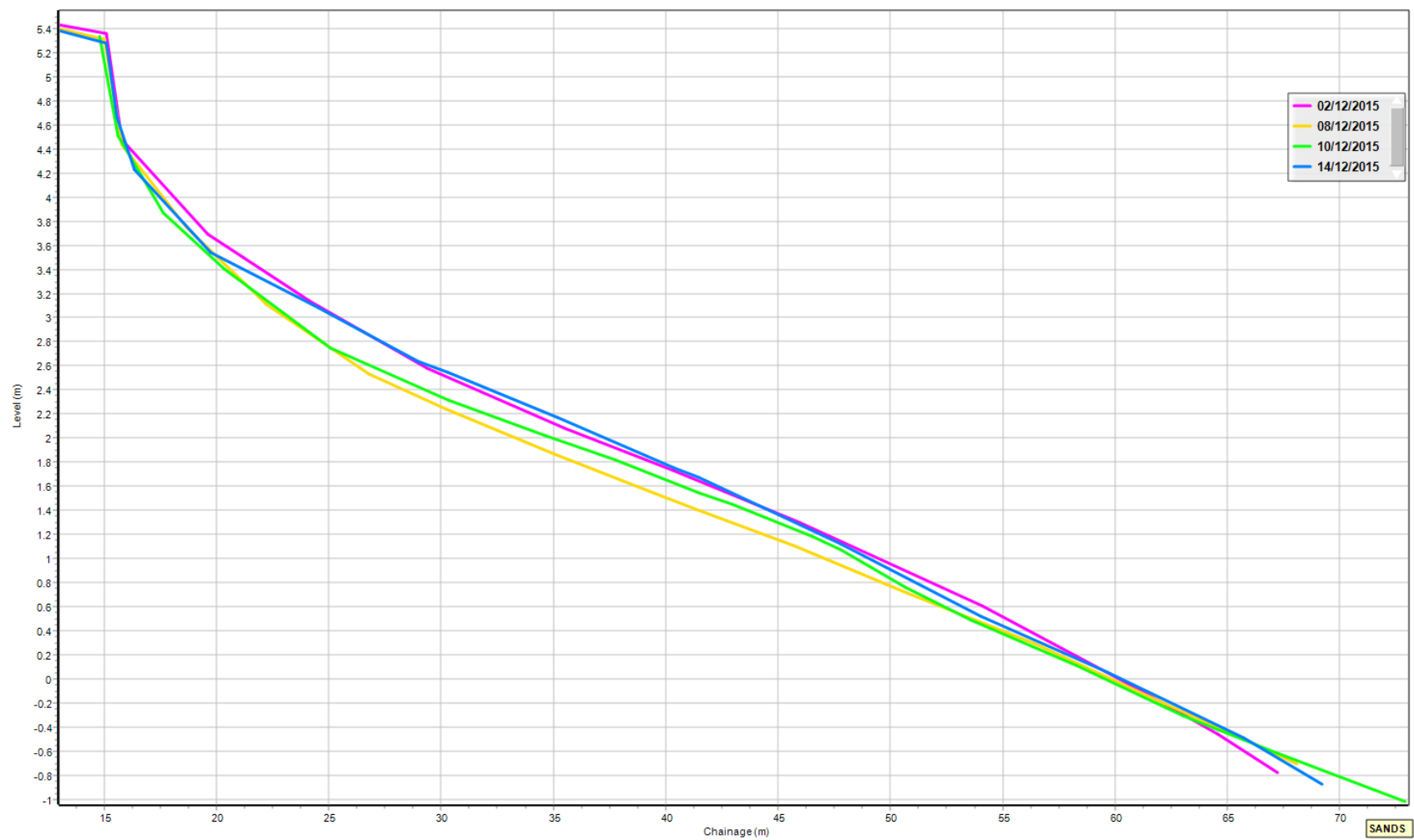


Figure B-19: dGPS profiles measured on Profile 3 during December 2015.

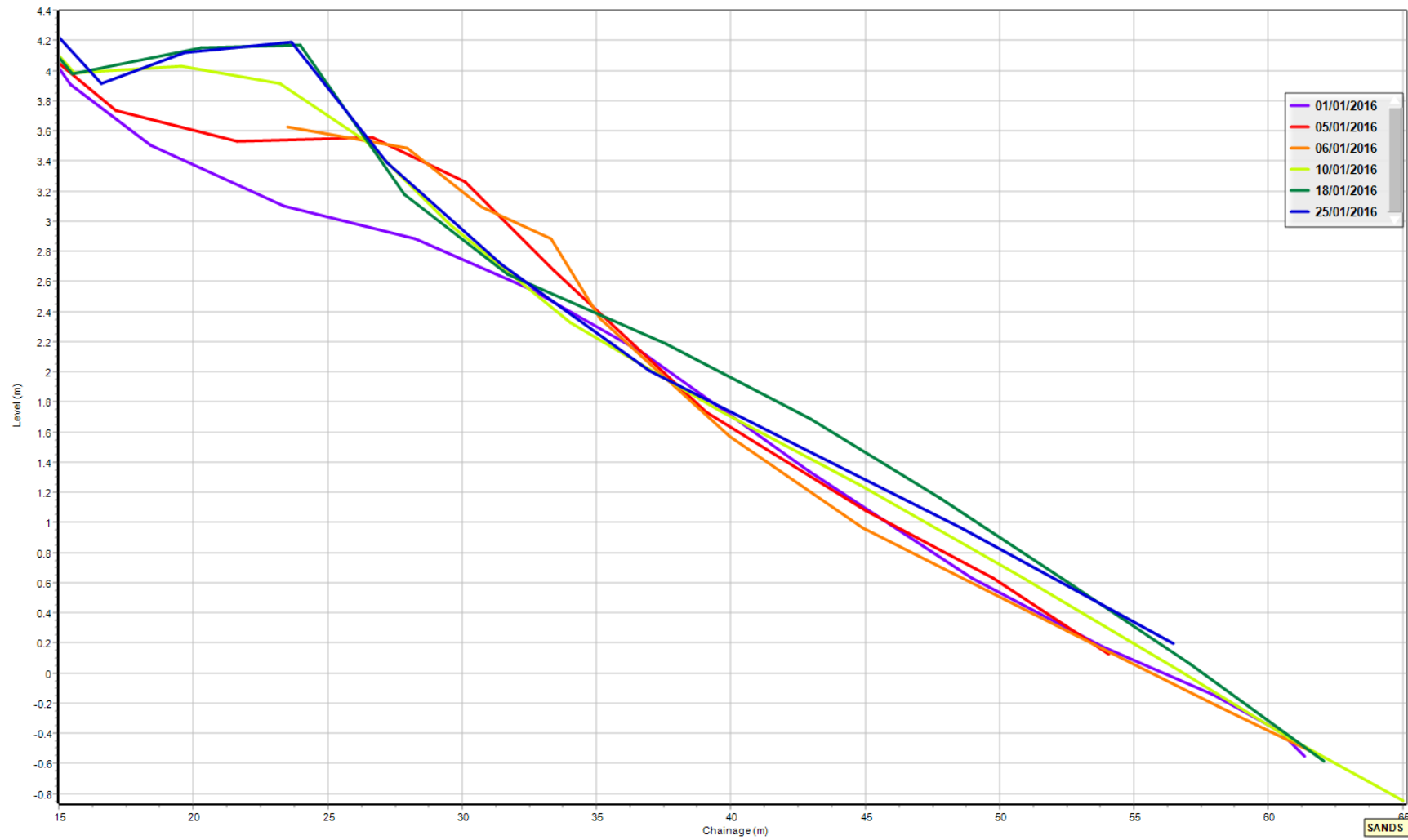


Figure B-20: dGPS profiles measured on Profile 1 during January 2016.

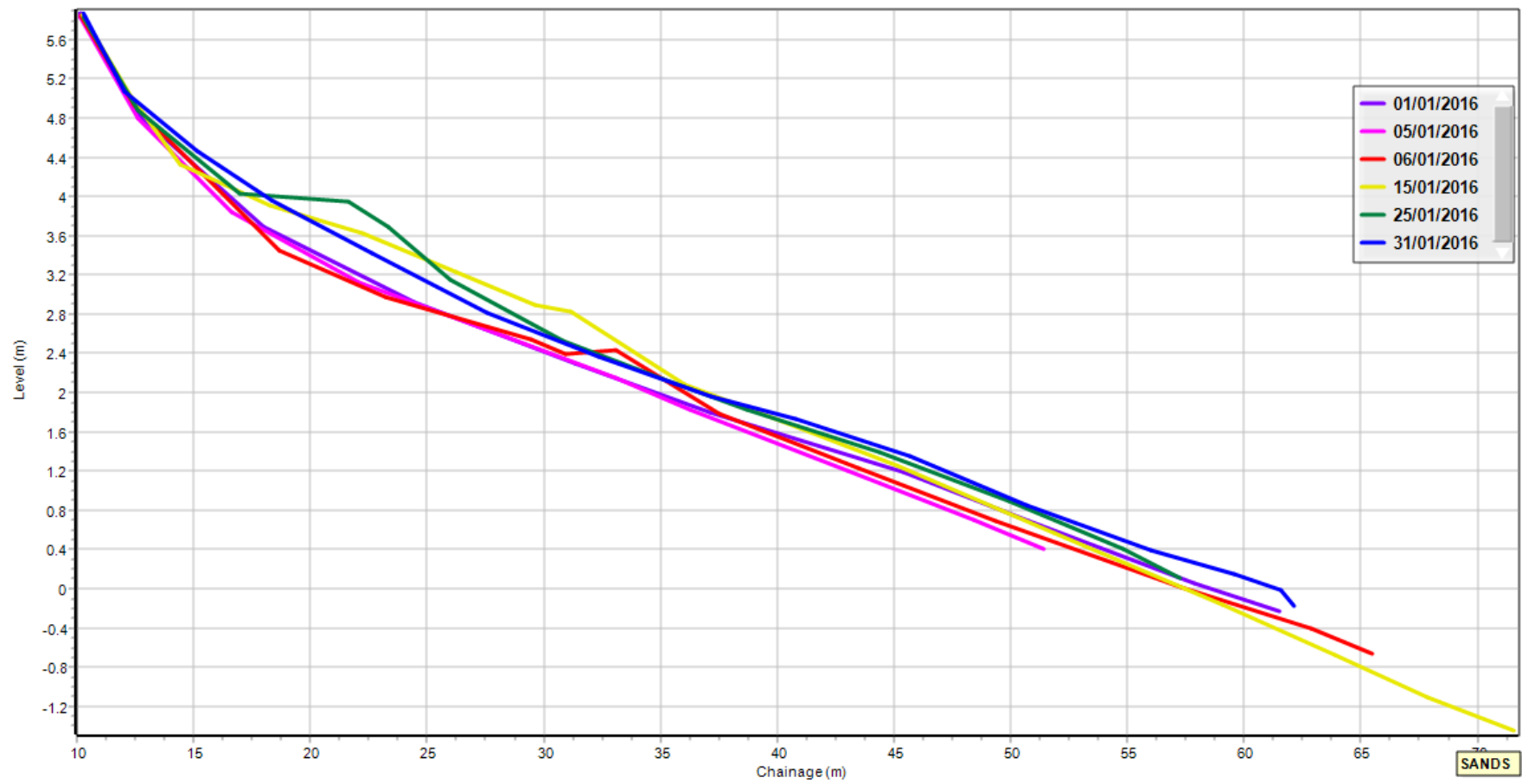


Figure B-21: dGPS profiles measured on Profile 2 during January 2016.

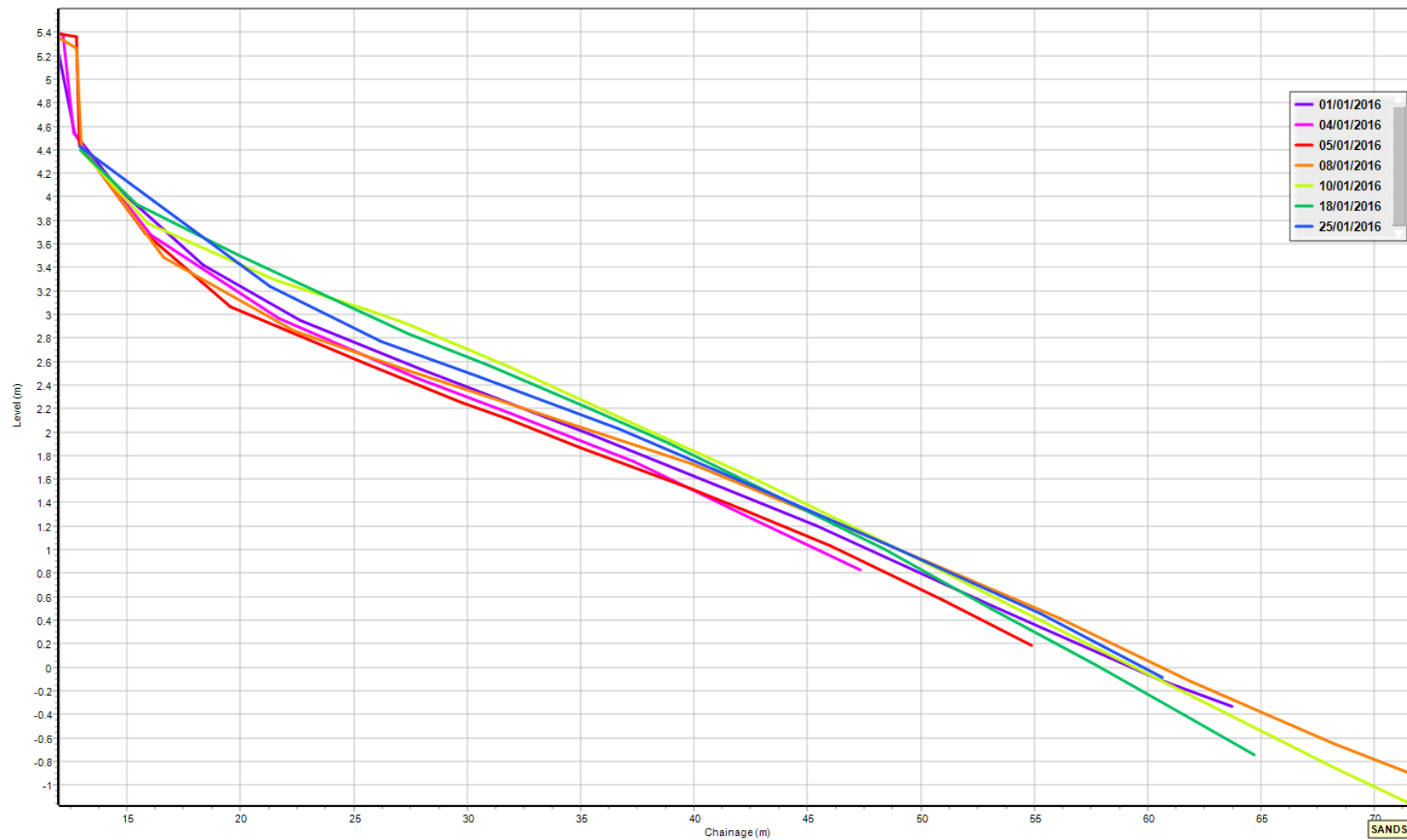


Figure B-22: dGPS profiles measured on Profile 3 during January 2016.

Appendix C : Mean profile and profile envelope for each profile during each study period

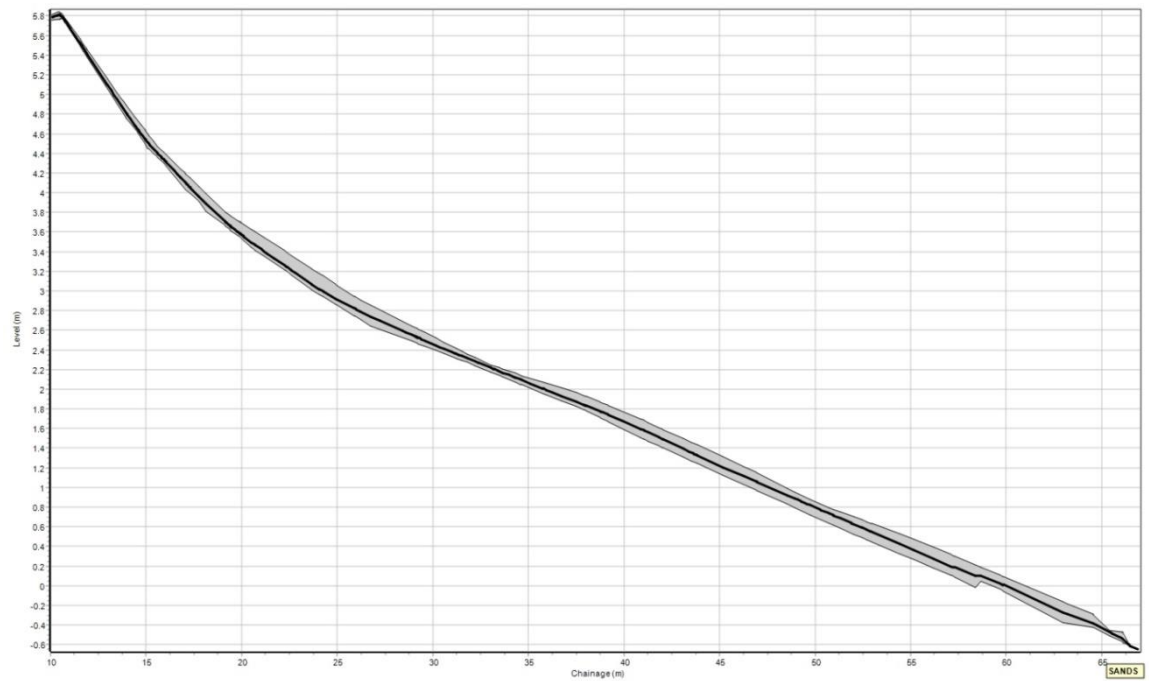


Figure C-1: Mean profile and profile envelopes from all dGPS profiles taken along Profile 2 in December 2014. Profiles 1 and 3 were not measured in December 2014.

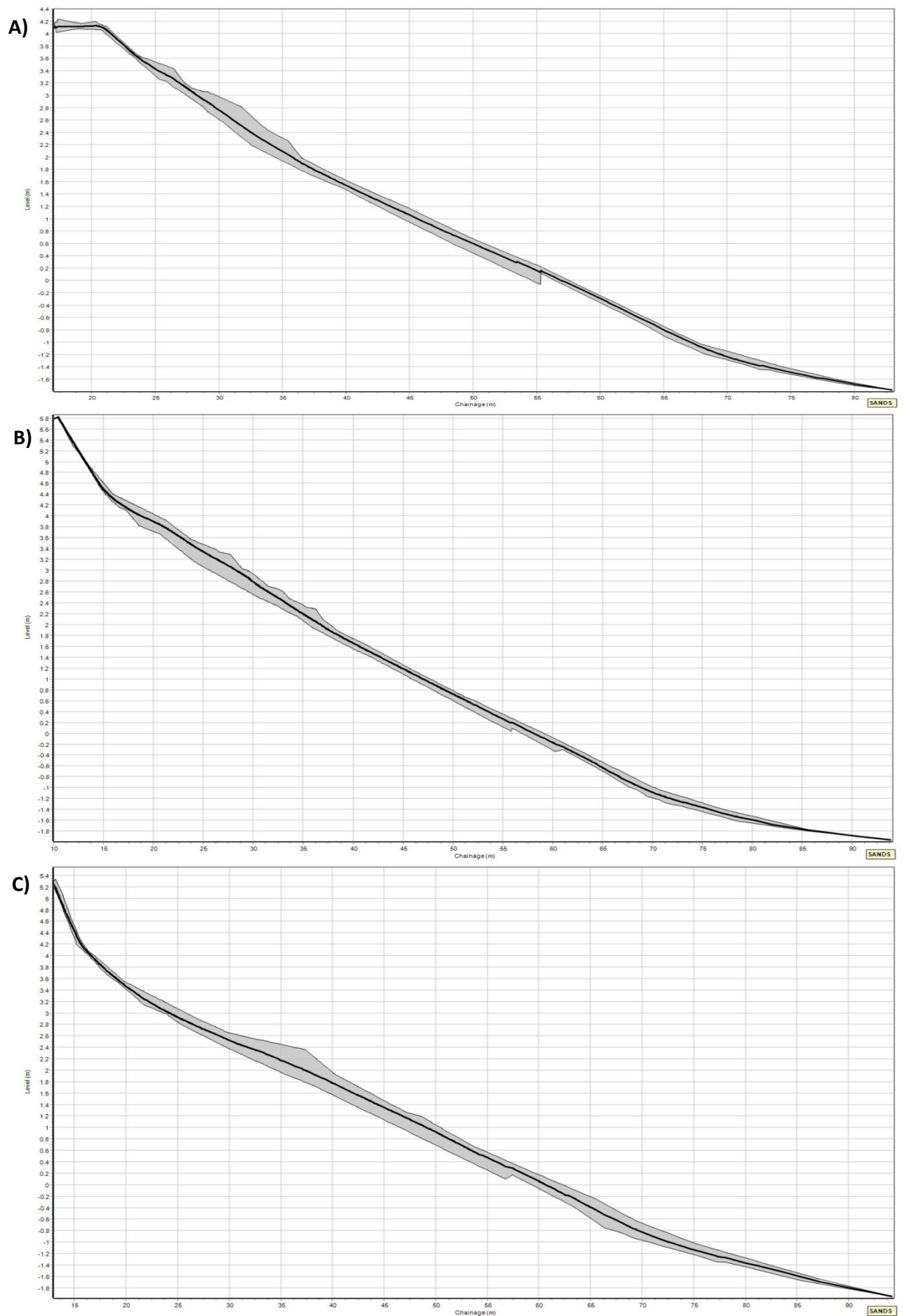


Figure C-2: Mean profile and profile envelopes from all dGPS profiles taken along A) Profile 1, B) Profile 2, and C) Profile 3 in January 2015.

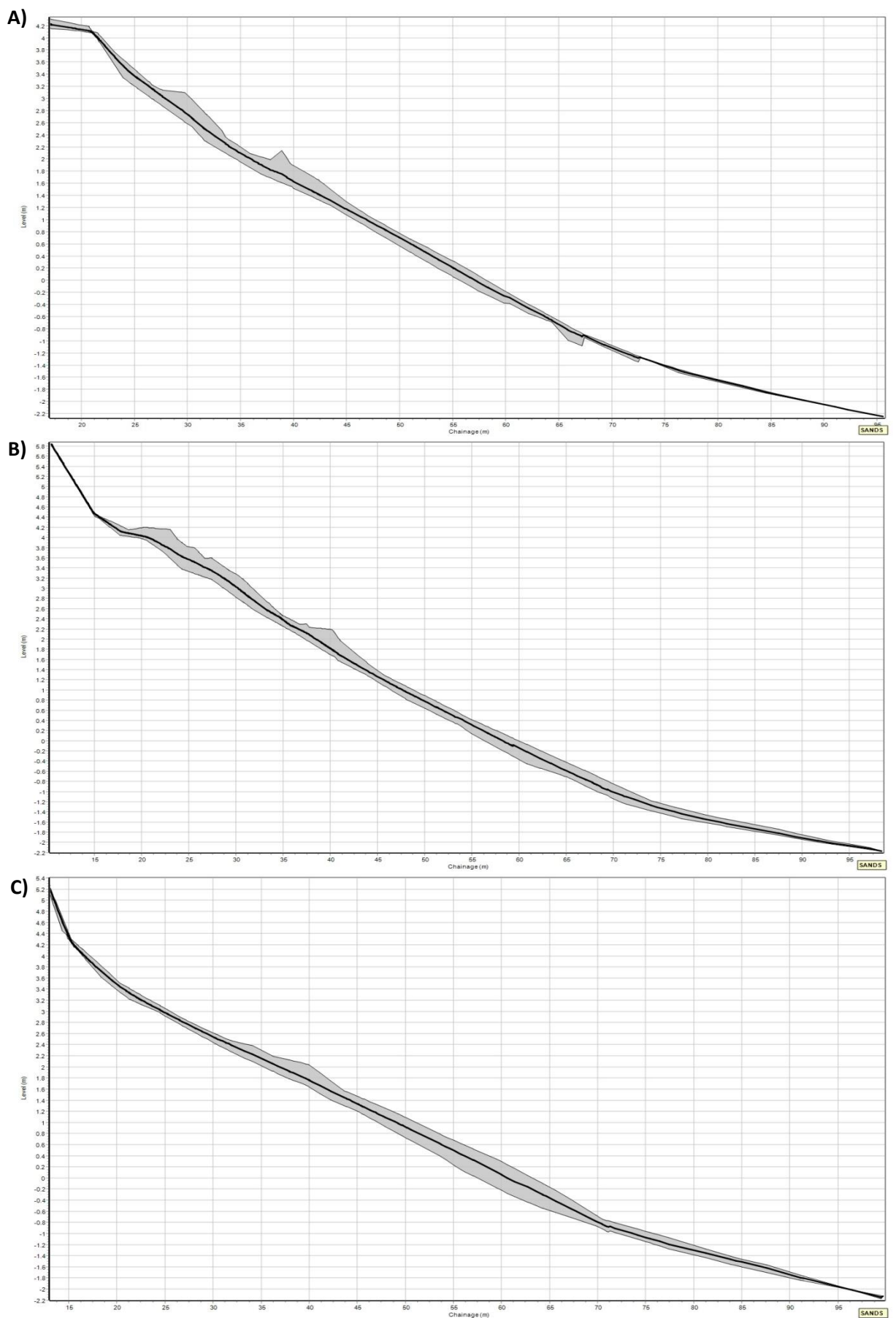


Figure C-3: Mean profile and profile envelopes from all dGPS profiles taken along A) Profile 1, B) Profile 2, and C) Profile 3 in February 2015.

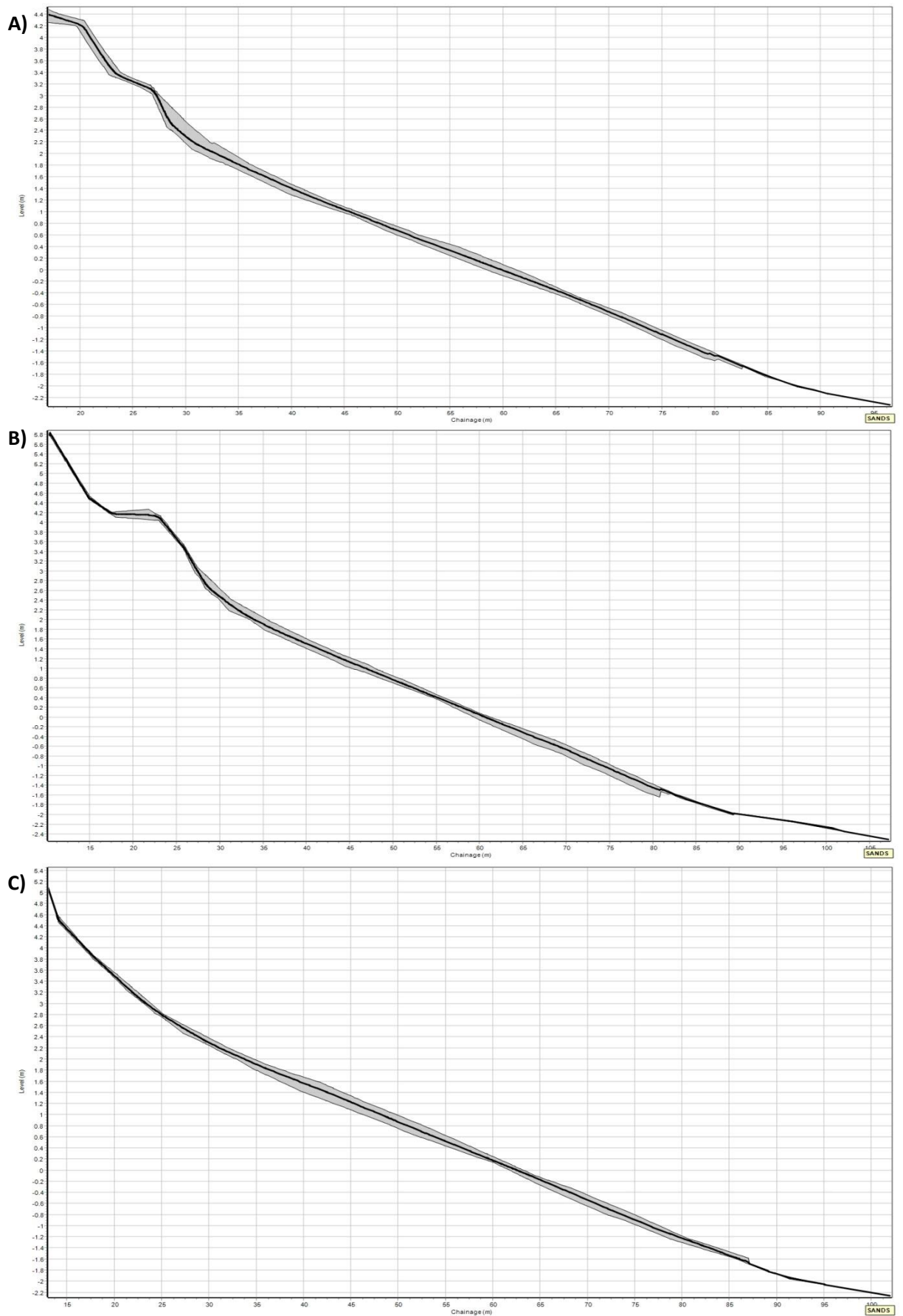


Figure C-4: Mean profile and profile envelopes from all dGPS profiles taken along A) Profile 1, B) Profile 2, and C) Profile 3 in March 2015.

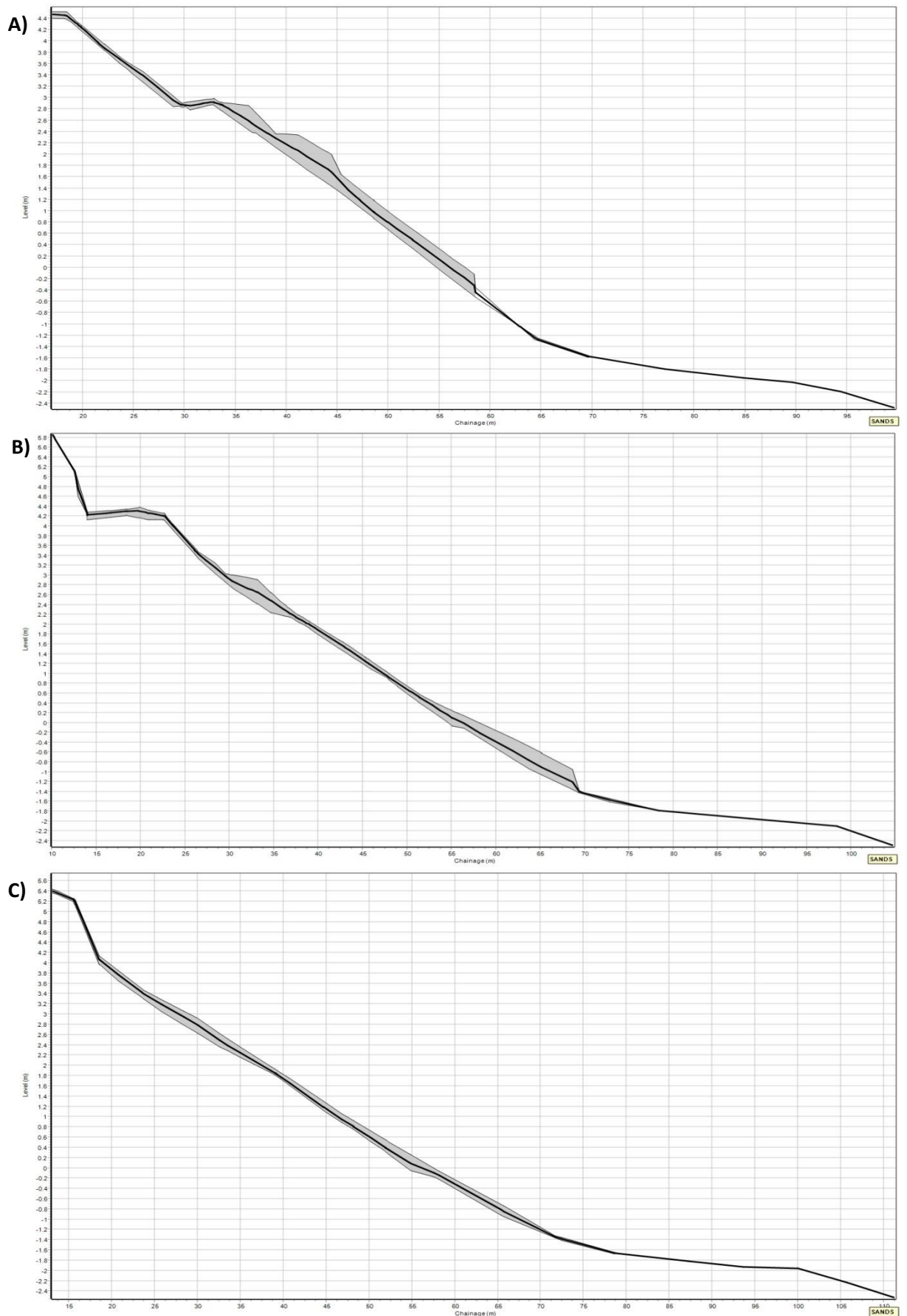


Figure C-5: Mean profile and profile envelopes from all dGPS profiles taken along A) Profile 1, B) Profile 2, and C) Profile 3 in October 2015.

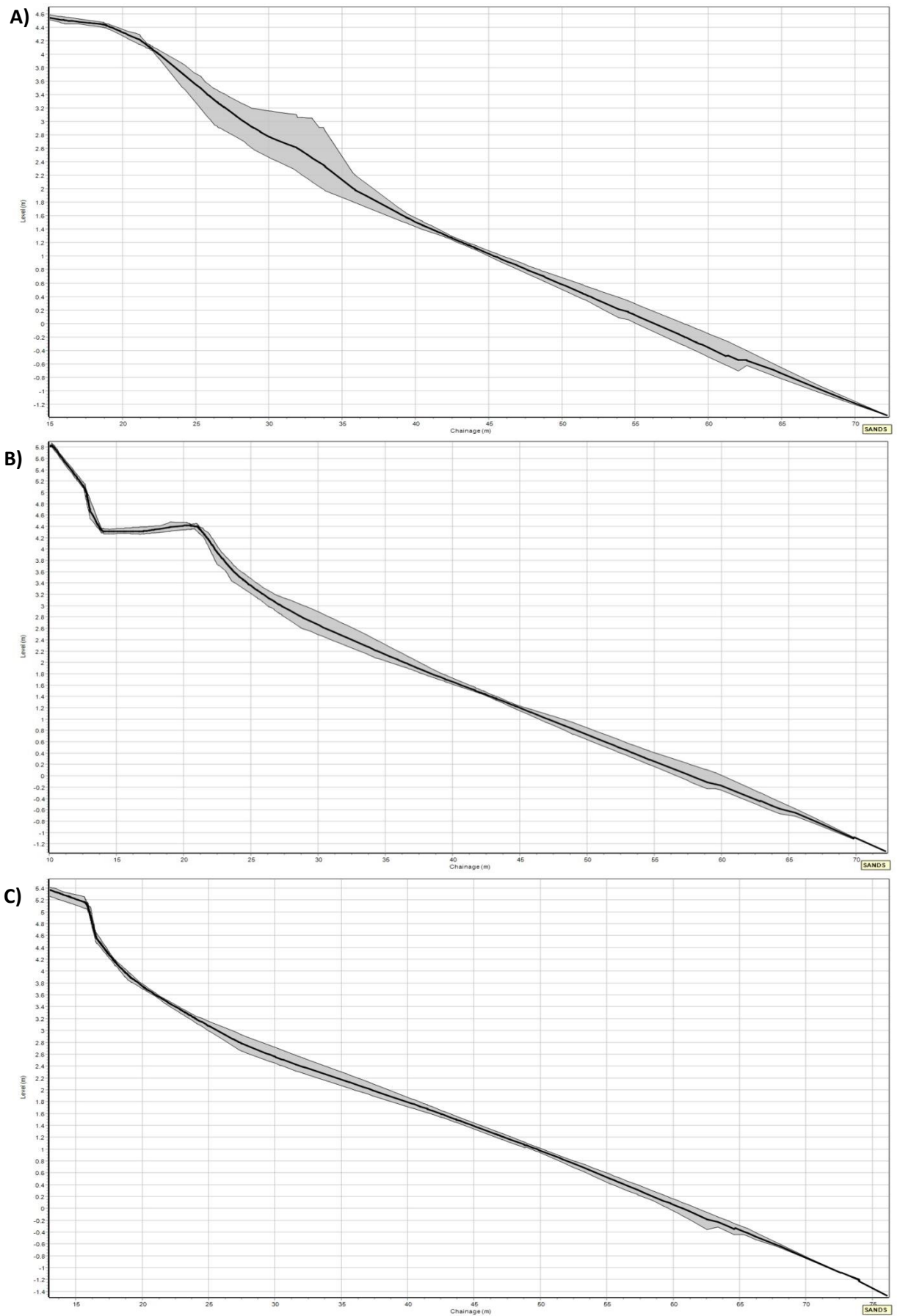


Figure C-6: Mean profile and profile envelopes from all dGPS profiles taken along A) Profile 1, B) Profile 2, and C) Profile 3 in November 2015.

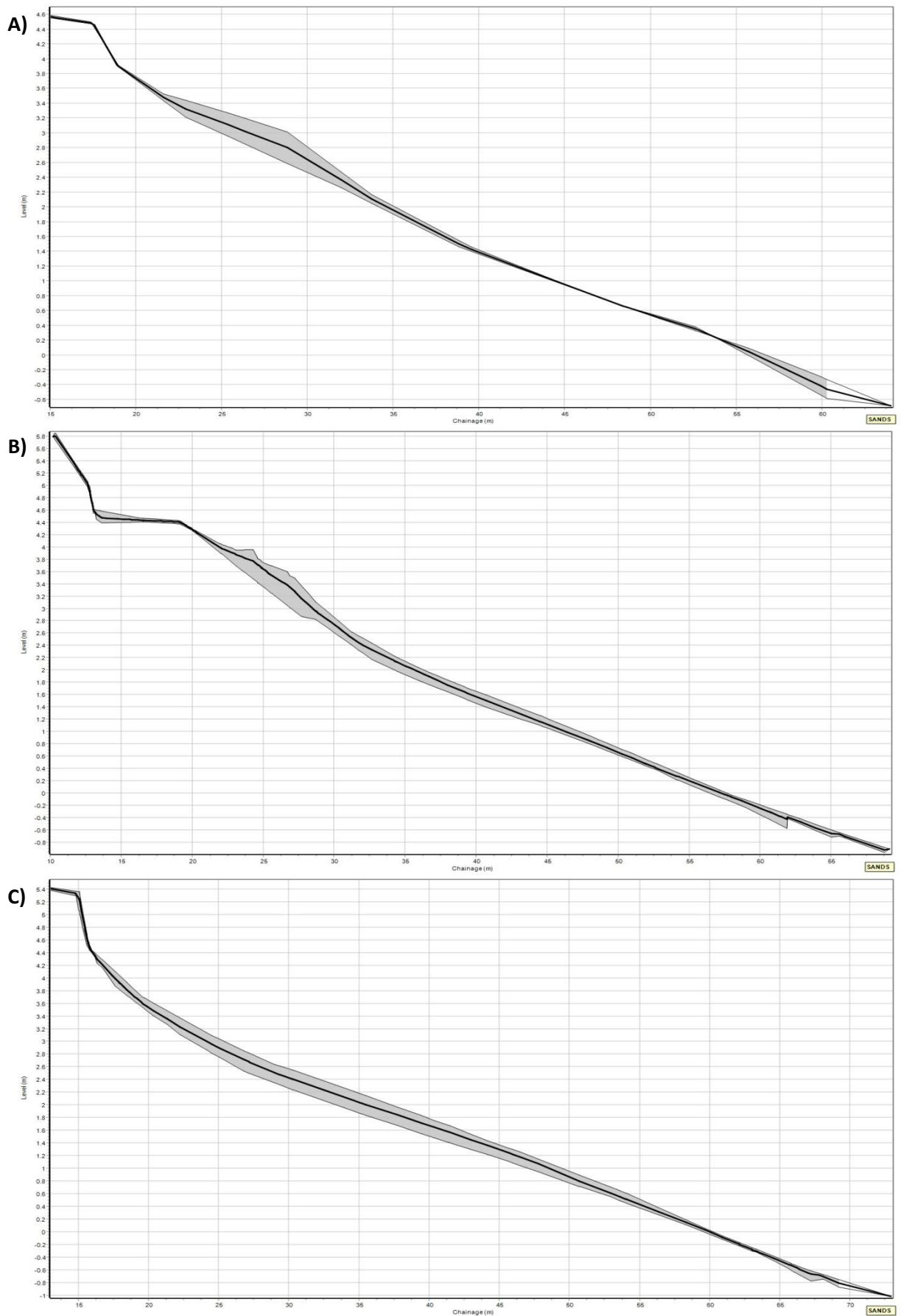


Figure C-7: Mean profile and profile envelopes from all dGPS profiles taken along A) Profile 1, B) Profile 2, and C) Profile 3 in December 2015.

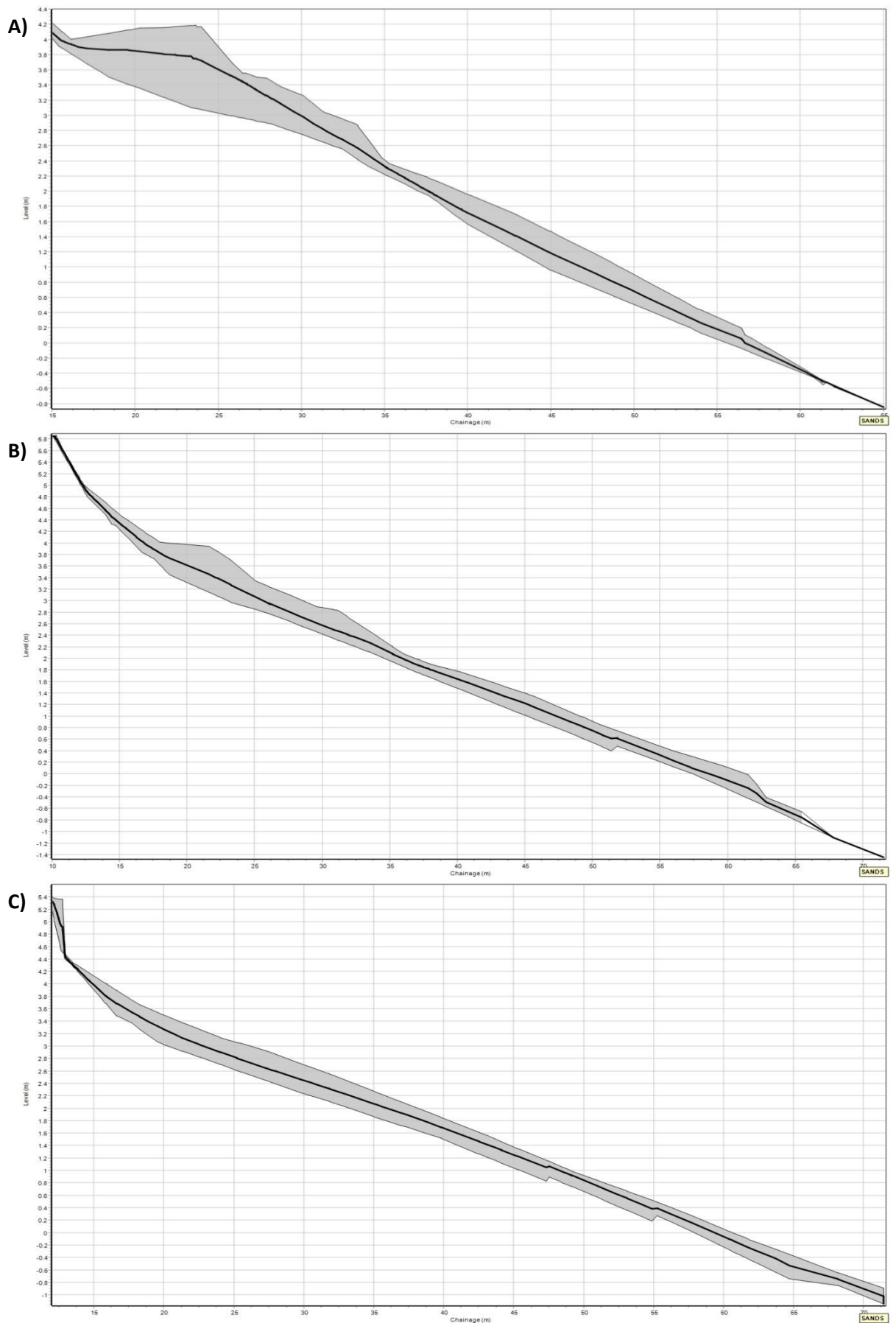


Figure C-8: Mean profile and profile envelopes from all dGPS profiles taken along A) Profile 1, B) Profile 2, and C) Profile 3 in January 2016.

Appendix D : Cross-shore variation between percentages of surface sediment codes during the first winter, with each profile’s results shown separately.

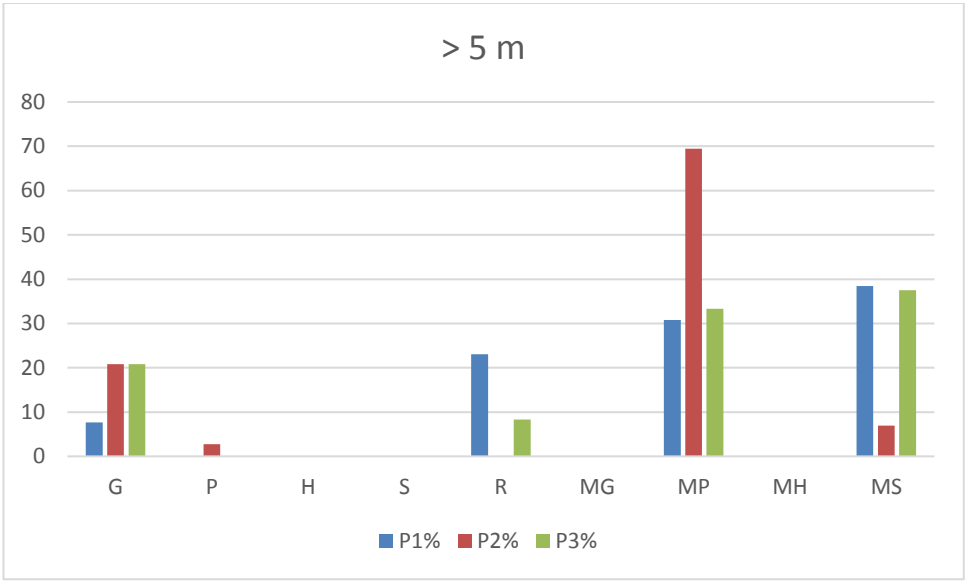


Figure D-1: Surface sediment codes at elevations over 5 m.

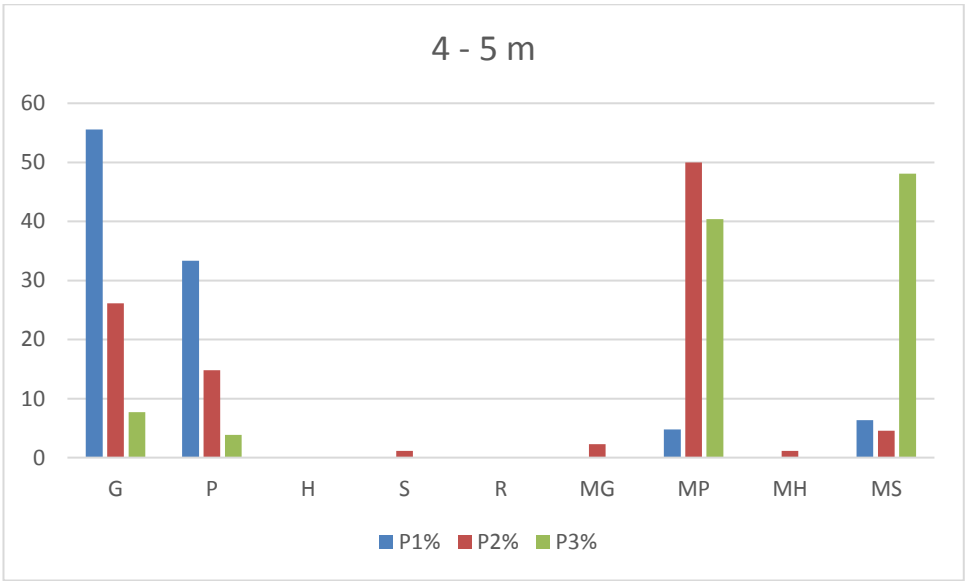


Figure D-2: Surface sediment codes at elevations of 4 - 5 m.

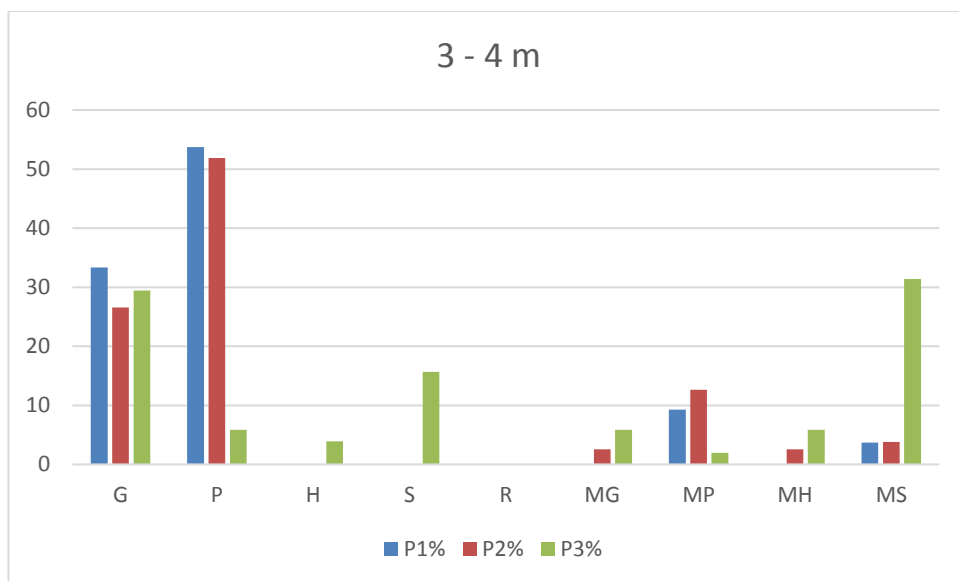


Figure D-3: Surface sediment codes at elevations of 3 - 4 m.

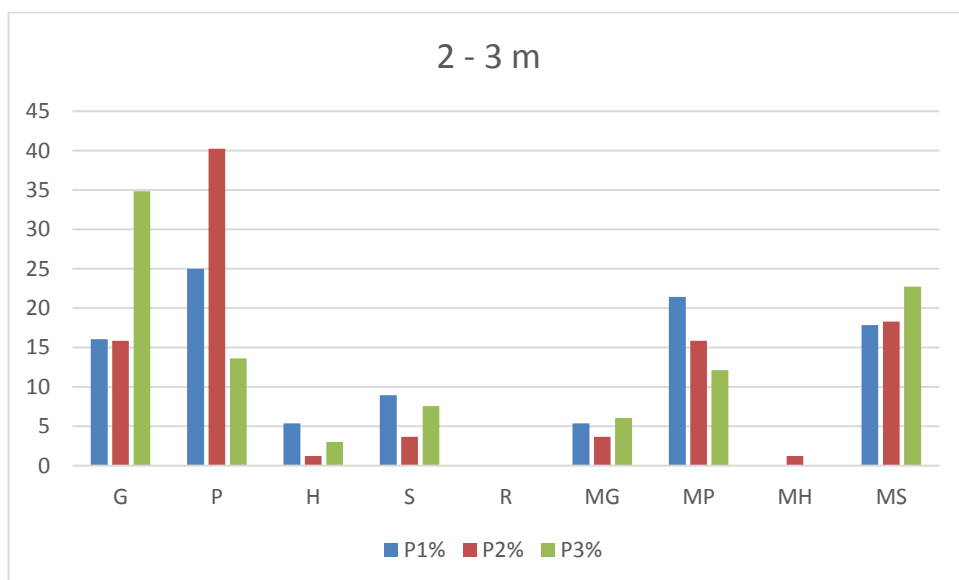


Figure D-4: Surface sediment codes at elevations of 2 - 3 m.

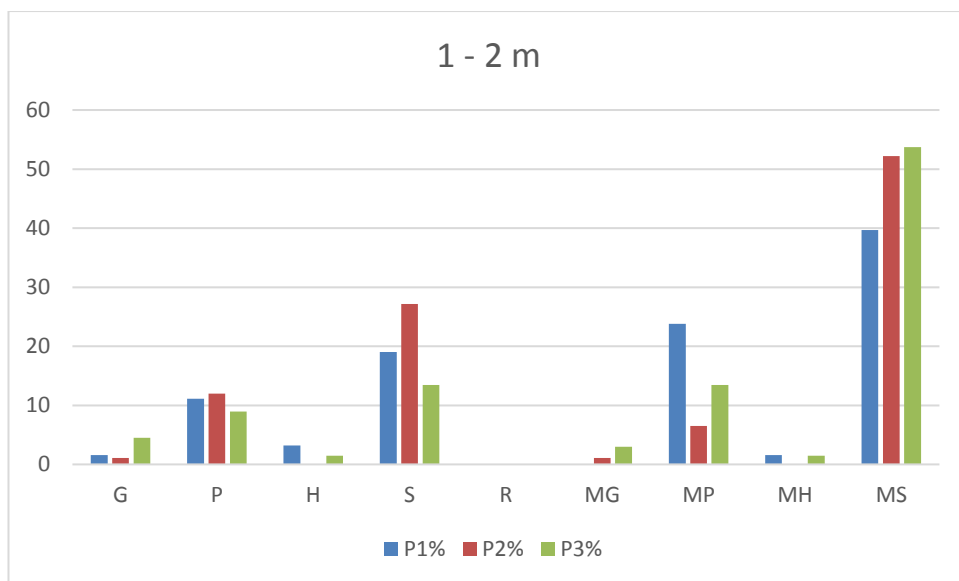


Figure D-5: Surface sediment codes at elevations of 1 - 2 m.

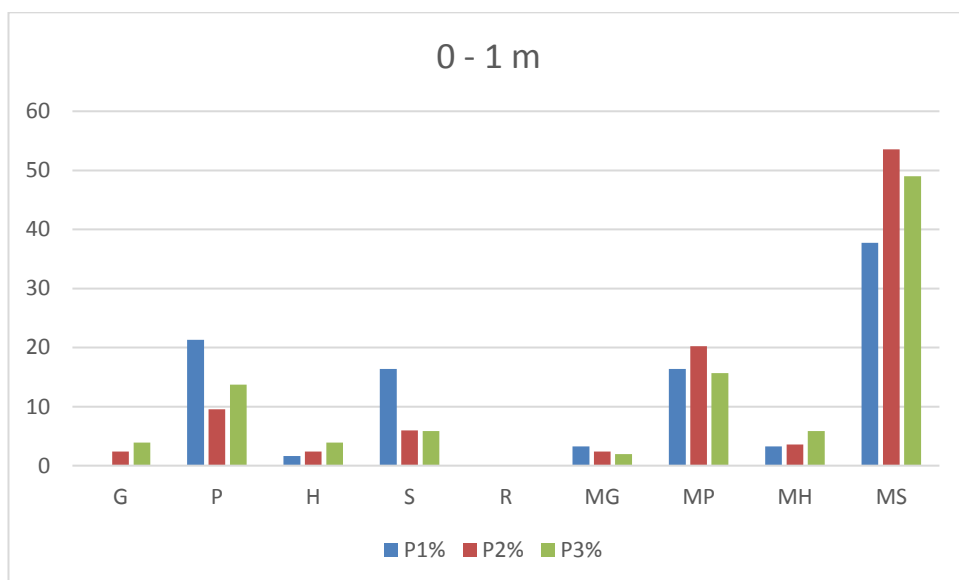


Figure D-6: Surface sediment codes at elevations of 0 - 1 m.

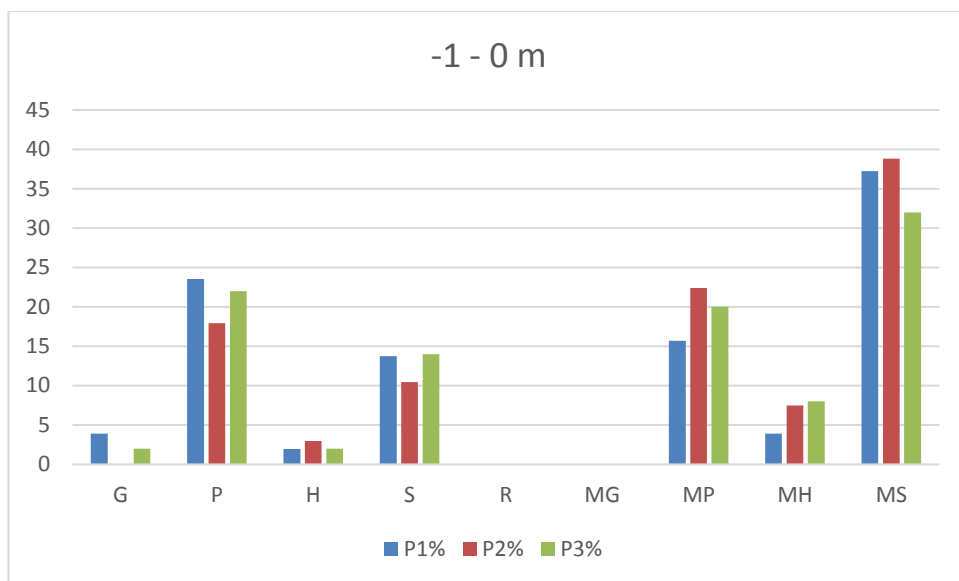


Figure D-7: Surface sediment codes at elevations of -1 - 0 m

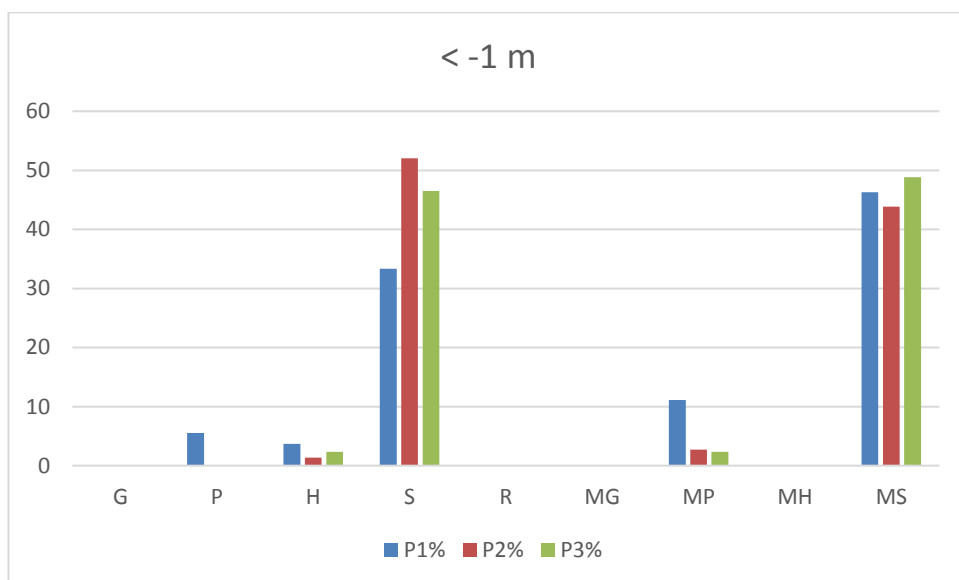


Figure D-8: Surface sediment codes at elevations less than -1 m

Appendix E : Comparison of surface codes to sieved sediment samples

Date and SID No	D ₅₀ (mm)	Sand % (< 1 mm)	Surface Code
4/12/14 C1	0.5	71.9	S
4/12/14 C3	8	17.3	G
4/12/14 C6	9	26.8	MS
4/12/14 C7	0.5	54.6	S
11/12/14 C3	7	18.6	P
11/12/14 C4	6	22.5	MS
11/12/14 C5	1	50.8	MS
12/12/14 C1	8	19.2	MH
12/12/14 C3	3	33.4	S
12/12/14 C5	5	30.5	MS
13/12/14 C1	9	17.1	P
13/12/14 C3	11	21.7	P
13/12/14 C4	9	29.7	S
15/12/14 C3	13	9.9	P
15/12/14 C4	7	23.6	MS
15/12/14 C5	9	26.5	MS
15/1/15 P1	8	29.4	MS
15/1/15 P2	11	22.1	MS
24/1/15 P1	9	23.7	MS
24/1/15 P2	13	20.0	MS
24/1/15 P3	8	23.8	MS
25/1/15 C1	10	18.9	MP
25/1/15 C3	3	42.8	MS
25/1/15 LTT	0.5	98.5	S
27/1/15 C2	6	18.8	MS
27/1/15 C5	13	2.6	H
27/1/15 C8	10	9.3	P
13/2/15 C2	10	23.2	MP
13/2/15 C4	3	32.5	MP
13/2/15 C5	10	10	H
13/2/15 C7	23	0.05	P
14/2/15 C2	5	31.8	MS
14/2/15 C4	3	35.2	MS
14/2/15 C6	6	5.3	P
14/2/15 C9	5	30.8	MS
15/2/15 C3	2	46.1	S
15/2/15 C5	4	44.8	S
15/2/15 C8	12	23.5	MS
17/2/15 C3	1	48.2	MP
17/2/15 C5	7	34.0	MP
17/2/15 C7	12	15.6	P
18/2/15 C2	12	10.0	P
18/2/15 C6	11	17.8	P
18/2/15 C8	9	21.6	MP

20/2/15 C2	7	0.7	P
20/2/15 C3	8	25.7	MP
20/2/15 C6	9	18.9	MS
20/2/15 C8	9	19.8	P
9/3/15 P1	3	42.8	S
9/3/15 P2	9	29.0	S
9/3/15 P3	1	60.2	S
13/3/15 P1	0.5	56.3	MS
13/3/15 P2	7	36.3	MS
13/3/15 P3	6	22.2	S
16/3/15 P1	5	29.0	MS
16/3/15 P2	3	36.5	S
16/3/15 P3	8	29.0	S

Appendix F : i) Database of AL measurements by date and location

Table F-1: AL measurements (cm (left, in black) and as a percentage of wave height (right, in blue)) during October 2014 field period.

Location	30/09/2014		01/10/2014		02/10/2014		03/10/2014		04/10/2014	
	cm	% H _s	cm	% H _s	cm	% H _s	cm	% H _s	cm	% H _s
1	4.2	11.68			16.8	49.32	12.6	35.82	4.2	6.744
2	8.4	23.36	8.4	17.26	16.8	49.32	8.4	23.88	12.6	20.23
3	4.2	11.68	16.8	34.52						
4										
5			8.4	17.26	8.4	24.66			4.2	6.744
6	8.4	23.36	4.2	8.629	8.4	24.66			4.2	6.744
7	4.2	11.68			8.4	24.66	8.4	23.88	4.2	6.744
8			4.2	8.629			42	119.4	12.6	20.23
9										
10										
11										
12					4.2	12.33	16.8	47.75		
13	12.6	35.04	8.4	17.26	8.4	24.66	12.6	35.82		
14	8.4	23.36	4.2	8.629			8.4	23.88	16.8	26.97
15	8.4	23.36								
16			8.4	17.26	12.6	36.99				
17	4.2	11.68	4.2	8.629	12.6	36.99	8.4	23.88	8.4	13.49
18	12.6	35.04	4.2	8.629	8.4	24.66	8.4	23.88	4.2	6.744

Table F-2: AL measurements (in cm (left, in black) and as a percentage of wave height (right, in blue)) during December 2014 field period.

Location	01/12/2014		02/12/2014		03/12/2014		04/12/2014		05/12/2014		06/12/2014		10/12/2014		11/12/2014		12/12/2014		13/12/2014	
	cm	%H _s	cm	%H _s	cm	%H _s	cm	%H _s	cm	%H _s	cm	%H _s	cm	%H _s	cm	%H _s	cm	%H _s	cm	%H _s
1	12.6	30.32			4.2	7.31	12.4	23.3	8.4	24.8	12.6	29.25	12.6	9.498			8.4	4.53	12.2	11.74
2																				
3									4.2	12.4	4.2	9.749	30.2	22.77	12.6	9.18	29.4	15.8	12.6	12.13
4	4.2	10.11	8.4	23.49	8.4	14.6	4.2	7.89	4.2	12.4	12.6	29.25	12.6	9.498	8.4	6.12	24.8	13.4	8.4	8.086
5	29.4	70.74	12.6	35.23	12.6	21.9	16.8	31.5	4.2	12.4	16.8	39	21	15.83	21	15.3	16.8	9.06	12.6	12.13
6	12.6	30.32	4.2	11.74	12.6	21.9	12.6	23.7	4.2	12.4	4.2	9.749	25.2	19						
7					4.2	7.31	4.2	7.89	4.2	12.4	4.2	9.749	33.6	25.33						
8	33.6	80.84	8.4	23.49	16.8	29.2	8.4	15.8	21	62	29.4	68.24	8.4	6.332						

Table F-3: AL measurements (in cm (left, in black) and as a percentage of wave height (right, in blue)) during January 2015 field period.

Location	10/01/2015		11/01/2015		14/01/2015		17/01/2015		18/01/2015		19/01/2015	
	cm	%H _s	cm	%H _s	cm	%H _s	cm	%H _s	cm	%H _s	cm	%H _s
1	25.2	13.3	16.8	11.9	12.6	8.948	25.2	27.3	29.4	45.8	4.2	13.44
2	21	11.1	12.6	8.95	12.6	8.948	12.6	13.7	12.6	19.6	8.4	26.88
3	25.2	13.3	16.8	11.9	12.6	8.948	16.8	18.2	21	32.7	12.6	40.32
4	26.8	14.2	12.6	8.95	12.6	8.948	4.2	4.55				
5	33.6	17.8	12.6	8.95	12.6	8.948	21	22.8	12.6	19.6	4.2	13.44
6	16.8	8.88	8.4	5.97								
7					21	14.91						
8					25.2	17.9	4.2	4.55				

Table F-4: AL measurements (in cm (left, in black) and as a percentage of wave height (right, in blue)) during February 2015 field period.

Location	12/02/2015		13/02/2015		14/02/2015		15/02/2015		16/02/2015		17/02/2015		18/02/2015		21/02/2015	
	cm	%H _s	cm	%H _s	cm	%H _s	cm	%H _s	cm	%H _s	cm	%H _s	cm	%H _s	cm	%H _s
1	21	89.21														
2	16.8	71.37	16.8	10.3	16.8	26.24	12.6	18.23	37.8	48.07	25.2	50.02	31.2	37.1	33.6	54.5
3	12.6	53.53	16.8	10.3	16.8	26.24	12.6	18.23	12.6	16.02	21	41.68	21	24.97	29.4	47.7
4	16.8	71.37	21	12.9	21	32.8										
5	4.2	17.84	29.4	18	21	32.8	12.6	18.23	16.8	21.37	12.6	25.01	8.4	9.99	12.6	20.4
6			8.4	5.15	4.2	6.56	12.6	18.23	12.6	16.02	16.8	33.34	21	24.97	21	34.1
7			4.2	2.57			21	30.39	8.4	10.68	4.2	8.336	16.8	19.98	12.6	20.4
8			33.6	20.6	16.8	26.24	12.6	18.23	12.6	16.02	16.8	33.34	33.6	39.96	37.8	61.3
9	25.2	107.1	12.6	7.72	16.8	26.24	21	30.39	12.6	16.02	12.6	25.01	12.6	14.98	33.6	54.5

Table F-5: AL measurements (in cm (left, in black) and as a percentage of wave height (right, in blue)) during February 2015 field period (continued).

Location	22/02/2015		25/02/2015		26/02/2015	
	cm	%H _s	cm	%H _s	cm	%H _s
1						
2	21	16.64	33.6	50.369	21	28.85
3	33.6	26.63	16.8	25.184	8.4	11.54
4						
5	12.6	9.987	12.6	18.888	12.6	17.31
6	16.8	13.32	4.2	6.2961		
7	12.6	9.987	4.2	6.2961		
8	12.6	9.987	12.6	18.888	16.8	23.08
9						

Table F-6: AL measurements (in cm (left, in black) and as a percentage of wave height (right, in blue)) during March 2015 field period.

Location	09/03/2015		10/03/2015		11/03/2015		12/03/2015		13/03/2015		14/03/2015		15/03/2015		16/03/2015		17/03/2015	
	cm	%H _s	cm	%H _s	cm	%H _s	cm	%H _s	cm	%H _s	cm	%H _s	cm	%H _s	cm	%H _s	cm	%H _s
1	16.8	25.78	16.8	27.59	12.6	22.82	16.8	31.95	12.6	21.83	25.2	34.16			16.8	21.13	8.4	16.2
2	12.6	19.34	8.4	13.79	8.4	15.21	8.4	15.97	31.2	54.06			25.2	40.1	12.6	15.85	4.2	8.08

Table F-7: AL measurements (in cm (left, in black) and as a percentage of wave height (right, in blue)) during October 2015 field period.

Location	29/09/2015		02/10/2015		03/10/2015		05/10/2015		06/10/2015		21/10/2015	
	cm	%H _s	cm	%H _s	cm	%H _s	cm	%H _s	cm	%H _s	cm	%H _s
1	4.2	5.91	8.4	13.5	4.2	9.87	21	19.17	4.2	4.242		
2	8.4	11.8	21	33.75	21	49.4	29.4	26.84	12.6	12.73	4.2	15.98
3											8.4	31.96
4	21	29.6	12.6	20.25	8.4	19.7	21	19.17	12.6	12.73	12.6	47.95
5	16.8	23.6	12.6	20.25	8.4	19.7	21	19.17	12.6	12.73		
6	12.6	17.7										
7			16.8	27								

Table F-8: AL measurements (in cm (left, in black) and as a percentage of wave height (right, in blue)) during November 2015 field period.

Location	04/11/2015		05/11/2015		07/11/2015		08/11/2015		09/11/2015		10/11/2015		11/11/2015		12/11/2015		14/11/2015	
	cm	%H _s	cm	%H _s	cm	%H _s	cm	%H _s	cm	%H _s	cm	%H _s	cm	%H _s	cm	%H _s	cm	%H _s
1	12.6	19.75	12.6	19.5									8.4	8.28	25.2	29.65	12.6	10.2
2	16.8	26.33	12.6	19.5	8.4	7.21	4.2	4.31			12.6	9.25	16.8	16.6	16.8	19.76	21	17
3					12.6	10.8	21	21.5	4.2	4.12	16.8	12.3	21	20.7	16.8	19.76	12.6	10.2
4	21	32.92	21	32.5	12.6	10.8	16.8	17.2	16.8	16.5	8.4	6.17	21	20.7	16.8	19.76	16.8	13.6
5	16.8	26.33	8.4	13	4.2	3.6	12.6	12.9	12.6	12.4	4.2	3.08	12.6	12.4	12.6	14.82	12.6	10.2
6	8.4	13.17	12.6	19.5	8.4	7.21	8.4	8.61	4.2	4.12	8.4	6.17	8.4	8.28	8.4	9.882	8.4	6.82
7	21	32.92	16.8	26	8.4	7.21	21	21.5	8.4	8.25	16.8	12.3	21	20.7	21	24.71	12.6	10.2
8	25.2	39.5	16.8	26	4.2	3.6	12.6	12.9	8.4	8.25	12.6	9.25	21	20.7	12.6	14.82	21	17
9	8.4	13.17					4.2	4.31	4.2	4.12	25.2	18.5	29.4	29	25.2	29.65	12.6	10.2
10	25.2	39.5	21	32.5							21	15.4	21	20.7	21	24.71	21	17
11	21	32.92													12.6	14.82		
12																		
13	16.8	26.33			12.6	10.8												
14	29.4	46.08	21	32.5	12.6	10.8	21	21.5	12.6	12.4	12.6	9.25	21	20.7	21	24.71	16.8	13.6
15	25.2	39.5	21	32.5	12.6	10.8	25.2	25.8	12.6	12.4	21	15.4	33.6	33.1	29.4	34.59	21	17
16	12.6	19.75	16.8	26	8.4	7.21	16.8	17.2	8.4	8.25	16.8	12.3	21	20.7	16.8	19.76	12.6	10.2

Table F-9: AL measurements (in cm (left, in black) and as a percentage of wave height (right, in blue)) during December 2015 field period.

Location	09/12/2015		10/12/2015		11/12/2015		14/12/2015		15/12/2015		16/12/2015	
	cm	%H _s	cm	%H _s	cm	%H _s	cm	%H _s	cm	%H _s	cm	%H _s
1	16.8	13.67	25.2	15.99	16.8	13.3	16.8	20.3	16.8	18.62	16.8	14.6
2	25.2	20.51	25.2	15.99	21	16.6	21	25.4	12.6	13.97	25.2	21.9
3	12.6	10.26	21	13.33	12.6	9.96	12.6	15.2	12.6	13.97	21	18.2
4	8.4	6.837	12.6	7.997	8.4	6.64	8.4	10.2	4.2	4.656	12.6	10.9
5	12.6	10.26	16.8	10.66	12.6	9.96	12.6	15.2	8.4	9.311	25.2	21.9
6	21	17.09	16.8	10.66	12.6	9.96	12.6	15.2				
7	16.8	13.67	25.2	15.99	12.6	9.96	21	25.4	12.6	13.97	16.8	14.6
8	16.8	13.67	16.8	10.66	8.4	6.64	16.8	20.3	8.4	9.311	12.6	10.9
9	12.6	10.26			8.4	6.64	21	25.4	12.6	13.97	16.8	14.6
10	12.6	10.26	12.6	7.997	8.4	6.64	4.2	5.08	10.2	11.31	22.6	19.6
11	25.2	20.51	16.8	10.66	16.8	13.3	16.8	20.3	21	23.28	25.2	21.9
12	21	17.09	21	13.33	16.8	13.3	16.8	20.3	16.8	18.62	25.2	21.9
13	16.8	13.67	16.8	10.66	12.6	9.96	8.4	10.2			21	18.2
14	12.6	10.26	16.8	10.66	8.4	6.64			8.4	9.311	16.8	14.6

Table F-10: AL measurements (in cm (left, in black) and as a percentage of wave height (right, in blue)) during January 2016 field period.

Location	08/01/2016		09/01/2016		10/01/2016		11/01/2016		12/01/2016		13/01/2016		15/01/2016		16/01/2016		19/01/2016	
	cm	%H _s	cm	%H _s	cm	%H _s	cm	%H _s	cm	%H _s	cm	%H _s	cm	%H _s	cm	%H _s	cm	%H _s
1	21	16.6	16.8	12	12.6	6.84	8.4	6.33	8.4	7.24	12.6	9.74						
2	25.2	19.9	16.8	12	16.8	9.13	16.8	12.7	8.4	7.24	16.8	13	12.6	15.6	8.4	14.76	12.6	14.05
3	21	16.6	21	14.9	29.4	16	12.6	9.49	16.8	14.5	16.8	13	8.4	10.4	16.8	29.53	16.8	18.73
4	21	16.6	12.6	8.97	12.6	6.84	21	15.8	12.6	10.9	21	16.2	8.4	10.4	8.4	14.76	8.4	9.367
5	16.8	13.3	4.2	2.99	8.4	4.56	8.4	6.33	8.4	7.24	8.4	6.5			4.2	7.382		
6	25.2	19.9	8.4	5.98	4.2	2.28	4.2	3.16	8.4	7.24	12.6	9.74	4.2	5.19	12.6	22.14	8.4	9.367
7	33.6	26.5	12.6	8.97	12.6	6.84	12.6	9.49	16.8	14.5	12.6	9.74	8.4	10.4	12.6	22.14	21	23.42
8	25.2	19.9	16.8	12	21	11.4	25.2	19	12.6	10.9	21	16.2			8.4	14.76	16.8	18.73
9	29.4	23.2	12.6	8.97	16.8	9.13	12.6	9.49	12.6	10.9	16.8	13						
10	16.8	13.3	12.6	8.97	8.4	4.56	12.6	9.49	16.8	14.5	12.6	9.74						
11	25.2	19.9	21	14.9	21	11.4	16.8	12.7	21	18.1	25.2	19.5	12.6	15.6	8.4	14.76		
12	21	16.6	16.8	12	16.8	9.13	21	15.8	12.6	10.9	21	16.2			8.4	14.76	16.8	18.73
13	29.4	23.2			21	11.4	21	15.8	12.6	10.9	12.6	9.74	8.4	10.4	4.2	7.382	21	23.42
14	16.8	13.3	12.6	8.97	16.8	9.13	16.8	12.7	8.4	7.24			12.6	15.6	4.2	7.382	4.2	4.684
15	16.8	13.3	8.4	5.98			8.4	6.33	8.4	7.24	8.4	6.5						

ii) Positions of SIDs during each field period

Table F-11: Locations (Easting/Northing) of SIDs in each study period.

Location	Oct-14		Dec-14		Jan-15		Feb-15		Mar-15		Oct-15	
1	474375.9	98005.58	474460.1	98004.17	474430.8	97986.03			474431.9	97985.97	474464	98002.71
2	474374.7	97999.26	474435.8	98014.12	474431.9	97991.2	474432	97985.89	474420.6	97997.98	474464.8	97994.55
3	474373.4	97994.52	474434.5	98008.13	474432.8	97996.72	474432.8	97992.44			474418.6	97996.91
4	474373.4	97990.84	474433.9	98002.01	474434	98001.91	474433.2	97996.8			474442.7	97997.25
5	474373.4	97987.2	474433.2	97992.4	474434.5	98008.08	474434.5	98002.31			474444.4	98002.43
6	474373.2	97983.72	474431.5	97984.41	474435.5	98012.23	474434.5	98008.09			474445.6	98008.11
7	474373	97980.41	474429.7	97976.01	474460.4	98004.29	474435.5	98012.26			474419.8	98003.48
8	474372.8	97975.05	474417.2	97997.91			474420.3	97992.32				
9	474406.1	97986.82					474420.7	97998				
10	474406.2	97992.43										
11	474407.8	97997.35										
12	474421.2	98005.56										
13	474420.7	98001.37										
14	474419.7	97995.88										
15	474418.5	97991.64										
16	474417.5	97985.62										
17	474416.7	97980.8										
18	474416.3	97977.25										

Table F-12: Locations (Easting/Northing) of SIDs in each study period (continued)

Location	Nov-15		Dec-15		Jan-16	
1	474422.6	98013.08	474421.6	98008.68	474421.4	98010.3
2	474421.1	98007.75	474421	98005.06	474420.2	97999.12
3	474420.8	98003.41	474419.4	97992.62	474419.7	97994.31
4	474420	97997.03	474418.4	97983.21	474419.1	97989.52
5	474419.3	97990.65	474445.6	97988.17	474418.4	97985.13
6	474445	97985.51	474443.4	97994.5	474444.7	97982.49
7	474445.8	97991.29	474446.9	98005.3	474445.1	97987.77
8	474446	97994.6	474447.2	98009.77	474444.5	97997.01
9	474446.9	98002.42	474467	98009.05	474446.8	98005.58
10	474446.9	98007.23	474466.5	98005.62	474467	98008.46
11	474447.6	98012.04	474465.9	98000.85	474465.2	97997.09
12	474468	98015.51	474464.8	97994.6	474464.7	97994.66
13	474467.1	98004.64	474464	97983.56	474463.8	97987.82
14	474464.8	97994.8	474463	97979.88	474463	97983.07
15	474464	97987.18			474462	97977.52
16	474462	97980.27				

Appendix G : Mean, maximum and standard deviation of AL depths per day.

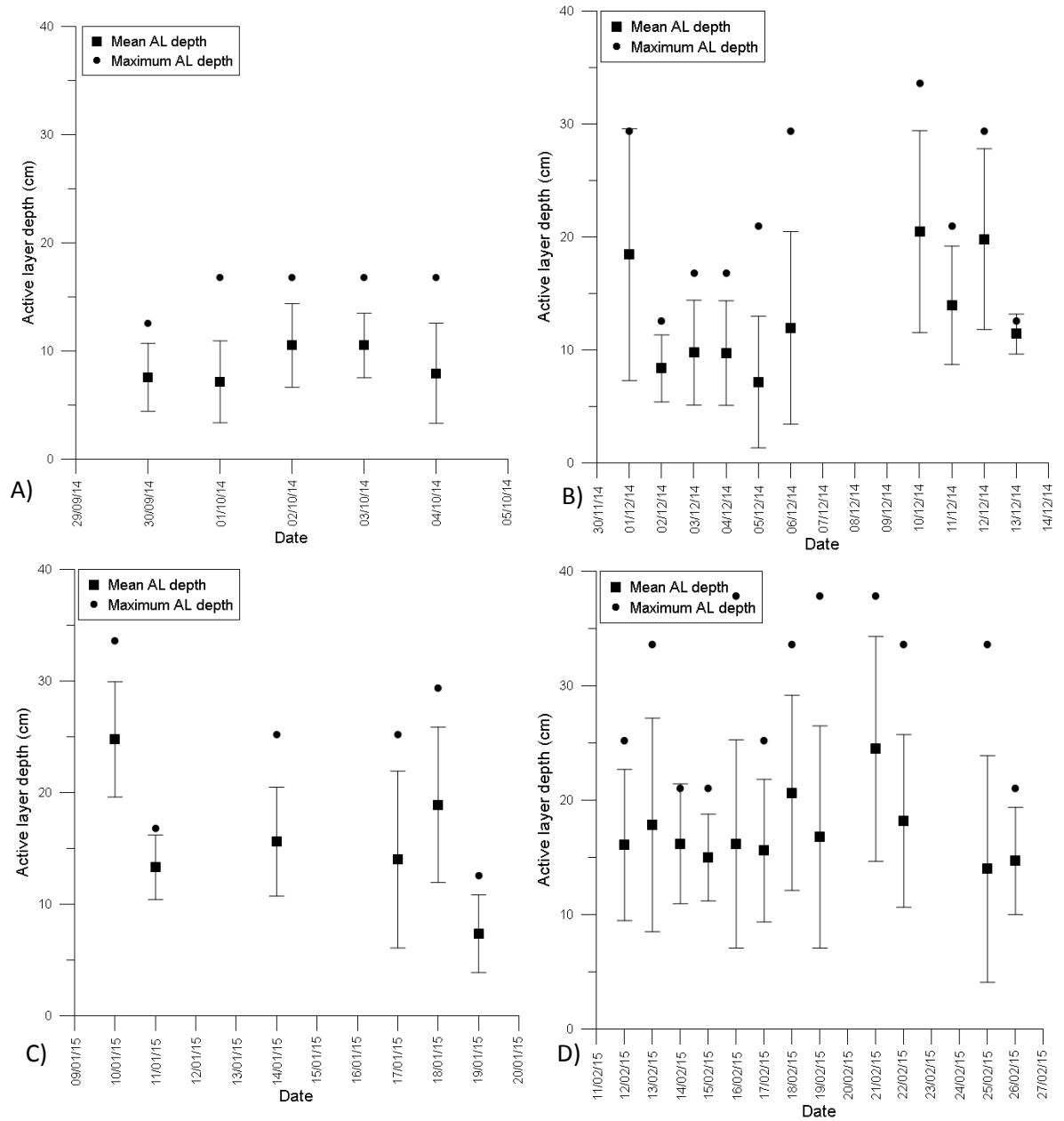


Figure G-1: Active layer variation for study periods during: A) October 2014, B) December 2014, C) January 2015, D) February 2015.

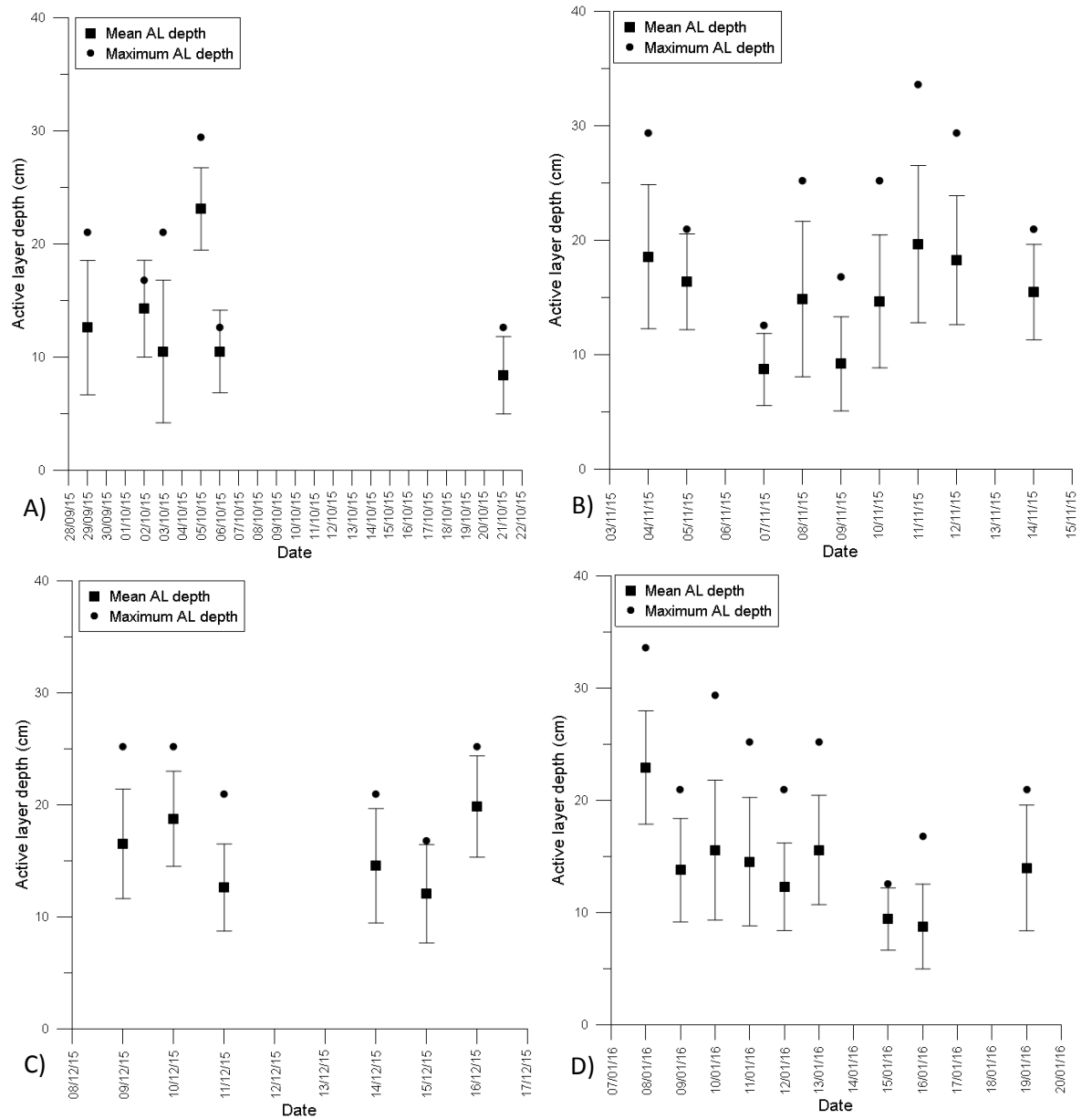
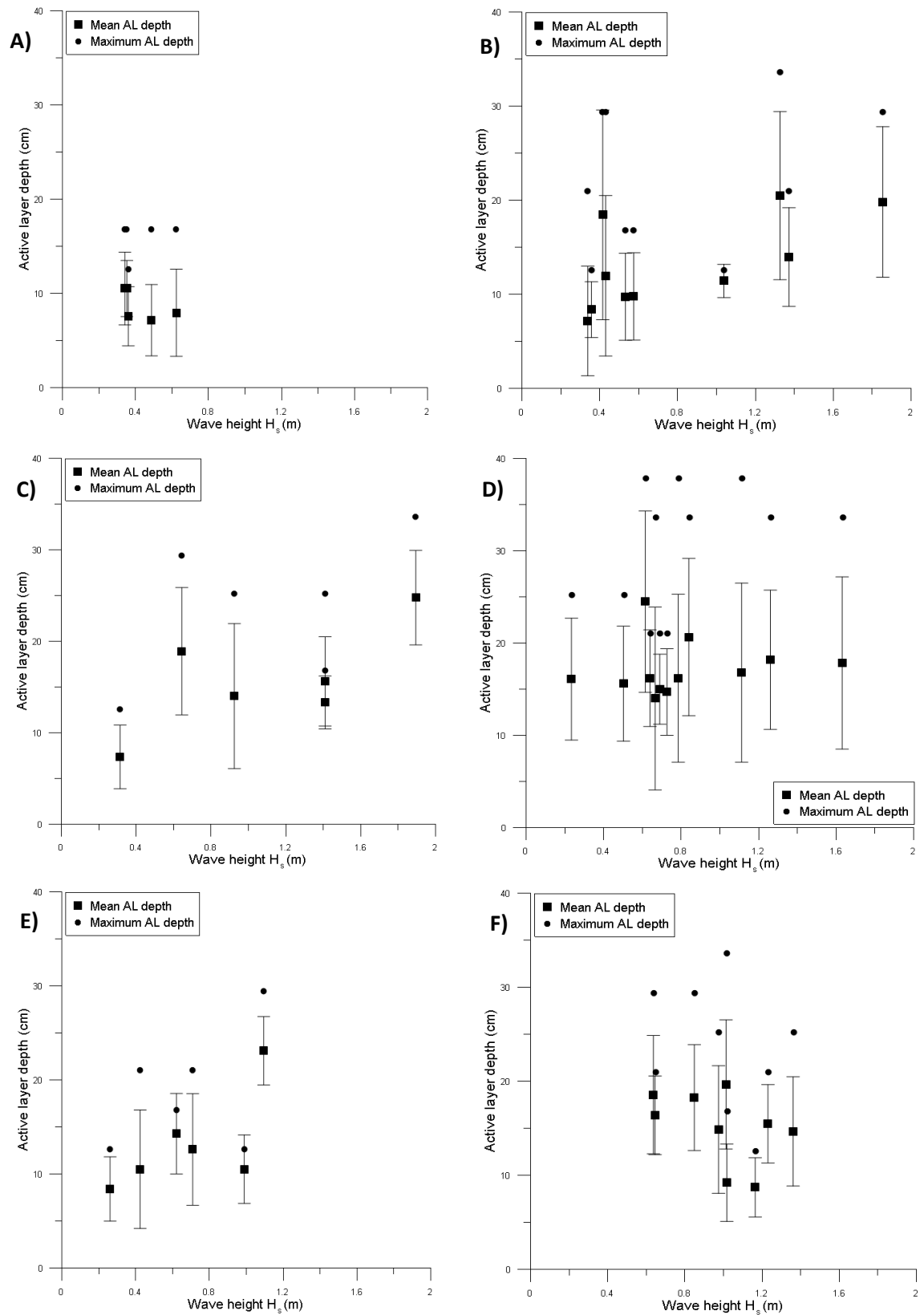


Figure G-2: Active layer variation for study periods during: A) October 2015, B) November 2015, C) December 2015, D) January 2016

Appendix H : Mean, maximum and standard deviations of daily AL measurements in relation to wave height, separated by study period.



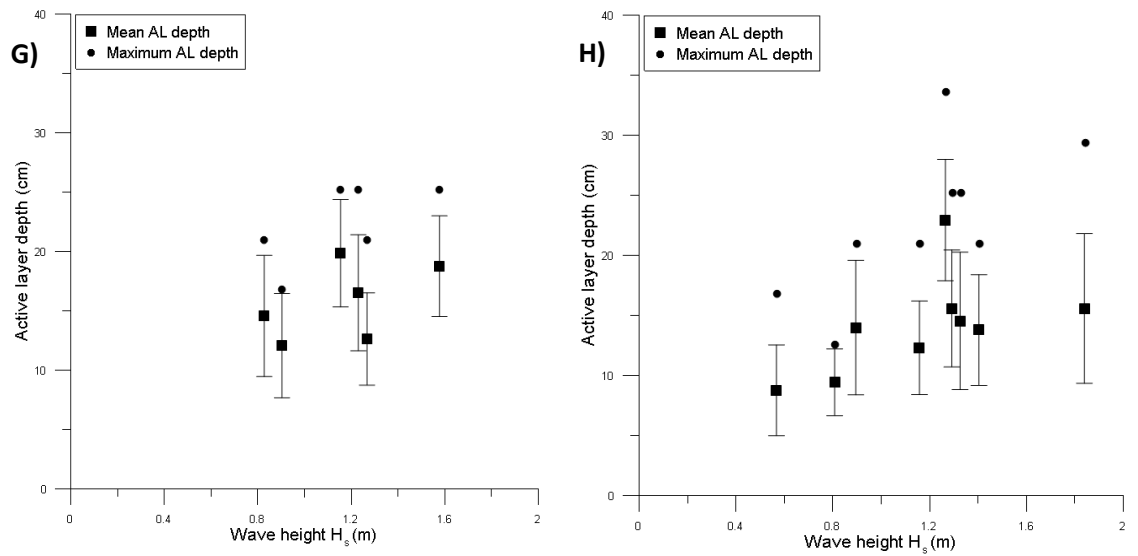
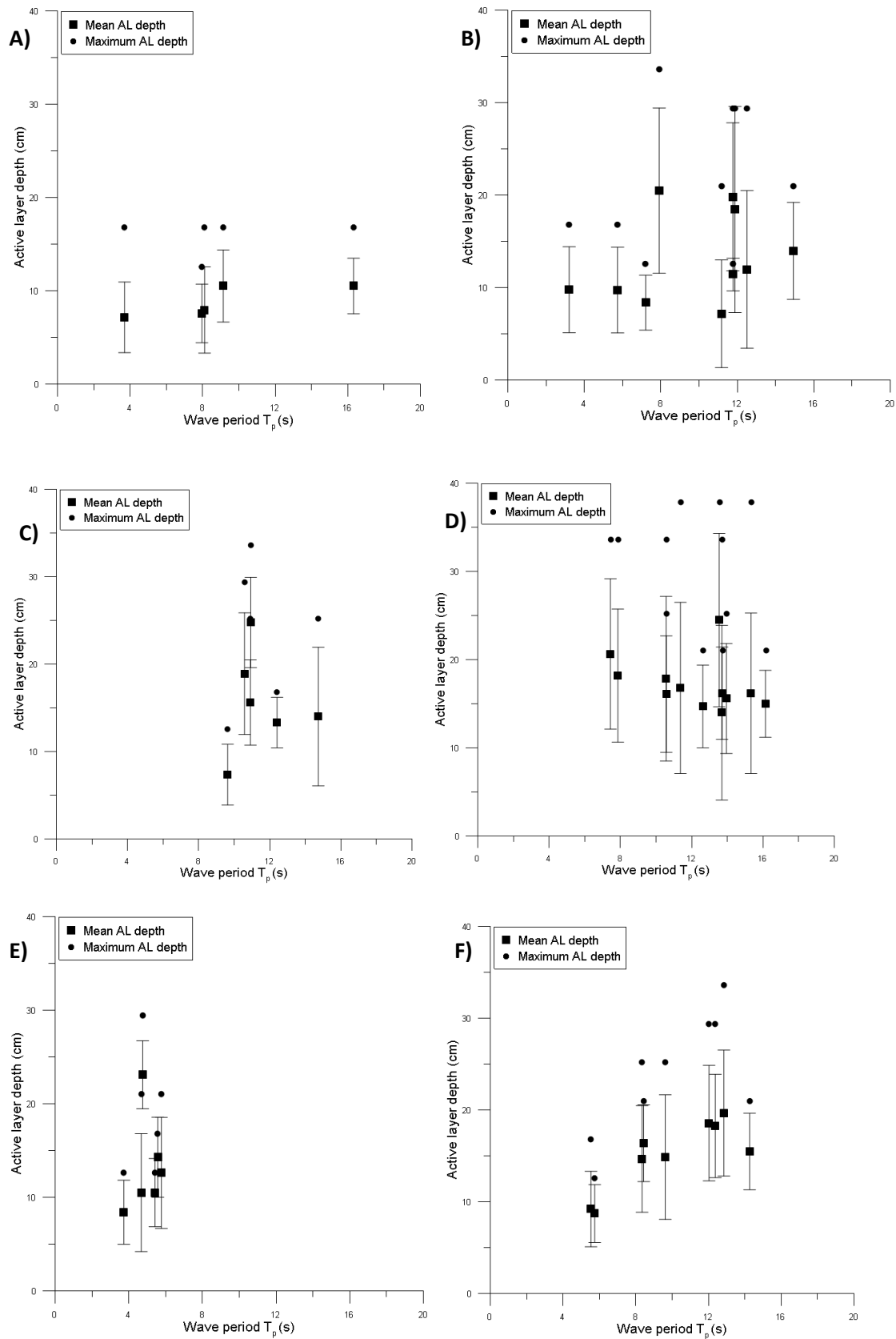


Figure H-1: Variation in daily mean and maximum AL depth on the mixed sediment beach, according to wave height (H_s) for A) October 2014, B) December 2014, C) January 2015, D) February 2015, E) October 2015, F) November 2015, G) December 2015, H) January 2016. Bars represent one standard deviation from the mean.

Appendix I : Mean, maximum and standard deviations of daily AL measurements in relation to wave period, separated by study period.



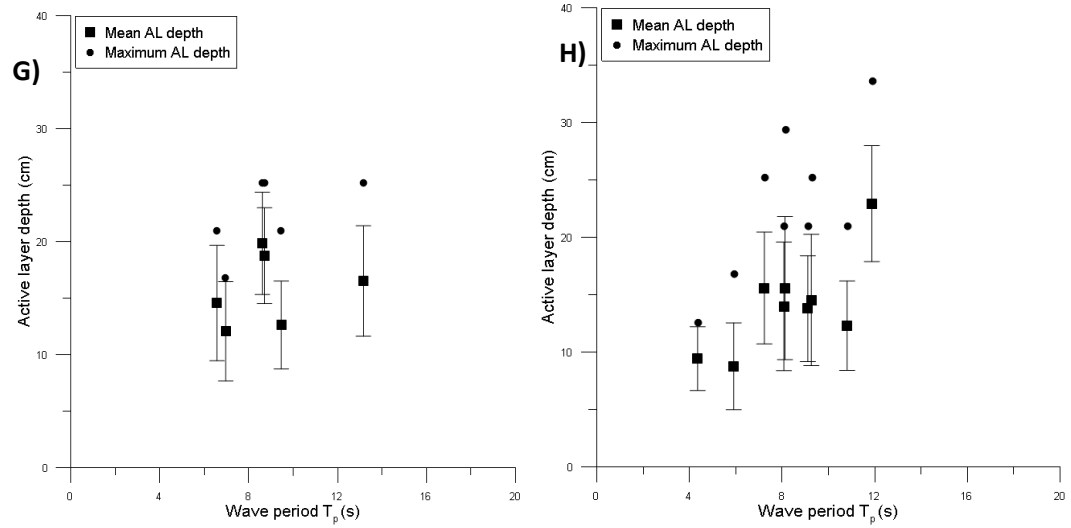


Figure I-1: Variation in average and maximum AL depth measurements according to wave period for each study period. A) October 2014, B) December 2014, C) January 2015, D) February 2015, E) October 2015, F) November 2015, G) December 2015, H) January 2016. Bars represent one standard deviation from the mean.

Appendix J : i) Daily mean AL measurements of each study period, in relation to wave direction (Winter 1).

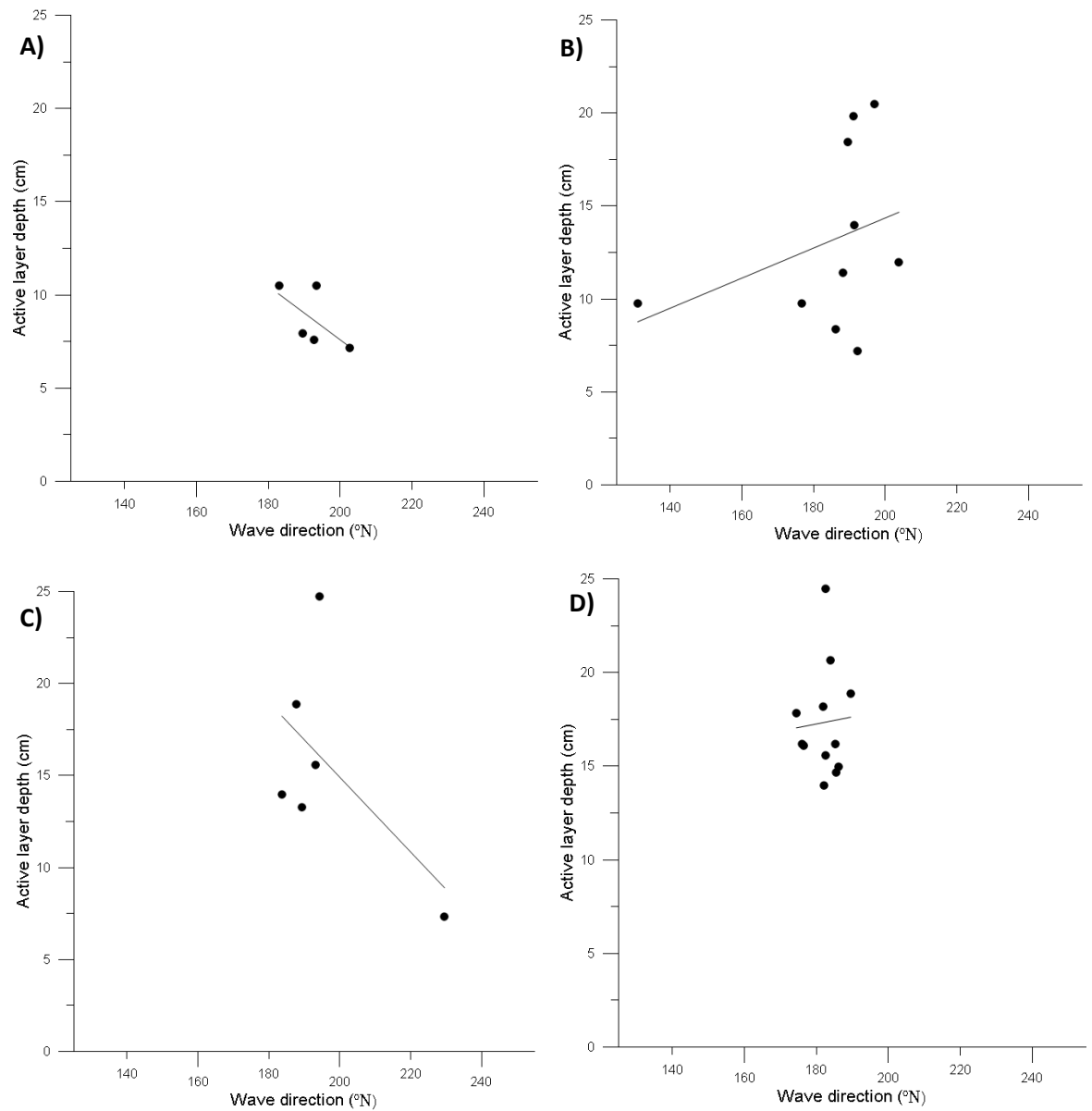


Figure J-1: Scatterplots showing daily average active layer measurements plotted against wave direction during each study period. A) October 2014, B) December 2014, C) January 2015, D) February 2015.

ii) Daily mean AL measurements of each study period, in relation to wave direction (Winter 2).

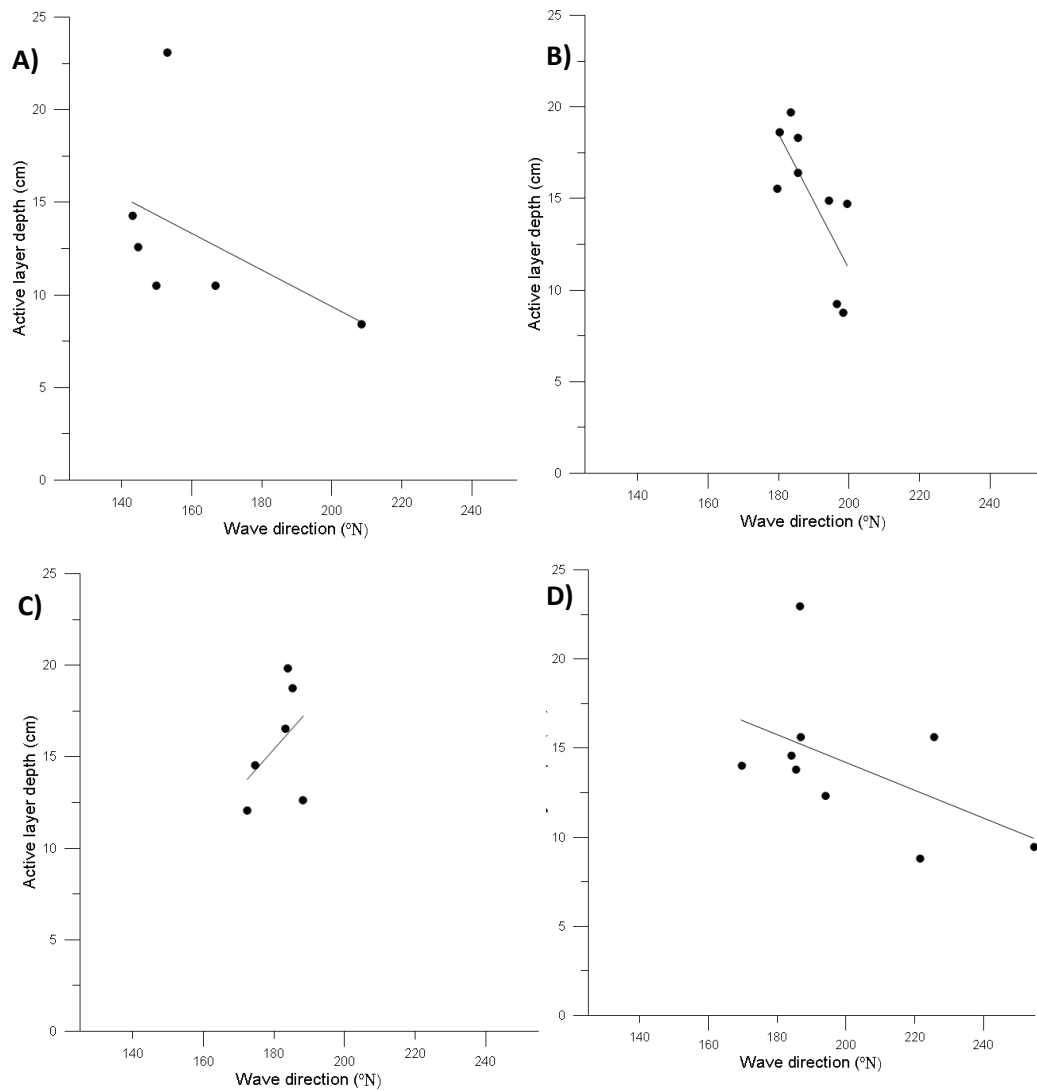


Figure J-2: Scatterplots showing daily average active layer measurements plotted against wave direction during each study period. A) October 2015, B) November 2015, C) December 2015, D) January 2016.

Appendix K : Relationship between average sand content and AL depth.

Table K-1: Variation in average sand content for each study period, alongside average AL depth values.

Month	Average sand content (%)	Average AL depth (cm)	Average AL depth as % Hs
October 2014	18.67	8.67	21.67
December 2014	26.62	12.99	20.72
January 2015	22.34	15.96	15.62
February 2015	24.28	17.33	25.74
March 2015	35.58	14.81	23.99
October 2015	20.65	13.3	20.99
November 2015	27.55	15.53	17.28
December 2015	20.18	15.73	13.86
January 2016	23.91	14.57	12.39

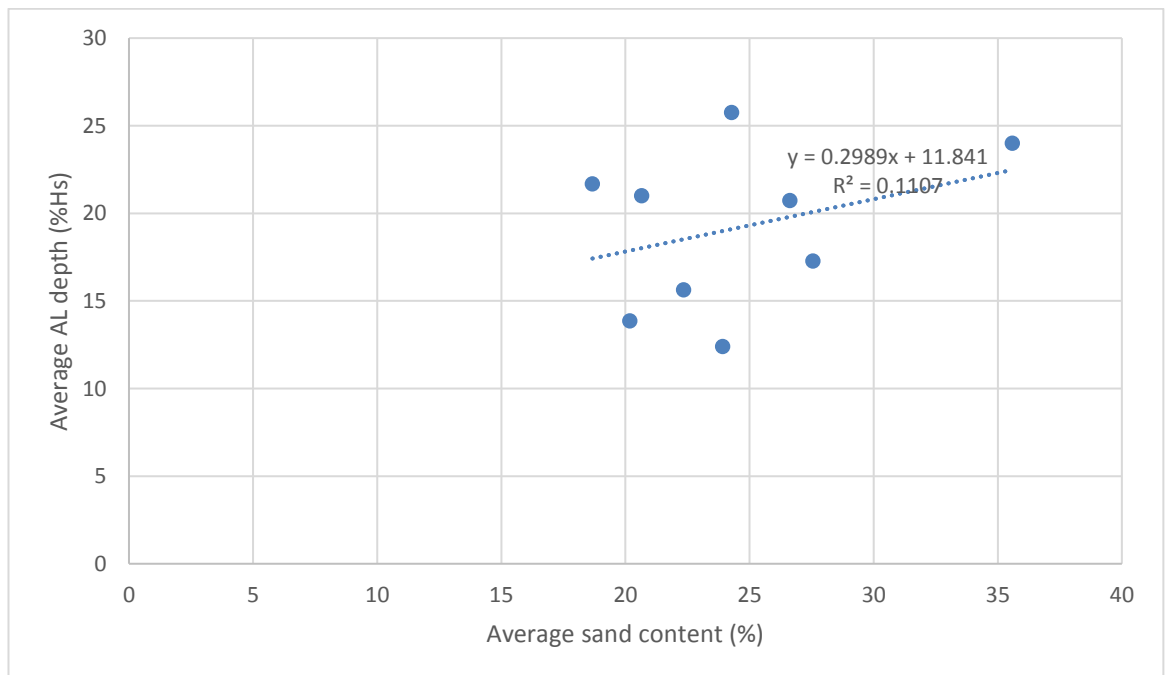
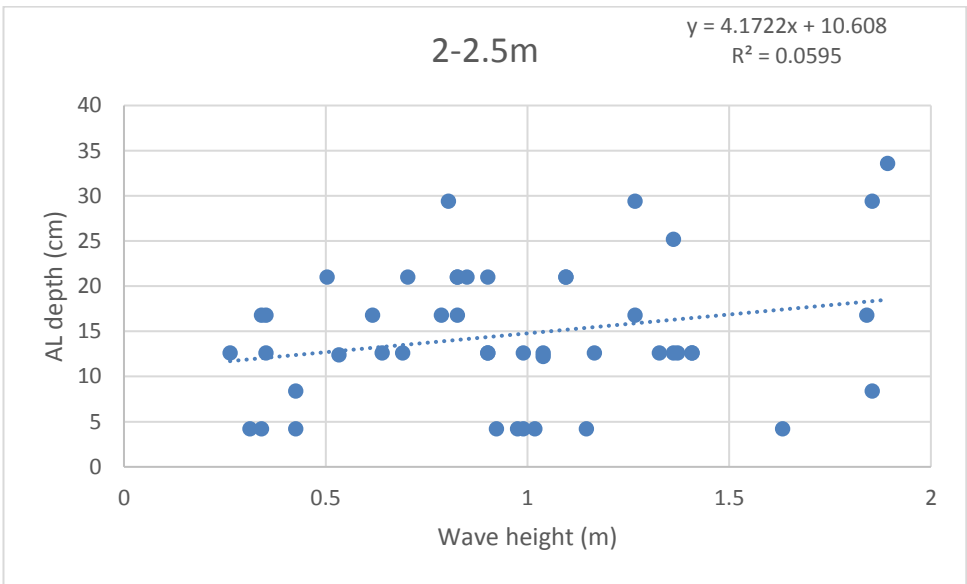
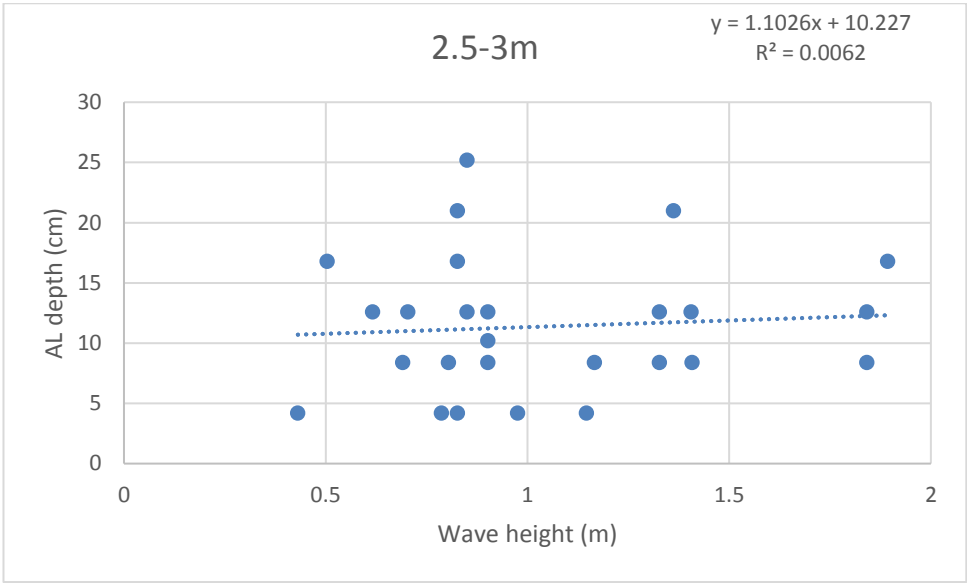
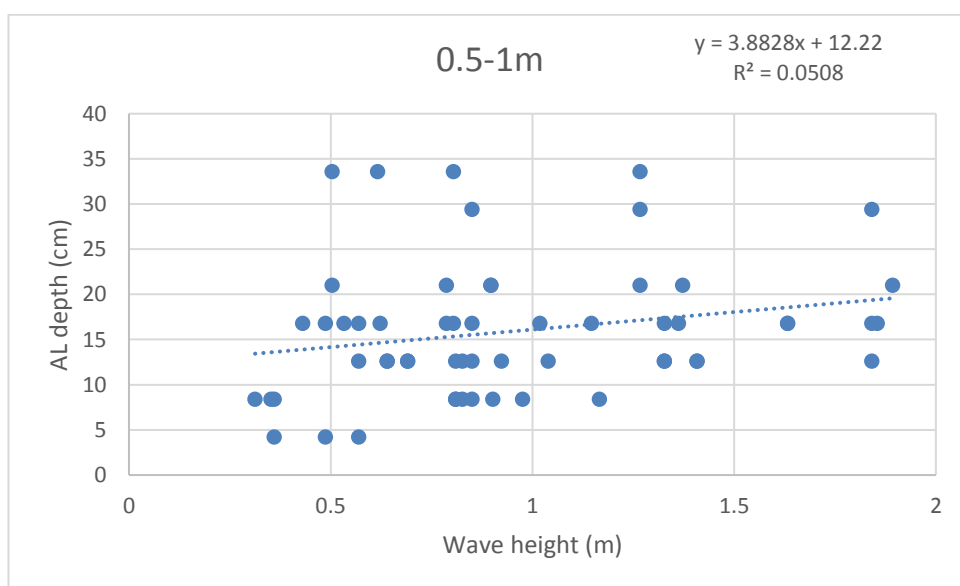
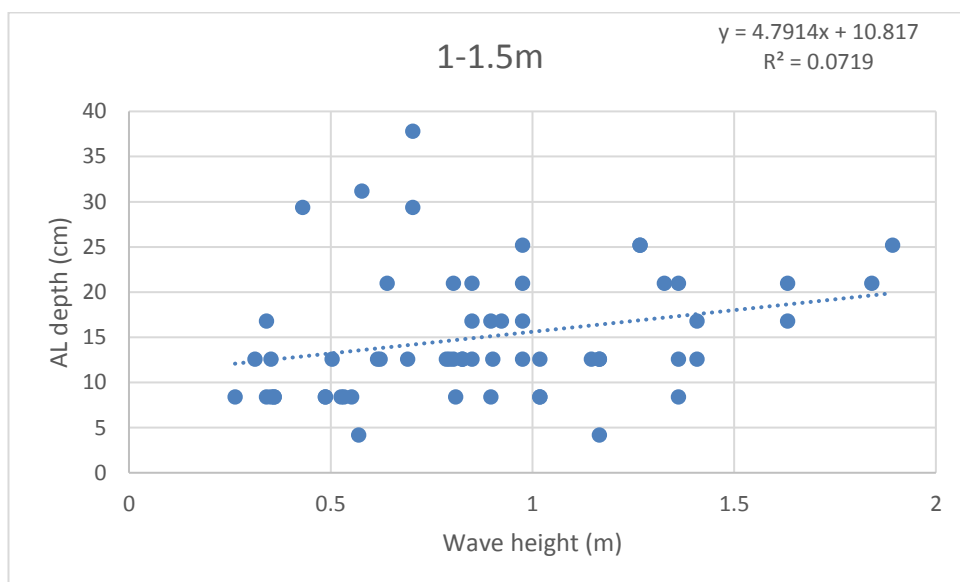
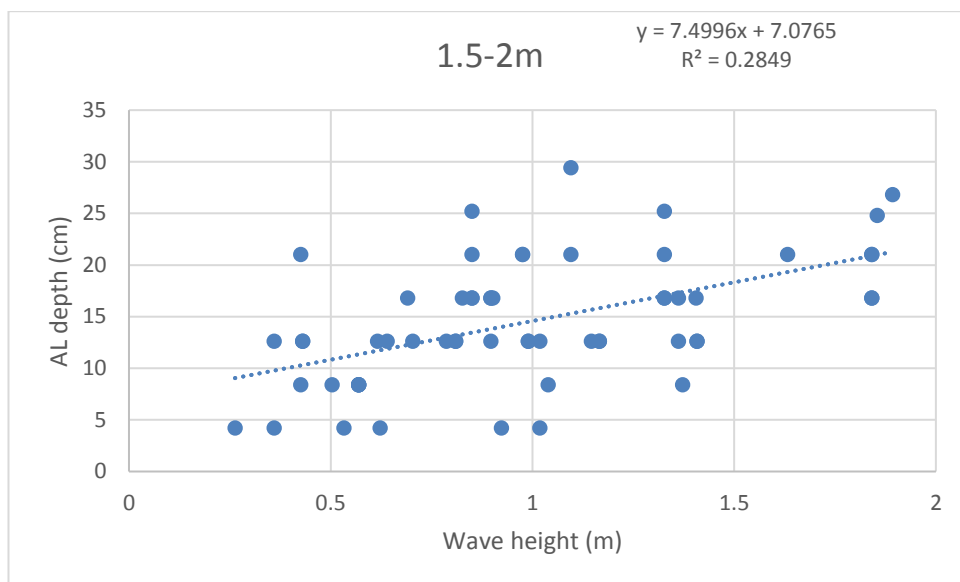
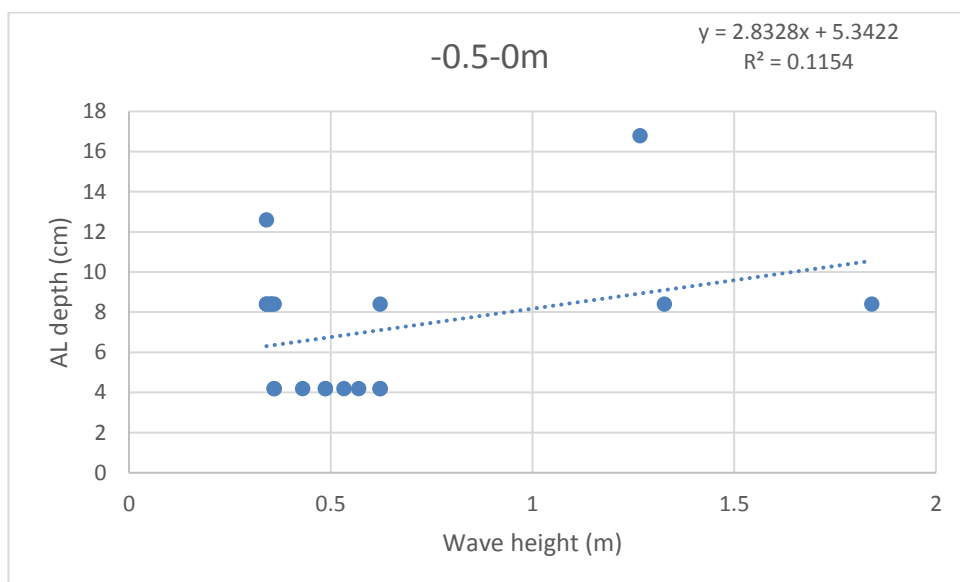
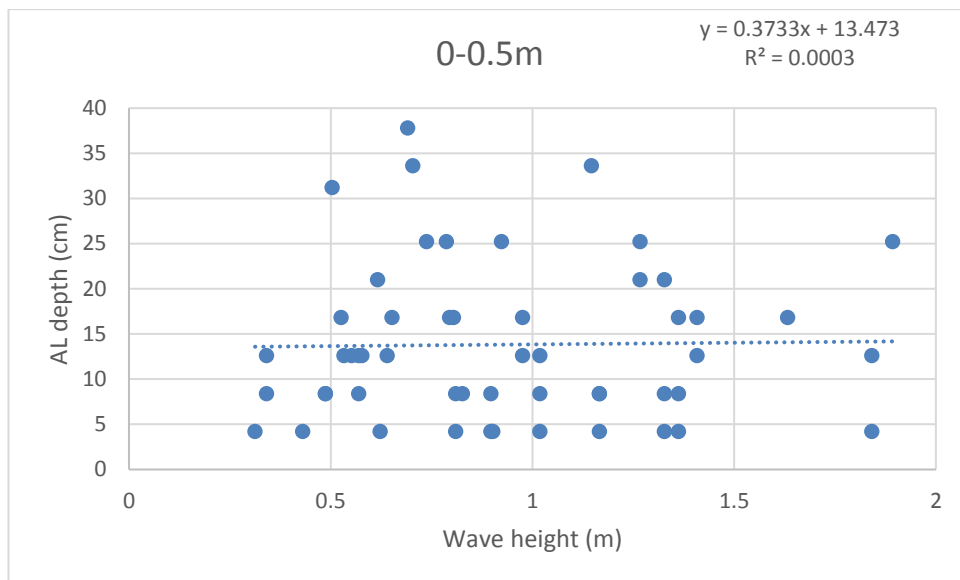


Figure K-1: Scatterplot showing monthly average sand content against monthly average AL depth as a percentage of wave height.

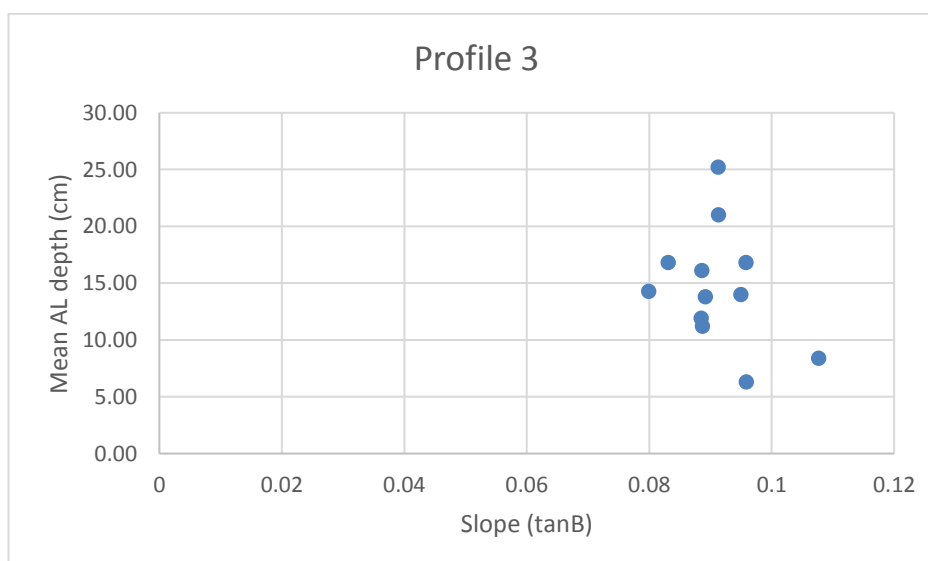
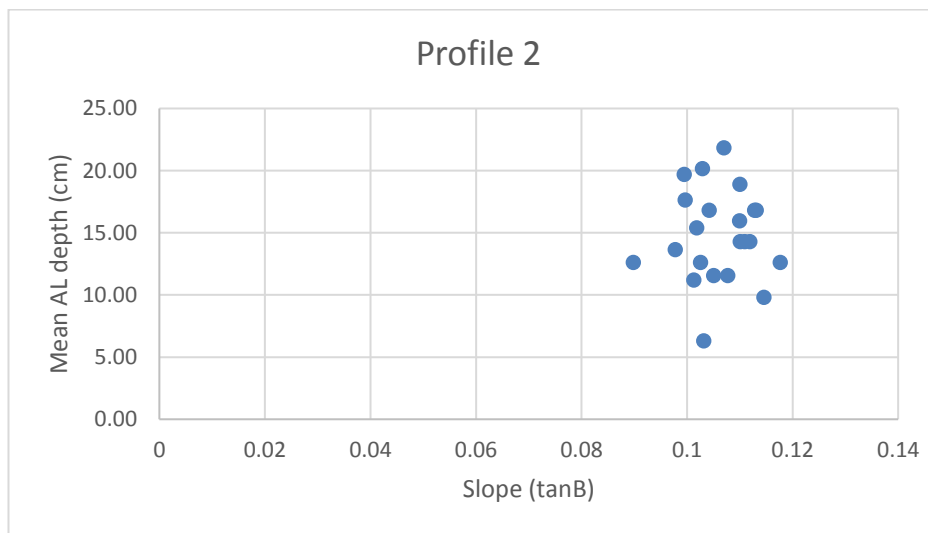
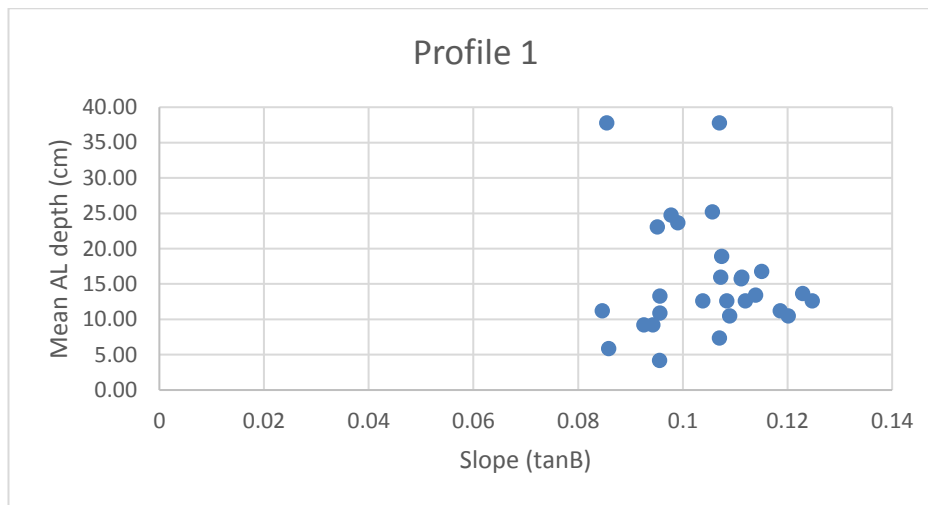
Appendix L : Scatterplots showing relationship between wave height and AL depth within each elevation zone.







Appendix M : Relationships between slope angle and AL depth for each profile



Appendix N : RFID detector tests

The range of the RFID detector was tested by burying pebbles in various sediment types on different parts of the beach profile, with the tags either perpendicular or parallel to the beach surface. This was intended to illustrate whether different sediment types have an impact on detection range, and whether tag orientation influences detection. Results are presented in the table below.

Location 1, lower beach. (Sandy, high groundwater levels)

Location 2, upper beach. (Pebbles.)

Location 3, mid beach. (Mainly sand, fairly dry) The experiment was not completed with parallel tag orientation at this location.

Table N-1: Detection depths from tests of RFID detector for different tag sizes in different sediments.

	Tag size (mm)	Depth (cm)		
		Location 1	Location 2	Location 3
Perpendicular tag orientation	32	40	45	40
	23	20	50	35
	12	< 20	< 20	< 10
Parallel tag orientation	32	30	65	-
	23	40	30	-
	12	20	< 20	-

Appendix O : Pebble deployments and distance between survey detections

Date	Easting	Northing	Elevation (m)	Depth (m)	Pebble Number	Distance since previous detection (m)																										
						23/02/2015	27/02/2015	09/03/2015	10/03/2015	11/03/2015	12/03/2015	15/03/2015	17/03/2015	23/03/2015	24/03/2015	10/04/2015	11/04/2015	14/04/2015	20/04/2015	04/05/2015	21/10/2015	10/11/2015	26/11/2015	03/12/2015	04/12/2015	07/01/2016	13/01/2016	14/01/2016	20/01/2016	24/01/2016	28/01/2016	27/02/2016
30/09/2014	474396.6	97987.36	0.553	0.08	193																											
				0.12	196																											
				0.17	209																											
				0.22	169																											
				0.28	152	125																										
				0.35	184																											
30/09/2014	474441.9	97983.71	0.394	0.40	213																											
				0.10	135																											
				0.16	175																											
				0.20	192																											
				0.25	134																											
				0.30	197																											
30/09/2014	474437.2	97989.13	0.732	0.39	150																											
				0.12	128																											
				0.19	211																											
				0.23	119																											
				0.28	202																											
				0.34	130	85																										
30/09/2014	474431.1	97993.5	0.959	0.40	146																											
				0.10	296																											
				0.14	214																											
				0.20	319																											
				0.28	267																											
				0.35	257																											
30/09/2014					0.42	260																										

[illegible]

Distance since previous detection (m)																															
27/02/2016	28/01/2016	24/01/2016	20/01/2016	14/01/2016	13/01/2016	07/01/2016	04/12/2015	03/12/2015	26/11/2015	10/11/2015	21/10/2015	04/05/2015	20/04/2015	14/04/2015	11/04/2015	10/04/2015	24/03/2015	23/03/2015	17/03/2015	15/03/2015	12/03/2015	11/03/2015	10/03/2015	09/03/2015	27/02/2015	23/02/2015	Pebble Number				
Depth (m)																															
Elevation (m)	1.089							-0.599							-0.157							1.072									
Northing	97996							97973.27							97979.68							97994.27									
Easting	474433							474430.2							474431							474433.4									
Date	09/03/2015							13/03/2015							13/03/2015							13/03/2015									

Date	Easting	Northing	Elevation (m)	Depth (m)	Pebble Number	Distance since previous detection (m)									
						10/11/2015	26/11/2015	03/12/2015	04/12/2015	07/01/2016	13/01/2016	14/01/2016	20/01/2016	24/01/2016	28/01/2016
20/10/2015	474444.1	97996.05	1.445	0.05	483										
				0.1	129										
				0.15	464	6.1									
				0.2	156		114								
				0.25	203										
				0.3	422	36									
				0.35	189										
				0.4	469										
20/10/2015	474444	97988.7	0.658	0.05	480										
				0.1	110	21		53							12
				0.15	413										
20/10/2015	474441.9	97979.39	-0.116	0.2	200	22									
				0	122										
				0.05	511	-29									
09/11/2015	474417.7	97991.63	0.423	0.1	390										
				0.15	383	18	-9								
				0.05	194	57									
09/11/2015	474419.5	98000.01	1.281	0.1	345										
				0.15	170	6.7	98								
				0.05	310			189							
				0.1	207	26	173								
09/11/2015	474420.3	98007.13	2.145	0.15	113		102								
				0.2	325			77				170			
				0.05	179			94							
				0.1	354			205							
02/12/2015	474444.4	97982.64	0.085	0.15	143		104								
				0.2	363										
				0.25	151	5.5	-19								
02/12/2015	474445.5	97990.27	0.897	0	347			-22							
				0.05	284			-15							
				0.1	507			-7							
02/12/2015	474446.5	97998.02	1.555	0.05	282						2		-15		
				0.1	225										
				0.15	123			-30							
				0.2	315										
				0.05	148										
02/12/2015	474446.5	97998.02	1.555	0.1	212										
				0.15	509										
				0.2	160										
				0.25	400										
02/12/2015	474446.5	97998.02	1.555	0.3	355										
				0.3	355										

Date	Easting	Northing	Elevation (m)	Depth (m)	Pebble Number	Distance since previous detection (m)						
						07/01/2016	13/01/2016	14/01/2016	20/01/2016	24/01/2016	28/01/2016	27/02/2016
06/01/2016	474465.9	98003.41	1.947	0.05	323							
				0.1	141	1			-5		14	
				0.15	142	1			4			
				0.2	341							
				0.25	314							
				0.3	195							
06/01/2016	474463.9	97992.3	1.284	0.05	232						-114	
				0.1	298				-1	-25		
				0.15	288							
				0.2	165							
				0.25	173							
				0.3	352							
06/01/2016	474461.2	97985.99	0.787	0.05	185		-16			2		-4
				0.1	289	-32	27					
				0.15	305							
				0.2	168							
				0.25	249						-31	
				0.3	205							
06/01/2016	474445.2	98000.63	1.785	0.05	340							
				0.1	111							
				0.15	350							
				0.2	161				-5			
				0.25	223							
				0.3	313							
06/01/2016	474443.2	97992.21	0.959	0.05	293		-9			0.9	16	
				0.1	262				35			
				0.15	408	-14						14
				0.2	109	-14			-2	7.1		
19/01/2016	474467.6	98012.28	3.183	0.05	269				1.2	-19		
				0.1	164				1.2	-16		
				0.15	320							
				0.2	172				1.2			
				0.25	318					2.2		
				0.3	159					2.2	-10	
19/01/2016	474466	98005.43	2.558	0.05	187					-13	14	
				0.1	120					-32		
				0.15	321					-60		
				0.2	238							
				0.25	258					-33		
				0.3	316							
19/01/2016	474465.1	97996.55	1.724	0.05	154				13	-10		
				0.1	107				-48			
				0.15	335				-4			
				0.2	201					-3	10	0
				0.25	250						84	
				0.3	138				5	-37		
19/01/2016	474462	97978.43	0.071	0.05	333				-7			
				0.1	167				-6			
				0.15	332				-1		82	
				0.2	121				0.7		22	

Date	Easting	Northing	Elevation (m)	Depth (m)	Pebble Number	Distance since previous detection (m)						
						07/01/2016	13/01/2016	14/01/2016	20/01/2016	24/01/2016	28/01/2016	27/02/2016
19/01/2016	474444.2	97980.29	0.043	0.05	149				6.3			
				0.1	294				27			
				0.15	132				26		20	
				0.2	351				31			
19/01/2016	474444.9	97988.22	0.821	0.05	538							
				0.1	116				-5			
				0.15	171				1.7		51	
				0.2	356				34			
				0.25	182				34	-50		
19/01/2016	474445.9	97996.77	1.595	0.05	242							
				0.1	216						46	
				0.15	336					5.6		
				0.2	180				4.2		17	
				0.25	251					-25		
19/01/2016	474447	98006.11	2.557	0.3	228					1.3	8	
				0.05	259							
				0.1	243							
				0.15	147							
				0.2	220							
				0.25	204							
25/01/2016	474447.6	98014.58	3.565	0.3	240							
				0.05	301							
				0.1	176							
				0.15	278							
				0.2	177						104	
25/01/2016	474446.9	98006.85	2.434	0.25	328							
				0.3	131							
				0.05	178							
				0.1	334							
				0.2	155							
25/01/2016	474445	97989.97	1.013	0.25	317							
				0.3	139							
				0.05	246							
				0.1	271							
				0.15	137							
25/01/2016	474421.7	98013.46	3.113	0.2	364							
				0.25	302							
				0.05	126						108	
				0.1	273							
				0.2	198							2.7
25/01/2016	474421	98001.21	1.654	0.25	272							
				0.35	245							
				0.05	274							
				0.1	199							
				0.15	306							
25/01/2016	474419	97991.23	0.767	0.2	112							
				0.25	174							
				0.3	140							
				0.05	145							
				0.1	295							
25/01/2016				0.15	396							
				0.2	163						82	
				0.25	136							

Appendix P : Pebble column detection rates in individual surveys

Deployment Date / Column	Detection rates of each survey [dates with correct location data available] (%)																									Total % detected		
	23/2/15	27/2/15	9/3/15	10/3/15	11/3/15	12/3/15	15/3/15	17/3/15	23/3/15	24/3/15	10/4/15	11/4/15	14/4/15	20/4/15	4/5/15	21/10/15	10/11/15	26/11/15	3/12/15	4/12/15	7/1/16	13/1/16	14/1/16	20/1/16	24/1/16		28/1/16	27/2/16
30/9/14 (1) n=7	14.3		14.3						14.3			14.3			14.3		14.3		14.3									85.7
30/9/14 (2) n=6																								16.7				33.3
30/9/14 (3) n=6	16.7			16.7					16.7	16.7	33.3				16.7				16.7			16.7						83.3
30/9/14 (4) n=6									16.7			16.7		16.7														50
30/9/14 (5) n=7																												42.9
30/9/14 (6) n=4																						25						75
30/9/14 (7) n=7																												50
30/9/14 (8) n=5																												40

Deploy- ment Date / Column	Detection rates of each survey [dates with correct location data available] (%)																									Total % detected	
	23/2/15	27/2/15	9/3/15	10/3/15	11/3/15	12/3/15	15/3/15	17/3/15	23/3/15	24/3/15	10/4/15	11/4/15	14/4/15	20/4/15	4/5/15	21/10/15	10/11/15	26/11/15	3/12/15	4/12/15	7/1/16	13/1/16	14/1/16	20/1/16	24/1/16		28/1/16
30/9/14 (9) n=5																											20
30/9/14 (10) n=7		14.3												14.3			14.3						14.3				42.9
4/12/14 (1) n=6					33.3	16.7	16.7	16.7	16.7	33.3											16.7	16.7					33.3
4/12/14 (2) n=5																											20
15/1/15 (1) n=5		20							20						20												60
15/1/15 (2) n=4	25	25									25				50				25			25	25				100
15/1/15 (3) n=5		40			20					20																	100
24/1/15 (1) n=5			40	40	20									20	20				20				20				80
24/1/15 (2) n=5					20					20	20				20												60
24/1/15 (3) n=8	17.5			25	25			17.5	25	25	37.5				17.5								17.5				75
9/3/15 (1) n=4				75			25	100	50	75	25				50					25							100

Deployment Date / Column	Detection rates of each survey [dates with correct location data available] (%)																									Total % detected			
					10/3/15	11/3/15	12/3/15	15/3/15	17/3/15	23/3/15	24/3/15	10/4/15	11/4/15	14/4/15	20/4/15	4/5/15	21/10/15	10/11/15	26/11/15	3/12/15	4/12/15	7/1/16	13/1/16	14/1/16	20/1/16		24/1/16	28/1/16	27/2/16
9/3/15 (2) n=6					83.3	83.3	50	50	33.3	33.3	33.3	33.3											16.7						100
9/3/15 (3) n=8					17.5	25	37.5	25	50	25	50	50			25	50													87.5
13/3/15 (1) n=4							50	75	25	25	25	25			25	50													100
13/3/15 (2) n=6							50	33.3	83.3	50	50					16.7			16.7										100
13/3/15 (3) n=5							20	60	40	20	40	40			20			20					20						100
16/3/15 (1) n=4								25	25		25	25			75	25													100
16/3/15 (2) n=5								20	40	40	40	40			20	20		20			20			20					80
16/3/15 (3) n=5								50	50	75	50	50			25		25	25		25			25	50					100
20/3/15 (1) n=4									50			25			25	25													75
20/3/15 (2) n=4									25			25				50									25				75
20/3/15 (3) n=3												33.3				66.7													100

Deployment Date / Column	Detection rates of each survey [dates with correct location data available] (%)																									Total % detected		
									23/3/15	24/3/15	10/4/15	11/4/15	14/4/15	20/4/15	4/5/15	21/10/15	10/11/15	26/11/15	3/12/15	4/12/15	7/1/16	13/1/16	14/1/16	20/1/16	24/1/16		28/1/16	27/2/16
20/3/15 (4) n=3									100	33.3				33.3														100
20/3/15 (5) n=4									25	50				75				25					25					100
20/3/15 (6) n=4									25	50	50			50				25	25				25					100
20/10/15 (1) n=8																	25	12.5										37.5
20/10/15 (2) n=4																	50		25							25		50
20/10/15 (3) n=4																	50	25										75
9/11/15 (1) n=3																	16.7	16.7	16.7									66.7
9/11/15 (2) n=4																	25	50	50					25				100
9/11/15 (3) n=5																	20	40	40									80
2/12/15 (1) n=3																			100									100
2/12/15 (2) n=4																			25				25		25			50

Deploy- ment Date / Column	Detection rates of each survey [dates with correct location data available] (%)																								Total % detected				
																			3/12/15	4/12/15	7/1/16	13/1/16	14/1/16	20/1/16		24/1/16	28/1/16	27/2/16	
2/12/15 (3) n=6																											0		
6/1/16 (1) n=6																					33.3				33.3	16.7		33.3	
6/1/16 (2) n=6																								16.7	16.7	16.7		33.3	
6/1/16 (3) n=6																					16.7	33.3			16.7	16.7	16.7	33.3	
6/1/16 (4) n=6																								16.7				16.7	
6/1/16 (5) n=4																					50	25			50	50	25	25	100
19/1/16 (1) n=6																									50	66.7	16.7		83.3
19/1/16 (2) n=6																									66.7	16.7			66.7
19/1/16 (3) n=6																									66.7	50	33.3	16.7	100
19/1/16 (4) n=4																									100		50		100

Deployment Date / Column	Detection rates of each survey [dates with correct location data available] (%)																								Total % detected
19/1/16 (5) n=4																									100
19/1/16 (6) n=5																									80
19/1/16 (7) n=6																									83.3
19/1/16 (8) n=6																									16.7
25/1/16 (1) n=6																									16.7
25/1/16 (2) n=6																									0
25/1/16 (3) n=5																									0
25/1/16 (4) n=5																								20	40
25/1/16 (5) n=6																								0	0
25/1/16 (6) n=5																								20	20

Appendix Q : Pilot Study (March 2014)

A three-week long pilot study has already been completed at Eastoke, Hayling Island (Figure Q-1). The aim of this was to test methods planned for measurement of sediment characteristics, porosity, and active layer depth. For the majority of the three-week period, wave conditions were gentle, and tides were moving towards springs for the first two weeks and then back towards neap again.

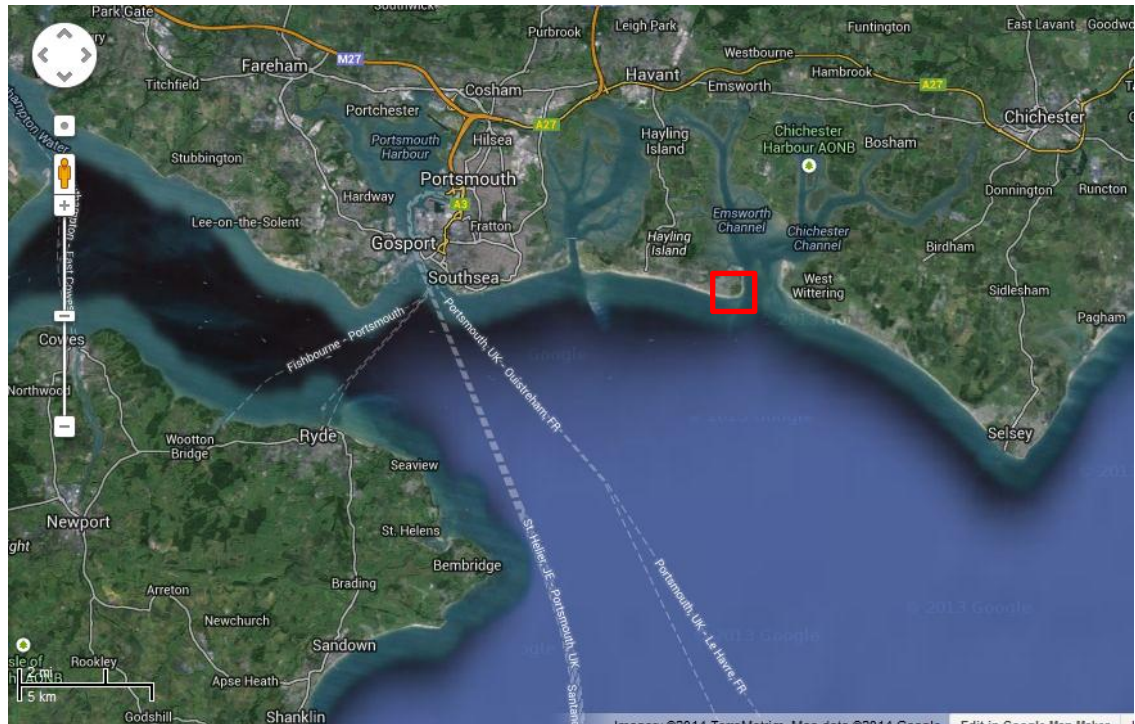


Figure Q-1: Location map of Eastoke, Hayling Island (source: www.maps.google.co.uk)

Trenching

What was done:

On March 10th, an excavator was used to dig five small trenches between the crest of the beach and the (neap) low water line. These ranged in depth from approximately 30 cm to 1.5 m, and their approximate locations can be seen in Figure Q-2 (though due to the multiple harsh storms over the winter, the aerial photography used does not accurately show the location of the beach crest; the topmost sliding indicator device was located at the base of the crest). Clear layers of sediment were visible within the beach subsurface, and the westerly wall of each trench was scanned at 2mm resolution with a Leica C10 terrestrial laser scanner (TLS).

The TLS data was imported and processed in Leica Cyclone, and was then exported as .xyz files and analysed for surface roughness indicators (standard deviation of the depth of points within

an area) using a programme created by Dr Jo Nield of Southampton University. The point clouds were also converted into DEMs using ArcMap.

Issues noted:

The trench was not directly aligned in either the x or y direction in the coordinate system of Leica Cyclone, which was a problem when analysing the data for surface roughness; the programme for these calculations does not take the angle of the trench face into account, and so the standard deviations produced are not solely the result of grain sizes.

This was also a problem when creating DEMs; one end of the DEM is lighter than the other and so increasing the contrast to show the topography of the trench was not successful.

Potential methods to resolve issues:

Scans could be taken face-on to the trench wall (though the intention behind doing two slightly angled scans of each trench is to reduce the shadow effect caused by larger grains in the wall), or, if possible, a coordinate system could be created within Cyclone so that the trench face lies in line with the x coordinates.



Figure Q-2: Locations of trenches, sediment baskets and sliding indicator devices

The trench walls were also photographed with a DSLR and a 14 megapixel Fujifilm digital camera to compare the variation in quality. Both sets of photographs of the individual trench walls were imported into Agisoft Photoscan. This is a programme that automatically aligns overlapping photographs to create a 3D model of the trench wall (Figure Q-3). The white squares visible in the image are the markers used to help Photoscan align the photographs; each one is slightly different, and the software can detect this. If a marker is in more than one photograph, Photoscan uses this to speed up the alignment process.

Overall there does not seem to be a noticeable difference between the outputs of the two cameras, but for Trench 1, which was partially shaded due to the angle of the sun at the time of photographing, the alignment of the Fujifilm camera's photographs did not work due to the shadows visible in most images. Although it is probably not as accurate as the laser scanner, it has the benefit of visually looking like the sediment, which makes identification of layers much simpler. It is hoped that the Photoscan data will produce better results for the surface roughness calculations, but these have not yet been run.

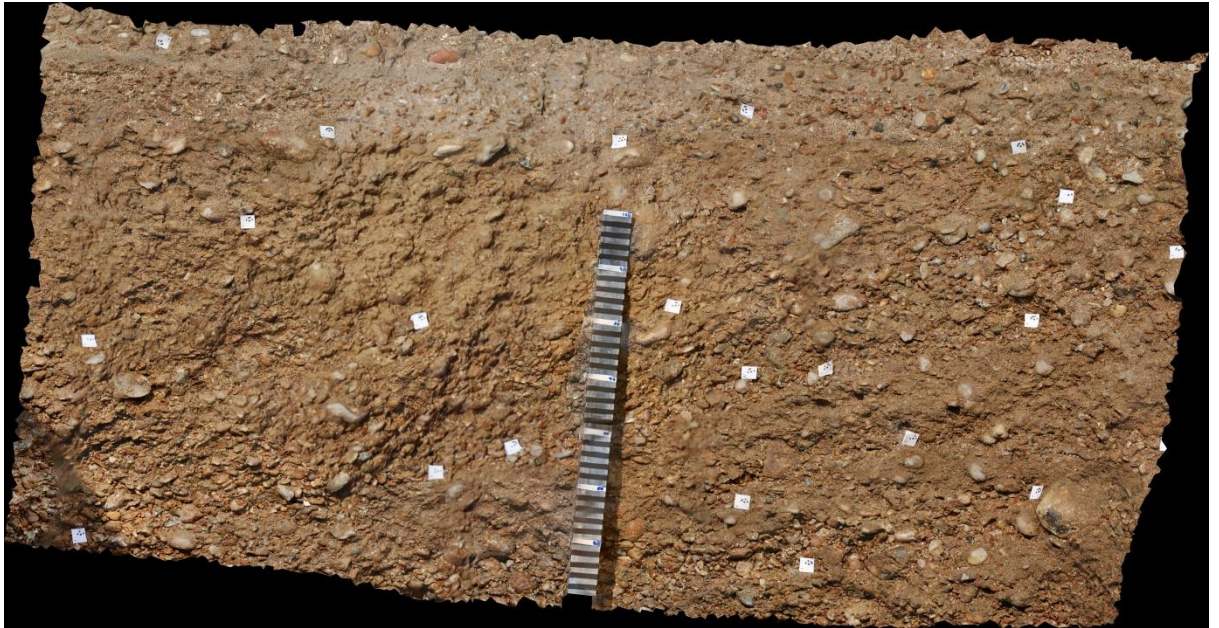


Figure Q-3: Photoscan 3D image of a trench wall

The metre rule was left in the trench for the photographs so that it could be used to mark an approximate scale for the 3D model. It is possible to run surface roughness calculations that avoid this area, but for future experiments it may be more helpful to measure distances between markers so that the metre rule does not need to be left in place.

In addition to laser scanning and photography, sediment samples were taken in each of the trenches for each visible layer. These were dried overnight in an oven and sieved in the lab at Sussex for 15 minutes each to give a clearer picture of the sediment characteristics at Eastoke, Hayling Island. The sieve sizes used were (in millimetres): 0.71, 1, 2, 4, 8, 11.2, 16. The D_{50} of the combined samples is 5 mm. The tables below show the percentage of sediment with grain sizes of <1 mm, and the D_{50} for each sample.

Table Q-1: Trench 1

Sample	% <1mm	D_{50}
T1 S1	17.32	7mm
T1 S2	7.55	9mm
T1 S3	30.97	16mm
T1 S4	8.24	>16 mm
T1 S5	18.16	>16 mm

Table Q-2: Trench 2

Sample	% <1mm	D_{50}
T2 S1	94.88	.5mm

T2 S2	27.88	3mm
T2 S3	48.82	1mm
T2 S4	11.87	9mm
T2 S5	66.79	.5mm
T2 S6	8.24	>16 mm

Table Q-3: Trench 3

Sample	%<1mm	D ₅₀
T3 S1	88.37	.5mm
T3 S2	44.39	1.5mm
T3 S3	78.50	.5mm
T3 S4	27.31	14mm

Table Q-4: Trench 4

Sample	%<1mm	D ₅₀
T4 S1	75.96	.5mm
T4 S2	28.68	6mm
T4 S3	7.74	13mm

Table Q-5: Trench 5

Sample	%<1mm	D ₅₀
T5 S1	53.11	1mm
T5 S2	16.53	10mm

Generally the results indicate that the surface of the beach contains a greater proportion of sand and thus has a smaller D₅₀ than samples taken from lower layers, with Trenches 1, 4 and 5 showing the clearest pattern. Trenches 2 and 3 display more disparity between layers, alternating between layers of finer particles and coarser particles.

Sediment packing patterns

3 sediment tubes were buried in the beach on March 10th, one in the upper section of the beach profile, and two towards the middle. Their locations can be seen in Figure Q-2.

The sediment tubes were made of soil pipe that had been cut with a Jigsaw; there were three different designs for the holes through which water would flow to redistribute the sediment

more naturally (Figure Q-4). The middle tube was created first, but it was decided that the holes were too small to allow sufficient mixing to mimic the natural processes, so the left-hand tube was created with six roughly equal full-length holes, and the right-hand tube had four slightly wider full-length holes. It became evident after burial that the plastic mesh would need to be attached to the top of the soil pipe in order to retain its shape while sediment is being transported in the vicinity. As such, one of the tubes was excavated early and redesigned so that it would better contain the sediment; the mesh was superglued to the top rim of the basket, and an extra layer of mesh was wrapped around the outside to help prevent sediment being trapped between the pipe struts and the mesh.



Figure Q-4: Initial designs of sediment tubes (photo credit: C. Moses)

After four days in-situ, the redesigned tube was excavated and allowed to dry before being transported to Southampton University's CT scanning facility for internal scanning. The tubes were buried containing pure gravel, but a significant amount of sand can be seen in the matrix after removal (Figure Q-5), which suggests that the beach is very active and mixing takes place quickly, even in gentle wave conditions. However, this method is not believed to allow the gravel a great enough freedom of movement to provide an accurate representation of the internal beach structure, so finding a better method has been suggested as a future research project.

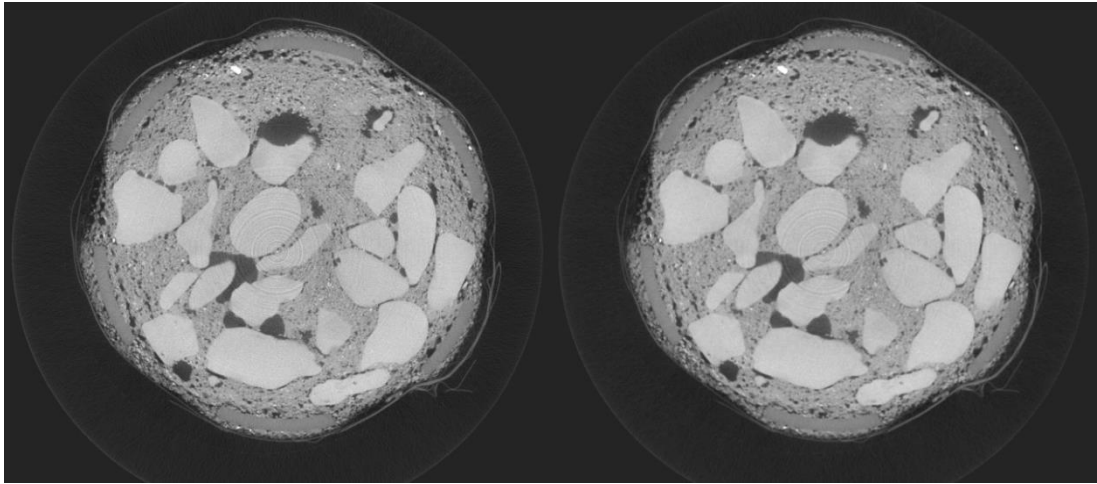


Figure Q-5: Initial scan of sediment packing patterns within sediment tube

Active layer measurements

14 sliding indicator devices were buried on March 10th. The sliding indicator devices are shown in Figure Q-6 and were made of washing line threaded with either plastic or foam golf balls, which were then attached to groyne offcuts provided by HBC. Each sliding indicator device has a foam golf ball attached to the end of the washing line to enable the string to float and help prevent it being covered by sediment as the active layer shifts.



Figure Q-6: Sliding indicator devices (photo credit: C. Moses)

The devices work by allowing the buoyant balls to float to the surface as the sediment around them is disturbed. As such, the number of balls found exposed each day gives an indication of the depth of the active layer. Daily measurements were taken of the number of balls and length of string found exposed, which indicate active depth and erosion/accretion respectively. The exposed balls were then reburied daily so that measurements could be taken for two-tide periods.

Overall, the sliding indicator devices worked well. However, they are susceptible to tampering by passersby, dogs and fishermen (e.g. Figure Q-7). It was noticeable how much less likely damage was when there were signs in the vicinity explaining what the equipment was there

for (the signs were taken away after two weeks), but these devices would still not be appropriate for use on a busier beach – for example in the summer months.



Figure Q-7: Broken sliding indicator device

It has been suggested that attaching a small tag to the end of each chain, with a note saying, for example, ‘do not tamper’ and providing a web address to go to for more details about the experiment may help to deter people, though this would obviously not work for dogs. Photographs were also taken of each sliding indicator device each day, and a view of the overall beach surface, as an indication of how the surface sediments changed over time.

Initial results suggest a correlation between active layer depth and both wave height and wave period. Results have not yet been analysed to determine what effect position on the beach profile has on active layer depth in different wave conditions, but using the average measured active layer depth for each day has provided good initial results. Devices outside of wave run up coverage and thus giving an active depth of 0 cm were excluded from the averages. Figure Q-8 shows the average active depths each day.

Figure Q-9 shows the relationship between average wave height and average active layer depth over approximately the same 24hr period. A Spearman’s Rank correlation coefficient was run on these values, giving a coefficient of $r = 0.44$. However, when the two outlying values were excluded, this coefficient increased dramatically to $r = 0.77$. The best correlation came from average wave period and average active layer depth though, with a value of $r = 0.82$; this is shown in Figure Q-10. This agrees with results found by Hoque and Asano (2007), that a longer wave period leads to a greater active depth measurement.

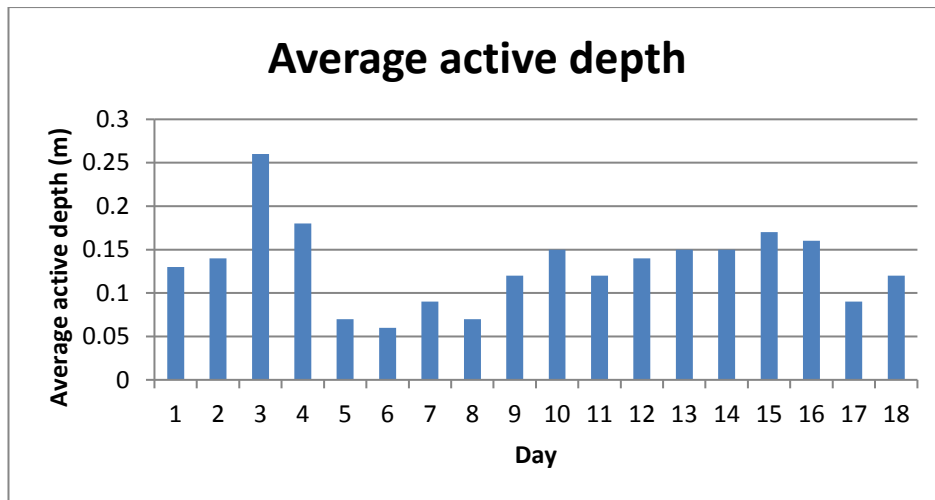


Figure Q-8: Average active layer depths each day after initial burial

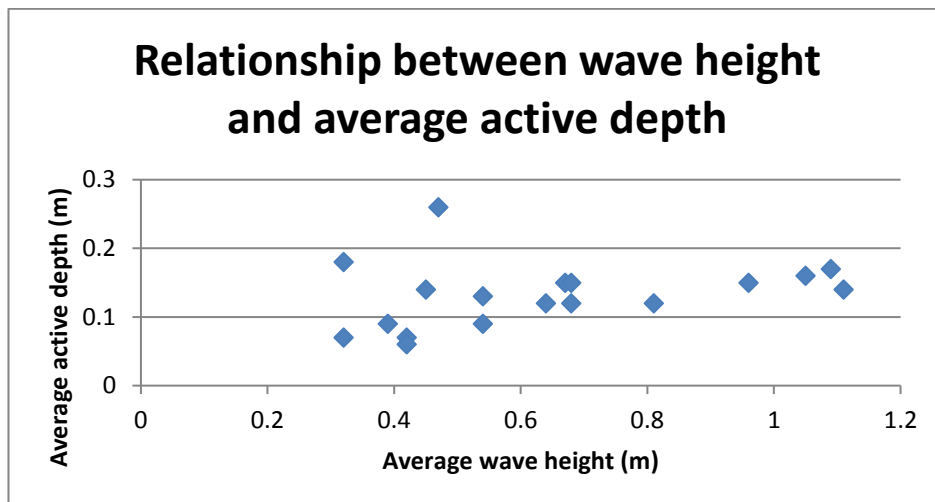


Figure Q-9: Relationship between average wave height and average active depth

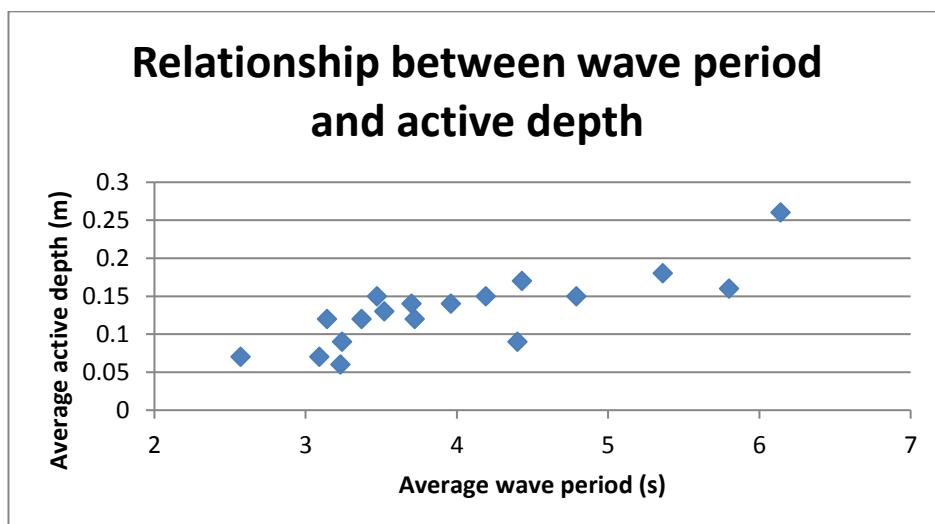


Figure Q-10: Relationship between average wave period and average active depth

Appendix R : Tracer guide

Step 1: Preparation

Choose appropriate tag sizes for the size of pebbles on the beach to be studied

- Bear in mind that smaller tags have a lower discovery rate, so use the largest size possible/appropriate.

Collection of pebbles

- Take large rubble bags to the chosen site
- Use a ruler to choose pebbles of an appropriate size – the C (short) axis needs to be the length of the tag +6mm minimum.
- Count the pebbles into the bags – don't overfill the bags if they need to be carried.
- Collect more than necessary in case of breakages during drilling (about 10% extra)

Drilling

- In the past, Waterloooville based company **ICEE** (icee.co.uk, brian.green@icee.co.uk) have water jetted the pebbles
- They will need to know what diameter of hole to drill – this varies depending on which size tag you are using (and remember to include the silicone sheaths as extra diameter)
- Pebbles need to be laid out in wooden trays, ready to be drilled through their C (short) axis



- In the past, we have used a type of wooden board with regularly spaced holes already drilled in it as the tray base to help lay out the pebbles evenly. Spacing between pebbles must be even as the drilling company set their water jetter to automatically drill a hole every few centimetres (you will need to know what you want them to set this to – it can be different for each tray, e.g. if you have a tray of large pebbles and a tray of small pebbles, so make a note on the side of each tray)

- Use expanding foam to fill the gaps between pebbles and seal the tray with screws and nails
- The trays will need to be transported to the jetting company and picked up after they have been drilled

Order tags



- 12mm, 23mm, or 32mm (Read-only Glass Transponders)
- And tag sleeves (aka Transponder Sheeting) – silicone cases to protect tags and help prevent shattering
- Supplier: **Texas Instruments (www.ti-rfid.com)**

Order resin

- Clear casting epoxy resin + hardener
- Supplier: **ABL (Stevens) Resin and Glass, 01720 766685**
- They should have a record of what HBC have previously purchased

Order talc

- HBC used to have a huge bucket of talc in the store room, but I think this was disposed of during the move to the new store.
- The Health and Safety sheet says it is 'Talc – Hydrated Magnesium Silicate'
- Supplied by **J M Loveridge plc (Southbrook Rd, Southampton. 023 8022 2008)**

Step 2: Tagging pebbles

Equipment required:

- Drilled pebbles
- Tags
- Tag sleeves
- Resin (2 parts (resin & hardener) + barrites/talc)
- Plastic cups
- Wooden spatulas (coffee stirrers/kebab sticks)
- Newspaper/disposable plastic covering for the work surface
- Sellotape
- Face mask
- Gloves (e.g. blue medical gloves) – although the resin is not necessarily harmful to skin, it is very sticky and difficult to wash off
- Weighing scales
- Callipers
- Small RFID detector (cricket bat)

- Laptop (Excel)
- Camera

Method

1. Scrub all drilled pebbles to remove excess packing foam
2. Stick a small square of sellotape over one side of each drilled hole. Place pebbles on the covered work surface with the taped side down
3. Insert tags into tag sleeves
4. Mix a batch of resin in a plastic cup ***
5. Scoop a small amount of resin into each pebble using a spatula (fill about halfway)



6. Push a tag into each hole
 7. Add more resin as necessary
- Repeat steps 3-6 until all tags have been inserted.
8. Once resin has hardened, catalogue pebbles and add data to Excel spreadsheet:
 - a. Check tag ID using small RFID detector (& add which size tag it is to a separate column of the spreadsheet, e.g. 32mm)



- b. Weigh pebble
- c. Measure A, B, C axes using callipers (optional, depending on what data you'll want to analyse later)
- d. Give each pebble a unique 3 or 4 digit number. Write this on pebble in permanent marker. (If possible, make sure these do not coincide with previous deployments on the same beach.)
- e. If necessary, photograph all pebbles.

*** Mixing the resin

Health & safety information on the resin packaging says to wear a face mask during mixing. Specifically, avoid breathing the dust of the talc.

Mix in small batches to reduce waste. Proportions for the resin will be on the bottle (usually 1 part hardener to 2 parts resin). Original methodology suggests adding 3 parts mixed resin to 5 parts talc (e.g. 60ml of resin to 100g of talc).

Depending on the temperature in the room, resin setting times can vary wildly. During winter months, it can take days to fully set, but during summer the resin becomes unusable quickly and sets solid within 24 hours.

Step 3: Deployment

Numbers

Between 30-100 pebbles per location, depending on how many locations / how often you plan to re-deploy.

Locations

- in previous surveys, MSL has most frequently been used
- I did a small pilot study to check detection rates of pebbles deployed at +2.1m, 0m and -1m OD. The lowest re-detection rates were for those pebbles deployed at -1m (average 11%, with 4 surveys returning 0 tagged pebbles), with the highest at 2.1m (39%) and 33% at 0m.

Mark deployment locations with dGPS

- marking the centre of the deployment square should be good enough, as the dGPS is a lot more accurate than the detection kit used later.

Deciding on survey frequencies

Previously, surveys have been done once every 3 months (after an initial check a few days after deployment).

Re-detection rates decrease rapidly after the first week or so. As such, I would recommend doing a couple of surveys in the first few weeks and then one per month for approximately 6 months. But it depends what data you want, and how much you have to spend / whether you can get casual workers or not.

The best tides are spring tides, which unfortunately tend to fall at the beginning and end of the day. Try to get the maximum amount of daylight on either side of the tide to maximise the survey time and thus area of beach covered per day.

Step 4: Surveys

ESCP kit

Pre-survey

- Charge lead batteries
- Charge GPS handset

At beach

Need: RFID antenna, backpack with box inside, lead batteries, handheld GPS (PDA), cable to connect GPS to RFID detector, tester pebbles (2), document explaining how to fix GPS-cycling issue

- Connect PDA to RFID box in backpack with cable (9-pin plugs either end)
- Plug in lead battery
- Switch on PDA, open RFID pocket programme
- Set up as follows:
 - GPS: comm port 2 (or 3, depending on which handset you are using), baud rate 4800. Note: if GPS box shows cycling data rather than just upwards-counting GGA data, follow the instructions in the 'common issues' section.
 - RFID: comm port 1, baud rate 9600. Once a pebble has been detected, the most recent tag ID will show in this box.
 - File name format: yyyyymmdd-initials. Click save **BEFORE** you start surveying, otherwise there will be no data recorded!
- Depending on the length of time you are surveying for, it may be necessary to change the battery in the backpack (detection range decreases the longer you are in the field for). I would recommend changing the battery halfway if you are surveying for much more than two hours.
- To change the battery, do not disconnect the PDA from the cable. Simple unplug the red and black cables and plug in a new battery. Test that the detector is still working with a tester pebble. If it doesn't show up in the RFID box on the screen of the PDA, click on this box and reset the comm port. Test again – it should work now. (Remember that the PDA will only show a new detection if it is different from the previous one, so you may need to use two pebbles.)

- At the end of the survey, exit the RFID pocket programme and click yes. Data will save automatically.
- If for any reason you need to stop mid-survey and restart the equipment etc., use a new file name when you restart (e.g. yyyyymmdd-initials-2), otherwise it will overwrite your previous data.
- Common problems are:-
 - (i) *GPS location info scrambling and numbers and letters randomly rotating.*
To fix this fault, the settings in SirfTech need to be changed.*
 - (ii) *GPS numbers static*
Part of the GPS coordinates info counts upwards in seconds. If it is not doing this, first try clicking on the GPS button, reselecting the [com] port, resetting the Baud rate to 4800 and clicking OK. If this does not work, you will need to reboot. If problem persists take the top off the handset and check the card is in correctly, you'll notice it is held in position with a wedge of paper, this is to prevent this GPS problem occurring and it may have slipped if handset has been knocked. You can get the top of the handset with a small coin on the plastic screws either side. Try rebooting first though.
 - (iii) RFID numbers recorded as squares is another problem (usually a battery connection problem inside the backpack) check connectors and tighten with pliers if necessary and reconnect.
 - (iv) Coordinates show some characters and lots of commas. This seems to occur when the handset is set up indoors. This should clear once the handset is in satellite view, but if it doesn't, go through the set up process again outdoors.

*To resolve RFID error where GPS box shows endlessly cycling data:

- The software should be set up to only use GGA, but rebooting the device or using the standard GPS software seems to reset this in RFID so the device is trying to use several protocols. The result is that instead of the GPS window showing the coordinates, it shows a cycling set of characters.
- To fix this, use the SirfTech application installed on the Recon. This is not shown under Programmes, but can be found using Start – File Explorer. (SirfTech guidance and screen shots are found here: <http://w5.nuinternet.com/s660100031/SirfTech.htm>)
- Click the SirfTech icon and it takes you to the start screen shown on the web page
- Click Com and set com port to 2 and baud rate to 4800. Baud is the SI unit for number of symbols or pulses per second, named after Emile Baudot, in case you ever need it in a pub quiz. Click Open and the NMEA messages number should start to change.
- Click OK
- From the main screen, click NMEA, Set Message Rate.
- In here you'll see a list of protocols and some of them might be time logging. Click the Message twisty to select each protocol. Choose GGA, set update rate to 1 and make sure the Use box is ticked. Press Set.
- Go through the process for all the others, setting update rate to 0 and unticking Use. I think you need to press Set after each one.

- Click OK
- From the main screen, NMEA, then Set Serial port (switch to Sirf)
- In here make sure Protocol is Sirf and Baud is 4800. NMEA time will be clocking. Click Set and wait, and Sirf time will start to clock, and NMEA will stop. Click =Baud.
- Click OK back to main screen
- Now the main screen should show some location data.
- Finally, click Sirf, Switch to NMEA and you'll see all the protocols listed. Set GGA to update rate =1 and all the others to 0. Sirftime will be clocking. Click set and wait. NMEA time will then start to clock. OK back to main screen.
- Start screen should still show the location data.
- Click Com, and you'll see port 2 is open and the clock and data count will be logging. Click Close and they will stop. This frees up port 2 to allow RFID to use the port.
- Open RFID and follow the instructions to connect
- Once RFID is running, the GPS window should now show GGA then the coordinates.

Selsey kit

Pre-survey

- Charge batteries for RFID (using Overlander RC-6S Pro charger)
 - If 'low voltage' error comes up, you have to charge in stages – choose a lower voltage to charge to first, and then later increase to full 14.8V.
- Check batteries in GPS and change if necessary (2x AAA batteries, need a flat screwdriver to access them)



- Check that GPS settings are correct (logging once per second – once set up it should remember its settings whenever you switch it on). Instructions are in the Instruction Manual (big white folder).
- Change date/time on detector so it will register accurate time stamps for pebbles detected

- To do this, you will need to plug in the cream-colour antenna loop (never switch on the detector box unless this or the main antenna is plugged in - & make sure it's plugged in properly, it may need an extra hard push)



- Switch on the box. All lights should flash initially, then only the red light to indicate it's on
- Connect the detector to a computer (probably easiest via bluetooth link – there is a Bluetooth connector. The code is 1234)
- Use Hyperlink or Putty to adjust the time to the nearest second (instructions for both of these are found in the yellow section (Command Line Interface) of the main Instruction Manual)

At beach

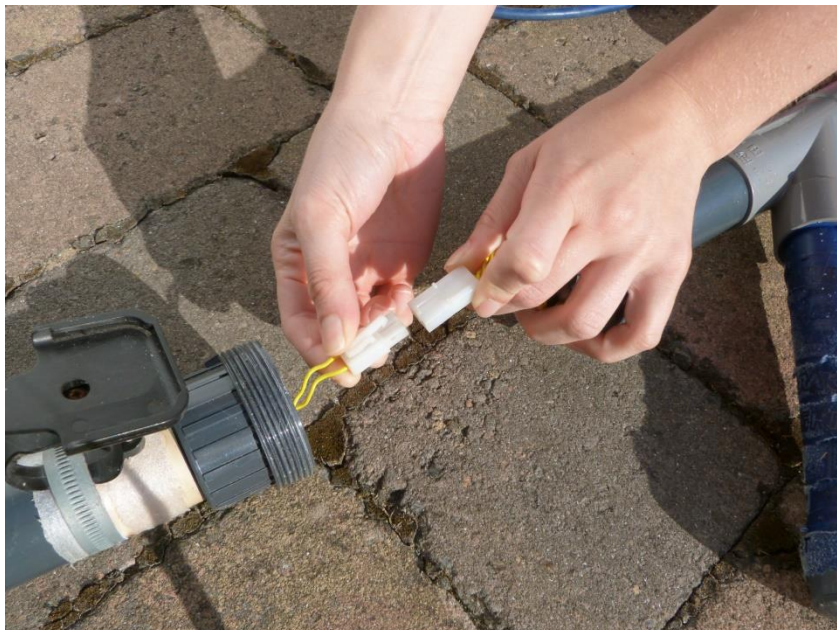
Need: Two sections of RFID antenna, backpack with box inside, Lipo battery (or batteries), GPS tracker, tester pebbles

- Turn on GPS by holding down power button. Wait for it to find satellites
- Connect LiPo battery to RFID detector and slot into backpack





- Join two parts of detector together, ensuring white clip is properly attached



- Plug antenna into box/backpack via 3-pin plug



- Turn on detector
- Ensure GPS is logging once per second (this will cause a small dot to appear on the screen. If it's not logging once per second the dot will flash up periodically).
- Clip GPS to detector

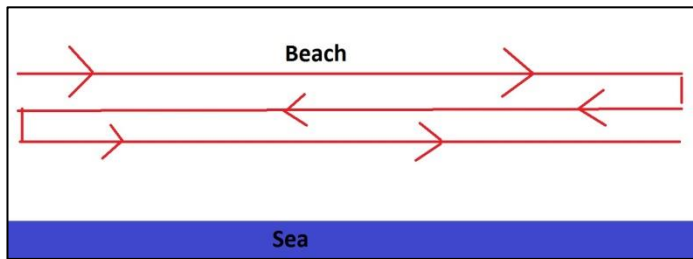


- Make sure detector is working by placing a pebble on the ground and sweeping the loop over it. The buzzer is broken, but it may make a sound. Also, the green 'detect' light will flash on the box in the backpack.

For both kits

Surveys should be done at low tide. It may be best to split the intended survey area into two sections, surveying one before the tide reaches its lowest, and one afterwards. In the first section, work from the top of the beach down to the water, and in the second section work from the water back up the beach.

Starting in the corner of the survey area, walk in a straight line from one end to the other, and then turn and follow the same line but approximately 2 metres away. Your survey path will look something like this:



As you walk, keep the antenna loop as close to the ground as possible. Sweep it from side to side at a steady pace (if you sweep too quickly, the detector may miss pebbles). Don't walk too fast, or you will miss large sections of beach between each sweep.

Whilst working on tricky shaped sections work logically using straight lines as often as possible and tackling odd shaped sections as a complete separate piece to reduce walking distance, think practically and logically. Some sections are accessible for a very short time at low tide so get those done first at low tide. Don't go out onto sand banks or parts that become cut off, you won't find any tags there as the sand is too deep and it's dangerous. Sandy sections on the beach still need doing because there may be tracers buried below the sandy surface. Don't get disheartened if you don't find any tags for long periods of time – if you've checked the equipment is still working fine with test pebbles it is not a problem.

Before finishing make sure each corner of the area scanned is marked by scanning the two test pebbles in each of the 4 corners that mark the top and bottom of the area you've covered for the day. Allow some overlap of 1 or 2 metres each day to ensure there are no gaps between each day's sections.

Step 5: Data Processing, Display & Analysis

ESCP kit

Download data from handheld GPS

- To download data plug in handset and download via pop up window or drive letter.
- Should download as .txt files
- Import data to Excel, delimited by commas

The data will be separated into columns.

N35																
	A	B	C	D	E	F	G	H	I	J	K	L	M	N	O	P
1	\$GPGGA	72159	5047.497 N		101.7861 W		1	7	1.2	5.3 M		47.4 M			0000*4E	R 0000 0000000168
2	\$GPGGA	72206	5047.497 N		101.7857 W		1	7	1.2	5.4 M		47.4 M			0000*4A	R 0000 0000000168
3	\$GPGGA	72208	5047.497 N		101.7858 W		1	7	1.2	5.7 M		47.4 M			0000*49	R 0000 0000000168
4	\$GPGGA	73350	5047.549 N		101.752 W		1	8	1	1 M		47.4 M			0000*4F	R 0000 0000000168
5	\$GPGGA	74414	5047.737 N		101.7751 W		1	8	1	0.9 M		47.4 M			0000*4A	R 0000 0000000168
6	\$GPGGA	74910	5047.639 N		101.7547 W		1	8	1	0.6 M		47.4 M			0000*42	R 0000 0000000168
7	\$GPGGA	75924	5047.585 N		101.756 W		1	9	0.9	1 M		47.4 M			0000*42	R 0000 0000000168
8	\$GPGGA	75945	5047.575 N		101.7537 W		1	10	0.9	0.9 M		47.4 M			0000*4C	R 0000 0000000168
9	\$GPGGA	80932	5047.617 N		101.7496 W		1	9	0.9	1.3 M		47.4 M			0000*45	R 0000 0000000168
10	\$GPGGA	81627	5047.595 N		101.7585 W		1	8	1	5.5 M		47.4 M			0000*49	R 0000 0000000168
11	\$GPGGA	82555	5047.542 N		101.7624 W		1	9	0.9	2.8 M		47.4 M			0000*48	R 0000 0000000168
12	\$GPGGA	82557	5047.542 N		101.7624 W		1	9	0.9	2.8 M		47.4 M			0000*48	R 0000 0000000168
13	\$GPGGA	85020	5047.793 N		101.9094 W		1	9	0.9	2 M		47.4 M			0000*43	R 0000 0000000168
14	\$GPGGA	90519	5047.493 N		101.7562 W		1	9	1	0.3 M		47.4 M			0000*41	R 0000 0000000168
15	\$GPGGA	92149	5047.536 N		101.7762 W		1	9	1	5.2 M		47.4 M			0000*47	R 0000 0000000168
16	\$GPGGA	92210	5047.536 N		101.7762 W		1	9	1	4.8 M		47.4 M			0000*43	R 0000 0000000168
17	\$GPGGA	94841	5047.662 N		101.7641 W		1	9	1	1.6 M		47.4 M			0000*42	R 0000 0000000168
18	\$GPGGA	95914	5047.795 N		101.8922 W		1	9	1	2.1 M		47.4 M			0000*4A	R 0000 0000000168
19																
20																
21																

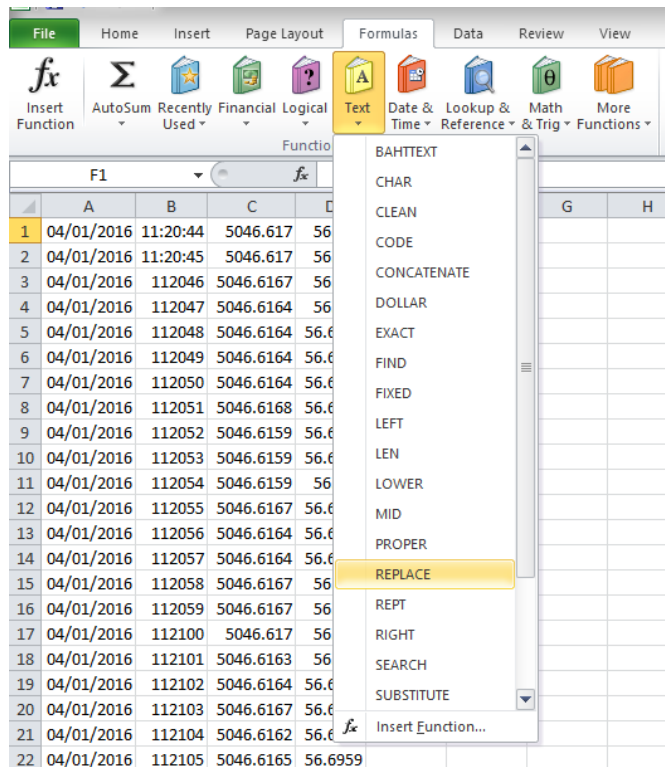
- The majority of this data set considered noise. Remove the highlighted columns shown below.

O1																
	A	B	C	D	E	F	G	H	I	J	K	L	M	N	O	P
1	\$GPGGA	72159	5047.5 N		101.786 W		1	7	1.2	5.3 M		47.4 M			0000*4E	R 0000 0000000168765983
2	\$GPGGA	72206	5047.5 N		101.786 W		1	7	1.2	5.4 M		47.4 M			0000*4A	R 0000 0000000168765980
3	\$GPGGA	72208	5047.5 N		101.786 W		1	7	1.2	5.7 M		47.4 M			0000*49	R 0000 0000000168765983
4	\$GPGGA	73350	5047.55 N		101.752 W		1	8	1	1 M		47.4 M			0000*4F	R 0000 0000000168765980
5	\$GPGGA	74414	5047.74 N		101.775 W		1	8	1	0.9 M		47.4 M			0000*4A	R 0000 0000000168765983
6	\$GPGGA	74910	5047.64 N		101.755 W		1	8	1	0.6 M		47.4 M			0000*42	R 0000 0000000168765980
7	\$GPGGA	75924	5047.57 N		101.756 W		1	9	0.9	1 M		47.4 M			0000*42	R 0000 0000000168765983
8	\$GPGGA	75945	5047.57 N		101.754 W		1	10	0.9	0.9 M		47.4 M			0000*4C	R 0000 0000000168765980
9	\$GPGGA	80932	5047.62 N		101.75 W		1	9	0.9	1.3 M		47.4 M			0000*45	R 0000 0000000168765983
10	\$GPGGA	81627	5047.6 N		101.759 W		1	8	1	5.5 M		47.4 M			0000*49	R 0000 0000000168765980
11	\$GPGGA	82555	5047.54 N		101.762 W		1	9	0.9	2.8 M		47.4 M			0000*4B	R 0000 0000000168765983
12	\$GPGGA	82557	5047.54 N		101.762 W		1	9	0.9	2.8 M		47.4 M			0000*48	R 0000 0000000168765980
13	\$GPGGA	85020	5047.79 N		101.909 W		1	9	0.9	2 M		47.4 M			0000*43	R 0000 0000000168765983
14	\$GPGGA	90519	5047.49 N		101.756 W		1	9	1	0.3 M		47.4 M			0000*41	R 0000 0000000168765980
15	\$GPGGA	92149	5047.54 N		101.776 W		1	9	1	5.2 M		47.4 M			0000*47	R 0000 0000000168765983
16	\$GPGGA	92210	5047.54 N		101.776 W		1	9	1	4.8 M		47.4 M			0000*43	R 0000 0000000168765980
17	\$GPGGA	94841	5047.66 N		101.764 W		1	9	1	1.6 M		47.4 M			0000*42	R 0000 0000000168765983
18	\$GPGGA	95914	5047.79 N		101.892 W		1	9	1	2.1 M		47.4 M			0000*4A	R 0000 0000000168765980
19																

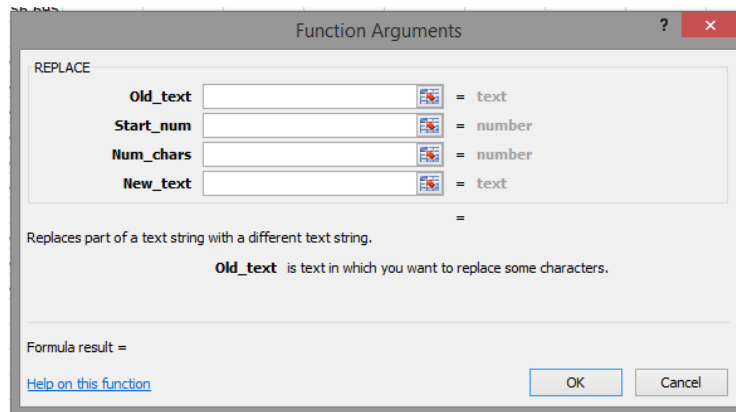
The remaining data depicts the Latitude (North) and Longitude (West) coordinates, Elevation and RFID number.

You now need to change the way the latitude and longitude are displayed. Use the 'replace' function in Excel:

- Select empty cell G1
- In the formulas tab, choose Text, and Replace



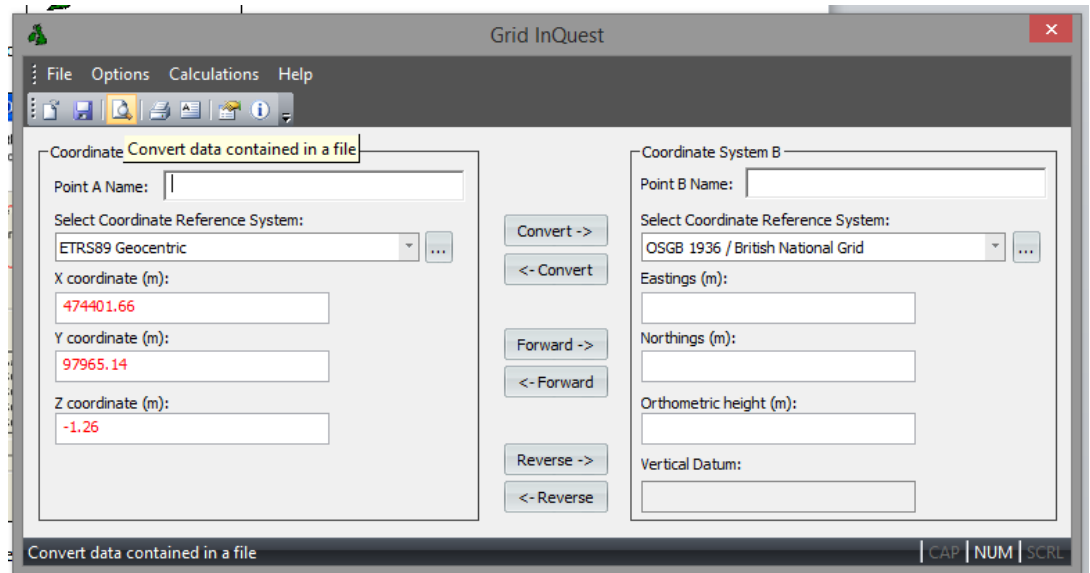
- The Function Arguments screen will pop up:



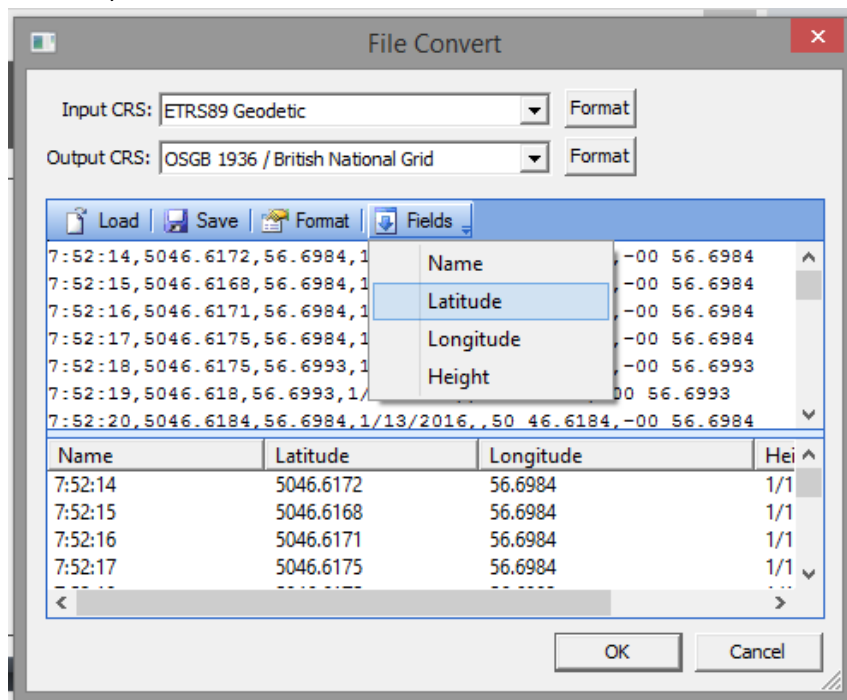
- Choose cell A1 for Old_text
- Start_num = **1**
- Num_chars = **2**
- Next_text = **"50 "** (There is a space after the fifty. Speechmarks are required, as Excel won't recognise the space without the speechmarks).
- Click OK
- Drag the right bottom corner of cell G1 to copy this formula to the bottom of the data set.
- Repeat this process in Column H for the data in column C, with the following:
 - Old_text = cell **C1**
 - Start_num = **1**
 - Num_chars = **1**
 - Next_text = **"-00 5"** (There is a space after the zeroes.)

- (This may be slightly different depending on which part of coast you have surveyed. If the W value doesn't start with a 5, then you will need to change what you write in the Next_text box.)
- Save as .xls(x) file

Use Grid Inquest to convert the lat/long to Eastings and Northings. (Use time column as 'name').



- Change the fields to the correct columns of the spreadsheet as necessary (for example, in the screenshot below, the lat and long need to be changed to the new/edited columns)



- Save as .csv file

Prepare the converted file for importing to ArcMap

- Columns required, with titles: PebbleID, Easting, Northing
- Save as .xls(x) file

Selsey kit

Download GPS data

- Use disc and cable to download GPS data – user manual kept with mini-disc explains how to do this
- Clear data log to free up space
- Data will save as two files - .kml and .nmea (You will need the .nmea files, which essentially open as text files)
- Make sure data is saved to the correct file path & has the date in its file name (yyyymmdd e.g. 20160729 for 29th July 2016). If more than one survey is done on the same day, differentiate these as appropriate.

Process GPS data in Excel

- 'Data' → 'from text'. Choose relevant .nmea file (if it doesn't show up initially, change to 'all files' in the drop down menu on the bottom right of the file selector)
- Text Import Wizard will pop up. Choose 'Delimited', click next
- Select 'comma' in delimiters list. Click next
- Click finish. Click yes to add to existing worksheet
- Delete unnecessary rows (assuming that your data looks the same as below, you need to **keep** rows B,D,F,J – the highlighted ones).

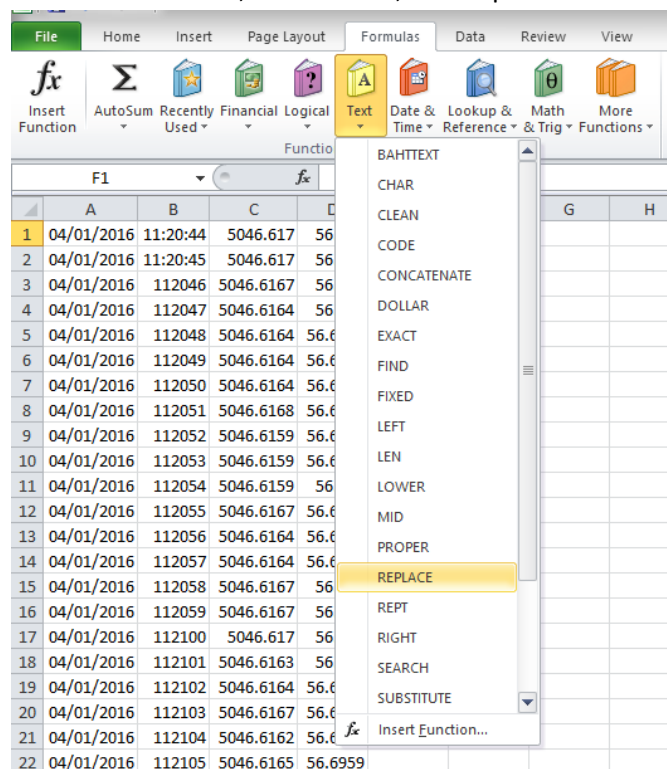
	A	B	C	D	E	F	G	H	I	J	K	L	M	N
1	\$GPRMC	112044	A	5046.617	N	56.695	W	0	0	40116			A*42	
2	\$GPRMC	112045	A	5046.617	N	56.695	W	0	0	40116			A*43	
3	\$GPRMC	112046	A	5046.6167	N	56.695	W	0	0	40116			A*46	
4	\$GPRMC	112047	A	5046.6164	N	56.695	W	0	0	40116			A*44	
5	\$GPRMC	112048	A	5046.6164	N	56.6959	W	0	0	40116			A*42	
6	\$GPRMC	112049	A	5046.6164	N	56.6959	W	0	0	40116			A*43	
7	\$GPRMC	112050	A	5046.6164	N	56.6959	W	0	0	40116			A*4b	
8	\$GPRMC	112051	A	5046.6168	N	56.6968	W	0	0	40116			A*44	
9	\$GPRMC	112052	A	5046.6159	N	56.6959	W	0	0	40116			A*47	
10	\$GPRMC	112053	A	5046.6159	N	56.6959	W	0	0	40116			A*46	
11	\$GPRMC	112054	A	5046.6159	N	56.695	W	0	0	40116			A*48	
12	\$GPRMC	112055	A	5046.6167	N	56.6959	W	0	0	40116			A*4d	

- Row J is the date (in this case, 4th January 2016). Change the first two cells to display it as 04/01/2016 and then highlight them both and drag (using the bottom right corner of the cells) to the end of your data set (assuming all your dates are the same. If not, first separate different dates into individual Excel spreadsheets).
- Then insert a new row before the time (row B in the above image) and move the dates over.
- Change the way the times are displayed so that they appear as 11:20:44, etc. (You can do this by adding the colons to the first two cells and then dragging down, assuming

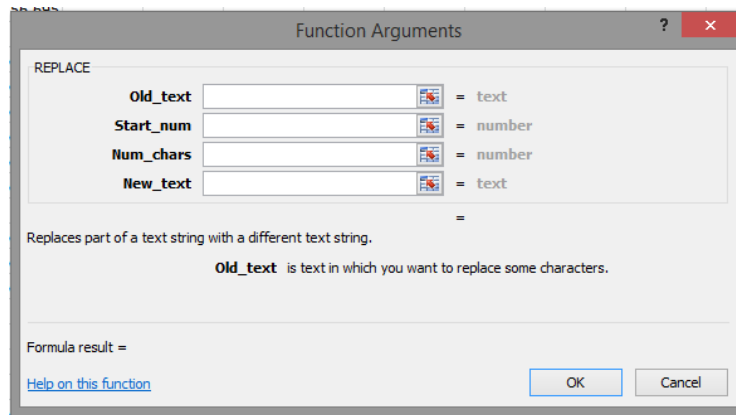
that all times are sequential. If there are gaps in the data where the GPS was switched off, you will first need to identify these.)

	A	B	C	D	E	F
1	04/01/2016	11:20:44	5046.617	56.695		
2	04/01/2016	11:20:45	5046.617	56.695		
3	04/01/2016	112046	5046.6167	56.695		
4	04/01/2016	112047	5046.6164	56.695		
5	04/01/2016	112048	5046.6164	56.6959		
6	04/01/2016	112049	5046.6164	56.6959		
7	04/01/2016	112050	5046.6164	56.6959		
8	04/01/2016	112051	5046.6168	56.6968		
9	04/01/2016	112052	5046.6159	56.6959		
10	04/01/2016	112053	5046.6159	56.6959		
11	04/01/2016	112054	5046.6159	56.695		
12	04/01/2016	112055	5046.6167	56.6959		
13	04/01/2016	112056	5046.6164	56.6959		
14	04/01/2016	112057	5046.6164	56.6959		

- You now need to change the way the latitude and longitude are displayed. Use the 'replace' function in Excel:
 - Select cell E1
 - In the formulas tab, choose Text, and Replace



- The Function Arguments screen will pop up:



- Choose cell **C1** for Old_text
- Start_num = **1**
- Num_chars = **2**
- Next_text = **"50 "** (There is a space after the fifty. Speechmarks are required, as Excel won't recognise the space without the speechmarks).
- Click OK
- Drag the right bottom corner of cell E1 to copy this formula to the bottom of the data set.
- Repeat this process in Column F for the data in column D, with the following:
 - Old_text = cell **D1**
 - Start_num = **1**
 - Num_chars = **1**
 - Next_text = **"-00 5"** (There is a space between the zeroes and the five.)
- Save as .xls(x) file

Use Grid Inquest to convert the lat/long to Eastings and Northings.

- Use time column as 'name'
- Save as .csv file

Download RFID data

- Plug cream colour antenna loop into detector box
- Switch datalogger box on
- Use Bluetooth antenna to connect to computer
 - code is 1234
 - alternatively, use a serial cable link
- Use Hyperlink or Putty to retrieve pebble detection data (instructions for these can be found in the big white folder 'Instruction Manual'
 - If using Hyperlink:
 - Save as text file by clicking 'Transfer'... 'Capture text'. Choose a file name that includes the survey date in the following format: yyyyymmdd
 - Then use command code 'UP' to download the data from the datalogger
 - Once it's complete, click 'Transfer'... 'Capture text'... 'Stop'.

- If using Putty, check the manual


Process RFID data in Excel

- Open file (Data→From text)
- Delimit by space
- Delete the first few rows (highlighted below)

	A1										
	A	B	C	D	E	F	G	H	I	J	
1	up										
2	Upload #29										
3	Reader: Noname	Site: AA									
4	-----	upload	29 start	-----							
5	E	07/01/2016	36:10.2	upload	28 complete						
6	E	13/01/2016	51:37.7	supply	power ok		14.8V				
7	E	13/01/2016	51:37.7	database	file opened						
8	E	13/01/2016	51:37.7	starting	reader after		power up				
9	D	13/01/2016	54:37.9	00:00.1	HR	0000_0000000179993301	2	1821			
10	D	13/01/2016	01:55.2	00:00.2	HR	0000_0000000184445482	3	4341			
11	D	13/01/2016	02:16.8	00:00.1	HR	0000_0000000184444906	2	212			
12	D	13/01/2016	02:18.1	00:00.3	HR	0000_0000000166941432	4	11			
13	D	13/01/2016	02:27.0	00:00.0	HR	0000_0000000184445170	1	84			
14	D	13/01/2016	02:27.2	00:00.1	HR	0000_0000000184445170	2	1			
15	D	13/01/2016	02:41.0	00:00.2	HR	0000_0000000184444453	3	135			
16	D	13/01/2016	09:41.3	00:00.1	HR	0000_0000000184445127	2	4171			
17	D	13/01/2016	14:20.4	00:00.2	HR	0000_0000000166941516	3	2770			
18	D	13/01/2016	15:03.5	00:00.1	HR	0000_0000000166941526	2	425			

- Delete columns A,D,E,G,H
- Format cells in New column B (right click, Format, cell type = time)

	A	B	C
1	13/01/2016	54:37.9	0000_00000001799933
2	13/01/2016	01:55.2	0000_00000001844454
3	13/01/2016	02:16.8	0000_00000001844449
4	13/01/2016	02:18.1	0000_00000001669414
5	13/01/2016	02:27.0	0000_00000001844451
6	13/01/2016	02:27.2	0000_00000001844451
7	13/01/2016	02:41.0	0000_00000001844444
8	13/01/2016	09:41.3	0000_00000001844451
9	13/01/2016	14:20.4	0000_00000001669415
10	13/01/2016	15:03.5	0000_00000001669415
11	13/01/2016	15:03.8	0000_00000001669415
12	13/01/2016	16:09.5	0000_00000001669414
13	13/01/2016	16:51.9	0000_00000001687654



	A	B	C
1	13/01/2016	07:54:38	0000_00000001799933
2	13/01/2016	08:01:55	0000_00000001844445
3	13/01/2016	08:02:17	0000_00000001844444
4	13/01/2016	08:02:18	0000_00000001669411
5	13/01/2016	08:02:27	0000_00000001844445
6	13/01/2016	08:02:27	0000_00000001844445
7	13/01/2016	08:02:41	0000_00000001844444
8	13/01/2016	08:09:41	0000_00000001844445
9	13/01/2016	08:14:20	0000_00000001669411
10	13/01/2016	08:15:04	0000_00000001669411
11	13/01/2016	08:15:04	0000_00000001669411
12	13/01/2016	08:16:09	0000_00000001669411
13	13/01/2016	08:16:52	0000_00000001687655

- 'Sort' data by tag ID (column C)
- Using the original tracer database (created when the pebbles were tagged), add each pebble's unique ID into column D. Duplicates can be ignored / deleted (for consistency, keep the first result for each tag ID – the GPS is only accurate to approximately 2 metres anyway, so this should not have much (if any) effect on the results).
- 'Sort' data by time (column B)
- Using the cleaned Eastings/Northings GPS file from the same survey, add the location data for each pebble detected (i.e. match the time of the pebble detection with the timestamp on a GPS location and copy across the Eastings and Northings)

	A	B	C	D	E	F
1	13/01/2016	07:54:38	0000_0000000179993301	014	474452.5	98021.16
2	13/01/2016	08:01:55	0000_0000000184445482	312	474445.2	97996.4
3	13/01/2016	08:02:17	0000_0000000184444906	342	474470.3	97991.2
4	13/01/2016	08:02:18	0000_0000000166941432	185	474471.4	97990.47

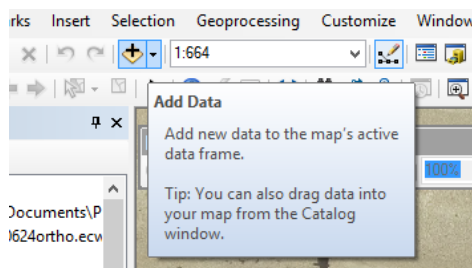
- Copy all of the data from columns D,E,F into a new spreadsheet. This is the data required for input into ArcMap. Use the first row of each column for a title: PebbleID, Easting, Northing.
Save the final file with the naming format: ProcessedYYYYMMDD (date of the survey). If more than one survey was done on the same day (e.g. by two different surveyors on neighbouring sections of beach) these can be placed in the same Excel file if necessary.

Data Display using ArcMap

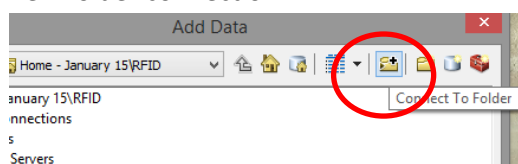
Data from both kits should now be in Excel spreadsheets containing information about the Pebble ID, Easting and Northing.

These are easily added to ArcMap.

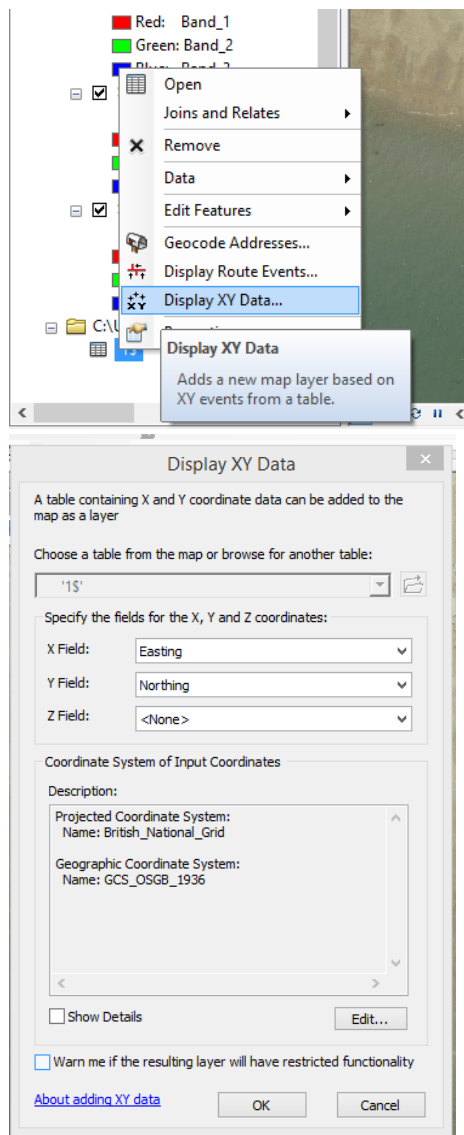
- Use CCO aerial imagery as a basemap
- Add the individual Excel worksheets as layers to the map



- If the folder you are looking for does not show up in the list, you will need to create a new folder connection:



- Once the layers have been added, right click on a layer in the Table of Contents on the left of the screen, select Display X Y data



- Choose Easting for X field and Northing for Y field, leave Z field blank
- Change the coordinate system by clicking 'edit' and choose British National Grid (located under 'Projected Coordinate Systems' → 'National Grids' → 'Europe')
- Uncheck the box to 'Warn me if the resulting layer will have restricted functionality' (the warning that shows up is completely irrelevant anyway and your data will still work fine).
- You can remove the original layers (with the spreadsheet symbol next to them) once all the point data has been converted.